Methods in Pharmacology and Toxicology

Series Editor
Y. James Kang

For further volumes:
http://www.springer.com/series/7653

TRP Channels in Drug Discovery

Volume II

Edited by

Arpad Szallasi

Monmouth Medical Center, Long Branch, NJ, USA

Tamás Bíró

Medical and Health Science Center, Department of Physiology,
University of Debrecen, Debrecen, Hungary

Humana Press

Editors
Arpad Szallasi
Monmouth Medical Center
Long Branch, NJ, USA

Tamás Bíró
Medical and Health Science Center
Department of Physiology
University of Debrecen
Debrecen, Hungary

ISSN 1557-2153 ISSN 1940-6053 (electronic)
ISBN 978-1-62703-094-6 ISBN 978-1-62703-095-3 (eBook)
DOI 10.1007/978-1-62703-095-3
Springer New York Heidelberg Dordrecht London

Library of Congress Control Number: 2012947027

Printed on acid-free paper

Humana Press is a brand of Springer
Springer is part of Springer Science+Business Media (www.springer.com)

Preface

With almost 600 reviews, Transient Receptor Potential (TRP) channels arguably represent today's most extensively reviewed pharmacological targets. The literature on TRP channels is vast and still growing: It has exploded from a mere 21 papers in 1995 to over 2,000 in the past 2 years. Yet, even the most studied TRP channels like TRPV1 continue to surprise: as Bernd Nilius points it out in his Introduction, "We are still at the beginning of the beginning."

Over the past decade, both gain- and loss-of-function mutations in TRP channels (so-called "TRP channelopathies") have been identified in human disease states ranging from focal segmental glomerulosclerosis (TRPC6) and familial episodic pain syndrome (TRPA1) through brachyolmia and hereditary arthropathy of hand and feet (TRPV4) to mucolipidosis type-4 (TRPML1) and amyotrophic lateralsclerosis and parkinsonism/dementia complex (TRPM7). These findings imply a therapeutic potential for drugs targeting TRP channels in a wide variety of diseases, many with no existing satisfactory treatment options. Indeed, a number of potent, small molecule TRPV1, TRPV3, and TRPA1 antagonists have already entered clinical trials, and many more are in preclinical development.

The TRP superfamily of ion channels in humans is a diverse family of 28 cation channels with varied physiological functions. Their name stems from their similarity on the sequence level to the original *trp* gene from *Drosophila* which, when mutated, resulted in a transient receptor potential in the presence of continued exposure to light. Overall, few generalizations can be made about TRP channels. Most family members share a low level of structural similarity, but some channels are very highly homologous to each other (e.g., TRPC3 and TRPC7; TRPV5 and TRPV6). Many TRP channels form functional channels as homotetramers, though heteromultimerization is not uncommon. The latter phenomenon may have important implications for drug discovery.

Consistent with their diverse structure, TRP channels also serve diverse functions including afferent sensory functions (mechanical, chemical, thermal, noxious, etc.) as well as efferent mechanisms (of growth control, cellular differentiation, vasoregulation, mediator release, etc.). While most family members are cation channels with limited selectivity for calcium, both calcium- (TRPV5 and TRPV6) and sodium-selective (TRPM4 and TRPM5) family members exist. In addition, some TRP channels transport noncanonical cations such as iron (TRPML1), magnesium (TRPV6), or zinc (TRPA1).

Of the 28 TRP channels discovered until today, seven sense hot or warm temperatures (TRPV1 to TRPV4, TRPM2, TRPM4, and TRPM5), whereas two (TRPA1 and TRPM8) are activated by cold. Together, these channels, referred to as "thermoTRPs," cover a wide temperature range with extremes that fall between 10 °C (TRPA1) and 53 °C (TRPV2). The temperature sensor is believed to be associated with the C terminus. In support of this model, swapping the C-terminal domain of TRPV1 with that of TRPM8 was shown to change the temperature sensitivity of TRPV1 from hot to cold.

Animal data and human genetic studies have shown that TRP channel dysfunction ("TRP channelopathy") can cause various pathological conditions. In fact, the TRML

(mucolipin) and TRPP (polycystin) families were named after the human diseases they are associated with (mucolipidosis and polycystic kidney disease, respectively). The founding member of the M (melastatin) family, TRPM1, was identified via comparative analysis of genes that distinguish benign nevi and malignant melanoma. The A (ankyrin) family has only one known member (TRPA1), and its name refers to the unusually high number of ankyrin repeats at the N terminus of the channel protein. Mammalian TRP channels that are most similar to those in *Drosophila* are referred to as canonical (TRPC). Last, the V (vanilloid) family came into existence by expression cloning of the capsaicin receptor TRPV1.

The aim of these volumes is ambitious: They open with a series of "state-of-the-art" minireviews on the most interesting TRP channels (from TRPA1 to TRPV4), followed by a collection of cookbook-like protocol chapters describing various methodologies (ranging from capsaicin inhalation test in humans through rodent models of anxiety to stroke, cancer, diabetes, and experimental colitis models) relevant to TRP channel research. Pain models (TRPs = "Targets for Relief of Pain") were previously detailed in our *Analgesia: Methods and Protocols* volume in the *Methods in Molecular Biology* series. Here, we focus on non-pain models in keeping with the alternative interpretation of TRPs: "Truly Remarkable Proteins."

It is our hope that this book will be useful for graduate students in academic laboratories as well as for scientists developing new drugs at Pharma and clinicians interested in novel drugs in the pipeline.

Long Branch, NJ, USA ***Arpad Szallasi***
Debrecen, Hungary ***Tamás Biró***

Contents

Contributors

Ovidiu Constantin Baltatu • *Universidade Camilo Castelo Branco, São José dos CamposSão Paulo, Brazil*

Heike Benecke • *Department of Cell Physiology, Ruhr-University Bochum, Bochum, Germany*

L. Ashley Blackshaw • *Nerve-Gut Research Laboratory, Department of Medicine, Faculty of Health Sciences, The University of Adelaide, Adelaide, SA, Australia; Department of Gastroenterology & Hepatology, Hanson Institute, Royal Adelaide Hospital, Adelaide, SA, Australia; Faculty of Health Sciences, The University of Adelaide, Adelaide, SA, Australia*

Kata Bölcskei • *Analgesic Research Laboratory, University of Pécs, Pécs, Hungary; Laboratory of Neuropharmacology, Pharmacological and Drug Safety Research, Gedeon Richter Plc., Budapest, Hungary*

Stuart M. Brierley • *Nerve-Gut Research Laboratory, Department of Medicine, Faculty of Health Sciences, The University of Adelaide, Adelaide, SA, Australia; Department of Gastroenterology & Hepatology, Hanson Institute, Royal Adelaide Hospital, Adelaide, SA, Australia; Department of Physiology, Faculty of Health Sciences, The University of Adelaide, Adelaide, SA, Australia*

Luciana Aparecida Campos • *Universidade Camilo Castelo Branco, São José dos CamposSão Paulo, Brazil*

Joel Castro • *Nerve-Gut Research Laboratory, Department of Medicine, Faculty of Health Sciences, The University of Adelaide, Adelaide, SA, Australia; Department of Gastroenterology & Hepatology, Hanson Institute, Royal Adelaide Hospital, Adelaide, SA, Australia*

Loris A. Chahl • *School of Biomedical Sciences and Pharmacy, University of Newcastle, Newcastle, NSW, Australia; Schizophrenia Research Institute, Sydney, NSW, Australia*

Sharon C. Cheetham • *RenaSci Limited, BioCityNottingham, UK*

Robert Cornell • *Department of Anatomy and Cell Biology, Carver College of Medicine, University of Iowa, Iowa City, IA, USA*

Jennifer L. Coyner • *Psychiatry and Neuroscience, School of Medicine, Uniformed Services University (USU), Bethesda, MD, USA; Center for Neuroscience and Regenerative Medicine (CNRM), Bethesda, MD, USA*

Michael F. Crutchlow • *Merck Sharp & Dohme Corp., Whitehouse Station, NJ, USA*

Amanda Decker • *Department of Anatomy and Cell Biology, Carver College of Medicine, University of Iowa, Iowa City, IA, USA*

Alisa S. Elliott • *Department of Neurosurgery and The Center for Neuroscience, West Virginia University, School of Medicine, Morgantown, WV, USA*

Lisa Foa • *School of Medicine, University of Tasmania, Tasmania, Australia*

Angela M. Gajda • *Research Diets, Inc., New Brunswick, NJ, USA*

Robert J. Gasperini • *Menzies Research Institute Tasmania, University of Tasmania, Tasmania, Australia*
José C. González-Cobos • *The Center for Cardiovascular Sciences, Albany Medical College, Albany, NY, USA*
Dorte X. Gram • *XENIA PHARMA, Copenhagen, Denmark; Department of Science, System, and Models, Roskilde University, Roskilde, Denmark*
Joel D. Greenspan • *Department of Neural and Pain Sciences and Brotman Facial Pain Center, University of Maryland Dental School, Baltimore, MD, USA*
Kelly E. Harmon • *The Center for Cardiovascular Sciences, Albany Medical College, Albany, NY, USA*
Andrea M. Harrington • *Nerve-Gut Research Laboratory, Department of Medicine, Faculty of Health Sciences, The University of Adelaide, Adelaide, SA, Australia; Department of Gastroenterology & Hepatology, Hanson Institute, Royal Adelaide Hospital, Adelaide, SA, Australia*
Rikard Holmdahl • *Medical Inflammation Research, Department of Medical Biochemistry and Biophysics, Karolinska Institute, Stockholm, Sweden*
Jason D. Huber • *The Center for Neuroscience and Department of Basic Pharmaceutical Sciences, West Virginia University, School of Medicine, Morgantown, WV, USA*
Patrick A. Hughes • *Nerve-Gut Research Laboratory, Department of Medicine, Faculty of Health Sciences, The University of Adelaide, Adelaide, SA, Australia; Department of Gastroenterology & Hepatology, Hanson Institute, Royal Adelaide Hospital, Adelaide, SA, Australia; Leukocyte Biology Laboratory, Women's and Children's Health Research Institute, North Adelaide, SA, Australia*
Yuko Iwata • *Department of Molecular Physiology, National Cerebral and Cardiovascular Center Research Institute, Osaka, Japan*
Helen C. Jackson • *RenaSci Limited, BioCity, Nottingham, UK*
Luke R. Johnson • *Psychiatry and Neuroscience, School of Medicine, Uniformed Services University (USU), Bethesda, MD, USA; Center for the Study of Traumatic Stress (CSTS), Bethesda, MD, USA; Center for Neuroscience and Regenerative Medicine (CNRM), Bethesda, MD, USA*
Sergii Khalimonchyk • *INSERM U-1003, Equipe labellisée par la Ligue Nationale contre le cancer, Villeneuve d'Ascq, FranceS. Khalimonchyk Université des Sciences et Technologies de Lille (USTL), Villeneuve d'Ascq, France*
V'yacheslav Lehen'kyi • *INSERM U-1003, Equipe labellisée par la Ligue Nationale contre le cancer, Villeneuve d'Ascq, France; Université des Sciences et Technologies de Lille (USTL), Villeneuve d'Ascq, France*
Matteo Levisetti • *Global Clinical Development, Pfizer, La Jolla, CA, USA*
Tobias Lotts • *Department of Dermatology, Clinical Neurodermatology, University of Münster, Münster, Germany*
Yan Ma • *Li Ka Shing Institute of Health Sciences, School of Biomedical Sciences, Chinese University of Hong Kong, Hong Kong, China*
Jennifer L. McGuire • *Psychiatry and Neuroscience, School of Medicine, Uniformed Services University (USU), Bethesda, MD, USA*
Laurent Misery • *Department of Dermatology, University Hospital of Brest and Laboratory of Neurosciences of Brest, University of Western Brittany, Brest, France*

Rajender K. Motiani • *The Center for Cardiovascular Sciences, Albany Medical College, Albany, NY, USA*
Kutty Selva Nandakumar • *Medical Inflammation Research, Department of Medical Biochemistry and Biophysics, Karolinska Institute, Stockholm, Sweden*
Michael A. Pellizzon • *Research Diets, Inc., New Brunswick, NJ, USA*
Michael P. Philpott • *Centre for Cutaneous Research, Blizard Institute, Barts and The London School of Medicine and Dentistry, Queen Mary College University of London, London, UK*
Albin Pourtier • *Institut de Biologie, UMR-8161, CNRS/Universités de Lille1 et Lille2/ Institut Pasteur de Lille, Lille, France*
Natalia Prevarskaya • *INSERM U-1003, Equipe labellisée par la Ligue Nationale contre le cancer, Villeneuve d'Ascq, France;*
Université des Sciences et Technologies de Lille (USTL), Villeneuve d'Ascq, France
Maylis Raphaël • *INSERM U-1003, Equipe labellisée par la Ligue Nationale contre le cancer, Villeneuve d'Ascq, France;*
Université des Sciences et Technologies de Lille (USTL), Villeneuve d'Ascq, France
Antonio Reboreda • *Section of Physiology, Department of Functional Biology and Health Sciences, School of Biology, University of Vigo, Vigo, Pontevedra, Spain*
Matthew R. Ricci • *Research Diets, Inc., New Brunswick, NJ, USA*
Caitlin J. Riebe • *Max Planck Institute of Psychiatry, Munich, Germany*
Charles L. Rosen • *Department of Neurosurgery and The Center for Neuroscience, West Virginia University, School of Medicine, Morgantown, WV, USA*
Katalin Sandor • *Department of Physiology and Pharmacology, Karolinska Institute, Stockholm, Sweden*
Koji Shibasaki • *Department of Molecular and Cellular Neurobiology, Gunma University Graduate School of Medicine, Maebashi, Japan*
Sonja Ständer • *Department of Dermatology, Clinical Neurodermatology, University of Münster, Münster, Germany*
Kenneth J. Sufka • *Department of Psychology, Department of Pharmacology, Research Institute of Pharmaceutical Sciences, University of Mississippi, Oxford, MI, USA*
Xiaojing Sun • *Department of Biochemistry and Molecular Biology, Mayo Clinic, Rochester, MN, USA;*
Division of Cardiovascular Diseases, Department of Medicine, Mayo Clinic, Rochester, MN, USA
Anish Suri • *Discovery Immunology, Bristol Myers Squibb, Princeton, NJ, USA*
Camilla I. Svensson • *Department of Physiology and Pharmacology, Karolinska Institute, Stockholm, Sweden*
Yung-Wui Tjong • *Li Ka Shing Institute of Health Sciences, School of Biomedical Sciences, Chinese University of Hong Kong, Hong Kong, China*
Mohamed Trebak • *The Center for Cardiovascular Sciences, Albany Medical College, Albany, NY, USA*
Ryan C. Turner • *Department of Neurosurgery and The Center for Neuroscience, West Virginia University, School of Medicine, Morgantown, WV, USA*
Shigeo Wakabayashi • *Department of Molecular Physiology, National Cerebral and Cardiovascular Center Research Institute, Osaka, Japan*
Janine Wäring • *Department of Cell Physiology, Ruhr-University Bochum, Bochum, Germany*

Stephen W. White • *Department of Psychology, University of Mississippi, Oxford, MI, USA*
Carsten T. Wotjak • *Max Planck Institute of Psychiatry, Munich, Germany*
Xiaolei Xu • *Department of Biochemistry and Molecular Biology, Mayo Clinic, Rochester, MN, USA;*
Division of Cardiovascular Diseases, Department of Medicine, Mayo Clinic, Rochester, MN, USA
Xiaoqiang Yao • *Li Ka Shing Institute of Health Sciences, School of Biomedical Sciences, Chinese University of Hong Kong, Hong Kong, China*
Wei Zhang • *The Center for Cardiovascular Sciences, Albany Medical College, Albany, NY, USA*
Xuexin Zhang • *The Center for Cardiovascular Sciences, Albany Medical College, Albany, NY, USA*
Beili Zhu • *Janey and Dolph Briscoe Division of Cardiology, Department of Medicine, The University of Texas Health Science Center at San Antonio, San Antonio, TX, USA*

Part I

TRPs and Cardiovascular Disease

Chapter 1

TRPs to Cardiovascular Disease

José C. González-Cobos, Xuexin Zhang, Rajender K. Motiani, Kelly E. Harmon, and Mohamed Trebak

Abstract

Transient receptor potential (TRP) is a large superfamily of cation channels comprising 28 members in mammals. TRP channels are ubiquitously expressed in human tissues, including the cardiovascular system where they have been associated with a number of physiological functions, such as proliferation, contraction, and migration. TRP channels comprise six large families of cation channels: TRPC, TRPM, TRPV, TRPP, TRPA, and TRPML with diverse ion selectivities and modes of activation. Depending on the isoform considered, activation of TRP channels can cause entry of Ca^{2+}, Na^{+}, or Mg^{2+} into cells. TRP channels have recently emerged as attractive drug targets for treatment of cardiovascular diseases since their expression and/or activation was shown to be disturbed in certain pathophysiological conditions, such as cardiac hypertrophy and hypertension. In this short review, we will summarize data on the expression of TRP channels in the three major cell types of the cardiovascular system: cardiomyocytes, endothelial cells, and smooth muscle cells and will review evidence for the involvement of TRP channels in mediating cardiovascular disease.

Key words: TRP channels, Cation channels, Cardiac hypertrophy, Smooth muscle remodeling, Endothelium-dependent vasorelaxation, Hypertension, Restenosis

1. Introduction

The cardiovascular system (CVS) comprises the heart muscle and the vascular system; its role is to maintain blood flow and secure oxygen transport and organ perfusion to match the body's metabolic demand. This function of the CVS is supported by a complex physiological network that includes both global and local control levels. While global circuits of control include baroreceptor firing, humoral factors, and vasoactive hormones secreted in response to general physiological changes (e.g., blood pressure), local control

Arpad Szallasi and Tamás Bíró (eds.), *TRP Channels in Drug Discovery: Volume II*, Methods in Pharmacology and Toxicology, DOI 10.1007/978-1-62703-095-3_1,

involves cell sensing and integration of specific physiological stimuli to generate appropriate tissue-specific cellular responses.

The transient receptor potential (TRP) is a large superfamily of cation channels related to *drosophilae trp*. The *trp* gene was identified from work in *Drosophila* phototransduction and is required for proper activation of a phospholipase C (PLC)-dependent calcium (Ca^{2+}) entry pathway in photoreceptor cells; in *trp* mutant flies, activation of photoreceptors developed a transient PLC-dependent Ca^{2+} entry in response to prolonged light stimulation, by comparison to the sustained Ca^{2+} entry observed in wild-type flies, resulting in impaired vision (1–7). All 28 mammalian TRP proteins form cation channels with an amazing diversity of cation selectivity and activation mechanisms (8). Some TRP channels function as cellular sensors and open upon direct binding of a ligand while others are activated through PLC-coupled receptors, such as G-protein-coupled receptors and receptor tyrosine kinase. The vast majority of TRP channels are nonselective cation channels that permeate Ca^{2+} ions. Notorious exceptions include TRPV5 and TRPV6 channels which are highly Ca^{2+} selective; TRPM6 and TRPM7 which are Mg^{2+} selective, and TRPM4 and TRPM5 that do not permeate Ca^{2+} (9–13).

Since the cloning of the first mammalian TRP nearly two decades ago, a number of studies contributed greatly to our understanding of the role of TRP channels in cellular sensory mechanisms and their implications in diverse physiological functions and pathophysiological situations. In this mini-review, we will summarize TRP channel contributions to the physiology of the cardiovascular system and their role in the development of cardiac and vascular pathologies.

2. TRP Channels: Biophysical Properties and Activation Mechanisms

Although all members of the TRP channel superfamily share structural similarities, such as the presence of six transmembrane (6TM) domains with a putative pore forming region between TM5 and TM6 and cationic permeability, sequence homologies found when comparing different members can be as low as 20% (14, 15). Based on sequence homology and functional similarities the 28 TRP members have been classified into six major families including the "classical" or "canonical" TRPs (TRP**C**); the vanilloids (TRP**V**); the melastatins (TRP**M**); the mucolipins (TRP**ML**); the polycystins (TRP**P**); and the ankyrin transmembrane protein 1 (TRP**A1**). A seventh family, TRPN, contributes proteins in flies and worms but has not been identified in higher organisms (15, 16). The biophysical properties and mechanisms of activation proposed for TRP channels will be briefly discussed below.

2.1. TRPCs

The canonical TRPs comprise seven members (TRPC1–TRPC7) of nonselective cationic channels (17, 18). This family shares the biggest similarity with the founding member *Drosophila trp* and is therefore referred to as classical or canonical (8). Based on structural homology, functional similarities, and direct protein–protein interactions, TRPC channels are further subdivided into four subfamilies: TRPC1, TRPC2, TRPC3/6/7, and TRPC4/5 (TRPC1 is sometimes included in the same subfamily as TRPC4/5) (19). TRPC2, although a pseudogene in humans, is known to encode functional channels in rodents and lower organisms. (For a comprehensive review the reader is referred to (20)). Overall, members of this family share the general TRP superfamily architectural features in addition to particular features, such as cytoplasmic N- and C-terminus where 3–4 ankyrin-like repeats (ANK1–4) and the invariant TRP signature motif (EWKFAR) are located, respectively (18, 21). The TRPC family displays conductances that range from 2 to 75 pico Siemens (pS) with cation permeability ratios P_{Ca}/P_{Na} ranging from 1 to 9, with nearly linear current–voltage relationship showing both inward and outward rectification and reversal potentials at or near 0 mV (0–20 mV), suggesting lack of cation selectivity (Table 1) (22–25).

Soon after their discovery, all TRPC channels were shown to be activated by PLC-coupled receptors such as G-protein-coupled receptors and receptor tyrosine kinases when ectopically expressed in HEK293 cells, and thus have been proposed to encode the then elusive store-operated Ca^{2+} (SOC) channels activated by depletion of inositol-1,4,5 trisphosphate (IP_3)-sensitive internal Ca^{2+} stores (18, 26–28). However, the lack of Ca^{2+} selectivity of TRPCs and the discovery 5 years ago of STIM and Orai proteins as the *bona fide* components of the highly Ca^{2+}-selective SOC pathway have cast doubts on the involvement of TRPCs as SOC channels (for review see (29, 30)). It is known that PLC activity leads to the concomitant production of IP_3 and diacylglycerol (DAG) and the production of an array of downstream intracellular second messengers; naturally, activation of PLC-coupled receptors can lead to the development of Ca^{2+} currents that could be activated by store-dependent as well as store-independent mechanisms related to the production of second messengers downstream the PLC pathway. In fact, it was promptly recognized that DAG analogues (e.g., oleyl-acetyl glycerol; OAG) and endogenous DAG could activate TRPC3/6/7 currents independently of Ca^{2+} store depletion (31, 32) (for review see (33)). The exact mechanism of activation of TRPC3/6/7 channels by DAG and whether DAG action is a direct or indirect one remain unknown. One argument in favor of an indirect action of DAG is the fact that under the cell-attached configuration of the patch clamp technique, TRPC7 channels could be activated by OAG, while OAG failed to activate TRPC7 channels in excised patches (34). Clearly, the activation of

Table 1
Biophysical properties, activators, and inhibitors of TRP channels

	Permeability (P_{Ca}/P_{Na})	Conductance (pS)	Activators/modes of activation	Inhibitors/modes of inhibition
TRPC1	Nonselective (199)	16 (199) 15, 29, 44 (169)	OAG (200), PLC (201), Angiotensin II (100 nM) (169), ET-1, SD (199, 202), Stretch (203–205)	SKF96365 (206), La^{3+}, Gd^{3+}, 2-APB (202), Chelerythrine, Wortmannin (20 μM) (200)
TRPC2	2.7 (207)	42 (207)	DAG, SAG (207), PLC (208), SD (209)	2-APB (207), SKF96365 (210)
TRPC3	1.62 (211)	23 (211) 17, 66 (212)	DAG, OAG (31, 32), IP_3, Carbachol (212, 213), UTP (214), ATP (215), PI(4,5)P_2(34)	2-APB (216), SKF96365 (217), PMA (32), Verapamil (217), La^{3+}, Gd^{3+}, Ni^{2+} (217)
TRPC4	1.1(218) 7 (219)	30 (220) 41 (221)	PLC, GTPγS, IP_3 (219, 221), ET-1 (171), Oxytocin (222), Acetylcholine (173), ATP (185), SD (185, 219), G proteins(38)	SKF96365 (223), ML204 (224), PI(4,5)P_2 (38)
TRPC5	1.8 (221) 9.5 (225)	30,47,66,70(226) 38 (227),63 (221)	PLC, GTPγS (221), ATP (225), Sphingosine-1-phosphate (176), SD (228), Genistein, La^{3+} (229), Acetylcholine, Carbachol (175), Gd^{3+}(230), Wortmannin, LY294002, PI(4,5)P_2(37)	2-APB (228), SKF96365, La^{3+} (225), Methoxyverapamil (228), Nifedipine (228), Flufenamate (175), PI(4,5)P_2(37)
TRPC6	5 (31)	2 (169) 15, 28, 44 (231) 35, 37 (31)	DAG, OAG, SAG, SLG (31), Stretch (232), 20-HETE (233), Angiotensin II (1 nM) (169, 231), Hyperforin (234), Acetylcholine (173), PI(4,5)P_2(34)	2-APB (176), SKF96365 (170), La^{3+}, Gd^{3+} (170), DiC8-PIP_2 (231), Angiotensin II (100 nM) (169)
TRPC7	1.9 (215)	75 (235)	DOG, OAG, ATP (215), SD (236), PI(4,5)P_2(34)	La^{3+}, SKF96365 (215)
TRPV1	10.2 (237) 9.6 (238)	35.4, 76.7 (238) 15(Ca^{2+}) (237) 63(Na^{+}) (237)	Capsaicin (239), 2-APB (75), Anandamide (240), RTX (241), DAG (242), protons (243), heat (threshold 42°C) (239), NADA (244)	Ruthenium red (69), Capsazepine (243, 245, 246), SB-366791 (246, 247), 5'-iodoresiniferatoxin (246), SB-452533 (248)
TRPV2	2.94 (249)	ND	Heat (threshold 52°C) (249), 2-APB (75), stretch (70)	Ruthenium red (70)

TRPV3	12.1 (71)	172 (71)	Heat (threshold 30°C) (71), Camphor (250), 2-APB (75)	Ruthenium red (71)
TRPV4	6.3 (251)	310 (252) 30(-60 mV) (251) 88 (60 mV) (251)	Osmotic cell swelling, Phorbols (79), heat (threshold 27°C) (253), 4α-PDD (254), EETs (160), GSK1016790A (255)	Ruthenium red (72)
TRPV5	>100 (9, 10)	77.5 (256)	Low intracellular Ca^{2+} (10), hyperpolarization (10), PIP_2 (257), SD (258)	Ruthenium red (73, 74), Econazole (73), 2-APB (258), high intracellular Mg^{2+} (257)
TRPV6	>100 (10)	40 (259)	Low intracellular Ca^{2+} (10), hyperpolarization (10)	Ruthenium red (74)
TRPM1	Nonselective (97)	ND	Constitutively activated (97)	Glutamate (97), La^{3+}, Gd^{3+} (260)
TRPM2	0.71(261)	65 (261) 58, 76 (262)	ADP-ribose (95, 100), cADP-ribose (95), NAD, H_2O_2 (263)	Flufenamic acid (264), 2-APB (265) Clotrimazole, Econazole (266)
TRPM3	1.57 (94)	65-133 (94)	Cell swelling (94), heat (108), Pregnenolone sulfate (267), D-erythro-sphingosine (94)	La^{3+}, Gd^{3+} (94), 2-APB (228)
TRPM4	Ca^{2+} impermeable (12)	25 (268) 20.9 (12)	Intracellular Ca^{2+} (12), Decavanadate (268), BTP2 (269), PKC, ATP (270), heat (104), $PI(4,5)P_2$ (271)	ATP_i, ADP_i, AMP_i (272), Flufenamic acid (273), Spermine (273), La^{3+}, Gd^{3+} (260)
TRPM5	Ca^{2+} impermeable (13)	23 (274) 25 (13)	Intracellular Ca^{2+} (13), $PI(4,5)P_2$ (13), heat (from15°C to 35°C) (104)	Flufenamic acid (273), Spermine (273), Decavanadate (268)
TRPM6	0.86 (11)	ND	Low intracellular Mg^{2+} (11)	High intracellular Mg^{2+} (11), Ruthenium red (275)
TRPM7	0.86 (11)	40-105 (276, 277)	Mg-ATP (278), $PI(4,5)P_2$ (279), low intracellular Mg^{2+} (11)	Spermine (280), Carbachol (279), high intracellular Mg^{2+} (11)
TRPM8	0.97 (103) 3.2 (105)	83 (105)	Cold (threshold of 21.8°C) (103), Menthol (103), Icilin (105)	Ruthenium red (103), 2-APB (281), SB-452533, BCTC (282), Capsazepine, CPTC (282)

(continued)

Table 1 (continued)

	Permeability (P_{Ca}/P_{Na})	Conductance (pS)	Activators/modes of activation	Inhibitors/modes of inhibition
TRPA1	0.84 (117)	40-105 (117)	Allicin, cold (average activation temperature of 17.5°C) (117), Methyl salicylate, Bradykinin, AITC, Cinnamaldehyde (283), Δ9 tetrahydrocannabinol (118), URB597 (284)	Ruthenium red (117, 283, 284)
TRPP2	Nonselective (285)	40-177 (111–113)	Gelsolin (286), EGF(287), hydro-osmotic pressure (288)	Anti-polycystin-2 antibody, Ca^{2+}, La^{3+}, Gd^{3+}, Diuretic amiloride (111), Li^{+} (289)
TRPP3	ND	137 (290)	Intracellular Ca^{2+} (290), Citric acid (291), removal of an acid stimulus (292)	ND
TRPP5	ND	300 (293)	Intracellular Ca^{2+}(293)	La^{3+}, Gd^{3+}, Amiloride (293)

ND, not determined; SD, store depletion; OAG, 1-oleoyl-2-acetyl-sn-glycerol; SKF96365, 1-[beta-[3-(4-methoxyphenyl)propoxy]-4-methoxyphenethyl]-1H-imidazole hydrochloride; Ang II, angiotensin II; DAG, diacylglycerol; SAG, 1-stearoyl-2-arachidonoyl-sn-glycerol; 2-APB, 2-aminoethoxydiphenyl borate; PMA,phorbol 12-myristate 13-acetate; ET-1, endothelin-1; SLG, 1-stearoyl-2-linoleoyl-sn-glycerol; DOG, 1,2-dioctanoylsn-glycerol; RTX, resiniferatoxin; SB-366791, N-(3-methoxyphenyl)-4-chlorocinnamide; SB-452533, N-(2-bromophenyl)-N-{2-[ethyl(3-methylphenyl)amino]ethyl}-urea; NADA, N-arachidonoyl-dopamine; 4α-PDD, 4 α-phorbol didecanoate; GSK1016790A, (N-((1S)-1-{[4-((2S)-2-{[(2,4-dichlorophenyl)sulfonyl]amino}-3-hydroxypropanoyl)-1-piperazinyl]carbonyl}-3-methylbutyl)-1-benzothiophene-2-carboxamide; EETs, epoxyeicosatrienoic acids; 20-HETE, 20-hydroxyeicosatetraenoic acid; NAD, nicotinamide adenine dinucleotide; BTP2, 3,5-bis(trifluoromethyl)pyrazole derivative; BCTC, N-(4-tertiarybutylphenyl)-4-(3-chloropyridin-2-yl) tetrahydropyrazine-1(2H)-carboxamide; CPTC, (2R)-4-(3-chloro-2-pyridinyl)-2-methyl-N-[4-(trifluoromethyl)phenyl]-1-piperazinecarboxamide; URB597, 3'-carbamoylbiphenyl-3-yl cyclohexylcarbamate; AITC, allyl isothiocyanate

TRPC3/6/7 by DAG is protein kinase C (PKC)-independent as PKC exerts a negative regulatory effect on these channels through phosphorylation (35). Activation of TRPC3/6/7 channels by phosphatidylinositol phosphates in excised patches has been reported. In fact, TRPC3/6/7 currents are robustly activated by application of $PI(4,5)P_2$ or ATP, but not by IP_3 in excised patches (34). The exact mechanisms of activation of TRPC1/4/5 under physiological conditions of stimulation by PLC-coupled receptors are even less clear. TRPC5 channels are activated by increases in local Ca^{2+} originating from Ca^{2+}-selective channels (36). TRPC5 channels are regulated by polyphosphoinositides in a complex manner. $PI(4,5)P_2$ and PI4P can activate TRPC5 channels in excised patches, but are inhibitory in the whole-cell configuration suggesting that membrane polyphosphoinositides have at least two independent roles in the regulation of TRPC5 channels (37). Otsuguro et al. showed that PIP_2 breakdown is required for the activation of the α-isoform of TRPC4. However, PIP_2 depletion was insufficient for channel opening; an additional requirement for Ca^{2+} and pertussis toxin-sensitive Gi/o proteins was noted (38).

As mentioned earlier, there is also a large body of literature suggesting TRPC channels as store-operated in a variety of cell types including endothelial cells and smooth muscle cells. Undeniably, all the TRPCs with the exception of TRPC6 were proposed to be sensitive to store depletion when studied either under endogenous conditions or overexpression systems (39–44). However, as pointed out earlier, major advances have been made regarding the molecular composition and activation mechanisms of SOC channels. Small interfering RNA (siRNA)-based high throughput screens coupled to the use of the SERCA pump inhibitor thapsigargin (to passively deplete the Ca^{2+} stores) by four independent groups have identified two conserved genes required for store-operated Ca^{2+} entry (SOCE): STIM1 and Orai1 (mammals have 2 STIMs and 3 Orais encoded by separate genes) (45–49). While STIM1 is the endoplasmic reticulum (ER)-resident Ca^{2+} sensor, Orai1 is the pore forming subunit of the archetypical SOC channel, CRAC (for Ca^{2+} release-activated Ca^{2+} current), at the plasma membrane. It is now well accepted that store depletion is sensed by a low-affinity Ca^{2+} binding EF hand located in the N-terminus of STIM1 facing the lumen of the ER resulting in STIM1 oligomerization and translocation to parts of the ER that are close to the plasma membrane (30, 50, 51). Recently, structure–function studies have identified a minimal conserved 100 amino acid region located in STIM1 C-terminus called STIM1 Orai1 Activating Region (SOAR) essential for the STIM–Orai physical coupling required for SOC channel activation, (For comprehensive reviews the reader is referred to (29, 52).) It is worth mentioning that in all of the screens noted above, none of the members of the wider TRP

superfamily gave a hit. Muallem and coworkers presented convincing biochemical evidence suggesting interactions of TRPC1/2/4/5 with the STIM1 ERM domain located in the C-terminus (53–55). Mutagenesis analysis showed that TRPC/STIM1 interactions are of electrostatic nature and occur in between two charged critical amino acids contained within the C-terminus of TRPC and STIM1 proteins. Other groups have reported the formation of ternary complexes between TRPC1, STIM1, and Orai1 that appear to be essential for the activation of nonselective channels in response to store depletion in human salivary gland cells and human platelets (56–58). However, an extensive study by DeHaven et al. demonstrated that the function of TRPC1, TRPC3, TRPC5, TRPC6, and TRPC7 does not depend on STIM1 or store depletion (59).

2.2. TRPVs

The vanilloid TRP channel family contains six members. The name vanilloid refers to the historical origin of its founding member TRPV1, first identified in sensory neurons as the extracellular vanilloid receptor (60). The members of this family are divided in two groups: TRPV1–TRPV4 and TRPV5/6 (61). While sharing the major TRP features (namely, 6TMs with a putative pore between TM5 and TM6, nonselective cationic permeability with the exception of TRPV5/6 which are Ca^{2+} selective (9, 10)), TRPV channels can be mainly differentiated by an ankyrin repeat domain composed of six ankyrin repeats that is located in the N-terminus, and by a version of the TRP box (VWKYQR) inserted within the TRP domain in the C-terminus (62–65). While ankyrin repeats in the N-terminus are believed to assist these channels in membrane trafficking and tetramerization, the TRP domain located in the C-terminus is thought to be a PIP_2 binding site required for modulation of TRPV channel activity and channel tetramerization (66–68).

Biophysically, the TRPV family displays differential Ca^{2+} selectivity expanding from nonselective to highly selective channels. TRPV1, TRPV2, TRPV3, and TRPV4 form nonselective cation channels with P_{Ca}/P_{Na} values that range from 1 to 12, depending on experimental conditions. In contrast, TRPV5 and TRPV6 have unusual Ca^{2+} selectivity with P_{Ca}/P_{Na} values that surpass 100, with current/voltage relationships displaying inward rectification (9, 10). Pharmacologically, all TRPVs are inhibited nonspecifically by ruthenium red and TRPV1–3 differentially potentiated by 2-aminoethoxydiphenyl borate (2-APB) (69–75). As it is the case with other TRPs, TRPVs can also form heterotetramers with distinct biophysical properties, thereby contributing to increased diversity of Ca^{2+} signals. This scenario has been reported for TRPV5 and TRPV6 and other studies suggest similar interactions between TRPVs and other TRPs (TRPM, TRPA) (76).

In general, TRPVs are polymodally activated channels with the capacity to integrate an array of physiological signals (77). Although

the founding member TRPV1 was first described as a chemical sensor (vanilloid receptor), it is now known that this family of cation channels is also responsive to other physiological stimuli including pain, temperature, osmotic/mechanical forces, lipid messengers, pH, intracellular Ca^{2+}, and a variety of synthetic compounds (78). Specifics about the activation mechanisms, gating, and channel regulation in response to these stimuli are starting to emerge and structure–function correlations for specific domains have been assigned. For example, activation of TRPV1 by capsaicin, the active component of hot chili peppers, has been suggested to occur intracellularly through a tyrosine–serine motif located in the intracellular loop between TM2 and TM3 regions (78). Similarly, TRPV4 sensitivity to phorbol esters, heat, and epoxyeicosatrienoic acid (EET) is compromised upon mutation of an analogous region located in the N-terminal end of TM3 (Tyr^{555} and Ser^{556}) (79). In addition, it has been suggested that responses to mechanical stimulus are indeed indirectly mediated by the actions of intracellular lipid mediators generated, whereby membrane stretching induces EET production and TRPV4 activation (80, 81); whether this lipid messenger acts directly or indirectly on the channel is still uncertain.

TRPV channels are known to contribute to physiological temperature regulation. Indeed, TRPV1, TRPV2, TRPV3, and TRPV4 channels are sensitive to a range of temperatures from warm to noxious heat and are collectively referred as thermo-TRPs (82, 83). Heterologous expression of these channels results in heat sensitivity with particular thresholds for each temperature-sensitive TRPV member: 42°C, 52°C, 30°C, and 27°C, for TRPV1 through 4, respectively (See Table 1). It is believed that temperature responsiveness is achieved through the C-terminus and the PIP_2 binding domain (84). Unlike other TRPVs, TRPV5 and TRPV6 channels are constitutively active, highly Ca^{2+} selective, and subject to complex Ca^{2+}-dependent inactivation mechanisms. They are responsive to 1,25-dihydroxyvitamin D_3 and are expressed in the apical side of epithelial cells consistent with their role in Ca^{2+} absorption. They are involved in renal, placental, and intestinal absorption of Ca^{2+} among other functions (85–87).

2.3. TRPMs

The TRPM channel family is composed of eight members with extreme functional and genetic diversity and is categorized in three main groups: TRPM1/3, TRPM4/5, and TRPM6/7 (TRPM2 and TRPM8 share low sequence homology and have not been grouped) (88, 89). This family is named after the founding member TRPM1 (melastatin), originally identified as a prognostic marker for metastasis of melanoma (90). Generally, TRPM channels share the typical TRP channel architecture including a TRP box similar to that of TRPCs, found in the C-terminus (65). However, this family shares a particular 700 amino acid-long

TRPM homology region located in the N-terminus (91). A feature unique to this family is the presence of enzymatically active protein domains in TRPM2, TRPM6, and TRPM7. While TRPM2 has a C-terminally located cytoplasmic Nudix box, a 22 amino acid-long consensus catalytic site for pyrophosphatases, TRPM6 and TRPM7 contain a serine/threonine protein kinase domain with homology to the eEF2 α-kinase family (92, 93).

Similar to TRPVs, TRPM channels display diversity of cation selectivities and biophysical properties. Overall, all members of this family are nonselective cation channels with TRPM4 and TRPM5 being Ca^{2+}-impermeable ($P_{Ca}/P_{Na} < 0.05$). TRPM unitary conductances range from ~25 pS for TRPM4/5 up to ~100 pS for TRPM3/7 depending on experimental conditions (See Table 1). Although TRPM channel Ca^{2+} permeability is not remarkable, agonist activation of TRPM-mediated currents leads to increased intracellular Ca^{2+} concentration in different cell lines. TRPM channels are differentially activated by a variety of physiological stimuli and second messengers including ADP-ribose (ADPR), temperature, reactive oxygen species, membrane stretching, and intracellular ionic levels (e.g., Mg^{2+}, Ca^{2+}) among others (See Table 1) (11, 94, 95).

Of all TRPM family members, TRPM1 was first to be discovered but not until recently examples of its function began to appear. Endogenous TRPM1 currents were described in primary human neonatal epidermal melanocytes and the magnitude of these currents correlated with TRPM1 mRNA levels in different melanomas (96). However, the mode of activation was not specified suggesting constitutive activity of the channel (97). In addition, TRPM1 currents were suggested to be required for the mediation of the depolarizing light response observed in retinal ON-bipolar cells (98).

The first TRPM2 activator identified was ADPR; this mode of activation was initially proposed given that ADPR was a putative substrate for the mitochondrial Nudix box-containing pyrophosphatase NUDT9 (nucleoside diphosphate-linked moiety X-type motif 9) (99). It has been suggested that TRPM2 channel activation might occur independently of activity of its catalytic domain. Along this line of thought, a splice variant lacking the C-terminus (TRPM2-ΔC) was shown to be responsive to H_2O_2 treatment, but could not be activated by ADPR dialysis (100). Conversely, subsequent studies suggested that TRPM2 sensitivity to H_2O_2 was conferred by cytosolic ADPR accumulation originating from the mitochondria. (For a comprehensive discussion in TRP channels as oxidative stress sensors the reader is referred to (99)). The idea of channel/enzyme independence is not unique to TRPM2 and has been proposed for TRPM7; TRPM7 channel activation occurs independently of autophosphorylation and kinase activity (101, 102). TRPM7 has been also proposed to be sensitive to reactive oxygen/nitrogen species, but this mechanism of activation remains unclear.

Other modes of TRPM activation include heat, cold, intracellular Ca^{2+}, and cell membrane stretching (94, 103). TRPM4 (TRPM4b) and TRPM5 have been reported to be sensitive to warm temperatures and intracellular Ca^{2+} (13, 104). Indeed, TRPM4- and TRPM5-mediated current amplitudes analyzed at +25 mV display 10-degree temperature coefficient values (Q_{10}) of 8.5 ± 0.6 between 15°C and 25°C arguing for strong temperature dependence; heat application shifted the activation curve towards negative potentials in a way analogous to that of TRPV1 (104). These channels have been also reported to be Ca^{2+}-sensitive although differing in the level of Ca^{2+} sensitivity: in both cases PIP_2 was identified as a channel modulator important in the mediation of channel desensitization and Ca^{2+} sensitivity. On the other hand, TRPM8 has been shown to be activated by cold temperature below 25°C and in response to the cooling compounds menthol and icilin (103, 105). In a manner analogous to TRPC5, PIP_2 differentially behaves as both a positive and negative TRPM8 channel modulator. While the presence of PIP_2 increases TRMP8 sensitivity to menthol and cold, depletion of membrane PIP_2 causes channel desensitization (106). This negative feedback mechanism is further amplified by PLC-coupled receptor activation resulting in PIP_2 breakdown and concomitant activation of PKC; PKC is another TRPM8 negative modulator. TRPM3 has been shown to form constitutively active channels whose activity can be potentiated in response to hypotonic stimulation resulting in membrane stretching (94). In HEK293 cells expressing TRPM3, application of a hypotonic extracellular solution (200 mOsm) resulted in a much stronger increase in intracellular Ca^{2+} concentration as compared to non-transfected controls. (For a review on TRPM3 variants, ion channel properties, and modes of activation the reader is referred to (107).) Most recently, TRPM3 has been also molecularly and functionally identified in a large subset of small-diameter sensory neurons from dorsal root and trigeminal ganglia where it supports the activation of nocifensive responses upon exposure to heat. This channel was reported to be steeply activated by heat and TRPM3-deficient animals displayed decreased avoidance to noxious heat (108).

2.4. TRPPs

The polycystin family of TRP channels is named after its founding member polycystic kidney disease-2 (TRPP2), a gene product mutated in the inherited human disorder known as autosomal dominant polycystic kidney disease (109). Structurally, this family of channels contains three members; PKD2, PKD2L1, and PKD2L2, currently known as TRPP2, TRPP3, and TRPP5, respectively (88). There is another genetically related locus also involved in polycystic kidney disease which encodes a large membrane protein (PKD1 or TRPP1) of unknown function. This family is characterized by structural features that include a putative large

extracellular loop located between TM1 and TM2, a coil-coiled domain in the C-terminal region, and a Ca^{2+} binding EF hand domain found specifically in TRPP2 and TRPP3 (110). TRPP2-related cation channels display large single-channel conductance ranging from 40 to 300 pS. In general, TRPP2-like proteins' P_{Ca}/P_{Na} ratios argue for their capacity to conduct both monovalent and divalent cations such as Na^+, K^+, Ba^{2+}, and Ca^{2+} with TRPP3 having the highest Ca^{2+} permeability ($P_{Ca}/P_{Na} = 4$) (111, 112). TRPP2 has been reported to localize to intracellular compartments and it has been proposed that TRPP2 plasma membrane localization and regulation require the formation of TRPP1/TRPP2 signaling complexes (113, 114).

2.5. TRPA

The ankyrin-rich TRP family consists of only one member TRPA1, previously known as ANKTM1 and P120. Like all other TRP families, the TRPA1 protein includes six TM spanning domains with a putative pore structure between TM5 and TM6, with cytosolic N- and C-terminus. The name ankyrin-rich refers to the structural characteristic of this protein containing up to 18 predicted ankyrin repeats located in its remarkably long N-terminus (115). These structural motifs are also present in other TRP channel subfamilies and have been long implicated in membrane localization, in channel tetramerization, and in the mediation of intramolecular interactions (64). TRPA1 channels are activated either directly or indirectly by a variety of agonists including exogenous pungent compounds (found in edibles like garlic, mustard oil, wasabi, horseradish, and brussels sprouts), bradykinin, endogenous proalgesic agents, cold, and mechanical stimuli (reviewed in (116)). TRPA1 is a nonselective cation channel with P_{Ca}/P_{Na} of 0.84 and P_{Mg}/P_{Na} of 1.23 with conductances ranging from 40 to 105 pS (Table 1). Although this channel displays low Ca^{2+} permeability its contribution to the development of physiologically relevant Ca^{2+} signals has been described. For example, mice with a deletion of part of the TRPA1 protein have been shown to have impaired Ca^{2+} influx in response to mustard oil and allicin (117–119). In addition, freshly dissociated trigeminal ganglion neurons from these mutated animals were insensitive to these inflammatory mediators resulting in protection from the neurogenic inflammation observed in wild-type animals (120).

3. TRP Channels in Cardiovascular Physiology and Pathophysiology

Since their discovery, TRP channels have been identified as molecular sensors of remarkable diversity involved in the translation of sensorial stimuli to electrical signals. These channels have pivotal roles in senses including vision, hearing, taste, and touch. Changes in TRP channel expression levels and patterns have been suggested

as a critical step in mediating pathophysiological responses in a variety of physiological systems. The contribution of TRP channels in mediating physiological and pathophysiological responses in the CVS will be briefly reviewed below.

3.1. TRP Channels in the Heart

Physiologically, the heart provides the body with the pressure gradient and blood flow necessary for proper organ perfusion. Control of blood flow or cardiac output in response to the body's metabolic demand is accomplished directly by neural and humoral control of two determinants of the heart performance: heart rate and cardiac contractility. Inherently, the cardiac rhythm is regulated by the rate of diastolic depolarization that occurs in the pacemaker cells of the sinoatrial (SA) node, and disturbances in their electrophysiological behavior serve as basis for development of cardiac arrhythmias. Although the conductance responsible of SA node pacing (hyperpolarization activated current, I_H) has been well characterized, whether TRP channel-mediated nonselective cation conductances contribute to pacemaking regulation downstream of G-protein-coupled activation is still elusive.

Expression of TRPM4 and all the TRPCs with the exception of TRPC5 has been reported by RT-PCR in SA node cells and atrial cardiomyocytes where they have been suggested to mediate transient inward cationic currents in response to intracellular Ca^{2+} and store depletion, respectively (115, 121). Incubation of SA node cells with Ca^{2+}-free media results in decreased resting intracellular Ca^{2+} concentrations and pacemaker activity suggesting a requirement for extracellular Ca^{2+} (122). SA node cell firing rate was decreased to 27% of that observed in control cells upon treatment with the nonspecific SOC inhibitor SK&F-96356 (122). These observations coupled to the expression of TRPC channel family members in SA node cells lead these authors to suggest the involvement of TRPC-mediated SOC activity in pacemaker activity. Another group reported increased expression of TRPC3 and TRPC6 in transgenic animals overexpressing constitutively active Gαq protein; these transgenic animals serve as an animal model of heart failure and display higher incidence of premature ventricular contractions that were reduced upon treatment with SK&F-96356 (123). Interestingly, the rate of these episodes was exacerbated by the use of OAG, a DAG analogue known to activate TRPC3/6/7, suggesting a possible role of TRPC channels in regulating cardiac rhythm and contractility upon sympathetic stimulation.

Delayed depolarization is another electrophysiological abnormality observed in conditions of Ca^{2+} overload, and TRPM4 sensitivity to increases in intracellular Ca^{2+} makes this protein a potential player in this condition. A recent study evaluated genetic predisposition factors in three families with autosomal dominant isolated cardiac conduction disease and identified independent heterozygous missense mutations of the TRPM4 gene in each family

(Arg164Trp, Ala432Thr, and Gly844Asp) (124, 125). When overexpressed in HEK 293 cells, these three mutations resulted in increased current density that correlated with elevated plasma membrane TRPM4 channel density secondary to impaired endocytosis and deregulation of Small Ubiquitin MOdifier conjugation (SUMOylation) (124). The selectively higher expression of TRPM4 in the heart's conductive system raises the interesting question of whether this channel is relevant in conditions of normal ventricular depolarization. Conduction abnormalities can also be secondary to cardiac fibrosis resulting in the pathogenesis of atrial fibrillation (AF). Recently, Du et al. reported the requirement of TRPM7 for development of the Ca^{2+} signal in response to transforming growth factor (TGF)-β1 in atrial fibroblasts (126). Analysis of cells that were freshly isolated from patients suffering from AF unveiled a striking increase in TRPM7-mediated Ca^{2+} current and Ca^{2+} influx resulting in differentiation of fibroblasts into myofibroblasts. TGF-β1-induced differentiation was attenuated by TRPM7-specific knockdown suggesting a central role for TRPM7 in fibroblast differentiation and induction of fibrogenesis partially responsible for human atrial fibrillation.

Under certain pathologies such as chronic hypertension and aortic valve stenosis, the heart muscle initiates compensatory mechanisms in order to generate enough pressure work to establish adequate blood flow. These elevated cardiac afterloads that result in sustained mechanical stress and in vivo pressure overload are generally compensated for by heart muscle hypertrophy which in the long term reduces cardiac output. Numerous studies have argued for the importance of Ca^{2+} signals in the development of cardiac hypertrophy (121). Early studies reported the upregulation of Ca^{2+}-sensitive effectors such as calmodulin (CaM)-dependent kinase (CaMK) and their involvement in the regulation of fetal gene program reminiscent of failing human hearts (127, 128). Likewise, overexpression of calcineurin, a Ca^{2+}–CaM-dependent serine/threonine phosphatase, induces massive hypertrophy (129). Calcineurin dephosphorylates the transcription factor, nuclear factor of activated T cells (NFAT) family, thereby inducing NFAT translocation and its association with responsive elements located in hypertrophic responsive genes (130). The evident role of Ca^{2+}-dependent transcription factors in the etiology of cardiac hypertrophy stimulated the search for the channels required for the mediation of the Ca^{2+}-dependent hypertrophic response, and as such several members of the TRPC, TRPV, and TRPM families have been implicated in the development of this pathology.

Activation of G-protein-coupled receptors is one of the initial steps involved in the hypertrophic response (131), and genetic overexpression of Gαq proteins in animal models of heart failure has been shown to cause upregulation of TRPC3 and TRPC6 (123). Interestingly, this upregulation has been reported

to be in part due to TRPC-mediated activation of NFAT signaling, positively inducing expression through two conserved NFAT consensus sites located in the TRPC6 promoter (132). TRPC6 upregulation has been also observed in mouse hearts expressing constitutively active calcineurin or in response to pressure overload. Conversely, knockdown of TRPC6 has been associated with decreased hypertrophy observed downstream of endothelin-1 and angiotensin II receptor activation (132). Angiotensin II-induced Ca^{2+} influx has been shown to be mediated by TRPC3 and TRPC6 in rat neonatal cardiomyocytes and knockdown of either of these proteins resulted in complete abrogation of angiotensin II-induced hypertrophy (133). These results raise the possibility of the existence of functional DAG-sensitive TRPC3/6 heterotetramers that would be capable of providing the Ca^{2+} signals that drive hypertrophy. Another study implicated TRPC3-mediated Ca^{2+} entry in cardiac hypertrophy. In this study it was shown that TRPC3 knockdown by siRNA resulted in decreased expression of hypertrophy-associated genes such as atrial and brain natriuretic peptides (ANP and BNP), with no effect on genes controlling cardiomyocyte size and contraction (134).

TRPC1 has also been proposed to somehow contribute to the hypertrophic response (135). It is believed that TRPC1 contribution to hypertrophy is mediated by heteromultimeric interactions with other TRPC members given the poor plasma membrane expression of TRPC1 in ectopic expression systems; plasma membrane localization of TRPC1 channel occurred only when it was co-expressed with other TRPC family members (136). However, another study that targeted hypertrophic signals downstream of another G-protein-coupled receptor $5HT_{2A}$ reported the selective upregulation of TRPC1, but not TRPC6 in response to 5-hydroxytyptamine (5HT) stimulation (137). In addition, knockdown of TRPC1 proteins resulted in diminished cardiac hypertrophy and TRPC1-deficient animals have been reported to be protected against pressure overload and hypertrophic response. Although it is established that TRPC3/6 opening in response to receptor activation is mediated through DAG, it is not clear what signal is mediating TRPC1 activation and its contribution to cardiac hypertrophy. A number of reports have suggested TRPC1 as a store-operated channel and that TRPC1 sensitivity to Ca^{2+} store depletion is conferred by the ER-resident Ca^{2+} sensor STIM1 (for review see (53)). Most recently, it was reported that the hypertrophic stimuli endothelin-1, phenylephrine, and angiotensin II upregulated TRPC1 proteins without altering STIM1 expression levels (138). However, knockdown of STIM1 prevented TRPC1 upregulation and NFAT nuclear translocation (138). It remains unclear whether the lack of NFAT nuclear translocation is due to STIM1 knockdown or to the fact that TRPC1 upregulation was prevented.

TRPM4 and TRPV1 have also been implicated in the development of several cardiac pathologies including hypertrophy, fibrosis, and remodeling. Increased TRPM4 protein levels were reported in cardiac hypertrophy induced in spontaneous hypertensive rats; increased TRPM4 levels correlated with the development of TRPM4-like currents that were not otherwise measurable in control animals (139). TRPV1 protein levels were also upregulated in animal models of hypertrophic cardiac failure (140). In these animals an evident increase in ventricle-to-body weight ratio was observed with significant linear correlation with TRPV1 transcripts. TRPV1$^{-/-}$ animals displayed decreased hypertrophy and decreased fibrosis, suggesting that TRPV1 channel is important in the pathogenesis of genetically associated heart hypertrophy (140). For a comprehensive summary of TRP channels and their physiological and pathophysiological implications in the heart, see Table 2.

3.2. TRP Channels in the Endothelium

The innermost layer of the vessels, the endothelium, is the interphase between the blood and the interstitial compartment and is known to integrate variables such as intramural pressure, shear stress, and inflammatory stimuli to control physiological and pathophysiological responses of the vascular system. The endothelium is a continuous monolayer of cells that tightly adhere to each other and to the basal lamina to establish a selective but permeable structure, dividing the blood components from the parenchymal tissue. It is the balance of cell–cell junction integrity between endothelial cells and the contractile forces generated within these cells that is critical for the transcellular pathway of endothelial permeability. Any signal that results in endothelial cell barrier destabilization such as thrombin and histamine causes a decreased barrier function increasing the interendothelial gap resulting in increased permeability. Abnormal barrier function results in infiltration of plasma, cells, and proteins and is widely observed under conditions of pulmonary edema, tissue inflammation, and atherosclerosis (141).

Endothelial cells are non-excitable cells and express a variety of Ca^{2+} channels that respond to PLC-coupled receptor stimulation. These responses are mediated by activation of store-dependent and store-independent Ca^{2+} channels. TRP channels, in particular TRPCs, are found ubiquitously expressed in endothelial cells from vessels of different calibers and their physiological contributions are starting to emerge (reviewed in (141)). A variety of agonists including inflammatory mediators such as thrombin, histamine, and several growth factors such as vascular endothelial growth factor (VEGF) have been recognized as agents affecting barrier function. These factors are believed to elicit the activation of intracellular Ca^{2+} signals that activate myosin light chain kinase (MLCK) leading to endothelial cell permeability. A different view has been proposed suggesting that rise in intracellular Ca^{2+} signals to cytoskeleton

Table 2
TRP channel physiological and pathophysiological implications

	Physiology	Pathophysiology
Heart TRPC1	Regulation of pacemaker firing rate in mouse sinoatrial node (294)	Cardiac hypertrophy (135, 295, 296), dilated cardiomyopathy (297, 298)
TRPC2	Regulation of pacemaker firing rate in mouse sinoatrial node (294)	
TRPC3	Regulation of pacemaker firing rate in mouse sinoatrial node (294)	Cardiac hypertrophy (299), hypertension (300), dilated cardiomyopathy via increased CaMKII activity and Nox-mediated oxidant production (301), hypertrophy of rat neonatal cardiomyocytes via angiotensin II-induced Ca^{2+} entry, and NFAT nuclear translocation (133)
TRPC4	Regulation of pacemaker firing rate in mouse sinoatrial node (294)	
TRPC5		Heart failure (299)
TRPC6	Regulation of pacemaker firing rate in mouse sinoatrial node (294), contractility via the α-(1A)-AR-Snapin-TRPC6-pathway (302)	Hypertrophy of rat neonatal cardiomyocytes via angiotensin II-induced Ca^{2+} entry and NFAT translocation (133), cardiac hypertrophy (132), heart failure (132)
TRPC7	Regulation of pacemaker firing rate in mouse sinoatrial node (294)	
TRPM4		Cardiac arrhythmias (303), cardiac hypertrophy (303), limiting catecholamine release from chromaffin cells leading to increased sympathetic tone and hypertension (304)
TRPM7		TGF-β1-elicited fibrogenesis in human atrial fibrillation (126)
TRPV1	Activating cardiac nociceptors by detection of tissue ischemia (305)	Cardiac hypertrophy (140)
TRPV2		Cardiac myopathy (121)
TRPV4	Regulation of Ca^{2+} in cardiac fibroblasts (306)	Hypertension, enhanced myogenic tone, and vascular remodeling (307)
TRPA1	Mediate cardiac mechanotransduction via Painless-TRPA channel (308)	
TRPP2	Induces left–right heart asymmetry development during embryogenesis (309)	Cardiac septation defects (310)

(continued)

Table 2 (continued)

	Physiology	Pathophysiology
Endothelium		
TRPC1	Endothelial permeability (induced by TNFα) (311, 312)	
TRPC2	Enhanced ATP-dependent Ca^{2+} influx in ewe uterine artery endothelial cells via pregnancy-enhanced interaction between TRPC3 and IP_3R2 (313)	
TRPC3	Monitor oxidative stress (314)	
TRPC4	Endothelial permeability in the lung (146), hypoxia-induced vascular remodeling (315), vascular tone (148), endothelium-dependent vasorelaxation, control of paracellular endothelial permeability (146), cystic fibrosis transmembrane conductance regulator (CFTR) function in vascular endothelial cells (316)	Angiogenesis (mediated by VEGF) (317)
TRPC6	Endothelial permeability (induced by VEGF) (151)	
TRPM2	Oxidative stress-induced endothelial permeability (154)	
TRPM7	Modulation of the angiogenic phenotype of human microvascular endothelial cells (318)	
TRPV1	Vascular tone (319)	
TRPV4	Vascular tone (320), vasodilation of mesenteric arteries in response to endothelial-derived factors (164)	Ciliary beating frequency regulation in association with COPD (321)
TRPA1	Endothelium-derived vasodilation (166)	
TRPP1	Fluid-flow sensation by the primary cilium in renal epithelium (162), NO production (322)	
TRPP2	Fluid-flow sensation by the primary cilium in renal epithelium (162), NO production (322)	
VSMCs		
TRPC1	Vascular smooth muscle cell proliferation (323), pulmonary smooth muscle cell proliferation (324), contractility (168), luminal injury response (178)	Vascular occlusive disease (178)
TRPC3	UTP-induced depolarization and constriction of cerebral arterial smooth muscle cell (214), TNFα-induced enhancement of Ca^{2+} mobilization in airway smooth muscle cells (325), regulation of myometrial intracellular Ca^{2+} during parturition and labor (326)	Idiopathic pulmonary arterial hypertension (183)
TRPC4	Regulation of myometrial intracellular Ca^{2+} during parturition and labor (326), gastrointestinal smooth muscle cell pacemaker oscillations (327), mICAT-regulated small intestinal motility (173)	

(continued)

Table 2 (continued)

	Physiology	Pathophysiology
TRPC5	Mediation of sphingosine-1-phosphate-induced migration (176), smooth muscle relaxation via enhanced NO production (328)	
TRPC6	mICAT-regulated small intestinal motility (173), regulation of myogenic tone (329)	Hypoxic pulmonary vasoconstriction (330), chronic hypoxia-induced pulmonary artery smooth muscle cell (179), idiopathic pulmonary arterial hypertension (183), mucus secretion in COPD (331)
TRPM3	Contraction and proliferation (332)	
TRPM4	Pressure-induced depolarization, vasoconstriction (195), auto-regulation of cerebral blood flow (214)	
TRPM7	Magnesium homeostasis during proliferation in response to angiotensin II (197), mediation of proinflammatory bradykinin signaling in vascular smooth muscle cell (333), interstitial cells of Cajal (ICC) pacemaker activity (334), defective vascular remodeling (335)	Hypertension (335)
TRPM8	Cooling-induced contraction of the gastric fundus (336)	
TRPV1	Gracilis arteriolar constriction (187)	Hypoxia-induced proliferation of pulmonary artery smooth muscle (188), renal hypertension (337)
TRPV2	Hypotonic response of nonselective cation channel in murine vascular myocytes (70)	
TRPV4	Vasodilation of mesenteric arteries in response to endothelial-derived factors (164)	Asthma (338)
TRPP1	Fluid-flow sensation by the primary cilium in renal epithelium (162), NO production (322)	
TRPP2	Fluid-flow sensation by the primary cilium in renal epithelium (162), NO production (322)	

CaMKII, Ca^{2+}/calmodulin-dependent protein kinases II; Nox-mediated ROS, NADPH oxidase-mediated reactive oxygen species; ROCE, receptor-operated calcium entry; NFAT, nuclear factor of activated T cells; α (1A)-AR-Snapin-TRPC6-pathway, α (1A)-adrenergic receptor-SNARE-associated modulatory protein; TGF-beta1, transforming growth factor beta 1; Ca^{2+}, calcium; ATP, adenosine triphosphate; IP_3R2, inositol 1,4,5-triphosphate receptor 2; VEGF, vascular endothelial growth factor; COPD, chronic obstructive pulmonary disease; UTP, uridine triphosphate; mICAT, muscarinic receptor-induced cation current; S1P, sphingosine-1-phosphate; NO, nitric oxide

organizing proteins causes destabilization and turnover of the cell–cell adherens junctions and subsequent endothelial permeability. Regardless of the downstream mechanisms resulting in endothelial permeability, it has been proposed that Ca^{2+} influx is required for this process and that members of the TRPC, TRPM, and TRPV subfamilies have been considered as molecular candidates that mediate this Ca^{2+} influx (142). Indeed, early studies conducted on both in vitro and in vivo models suggested the requirement of Ca^{2+} influx for endothelial permeability since Ca^{2+} chelation with quin-2 was able to reduce by 50% the thrombin-induced increase in transendothelial ^{125}I-albumin permeability (143).

TRPC1 has been suggested to be activated downstream of thrombin stimulation following a store-dependent mechanism to modulate the endothelial barrier function (144). Arguing for the relevance of store depletion in the development of the Ca^{2+} signal required for endothelial permeability, earlier studies reported that the increased Ca^{2+} influx associated with inhibition of the SERCA pump by thapsigargin or 2,5-di(tert-butyl)-1,4-benzohydroquinone (BHQ) could recapitulate the hyperpermeability and stress fiber formation observed in response to inflammatory mediators (143, 145, 146). Despite repeated attempts by our laboratory, we failed to observe an enhanced endothelial permeability in response to thapsigargin reminiscent of that observed with thrombin (unpublished). In human pulmonary artery endothelial cells knockdown of TRPC1 resulted in significant SOC abrogation (147). Similarly, another study reported that SOC activation in mouse macrovascular endothelial cells isolated from TRPC4-deficient mice was significantly abrogated, which correlated with a 50% decrease in maximal lung vascular permeability (146, 148). Endothelial cells obtained from TRPC4-deficient animals display poor Ca^{2+} signals in response to thrombin or PAR-1 activating peptide (146). Heteromultimers of TRPC4 and TRPC1 were proposed to mediate SOC and thrombin-stimulated hyperpermeability in endothelial cells (149). As pointed out earlier, the idea of TRPCs as SOCs remains largely controversial, especially after the discovery of STIM1 and Orai1, two proteins that together recapitulate the archetypical Ca^{2+}-released activated Ca^{2+} (CRAC) current originally described in leukocytes. Our laboratory has previously shown in human umbilical vein and pulmonary artery endothelial cells that passive store depletion with either BAPTA or thapsigargin leads to the development of small CRAC currents that display amplification in divalent free solutions and typical inward rectification (150). In these cells knockdown of Orai1 and STIM1, but not TRPC1 or TRPC4, completely abrogated SOC channel-mediated Ca^{2+} influx and CRAC currents.

Other factors known to influence endothelial permeability include VEGF and reactive oxygen species. TRPC6-mediated Ca^{2+} influx has been associated with RhoA-dependent changes in

endothelial cell shape observed in response to modulators of endothelial permeability (151). In human microvascular endothelial cells, TRPC6-like cation conductances can be activated downstream of VEGF receptor; these currents recapitulate VEGF-activated TRPC conductances recorded from cells ectopically expressing VEGFR2 and TRPC3 or TRPC6 (151, 152). Similarly, TRPM2, a ROS-sensitive TRP, has been shown to contribute to pulmonary artery endothelial barrier regulation (153). Knockdown of TRPM2 with siRNA reduced the H_2O_2-induced increase in endothelial permeability (154, 155). A short TRPM2 variant that lacks the pore domain acted as dominant negative and significantly inhibited endothelial permeability (155). TRPM4 has also been suggested to somehow regulate barrier function. A rat model of secondary spinal hemorrhage induced by spinal cord injury is characterized by disruption of capillary integrity which contributes to post-trauma secondary hemorrhage (156). In this animal model, knockdown or knockout of TRPM4 caused a reduction in secondary hemorrhage observed upon injury (156).

Endothelial cells are subjected to biomechanical forces exerted by the phasic blood flow occurring during the cardiac cycle. These hemodynamic forces can be in the form of intramural pressure, resulting in arterial strain, and shear stress. Differences in fluid flow lead to differences in endothelial phenotypes but in some cases can lead to development of vascular pathologies (157). For example, high physiological shear stress contributed by laminar blood flow correlates with the synthesis of vasoactive mediators such as nitric oxide (NO) and prostacyclin that contribute to the antithrombotic endothelial properties and smooth muscle homeostasis (141, 158). In contrast, low shear stress or turbulent flow correlates with endothelial dysfunction and formation of atheromatous lesions (159). Although direct correlation has been observed between fluid flow and endothelial phenotype, the mechanical stress sensor has not been unveiled. Many proteins and cellular signaling components such as G proteins, cytoskeleton, focal adhesion proteins, and mechanosensitive ion channels have been suggested to serve as local cellular sensors of mechanical stimulation. The polymodal nature of TRP channel activation and their known contribution to physiological functions have made them attractive candidates as sensors of mechanical inputs in endothelia.

The endothelial response to shear stress includes the elevation of intracellular Ca^{2+} concentrations via both intracellular Ca^{2+} release and subsequent entry through plasma membrane Ca^{2+} channels. This response has been shown to be inhibited by strong extracellular Ca^{2+} buffering or by the use of TRP channels inhibitors (153). TRPV4 channels have been proposed to mediate the Ca^{2+} influx that occurs in response to shear flow resulting in arterial dilation (61). Studies demonstrated that both shear flow and 4α-phorbol 12,13-didecanoate (4α-PDD), a TRPV4 activator,

were able to vasodilate carotid arteries and this effect could be abrogated by employing a nonselective TRP channel, ruthenium red. Similarly, it was shown that flow-induced endothelium-dependent arterial dilation was greatly reduced in TRPV4$^{-/-}$ mice (160). Despite these early reports suggesting TRPV4 mechanosensitivity, it was later reported that TRPV4 sensitivity to membrane stretch was mediated by activation of a swelling-sensitive phospholipase A2 and secondary production of arachidonic acid and its metabolites (80). Specifically, the TRPV4-mediated vasodilatory effect was dependent on the epoxygenase activity of cytochrome P_{450} resulting in the generation of EETs, previously reported to activate TRPV4 channels (161). These results question the ability of TRPV4 to be a mechanoreceptor per se, but highlight a role for this channel as a component of flow-induced vasodilatory response. Other examples of TRP channels as mechanosensors include TRPP1 and TRPP2. Mutations in the pkd1 and pkd2 genes, which encode TRPP1 and TRPP2 respectively, lead to autosomal dominant polycystic kidney disease (109). In the kidney, TRPP1 and TRPP2 localize to the primary cilium membrane where they have been shown to play a flow-sensing role (162). Similarly, these ciliary structures have been reported in endothelial cells and contain TRPP1 and TRPP2 proteins. Knockdown of these proteins was reported to drastically abrogate the typical Ca^{2+} signal and NO production observed upon shear stress stimulation (163). Most interestingly, primary cilium formation in endothelial cells is stimulated in areas of turbulent flow while cilium formation is inhibited in areas of laminar flow, perhaps serving as a signaling mechanism to hinder the progression of endothelial dysfunction. Although the presence of other TRP channels in ciliary structures in endothelial and smooth muscle cells has not be reported, their contribution in physiological signal sensing is an interesting question waiting to be answered.

Physiologically, the endothelium can modulate the vascular tone by synthesizing a variety of vasoactive compounds that can exert their functions on vascular smooth muscle cells (VSMCs) located in the medial or intermediate layer. Engagement of vasoactive compound receptors in VSMCs results in Ca^{2+} influx required for smooth muscle contraction. Similarly, the synthesis of second messengers such as NO and endothelium-dependent hyperpolarizing factors (EDHFs) contributes to the control of vascular tone by their direct vasodilatory effect on VSMCs. The production of these vasodilators depends on the development of intracellular Ca^{2+} signals, whereby rises in intracellular Ca^{2+} activate NO synthase and phospholipase A2 resulting in the production of NO and EETs (EDHF), respectively. Once produced, NO diffuses to nearby VSMCs resulting in the activation of cytosolic guanylate cyclase to reverse the Ca^{2+}-dependent pathways resulting in muscle relaxation (115, 141).

Data obtained with both TRPC4 and TRPV4 knockout animals showed reduced Ca^{2+} signals downstream receptor stimulation of endothelial cells; these results also correlated with diminished endothelium-dependent vasorelaxation observed in these animals (148, 164). In freshly isolated cerebral myocytes, Earley et al. showed that outwardly rectifying whole-cell currents activated by the TRPV4 agonists 4α-PDD and the endothelium-derived arachidonic acid metabolite 11,12 epoxyeicosatrienoic acid (11,12 EET) had biophysical properties consistent with those obtained from ectopically expressed TRPV4 channels (164, 165). Activation of these Ca^{2+} channels correlated with an increased frequency of unitary Ca^{2+} release events via ryanodine receptors (Ca^{2+} sparks) leading to the activation of spontaneous transient outward currents (STOCs) resulting in smooth muscle relaxation (165). A more recent study by Earley and coworkers suggested that TRPA1 causes endothelium-dependent vasodilation and that Ca^{2+} entry through endothelial TRPA1 channels causes vasodilation of cerebral arteries via activation of endothelial Ca^{2+}-activated K^+ channels and artery smooth muscle inwardly rectifying K^+ channels. Stimulation of TRPA1, found expressed in endothelial cell membrane projections proximal to vascular smooth muscle cells, by the mustard oil component, allyl isothiocyanate (AITC), induced dilation of pressurized vessels and caused decrease in smooth muscle intracellular Ca^{2+}; AITC-induced dilation was reduced by disruption of the endothelium (166). Unlike TRPV4 and TRPA1, the TRPV1 contribution to endothelium-dependent vasorelaxation has been explained by its capacity to induce NO production (166).

3.3. TRP Channels in Smooth Muscle

All seven members of the TRPC family, TRPC1–TRPC7, have been reported to be expressed in smooth muscle cells from various vascular beds (167). With the exception of TRPC2, a pseudogene in humans, all other TRPCs are known to form functional channels in some type of smooth muscle cells (20). As discussed previously, TRPC proteins have been suggested to form both SOC channels and receptor-activated channels in smooth muscle cells. Several studies have proposed that these channels help regulate vascular tone upon stimulation with vasoactive compounds such as angiotensin II, vasopressin, norepinephrine, and endothelin-1 (168–170). One of such examples is the activation of TRPC1 and TRPC6 upon stimulation with angiotensin II in freshly isolated mesenteric artery smooth muscle cells from rabbit (169). These studies suggested that low and high concentrations of angiotensin II can activate two different conductances in these cells (169). Using antibodies targeting TRPC1 and TRPC6 it was suggested that these conductances were contributed by TRPC1 and TRPC6 channels (169). Similarly, it has been shown that antibody against TRPC1 can reduce endothelin-1-induced smooth muscle cell contraction (168). In canine subarachnoid arteries, antibodies targeting either

TRPC1 or TRPC4 were shown to inhibit Ca^{2+} entry and vasoconstriction induced by endothelin-1 (171). The role of TRPC1 in mediating endothelin-1-induced Ca^{2+} entry was confirmed in rat aortic smooth muscle cells subjected to TRPC1 knockdown (172). Acetylcholine has been reported to activate TRPC4 and TRPC6 in smooth muscle cells lining the gastrointestinal tract which in turn regulate smooth muscle cell contraction and gastrointestinal motility (173). Another report suggested that IP_3 can induce vasoconstriction in cerebral arteries via activation of channels contributed by TRPC3; IP_3 caused IP_3 receptor-dependent activation of TRPC3 independently of Ca^{2+} release from the SR. TRPC3-mediated Na^+ entry and subsequent membrane depolarization were proposed to induce Ca^{2+} entry in smooth muscle via voltage-dependent Ca^{2+} channels and cause vasoconstriction (174). Muscarinic stimulation by agonists like acetylcholine has been shown to activate TRPC5 currents in smooth muscle cells obtained from murine stomach (175). In addition, it was proposed that sphingosine-1-phosphate can activate TRPC5 which in turn can regulate vascular smooth muscle cell motility (176).

Apart from contractility, a frequent cause of many smooth muscle cell-related disorders is the phenotypic switching of these cells from quiescent contractile cells to synthetic proliferative and migratory cells. The expression of TRPC channels has been reported to be increased in the synthetic smooth muscle cells in comparison to quiescent cells (158, 177). TRPC1 has been reported to be involved in mediating diseases contributed by proliferative VSMC phenotypes such as restenosis, atherosclerosis, and pulmonary hypertension (177–179). The expression of TRPC1 was reported to be increased upon balloon angioplasty in internal mammary artery (180). TRPC1 was proposed to contribute to VSMC remodeling in vivo upon vascular injury in human saphenous vein as antibody targeting TRPC1 was able to significantly reduce neointima formation (178). Similarly, TRPC1, TRPC3, TRPC4, and TRPC6 have been implicated in the development of pulmonary hypertension (179, 181). In an animal model of hypoxia-induced pulmonary hypertension TRPC1 and TRPC6 were reported to be upregulated and it was shown that their expression is regulated by hypoxia inducible factor 1(HIF1) (182–184). Additionally, it was reported that mitogenic activities of ATP in human pulmonary smooth muscle cells are at least in part mediated via increased expression and activation of TRPC4 channel (185). These data suggest a potential involvement of TRPC4 in phenotypic switching of pulmonary smooth muscle cells in response to mitogenic stimulation and subsequent development of pulmonary hypertension. Similarly, the expression of TRPC6 has been reported to be upregulated in pulmonary artery smooth muscle cells obtained from rats with hypoxic pulmonary hypertension

(179). Human pulmonary artery smooth muscle cells obtained from patients with pulmonary arterial hypertension have elevated expression and activity of TRPC3 and TRPC6 (183). Importantly, knockdown of TRPC6 using siRNA significantly attenuated the proliferation of these cells suggesting that the increase in TRPC6 expression can contribute to the development of pulmonary hypertension (183).

Out of six TRPV channels, four TRPVs (TRPV1–TRPV4) have been reported to be expressed in smooth muscle cells from various vascular beds and visceral organs (186). TRPV1 channel is the capsaicin receptor, the active ingredient of hot chili pepper, in smooth muscle cells (60). It has been reported that capsaicin can directly act on smooth muscle TRPV1 channels and can induce vasoconstriction in isolated rat gracilis arterioles (187). This suggests that TRPV1 can regulate vasoconstriction upon exposure to dietary ligands. Moreover, TRPV1 expression is reported to be increased in human pulmonary artery smooth muscle cells subjected to hypoxic conditions (188). This increased TRPV1 expression resulted in elevated levels of Ca^{2+} influx which in turn resulted in higher cell proliferation (188). Using capsazepine, a TRPV1 antagonist, these authors further demonstrated that inhibition of TRPV1 can decrease hypoxia-induced Ca^{2+} influx and the resulting increase in smooth muscle cell proliferation (188). Contrary to TRPV1, TRPV2 has been reported to be an osmotic sensor in mouse aortic smooth muscle cells (70). Muraki et al. demonstrated that hypotonic swelling of aortic smooth muscle cells results in activation of a Ca^{2+} current mediated by TRPV2 (70), therefore suggesting a potential role for TRPV2 in regulating pressure-induced vasoconstriction. TRPV4 is known to be involved in regulating vasodilation (165). As discussed above, TRPV4 is activated by EETs which are vasodilators released by endothelial cells and can hyperpolarize smooth muscle cells (165); activation of TRPV4 in cerebral artery smooth muscle cells by EETs causes hyperpolarization and subsequent dilation of the arteries (165). Similar role for TRPV4 has been also reported in mesenteric artery smooth muscle cells. Using TRPV4 knockout mice, Earley et al. convincingly showed that EET- mediated vasodilation of mesenteric arteries was present in wild-type mice but not in TRVP4 knockout mice (164).

With the exception of TRPM1, all other TRPM family members have been reported to be expressed in pulmonary artery and aorta (186, 189). Although several TRPs can be activated by oxidative stress, TRPM2 appears to be most important player involved in mediating oxidant effects (91). Several groups have suggested a potential role for TRPM2 in a plethora of pathophysiological outcomes arising from oxidant-induced vascular injury such as cerebral ischemia and stroke (190–194). Similar to TRPV2, TRPM4 has

been demonstrated to play a very important role in pressure-induced vasoconstriction via smooth muscle depolarization. Downregulation of TRPM4 in intact cerebral arteries results in significant reduction in smooth muscle cell depolarization and pressure-induced vasoconstriction (195). TRPM6 and TRPM7 are involved in magnesium (Mg^{2+}) homeostasis. Mg^{2+} is known to play a very important role in vascular smooth muscle cell growth, in vascular remodeling upon injury, and in hypertension (196). Mg^{2+} is also reported to inhibit vascular contractility induced upon stimulation with agonists. Using angiotensin II and aldosterone, He et al. showed that upon treatment with these vasoactive compounds the plasma membrane expression of TRPM7 was increased in rat VSMCs (197). Along with its expression level, TRPM7 activity was also enhanced. The resulting increase in intracellular concentration of Mg^{2+} was proposed to cause increased VSMC proliferation (197); these authors showed that knockdown of TRPM7 resulted in decrease in both Mg^{2+} levels and cell proliferation (197). TRPM8 has been reported to be expressed in rat aortic artery, mesenteric artery, and pulmonary artery smooth muscle cells (198). Johnson et al. showed that activation of TRPM8 with menthol and icilin causes dilation of preconstricted rat mesenteric artery and thoracic aorta. These authors further confirmed that the dilation was mainly due to activation of TRPM8 expressed on smooth muscle cells as dilation was independent of nitric oxide synthase activity and endothelium removal (198).

4. Concluding Remarks

Table 1 summarizes the biophysical properties and different activators and inhibitors of TRP channels, while Table 2 shows the physiological functions where TRPs were shown to play a role and the disease states where TRP channels are involved. Much has been learned about TRP channel mechanisms of regulation and roles in disease progression since their discovery almost two decades ago. Yet, the exact activation mechanisms and physiological function of many TRP isoforms remain unclear. The potential of TRP channels to heteromultimerize and form a large repertoire of native cation channels in different cell types with distinct biophysical properties, pharmacology, and mode of activation highlights the need for continued research on this highly ubiquitous family of proteins. Future studies are likely to unravel novel TRP channel heteromultimers, additional physiological functions, and disease conditions where TRP isoforms play a major role and bring us closer to fulfill the potential of TRP proteins as targets for human disease therapy.

References

1. Hardie RC (2004) Regulation of Drosophila TRP channels by lipid messengers. Novartis Found Symp 258:160–167, discussion 167–171, 263–266
2. Hardie RC (2007) TRP channels and lipids: from Drosophila to mammalian physiology. J Physiol 578(Pt 1):9–24
3. Hardie RC, Minke B (1993) Novel Ca2+ channels underlying transduction in Drosophila photoreceptors: implications for phosphoinositide-mediated Ca2+ mobilization. Trends Neurosci 16(9):371–376
4. Minke B (2006) TRP channels and Ca2+ signaling. Cell Calcium 40(3):261–275
5. Minke B, Cook B (2002) TRP channel proteins and signal transduction. Physiol Rev 82(2):429–472
6. Montell C (2005) Drosophila TRP channels. Pflugers Arch 451(1):19–28
7. Nilius B (2007) TRP channels in disease. Biochim Biophys Acta 1772(8):805–812
8. Montell C (2001) Physiology, phylogeny, and functions of the TRP superfamily of cation channels. Sci STKE 2001:RE1
9. Yue L et al (2001) CaT1 manifests the pore properties of the calcium-release-activated calcium channel. Nature 410(6829):705–709
10. Vennekens R et al (2000) Permeation and gating properties of the novel epithelial Ca(2+) channel. J Biol Chem 275(6):3963–9
11. Gwanyanya A et al (2004) Magnesium-inhibited, TRPM6/7-like channel in cardiac myocytes: permeation of divalent cations and pH-mediated regulation. J Physiol 559(Pt 3):761–776
12. Demion M et al (2007) TRPM4, a Ca2+-activated nonselective cation channel in mouse sino-atrial node cells. Cardiovasc Res 73(3): 531–538
13. Prawitt D et al (2003) TRPM5 is a transient Ca2+-activated cation channel responding to rapid changes in [Ca2+]i. Proc Natl Acad Sci USA 100(25):15166–15171
14. Clapham DE et al (2003) International Union of Pharmacology. XLIII. Compendium of voltage-gated ion channels: transient receptor potential channels. Pharmacol Rev 55(4):591–596
15. Flockerzi V (2007) An introduction on TRP channels. Handbook of Experimental Pharmacology 179:1–19
16. Damann N, Voets T, Nilius B (2008) TRPs in our senses. Curr Biol 18(18):R880–9
17. Trebak M (2006) Canonical transient receptor potential channels in disease: targets for novel drug therapy? Drug Discov Today 11(19–20):924–930
18. Trebak M et al (2007) Phospholipase C-coupled receptors and activation of TRPC channels. Handb Exp Pharmacol 179: 593–614
19. Vazquez G et al (2004) The mammalian TRPC cation channels. Biochim Biophys Acta 1742(1–3):21–36
20. Yildirim E, Birnbaumer L (2007) TRPC2: molecular biology and functional importance. Handb Exp Pharmacol 179:53–75
21. Gonzalez-Cobos JC, Trebak M (2010) TRPC channels in smooth muscle cells. Front Biosci 15:1023–1039
22. Owsianik G et al (2006) Permeation and selectivity of TRP channels. Annu Rev Physiol 68:685–717
23. Liu X, Singh BB, Ambudkar IS (2003) TRPC1 is required for functional store-operated Ca2+ channels. Role of acidic amino acid residues in the S5-S6 region. J Biol Chem 278(13): 11337–11343
24. Plant TD, Schaefer M (2003) TRPC4 and TRPC5: receptor-operated Ca2+-permeable nonselective cation channels. Cell Calcium 33(5–6):441–50
25. Wang YX, Zheng YM (2011) Molecular expression and functional role of canonical transient receptor potential channels in airway smooth muscle cells. Adv Exp Med Biol 704: 731–747
26. Pedersen SF, Owsianik G, Nilius B (2005) TRP channels: an overview. Cell Calcium 38(3–4):233–52
27. Vennekens R et al (2002) Current understanding of mammalian TRP homologues. Cell Calcium 31(6):253–264
28. Birnbaumer L (2009) The TRPC class of ion channels: a critical review of their roles in slow, sustained increases in intracellular Ca(2+) concentrations. Annu Rev Pharmacol Toxicol 49:395–426
29. Hogan PG, Lewis RS, Rao A (2010) Molecular basis of calcium signaling in lymphocytes: STIM and ORAI. Annu Rev Immunol 28:491–533
30. Potier M, Trebak M (2008) New developments in the signaling mechanisms of the store-operated calcium entry pathway. Pflugers Arch 457(2):405–415
31. Hofmann T et al (1999) Direct activation of human TRPC6 and TRPC3 channels by diacylglycerol. Nature 397(6716):259–263

32. Trebak M et al (2003) Signaling mechanism for receptor-activated canonical transient receptor potential 3 (TRPC3) channels. J Biol Chem 278(18):16244–16252
33. Trebak M et al (2003) The TRPC3/6/7 subfamily of cation channels. Cell Calcium 33(5–6):451–461
34. Lemonnier L, Trebak M, Putney JW Jr (2008) Complex regulation of the TRPC3, 6 and 7 channel subfamily by diacylglycerol and phosphatidylinositol-4,5-bisphosphate. Cell Calcium 43(5):506–514
35. Trebak M et al (2005) Negative regulation of TRPC3 channels by protein kinase C-mediated phosphorylation of serine 712. Mol Pharmacol 67(2):558–563
36. Gross SA et al (2009) TRPC5 is a Ca2+-activated channel functionally coupled to Ca2+-selective ion channels. J Biol Chem 284:34423–34432
37. Trebak M et al (2009) Complex functions of phosphatidylinositol 4,5-bisphosphate in regulation of TRPC5 cation channels. Pflugers Arch 457(4):757–769
38. Otsuguro K et al (2008) Isoform-specific inhibition of TRPC4 channel by phosphatidylinositol 4,5-bisphosphate. J Biol Chem 283(15):10026–10036
39. Rychkov G, Barritt GJ (2007) TRPC1 Ca(2+)-permeable channels in animal cells. Handb Exp Pharmacol 179:23–52
40. Eder P, Poteser M, Groschner K (2007) TRPC3: a multifunctional, pore-forming signalling molecule. Handb Exp Pharmacol 179:77–92
41. Cavalie A (2007) Ionic channels formed by TRPC4. Handb Exp Pharmacol 179:93–108
42. Beech DJ (2007) Canonical transient receptor potential 5. Handb Exp Pharmacol 179:109–123
43. Dietrich A, Gudermann T (2007) Trpc6. Handb Exp Pharmacol 179:125–141
44. Numaga T, Wakamori M, Mori Y (2007) Trpc7. Handb Exp Pharmacology 179:143–151
45. Feske S et al (2006) A mutation in Orai1 causes immune deficiency by abrogating CRAC channel function. Nature 441(7090):179–185
46. Liou J et al (2005) STIM is a Ca2+ sensor essential for Ca2+-store-depletion-triggered Ca2+ influx. Curr Biol 15(13):1235–1241
47. Roos J et al (2005) STIM1, an essential and conserved component of store-operated Ca2+ channel function. J Cell Biol 169(3):435–445
48. Vig M et al (2006) CRACM1 is a plasma membrane protein essential for store-operated Ca2+ entry. Science 312(5777):1220–1223
49. Zhang SL et al (2005) STIM1 is a Ca2+ sensor that activates CRAC channels and migrates from the Ca2+ store to the plasma membrane. Nature 437(7060):902–905
50. Bird GS et al (2008) Methods for studying store-operated calcium entry. Methods 46(3): 204–212
51. Draber P, Draberova L (2005) Lifting the fog in store-operated Ca2+ entry. Trends Immunol 26(12):621–624
52. Parekh AB, Putney JW Jr (2005) Store-operated calcium channels. Physiol Rev 85(2): 757–810
53. Yuan JP et al (2009) TRPC channels as STIM1-regulated SOCs. Channels (Austin) 3(4):221–225
54. Zeng W et al (2008) STIM1 gates TRPC channels, but not Orai1, by electrostatic interaction. Mol Cell 32(3):439–448
55. Yuan JP et al (2007) STIM1 heteromultimerizes TRPC channels to determine their function as store-operated channels. Nat Cell Biol 9(6):636–645
56. Jardin I, Salido GM, Rosado JA (2008) Role of lipid rafts in the interaction between hTRPC1, Orai1 and STIM1. Channels 2(6):401–403
57. Ong HL et al (2007) Dynamic assembly of TRPC1-STIM1-Orai1 ternary complex is involved in store-operated calcium influx. Evidence for similarities in store-operated and calcium release-activated calcium channel components. J Biol Chem 282(12):9105–9116
58. Ong HL, Ambudkar IS (2011) The dynamic complexity of the TRPC1 channelosome. Channels 5(5):424–431
59. Dehaven W et al (2009) TRPC channels function independently of STIM1 and Orai1. J Physiol 587:2275–2298
60. Caterina MJ et al (1997) The capsaicin receptor: a heat-activated ion channel in the pain pathway. Nature 389(6653):816–824
61. Earley S, Reading S, Brayden JE (2007) Functional significance of transient receptor potential channels in vascular function. In: Liedtke WB, Heller S (eds) TRP Ion Channel Function in Sensory Transduction and Cellular Signaling. CRC Presss, Boca Raton (FL)
62. Jin X, Touhey J, Gaudet R (2006) Structure of the N-terminal ankyrin repeat domain of the TRPV2 ion channel. J Biol Chem 281(35):25006–25010
63. McCleverty CJ et al (2006) Crystal structure of the human TRPV2 channel ankyrin repeat domain. Prot Sci 15(9):2201–2206
64. Latorre R, Zaelzer C, Brauchi S (2009) Structure-functional intimacies of transient

receptor potential channels. Quart Rev Biophys 42(3):201–246
65. Ramsey IS, Delling M, Clapham DE (2006) An introduction to TRP channels. Annu Rev Physiol 68:619–647
66. Erler I et al (2004) Ca2+-selective transient receptor potential V channel architecture and function require a specific ankyrin repeat. J Biol Chem 279(33):34456–34463
67. Arniges M et al (2006) Human TRPV4 channel splice variants revealed a key role of ankyrin domains in multimerization and trafficking. J Biol Chem 281(3):1580–1586
68. Rohacs T et al (2005) PI(4,5)P2 regulates the activation and desensitization of TRPM8 channels through the TRP domain. Nat Neurosci 8(5):626–634
69. Dray A, Forbes CA, Burgess GM (1990) Ruthenium red blocks the capsaicin-induced increase in intracellular calcium and activation of membrane currents in sensory neurones as well as the activation of peripheral nociceptors in vitro. Neurosci Lett 110(1–2):52–59
70. Muraki K et al (2003) TRPV2 is a component of osmotically sensitive cation channels in murine aortic myocytes. Circ Res 93(9):829–838
71. Xu H et al (2002) TRPV3 is a calcium-permeable temperature-sensitive cation channel. Nature 418(6894):181–186
72. Voets T et al (2002) Molecular determinants of permeation through the cation channel TRPV4. J Biol Chem 277(37):33704–33710
73. Nilius B et al (2001) Pharmacological modulation of monovalent cation currents through the epithelial Ca2+ channel ECaC1. Br J Pharmacol 134(3):453–462
74. Hoenderop JG et al (2001) Function and expression of the epithelial Ca(2+) channel family: comparison of mammalian ECaC1 and 2. J Physiol 537(Pt 3):747–761
75. Colton CK, Zhu MX (2007) 2-Aminoethoxydiphenyl borate as a common activator of TRPV1, TRPV2, and TRPV3 channels. Handb Exp Pharmacol 179:173–187
76. Kottgen M et al (2008) TRPP2 and TRPV4 form a polymodal sensory channel complex. J Cell Biol 182(3):437–447
77. Nilius B, Voets T (2004) Diversity of TRP channel activation. Novartis Found Symp 258:140–149, discussion 149–159, 263–266
78. Pingle SC, Matta JA, Ahern GP (2007) Capsaicin receptor: TRPV1 a promiscuous TRP channel. Handb Exp Pharmacol 179: 155–171
79. Vriens J et al (2004) Cell swelling, heat, and chemical agonists use distinct pathways for the activation of the cation channel TRPV4. Proc Natl Acad Sci USA 101(1):396–401
80. Plant TD, Strotmann R (2007) Trpv4. Handb Exp Pharmacol 179:189–205
81. Watanabe H et al (2003) Modulation of TRPV4 gating by intra- and extracellular Ca2+. Cell Calcium 33(5–6):489–495
82. Tominaga M (2007) The role of TRP channels in thermosensation. In: Liedtke WB, Heller S (eds) TRP Ion Channel Function in Sensory Transduction and Cellular Signaling, Boca Raton (FL).
83. Clapham DE (2003) TRP channels as cellular sensors. Nature 426(6966):517–524
84. Brauchi S et al (2006) A hot-sensing cold receptor: C-terminal domain determines thermosensation in transient receptor potential channels. J Neurosci 26(18):4835–4840
85. Peng JB (2011) TRPV5 and TRPV6 in transcellular Ca(2+) transport: regulation, gene duplication, and polymorphisms in African populations. Adv Exp Med Biol 704:239–275
86. Mensenkamp AR, Hoenderop JG, Bindels RJ (2007) TRPV5, the gateway to Ca2+ homeostasis. Handb Exp Pharmacol 179:207–220
87. Wissenbach U, Niemeyer BA (2007) Trpv6. Handb Exp Pharmacol 179:221–234
88. Montell C (2005) The TRP superfamily of cation channels. Sci STKE 2005(272):re3
89. Fleig A, Penner R (2004) The TRPM ion channel subfamily: molecular, biophysical and functional features. Trends Pharmacol Sci 25(12):633–639
90. Duncan LM et al (1998) Down-regulation of the novel gene melastatin correlates with potential for melanoma metastasis. Cancer Res 58(7):1515–1520
91. Eisfeld J, Luckhoff A (2007) Trpm2. Handb Exp Pharmacol 179:237–252
92. Bessman MJ, Frick DN, O'Handley SF (1996) The MutT proteins or "Nudix" hydrolases, a family of versatile, widely distributed, "housecleaning" enzymes. J Biol Chem 271(41): 25059–25062
93. Dunn CA et al (1999) Studies on the ADP-ribose pyrophosphatase subfamily of the nudix hydrolases and tentative identification of trgB, a gene associated with tellurite resistance. J Biol Chem 274(45):32318–32324
94. Grimm C et al (2003) Molecular and functional characterization of the melastatin-related cation channel TRPM3. J Biol Chem 278(24):21493–21501
95. Kolisek M et al (2005) Cyclic ADP-ribose and hydrogen peroxide synergize with ADP-ribose in the activation of TRPM2 channels. Mol Cell 18(1):61–69

96. Oancea E et al (2009) TRPM1 forms ion channels associated with melanin content in melanocytes. Sci Signal 2(70):re21
97. Koike C et al (2010) TRPM1 is a component of the retinal ON bipolar cell transduction channel in the mGluR6 cascade. Proc Natl Acad Sci USA 107(1):332–337
98. Morgans CW et al (2009) TRPM1 is required for the depolarizing light response in retinal ON-bipolar cells. Proc Natl Acad Sci USA 106(45):19174–19178
99. Miller BA, Zhang W (2011) TRP channels as mediators of oxidative stress. Adv Exp Med Biol 704:531–544
100. Wehage E et al (2002) Activation of the cation channel long transient receptor potential channel 2 (LTRPC2) by hydrogen peroxide. A splice variant reveals a mode of activation independent of ADP-ribose. J Biol Chem 277(26):23150–23156
101. Schmitz C et al (2003) Regulation of vertebrate cellular Mg2+ homeostasis by TRPM7. Cell 114(2):191–200
102. Matsushita M et al (2005) Channel function is dissociated from the intrinsic kinase activity and autophosphorylation of TRPM7/ChaK1. J Biol Chem 280(21):20793–20803
103. Peier AM et al (2002) A TRP channel that senses cold stimuli and menthol. Cell 108(5): 705–715
104. Talavera K et al (2005) Heat activation of TRPM5 underlies thermal sensitivity of sweet taste. Nature 438(7070):1022–1025
105. McKemy DD, Neuhausser WM, Julius D (2002) Identification of a cold receptor reveals a general role for TRP channels in thermosensation. Nature 416(6876):52–58
106. Liman ER (2007) TRPM5 and taste transduction. Handb Exp Pharmacol 179:287–298
107. Oberwinkler J, Phillipp SE (2007) Trpm3. Handb Exp Pharmacol 179:253–267
108. Vriens J et al (2011) TRPM3 is a nociceptor channel involved in the detection of noxious heat. Neuron 70(3):482–494
109. Mochizuki T et al (1996) PKD2, a gene for polycystic kidney disease that encodes an integral membrane protein. Science 272(5266): 1339–1342
110. Giamarchi A, Delmas P (2007) Activation mechanisms and functional roles of TRPP2 cation channels. In: Liedtke WB, Heller S (eds) TRP Ion Channel Function in Sensory Transduction and Cellular Signaling, Boca Raton (FL) 189–202
111. Gonzalez-Perrett S et al (2001) Polycystin-2, the protein mutated in autosomal dominant polycystic kidney disease (ADPKD), is a Ca2+-permeable nonselective cation channel. Proc Natl Acad Sci USA 98(3):1182–1187
112. Luo Y et al (2003) Native polycystin 2 functions as a plasma membrane Ca2+-permeable cation channel in renal epithelia. Mol Cell Biol 23(7):2600–2607
113. Koulen P et al (2002) Polycystin-2 is an intracellular calcium release channel. Nat Cell Biol 4(3):191–197
114. Delmas P (2005) Polycystins: polymodal receptor/ion-channel cellular sensors. Pflugers Archiv: Eur J Physiol 451(1):264–276
115. Dietrich A, Gudermann T (2011) TRP channels in the cardiopulmonary vasculature. Adv Exp Med Biol 704:781–810
116. Garcia-Anoveros J, Nagata K (2007) Trpa1. Handb Exp Pharmacol 179:347–362
117. Story GM et al (2003) ANKTM1, a TRP-like channel expressed in nociceptive neurons, is activated by cold temperatures. Cell 112(6): 819–829
118. Jordt SE et al (2004) Mustard oils and cannabinoids excite sensory nerve fibres through the TRP channel ANKTM1. Nature 427(6971):260–265
119. Bautista DM et al (2005) Pungent products from garlic activate the sensory ion channel TRPA1. Proc Natl Acad Sci USA 102(34): 12248–12252
120. Bautista DM et al (2006) TRPA1 mediates the inflammatory actions of environmental irritants and proalgesic agents. Cell 124(6): 1269–1282
121. Watanabe H et al (2009) The pathological role of transient receptor potential channels in heart disease. Circ J 73(3):419–427
122. Ju YK et al (2007) Store-operated Ca2+ influx and expression of TRPC genes in mouse sinoatrial node. Circ Res 100(11):1605–1614
123. Hirose M et al (2011) Diacylglycerol kinase zeta inhibits ventricular tachyarrhythmias in a mouse model of heart failure. Circ J 75(10): 2333–2342
124. Kruse M et al (2009) Impaired endocytosis of the ion channel TRPM4 is associated with human progressive familial heart block type I. J Clin Invest 119(9):2737–2744
125. Liu H et al (2010) Gain-of-function mutations in TRPM4 cause autosomal dominant isolated cardiac conduction disease. Circ Cardiovasc Genet 3(4):374–385
126. Du J et al (2010) TRPM7-mediated Ca2+ signals confer fibrogenesis in human atrial fibrillation. Circ Res 106(5):992–1003
127. Ramirez MT et al (1997) The nuclear deltaB isoform of Ca2+/calmodulin-dependent protein kinase II regulates atrial natriuretic factor

gene expression in ventricular myocytes. J Biol Chem 272(49):31203–31208
128. Kirchhefer U et al (1999) Activity of cAMP-dependent protein kinase and Ca2+/calmodulin-dependent protein kinase in failing and nonfailing human hearts. Cardiovasc Res 42(1):254–261
129. Molkentin JD et al (1998) A calcineurin-dependent transcriptional pathway for cardiac hypertrophy. Cell 93(2):215–228
130. Frey N, McKinsey TA, Olson EN (2000) Decoding calcium signals involved in cardiac growth and function. Nature Med 6(11): 1221–1227
131. Molkentin JD, Dorn GW 2nd (2001) Cytoplasmic signaling pathways that regulate cardiac hypertrophy. Annu Rev Physiol 63: 391–426
132. Kuwahara K et al (2006) TRPC6 fulfills a calcineurin signaling circuit during pathologic cardiac remodeling. J Clin Invest 116(12): 3114–3126
133. Onohara N et al (2006) TRPC3 and TRPC6 are essential for angiotensin II-induced cardiac hypertrophy. EMBO J 25(22):5305–5316
134. Brenner JS, Dolmetsch RE (2007) TrpC3 regulates hypertrophy-associated gene expression without affecting myocyte beating or cell size. PloS one 2(8):e802
135. Ohba T et al (2007) Upregulation of TRPC1 in the development of cardiac hypertrophy. J Mol Cell Cardiol 42(3):498–507
136. Hofmann T et al (2002) Subunit composition of mammalian transient receptor potential channels in living cells. Proc Natl Acad Sci USA 99(11):7461–7466
137. Vindis C et al (2010) Essential role of TRPC1 channels in cardiomyoblasts hypertrophy mediated by 5-HT2A serotonin receptors. Biochem Biophys Res Commun 391(1):979–983
138. Ohba T et al (2009) Essential role of STIM1 in the development of cardiomyocyte hypertrophy. Biochem Biophys Res Commun 389(1):172–176
139. Guinamard R et al (2006) Calcium-activated nonselective cation channels in mammalian cardiomyocytes. Trends Cardiovasc Med 16(7):245–250
140. Thilo F et al (2010) Increased transient receptor potential vanilloid type 1 (TRPV1) channel expression in hypertrophic heart. Biochem Biophys Res Commun 401(1):98–103
141. Wong CO, Yao X (2011) TRP channels in vascular endothelial cells. Adv Exp Med Biol 704:759–780
142. Ahmmed GU, Malik AB (2005) Functional role of TRPC channels in the regulation of endothelial permeability. Pflugers Arch 451(1):131–142
143. Lum H et al (1989) Calcium dependence of the thrombin-induced increase in endothelial albumin permeability. J Appl Physiol 66(3): 1471–1476
144. Ahmmed GU et al (2004) Protein kinase Calpha phosphorylates the TRPC1 channel and regulates store-operated Ca2+ entry in endothelial cells. J Biol Chem 279(20):20941–20949
145. Moore TM et al (1998) Store-operated calcium entry promotes shape change in pulmonary endothelial cells expressing Trp1. Am J Physiol 275(3 Pt 1):L574–L582
146. Tiruppathi C et al (2002) Impairment of store-operated Ca2+ entry in TRPC4(-/-) mice interferes with increase in lung microvascular permeability. Circ Res 91(1):70–76
147. Brough GH et al (2001) Contribution of endogenously expressed Trp1 to a Ca2+-selective, store-operated Ca2+ entry pathway. FASEB J 15(10):1727–1738
148. Freichel M et al (2001) Lack of an endothelial store-operated Ca2+ current impairs agonist-dependent vasorelaxation in TRP4-/- mice. Nat Cell Biol 3(2):121–127
149. Cioffi DL et al (2009) TRPing on the lung endothelium: calcium channels that regulate barrier function. Antioxid Redox Signal 11(4):765–776
150. Abdullaev IF et al (2008) Stim1 and Orai1 mediate CRAC currents and store-operated calcium entry important for endothelial cell proliferation. Circ Res 103(11):1289–1299
151. Pocock TM, Foster RR, Bates DO (2004) Evidence of a role for TRPC channels in VEGF-mediated increased vascular permeability in vivo. Am J Physiol Heart Circ Physiol 286(3):H1015–H1026
152. Cheng HW et al (2006) VEGF activates receptor-operated cation channels in human microvascular endothelial cells. Arterioscler Thromb Vasc Biol 26(8):1768–1776
153. Mehta D, Malik AB (2006) Signaling mechanisms regulating endothelial permeability. Physiol Rev 86(1):279–367
154. Hecquet CM, Malik AB (2009) Role of H(2)O(2)-activated TRPM2 calcium channel in oxidant-induced endothelial injury. Thromb Haemost 101(4):619–625
155. Hecquet CM et al (2008) Role of TRPM2 channel in mediating H2O2-induced Ca2+ entry and endothelial hyperpermeability. Circ Res 102(3):347–355
156. Gerzanich V et al (2009) De novo expression of Trpm4 initiates secondary hemorrhage in spinal cord injury. Nat Med 15(2):185–191

157. Paszkowiak JJ, Dardik A (2003) Arterial wall shear stress: observations from the bench to the bedside. Vasc Endovascu Surg 37(1): 47–57
158. House SJ et al (2008) The non-excitable smooth muscle: calcium signaling and phenotypic switching during vascular disease. Pflugers Arch 456(5):769–785
159. Yoshizumi M et al (2003) Stress and vascular responses: atheroprotective effect of laminar fluid shear stress in endothelial cells: possible role of mitogen-activated protein kinases. J Pharmacol Sci 91(3):172–176
160. Vriens J et al (2005) Modulation of the Ca2 permeable cation channel TRPV4 by cytochrome P450 epoxygenases in vascular endothelium. Circ Res 97(9):908–915
161. Nilius B et al (2004) TRPV4 calcium entry channel: a paradigm for gating diversity. Am J Physiol Cell Physiol 286(2):C195–C205
162. Nauli SM et al (2003) Polycystins 1 and 2 mediate mechanosensation in the primary cilium of kidney cells. Nat Genet 33(2): 129–137
163. AbouAlaiwi WA et al (2009) Ciliary polycystin-2 is a mechanosensitive calcium channel involved in nitric oxide signaling cascades. Circ Res 104(7):860–869
164. Earley S et al (2009) TRPV4-dependent dilation of peripheral resistance arteries influences arterial pressure. Am J Physiol Heart Circ Physiol 297(3):H1096–H1102
165. Earley S et al (2005) TRPV4 forms a novel Ca2+ signaling complex with ryanodine receptors and BKCa channels. Circ Res 97(12): 1270–1279
166. Earley S, Gonzales AL, Crnich R (2009) Endothelium-dependent cerebral artery dilation mediated by TRPA1 and Ca2+-activated K+ channels. Circ Res 104(8):987–994
167. Watanabe H et al (2008) TRP channel and cardiovascular disease. Pharmacol Ther 118(3):337–351
168. Bergdahl A et al (2003) Cholesterol depletion impairs vascular reactivity to endothelin-1 by reducing store-operated Ca2+ entry dependent on TRPC1. Circ Res 93(9):839–847
169. Saleh SN et al (2006) Angiotensin II activates two cation conductances with distinct TRPC1 and TRPC6 channel properties in rabbit mesenteric artery myocytes. J Physiol 577(Pt 2):479–495
170. Inoue R et al (2001) The transient receptor potential protein homologue TRP6 is the essential component of vascular alpha(1)-adrenoceptor-activated Ca(2+)-permeable cation channel. Circ Res 88(3):325–332
171. Xie A et al (2007) Novel mechanism of endothelin-1-induced vasospasm after subarachnoid hemorrhage. J Cereb Blood Flow Metab 27(10):1692–1701
172. Tai K et al (2008) Agonist-evoked calcium entry in vascular smooth muscle cells requires IP3 receptor-mediated activation of TRPC1. Eur J Pharmacol 583(1):135–147
173. Tsvilovskyy VV et al (2009) Deletion of TRPC4 and TRPC6 in mice impairs smooth muscle contraction and intestinal motility in vivo. Gastroenterology 137(4):1415–1424
174. Xi Q et al (2008) IP3 constricts cerebral arteries via IP3 receptor-mediated TRPC3 channel activation and independently of sarcoplasmic reticulum Ca2+ release. Circ Res 102(9): 1118–1126
175. Lee YM et al (2003) TRPC5 as a candidate for the nonselective cation channel activated by muscarinic stimulation in murine stomach. Am J Physiol Gastrointest Liver Physiol 284(4):G604–G616
176. Xu SZ et al (2006) A sphingosine-1-phosphate-activated calcium channel controlling vascular smooth muscle cell motility. Circ Res 98(11):1381–1389
177. Golovina VA et al (2001) Upregulated TRP and enhanced capacitative Ca(2+) entry in human pulmonary artery myocytes during proliferation. Am J Physiol Heart Circ Physiol 280(2):H746–H755
178. Kumar B et al (2006) Upregulated TRPC1 channel in vascular injury in vivo and its role in human neointimal hyperplasia. Circ Res 98(4):557–563
179. Lin MJ et al (2004) Chronic hypoxia-induced upregulation of store-operated and receptor-operated Ca2+ channels in pulmonary arterial smooth muscle cells: a novel mechanism of hypoxic pulmonary hypertension. Circ Res 95(5):496–505
180. Bergdahl A et al (2005) Plasticity of TRPC expression in arterial smooth muscle: correlation with store-operated Ca2+ entry. Am J Physiol Cell Physiol 288(4):C872–C880
181. Wang J et al (2005) Acute hypoxia increases intracellular [Ca2+] in pulmonary arterial smooth muscle by enhancing capacitative Ca2+ entry. Am J Physiol Lung Cell Mol Physiol 288(6):L1059–L1069
182. Wang J et al (2006) Hypoxia inducible factor 1 mediates hypoxia-induced TRPC expression and elevated intracellular Ca2+ in pulmonary arterial smooth muscle cells. Circ Res 98(12):1528–1537
183. Yu Y et al (2004) Enhanced expression of transient receptor potential channels in idiopathic

pulmonary arterial hypertension. Proc Natl Acad Sci USA 101(38):13861–13866

184. Firth AL, Remillard CV, Yuan JX (2007) TRP channels in hypertension. Biochim Biophys Acta 1772(8):895–906
185. Zhang S et al (2004) ATP-induced mitogenesis is mediated by cyclic AMP response element-binding protein-enhanced TRPC4 expression and activity in human pulmonary artery smooth muscle cells. Am J Physiol Cell Physiol 287(5):C1192–C1201
186. Earley S (2010) Vanilloid and melastatin transient receptor potential channels in vascular smooth muscle. Microcirculation 17(4): 237–249
187. Kark T et al (2008) Tissue-specific regulation of microvascular diameter: opposite functional roles of neuronal and smooth muscle located vanilloid receptor-1. Mol Pharmacol 73(5): 1405–1412
188. Wang YX et al (2008) Functional expression of transient receptor potential vanilloid-related channels in chronically hypoxic human pulmonary arterial smooth muscle cells. J Membr Biol 223(3):151–159
189. Yang XR et al (2006) Functional expression of transient receptor potential melastatin- and vanilloid-related channels in pulmonary arterial and aortic smooth muscle. Am J Physiol Lung Cell Mol Physiol 290(6):L1267–L1276
190. Simard JM, Tarasov KV, Gerzanich V (2007) Non-selective cation channels, transient receptor potential channels and ischemic stroke. Biochim Biophys Acta 1772(8):947–957
191. McNulty S, Fonfria E (2005) The role of TRPM channels in cell death. Pflugers Archiv: Eur J Physiol 451(1):235–242
192. Perraud AL et al (2005) Accumulation of free ADP-ribose from mitochondria mediates oxidative stress-induced gating of TRPM2 cation channels. J Biol Chem 280(7):6138–6148
193. Kaneko S et al (2006) A critical role of TRPM2 in neuronal cell death by hydrogen peroxide. J Pharmacol Sci 101(1):66–76
194. Kuhn FJ, Heiner I, Luckhoff A (2005) TRPM2: a calcium influx pathway regulated by oxidative stress and the novel second messenger ADP-ribose. Pflugers Arch 451(1): 212–219
195. Earley S, Waldron BJ, Brayden JE (2004) Critical role for transient receptor potential channel TRPM4 in myogenic constriction of cerebral arteries. Circ Res 95(9):922–929
196. Zholos A et al (2011) TRPM channels in the vasculature. Adv Exp Med Biol 704:707–729
197. He Y et al (2005) Transient receptor potential melastatin 7 ion channels regulate magnesium homeostasis in vascular smooth muscle cells: role of angiotensin II. Circ Res 96(2):207–215
198. Johnson CD et al (2009) Transient receptor potential melastatin 8 channel involvement in the regulation of vascular tone. Am J Physiol Heart Circ Physiol 296(6):H1868–H1877
199. Zitt C et al (1996) Cloning and functional expression of a human Ca2+-permeable cation channel activated by calcium store depletion. Neuron 16(6):1189–1196
200. Saleh SN, Albert AP, Large WA (2009) Activation of native TRPC1/C5/C6 channels by endothelin-1 is mediated by both PIP3 and PIP2 in rabbit coronary artery myocytes. J Physiol 587(Pt 22):5361–5375
201. Tu CL, Chang W, Bikle DD (2005) Phospholipase cgamma1 is required for activation of store-operated channels in human keratinocytes. J Invest Dermatol 124(1): 187–197
202. Delmas P et al (2002) Signaling microdomains define the specificity of receptor-mediated InsP(3) pathways in neurons. Neuron 34(2):209–220
203. Allen DG, Whitehead NP, Yeung EW (2005) Mechanisms of stretch-induced muscle damage in normal and dystrophic muscle: role of ionic changes. J Physiol 567(Pt 3):723–735
204. Nilius B et al (2007) Transient receptor potential cation channels in disease. Physiol Rev 87(1):165–217
205. Formigli L et al (2009) Regulation of transient receptor potential canonical channel 1 (TRPC1) by sphingosine 1-phosphate in C2C12 myoblasts and its relevance for a role of mechanotransduction in skeletal muscle differentiation. J Cell Sci 122(Pt 9): 1322–1333
206. Kim SJ et al (2003) Activation of the TRPC1 cation channel by metabotropic glutamate receptor mGluR1. Nature 426(6964):285–291
207. Lucas P et al (2003) A diacylglycerol-gated cation channel in vomeronasal neuron dendrites is impaired in TRPC2 mutant mice: mechanism of pheromone transduction. Neuron 40(3):551–561
208. Tong Q et al (2004) Erythropoietin-modulated calcium influx through TRPC2 is mediated by phospholipase Cgamma and IP3R. Am J Physiol Cell Physiol 287(6):C1667–C1678
209. Vannier B et al (1999) Mouse trp2, the homologue of the human trpc2 pseudogene, encodes mTrp2, a store depletion-activated capacitative Ca2+ entry channel. Proc Natl Acad Sci USA 96(5):2060–2064

210. Zhang P, Yang C, Delay RJ (2010) Odors activate dual pathways, a TRPC2 and a AA-dependent pathway, in mouse vomeronasal neurons. Am J Physiol Cell Physiol 298(5):C1253–C1264
211. Kamouchi M et al (1999) Properties of heterologously expressed hTRP3 channels in bovine pulmonary artery endothelial cells. J Physiol 518(Pt 2):345–358
212. Kiselyov K et al (1998) Functional interaction between InsP3 receptors and store-operated Htrp3 channels. Nature 396(6710):478–482
213. Trebak M et al (2002) Comparison of human TRPC3 channels in receptor-activated and store-operated modes. Differential sensitivity to channel blockers suggests fundamental differences in channel composition. J Biol Chem 277(24):21617–21623
214. Reading SA et al (2005) TRPC3 mediates pyrimidine receptor-induced depolarization of cerebral arteries. Am J Physiol Heart Circ Physiol 288(5):H2055–H2061
215. Okada T et al (1999) Molecular and functional characterization of a novel mouse transient receptor potential protein homologue TRP7. Ca(2+)-permeable cation channel that is constitutively activated and enhanced by stimulation of G protein-coupled receptor. J Biol Chem 274(39):27359–27370
216. Ma HT et al (2000) Requirement of the inositol trisphosphate receptor for activation of store-operated Ca2+ channels. Science 287(5458):1647–1651
217. Zhu X, Jiang M, Birnbaumer L (1998) Receptor-activated Ca2+ influx via human Trp3 stably expressed in human embryonic kidney (HEK)293 cells. Evidence for a non-capacitative Ca2+ entry. J Biol Chem 273(1):133–142
218. McKay RR et al (2000) Cloning and expression of the human transient receptor potential 4 (TRP4) gene: localization and functional expression of human TRP4 and TRP3. Biochem J 351(Pt 3):735–746
219. Philipp S et al (1996) A mammalian capacitative calcium entry channel homologous to Drosophila TRP and TRPL. Embo J 15(22):6166–6171
220. Schaefer M et al (2002) Functional differences between TRPC4 splice variants. J Biol Chem 277(5):3752–3759
221. Schaefer M et al (2000) Receptor-mediated regulation of the nonselective cation channels TRPC4 and TRPC5. J Biol Chem 275(23):17517–17526
222. Ulloa A et al (2009) Reduction in TRPC4 expression specifically attenuates G-protein coupled receptor-stimulated increases in intracellular calcium in human myometrial cells. Cell calcium 46(1):73–84
223. Fowler MA et al (2007) Corticolimbic expression of TRPC4 and TRPC5 channels in the rodent brain. PLoS One 2(6):e573
224. Miller MR et al. (2010) Novel Chemical Inhibitor of TRPC4 Channels. Probe Reports from the NIH Molecular Libraries Program [Internet]. Bethesda (MD): National Center for iotechnology Information (US); 2010 Dec 15 [updated 2011 May 26]
225. Okada T et al (1998) Molecular cloning and functional characterization of a novel receptor-activated TRP Ca2+ channel from mouse brain. J Biol Chem 273(17):10279–10287
226. Dresviannikov AV, Bolton TB, Zholos AV (2006) Muscarinic receptor-activated cationic channels in murine ileal myocytes. Br J Pharmacol 149(2):179–187
227. Strubing C et al (2001) TRPC1 and TRPC5 form a novel cation channel in mammalian brain. Neuron 29(3):645–655
228. Xu SZ et al (2005) Block of TRPC5 channels by 2-aminoethoxydiphenyl borate: a differential, extracellular and voltage-dependent effect. Br J Pharmacol 145(4):405–414
229. Wong CO, Huang Y, Yao X (2010) Genistein potentiates activity of the cation channel TRPC5 independently of tyrosine kinases. Br J Pharmacol 159(7):1486–1496
230. Jung S et al (2003) Lanthanides potentiate TRPC5 currents by an action at extracellular sites close to the pore mouth. J Biol Chem 278(6):3562–3571
231. Albert AP, Saleh SN, Large WA (2008) Inhibition of native TRPC6 channel activity by phosphatidylinositol 4,5-bisphosphate in mesenteric artery myocytes. J Physiol 586(13):3087–3095
232. Spassova MA et al (2006) A common mechanism underlies stretch activation and receptor activation of TRPC6 channels. Proc Natl Acad Sci USA 103:16586–16591
233. Basora N et al (2003) 20-hydroxyeicosatetraenoic acid (20-HETE) activates mouse TRPC6 channels expressed in HEK293 cells. J Biol Chem 278(34):31709–31716
234. Leuner K et al (2007) Hyperforin—a key constituent of St. John's wort specifically activates TRPC6 channels. Faseb J 21(14):4101–4111
235. Vazquez G et al (2006) Native TRPC7 channel activation by an inositol trisphosphate receptor-dependent mechanism. J Biol Chem 281(35):25250–25258
236. Lievremont JP, Bird GS, Putney JW Jr (2004) Canonical transient receptor potential TRPC7

can function as both a receptor- and store-operated channel in HEK-293 cells. Am J Physiol Cell Physiol 287(6):C1709–C1716

237. Samways DS, Egan TM (2011) Calcium-dependent decrease in the single-channel conductance of TRPV1. Pflugers Archiv: Eur J Physiol 462(5):681–691
238. Mohapatra DP et al (2003) A tyrosine residue in TM6 of the Vanilloid Receptor TRPV1 involved in desensitization and calcium permeability of capsaicin-activated currents. Mol Cell Neurosci 23(2):314–324
239. Tominaga M et al (1998) The cloned capsaicin receptor integrates multiple pain-producing stimuli. Neuron 21(3):531–543
240. Zygmunt PM et al (1999) Vanilloid receptors on sensory nerves mediate the vasodilator action of anandamide. Nature 400(6743):452–457
241. Szallasi A et al (1999) The cloned rat vanilloid receptor VR1 mediates both R-type binding and C-type calcium response in dorsal root ganglion neurons. Mol Pharmacol 56(3):581–587
242. Woo DH et al (2008) Direct activation of transient receptor potential vanilloid 1(TRPV1) by diacylglycerol (DAG). Mol Pain 4:42
243. McIntyre P et al (2001) Pharmacological differences between the human and rat vanilloid receptor 1 (VR1). Br J Pharmacol 132(5):1084–1094
244. Huang SM et al (2002) An endogenous capsaicin-like substance with high potency at recombinant and native vanilloid VR1 receptors. Proc Natl Acad Sci USA 99(12):8400–8405
245. Bevan S et al (1992) Capsazepine: a competitive antagonist of the sensory neurone excitant capsaicin. Br J Pharmacol 107(2):544–552
246. Poblete IM et al (2005) Anandamide elicits an acute release of nitric oxide through endothelial TRPV1 receptor activation in the rat arterial mesenteric bed. J Physiol 568(Pt 2):539–551
247. Gunthorpe MJ et al (2004) Identification and characterisation of SB-366791, a potent and selective vanilloid receptor (VR1/TRPV1) antagonist. Neuropharmacology 46(1):133–149
248. Rami HK et al (2004) Discovery of small molecule antagonists of TRPV1. Bioorg Med Chem Lett 14(14):3631–3634
249. Caterina MJ et al (1999) A capsaicin-receptor homologue with a high threshold for noxious heat. Nature 398(6726):436–441
250. Moqrich A et al (2005) Impaired thermosensation in mice lacking TRPV3, a heat and camphor sensor in the skin. Science 307(5714): 1468–1472
251. Strotmann R et al (2000) OTRPC4, a nonselective cation channel that confers sensitivity to extracellular osmolarity. Nat Cell Biol 2(10):695–702
252. Liedtke W et al (2000) Vanilloid receptor-related osmotically activated channel (VR-OAC), a candidate vertebrate osmoreceptor. Cell 103(3):525–535
253. Guler AD et al (2002) Heat-evoked activation of the ion channel, TRPV4. J Neurosci 22(15):6408–6414
254. Birder L et al (2007) Activation of urothelial transient receptor potential vanilloid 4 by 4alpha-phorbol 12,13-didecanoate contributes to altered bladder reflexes in the rat. J Pharmacol Exp Ther 323(1):227–235
255. Thorneloe KS et al (2008) N-((1 S)-1-{[4-((2 S)-2-{[(2,4-dichlorophenyl)sulfonyl] amino}-3-hydroxypropa noyl)-1-piperazinyl] carbonyl}-3-methylbutyl)-1-benzothiophene-2-carboxamid e (GSK1016790A), a novel and potent transient receptor potential vanilloid 4 channel agonist induces urinary bladder contraction and hyperactivity: Part I. J Pharmacol Exp Ther 326(2):432–442
256. Nilius B et al (2000) Whole-cell and single channel monovalent cation currents through the novel rabbit epithelial Ca2+ channel ECaC. J Physiol 527(Pt 2):239–248
257. Lee J et al (2005) PIP2 activates TRPV5 and releases its inhibition by intracellular Mg2+. J Gen Physiol 126(5):439–451
258. Schindl R et al (2002) Store depletion-activated CaT1 currents in rat basophilic leukemia mast cells are inhibited by 2-aminoethoxydiphenyl borate. Evidence for a regulatory component that controls activation of both CaT1 and CRAC (Ca(2+) release-activated Ca(2+) channel) channels. J Biol Chem 277(30):26950–26958
259. Bakowski D, Parekh AB (2002) Permeation through store-operated CRAC channels in divalent-free solution: potential problems and implications for putative CRAC channel genes. Cell Calcium 32(5–6):379–391
260. Xu XZ et al (2001) Regulation of melastatin, a TRP-related protein, through interaction with a cytoplasmic isoform. Proc Natl Acad Sci USA 98(19):10692–10697
261. Kraft R et al (2004) Hydrogen peroxide and ADP-ribose induce TRPM2-mediated calcium influx and cation currents in microglia. Am J Physiol Cell Physiol 286(1): C129–C137
262. Sano Y et al (2001) Immunocyte Ca2+ influx system mediated by LTRPC2. Science 293(5533):1327–1330

263. Naziroglu M (2007) New molecular mechanisms on the activation of TRPM2 channels by oxidative stress and ADP-ribose. Neurochem Res 32(11):1990–2001
264. Hill K et al (2004) Flufenamic acid is a pH-dependent antagonist of TRPM2 channels. Neuropharmacology 47(3):450–460
265. Togashi K, Inada H, Tominaga M (2008) Inhibition of the transient receptor potential cation channel TRPM2 by 2-aminoethoxydiphenyl borate (2-APB). Br J Pharmacol 153(6):1324–1330
266. Hill K, McNulty S, Randall AD (2004) Inhibition of TRPM2 channels by the antifungal agents clotrimazole and econazole. Naunyn Schmiedebergs Arch Pharmacol 370(4):227–237
267. Lambert S et al (2011) Transient receptor potential melastatin 1 (TRPM1) is an ion-conducting plasma membrane channel inhibited by zinc ions. J Biol Chem 286(14): 12221–12233
268. Nilius B et al (2004) Decavanadate modulates gating of TRPM4 cation channels. J Physiol 560(Pt 3):753–765
269. Takezawa R et al (2006) A pyrazole derivative potently inhibits lymphocyte Ca2+ influx and cytokine production by facilitating transient receptor potential melastatin 4 channel activity. Mol Pharmacol 69(4):1413–1420
270. Nilius B et al (2005) Regulation of the Ca2+ sensitivity of the nonselective cation channel TRPM4. J Biol Chem 280(8):6423–6433
271. Nilius B et al (2006) The Ca2+-activated cation channel TRPM4 is regulated by phosphatidylinositol 4,5-biphosphate. EMBO J 25(3):467–478
272. Nilius B et al (2004) Intracellular nucleotides and polyamines inhibit the Ca2+-activated cation channel TRPM4b. Pflugers Archiv: Eur J Physiol 448(1):70–75
273. Ullrich ND et al (2005) Comparison of functional properties of the Ca2+-activated cation channels TRPM4 and TRPM5 from mice. Cell calcium 37(3):267–278
274. Hofmann T et al (2003) TRPM5 is a voltage-modulated and Ca(2+)-activated monovalent selective cation channel. Curr Biol 13(13):1153–1158
275. Voets T et al (2004) TRPM6 forms the Mg2+ influx channel involved in intestinal and renal Mg2+ absorption. J Biol Chem 279(1):19–25
276. Runnels LW, Yue L, Clapham DE (2001) TRP-PLIK, a bifunctional protein with kinase and ion channel activities. Science 291(5506):1043–1047
277. Kerschbaum HH, Cahalan MD (1999) Single-channel recording of a store-operated Ca2+ channel in Jurkat T lymphocytes. Science 283(5403):836–839
278. Nadler MJ et al (2001) LTRPC7 is a Mg.ATP-regulated divalent cation channel required for cell viability. Nature 411(6837): 590–595
279. Runnels LW, Yue L, Clapham DE (2002) The TRPM7 channel is inactivated by PIP(2) hydrolysis. Nat Cell Biol 4(5):329–336
280. Kerschbaum HH, Kozak JA, Cahalan MD (2003) Polyvalent cations as permeant probes of MIC and TRPM7 pores. Biophys J 84(4): 2293–2305
281. Hu HZ et al (2004) 2-aminoethoxydiphenyl borate is a common activator of TRPV1, TRPV2, and TRPV3. J Biol Chem 279(34): 35741–35748
282. Weil A et al (2005) Conservation of functional and pharmacological properties in the distantly related temperature sensors TRVP1 and TRPM8. Mol Pharmacol 68(2):518–527
283. Bandell M et al (2004) Noxious cold ion channel TRPA1 is activated by pungent compounds and bradykinin. Neuron 41(6):849–857
284. Niforatos W et al (2007) Activation of TRPA1 channels by the fatty acid amide hydrolase inhibitor 3'-carbamoylbiphenyl-3-yl cyclohexylcarbamate (URB597). Mol Pharmacol 71(5):1209–1216
285. Hanaoka K et al (2000) Co-assembly of polycystin-1 and -2 produces unique cation-permeable currents. Nature 408(6815): 990–994
286. Montalbetti N et al (2005) Cytoskeletal regulation of calcium-permeable cation channels in the human syncytiotrophoblast: role of gelsolin. J Physiol 566(Pt 2):309–325
287. Bai CX et al (2008) Activation of TRPP2 through mDia1-dependent voltage gating. EMBO J 27(9):1345–1356
288. Montalbetti N et al (2005) Effect of hydro-osmotic pressure on polycystin-2 channel function in the human syncytiotrophoblast. Pflugers Archiv: Eur J Physiol 451(1):294–303
289. Cantero Mdel R, Cantiello HF (2011) Effect of lithium on the electrical properties of polycystin-2 (TRPP2). Eur Biophys J 40(9):1029–1042
290. Chen XZ et al (1999) Polycystin-L is a calcium-regulated cation channel permeable to calcium ions. Nature 401(6751):383–386
291. Ishimaru Y et al (2006) Transient receptor potential family members PKD1L3 and PKD2L1 form a candidate sour taste receptor. Proc Natl Acad Sci USA 103(33):12569–12574

292. Inada H et al (2008) Off-response property of an acid-activated cation channel complex PKD1L3-PKD2L1. EMBO Rep 9(7):690–697
293. Volk T et al (2003) A polycystin-2-like large conductance cation channel in rat left ventricular myocytes. Cardiovasc Res 58(1):76–88
294. Ju YK, Allen DG (2007) Store-operated Ca2+ entry and TRPC expression; possible roles in cardiac pacemaker tissue. Heart Lung Circ 16(5):349–355
295. Nishida M et al (2010) Regulation of cardiovascular functions by the phosphorylation of TRPC channels. Yakugaku Zasshi 130(11): 1427–1433
296. Wilkins BJ, Molkentin JD (2004) Calcium-calcineurin signaling in the regulation of cardiac hypertrophy. Biochem Biophys Res Commun 322(4):1178–1191
297. Ward ML et al (2008) Stretch-activated channels in the heart: contributions to length-dependence and to cardiomyopathy. Prog Biophys Mol Biol 97(2–3):232–249
298. Williams IA, Allen DG (2007) Intracellular calcium handling in ventricular myocytes from mdx mice. Am J Physiol Heart Circ Physiol 292(2):H846–H855
299. Bush EW et al (2006) Canonical transient receptor potential channels promote cardiomyocyte hypertrophy through activation of calcineurin signaling. J Biol Chem 281(44): 33487–33496
300. Liu D et al (2006) Transient receptor potential channels in essential hypertension. J Hypertens 24(6):1105–1114
301. Kitajima N et al (2011) TRPC3-mediated Ca2+ influx contributes to Rac1-mediated production of reactive oxygen species in MLP-deficient mouse hearts. Biochem Biophys Res Commun 409(1):108–113
302. Mohl MC et al (2011) Regulation of murine cardiac contractility by activation of alpha(1A)-adrenergic receptor-operated Ca(2+) entry. Cardiovasc Res 91(2):310–319
303. Guinamard R et al (2006) Functional expression of the TRPM4 cationic current in ventricular cardiomyocytes from spontaneously hypertensive rats. Hypertension 48(4):587–594
304. Mathar I et al (2010) Increased catecholamine secretion contributes to hypertension in TRPM4-deficient mice. J Clin Invest 120(9): 3267–3279
305. Pan HL, Chen SR (2004) Sensing tissue ischemia: another new function for capsaicin receptors? Circulation 110(13):1826–1831
306. Hatano N, Itoh Y, Muraki K (2009) Cardiac fibroblasts have functional TRPV4 activated by 4alpha-phorbol 12,13-didecanoate. Life Sci 85(23–26):808–814
307. Yang XR et al (2011) Upregulation of osmomechanosensitive TRPV4 channel facilitates chronic hypoxia induced myogenic tone and pulmonary hypertension. Am J Physiol Lung Cell Mol Physiol 302:L555–L568
308. Senatore S et al (2010) Response to mechanical stress is mediated by the TRPA channel painless in the Drosophila heart. PLoS Genet 6(9):e1001088
309. Pennekamp P et al (2002) The ion channel polycystin-2 is required for left-right axis determination in mice. Curr Biol 12(11): 938–943
310. Wu G et al (2000) Cardiac defects and renal failure in mice with targeted mutations in Pkd2. Nat Genet 24(1):75–78
311. Paria BC et al (2003) Tumor necrosis factor-alpha induces nuclear factor-kappaB-dependent TRPC1 expression in endothelial cells. J Biol Chem 278(39):37195–37203
312. Paria BC et al (2004) Tumor necrosis factor-alpha-induced TRPC1 expression amplifies store-operated Ca2+ influx and endothelial permeability. Am J Physiol Lung Cell Mol Physiol 287(6):L1303–L1313
313. Gifford SM, Yi FX, Bird IM (2006) Pregnancy-enhanced store-operated Ca2+ channel function in uterine artery endothelial cells is associated with enhanced agonist-specific transient receptor potential channel 3-inositol 1,4,5-trisphosphate receptor 2 interaction. J Endocrinol 190(2):385–395
314. Balzer M, Lintschinger B, Groschner K (1999) Evidence for a role of Trp proteins in the oxidative stress-induced membrane conductances of porcine aortic endothelial cells. Cardiovasc Res 42(2):543–549
315. Fantozzi I et al (2003) Hypoxia increases AP-1 binding activity by enhancing capacitative Ca2+ entry in human pulmonary artery endothelial cells. Am J Physiol Lung Cell Mol Physiol 285(6):L1233–L1245
316. Wei L et al (2001) Functional interaction between TRP4 and CFTR in mouse aorta endothelial cells. BMC Physiol 1:3
317. Ge R et al (2009) Critical role of TRPC6 channels in VEGF-mediated angiogenesis. Cancer Lett 283(1):43–51
318. Baldoli E, Maier JA (2011) Silencing TRPM7 mimics the effects of magnesium deficiency in human microvascular endothelial cells. Angiogenesis 15:0969–6970
319. Domenicali M et al (2005) Increased anandamide induced relaxation in mesenteric arteries of cirrhotic rats: role of cannabinoid and vanilloid receptors. Gut 54(4):522–527
320. Zhang DX et al (2009) Transient receptor potential vanilloid type 4-deficient mice

exhibit impaired endothelium-dependent relaxation induced by acetylcholine in vitro and in vivo. Hypertension 53(3):532–538

321. Zhu G et al (2009) Association of TRPV4 gene polymorphisms with chronic obstructive pulmonary disease. Hum Mol Genet 18(11): 2053–2062
322. Kwan HY, Huang Y, Yao X (2007) TRP channels in endothelial function and dysfunction. Biochim Biophys Acta 1772(8):907–914
323. Ng LC et al (2009) TRPC1 and STIM1 mediate capacitative Ca2+ entry in mouse pulmonary arterial smooth muscle cells. J Physiol 587(Pt 11):2429–2442
324. Sweeney M et al (2002) Inhibition of endogenous TRP1 decreases capacitative Ca2+ entry and attenuates pulmonary artery smooth muscle cell proliferation. Am J Physiol Lung Cell Mol Physiol 283(1):L144–L155
325. White TA et al (2006) Role of transient receptor potential C3 in TNF-alpha-enhanced calcium influx in human airway myocytes. Am J Respir Cell Mol Biol 35(2):243–251
326. Dalrymple A et al (2004) Physiological induction of transient receptor potential canonical proteins, calcium entry channels, in human myometrium: influence of pregnancy, labor, and interleukin-1 beta. J Clin Endocrinol Metab 89(3):1291–1300
327. Torihashi S et al (2002) Calcium oscillation linked to pacemaking of interstitial cells of Cajal: requirement of calcium influx and localization of TRP4 in caveolae. J Biol Chem 277(21):19191–19197
328. Yoshida T et al (2006) Nitric oxide activates TRP channels by cysteine S-nitrosylation. Nat Chem Biol 2(11):596–607
329. Welsh DG et al (2002) Transient receptor potential channels regulate myogenic tone of resistance arteries. Circ Res 90(3):248–250
330. Weissmann N et al (2006) Classical transient receptor potential channel 6 (TRPC6) is essential for hypoxic pulmonary vasoconstriction and alveolar gas exchange. Proc Natl Acad Sci USA 103(50):19093–19098
331. Nassini R et al (2010) Transient receptor potential channels as novel drug targets in respiratory diseases. Curr Opin Investig Drugs 11(5):535–542
332. Naylor J et al (2010) Pregnenolone sulphate- and cholesterol-regulated TRPM3 channels coupled to vascular smooth muscle secretion and contraction. Circ Res 106(9): 1507–1515
333. Yogi A et al (2009) Bradykinin regulates calpain and proinflammatory signaling through TRPM7-sensitive pathways in vascular smooth muscle cells. Am J Physiol Regul Integr Compar Physiol 296(2):R201–R207
334. Kim BJ et al (2005) Melastatin-type transient receptor potential channel 7 is required for intestinal pacemaking activity. Gastroenterology 129(5):1504–1517
335. Touyz RM et al (2006) Differential regulation of transient receptor potential melastatin 6 and 7 cation channels by ANG II in vascular smooth muscle cells from spontaneously hypertensive rats. Am J Physiol Regul Integr Compar Physiol 290(1): R73–R78
336. Mustafa S, Oriowo M (2005) Cooling-induced contraction of the rat gastric fundus: mediation via transient receptor potential (TRP) cation channel TRPM8 receptor and Rho-kinase activation. Clin Exp Pharmacol Physiol 32(10):832–838
337. Wang Y et al (2008) Deletion of transientreceptor potential vanilloid type 1 receptors exaggerates renal damage in deoxycorticosterone acetate-salt hypertension. Hypertension 52(2):264–270
338. Liedtke W, Simon SA (2004) A possible role for TRPV4 receptors in asthma. Am J Physiol Lung Cell Mol Physiol 287(2):L269–L271

Chapter 2

Anemic Zebrafish Models of Cardiomyopathy

Xiaojing Sun and Xiaolei Xu

Abstract

Cardiomyopathy refers to the cardiac remodeling process in response to a variety of intrinsic and extrinsic stimuli that stress the heart. To discover novel therapeutic strategies for the disease, we are establishing and characterizing adult zebrafish models of cardiomyopathy. One of the models is *tr265/tr265*, a line that becomes anemic due to a mutation that ablates erythroid-specific Band 3 protein. Although Band 3 does not express in the heart, the chronic anemic stress induces profound cardiac enlargement and cardiomyopathy-like pathogenesis. Phenylhydrazine hydrochloride (PHZ)-induced anemia model has been established which enables application of anemia stress to any adult fish. In this chapter, we provide detailed information on generation of two anemic models in zebrafish; measurement of the anemia level; determination of enlarged hearts in either organ level or cellular level; and detection of cardiomyocyte hyperplasia, as well as survival rate recording. The protocols described here can be applied to other adult zebrafish models of cardiomyopathy.

Key words: Zebrafish, Anemia, Tr265, Cardiomyopathy, Phenylhydrazine hydrochloride (PHZ)

1. Introduction

A heart remodels in response to a variety of extrinsic and intrinsic stimuli that impose biomechanical stresses. During the compensational remodeling phase, a heart can adapt itself to deal with stresses by increasing the size of cardiomyocytes. Initially, this adaptive response improves cardiac function. However, sustained stresses trigger a switch from compensational to decompensational remodeling, which is followed by cardiomyopathy and heart failure (1). The hallmarks of cardiomyopathy in humans include enlargement of individual cardiomyocytes, decreased cardiac function, disarray of myofibrils, fibrosis in the extracellular matrix, and re-activation of fetal transcriptional programs (1). Various model organisms have been utilized to understand the molecular mechanisms of cardiomyopathy. Larger mammals, such as cats, dogs,

Arpad Szallasi and Tamás Bíró (eds.), *TRP Channels in Drug Discovery: Volume II*, Methods in Pharmacology and Toxicology,
DOI 10.1007/978-1-62703-095-3_2,

pigs, and primates, boast similar cardiac physiology to that of humans, but genetic manipulation is difficult (2). Therefore, smaller mammals (e.g., mice, rats, and rabbits) are the major vertebrate models for molecular genetic studies of cardiomyopathy (3). To facilitate the identification of novel genes and signaling pathways by forward genetic screen, *Drosophila* has been adopted to study heart diseases (4). However, its primitive heart structure prevents it from being a bona fide model to accurately recapitulate cardiac hypertrophic responses. Acclaimed as *Drosophila* in the vertebrate, the zebrafish model has proven to be convenient for forward genetic screens (5, 6). Additionally, since small molecules can be absorbed through their skin (and later gills), zebrafish are ideal for chemical screens to discover novel therapeutic drugs (7). Despite these potential advantages and its wide application in studying cardiogenesis (8), zebrafish is still an under-utilized organism for studying cardiac remodeling in adults (9).

To generate the first adult fish model of heart failure, we characterized the zebrafish mutant *tr265/tr265* (10) whose Band 3 mutation disrupts erythrocyte formation and results in anemia (11). Chronic anemia imposes biomechanical stress to the heart and results in cardiomegaly (Fig. 1). Despite their anemic condition,

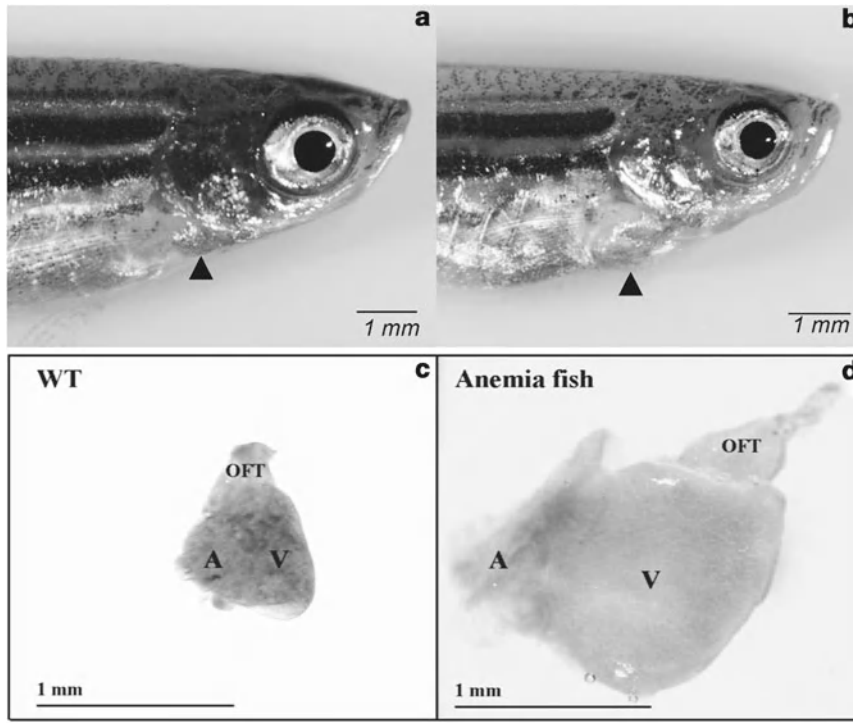

Fig. 1. Chronic anemia induces enlarged heart in *tr265/tr265* zebrafish. (**a**, **b**) Cardiomegaly is noted in a week-8 *tr265/tr265* fish (**b**) but not wild-type sibling (**a**). *Arrowheads* indicate the heart region. (**c**, **d**) Dissected hearts of either the sibling (**c**) or *tr265/tr265* fish (**d**). *A* atrium, *V* ventricle, OFT out flow tract. Bar = 1 mm.

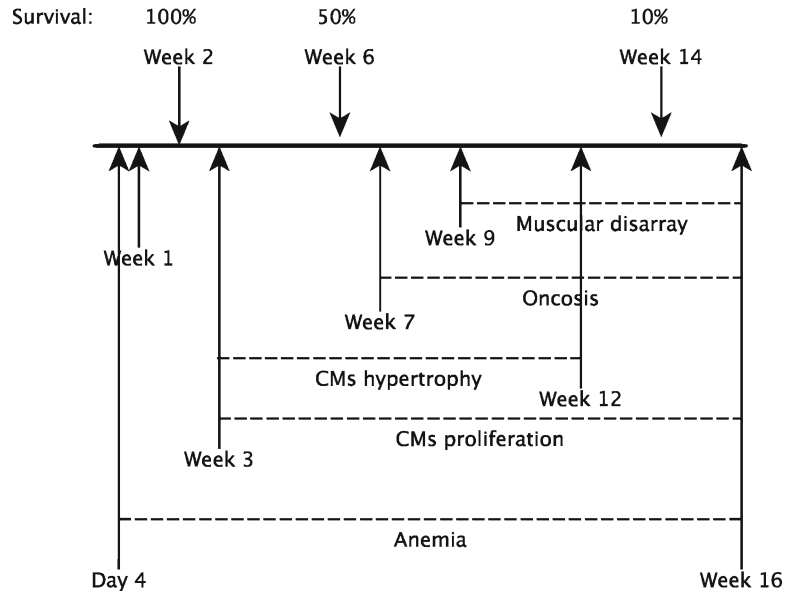

Fig. 2. Time course of cardiac remodeling events in *tr265/tr265*. Chronic anemia stress starts at day 4. Increased ventricular size can be detected at week 3, consisting of both myocyte hypertrophy and myocyte hyperplasia. Muscular disarray is detected from week 9 and thereafter, while oncosis is detectable starting from week 7. Large cardiomyocytes disappear at week 12, while proliferation of cardiomyocytes is detectable in *tr265/tr265* throughout its lifespan.

tr265/tr265 can survive to adulthood and reach sexual maturity. The following time course of cardiac remodeling events is shown in Fig. 2: chronic anemic stress starts at day 4 postfertilization (dpf). Increased ventricular size can be detected at week 3, consisting of both cardiomyocyte hypertrophy and cardiomyocyte hyperplasia. Muscular disarray is detected from week 9 and thereafter, while oncosis is detectable starting from week 7. Large cardiomyocytes disappear at week 12, while cardiomyocyte proliferation is detectable in *tr265/tr265* fish throughout its lifespan.

Our study of *tr265/tr265* indicated that cardiomyopathy-like responses exist in zebrafish. Of note, only in zebrafish does cardiomyocyte hyperplasia contribute significantly to the cardiac remodeling process. On the one hand, this model allows us to assess underlying signaling pathways and the relationship of cardiomyocyte hypertrophy and hyperplasia, and to investigate the roles of cardiomyocyte hyperplasia in heart failure as well as evaluate potential therapeutic strategies via promoting cardiomyocyte proliferation. On the other hand, the significant contribution of cardiomyocyte hyperplasia to the cardiac remodeling process, which occurs at a much lesser extent in human patients, raises concern on the conservation of the adult zebrafish model. Our characterization of Doxorubicin (DOX)-induced cardiomyopathy partially addressed this concern (12). DOX is an anthracyclin drug used in the treatment of a broad spectrum of cancers (13). However, overdose

of DOX imposes cardiac toxicity in human patients (14) as well as in animal models (15, 16), including zebrafish (12). We found that the zebrafish DOX model exhibits different cardiac remodeling processes than the anemia model. Cardiomyocyte hyperplasia does not contribute to cardiomyopathy in the DOX model (12), indicating cardiomyocyte hyperplasia is not a default remodeling mechanism in an adult fish heart. Together, these data underscore the value of the anemia model in studies of cardiomyocyte hyperplasia.

We also found the cardiac hypertrophy process can be recapitulated in wild-type fish using phenylhydrazine (PHZ), an anemia-inducing drug (10). PHZ has been previously used to induce cardiac hypertrophy in rats and trout (17, 18). Compared to the tr265 model, the PHZ model is less labor intensive and can be used to induce cardiac remodeling in adult fish in any fish line at any age. These unique features are extremely valuable for mutagenesis screens. However, it remains to be established whether prolonged PHZ treatment can be conducted to induce later pathological responses.

In this chapter, we provide detailed step-by-step instructions on how to generate these two anemia-induced cardiomyopathy models in adult zebrafish, as well as the protocols to define key remodeling events.

2. Materials

2.1. Equipment

1. Nursery tube (0.125 L) (Aquatic Habitats Inc., Allentown, NJ).
2. Fish tank (1 L, 2.5 L and 9 L) (Aquatic Habitats Inc.).
3. Zeiss Axioplan 2 microscope (Carl Zeiss, Thornwood, NY) for imaging.
4. Leica MZ FLI III microscope (North Central Instruments, Inc. Plymouth, MN) for imaging.
5. Nikon COOLPIX 8700 digital camera (Nikon Instruments Inc. Melville, NY) for imaging.
6. Confocal laser scanning microscopy (Zeiss LSM510, Carl Zeiss).
7. Dumont #5 Biologie Inox forceps (Fine Science Tools, Foster City, CA) was used to puncture the gill to induce bleeding.
8. L calibrated micropipette (Drummond Scientific Company, Foster City, CA) for collecting blood from live fish.
9. AG204 DeltaRange scale (Mettler Toledo, Columbus, OH) for measuring body weight.
10. Microtome Blade (Thermo Scientific, Wilmington, DE) for cutting heart samples.

11. Disposable vinyl specimen molds (10×10×5 mm) (Electron Microscopy Sciences, Torrance, CA)—container for fish hearts.
12. Poly-Prep slides (Sigma, St. Louis, MO) for collecting heart samples after frozen section.
13. Motorized Research Cryostat (Leica CM3050S) (North Central Instruments Inc. Plymouth, MN) for frozen section.
14. 8- or 16-well chamber slide (Nalge Nunc Internationalm, Rochester, NY) for cardiomyocyte culture.
15. 34-Gauge NanoFil beveled needle and 10 μL syringes (World Precision Instruments; Sarasota, Florida) for 5-bromo-2-deoxyuridine (BrdU) injection.
16. Software: AxioVision software (Carl Zeiss) was used to calculate the area of the ventricle from these images in pixels squared; NanoDrop ND-1000 and V3.1.2 software (Thermo Scientific) for measurement of hemoglobin concentration; ImageJ software for cardiomyocyte size quantification.

2.2. Reagents and Solutions

1. 0.16 mg/mL tricaine (Western Chemical, Redmond, Washington, DC) solution.
2. E3 water: 5 mM NaCl, 0.17 mM KCl, 0.33 mM $CaCl_2$, and 0.33 mM $MgSO_4$ in distilled water.
3. Drabkin's containing Brij solution (Sigma): Reconstitute one vial of the Drabkin's Reagent with 1,000 mL of water. Then add 0.5 mL of the 30% Brij 35 Solution (Sigma) to the 1,000 mL of reconstitute solution; mix well and filter if there are insoluble particles remain.
4. 0.5 M pH 8 EDTA (Promega, Madison, WI).
5. 10× PBS (Bio-Rad, Hercules, CA).
6. 4% formaldehyde: dilute 10% formaldehyde (Polysciences, Warrington, PA) with 1× PBS. Prepare freshly.
7. Tissue freezing medium (Thermo Scientific Inc. Hatfield, PA) for frozen fish heart.
8. PBD (1% albumin bovine serum (Sigma), 1% dimethyl sulfoxide (Mallinckrodt Baker, Phillipsburg, NJ), 1× PBS). Store at 4°C, stable at 4°C for up to 2 weeks.
9. Vectashield mounting medium for fluorescence with DAPI (Vector Laboratories, Inc., Burlingame, CA).
10. Microscope cover glass (Fisher Scientific, Dubuque, IA).
11. Cardiomyocyte dissociation buffer:
    (a) Solution A: 135 mM NaCl, 5.4 mM KCl, 1 mM $MgCl_2$, 10 mM HEPES, pH 7.2 with NaOH, 200 IU/mL Penicillin G, 200 μg/mL Streptomycin, filter and stored at 4°C for 1 week.

(b) Solution B: Solution A containing 2 mg/mL collagenase and 0.28 mg/mL protease XIV (Sigma). Prepare freshly.

12. L-15 Medium (with 2.05 mM L-Glutamine) (HyClone, Waltham, MA), store at 4°C.
13. PBT: PBS + 1% Tween-20 (PBT), NCSPBT: 10% fetal calf serum, 1% DMSO in PBT.
14. Phenylhydrazine hydrochloride (PHZ, Sigma): 2.5 mg/mL (light sensitive). Store at 4°C, stable at 4°C for up to 1 month.
15. BrdU (Sigma): 2.5 mg/mL dissolved in E3 water. Store at 4°C, stable at 4°C for up to 1 month.
16. Alexa Fluor-568 or 488 phalloidin (Invitrogen, Eugene, OR).
17. Primary antibody: anti-Mef2 (Santa Cruz Biotechnology, Santa Cruz, CA); anti-PCNA (Sigma); anti-BrdU (Sigma). Secondary antibody: AlexFluor-conjugated antimouse 568 or antirabbit 488 IgG (Invitrogen).

3. Methods

3.1. Generation of Anemia Models of Cardiomyopathy

3.1.1. Tr265 Model

1. *tr265/tr265* is a zebrafish mutant line identified from an ENU mutagenesis screen. There are two methods to identify heterozygous tr265 fish: either by PCR-based genotyping (11) or by crossing and phenotyping. In the latter method, about 25% of embryos will exhibit the anemia phenotype if both parents are tr265 heterozygous fish. Identified tr265 heterozygous fish are maintained in 2.5 L tanks in a circulation system (Note 1).
2. Set up several pairs of tr265 heterozygous fish. Embryos are collected the following day. At 4 dpf, *tr265/tr265* embryos are manually sorted from their siblings under a dissecting microscope. *tr265/tr265* can be clearly identified based on the amount of red blood cells in either the heart or the trunk region (Fig. 3).
3. Fifty *tr265/tr265* and fifty wild-type siblings are accommodated in separate nursery tubes at 5 dpf. Due to the high death rate during the first 2 weeks, the fish number will be adjusted at the end of week 2, so that the number of *tr265/tr265* fish and the number of sibling fish will be the same in each tube.
4. Juvenile fish will be transferred to separate 2.5 L tanks at week 4.
5. The fish heart can be collected for experiments after week 4 when *tr265/tr265* mutants develop an enlarged heart.

3.1.2. Phenylhydrazine Hydrochloride Model

1. Prepare 2.5 mg/mL PHZ stock solution with ddH_2O. Store at 4°C, protect stock solution from light by using foil to cover the tube. Prepare PHZ working solution by diluting stock solution with E3 water (see Sect. 2) (2.5 μg/mL, 1:1,000 dilution) (Note 2).

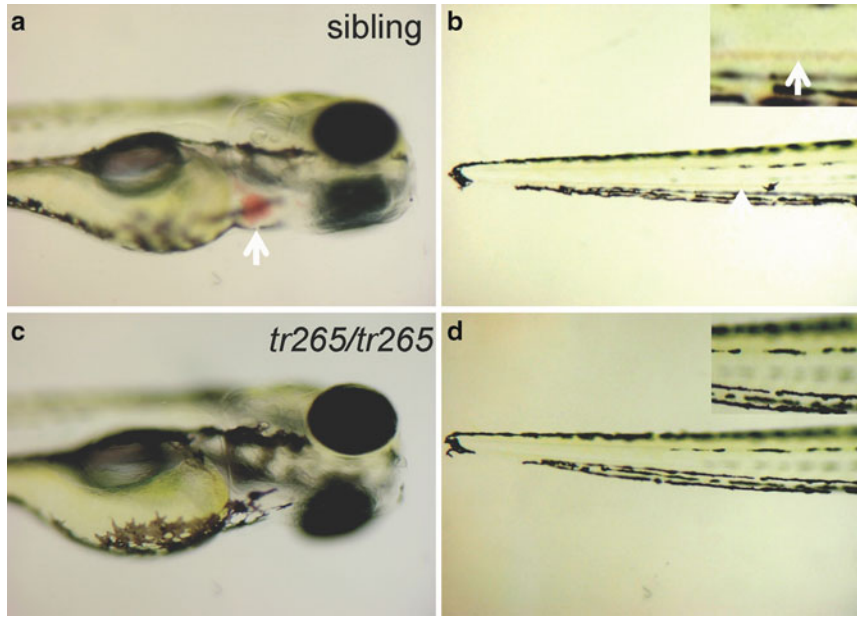

Fig. 3. Anemia can be visually detected in *tr265/tr265* fish. Shown are lateral views of fish embryos at 4 days postfertilization under a dissecting microscope. Red blood cells can be observed in the heart and tail region in wild-type siblings (**a**, **b**) but not *tr265/tr265* fish (**c**, **d**). *Arrows* indicate blood cells in either the heart or the trunk region.

2. Pick up adult fish for treatment. Typically, more than five fish are included for each treatment group. The fish can be put into a nursery tube with a netted bottom to facilitate handling. The treatment and washing steps can be done by transferring the nursery tube between tanks with fresh water and a container with 200–300 mL PHZ solution. In our lab, we used the cap from 1 mL pipette tips box as the container (Fig. 4).
3. Fish in nursery tubes were incubated for 1 h at room temperature, and then rinsed at least three times in fish water to get rid of residual PHZ (Note 3).
4. Put fish back in fishroom for circulating water and feeding.
5. Every other day, repeat steps 2–4.
6. The fish can be used for phenotype analysis after 3 weeks.

3.2. Assessment of Anemia in Adult Zebrafish

Hemoglobin concentration can be quantified by a colorimetric cyanmethemoglobin method since total hemoglobin at alkaline pH is rapidly converted to the cyanoderivative. The absorbance of the cyanoderivative is measured to estimate hemoglobin concentration (19).

1. Anesthetize fish in 0.16 mg/mL tricaine solution for 1–2 min.
2. Dry the gill region with a paper towel. Use a Dumont #5 Biologie Inox forceps to puncture the gill to induce bleeding.

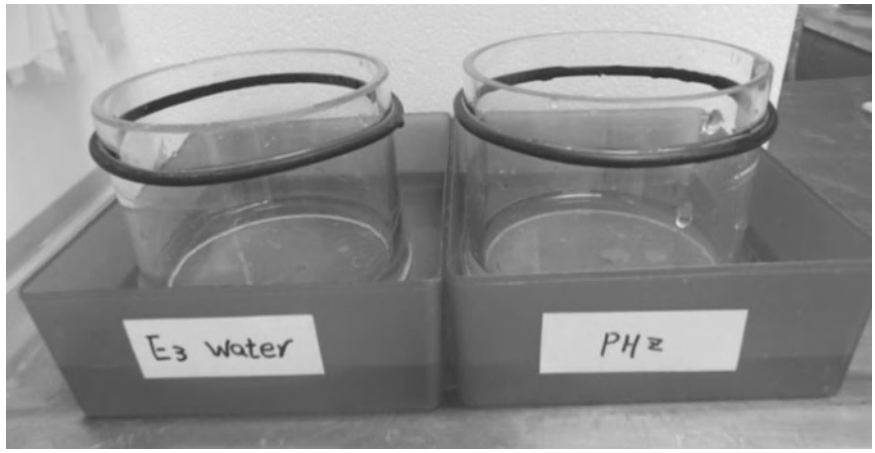

Fig. 4. PHZ treatment. Each group of fish is accommodated within a nursery tube. Fish is treated by transferring the nursery tubes into a box containing either E3 water as a control or PHZ solution.

3. Collect at least 0.5 μL of blood with a 1–5 μL calibrated micropipette containing approximately 0.5 μL 0.5 M pH 8 EDTA to prevent blood clotting. Mix the blood with 200 μL (for siblings) or 20 μL (for *tr265/tr265*) Drabkin's containing Brij solution (Note 4).
4. Incubate the blood with Drabkin's containing Brij solution at room temperature for at least 15 min.
5. Measure the absorbance at 540 nm with NanoDrop ND-1000 and V3.1.2 software (Note 5).
6. Calculate final hemoglobin concentration using the following equation: (absorbance/slope of the standard curve equation)/(volume of fish blood/final diluted volume). Calculate percent relative hemoglobin by dividing the mutant value by the sibling value and multiplying by 100.

3.3. Assessment of Cardiac Enlargement

If the fish is younger than 3 months, the enlarged heart will be measured by ventricle area to body length, since body length is the recommended stage marker (20). If the fish is older than 3 months, the enlarged heart will be measured by ventricle area to body weight, since the body weight changes more significantly at older ages.

3.3.1. Quantification of Body Length

1. Anesthetize fish in 0.16 mg/mL tricaine solution for 1–2 min.
2. Lay the fish down laterally on top of the paper towel with head to the left and tail to the right.
3. Measure the body length manually with a millimeter ruler, starting from the tip of the mouth to the body/caudal fin juncture.

3.3.2. Quantification of Body Weight

1. Reset an AG204 DeltaRange scale loaded with a small beaker filled with E3 water.
2. Collect each fish using a net and briefly dab the net on paper towels to wick excess water away from the fish before transfer to the beaker.
3. Transfer fish to the small beaker; record the weight of the fish in the beaker.

3.3.3. Quantification of Ventricle Area to Body Length/Body Weight

1. Anesthetize fish in 0.16 mg/mL tricaine solution for 1–2 min. Dissect the fish heart under a microscope.
2. Image dissected hearts next to a millimeter ruler with a Nikon COOLPIX 8700 digital camera attached to a Leica MZ FLI III microscope. Calculate the area of the ventricle from these images in pixels squared using AxioVision software. Calculate the number of pixels per mm in order to convert the ventricle area into mm^2.
3. Divide the ventricle area in mm^2 by body length (in mm) in order to determine ventricle area to body length. Divide the ventricle area in mm^2 by body weight (in g) to determine ventricle area to body weight.

3.4. Assessment of Cardiac Remodeling at the Cellular Level

We used three methods to quantify cardiomyocyte hypertrophy at the cellular level. First, we used β-catenin antibody to label the border of cardiomyocytes, which can be used to directly quantify cardiomyocyte cell size. Second, we use Mef2 antibody to label the nuclei of cardiomyocytes. The density of cardiomyocytes can be calculated, which indirectly reflects cardiomyocyte cell size. Third, we measure single cardiomyocyte size by dissociating the heart and culture cardiomyocytes in vitro, which can be used to quantify cardiomyocyte cell size. Below are detailed protocols for these methods.

3.4.1. Assessment of Cardiomyocyte Hypertrophy via Immunostaining of Tissue Sections

1. Anesthetize fish in 0.16 mg/mL tricaine solution for 1–2 min.
2. Dissect the fish heart under a microscope. Put 2–5 hearts into a disposable vinyl specimen mold. Remove extra buffer and add tissue freezing medium. Snap-freeze the mold on dry ice for several min (Note 6).
3. Cryosection the frozen heart (10–14 μM) on Leica CM3050S cryostat. Collect heart tissues on Poly-Prep slides (Note 7).
4. Affix freshly prepared 4% formaldehyde (see Sect. 2.2) on slides for 10 min.
5. Rinse with PBD twice (see Sect. 2.2).
6. Permeabilize samples for desired time (e.g., 0.1% Triton X-100/1% SDS in PBD for 45 min) (Note 8).
7. Rinse with PBD twice.

8. Block in 2% sheep serum blocking solution (PBD + 2% sheep serum) for 25 min.
9. Incubate with primary antibody (e.g., anti-mef2 or anti-β-catenin (1:50–1:200)) for 2 h at room temperature.
10. Rinse with PBD twice.
11. Wash with PBD four times, 5 min each time (Note 9).
12. Incubate with secondary antibody (e.g., AlexFluor-conjugated antimouse 568 or antirabbit 488 IgG (1:50–1:200) in PBD) for 30 min at room temperature (Note 10).
13. Rinse with PBD twice.
14. Wash with PBD four times, 5 min each time (Note 9).
15. Add one drop mounting medium. Cover with a microscope cover glass.
16. Image slides with a Zeiss Axioplan 2 microscope equipped with ApoTome and AxioVision software (Carl Zeiss) (Note 11).
17. Measure the β-catenin surface area of Mef2+ cells using AxioVision software (Carl Zeiss). Count 20–30 cardiomyocytes per ventricle section to measure cardiomyocyte cell size using β-catenin staining. Use 3–5 hearts for quantification. Analyze a square of at least 5,000 μm^2 drawn using AxioVision software (Carl Zeiss) per ventricle section per fish for cell density. Select 3–4 squares for quantification per ventricle section. Statistical analysis requires 2–3 slides for each heart. Count the cells in that square and divide by the square area to get cell density (cells per mm^2) (Note 12). The experiments usually were repeated three times.

3.4.2. Assessment of Cardiomyocyte Cell Size via Dissociation of a Zebrafish Heart

Three methods can be used to distinguish cardiomyocytes from other cell types. The first method is based on the unique morphology of cardiomyocytes, which can be distinguished by their striated sarcomere structure under DIC lighting conditions as well as their beating behavior. Secondly, cardiomyocytes can be labeled with fluorescence in cardiac-specific transgenic fish lines with GFP or RFP reporters. Thirdly, phalloidin staining can be easily conducted to label cardiomyocytes, as detailed below:

1. Anesthetize fish in 0.16 mg/mL tricaine solution for 1–2 min.
2. Sterilize fish for ~15 s in 70% EtOH.
3. Position fish on a sterilized sponge; remove the heart with sterilized forceps.
4. Place heart into solution A (see Sect. 2.2) in a six-well plate.
5. Remove the atrium.
6. Open the ventricle widely with forceps (Note 13).
7. Equilibrate ventricle in solution A for 10 min.

When possible, perform the steps below in a cell culture hood:

1. Transfer ventricles with sterile forceps to an Eppendorf tube containing 1 mL solution B (see Sect. 2.2). Rock for ~60 min to digest the ventricle (Note 14).
2. Pellet cells by spinning at 2,000 rpm for 2 min.
3. Remove and discard supernatant.
4. Add 1 mL of L15 medium supplemented with Penicillin/Streptomycin (see Sect. 2.2).
5. Pellet cells at 2,000 rpm for 2 min.
6. Remove and discard supernatant.
7. Add 500 μL of L15 supplemented with Penicillin/Streptomycin.
8. Dissociate cells by gentle titration using a 1 mL Pipetman.
9. Aliquot cells into an 8- or 16-well chamber slide (Note 15).
10. Add L15 supplemented with Penicillin/Streptomycin to the cells (500 μL max capacity).
11. Incubate cells at 28.5°C for 4 h (Note 16).

Below is the protocol for phalloidin staining of cardiomyocytes:

1. Remove the solution, fix with 4% formaldehyde for 10 min.
2. Remove the solution.
3. Rinse with PBD twice.
4. Permeabilize samples with PBDT for 15 min.
5. Rinse with PBD twice.
6. Incubate with phalloidin (1:50 dilution in PBD) for 30 min (cover the slide with foil).
7. Rinse with PBD twice.
8. Wash with PBD four times, 5 min each time.
9. Remove the medium; add one drop mounting medium; cover with a microscope cover glass. Capture both phase contrast and fluorescent images with a confocal laser scanning microscopy (Zeiss LSM510; Carl Zeiss). Randomly choose 20–30 dissociated cardiomyocytes per condition for cell area quantification using ImageJ software.

3.5. Assessment of Cardiomyocyte Hyperplasia via Immunostaining and BrdU-Incorporation

We developed two methods to quantify cardiomyocyte hyperplasia. First, we assessed cardiomyocyte hyperplasia by immunostaining with a PCNA antibody. For the detailed protocol, refer to Sect. 3.4.1. PCNA antibody was diluted in PBD (1:3,000). For PCNA + Mef2+ cell proliferation studies, the total number of PCNA + Mef2+ cells in each 10–14 μm ventricle section was divided by the estimated total number of Mef2+ cells in the ventricle section (estimated by multiplying Mef2+ cell density with the area of the ventricle section). Secondly, we assessed cardiomyocyte hyperplasia by BrdU incorporation assay, as detailed below:

1. Anesthetize fish in 0.16 mg/mL tricaine for 1–2 min.
2. Inject the fish intraperitoneally using a 34-gauge NanoFil beveled needle and 10 μL syringes with 10 μL of 2.5 mg/mL BrdU. Conduct three daily injections before harvesting the fish for antibody staining.
3. Subject the slides to Mef2 staining to identify cardiomyocyte (see Sect. 3.4.1, stop at step 14) after isolating the heart and conducting the frozen sections.
4. The slides were then followed by the BrdU staining
5. Refix cell in 4% formaldehyde for 10 min.
6. Rinse twice in PBT (see Sect. 2.2).
7. Incubate in 2 M HCl for 30 min.
8. Wash in PBT three times, 5 min each time.
9. Block in NCSPBT (see Sect. 2.2) for 60 min at 37°C.
10. Incubate with anti-BrdU (1:200 dilutions in NCSPBT) for 3 h at 37°C.
11. Wash in PBS four times, 5 min each time.
12. Incubate in NCSPBT for 1 h at 37°C with a 1:200 dilution of antimouse secondary antibody conjugated to the Alexa 488 or 568.
13. Wash four times in PBS, 5 min each time.
14. Mount slides in Vectashield mounting medium with DAPI, and image using Zeiss microscopy. Image random areas of each chamber using a Zeiss Axioplan 2 microscope (Carl Zeiss). BrdU index is defined as the ratio between the number of BrdU+/Mef2+ cells divided by the number of all cardiomyocytes revealed by Mef2+.

3.6. Survival Curve

As shown in Fig. 2, *tr265/tr265* fish exhibit high fatality. Only 50% homozygous mutant fish can survive to week 7 and less than 10% of mutants survive to week 16 (10). Below is the protocol to record survival curve:

1. Sort 50 WT siblings or *tr265/tr265* base on their red blood cell level at 4 dpf.
2. Put each group in separate nursery tubes. Adjust the fish number to be equal at the end of week 2. Discard extra fish.
3. Transfer fish to 2.5 L tanks at week 4.
4. Every 10 days, starting at 15 dpf, count the number of fish in each tube/tank. Calculate the survival rate by dividing the remaining fish number by the fish number at day 15 (see Note 17) in order to exclude the effect of normal die off that occurs during the first 2 weeks postfertilization.

5. Summarize the survival curve using Kaplan–Meier plot. Use the log-rank test to determine the statistical difference (Note 18).

4. Notes

1. Put 1–8 fish in small tank (1 L), 8–20 fish in an average tank (2.5 L) and 20–100 fish in a large tank (9 L).
2. PHZ is also toxic to humans. It is important to handle PHZ solutions with gloves, face shield, and safety glasses.
3. Fish are usually sensitive to the initial treatment of PHZ. For the first treatment, it is better to use low concentration solution (1.25 μg/mL) for 30 min.
4. Manually measure with a millimeter (mm) ruler the amount of EDTA in the micropipette prior to blood collection. After blood collection, measure the total volume in mm. Determine the number of mm to the 1 μL calibrated mark on the micropipette to convert mm to μL.
5. All absorbances should fall within the values used for the standard curve made with human hemoglobin from a stock concentration of 0.8 mg/mL human hemoglobin in Drabkin's with Brij.
6. The fish sample can be stored at −80°C for several months before sectioning.
7. Store the slides at 4°C for 1 week. Antibody staining will not work well after 1 week storage.
8. Permeabilization with 0.1% Triton X-100 is sufficient for most antibodies. For PCNA antibody only, permeabilization with 1% SDS leads to a better result. When co-staining with PCNA and other antibody, 0.05% Triton X-100/0.5% SDS can be used for permeabilization.
9. Increasing the number of washes can help to reduce background.
10. Once incubation has begun, the sample should be protected from light by using foil to cover the sample.
11. The sample can be stored at 4°C for 1–2 weeks without affecting the signal.
12. It is important to avoid the empty space when choosing the ventricle area for quantification, as it can reduce the variation.
13. Widely opening the ventricle is critical to effectively dissociate cardiomyocytes.
14. Rocking should be monitored carefully to avoid either over- or under-digestion. Proper digestion time depends on fish age and/or heart size.
15. Depending on desired density of the cardiomyocyte cells, 500 μL L15 medium can be aliquoted into 1–4 wells.

16. Cardiomyocyte cells exhibit a typical cardiomyocyte cell shape. The size and shape of cardiomyocytes will change after culture for more than 24 h (12).
17. The density and feeding protocol might result in significant variation of survival curve. Therefore, wild-type fish of the same density is a critical control.
18. More than 20 fish for each group was recommended for survival rate studies.

References

1. Ahmad F, Seidman JG, Seidman CE (2005) The genetic basis for cardiac remodeling. Annu Rev Genomics Hum Genet 6:185–216
2. Hasenfuss G (1998) Animal models of human cardiovascular disease, heart failure and hypertrophy. Cardiovasc Res 39:60–76
3. Molkentin JD, Robbins J (2008) With great power comes great responsibility: using mouse genetics to study cardiac hypertrophy and failure. J Mol Cell Cardiol 46:130–136
4. Wolf MJ, Amrein H, Izatt JA, Choma MA, Reedy MC, Rockman HA (2006) Drosophila as a model for the identification of genes causing adult human heart disease. Proc Natl Acad Sci USA 103:1394–1399
5. Chen JN, Haffter P, Odenthal J, Vogelsang E, Brand M, van Eeden FJ, Furutani-Seiki M, Granato M, Hammerschmidt M, Heisenberg CP, Jiang YJ, Kane DA, Kelsh RN, Mullins MC, Nusslein-Volhard C (1996) Mutations affecting the cardiovascular system and other internal organs in zebrafish. Development 123:293–302
6. Stainier DY, Fouquet B, Chen JN, Warren KS, Weinstein BM, Meiler SE, Mohideen MA, Neuhauss SC, Solnica-Krezel L, Schier AF, Zwartkruis F, Stemple DL, Malicki J, Driever W, Fishman MC (1996) Mutations affecting the formation and function of the cardiovascular system in the zebrafish embryo. Development 123:285–292
7. Zon LI, Peterson RT (2005) In vivo drug discovery in the zebrafish. Nat Rev Drug Discov 4:35–44
8. Stainier DY (2001) Zebrafish genetics and vertebrate heart formation. Nat Rev Genet 2:39–48
9. Chico TJ, Ingham PW, Crossman DC (2008) Modeling cardiovascular disease in the zebrafish. Trends Cardiovasc Med 4:150–155
10. Sun X, Hoage T, Bai P, Ding Y, Chen Z, Zhang R, Huang W, Jahangir A, Paw B, Li YG, Xu X (2009) Cardiac hypertrophy involves both myocyte hypertrophy and hyperplasia in anemic zebrafish. PLoS One 4:e6596
11. Paw BH, Davidson AJ, Zhou Y, Li R, Pratt SJ, Lee C, Trede NS, Brownlie A, Donovan A, Liao EC, Ziai JM, Drejer AH, Guo W, Kim CH, Gwynn B, Peters LL, Chernova MN, Alper SL, Zapata A, Wickramasinghe SN, Lee MJ, Lux SE, Fritz A, Postlethwait JH, Zon LI (2003) Cell-specific mitotic defect and dyserythropoiesis associated with erythroid band 3 deficiency. Nat Genet 34:59–64
12. Ding Y, Sun X, Huang W, Hoage T, Redfield M, Kushwaha S, Sivasubbu S, Lin X, Ekker S, Xu X (2011) Haploinsufficiency of target of rapamycin attenuates cardiomyopathies in adult zebrafish. Circ Res 109:658–669
13. Simunek T, Sterba M, Popelova O, Adamcova M, Hrdina R, Gersl V (2009) Anthracycline-induced cardiotoxicity: overview of studies examining the roles of oxidative stress and free cellular iron. Pharmacol Rep 61:154–171
14. Christiansen S, Autschbach R (2006) Doxorubicin in experimental and clinical heart failure. Eur J Cardiothorac Surg 30:611–616
15. Yi X, Bekeredjian R, DeFilippis NJ, Siddiquee Z, Fernandez E, Shohet RV (2006) Transcriptional analysis of doxorubicin-induced cardiotoxicity. Am J Physiol Heart Circ Physiol 290:H1098–H1102
16. Robert J (2007) Preclinical assessment of anthracycline cardiotoxicity in laboratory animals: predictiveness and pitfalls. Cell Biol Toxicol 23:27–37
17. Norman TD, Mc BR (1958) Cardiac hypertrophy in rats with phenylhydrazine anemia. Circ Res 6:765–770
18. Simonot DL, Farrell AP (2007) Cardiac remodelling in rainbow trout Oncorhynchus mykiss Walbaum in response to phenylhydrazine-induced anaemia. J Exp Biol 210:2574–2584
19. Danilova N, Sakamoto KM, Lin S (2008) Ribosomal protein S19 deficiency in zebrafish leads to developmental abnormalities and defective erythropoiesis through activation of p53 protein family. Blood 112:5228–5237
20. Kimmel CB, Ballard WW, Kimmel SR, Ullmann B, Schilling TF (1995) Stages of embryonic development of the zebrafish. Develop Dynam 203:253–350

Chapter 3

Methods to Study the Effects of TRP Channel Drugs on Vascular Endothelial Cell Function

Yan Ma, Yung-Wui Tjong, and Xiaoqiang Yao

Abstract

Transient receptor potential (TRP) channels are abundantly expressed in vascular endothelium where the channels play important functional roles. In this chapter, we describe some well-established approaches, from molecular detection to functional assays, to study the role of TRP channels in endothelial cells. Comprehensive step-by-step instructions and representative figures are provided on the following methods: (1) isolation and culture of vascular endothelial cells; (2) determination of the TRP channel interaction [co-immunoprecipitation, double immunofluorescence staining, chemical cross-linking, and Förster resonance energy transfer (FRET) detection]; (3) detection of TRP channel-mediated intracellular Ca^{2+} changes using fluorescence microscopy; (4) determination of the electrophysiological properties by whole-cell patch clamp and examination of TRP channel function in vascular tone control using isometric tension measurement.

Key words: TRP channels, Protein interaction, Electrophysiology, Intracellular Ca^{2+} detection, Vascular function

1. Introduction

The transient receptor potential (TRP) channels are mostly situated at the plasma membrane. These channels can be gated by temperature, light, pressure, and/or chemical stimuli. Functional TRP channels are composed of four subunits, each containing six membrane-spanning helices linked by similar lengths of intracellular or extracellular loops. Most TRP channels are nonselective cationic channels, with Na^+, Ca^{2+}, and Mg^{2+} all permeating through the channels (1). TRP channels are categorized into two groups. Group 1 contains TRPC (TRP canonical), TRPV (TRP vanilloid), TRPM (TRP melastatin), TRPN (TRP NOMPC), and TRPA

Arpad Szallasi and Tamás Bíró (eds.), *TRP Channels in Drug Discovery: Volume II*, Methods in Pharmacology and Toxicology, DOI 10.1007/978-1-62703-095-3_3,

(TRP ankyrin), which share substantial sequence similarity in the transmembrane domains. Group 2 contains TRPP (TRP polycystin) and TRPML (TRP mucoliptin) which have relatively low sequence similarity. In addition, they have a large extracellular loop between the first and the second transmembrane segments (1).

TRP subunits interact with each other to form homotetrameric or heterotetrameric channels (2, 3). TRP channels may also interact with other proteins to form signaling complexes (4, 5). These interactions play a vital role in regulating vascular function. One of the most commonly used methods for determining TRP protein interaction is co-immunoprecipitation. Co-immunoprecipitation utilizes an antibody that targets a bait protein. The antigen–antibody complex is then allowed to bind to protein A agarose, and irrelevant proteins are washed out. The target protein in the bait protein complex can be determined by Western blotting (6). Another independent method for determining protein interaction is chemical cross-linking. Cross-linking reagents carrying reactive moieties bind to specific amino acids on target proteins, including antibodies. Two closely associated proteins can be cross-linked by this type of small-molecule cross-linker, and the complex be detected by Western blotting (7). The third method to study protein–protein interaction is fluorescence double immunostaining. In this method, specific fluorescent dye-labeled antibodies are allowed to bind to their specific targets in the cells, and the distribution of the target proteins can be visualized under fluorescent microscopy (8). Another highly useful method for studying protein–protein interaction is Förster resonance energy transfer (FRET). FRET is based on the principle that a donor chromophore transfers its energy to an acceptor chromophore if their mutual distance is less than 10 nm (8, 9). Cyan fluorescence protein (CFP)–yellow fluorescence protein (YFP) pair is one of the most popular donor–acceptor pairs for biological approach (10).

Commonly used methods to study TRP channel function in vascular endothelial cells include fluorescent cytosolic Ca^{2+} measurement, patch clamp, isometric vessel tension study, and isobaric vessel diameter measurement. Ca^{2+} influx in vascular cells is in part mediated by TRP channels, and Ca^{2+}-related signaling cascade is important for vascular contraction/relaxation. Fluorescent probes enable the quantitative analysis for changes in intracellular Ca^{2+} concentration ($[Ca^{2+}]_i$) (11, 12). The electrophysiological properties of functional channels can be determined by patch clamp technique. Patch clamp recording uses a chloride-coated silver wire in contact with the extracellular solution (bath solution) as the reference electrode. Another electrode is a glass micropipette with an open tip diameter of about 1 μm. This micropipette is filled with pipette solution and is used to "patch" a surface area containing one or a few ion channels and measure the changes in electrical current. The method can also measure membrane potential

(13, 14). Measurement of isometric tension and/or isobaric diameter of blood vessels in vitro can be used to determine vascular tone regulation and TRP channel involvement in these functions (15). Wire myograph and pressure myograph instruments are used in these experiments.

2. Materials

2.1. Equipment

1. Epoch Microplate Spectrophotometer (BioTek, Winooski, VT) for reading protein absorbance at 630 nm and calculating protein concentration.
2. Mini-PROTEIN Tetra System (Bio-Rad, Hercules, CA) equipped with a PowerPac™ Basic Power Supply (Bio-Rad) for protein electrophoresis.
3. Trans-Blot SD Semi-Dry Transfer Cell (Bio-Rad) equipped with a PowerPac™ Universal Power Supply (Bio-Rad) for protein transfer from within the SDS-PAGE gel onto a PVDF membrane.
4. FluorChem 8000 system (ProteinSimple, Santa Clara, CA) for protein bands detection.
5. FV1000 confocal system (Olympus, Tokyo) for fluorescence detection.
6. Software: FV10-ASW 1.5 software (Olympus) for quantitative analysis of protein co-localization.
7. Olympus IX 81 microscope (Olympus) equipped with a FRET filter set (Olympus) for FRET detection.
8. EPC-9 patch amplifier (HEKA, Lambrecht/Pfalz, Germany) for whole-cell patch clamp recording.
9. P-97 micropipette puller (Sutter Instrument, Novato, CA) for pulling micropipette.
10. Software: PulseFit (HEKA) for whole-cell patch clamp data analysis.
11. Isometric tension myograph (model 610M, Danish Myotechnology, Aarhus, Denmark) for blood vessel isometric tension measurement.
12. Software: PowerLab (AD Instruments, Sydney, Australia) and LabChart (AD Instruments) for blood vessel isometric tension analysis.
13. Pressure myograph (model 110P, Danish Myotechnology) for blood vessel isobaric diameter measurement.
14. Software: MyoView software (GE Healthcare, Piscataway, NJ) for blood vessel isobaric diameter analysis.

2.2. Reagents and Solutions

1. Cell lysis buffer: 50 mM Tris (Sigma-Aldrich), pH 7.5, 150 mM NaCl (Sigma-Aldrich), 50 mM NaF (Sigma-Aldrich), 1.5% NP-40 (Sigma-Aldrich), 0.5% sodium deoxycholate (Sigma-Aldrich), and protease inhibitor cocktail tablet (Roche, Mannheim, Germany).
2. Lowry assay reagents for protein concentration calibration: reagent A, reagent B, and reagent S (Bio-Rad).
3. ECL Western blotting detection reagents (GE Healthcare).
4. Protein A agarose suspension (Roche).
5. Chemical cross-linking quenching solution: 50 mM Tris (Sigma-Aldrich).
6. Calcium Calibration Buffer Kit (Invitrogen, Carlsbad, CA).
7. Normal physiological salt solution (NPSS): 140 mM NaCl (Sigma-Aldrich), 1 mM KCl (Sigma-Aldrich), 1 mM $CaCl_2$ (Sigma-Aldrich), 1 mM $MgCl_2$ (Sigma-Aldrich), 10 mM glucose (Sigma-Aldrich), and 5 mM Hepes (Sigma-Aldrich), pH 7.4.
8. Krebs Henseleit solution: 118 mM NaCl (Sigma-Aldrich), 4.7 mM KCl (Sigma-Aldrich), 2.5 mM $CaCl_2$ (Sigma-Aldrich), 1.2 mM KH_2PO_4 (Sigma-Aldrich), 1.2 mM $MgSO_4 \cdot 7H_2O$ (Sigma-Aldrich), 25.2 mM $NaHCO_3$ (Sigma-Aldrich), and 11.1 mM glucose (Sigma-Aldrich), pH 7.4.
9. 60 mM K^+ solution for isometric tension measurement: 58 mM NaCl (Sigma-Aldrich), 64.7 mM KCl (Sigma-Aldrich), 2.5 mM $CaCl_2$ (Sigma-Aldrich), 1.2 mM KH_2PO_4 (Sigma-Aldrich), 1.2 mM $MgSO_4 \cdot 7H_2O$ (Sigma-Aldrich), 25.2 mM $NaHCO_3$ (Sigma-Aldrich), and 11.1 mM glucose (Sigma-Aldrich), pH 7.4.

3. Methods

3.1. Problems on the Study of TRP Channel Function in Vascular Endothelium

1. For some TRP channels such as TRPV1, TRPV4, and TRPC3, highly specific activators/inhibitors are available (16–18). However, for other TRP channels such as most TPRCs, there are no specific activators/inhibitors. Therefore, siRNA and dominant-negative molecular constructs need to be used.
2. Primary cultured vascular endothelial cells are easily to be contaminated by other cells such as smooth muscle cells and neuronal cells during cell culture procedure. The identity of the primary cultured endothelial cells should be verified by immunostaining using antibodies against von Willebrand factor and platelet endothelial cell adhesion molecule (PECAM) (19).

3. Prolonged culture of endothelial cells will result in loss of some endothelial cell properties. For example, Draijer and co-workers found that cGMP-PK type I expression decreases during serial passage of endothelial cells (20). To avoid this issue, only cells from the first four passages, preferably the first two passages, should be used for experiments.
4. In the functional studies such as isomeric tension and isobaric diameter measurement described in the following sections, endothelium-denuded vessels can be used as negative control to confirm whether a certain response is related to endothelium or not.

3.2. Endothelial Cell Preparation and Culture for Rat Mesenteric Artery

All animal experiments should be conducted in accordance with the regulation of the U.S. National Institute of Health (NIH publication No. 8523). Vascular endothelial cells are isolated from male Sprague–Dawley rats of approximately 250–300 g by an enzymatic digestion method. The primary rat mesenteric arterial endothelial cells (MAECs) are cultured in endothelial growing medium (Lonza, Walkersville, MD) with 1% bovine brain extract, 100 U/ml penicillin, and 100 μg/ml streptomycin.

1. Prepare 10 ml endothelial basic medium (Lonza) with 0.02% collagenase IA: dilute 2 mg collagenase IA in 10 ml endothelial basic medium.
2. Prepare 5 ml endothelial growing medium with 1% bovine brain extract, 100 U/ml penicillin, and 100 μg/ml streptomycin: dilute 0.05 g bovine brain extract in 5 ml endothelial growing medium, add 50 μl 100X Penicillin Streptomycin (Invitrogen).
3. Open the rat abdomen, and use PBS (Invitrogen) to perfuse the heart in order to remove circulating blood from blood vessels.
4. Dissect the small intestine and excise all the vein branches.
5. Digest the remained arterial branches with 10 ml 0.02% collagenase IA in endothelial basic medium for 45 min at 37°C.
6. Centrifuge at $1600 \times g$ for 5 min at room temperature.
7. Resuspend the pelleted cells in 5 ml endothelial growing medium supplemented with 1% bovine brain extract, 100 U/ml penicillin, and 100 μg/ml streptomycin.
8. Place the resuspended cells in a 25-cm^2 culture flask.
9. Remove the nonadherent cells after 1 h.
10. Culture the adherent cells at 37°C in a 5% CO_2 humidified incubator.

3.3. Western Blotting and Co-immunoprecipitation

3.3.1. Protein Quantification (Lowry Assay)

1. Thaw samples to be assayed on ice.
2. Prepare the BSA standards with final concentration ranging of 0, 0.1, 0.2, 0.4, 0.6, 0.8, 1.2, 1.6, 2.0 μg/ml.
3. Pipette the BSA standard curve (0–2.0 μg/ml) and samples into triplicated wells of 96-well plate with 5 μl/well.
4. Mix the reagent A (Bio-Rad) and reagent S (Bio-Rad) at 50:1 ratio, and add the mixture to 96-well plate with 25 μl/well.
5. Add reagent B (Bio-Rad) as 200 μl/well.
6. Place the 96-well plate in dark for 15-min incubation.
7. Read the absorbance at 630 nm by a Microplate UV/VIS Spectrophotometer (BioTek).
8. The concentration of protein is calculated with reference to the standard protein curve.

3.3.2. Western Blotting

1. Prepare the SDS-PAGE gel.
2. Calibrate protein samples to equal amounts based on the standard curve obtained by Lowry assay (see Sect. 3.3.1).
3. Denature the samples with SDS-PAGE loading dye (5 min, 95°C) and load at ~20 μg into each lane of polyacrylamide gel and separated by a 7.5% SDS-PAGE gel with 100 V constant voltage. Run until the front of the bromophenol dye is approximately 1 cm from the gel bottom (50 min–1.5 h).
4. Prewet a PVDF membrane in methanol.
5. Move the proteins from within the SDS-PAGE gel onto the PVDF membrane, with 15 V constant voltage (1–2 h).
6. Immerse the PVDF membrane in a blocking solution containing 5% nonfat milk and 0.1% Tween-20 in PBS for 1 h at room temperature with constant shaking (Note 1).
7. Incubate with the primary antibody (1:500) at 4°C overnight with constant shaking.
8. Rinse the membrane three times for 5 min each with 15 ml of PBST to remove unbound primary antibody.
9. Incubate with secondary antibody (1:5,000) conjugated with horseradish peroxidase at room temperature for 1 h with constant shaking.
10. Rinse the membrane three times for 5 min each with 15 ml of PBST to remove unbound secondary antibody.
11. Incubate with ECL Western blotting detection reagents (GE Healthcare) for 5 min at room temperature.

12. Exposure the membrane to X-ray film.
13. Detect the intensity of the protein blotting bands by FluorChem 8000 system (ProteinSimple, Santa Clara, CA).

3.3.3. Co-immuno-precipitation

1. Incubate extracted proteins (~800 μg) with 50 μl protein A agarose suspension (Roche) (Note 2) and incubate for 3 h at 4°C on a rocking platform.
2. Pellet agarose beads by centrifuging in a microcentrifuge (12,000 × *g*) at 4°C for 2 min. Transfer supernatant to a fresh tube.
3. Add 7 mg of pulling antibody [or preimmune IgG (Note 3) as negative control] to the sample and incubate on a rocking platform for 2 h at 4°C.
4. Add 100 μl protein A agarose suspension to the mixture and incubate on a rocking platform overnight at 4°C.
5. Centrifuge (12,000 × *g*) for 2 min at 4°C and collect agarose–antibody–antigen complexes. Discard the supernatant.
6. Resuspend the pellet in 1 ml lysis buffer (see Sect. 2.2) and incubate for 30 min at 4°C on a rocking platform.
7. Pellet the beads again and discard supernatant.
8. Repeat step 6–7 for two times.
9. Resuspend pellet by 25 μl of gel-loading buffer.
10. Denature proteins by heating the sample for 5 min at 95°C.
11. Centrifuge the suspension (12,000 × *g*) for 2 min at 4°C.
12. Analyze the supernatant by gel electrophoresis and Western blotting (see Sect. 3.3.2) (Fig. 1).

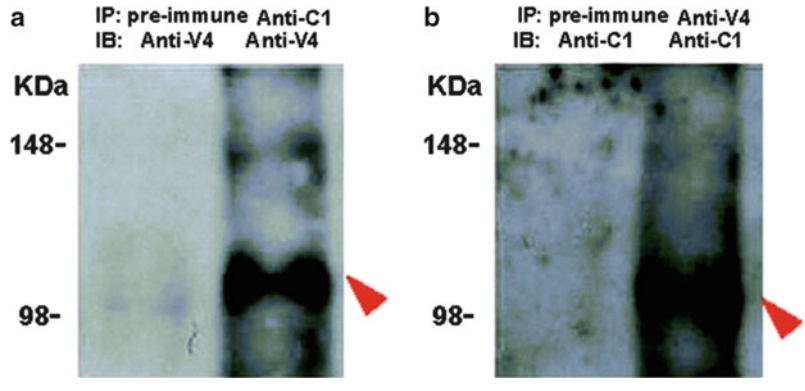

Fig. 1. Representative images of co-immunoprecipitation followed by immunoblots in primary cultured MAECs (12). The pulling and blotting antibodies are indicated. Control immunoprecipitation was performed using the preimmune IgG (labeled as preimmune). Anti-C1 indicates anti-TRPC1; anti-V4, anti-TRPV4; IB, immunoblot; IP, immunoprecipitation.

Pros

1. Protein samples can be obtained from cell line or animal tissues.
2. Protein interaction can be detected in native concentration or in over-expressed system (transfection).
3. This method is able to detect interaction between two (one-step co-immunoprecipitation) or three proteins (two-step co-immunoprecipitation).

Cons

1. Co-immunoprecipitation only detects stable protein–protein interaction.
2. This method does not indicate whether the interaction is direct.
3. Specific antibody is required.
4. Homogenization of cellular components may result in false positive interaction.

3.4. Double Immunofluorescence Staining

Double immunofluorescence staining is used to determine subcellular protein localization by fluorescence detection.

1. Seed freshly dispersed or cultured cells on glass coverslips.
2. Rinse the cells with PBS for three times.
3. Fix the cells with 3.7% formaldehyde (Sigma-Aldrich) at room temperature for 20 min.
4. Permeabilize the cells with 0.1% Triton X-100 (Sigma-Aldrich) at room temperature for 15 min.
5. Incubate the cells with 2% BSA in PBS for 1 h at room temperature to block the nonspecific immunostaining.
6. Incubate the cells with a mixture of primary antibodies at 4°C overnight.
7. Rinse the cells with PBS for three times.
8. Incubate with a mixture of secondary antibodies conjugated to proteins with different excitation wavelengths (e.g. Alexa Fluor 488 and Alexa Fluor 546) for 2 h at room temperature.
9. After washing and mounting, detect immunofluorescence by FV1000 confocal system (Olympus) (Fig. 2).
10. Carry out the quantitative analysis of the co-localization using FV10-ASW 1.5 software (Olympus).

Pros

1. This method can visualize protein distribution directly.
2. Procedure is simple and takes shorter time.

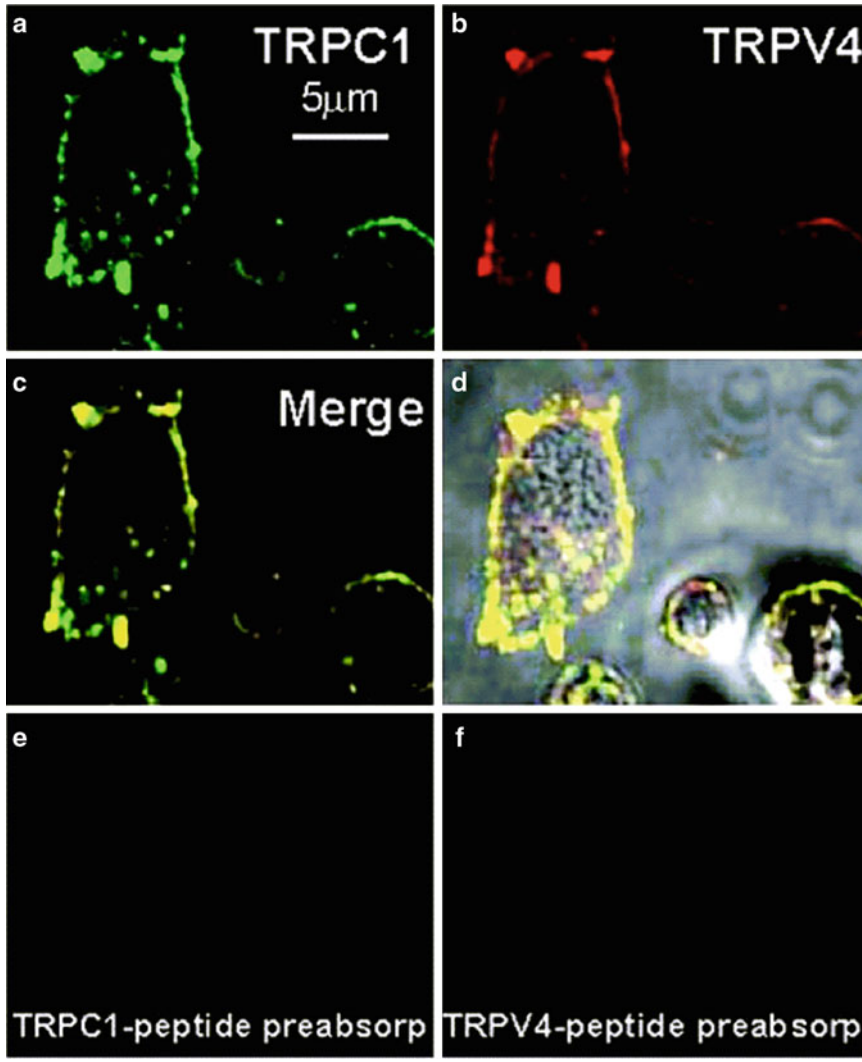

Fig. 2. Representative co-localization of TRPV4 and TRPC1 in the primary cultured rat MAECs (12). (**a**, **b**) Representative images of TRPC1 (**a**, *green*) and TRPV4 (**b**, *red*) in plasma membrane. (**c**) Overlay image of (**a** and **b**). (**d**) Bright field image of the same cell together with merged fluorescence. (**e**) TRPC1 antibody was preabsorbed with excessive TRPC1 peptide. (**f**) TRPV4 antibody was preabsorbed with excessive TRPV4 peptide.

Cons

1. Optical imaging systems do not offer good enough resolution to determine direct protein interaction. Only rough estimation can be made.

3.5. Chemical Cross-linking

Cross-linking reagents carrying reactive moieties can bind to specific amino acids on target proteins, including antibodies. Commercially available cross-linking reagents have different characteristics, differed in specificity, water solubility, cleavability, etc.

DTSSP [3,3′-Dithiobis (sulfosuccinimidylpropionate)] and DSS (disuccinimidylsuberate) are two of the commonly used cross-linking reagents. DTSSP contains an amine-reactive N-hydroxysulfosuccinimide (sulfo-NHS) ester that reacts with primary amines at pH 7–9 to form stable amide bonds. DSS is the nonsulfonated analog of DTSSP. DTSSP is membrane impermeable cross-linker whereas DSS is membrane permeable. Generally, cells are incubated with the cross-linking reagent at an appropriate concentration. Then the reaction is quenched by quenching solution, followed by nonreducing SDS-PAGE to visualize cross-linked protein complexes.

1. Prepare the nonreducing SDS-PAGE loading dye: dissolve 4.0 g sucrose, 0.8 g SDS, 1 mol/l Tris–HCl in 2 ml H_2O, adjust pH to 6.8, and then add 0.001% bromophenol blue.
2. Dissolve DTSSP (Thermo Scientific, Rockford, IL) in water at 10–25 mmol/l (Note 4, 5).
3. Wash culture flask with PBS to remove residual media (Note 6).
4. Add DTSSP to a final concentration of 5 mmol/l (Note 7).
5. Incubate the reaction mixture on ice for 2 h (Note 7).
6. Quench the reactions by adding quenching solution (see Sect. 2.2) and incubate at room temperature for 30 min (Note 7).
7. Discard the solutions, and treat the cells with cell lysis buffer (see Sect. 2.2) on ice for 30 min.
8. Scrape, collect, and centrifuge the cell lysates at 4°C.
9. Keep the supernatant and discard the cell debris at the bottom.
10. Add nonreducing SDS-PAGE loading dye, and run nonreducing SDS-PAGE (Note 8).
11. Detect the cross-linked products by Western blotting (Fig. 3). This may be a complete linkage (Fig. 3, upper bands, ~500 kDa) or partial linkage (Fig. 3, lower bands, ~250 kDa).

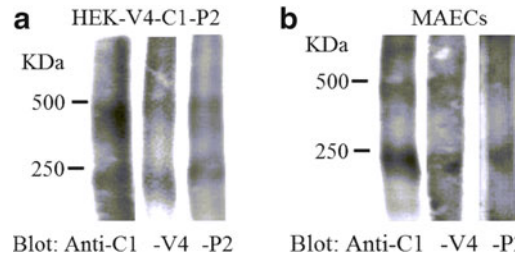

Fig. 3. Representative chemical cross-linking of TRPV4, TRPC1, and TRPP2 in transfected HEK cells (**a**) and primary cultured rat MAECs (**b**). These bands were recognized by anti-TRPC1, anti-TRPV4, or anti-TRPP2 antibody (21).

Pros

1. Protein interaction is detected in their native state.
2. Transient protein interactions can be detected.
3. Cross-linking reagents for different situations are well developed.

Cons

1. This method cannot differentiate the direct or indirect interaction.
2. Need specific antibody.
3. It is technically difficult to control the degree of cross-linking. Over cross-linking results in high background noise on Western blots.

3.6. Förster Resonance Energy Transfer Detection

TRP channel interaction is critical for many cellular processes in mammalian cells. The protein–protein interaction can be detected by a fluorescence microscope approach, which is called FRET detection. First, target proteins are fused with CFP and/or YFP. The fluorescence from CFP-, YFP-, and FRET-channels is recorded, and FRET ratio be calculated by the formula.

The following is a step-by-step protocol.

1. Seed cells on coverslips.
2. Transfect the following fusion proteins into cultured mammalian cells:
   (a) CFP fused to YFP (positive control).
   (b) Unfused, free CFP and unfused, free YFP (negative control).
   (c) Protein 1-CFP and Protein 2-YFP.
   (d) Protein 1-YFP and Protein 2-CFP.
3. Place the coverslip in a chamber 12–24 h after transfection.
4. Mount the chamber on an inverted microscope equipped with a CCD camera and three-cube FRET filters including (excitation, dichroic, emission): YFP (S500/20 nm; Q515lp; S535/30 nm); FRET (S430/25 nm; 455dclp; S535/30 nm); and CFP (S430/25 nm; 455dclp; S470/30 nm) (Olympus).
5. Subtract the average background signal.
6. Capture the fluorescence images of the transfected cells at CFP-, YFP-, and FRET-channels, respectively.
7. Calculate the FRET ratio (FR) (Fig. 4) by the following equation:

$$\mathrm{FR} = F_{\mathrm{AD}} / F_{\mathrm{A}} = \left[S_{\mathrm{FRET}}(\mathrm{DA}) - R_{\mathrm{D1}} * S_{\mathrm{CFP}}(\mathrm{DA})\right] / R_{\mathrm{A1}} * \left[S_{\mathrm{YFP}}(\mathrm{DA}) - R_{\mathrm{D2}} * S_{\mathrm{CFP}}(\mathrm{DA})\right]$$

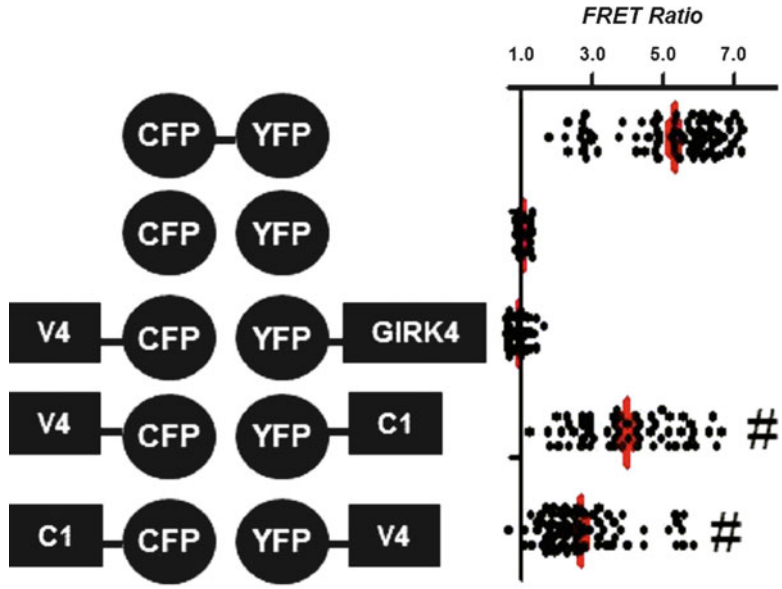

Fig. 4. FRET detection for the interaction between TRPV4 and TRPC1. *Horizontal axes* indicate FRET ratio of living cells expressing the indicated constructs (12). *Each point* represents the FRET ratio of a single cell. The *red lines* and *error bars* indicate the average FRET ratio values and SE. When the FRET ratio is 1, there is no FRET; when the FRET ratio is greater than 1, there is FRET. Data are given as mean ± SE (n = 50–81). GIRK, G-protein-activated inwardly rectifying K^+ channels.

where F_{AD} represents the total YFP emission with 430/25-nm excitation, and F_A represents the direct YFP emission with 500/20-nm excitation. In S_{CUBE}(SPECIMEN), CUBE indicates the filter cube (CFP, YFP, or FRET), and SPECIMEN indicates whether the cell is expressing donor (D, CFP), acceptor (A, YFP), or both (DA). $R_{D1} = S_{FRET}(D)/S_{CFP}(D)$, $R_{D2} = S_{YFP}(D)/S_{CFP}(D)$, and $R_{A1} = S_{FRET}(A)/S_{YFP}(A)$ are predetermined constants that require measurement of the bleed-through of the emission of only CFP- or YFP-tagged molecules into the FRET channel and the emission of only CFP-tagged molecules into the YFP channel.

Pros

1. FRET detection usually only detect direct protein interactions.
2. FRET detection can measure real-time protein interaction in living cells and in normal conditions.

Cons

1. CFP- and YFP-tagged constructs are transfected (over-expressed) in the target cells, thus may not reflect the processes in native cells.
2. Highly specialized FRET detection equipment with defined wavelength is needed.

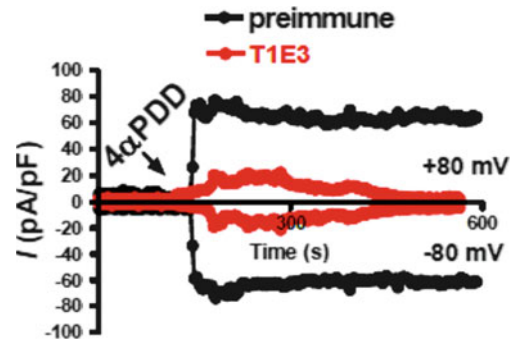

Fig. 5. Representative trace for time course of 4α-PDD (5 μmol/l)-stimulated whole-cell current in human umbilical vein endothelial cells (12). Cells were preincubated with T1E3 (1:100) or preimmune IgG (1:100, as control) for 1 h at 37°C prior to the experiment.

3.7. Whole-Cell Patch Clamp

1. Seed cells on coverslips.
2. Prepare appropriate pipette solution and bath solution.
3. Place a coverslip in a chamber containing bath solution and mount the chamber on a microscope.
4. Pull a glass micropipette with P-97 micropipette puller (Sutter Instrument) and fill the pipette tip with pipette solution.
5. Lower the pipette towards the cell. When the pipette tip is in contact with the cell membrane, apply suction through the pipette pressure tubing to make the gigaseal on cell membrane (Note 9).
6. Switch to voltage clamp. Record the whole cell current density (pA/pF) by an EPC-9 patch amplifier (HEKA) in response to successive voltage pulses of +80 mV and −80 mV for 100 ms duration (Fig. 5).
7. Plot the whole cell current values vs. time (Fig. 5).

Pros

1. Patch clamp is the most sensitive and reliable technique to measure electrical activity of living cell membrane.
2. Patch clamp can be combined with other techniques such as fluorescence microscopy and wire myograph to produce more powerful outcome.

Cons

1. Patching primary cultured cells may be technically challenging.
2. Relatively slow outputs.

3.8. Fluorescence Measurement of Intracellular Ca^{2+} Concentration ($[Ca^{2+}]_i$)

Fluorescent probes, or fluorescent dyes, are molecular probes which show a spectral response upon binding Ca^{2+}. Once cells are loaded with these dyes, it is possible to measure the intracellular Ca^{2+} changes using fluorescent microscopy.

1. Prepare 0.02% pluronic F127: add 0.2 mg pluronic F127 to 1 ml H_2O.
2. Prepare normal physiological salt solution (NPSS) (See Sect. 2.2).
3. Seed cells on coverslips.
4. Load 10 μmol/l Fura-2/AM and 0.02% pluronic F-127 for 30 min in dark at 37°C in NPSS.
5. Mount the cell coverslip onto the recording chamber and place on the stage of an inverted microscope (Olympus IX81, Olympus).
6. Record the $[Ca^{2+}]_i$ fluorescence using a fluorescence imaging system (Olympus) at excitation wavelength 340 and 380 nm.
7. Analyze the data by MetaFluor Analyst software (Molecular Devices, Sunnyvale, CA). The changes in $[Ca^{2+}]_i$ are indicated by the changes of the ratio of the fluorescence under 340 nm relative to the fluorescence under 380 nm (F340/F380) (Fig. 6).
8. If necessary, convert the Fura-2 ratio F340/F380 to $[Ca^{2+}]_i$ based on the calibration using Calcium Calibration Buffer Kit (Invitrogen) (Fig. 7).

Pros

1. Fluorescent dyes are highly sensitivity to changes in cytosolic Ca^{2+}.
2. This method measures real-time $[Ca^{2+}]_i$ in living cells under physiological/pathological conditions.

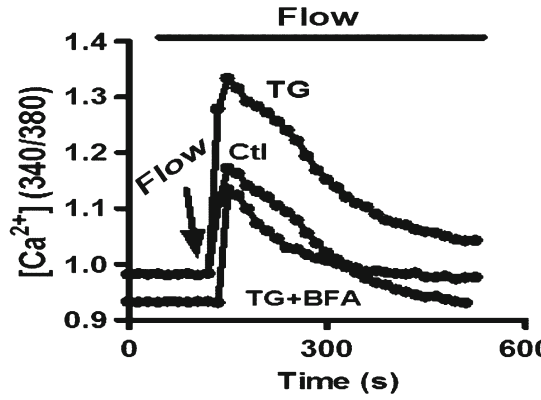

Fig. 6. Representative traces for the potentiation of flow-induced Ca^{2+} influx in human umbilical vein endothelial cells (22). TG, thapsigargin, 4 μmol/l, was given for 15 min; BFA, brefeldin A, 5 μmol/l, was given for 30 min before TG.

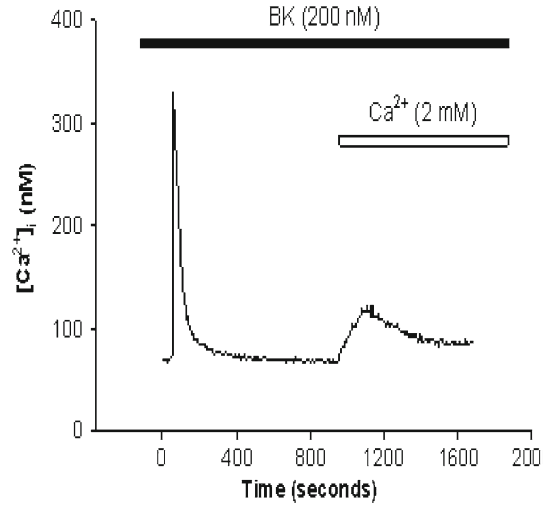

Fig. 7. Bradykinin-induced Ca^{2+} entry (23). A representative trace of Fura-2 fluorescence in rat aortic endothelial cells bathed in $0Ca^{2+}$-PSS in response to bradykinin (200 nM) challenge.

Cons

1. Due to difference in hardware and software, different detection systems may give out very different values of fluorescence intensity and/or changes in fluorescence intensity (or ratios). This makes data comparison difficult. In this regard, ratiometric dyes such as Fura-2 is preferred, because the values can be converted into Ca^{2+} concentration after careful calibration.

3.9. Isometric Tension Measurement

The mouse aorta is isolated and mounted onto two thin stainless steel holders (Danish Myotechnology). One holder is connected to a force displacement transducer. The other one is connected to a movable device that allowed the application of an appropriate passive tension, which is determined to be the optimal resting tension for obtaining the maximal active tension induced by 60 mM K^+ solution (see Sect. 2.2) bubbled with 95% O_2 + 5% CO_2 (Note 10). The vessel tension is measured by an isometric tension myograph (model 610 M, Danish Myotechnology). Data were acquired and analyzed using PowerLab (AD Instruments) and LabChart (AD Instruments).

1. Kill the male C57BL mice (~5 week-old) by cervical dislocation.
2. Cut out the thoracic aorta and place it into an ice-cold Krebs–Henseleit solution (see Sect. 2.2) bubbled with a gas mixture of 95% O_2 and 5% CO_2.
3. Remove the fat and peripheral tissues under dissection microscope.

4. Cut the aorta into 2-mm segments.
5. Mount the aortic rings onto two thin stainless steel holders (supplied by the isometric tension myograph) in 5 ml organ baths containing Krebs–Henseleit solution bubbled with a gas mixture of 95% O_2 and 5% CO_2 at 37°C.
6. Equilibrate the aortic rings for about 30 min (Note 11).
7. Apply 60 mM K^+ solution to test the contractile function of the aortic rings.
8. Wash out with Krebs–Henseleit solution for two times.
9. Repeat step 7–8.
10. Preconstrict the aortic rings with 10 μM phenylephrine to achieve sustained contraction.
11. Apply acetylcholine with cumulative concentrations into the bath solution to test the integrity of endothelium.
12. Wash out with Krebs–Henseleit solution for three times.
13. Repeat step 10.
14. Apply cumulative chemicals into the bath solution to test its relaxation effect.
15. Acquire and analyze data by PowerLab and LabChart (Fig. 8).

Pros

1. Isometric tension measurement allows direct measurement of contractile force generated from blood vessels.
2. Wire myograph can be combined with fluorescent microscopy to detect the vessel contraction and intracellular Ca^{2+} changes simultaneously.

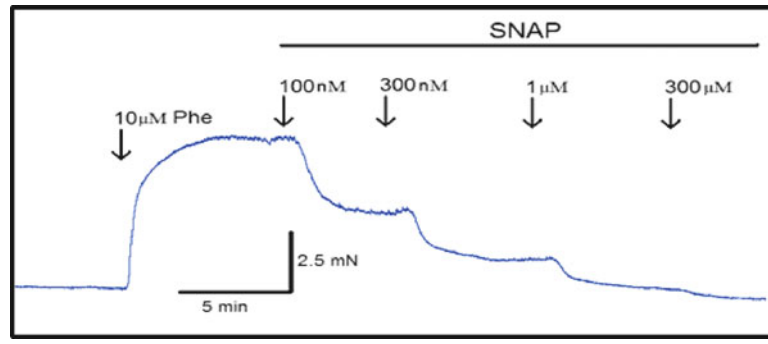

Fig. 8. Representative time courses of isometric tension in isolated mouse aortic segments in response to cumulatively increasing concentrations of SNAP applied to the bath (24). The aortic segments (~2 mm in length) were preconstricted with 10 μM phenylephrine (Phe). SNAP, S-nitroso-N-acetylpenicillamine.

Cons

1. Wire myograph only measures small vessels (internal diameter 60 μm–3 mm), whereas contractility of large blood vessels are measured in isolated organ bath.
2. The vessels under measurement are not exposed to hydrostatic pressure. The conditions are not physiological.

3.10. Isobaric Diameter Measurement

The rat mesenteric artery is isolated and mounted onto a pressure myograph chamber (model 110P, Danish Myotechnology). External diameter is recorded using a CCD camera. Flow is initiated by creating a pressure different between inflow and outflow. The mean intraluminal pressure is maintained at 50 mmHg throughout whole procedure. Data were acquired and analyzed by MyoView software (GE Healthcare).

1. Kill the Sprague–Dawley rats by inhalation of CO_2.
2. Remove the ileum and immerse the mesentery in Krebs–Henseleit solution (see Sect. 2.2) bubbled with a gas mixture of 95% O_2 and 5% CO_2.
3. Carefully dissect the third- or fourth-order mesenteric artery (~2–3 mm long).
4. Transfer the artery to a pressure myograph chamber (model 110P, Danish Myotechnology) filled with oxygenated Krebs–Henseleit solution at 37°C.
5. Cannulate one glass micropipette (tip diameter ~125 μm) into the proximal part and the other into distal end of the artery and secure with two fine nylon sutures.
6. Connect both cannulation pipettes to independent reservoirs set at the same height and solution level to ensure there is no flow.
7. Set the intraluminal pressure to 50 mmHg and equilibrate the artery for 30 min at 37°C by oxygenated Krebs–Henseleit solution (flow rate ~2–3 ml/min).
8. Pressurize the artery to 80 mmHg, and apply a longitudinal force to stretch the vessel until it appears straight and then by an extra 10%.
9. Decrease the pressure back to 50 mmHg, and incubate the vessel for another 10 min before an experimental maneuver.
10. Monitor the artery by a charge-coupled device camera (video camera module) attached to a light inverted microscope.
11. Analyze the external diameter of the vessel and luminal pressure by MyoView software (GE Healthcare) (Fig. 9).

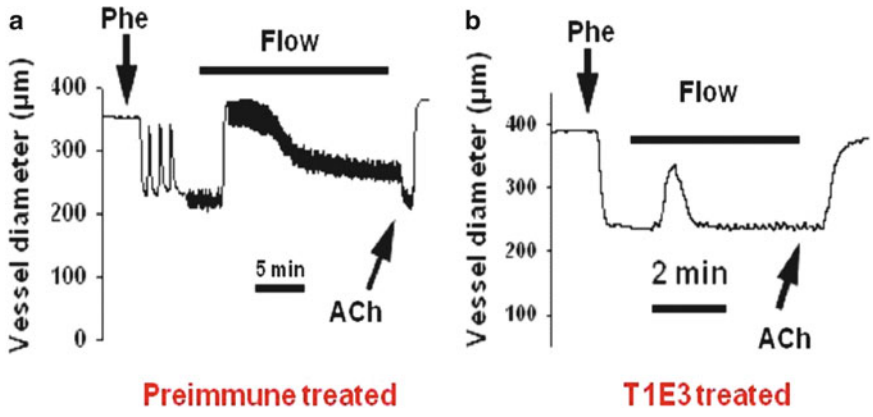

Fig. 9. Representative traces showing the effect of T1E3, a TRPC1 blocking antibody, on flow-induced vascular isobaric diameter changes in isolated mice mesenteric arteries (12). Arteries were preincubated with preimmune IgG (1:50) or T1E3 (1:50) overnight. The *solid bar* on the top of the trace indicates the period when intraluminal flow (Kreb's solution with 1% BSA) was applied. The arteries were preconstricted with phenylephrine (Phe).

Pros

1. Pressure myograph allows blood vessels to assume the stereological conformation as they would be in vivo.
2. Pressure myograph can be combined with fluorescent microscopy to detect the vessel diameter and intracellular Ca^{2+} changes simultaneously.

Cons

1. Arteries with an internal diameter smaller than 60 μm are difficult to be cannulated and recorded by pressure myograph.
2. Only one vessel can be studied in each experiment, namely slow output.

4. Notes

1. Always wear gloves when handling the PVDF membrane, otherwise it may be damaged or contaminated.
2. Check the affinities of protein A agarose for various IgG subclasses before use. Consider other kind of protein agarose (e.g., protein G agarose) if the binding capacity of protein A agarose is low for some certain species.
3. Preimmune IgG should be used as control if antibodies are to be used for experiments.

4. Use DTSSP and DSP for cross-linking molecules at the cell surface and within the cell, respectively.
5. Do not prepare stock solutions for the cross-linkers. The NHS-ester moieties become nonreactive due to hydrolyzation. Reconstitute the cross-linkers immediately before use and discard any unused reconstituted cross-linkers.
6. Use micromolar concentrations of proteins to compensate the protein loss from during chemical cross-linking.
7. The concentration of DTSSP and the incubation duration should be determined empirically.
8. Cross-linked protein complexes often appear fuzzy on the X-ray film.
9. In patch clamp, the starting seal membrane resistance must achieve 1 GΩ.
10. In myograph, determine the passive tension carefully. Too much higher tension will cause the vessel rings injury.
11. If the basal tension is still not stable after 30 min, a longer time of equilibrium is needed.

Acknowledgments

This work was supported by CUHK478011, CUHK479109, and CUHK478710 from the Hong Kong RGC, Strategic Investment Scheme C and Group Research Grant from Chinese University of Hong Kong.

References

1. Venkatachalam K, Montell C (2007) TRP channels. Annu Rev Biochem 76:387–417
2. Kobori T, Smith GD, Sandford R, Edwardson JM (2009) The transient receptor potential channels TRPP2 and TRPC1 form a heterotetramer with a 2:2 stoichiometry and an alternating subunit arrangement. J Biol Chem 284:35507–35513
3. Ma X, Qiu S, Luo JH, Ma Y, Ngai CY, Shen B, Wong CO, Huang Y, Yao XQ (2010) Functional role of vanilloid transient receptor potential 4-canonical transient receptor potential 1 complex in flow-induced Ca(2+) influx. Arterioscler Thromb Vasc Biol 30:851–858
4. Adebiyi A, Zhao G, Narayanan D, Thomas-Gatewood CM, Bannister JP, Jaggar JH (2010) Isoform-selective physical coupling of TRPC3 channels to IP3 receptors in smooth muscle cells regulates arterial contractility. Circ Res 106:1603–1612
5. Kwan HY, Shen B, Ma X, Kwok YC, Huang Y, Man YB, Yu S, Yao X (2009) TRPC1 associates with BK(Ca) channel to form a signal complex in vascular smooth muscle cells. Circ Res 104:670–678
6. Masters SC (2004) Co-immunoprecipitation from transfected cells. Methods Mol Biol 261: 337–350
7. Miernyk JA, Thelen JJ (2008) Biochemical approaches for discovering protein-protein interactions. Plant J 53:597–609
8. Lalonde S, Ehrhardt DW, Loque D, Chen J, Rhee SY, Frommer WB (2008) Molecular and cellular approaches for the detection of protein-protein interactions: latest techniques and current limitations. Plant J 53:610–635

9. Herman B, Krishnan RV, Centonze VE (2004) Microscopic analysis of fluorescence resonance energy transfer (FRET). Methods Mol Biol 261:351–370
10. Latif R, Graves P (2000) Fluorescent probes: looking backward and looking forward. Thyroid 10:407–412
11. Rao GH, Peller JD, White JG (1985) Measurement of ionized calcium in blood platelets with a new generation calcium indicator. Biochem Biophys Res Commun 132:652–657
12. Ma X, Qiu S, Luo J, Ma Y, Ngai CY, Shen B, Wong CO, Huang Y, Yao X (2010) Functional role of vanilloid transient receptor potential 4-canonical transient receptor potential 1 complex in flow-induced Ca2+ influx. Arterioscler Thromb Vasc Biol 30:851–858
13. Neher E, Sakmann B, Steinbach JH (1978) The extracellular patch clamp: a method for resolving currents through individual open channels in biological membranes. Pflugers Arch 375:219–228
14. Hamill OP, Marty A, Neher E, Sakmann B, Sigworth FJ (1981) Improved patch-clamp techniques for high-resolution current recording from cells and cell-free membrane patches. Pflugers Arch 391:85–100
15. Shen B, Cheng KT, Leung YK, Kwok YC, Kwan HY, Wong CO, Chen ZY, Huang Y, Yao X (2008) Epinephrine-induced Ca2+ influx in vascular endothelial cells is mediated by CNGA2 channels. J Mol Cell Cardiol 45: 437–445
16. Czikora A, Lizanecz E, Bako P, Rutkai I, Ruzsnavsky F, Magyar J, Porszasz R, Kark T, Facsko A, Papp Z, Edes I, Toth A (2012) Structural activity relationships of vanilloid receptor agonists for arteriolar TRPV1, Br J Pharmacol 165 (5):1801–1812
17. Watanabe H, Davis JB, Smart D, Jerman JC, Smith GD, Hayes P, Vriens J, Cairns W, Wissenbach U, Prenen J, Flockerzi V, Droogmans G, Benham CD, Nilius B (2002) Activation of TRPV4 channels (hVRL-2/mTRP12) by phorbol derivatives. J Biol Chem 277:13569–13577
18. Kiyonaka S, Kato K, Nishida M, Mio K, Numaga T, Sawaguchi Y, Yoshida T, Wakamori M, Mori E, Numata T, Ishii M, Takemoto H, Ojida A, Watanabe K, Uemura A, Kurose H, Morii T, Kobayashi T, Sato Y, Sato C, Hamachi I, Mori Y (2009) Selective and direct inhibition of TRPC3 channels underlies biological activities of a pyrazole compound. Proc Natl Acad Sci USA 106:5400–5405
19. Kottgen M (2007) TRPP2 and autosomal dominant polycystic kidney disease. Biochim Biophys Acta 1772:836–850
20. Draijer R, Vaandrager AB, Nolte C, de Jonge HR, Walter U, van Hinsbergh VW (1995) Expression of cGMP-dependent protein kinase I and phosphorylation of its substrate, vasodilator-stimulated phosphoprotein, in human endothelial cells of different origin. Circ Res 77:897–905
21. Du J, Ma X, Hung Y, Lutz B, Yao X (2012) Heteromeric coassembly of TRPV4, TRPC1 and TRPP2 to form a flow-sensitive channel, in preparation
22. Ma X, Cao J, Luo J, Nilius B, Huang Y, Ambudkar IS, Yao X (2010) Depletion of intracellular Ca2+ stores stimulates the translocation of vanilloid transient receptor potential 4-c1 heteromeric channels to the plasma membrane. Arterioscler Thromb Vasc Biol 30:2249–2255
23. Leung PC, Cheng KT, Liu C, Cheung WT, Kwan HY, Lau KL, Huang Y, Yao X (2006) Mechanism of non-capacitative Ca2+ influx in response to bradykinin in vascular endothelial cells. J Vasc Res 43:367–376
24. Wong CO, Sukumar P, Beech DJ, Yao X (2010) Nitric oxide lacks direct effect on TRPC5 channels but suppresses endogenous TRPC5-containing channels in endothelial cells. Pflugers Arch 460:121–130

Chapter 4

Atherosclerosis Models with Cell-Mediated Calcification

Beili Zhu

Abstract

This protocol describes a novel chronic total occlusion (CTO) model that features cell-mediated calcium deposits in rabbit femoral arteries. CTO is the most severe case of atherosclerosis, and it remains a big challenge in cardiology. There are urgent needs to establish a CTO animal model in order to develop new devices and drugs. The purpose of this protocol is to provide such a platform for advancing the treatment of CTOs.

Our CTO model features the following four prominent characteristics of a clinical calcified atherosclerosis: (1) The occlusion site occurs gradually. (2) Calcium deposits are mediated by cells and they progress over time. (3) Acute and chronic inflammation at occlusion sites. (4) Recanalization (new vessel formation) at occlusion sites. These facts indicate that our model bears great similarities to clinical CTO disease. The strategy we apply here is to implant tissue-engineering scaffolds into rabbit femoral arteries and induce the cells on scaffolds to deposit calcium themselves.

In this chapter, we first describe a detailed protocol of scaffold fabrication, growth factor coating on scaffolds, and the initiation of cellular calcification. We then provide easy-to-follow steps to implant cellular constructs into animal arteries using interventional techniques. Finally, we describe the methods to detect calcium in CTOs and the staining approaches to identify other pathological characteristics at the occlusion sites. Additionally, we provide notes to highlight the critical steps in order to successfully carry out this protocol. An animal CTO model generated by the above techniques will provide a useful platform to develop new devices and test novel drugs for treatment of the most severe case of atherosclerotic calcification.

Key words: Atherosclerosis, Chronic total occlusion, Calcium, Inflammation, Recanalization, Tissue engineering scaffolds, Polycaprolactone, Primary human osteoblasts, TGF-β1

1. Introduction

Atherosclerosis is a leading cause of death in North America, and more than nine million people suffer from this disease each year (1). Chronic total occlusion (CTO) is the most severe case of atherosclerosis. It features various degrees of calcium deposits and thrombus in completely obstructed arteries (2).

Arpad Szallasi and Tamás Bíró (eds.), *TRP Channels in Drug Discovery: Volume II*, Methods in Pharmacology and Toxicology,
DOI 10.1007/978-1-62703-095-3_4,

Intracellular traffic is a highly regulated process (3–5). In the same way, calcification in CTO is an active, cell-mediated progression that is similar to osteogenesis in bone (6, 7). CTO only occurs in 10% of all percutaneous coronary interventions (PCIs), but it reflects the most severe case in atherosclerosis and is so-called the final frontier in cardiology (8). Therefore, there is a strong need to develop CTO models that simulate this most severe stage of atherosclerosis in human. Such models will be extremely useful for the development of novel interventional devices and drugs to treat CTOs.

Many approaches have been explored to create animal models of CTO. In most animal models, arterial occlusion was achieved by blocking the blood flow using ligation (9, 10). This abrupt blockage does not mimic the gradual progression of vessel occlusion in atherosclerosis. The most recent models implanted gelatin sponges with bone powder or Ca^{2+} dip-coated poly-L-lactone scaffolds in arteries (11, 12). Calcium was detected at occlusion sites in these studies. However, there is a concern whether these non-cell generated calcium is similar to the pathological form found in human CTOs.

In this protocol, we present an advanced gradual occlusion model of CTO. It features calcium deposits that progress over time and is mediated by cells just like in human conditions. Besides, the two prominent features of atherosclerosis: chronic inflammation and recanalization (new vessel formation) are also found in this CTO model (13). Our tissue-engineering approach is to culture primary human osteoblasts on TGF-β1-coated polycaprolactone scaffolds. Then, by catheter-based interventional techniques, we implant cellular scaffolds into rabbit femoral arteries.

In atherosclerotic calcification, calcium deposits are the products of vascular cells which have been differentiated into osteoblast lineage (6, 7). In this study, in order to initiate calcification earlier, primary osteoblasts (HOBs) were directly chosen as the cell type to deposit calcium. The most common approach to induce in vitro calcification of HOB cultures is the addition of β-glycerophosphate and dexamethasone (Dex) to cell culture medium (14). Another frequently used method is to treat osteoblasts with BMP-2, TGF-β1, or leptin in medium (15–18). Among these growth factors, TGF-β1 is secreted by osteoblast lineage cells (19, 20) and is a sufficient growth factor in bone matrix. Therefore, we design the coating of TGF-β1 on scaffolds and then the seeding of primary human osteoblasts on top of them (21). By direct contact between osteoblasts and TGF-β1, cells will continuously deposit calcium in blood flows. The scaffold carrier we choose is polycaprolactone (PCL), which is a biodegradable polymer that has been widely used as scaffolding material in bone tissue engineering (22).

In this proposal, we describe how to fabricate scaffolds from PCL raw material, to prepare TGF-β1 coating on scaffolds, and to culture HOBs in vitro on scaffolds for precalcification treatment. We also provide a step-by-step protocol on how to implant these HOB-PCL constructs into rabbit femoral arteries using catheter-based techniques. Finally, we show a detailed guide on how to detect calcium deposits and other pathological markers in CTO using chemical detection methods and imaging approaches.

2. Materials

2.1. Fabrication of PCL scaffolds

1. Polycaprolactone (IV = 1.0–1.3; GMP grade) (Lactel Durect Co., Birmingham, AL, USA)
2. Sodium Chloride (Sigma, St. Louis, MO, USA)
3. Glass Scintillation Vials, 20 ml (Wheaton, Millville, NJ, USA)
4. Pouches 7-1/2 × 13″ cool box (Certol, Commerce City, CO, USA)
5. A set of sieves: 250–500 μm in mesh size
   (a) Stainless steel pan (VWR, Sugar Land, TX, USA)
   (b) Stainless steel cover (VWR)
   (c) 500 μm sieve (VWR)
   (d) 250 μm sieve (VWR)
6. Dichloromethane (purity ≥ 98%, Sigma)
7. Virgin PTFE Rod (Molds) (MSC Industrial, San Antonio, TX, USA)

2.2. TGF-β1 Coating on PCL Scaffolds

1. TGF-β1 (R&D Systems, Minneapolis, MN, USA)
2. Bovine Serum Albumin low endotoxin, cell culture tested (Sigma)
3. Low binding tubes (GLP-PGC Scientifics, Palm Desert, CA, USA)
4. Fibronectin 1 mg/ml (Sigma)
5. BD syringes with Luer-Lok tips 60 ml (BD Biosciences, San Jose, CA, USA)
6. 25 Gauge Syringe needle (BD Medical, Franklin Lakes, NJ, USA)
7. Corning Ultra-Low Attachment 96 well plates (Corning, Corning, NY, USA)
8. Corning Ultra-Low Attachment 24 well plates (Fisher Scientific, Houston, TX, USA)

2.3. In Vitro Culture and Differentiation of Primary Human Osteoblasts

1. Primary Human Osteoblasts (HOBs) (Lonza, Walkersville, MD)
2. Minimal essential medium-Alpha (αMEM), no nucleosides (Invitrogen, Carlsbad, CA, USA)
3. L-ascorbic acid (Sigma)
4. β-glycerophosphate (Sigma)
5. Dexamethasone (Sigma)
6. Osteoblast basal media (Lonza)
7. Single Quotes (Lonza)
8. Trypsin-EDTA (Lonza)
9. Nalgene Sterile Disposable Filter Units (Thermo Scientific, Logan, UT, USA)

2.4. Implantation of PCL-HOB Scaffolds into Rabbit Artery

1. New Zealand White Rabbits, male, weighing 4.5–5 kg (Myrtle's Rabbitry, Thompsons Station, TN, USA)
2. French introducer sheath (Boston Scientific, Natick, MA, USA)
3. 5 French Angled Glide-catheter (Terumo Medical, Somerset, NJ, USA)
4. 0.014 in. guide wire (Boston Scientific)
5. 5 French straight XP Glide-catheter (Terumo Medical)

2.5. Characterization of Calcification and Pathological Features at Chronic Total Occlusion Sites

1. Tissue-Tek OCT compound 4583 (Electron Microscopy Sciences, Hatfield, PA, USA)
2. Formalin Solution, neutral buffered, 10% (Sigma)
3. Transfer pipette (VWR)
4. Silane Coated Slides (Electron Microscopy Sciences)
5. Ca^{2+}-free PBS (Invitrogen)
6. OsteoImage Bone Mineralization Assay (Lonza)
7. Aqueous Mounting Medium (Vector Laboratories, Burlingame, CA, USA)
8. Cover Glass 22 × 50 mm (Fisher)
9. Microscope slide super PAP Pen, Fine tip 2.5 mm (Polysciences, Warrington, PA, USA)
10. Harleco Hematoxylin, Gill III (EMD chemicals, Billerica, MA, USA)
11. Harleco Eosin Y Solution, Aqueous, (EMD chemicals)
12. Tissue Path Disposable Base Molds (15 × 15 × 5 mm) (Fisher Scientific)
13. Sodium Bicarbonate Powder (Sigma)

2.6. Instruments

1. Scanning Electron Microscope (JEOL JSM-6610LV, Peabody, MA, USA)
2. Energy-dispersive X-ray spectroscopy (EDS) detector (EDAX Apollox System, Mahwah, NJ, USA)
3. Leica Cryostat (Leica Microsystems, Buffalo Grove, IL, USA)
4. Confocal Microscope (Olympus FV-1000, Olympus, Center Valley, PA, USA)
5. Light Microscope (Olympus)

3. Methods

3.1. Fabrication of PCL Scaffolds

PCL scaffolds were fabricated by the vibration particle technique (21, 23–25). All tools, PTFE molds, and beakers are cleaned and placed in a sterile pouch and autoclaved prior to all experiments (Note 1).

1. Select sodium chloride by sieves at mesh sizes of 250 and 500 μm. Only particles in the range of 250 μm–500 μm are used in this experiment.
2. Pour NaCl (250–500 μm) into a clean dry 250 ml beaker. Cover the beaker with aluminum foil and punch some holes on top for ventilation purposes.
3. Place the beaker in a furnace at 200°C and bake for at least2 h. Take it out to room temperature right before the experiment.
4. Pour 11.37 ml dichloromethane and 1.33 g poly-(ε-caprolactone) in a 20 ml scintillation vial. Close the cap and vortex at maximum speed on a vortex meter for 20 min until PCL dissolves completely in dichloromethane.
5. Spread 7.875 g NaCl evenly at the bottom of a PTFE mold. The mold is machined to have a rectangular cavity of $33 \times 20 \times 15$ mm.
6. Once the polymer solution is added on top of the mold, vortex the mold continuously for 2 min (Note 2).
7. Add the second set of NaCl at 7.87 g evenly into the mold on top of the previous polymer–salt mixture. Continue the vigorous vortexing to mix the salt and polymer solution well.
8. After about a minute or two, the polymer solution tends to dry and is too stiff to vortex anymore. Before it totally dries out, stop the vortex mixer and spread the last set of salt (3.50 g) into the mold to evenly cover the top of the polymer solution (Note 3).

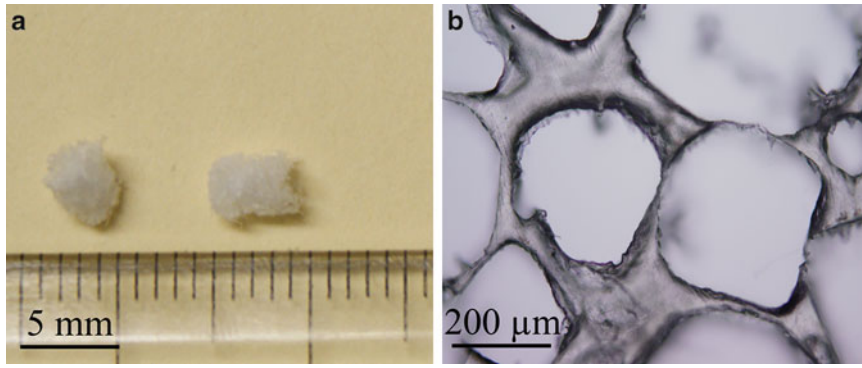

Fig. 1. (**a**) Polycaprolactone (PCL) scaffolds (diameter = 3 mm; length = 5 mm). (**b**) Cross-sections of polycaprolactone scaffolds under light microscopy (13). Reproduced by permission of John Wiley & Sons, Inc.

9. It is recommended to make 2–3 molds of polymer–salt mixture at once to yield sufficient amount of scaffolds for in vitro and in vivo experiments.
10. The polymer–salt mixture in the PTFE molds was left in customized plexiglass operation box for 24 h at room temperature. It is under the continuous air flow generated by two fans on two opposite sides of the box.
11. Place molds in a vacuum oven (500 mTorr) at 45°C for another 24 h.
12. Screw a metal circular punch (Inner diameter 3 mm) onto an arbor press, and punch scaffolds out of the molds (Note 4). Each mold can yield 50 scaffolds at a diameter of 3 mm.
13. Place scaffolds from each mold in a separate 1 L beaker filled with 800 ml of ddH_2O for 2 days at room temperature. Change water once after 24 h.
14. Collect porous scaffolds floating in water into a 15 ml centrifuge tube. Unscrew the cap and dry them in a lyophilizer for 24 h. The lyophilizer is set at −40°C under vacuum.
15. Take out ready-to-use scaffolds from lyophilizer, seal the cap, and store them at −20°C.
16. Check the pores of scaffolds under a light microscope. The pore size ranges from 200 to 600 μm, and the porosity is ≥90% (Fig. 1).

3.2. TGF-β1 Coating on PCL Scaffolds (Note 5)

1. Place 30 scaffolds in a 60 ml syringe. Fill in 15 ml of 75% ethanol in ddH_2O. Remove air from the syringe, put on a 25-Gauge syringe needle, and obstruct the needle tip with a piece of clean Styrofoam.
2. Vigorously plunge the syringe for about a minute in order to remove air from scaffolds and allow 75% ethanol to penetrate inside pores.

3. Scaffolds are floating on ethanol at first, and once they all sink to the bottom of the syringe, it indicates fluids get inside the pores. You can stop plunging at that time.
4. Let scaffolds sit in syringe for 15 min for sterilization.
5. Take scaffolds out from 75% ethanol and place them in a new 20 ml syringe. Fill syringe with PBS and repeat steps 1–4.
6. In order to wash out any residual ethanol. Change PBS two more times and repeat steps 1–3.
7. Aliquote 1 mg/ml fibronectin into 200 μl volume and store at –20°C.
8. Prepare fresh fibronectin solution at a concentration of 20 μg/ml in PBS for each experiment.
9. Place scaffolds in a new 60 ml syringe and fill the syringe with 15 ml fibronectin solution at a concentration of 20 μg/ml. Repeat steps 1–4.
10. Take scaffolds out of the syringe and place each one in an individual well of a regular 96-well plate.
11. Fill each well with 300 μl fibronectin solution at a concentration of 20 μg/ml (Note 6).
12. Seal the 96-well plate with parafilm and place it on ice at 4°C fridge overnight (Note 7).
13. The next morning, prepare 4 mM HCl using ddH_2O and sterilize it by filtering through a 0.2 μm membrane.
14. Reconstitute TGF-β1 powder in 4 mM HCl to prepare a stock solution at a concentration of 40 ng/μl in low binding tubes.
15. Prepare 1% BSA by adding 0.1 g bovine serum albumin in 10 ml ddH_2O.
16. Dilute TGF-β1 stock solution to 5 ng/20 μl volume using 1% BSA (Note 8).
17. Take out PCL scaffolds coated with fibronectin from 4°C. Put them on a sterile gauze to suck out liquid and then move them to an ultra-low attachment 96-well plate. Each well holds one scaffold.
18. Drop load 20 μl of TGF-β1 solution (as prepared in step 16) onto each scaffold using a micropipette.
19. After all scaffolds are loaded with TGF-β1, the ultra-low attachment 96-well plate is placed on ice at 4°C for 3 h.

3.3. Precalcification of Primary Human Osteoblast Cultures on TGF-β1 Coated Scaffolds

1. Culture Human Osteoblasts (HOBs) in osteoblast basal medium supplemented with single quotes in a humidified incubator at 37°C with 5% CO_2.
2. Culture cells in T-150 flasks, and change medium every 2 days.

3. Passage cells using trypsin–EDTA when cultures reached 80–90% confluence. HOBs at third passage are used for all cell culture experiments.
4. The medium used for precalcification is α-MEM supplemented with 7% FBS, 1% antibiotic/antimycotic, 100 μg/ml ascorbic acid, 5 mM β-glycerolphosphate, and 10^{-10} M dexamethasone. Medium was sterilized by passing through a 0.2 μm filter.
5. Take out scaffolds from 4°C and put them on a sterile gauze to suck out liquid. Move scaffolds to a dry ultra-low attachment 24-well plate. A total number of 2×10^5 HOBs are seeded on each scaffold in each well.
6. Put the plate inside an incubator for 2 h.
7. Take the plate out and add 1 ml precalcification medium into each well.
8. Medium is changed every 3 days, and HOB-PCL constructs are harvested for implantation after 28 days of culture.

3.4. Implantation of Precalcified HOB-PCL Constructs into Rabbit Femoral Arteries via Catheterization (Note 9)

1. The animals are preanesthetized using a mixture of ketamine (30 mg/kg) and midazolam (0.2 mg/kg) administered intramuscularly (i.m.). The animals are intubated and anesthesia was maintained using isoflorane inhalant (1–2%) administered with 100% O_2.
2. Each rabbit receives a control PCL scaffold and a test scaffold with osteoblasts and TGF-β1, and two time points (10 and 28 days) can be used for the study.
3. The control PCL scaffold only has the loading of fibronectin, but without TGF-β1 or osteoblasts.
4. Perform a right common carotid artery cut-down, and place a 5 French introducer sheath into the artery.
5. Advance a 0.014 in. guide wire first across the aortic arch.
6. Use a 5 French angled Glide-catheter to follow over the wire, go pass the aortic arch, and advance to a point proximal to the iliac bifurcation.
7. Perform a baseline angiogram of femoral arteries on both sides of the body.
8. Advance the guide wire down into one femoral artery to just proximal to the stifle.
9. Retract the Glide-catheter and leave the 0.014 wire in place.
10. Thread a treated PCL scaffold onto the end of the wire and push the scaffold down to the mid-thigh area of one femoral artery using a 5 Fr straight XP Glide-catheter (Fig. 2a).
11. Use the same technique and place a control scaffold in a similar position of the contralateral femoral artery (Fig. 2b).

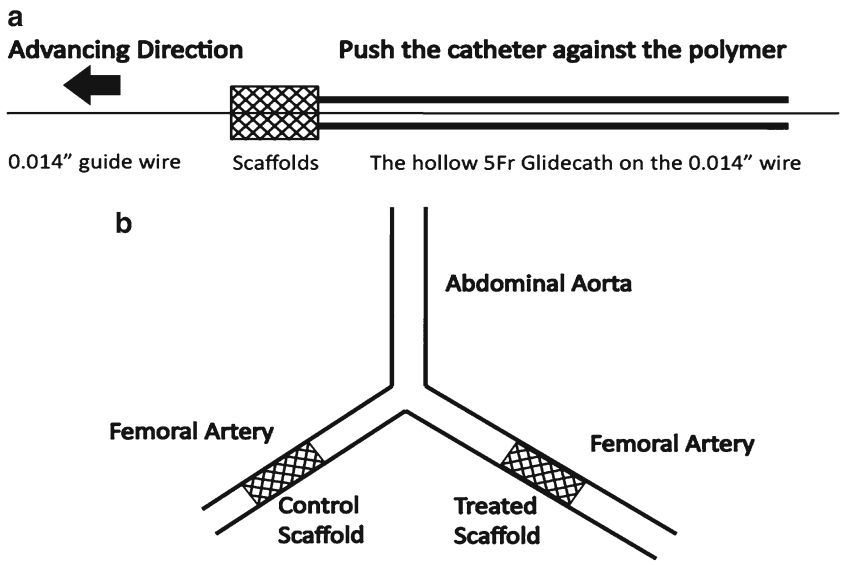

Fig. 2. (**a**) Schematic description of scaffold delivery to create chronic total occlusion (CTO) in a rabbit femoral artery. (**b**) Location of CTO sites in targeted femoral arteries (13). Reproduced by permission of John Wiley & Sons, Inc.

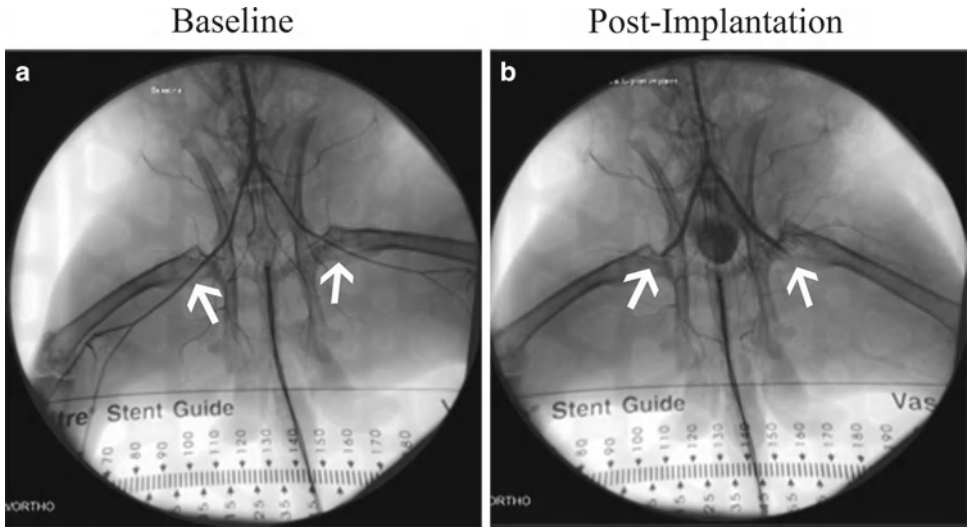

Fig. 3. Angiogram of both left and right femoral arteries before implantation: baseline (**a**), and after implantation of scaffolds (**b**) from the same animal (13). Reproduced by permission of John Wiley & Sons, Inc.

12. Perform a postscaffold implantation angiogram immediately.
13. Document the deployment of the constructs and verify the percentage occlusion of the vessels (Fig. 3).
14. Remove the catheter and the wire.
15. Ligate the right carotid artery with 4-0 silk suture.

16. Use a 3-0 absorbable suture to close incision in two layers.
17. Allow rabbits to recover and monitor their health until the end study days of 10 and 28.

3.5. Harvest of Femoral Arteries

1. Sedate the rabbit and intubate it as stated in Sect. 1.4 step 1 (13).
2. Make an abdominal incision and isolate the abdominal aorta.
3. Place a 5 Fr introducer sheath inside the vessel.
4. Perform an angiography to document the percentage occlusion of both femoral arteries at day 10 and day 28 time points.
5. Euthanize the rabbits while they are still under anesthesia.
6. Flush femoral arteries with saline.
7. Excise the arteries.

3.6. Tissue Preservation

1. Fix femoral arteries in 10% neutral buffered formalin for 24 h.
2. Cut arteries cross-sectionally into small tubes.
3. Embed artery segments in Tissue-Tek OCT compound.
4. Cut sections in 60 μM thickness using a Leica cryostat (Note 10).
5. Mount tissue onto silane-coated microscope slides.

3.7. Detection of Calcium Element in CTO

1. Wash tissue on slides with Ca^{2+} free PBS gently using transfer pipets.
2. Place slides flat in chemical hood and air-dry them overnight.
3. Examine the dry specimen using a scanning electron microscope equipped with an energy-dispersive X-ray Spectroscopy (EDS) detector (EDAX Apollox system).
4. CTO specimen containing calcium elements will show a signal peak at 3.8 kev range (Fig. 4).

3.8. Fluorescent Imaging of Calcium and Cell Nuclei

1. Circle the staining area on slides using a microscope slide marker, and perform the staining when slides are in horizontal position.
2. Wash tissue on slides three times in PBS.
3. Use Osteo Image mineralization assay to stain calcium deposits.
4. Dilute wash buffer 1:10 in de-ionized water.
5. Wash slides twice with 1× wash buffer.
6. Dilute staining reagent 1:100 in staining reagent dilution buffer.
7. Add fresh ddH_2O and incubate on slides for another 5 min.
8. Add 200 μl diluted sterilizing reagent to each slide.

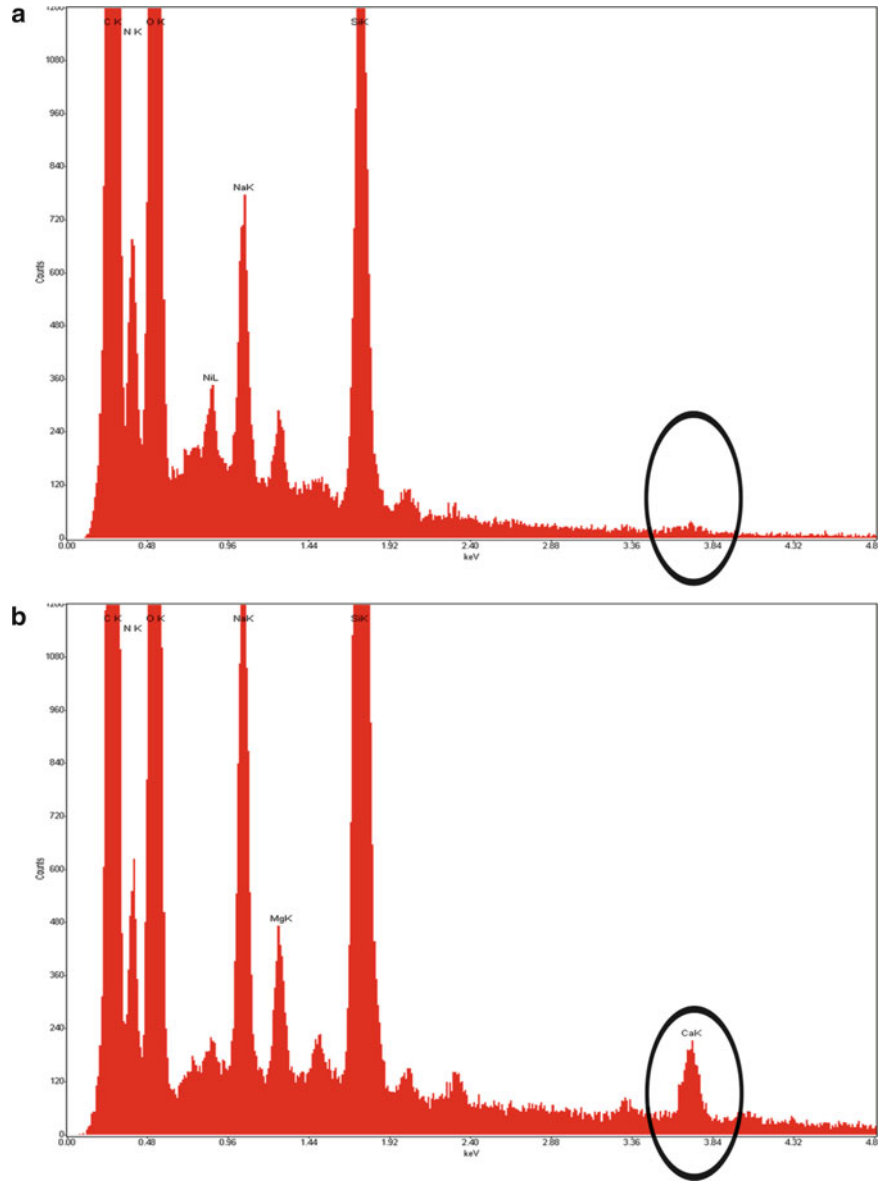

Fig. 4. EDS profile of chronic total occlusion (CTO) arteries at day 28 with control scaffolds (**a**), and treated scaffolds (**b**) (13). Reproduced by permission of John Wiley & Sons, Inc.

9. Incubate slides in dark for 30 min at room temperature.
10. Aspirate staining reagent using a transfer pipette.
11. Wash slides gently three times with wash buffer.
12. Counterstain cell nuclei with DAPI.
13. Mount slides with mounting medium.
14. View slides under the FITC channel for calcium and DAPI channel for cell nuclei using a confocal microscope (Fig. 5).

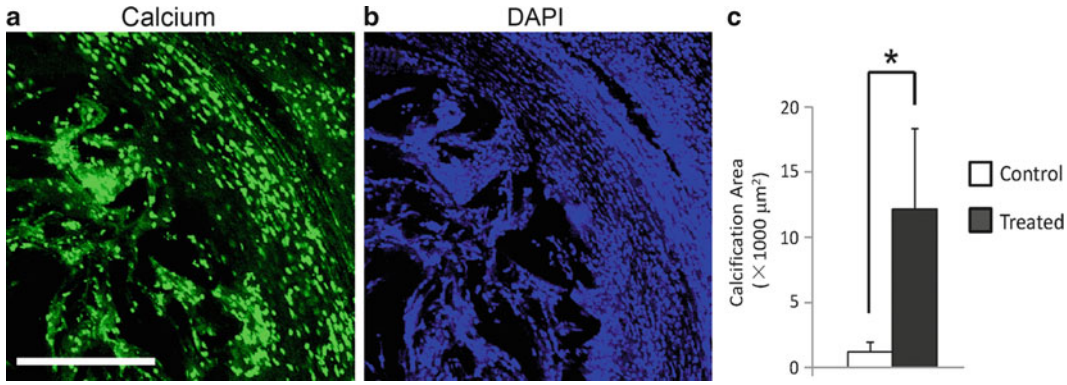

Fig. 5. Stains for calcium (*green fluorescence*) at chronic total occlusion (CTO) sites of rabbit femoral arteries with scaffold implantation at 10 days (**a**). Nuclei were counterstained with DAPI (*blue fluorescence*) from the same location (**b**). Scale bar was 250 μm. (**c**) Quantitative area of calcium deposits in treated and control CTO sites at 10 days (*$p<0.05$) (13). Reproduced by permission of John Wiley & Sons, Inc.

3.9. Hematoxylin and Eosin Staining

1. Take out slides from freezer to room temperature and wait 10 min for slides to dry.
2. Circle the staining area on slides using a microscope slide marker, and perform the staining when slides are in horizontal position.
3. Incubate slides with ddH_2O for 5 min.
4. Suck out H_2O on slides using a transfer pipette.
5. Add fresh ddH_2O and incubate on slides for another 5 min.
6. Remove H_2O from slides using a transfer pipette.
7. Stain slides with hematoxylin solution for 2 min.
8. Wash slides twice with H_2O, 5 min incubation each time (Note 11).
9. Stain tissue with 0.1% sodium bicarbonate (bluing agent; 0.05 g sodium bicarbonate in 50 ml ddH_2O) for 30 s, and no more than 30 s.
10. Incubate slides with 70% ethanol for 2 min and then remove the solution.
11. Incubate slides with 90% ethanol for 2 min and remove the solution.
12. Incubate slides with 95% ethanol for 2 min and remove the solution.
13. Stain tissue sections with 1% Eosin Y solution for 2 min.
14. Rinse slides with ddH_2O twice, 10 s for each time.
15. Air-dry the slides.
16. Mount slides with aqueous mounting media (Note 12).
17. Image slides under a light microscope (Figs. 6 and 7).

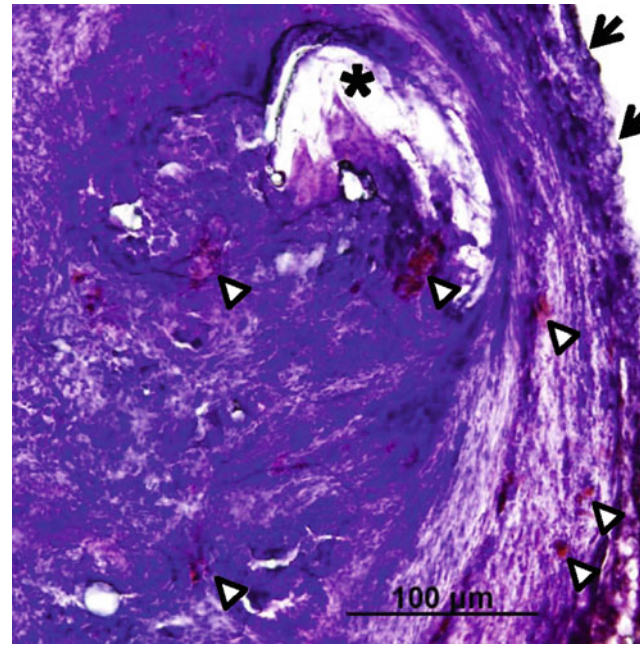

Fig. 6. Recanalization, the new blood formation in control and treated CTO sites at 28 days using hematoxylin–eosin staining. *Arrow heads* point to the small new blood vessels, and *asterisks* show the location of scaffolds. *Arrows* identify the elastic lamina of arteries (13). Reproduced by permission of John Wiley & Sons, Inc.

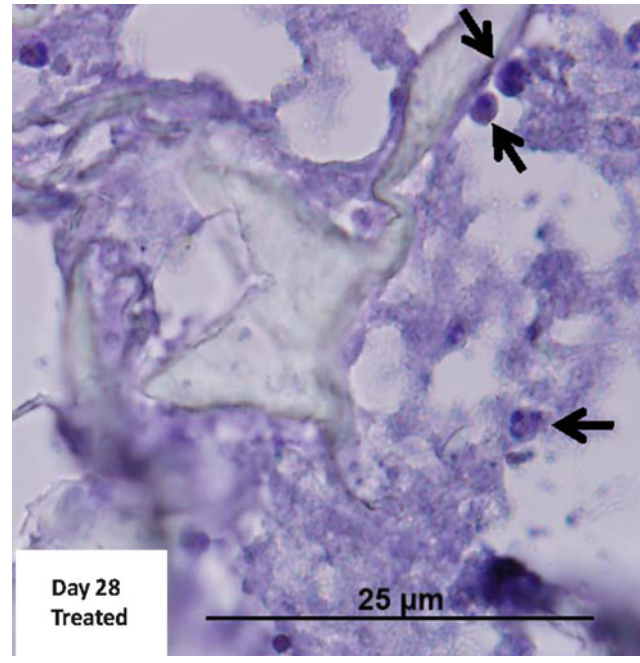

Fig. 7. Acute and chronic inflammatory response in control and treated CTO sites at 28 days using hematoxylin–eosin staining. *Arrows* point to leukocytes, and *arrow heads* show lymphocytes (13). Reproduced by permission of John Wiley & Sons, Inc.

4. Notes

1. All the experimental procedures should be performed under sterile conditions.
2. It is essential to vortex the polymer and salt mixture continuously at a speed that the top of the solution vigorously moves throughout the whole process. Vortexing is critical to make NaCl particles distribute evenly inside the polymer solution. The resulting scaffolds yield evenly distributed pores.
3. Adding the last set of salt is very important to achieve good quality scaffolds. If polymer solution is still very wet after the last addition of salt (3.5 g) has been added, pour another 3.5 g NaCl into the mold to see if that can dry the solution out. However, by doing so, you increase the length of your scaffolds and make them difficult to punch out in the follow-up steps. If polymer solution is already dry before the last set of salt has been added, drop an additional 0.5–1 ml dichloromethane into the mold and vortex continuously. Repeat step 7.
4. The inner diameter of the metal circular punch determines the diameter of scaffolds. The rim at the tip of the punch should be sharpened so that extraction process can be easy.
5. All steps in this section should be performed in biological hoods.
6. Scaffolds should all sink to the bottom of the wells after the addition of fibronectin solution. If some of them still float, that means the majority of the pores in that scaffold is not penetrated by fibronectin and they should not be used for the follow-up experiments.
7. PCL is hydrophobic by nature and does not favor the attachment of cells. Fibronectin acts as a glue to bind both TGF-β1 and cells onto the scaffolds.
8. Aliquote stock TGF-β1 to the amount needed for each experiment and store them at −80°C. Avoid repeated freeze thawing cycles.
9. The weight of rabbits need to be in the range of 4.5–5 kg or larger. A 5 Fr catheter cannot fit in the femoral arteries of rabbits that are less than 3 kg in weight.
10. Sections must be 60 μm or thicker to maintain the integrity of OCT sites. Slides thinner than 60 μm will experience hollow defects in the area of scaffold cross-sections. It is key to the success of the following staining and calcium detection experiments.

11. It is suggested to test different incubation time and concentration of hematoxyline and eosin used to achieve a good balance of blue and pink color for good imaging effect.
12. Only aqueous mounting media can be used. Polycaprolactone (PCL) is soluble in some organic solvents including xylene, and thus organic solvents must be eliminated through the whole process of staining.

References

1. Shamoun F, Sural N, Abela G (2008) Peripheral artery disease: therapeutic advances. Expert Rev Cardiovasc Ther 6(4):539–553
2. Soon KH, Selvanayagam JB, Cox N, Kelly AM, Bell KW et al (2007) Percutaneous revascularization of chronic total occlusions: review of the role of invasive and non-invasive imaging modalities. Int J Cardiol 116(1):1–6
3. Cabrera R, Sha Z, Vadakkan TJ, Otero J, Kriegenburg F et al (2010) Proteasome nuclear import mediated by Arc3 can influence efficient DNA damage repair and mitosis in *Schizosaccharomyces pombe*. Mol Biol Cell 21(18):3125–3136
4. Sha Z, Brill LM, Cabrera R, Kleifeld O, Scheliga JS et al (2009) The eIF3 interactome reveals the translasome, a supercomplex linking protein synthesis and degradation machineries. Mol Cell 36(1):141–152
5. Sha Z, Yen HC, Scheel H, Suo J, Hofmann K et al (2007) Isolation of the Schizosaccharomyces pombe proteasome subunit Rpn7 and a structure-function study of the proteasome-COP9-initiation factor domain. J Biol Chem 282(44):32414–32423
6. Giachelli CM (2004) Vascular calcification mechanisms. J Am Soc Nephrol 15(12): 2959–2964
7. Montecucco F, Steffens S, Mach F (2007) The immune response is involved in atherosclerotic plaque calcification: could the RANKL/RANK/OPG system be a marker of plaque instability? Clin Dev Immunol 2007:75805
8. Bhambhani A, Gadkar N, Cook S (2007) Intravascular ultrasound guided percutaneous coronary intervention for chronic toal occlusion of left anterior descending artery. Kardiovaskulare Medizin 10:78–80
9. Radke PW, Heinl-Green A, Frass OM, Post MJ, Sato K et al (2006) Evaluation of the porcine ameroid constrictor model of myocardial ischemia for therapeutic angiogenesis studies. Endothelium 13(1):25–33
10. Segev A, Nili N, Qiang B, Charron T, Butany J et al (2005) Human-grade purified collagenase for the treatment of experimental arterial chronic total occlusion. Cardiovasc Revasc Med 6(2):65–69
11. Suzuki Y, Oyane A, Ikeno F, Lyons JK, Yeung AC (2009) Development of animal model for calcified chronic total occlusion. Catheter Cardiovasc Interv 74(3):468–475
12. Suzuki K, Saito N, Zhang G, Conditt G, McGregor J et al (2008) Development of a novel calcified total occlusion model in porcine coronary arteries. J Invasive Cardiol 20(6): 296–301
13. Zhu B, Bailey SR, Elliott J, Li X, Escobar GP et al (2012) Development of a total atherosclerotic occlusion with cell-mediated calcium deposits in a rabbit femoral artery using tissue-engineering scaffolds. J Tissue Eng Regen Med 6(3):193–204. doi:10.1002/term.413
14. Jones JR, Tsigkou O, Coates EE, Stevens MM, Polak JM et al (2007) Extracellular matrix formation and mineralization on a phosphate-free porous bioactive glass scaffold using primary human osteoblast (HOB) cells. Biomaterials 28(9):1653–1663
15. Eichner A, Brock J, Heldin CH, Souchelnytskyi S (2002) Bone morphogenetic protein-7 (OP1) and transforming growth factor-beta1 modulate 1,25(OH)2-vitamin D3-induced differentiation of human osteoblasts. Exp Cell Res 275(1):132–142
16. Jorgensen NR, Henriksen Z, Sorensen OH, Civitelli R (2004) Dexamethasone, BMP-2, and 1,25-dihydroxyvitamin D enhance a more differentiated osteoblast phenotype: validation of an in vitro model for human bone marrow-derived primary osteoblasts. Steroids 69(4):219–226
17. Lecanda F, Avioli LV, Cheng SL (1997) Regulation of bone matrix protein expression and induction of differentiation of human osteoblasts and human bone marrow stromal cells by bone morphogenetic protein-2. J Cell Biochem 67(3):386–396
18. Gordeladze JO, Drevon CA, Syversen U, Reseland JE (2002) Leptin stimulates human osteoblastic cell proliferation, de novo collagen

synthesis, and mineralization: impact on differentiation markers, apoptosis, and osteoclastic signaling. J Cell Biochem 85(4):825–836

19. Zhang H, Ahmad M, Gronowicz G (2003) Effects of transforming growth factor-beta 1 (TGF-beta1) on in vitro mineralization of human osteoblasts on implant materials. Biomaterials 24(12):2013–2020
20. Zhang H, Aronow MS, Gronowicz GA (2005) Transforming growth factor-beta 1 (TGF-beta1) prevents the age-dependent decrease in bone formation in human osteoblast/implant cultures. J Biomed Mater Res A 75(1):98–105
21. Zhu B, Bailey SR, Mauli Agrawal C (2011) Engineering calcium deposits on polycaprolactone scaffolds for intravascular applications using primary human osteoblasts. J Tissue Eng Regen Med 5(4):324–336
22. Ciapetti G, Ambrosio L, Savarino L, Granchi D, Cenni E et al (2003) Osteoblast growth and function in porous poly epsilon -caprolactone matrices for bone repair: a preliminary study. Biomaterials 24(21):3815–3824
23. Chim H, Ong JL, Schantz JT, Hutmacher DW, Agrawal CM (2003) Efficacy of glow discharge gas plasma treatment as a surface modification process for three-dimensional poly (D, L-lactide) scaffolds. J Biomed Mater Res A 65(3):327–335
24. Zhu B, Bailey SR, Mauli Agrawal C (2011) Calcification of primary human osteoblast cultures under flow conditions using polycaprolactone scaffolds for intravascular applications. J Tissue Eng Regen Med. doi: 10.1002/term.472
25. Lin J, Lindsey ML, Zhu B, Agrawal CM, Bailey SR (2007) Effects of surface-modified scaffolds on the growth and differentiation of mouse adipose-derived stromal cells. J Tissue Eng Regen Med 1(3):211–217

Chapter 5

Models of Hypertension and Blood Pressure Recording

Luciana Aparecida Campos and Ovidiu Constantin Baltatu

Abstract

Hypertension and cardiovascular events continue to constitute the leading global diseases affecting around 20% of the world's population. Although there have been significant advances in the treatment and prevention of these diseases, important efforts are being made aiming at deciphering the outstanding issues in the areas of cardiovascular physiology and pathology, positively impacting the development of new strategies applied to the diagnosis and treatment of hypertension. In this search, many animal models of disease have been developed and are currently being employed, demonstrating a most valuable tool in understanding the biological bases of the disease.

Key words: Hypertension, Experimental model, Blood pressure monitoring, End-organ damage

1. Introduction

Hypertension is not a modern phenomenon. Although blood pressure was first measured in a dying mare in 1733 by Stephen Hales, it was not until 1950s, when the first articles on the disease started to appear, that we became aware of the relationship between high blood pressure and cardiovascular diseases that continue to constitute up-to-date the leading global diseases affecting about 20% of the world's population (1).

There was a longstanding theory that body pressor substances caused hypertension due to their actions on the peripheral blood vessels. The substance or its site of synthesis was yet to be discovered. It was only in 1898 that a substance called renin was discovered by Robert Tigerstedt and Bergman, his pupil. Their basic hypothesis was that "…a blood-pressure raising substance is formed in the kidneys and passed into the blood." (2). To test this hypothesis, they homogenized fresh rabbit kidney in saline, centrifuged it, and then injected the supernatant fluid into other rabbits. The

Arpad Szallasi and Tamás Bíró (eds.), *TRP Channels in Drug Discovery: Volume II*, Methods in Pharmacology and Toxicology, DOI 10.1007/978-1-62703-095-3_5, © Springer Science+Business Media, LLC 2012

outcome was that the injections resulted in an increase in blood pressure in the recipient rabbits. Their experiments did not stop there. Through various other experiments, Tigerstedt and Bergman demonstrated that the pressor substance, discovered and named by the authors as renin, was water soluble and heat labile, all of which pointed renin as being a protein. Also, they showed that renin could only be extracted from renal cortex and renal venous blood, and that the pressor action appeared to be mediated by an effect on vascular smooth muscle, although not necessarily a direct effect.

Hypertension became known when Harry Goldblatt established renovascular hypertension in the 1930s by clipping the renal artery of a dog and producing, thus, the first animal model of secondary form of hypertension (3). Since then, many attempts have been performed to develop experimental nongenetic and genetic models of hypertension targeting the system.

Over the past 60 years various animal models of hypertension have been developed, mainly rats. In this chapter we will summarize the most frequently used experimental animal models of hypertension with its predominant characteristic phenotypes, mentioning strains of animals other than rats used as models of hypertension. Recent articles on hypertension can be reviewed (2, 4–8).

An animal model of hypertension should fulfill the following criteria:

1. It should have persistently elevated levels of arterial pressure comparable to human hypertension.
2. It should have functional injury and pathology correlating to a clinical scenario.
3. It should be reproducible between and among experiments.
4. It should be a simple and cost-effective model for pharmaceutical development.
5. It should allow cross-over testing of a series of compounds.

The most used experimental species is the rat due to the extensive characterization of its cardiovascular physiology which has many similarities with the human one, ease to breed and reproduce, and cost-effective. Transgenic rats have been developed to target specific genes of regulatory systems in order to progress our understanding on cardiovascular system. Knockout mice have been also developed and recognized as useful for cardiovascular pathophysiology, although cardiovascular phenotyping has been proven to be more challenging. Large animal species such as dogs, pigs, and monkeys are also used to produce experimental hypertension. However, breeding and costs made such large animals not suitable for routine testing.

Various models of hypertension are utilized to study different human forms of hypertension. The mostly utilized model for human essential hypertension is the spontaneously hypertensive rat that does not have a known cause of hypertension. Several other models have been developed and employed (Table 1) to progress

Table 1
The most common models of hypertension and their phenotypes

Animal models	Main phenotype
Renovascular hypertension 2K1C or 1K1C (Goldblatt hypertension) (9) Renal artery clipped/mechanic type of hypertension in rabbits, dogs, pigs, monkeys, mice, and rats. Clipping one renal artery and preserving both kidneys (two-kidney one-clip model—2K1C) or removing the contralateral one (one-kidney one-clip—1K1C) leads to hypertension that develops progressively and reaches around 180 mmHg systolic 3 weeks after surgery	Cardiac hypertrophy (50%) Renal hemodynamic and excretory alterations, particularly in the nonclipped kidney: – In 2K1C plasma renin activity is increased; there is no salt and water retention because of the other normal kidney that is intact – In 1K1C plasma renin activity is normal and rapid salt and water retention because of no pressure diuresis and natriuresis
Pharmacological models for systemic hypertension—endocrine etiology	
Angiotensin II-Induced Hypertension (10) Infused doses of Ang II of 50–250 ng/kg per minute subcutaneously, which do not produce direct vasoconstriction are described as "subpressor" or "slow pressor" and can induce a gradual increase of blood pressure in days to weeks. It is a model of renovascular hypertension with low plasma renin activity	Cardiac hypertrophy and fibrosis Inversion of circadian rhythm of blood pressure in rats (model of nondipper hypertension)
DOCA–salt—endocrine hypertension (11) The administration for at least 6 weeks of 10–20 mg/kg/week DOCA (deoxycorticosterone acetate) subcutaneously in combination with a drinking saline (0,9.2% NaCl) and with unilateral nephrectomy induces a low renin form of hypertension in rats, mice, dogs, and pigs	Cardiac hypertrophy (30%, with no cardiac failure) Impaired renal function—proteinuria, glomerulosclerosis Impaired endothelium-dependent vascular relaxation.
L-NAME-induced hypertension (12) L-NAME (NG-nitro-l-arginine methyl ester) given at 20–40 mg/kg body weight, intraperitoneally or orally decreases NO production leading to hypertension in rats, dogs, and pigs	Hypertension of about 180 mmHg systolic; most of in-life studies are investigating pathophysiology and treatment at 4 weeks Early generalized impairment of endothelial function Progressive kidney damage (proteinuria, intrarenal vascular, tubular and glomerular lesions)
Genetic models for systemic hypertension	
Spontaneously Hypertensive Rats (SHR) (13) Selective inbreeding of Wistar Kyoto (WKY) rats with the highest blood pressure. It is the most commonly used animal model of primary (essential) hypertension. Hypertension starts at 5–6 weeks of age and the systolic pressure may reach 180–200 mmHg in the adult, depending on strain and gender	Cardiac hypertrophy (30%, with normal cardiac output) and increased total peripheral resistance Impaired endothelium-dependent vascular relaxation After 24 months of age, may develop manifest heart failure

(continued)

Table 1 (continued)

Animal models	Main phenotype
SHR Stroke Prone (SHR-SP) (14) It is a substrain of SHR that develop cerebrovascular lesions spontaneously in over 80% of rats	Tendency to die from cerebrovascular, i.e., stroke and renal lesions
Milan Hypertensive rat (MHS) (15) Breeding of a hypertensive rat strain that develops alterations in renal sodium and water metabolism with consequent hypertension.	1. Hypertension develops at 8 weeks of age and reaches systolic levels of 160-175 mmHg at 10 weeks of age 2. Cardiac hypertrophy (10%) 3. Increased renal sodium reabsorption
Lyon Hypertensive Rats (16) Lyon Hypertensive (LH/Mav) rats obtained through selective breeding have spontaneous and salt-sensitive hypertension in comparison with the normotensive control LN (Lyon Normotensive), the high genetic similarity between these two strains, simultaneously selected from the same colony of outbred Sprague-Dawley	Hypertension develops at 6 weeks of age, reaching levels of 175 mmHg systolic at adult age; salt diet further increase blood pressure Renal damage (exaggerated proteinuria) High body weight Hyperlipidemia Elevated insulin-to-glucose ratio
New Zealand genetically Hypertensive rats (17) New Zealand genetically hypertensive (NZGH) rat was derived from the same Wistar background as the SHR. The NZGH rat has similar time course in the development of hypertension as the SHR	Hypertension develops early after birth reaching systolic arterial pressure of more than 200 mmHg at 10 weeks of age Elevated left ventricular mass Alterations in hemodynamics and vascular reactivity Increased renal afferent arteriole
Dahl-rat—genetic hypertension (18) Dahl salt-sensitive (DS) and salt-resistant (DR) inbred rat strains with 8% NaCl diet develop hypertension (>140 mmHg systolic arterial pressure) On 8% NaCI diet, DS rats develop fulminant hypertension and marked vascular and renal lesions after 3–4 weeks and die within 8 weeks. In contrast, DR rats on 8% NaCI diet develop hypertension and associated vascular and renal lesions in 3–4 months	Hypertension develops with salt diet with systolic arterial pressure levels of about 185 mmHg Cardiac hypertrophy with subsequent severe heart failure Renal damage (severe and early proteinuria) Impaired endothelium-dependent vascular relaxation
Sabra rat (19) Sabra salt-sensitive rat (SBH/y) in contrast to the resistant SBN/y rat becomes hypertensive under a high-salt diet (1% NaCl in drinking water) and DOCA (subcutaneous 25-mg DOCA tablet) in 3 weeks	Hypertension develops with values above 200 mmHg systolic blood pressure Model used to study the genetics of salt sensitivity
Transgenic models for hypertension—models of hypertension with a defined genetic cause	
TGR (mRen 2)27 (20) Transgenic rat carrying the mouse renin Ren-2d as transgene. It develops fulminant hypertension at an early age and end-organ damage similarly to human malignant phase hypertension. Homozygote rats die at 2 months of age	Cardiac hypertrophy (40%) and fibrosis Renal damage (proteinuria, structural changes) Impaired endothelial-dependent relaxations

(continued)

Table 1
(continued)

Animal models	Main phenotype
Human Renin—Human Angiotensinogen Double Transgenic Rats (21) Breeding of transgenic human renin female TGR(hREN) with transgenic angiotensinogen male TGR(hAOGEN), double-transgenic rats (dTGR) expressing human renin and angiotensinogen are generated	Fulminant hypertension followed by overt organ damage of heart and kidney comparable to malignant hypertensive patients Early mortality
Transgenic rats with inducible renin expression (22) The same mouse Ren-2 gene has been used to generate a transgenic rat with inducible hypertension under the transcriptional control of the cytochrome P450, Cyp1a1 promoter, which can be induced by treating the animals with indole-3 carbinol, a xenobiotic drug	Vessel wall changes in peripheral tissues—kidney, heart, and mesentery—with medial thickening and fibrinoid necrosis Multiple small hemorrhagic lesions Stroke lesions with 0.9% saline in addition to drinking water
TGM(rAOGEN)123 (23) Overexpression of the rat angiotensinogen gene in mice leads to hypertension	Cardiac hypertrophy and fibrosis Renal dysfunction, albuminuria, and fibrosis
Mice lacking Atrial Natriuretic Peptide (ANP) (24) Disruption of the proANP gene in homozygous mutants leads to no circulating of atrial ANP and hypertension, and in heterozygotes leads to normal circulating ANP levels and normal blood pressure	Develop hypertension when fed a high salt diet
Mice lacking the guanylyl cyclase-A receptor for atrial natriuretic peptide (25) Mice lacking a functional Npr1 gene coding for natriuretic peptide receptor A have hypertension. Described as a model of resistant to salt (blood pressure does not change by more than 5 mm Hg when salt intake is high)	Cardiac hypertrophy Mice may die through congestive heart failure or aortic dissection
Mice lacking the proatrial natriuretic peptide convertase corin (26) Corin-deficient ($Cor^{-/-}$) mice have spontaneous hypertension, which is enhanced with dietary salt loading	Cardiac hypertrophy Pregnant $Cor^{-/-}$ mice demonstrate late-gestation proteinuria and enhanced high blood pressure during pregnancy
eNOS mutant mice (27) Knockout mice homozygous but not heterozygous for disruption of the gene endothelial nitric oxide synthase ($eNOS^{-/-}$) mice develop mild hypertension	Increase in wall thickness Abnormal microvascular density

Besides experimental hypertension induced through surgical and/or pharmacological manipulation of experimental animal, there are also models obtained through transgenic manipulations or selective inbreeding. The most characterized experimental animal models of hypertension with their main phenotype are presented in the table above

our understanding on numerous forms of human secondary hypertension of a known cause. Experimental hypertension can be achieved through:

1. Surgical and/or pharmacological manipulation of experimental animal.
2. Genetic manipulation by targeting a specific gene of interest through the stimulation, inhibition, or ablation (knock out) of its synthesis.
3. Selective inbreeding of hypertensive animals.

2. Materials

2.1. Renovascular Hypertension 2K1C or 1K1C (Goldblatt Hypertension)

1. Rats weighing from 120 to 200 g are used.
2. U-shaped silver ribbon clip or with 4-0 silk suture.

2.2. Angiotensin II-Induced Hypertension

1. Adult rats at least 3 months old are used.
2. Osmotic minipumps (Alzet, Alza Corp, St. Paul, MN) with different infusion and duration rates are utilized, depending of the intended duration of the angiotensin II administration.
3. Angiotensin II (Sigma-Aldrich, St. Louis, MO) is dissolved in 0.9% saline at a concentration calculated to allow the desired infusion rate (i.e., of 50–250 ng Ang II per kilogram per minute).

2.3. DOCA–Salt-Induced Endocrine Hypertension

1. Deoxycorticosterone acetate, DOCA (Sigma-Aldrich).

3. Methods

3.1. Renovascular Hypertension 2K1C or 1K1C (Goldblatt Hypertension)

Clipping one renal artery and preserving both kidneys (two-kidney one-clip model—2K1C) or removing the contralateral one (one-kidney one-clip—1K1C) leads to hypertension.

1. Induce anesthesia with a commonly used anesthetic such as 36 mg/kg body weight of 3% sodium pentobarbital intraperitoneally (Note 1).
2. Make a median longitudinal incision in the abdominal wall.

3. The left renal artery is reached through the median abdominal incision and constricted with a U-shaped silver ribbon clip or with 4-0 silk suture; constriction of renal artery should be more than 50% (Note 2).
4. Close the abdominal incision at muscle and then skin layers with silk sutures.
5. The experimental model is considered successful if hypertensive with systolic BP more than 160 mmHg for 2 consecutive days after 4 weeks of ligation.

3.2. Angiotensin II-Induced Hypertension

Chronic infusion of angiotensin II at doses which do not produce an acute increase in blood pressure leads to hypertension.

1. Fill the minipumps with the angiotensin II solution following the Alzet instructions for filling procedure (Note 3).
2. Rats are anaesthetized with ether.
3. A subcutaneous tunneling is made with a bunt-tip forceps through a 1.5 cm incision in the retroscapular area and the minipumps filled with the angiotensin II solution are implanted subcutaneously.

3.3. DOCA–Salt-Induced Endocrine Hypertension

Administration of deoxycorticosterone acetate (DOCA) to uninephrectomized rats receiving drinking water containing 1% NaCl causes endocrine hypertension resulting from hypervolemia and high salt intake.

1. Rats are anesthetized (i.e., with pentobarbital sodium—60 mg/kg ip).
2. An incision in the left flank of the lumbar region is performed.
3. The left kidney is exposed from the perirenal fat (Note 4).
4. The renal pedicle is isolated, two ligatures are tied on it and thereafter it is sectioned distally from the ligatures and the left kidney is removed.
5. The DOCA pellet is placed through the incision in a subcutaneous tunneling made with surgical forceps with blunt tip (Note 5).
6. The incision wound is closed with surgical clippers or silk sutures.

3.4. Methods for Blood Pressure Measurements

3.4.1. Indirect Measurements: The Oscillometric Method

It uses the same principle of oscillometric determinations of arterial pressure in humans. This method can be used in large animals (dogs, rabbits) by placing the cuff on forelimb (radial artery) or hindlimb (tibial artery), or in small animals (rats, mice) by placing the cuff on tail (tail artery). The cuff connected to a sphygmomanometer or pressure transducer is inflated above the systolic pressure and then deflated. When cuff is deflated pulsations start

appearing when pressure in the cuff equals systolic pressure. This method affects heart rate, stress hormones, and consequently, blood pressure due to the stress imposed to the restrained animal.

3.4.2. Direct Measurements: Intra-arterial Cannulation

A catheter is implanted in carotid or femoral artery and exteriorized through a tunneling under the skin. The catheter is filled with 1% heparin in normal saline and connected to a pressure transducer and then to the preamplifier and recorded on the polygraph or physiography. Although more reliable, it has many drawbacks and limitations, such as easy blockage of the system by blood clots, and decreased blood flow to the brain and to inferior limbs, with catheter placed in jugular and femoral arteries, respectively.

3.4.3. Direct Measurements: Intra-arterial Cannulation and Telemetry Recordings

Telemetry is the actual gold standard for blood pressure measurement chronically for weeks or months. The blood pressure transmitter has an intra-arterial catheter and a wireless transmitter. A receiver with data acquisition system allows continuous monitoring of blood pressure in conscious and unrestrained animals that have implanted the telemetry transmitter.

4. Notes

1. In order to achieve a proper experimental group of rats, 2K1C/1K1C should be induced in a number of animals at least double of the targeted group number, since only 45–50% develop stable hypertension.
2. To produce the 1K1C model, the left kidney is exposed from the perirenal fat; the renal pedicle is isolated, two ligatures are tied on it and thereafter it is sectioned distally from the ligatures and the left kidney is removed.
3. The most important step is the filling of the minipumps—the pump should be filled completely with drug solution and no air bubbles should be allowed to be trapped within the body of the pump; handle with gloves to avoid deposition of skin oils.
4. When exposing the kidney from the perirenal fat care should be taken not to remove the adrenal gland besides the kidney.
5. A mild DOCA-salt hypertension model that might allow studying mechanisms that serve as a primary cause of hypertension development has been recently described by Kandlikar and Fink (28). In this model, no nephrectomy is performed and a lower dose of DOCA is used in rats receiving drinking water containing 1% NaCl and 0.2% KCl to induce an increase of blood pressure of about 20 mmHg.

References

1. Ezzati M, Lopez AD, Rodgers A, Vander Hoorn S, Murray CJ (2002) Selected major risk factors and global and regional burden of disease. Lancet 360:1347–1360
2. Phillips MI, Schmidt-Ott KM (1999) The discovery of Renin 100 years ago. News Physiol Sci 14:271–274
3. Goldblatt H, Weinstein H, Kahn JR (1941) Studies on experimental hypertension: Xiv. The effect of intermittent renal arterial occlusion on the blood pressure of the dog. J Exp Med 73:439–451
4. Pinto YM, Paul M, Ganten D (1998) Lessons from rat models of hypertension: from Goldblatt to genetic engineering. Cardiovasc Res 39:77–88
5. Bader M (2010) Rat models of cardiovascular diseases. Methods Mol Biol 597:403–414
6. Osborn JW, Fink GD (2010) Region-specific changes in sympathetic nerve activity in angiotensin II-salt hypertension in the rat. Exp Physiol 95:61–68
7. Hainsworth AH, Markus HS (2008) Do in vivo experimental models reflect human cerebral small vessel disease? A systematic review. J Cereb Blood Flow Metab 28:1877–1891
8. Yagil Y, Yagil C (1998) Genetic basis of salt-susceptibility in the Sabra rat model of hypertension. Kidney Int 53:1493–1500
9. Laragh JH (1991) On the mechanisms and clinical relevance of one-kidney, one-clip hypertension. Am J Hypertens 4:541S–545S
10. Simon G, Abraham G, Cserep G (1995) Pressor and subpressor angiotensin II administration. Two experimental models of hypertension. Am J Hypertens 8:645–650
11. Schenk J, McNeill JH (1992) The pathogenesis of DOCA-salt hypertension. J Pharmacol Toxicol Methods 27:161–170
12. Jover B, Mimran A (2001) Nitric oxide inhibition and renal alterations. J Cardiovasc Pharmacol 38(Suppl 2):S65–S70
13. Trippodo NC, Frohlich ED (1981) Similarities of genetic (spontaneous) hypertension. Man and rat. Circ Res 48:309–319
14. Okamoto K, Tabei R, Fukushima M, Nosaka S, Yamori Y (1966) Further observations of the development of a strain of spontaneously hypertensive rats. Jpn Circ J 30:703–716
15. Bianchi G, Ferrari P, Cusi D, Salardi S, Guidi E et al (1986) Genetic and experimental hypertension in the animal model-similarities and dissimilarities to the development of human hypertension. J Cardiovasc Pharmacol 8(Suppl 5):S64–S70
16. Julien C, Bertolino S, Medeiros IA, Barres C, Sassard J (1997) Renin secretion in Lyon hypertensive rats. Clin Exp Hypertens 19: 699–711
17. Ledingham JM, Laverty R (1998) Renal afferent arteriolar structure in the genetically hypertensive (GH) rat and the ability of losartan and enalapril to cause structural remodelling. J Hypertens 16:1945–1952
18. Rapp JP, Dene H (1985) Development and characteristics of inbred strains of Dahl salt-sensitive and salt-resistant rats. Hypertension 7:340–349
19. Yagil C, Katni G, Rubattu S, Stolpe C, Kreutz R et al (1996) Development, genotype and phenotype of a new colony of the Sabra hypertension prone (SBH/y) and resistant (SBN/y) rat model of slat sensitivity and resistance. J Hypertens 14:1175–1182
20. Mullins JJ, Peters J, Ganten D (1990) Fulminant hypertension in transgenic rats harbouring the mouse Ren-2 gene. Nature 344:541–544
21. Ganten D, Wagner J, Zeh K, Bader M, Michel JB et al (1992) Species specificity of renin kinetics in transgenic rats harboring the human renin and angiotensinogen genes. Proc Natl Acad Sci USA 89:7806–7810
22. Kantachuvesiri S, Fleming S, Peters J, Peters B, Brooker G et al (2001) Controlled hypertension, a transgenic toggle switch reveals differential mechanisms underlying vascular disease. J Biol Chem 276:36727–36733
23. Kimura S, Mullins JJ, Bunnemann B, Metzger R, Hilgenfeldt U et al (1992) High blood pressure in transgenic mice carrying the rat angiotensinogen gene. EMBO J 11:821–827
24. John SW, Krege JH, Oliver PM, Hagaman JR, Hodgin JB et al (1995) Genetic decreases in atrial natriuretic peptide and salt-sensitive hypertension. Science 267:679–681
25. Lopez MJ, Wong SK, Kishimoto I, Dubois S, Mach V et al (1995) Salt-resistant hypertension in mice lacking the guanylyl cyclase-A receptor for atrial natriuretic peptide. Nature 378:65–68
26. Chan JC, Knudson O, Wu F, Morser J, Dole WP et al (2005) Hypertension in mice lacking the proatrial natriuretic peptide convertase corin. Proc Natl Acad Sci USA 102:785–790
27. Shesely EG, Maeda N, Kim HS, Desai KM, Krege JH et al (1996) Elevated blood pressures in mice lacking endothelial nitric oxide synthase. Proc Natl Acad Sci USA 93:13176–13181
28. Kandlikar SS, Fink GD (2011) Mild DOCA-salt hypertension: sympathetic system and role of renal nerves. Am J Physiol Heart Circ Physiol 300:H1781–H1787

Chapter 6

Balloon Injury in Rats as a Model for Studying TRP Channel Contribution to Vascular Smooth Muscle Remodeling

Wei Zhang and Mohamed Trebak

Abstract

Many vascular occlusive diseases are characterized by endothelial dysfunction and phenotypic switch of vascular smooth muscle cell (VSMC) from quiescent contractile to proliferative migratory phenotypes. These cellular responses can be recapitulated and studied in vivo in animal models of vascular injury. A typical example is the balloon injury model which causes endothelial denudation and distending mural injury in the operated blood vessel wall. VSMCs respond to this vascular injury by enhanced proliferation and migration, neointimal growth, and subsequent vascular occlusion. In these protocols, a balloon catheter (a catheter with a tiny balloon at the tip) is inserted into a blood vessel (usually the carotid artery) lumen and then the balloon is inflated and dragged in the vessel in order to cause endothelial denudation and distending mural injury. Many ion channels, including isoforms of STIM/Orai and transient receptor potential (TRP) channels have showed altered expression during the process of VSMC phenotypic switch. The vascular injury model offers means to study the in vivo contribution of changes in expression of these ion channels to vascular occlusion. After injury, expression of TRP channels in injured vessel section can be altered positively or negatively by transducing these vessel sections with viral particles encoding either cDNA clones or shRNA constructs specific to a given ion channel.

Key words: Balloon angioplasty, Neointima, Smooth muscle remodeling, Rat carotid artery, Viral transduction, Ion channels

1. Introduction

Endothelial dysfunction and vascular smooth muscle cell (VSMC) proliferation/migration are involved in many vascular occlusive diseases (1–4). Animal models are experimental animals carrying diseases or disorders which in some aspects mimic certain human diseases. They are used for etiological study and potential drug screening. Animal models are either spontaneous or induced. The balloon injury model is a physically induced animal model, which

Arpad Szallasi and Tamás Bíró (eds.), *TRP Channels in Drug Discovery: Volume II*, Methods in Pharmacology and Toxicology,
DOI 10.1007/978-1-62703-095-3_6,

has been in use since 1983 (5–7). The distinguishing feature of this model is that it mimics the complications of a therapeutic procedure called angioplasty which is performed on patients to restore blood flow in an artery clogged by atherosclerotic plaque. Angioplasty is a clinically widespread procedure which crushes the atherosclerotic plaque in narrowed sections of an artery using a balloon that is guided by a catheter to the site of plaque deposit, and then inflated with water pressure 75–500 times the normal blood pressure. Mechanical stress caused by the inflated balloon crushes the plaque but also causes damages to the blood vessel wall, including partial loss of the endothelial layer and distending injury in the media layer. The loss of endothelial integrity exposes the media layer containing VSMCs to the blood and multiple stimuli it contains. Stimuli such as platelet-derived growth factor (PDGF) trigger VSMC to proliferate and migrate. These proliferative migratory VSMC will produce and secrete extracellular matrix proteins. VSMCs and extracellular matrix thus form a new mural structure called neointima, which occupies part of the vessel lumen and causes artery narrowing, blood flow reduction, and occlusion.

Rat is the most commonly used animal species for balloon injury model. The carotid artery is used as the target vessel of injury due to the easy access and minor pain or harm to the animal. There are two carotid arteries symmetrically located on the left and right side of trachea in the neck. Balloon injury is usually performed on the left one (left carotid artery), while the right one is used as an internal control. Local drug/gene delivery in the injured carotid artery wall is a tool for investigation of the molecular biological mechanism and potential therapeutic targets of VSMC proliferative disorders. Viruses encoding either cDNA clones or shRNA constructs specific to a given gene are administered in the vessel lumen right after balloon injury. These viral strategies are used to either express a protein (cDNA) that is thought beneficial or prevent the upregulation of a protein (shRNA) that is thought detrimental to vessel healing. Typically, these viral particles encode a marker such as the green fluorescent protein (GFP) under a separate promoter for visualization of extent of medial infection by the virus.

2. Materials

2.1. Animals

1. The use of rats for these experiments has to be reviewed and approved by the Institutional Animal Care and Use Committee (IACUC) or equivalent at the host institution's Animal Resource Facility. Such animal facility should be licensed by the US Department of Agriculture and the Division of

Laboratories and Research of the Department of Public Health of its corresponding State and should be accredited by the American Association for the Accreditation of Laboratory Animal Care. The most highly used and best characterized strain of rat for balloon injury model is Sprague–Dawley (SD rats).

2. Animals are fed with normal diet perioperatively. Male rats are preferred since the female hormone estrogen modulates neointima formation in response to balloon injury (8). Animal weights that have been mostly reported in literature are between 350 and 500 g. According to the authors' experience, the optimal size of SD rats for balloon injury is between 400 and 500 g. The fully grown animal has a carotid artery with large diameter and thick walls which allows the balloon catheter easy access into the vessel lumen and avoids severe damage to the blood vessel wall. Severe damage to the vessel will lead to blood leakage and thrombosis.

2.2. Preoperative Procedures: Solutions and Supplies

1. Povidone–Iodine scrub or other topical antiseptic/bactericide agent
2. Absolute alcohol

2.2.1. Solutions

3. Artificial Tears Ointment (Rugby Laboratories, Duluth, GA)
4. Anesthetic drugs (e.g. Ketamine + Xylazine) (Sigma-Aldrich, St. Louis, MO)

2.2.2. Supplies

1. Autoclave
2. Hair remover
3. Sterile cover sheet (surgical blanket)
4. Heat pad (Braintree Scientific, Inc., Braintree, MA) or alternative heating source
5. Lamp (Fisher Scientific LED light source)
6. Needles and syringes
7. Surgical gauze
8. Cotton-tipped applicators
9. Tape
10. Surgery platform (Braintree Scientific, Inc.)
11. Animal weighing scale
12. Personal Protective Equipment: surgical gown, hair cover, surgical mask, surgical gloves, goggles, or safety glasses

2.3. Surgical Procedures: Solutions and Supplies

1. Sterile saline solution
2. Lidocaine hydrochloride (10 mg/mL, Hospira, Inc., Lake Forest, IL)

2.3.1. Solutions

3. Ketamine HCl (100 mg/mL, Vedco Inc., St. Joseph, MO)

4. Xylazine (100 mg/mL, Webster Veterinary, Devens, MA) diluted to 20 mg/mL
5. Absolute alcohol

2.3.2. Supplies

1. Heat pad (Braintree Scientific, Inc.) or alternative heating source
2. Lamp (Fisher Scientific LED light source)
3. Needles and syringes
4. Surgical gauze
5. Cotton-tipped applicators
6. Fogarty balloon embolectomy catheters, 2 French (Edwards Lifesciences, Germany)
7. Trocar guiding needle
8. Inflation device for balloon catheter
9. Suture: 4-0/3-0 black braided silk (Roboz Surgical Instrument Company, Inc., Gaithersburg, MD)

2.3.3. Surgical Instruments (Fig. 1)

1. Scalpels and surgical blades
2. Operating scissors (Roboz)
3. Microdissecting scissors (Roboz)
4. Small curved forceps (Hartmann Mosquito Forceps 4″ curved, Apiary Medical, Inc. San Diego, CA,)
5. Microclips (Roboz)
6. Microclip applying forceps (Roboz)
7. Angled microdissecting forceps (Roboz)
8. Tissue forceps (Roboz)
9. Retractors (Crile Retractor 4″ double ended, Apiary Medical, Inc.)
10. Intravascular Over-the-Needle Teflon Catheter (24G, Baxter Travenol Laboratories, Deerfield, IL)
11. Suture (Roboz)
12. Needle and needle holder

2.4. Postoperative Procedures: Solutions and Supplies

1. Povidone–Iodine scrub (Aplicare, Inc., Meridien, CT), or other topical antiseptic/bactericide agent
2. Buprenex (buprenorphine, Signa-Aldrich)

2.4.1. Solutions

2.4.2. Supplies

1. Surgical gauze
2. Heat pad (Braintree Scientific, Inc.)
3. Animal cage with water supply

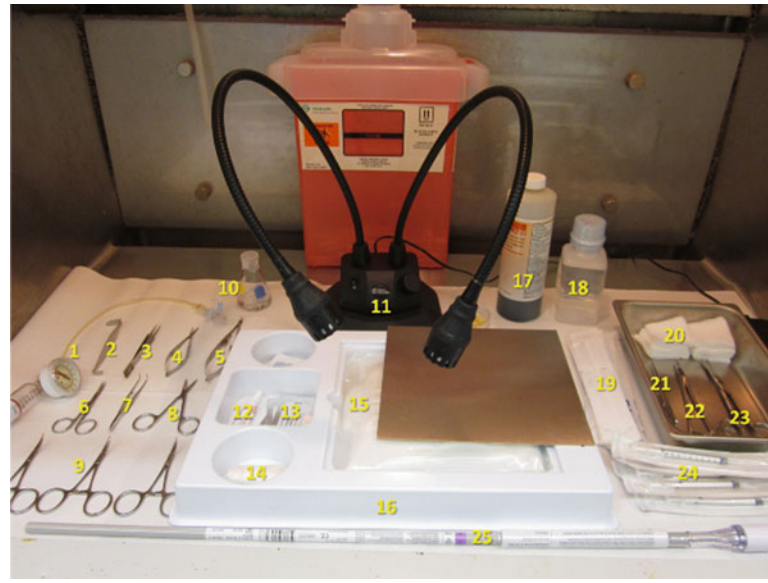

Fig. 1. Surgical setup and surgical equipment. 1. Inflation device for balloon catheter; 2. Retractor; 3. Angled microdissecting forceps; 4. Microdissecting spring scissors(VANNAS); 5. Microsuturing needle holder; 6. Microdissecting scissors, curved blade; 7. Microdissecting forceps, curve tip width 0.8 mm; 8. Microdissecting scissors; 9. Hemostatic forceps, curved; 10. Absolute alcohol with small arterial clamps soaked in; 11. Lamp; 12. Artificial tears ointment; 13. Scalpel; 14. Pillow made from paper towel; 15. Heatpad; 16. Surgery platform; 17. Povidone–Iodine scrub; 18. Saline; 19. Cotton-tipped applicators; 20. Gauze; 21. Tissue forceps; 22. Needle holder; 23. Operating scissors; 24. Syringes; 25. Fogarty balloon catheter.

3. Methods

3.1. Preoperative Procedures

1. Autoclave surgical tools.
2. Weigh animals and calculate the dose of anesthetic drugs (ketamine 70 mg/kg + xylazine 6 mg/kg).
3. Administer the anesthetic drugs intraperitoneally (i.p.) (Note 1). It usually takes 5–10 min for the rat to be sedated to a surgical level of anesthesia (verified by toe pinch). An additional small dose of anesthetic drugs (ketamine 7 mg/kg + xylazine 0.6 mg/kg) will be administered if the rat was not adequately sedated >10 min after the initial dose (Note 2).
4. Place the sedated animal carefully on the surgical platform supinely with head towards the surgeon (Note 3). We suggest putting a small pillow (made by paper towel or gauze, 5 cm × 3 cm × 1.5 cm) under the animal's neck. This will reduce the stress on the animal's neck and also make it easier for the surgeon to shave and to perform the surgery.

5. Use tape to fix the animal on the surgical platform with heat pad.
6. Use the hair remover to remove the hair in the ventral neck region.
7. Swab this area with Povidone–Iodine scrub and 70% alcohol.
8. Cover the animal body with a sterile cover sheet, but expose the surgical area.

3.2. Surgery

The surgeon should wear all the surgical personal protective equipment, including surgical mask, hair cover, surgical gloves, glasses, and gown during the surgery procedures.

1. Use a scalpel to make a straight longitudinal incision in the skin and make sure not to cut the tissue underneath. The length of the incision is 3–4 cm.
2. Use dull forceps to blunt dissect the connective tissue from the skin. Keep the forceps tips up and make sure not to puncture the skin or the underlying tissue.
3. Use medium scissors to cut the connective tissues overlying the glands and keep the tips up when cutting. When seeing the two glands use dull forceps to separate them gently.
4. Use dull forceps to dissect muscle layers longitudinally along with the left side of trachea. Make sure not to puncture or press the trachea. Add sterile saline in the surgical area once in a while to keep the tissue moist. Carefully separate muscular tissues to expose the left common carotid artery. Use retractor(s) to hold the skin and muscle tissues back so that the carotid vasculature would be accessed.
5. Dissect muscle bluntly along the common carotid artery toward its distal end (head) until seeing the bifurcation and two branches—external carotid artery and internal carotid artery. At this point the surgeon has to be extremely careful not to injure the vagus nerve, the fine white string adjacent to the common carotid artery. Separate the vagus nerve from the carotid vasculature carefully and bluntly. Dissect away the nerve and all adjacent tissues from the artery and expose an isolated part of the artery which is 1.5–2 cm long starting from the bifurcation of carotid artery towards the proximal end.
6. Bluntly dissect away the connective tissue surrounding the bifurcation and the external/internal carotid arteries. The surgeon needs to be very careful not to tear the blood vessels including small branches. If necessary the small blood vessels could be ligated and then cut off to avoid bleeding. It is very common to tear a small blood vessel apart when dissecting the adjacent tissues. If bleeding occurs, immediately clamp the broken end of the blood vessel to stop bleeding, and use saline

and gauze to clean the blood in the surgical area. Then permanently ligate the broken blood vessel with sutures.

7. Keep dissecting to isolate the external carotid artery from the adjacent tissues. The length of that portion of external carotid artery that one could be able to isolate from the surrounding tissues is approximately 3–6 mm, from the bifurcation to its distal end (towards the head). Place two pieces of 4-0 silk suture around the external carotid artery. Hold one piece of the suture to slightly lift up the bifurcation in order to get access to the internal carotid artery underneath (ventral aspect). Carefully and bluntly dissect the adjacent tissue on the internal carotid artery, except a small gland cling on it. In most cases, it is very difficult to isolate that gland from the internal carotid artery. The length of the isolated portion of internal carotid artery should be about 2 mm, sufficient for placing an artery clip on it.
8. Ligate the distal end of external carotid artery. Make a double-knot tie on the most distal end of the isolated portion of external carotid artery. At this point do not cut the extra suture since it will be used to retract the external carotid artery during the following processes. Place a microclip on the common carotid artery at the proximal end of the isolated portion. Gently lift up the suture around the external carotid artery near the bifurcation and place another clip on the internal carotid artery (clip the gland too if it could not be separated from the internal carotid artery). When applying microclip, the use of forceps is recommended to easily place the clip on internal carotid artery. Now the blood flow has been stopped by the clips (Fig. 2).
9. Gently retract the distal suture on the external carotid artery and make an arteriotomy incision on it by the small microscissors. The incision should be made as close as possible to the suture knot and its size should be less than half of the vessel circumference. Blood in the closed portion of carotid artery will flow out from the incision and should be cleaned away with saline and gauze.
10. Slightly pull the distal suture on external carotid artery with a clamp, in order to tense the blood vessels. Use the angled microdissecting forceps to prop the arteriotomy hole open and insert the uninflated 2F balloon catheter into the vessel lumen. Be careful not to puncture the balloon with the forcep tips. Advance the balloon catheter proximally through external carotid artery to the common carotid artery. Try not to prop up the vessel wall with the balloon catheter tip when advancing; otherwise the vessel wall will be punctured and leaky. Insert the balloon catheter all the way to the proximal site where the clip is.

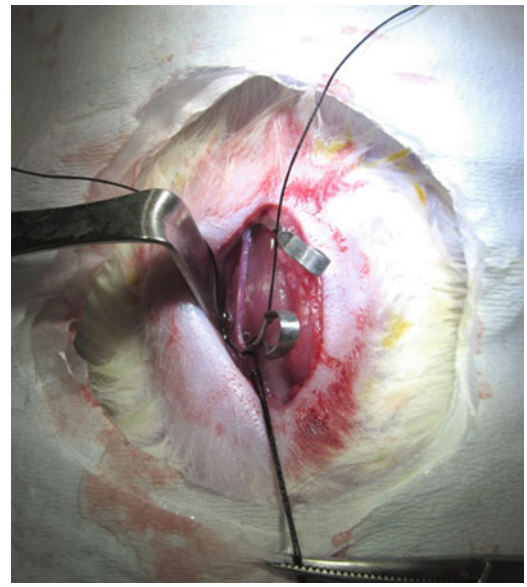

Fig. 2. Application of microclips to carotid artery to stop blood flow. The disposable sterile cover sheet (Polylined sterile field, Busse Hospital Disposables, NY) was cut a hole in the middle to expose the surgical area. The carotid artery was dissected away from the surrounding tissues. External carotid artery was ligated at its distal end of the dissected portion. Two microclips were placed on the internal carotid artery and at the proximal end of the dissected portion of common carotid artery, respectively. The extra suture of the tie on external carotid artery was not cut off and was pulled distally by the forceps in order to tense the blood vessel.

11. Slowly inflate the balloon with 1.4–1.8 atm pressure, depending on the diameter of the carotid artery. Slightly pull the balloon catheter back to check the resistance of the vessel wall. Adjust the pressure of the balloon in order to make sure that the balloon can slowly be pulled back while avoiding excessive stretching of the artery. Lock the stopcock and the pump to maintain the pressure. Gently pull the balloon with rotation back to the bifurcation (Fig. 3). Avoid withdrawing the balloon too close to the arteriotomy hole since the inflated balloon would easily slip out of the hole. Deflate the balloon and re-insert it proximally to the site of the clip on the common carotid artery. Inflate the balloon again with the same pressure and repeat the same procedure a total of three times. During these procedures lidocaine should be dispensed on top of carotid artery in order to relax the vessel.
12. Deflate and withdraw the balloon out of the vessel lumen. If treatment with virus-encoding cDNA clone or shRNA is intended, thaw the appropriate virus and prepare a 1 mL syringe and an intravascular over-the-needle catheter (Note 4). Remove the needle, and set the catheter on the syringe. Suck up the virus solution (30–50 μL) into the catheter and syringe; insert

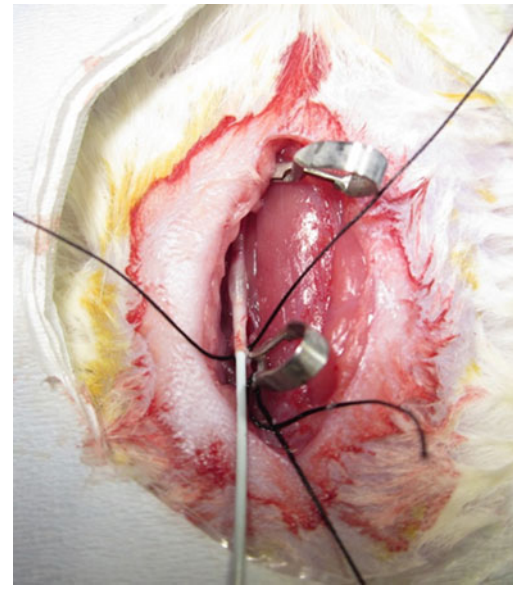

Fig. 3. Balloon inflation in the carotid artery. The balloon catheter was inserted into the carotid artery and inflated with 1.5 atm pressure.

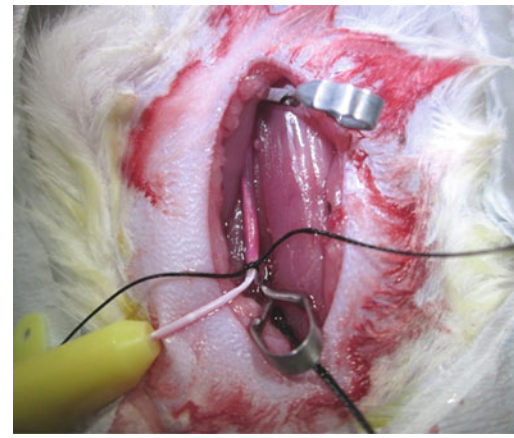

Fig. 4. Viral transduction into the carotid artery. After injury and withdrawal of the balloon catheter, lentivirus solution was provided intravascularly through the Teflon catheter and syringe.

the catheter into the arteriotomy hole. Advance the catheter tip into the common carotid artery and tie the suture with a single knot on the external carotid artery to fix the catheter and close the hole. Inject the virus solution into the lumen of common carotid artery while avoiding air bubbles. Maintain the virus solution in the artery lumen for 30 min (Fig. 4). Keep the exposed tissue moist by covering it with a piece of moist gauze. Administer 10% initial dose of the anesthetic drug through i.p. to the animal. Keep an eye on the animal during these 30 min

in case it wakes up. When the virus treatment is done, suck back the virus solution into the syringe to avoid virus entering the blood circulation. Loosen the tie and withdraw the catheter.

13. Right after the virus treatment is completed, or right after completion of balloon injury (if no virus treatment is required), tie the suture on external carotid artery and proximal to the arteriotomy hole. Make the knot close to the bifurcation in order to reduce the risk of leak and thrombosis. Make sure not to tie the surrounding tissues.
14. Slightly loosen the clip on the internal carotid artery (do not remove) by applying forceps and check if there is bleeding; the surgical procedures may cause leak or puncture on the blood vessel. If you notice excessive bleeding, quickly clip it back and remove the forceps. If there is a puncture on external carotid artery, make one more tie if possible. If bleeding occurs because of a leak from the common carotid artery, press a piece of gauze on the leaky site until it stops bleeding. Then remove both clips to restore blood flow.
15. Remove all clamps or other surgical instruments and cut off excess suture. Place the retracted tissues such as muscles and glands back on top of the carotid vasculature layer by layer. Close skin using 4-0 black silk sutures and a running (continuous) suture. Double-knot both ends.
16. Swab on all sides of the closed wound with the Povidone–Iodine or other antiseptic/bactericide/virucide agent to reduce risks of infection.

3.3. Postoperative Procedures

1. Keep rats on heat pad after surgery to avoid hypothermia; postsurgical hypothermia is major cause of postsurgery deaths in rodents. However, hyperthermia caused by hot heat pad may also be lethal; cover the heat pad with towels before placing rat on it.
2. Postsurgical analgesia: Administer one dose of 0.05–0.2 mg/kg buprenorphine via intramuscular injection (i.m.) to the rat.
3. The animals should be closely and continuously monitored after surgery. When the rat is awake and ambulant, put it back into its cage and provide sufficient water and food.
4. Carefully clean the balloon catheter with water and alcohol. Check the balloon to make sure it could still be inflated and has no leak; it could be reused several times in future surgeries if properly cleaned with alcohol and saline every time before use.
5. Clean the virus-contaminated catheter and syringe with bleach. The catheter can be reused after being cleaned with bleach and rinsed with alcohol and distilled water.
6. Clean all the stainless steel instruments with soap and water and then spread them on paper towels to air-dry.

4. Notes

1. Anesthetic drugs and analgesic drugs are generally controlled substances. They must be approved for use in rats and handled by licensed/authorized personnel following the strict guidelines and policies of the research institution.
2. If a supplemental dose of anesthetic drugs (10–20% of original dose) is deemed necessary it is usually administered around 1 h after the initial dose was given, according to the surgeon's experience.
3. Rat should be monitored during all the surgical procedures. Some may need more anesthetic drugs to keep them sedated due to individual heterogeneity between animals.
4. Lentivirus was stored at −80°C and thawed on ice before use. Open the tube cap and suck up virus in a hood in order to avoid inhalation of viral aerosol.

Acknowledgments

Work in the authors' laboratory is supported by the National Institutes of Health grant HL097111 to MT.

References

1. Heitzer T, Schlinzig T, Krohn K, Meinertz T, Munzel T (2001) Endothelial dysfunction, oxidative stress, and risk of cardiovascular events in patients with coronary artery disease. Circulation 104:2673–2678
2. Celermajer DS, Sorensen KE, Gooch VM, Spiegelhalter DJ, Miller OI, Sullivan ID, Lloyd JK, Deanfield JE (1992) Non-invasive detection of endothelial dysfunction in children and adults at risk of atherosclerosis. Lancet 340:1111–1115
3. Ip JH, Fuster V, Badimon L, Badimon J, Taubman MB, Chesebro JH (1990) Syndromes of accelerated atherosclerosis: role of vascular injury and smooth muscle cell proliferation. J Am Coll Cardiol 15:1667–1687
4. Owens GK, Kumar MS, Wamhoff BR (2004) Molecular regulation of vascular smooth muscle cell differentiation in development and disease. Physiol Rev 84:767–801
5. Clowes AW, Reidy MA, Clowes MM (1983) Kinetics of cellular proliferation after arterial injury. I. Smooth muscle growth in the absence of endothelium. Lab Invest 49:327–333
6. Clowes AW, Reidy MA, Clowes MM (1983) Mechanisms of stenosis after arterial injury. Lab Invest 49:208–215
7. Tulis DA (2007) Rat carotid artery balloon injury model. Methods Mol Med 139:1–30
8. Oparil S, Chen SJ, Chen YF, Durand JN, Allen L, Thompson JA (1999) Estrogen attenuates the adventitial contribution to neointima formation in injured rat carotid arteries. Cardiovasc Res 44:608–614

Part II

TRPs and the Brain

Chapter 7

TRP Channels in the Brain

Antonio Reboreda

Abstract

In the past few years the presence of one or another member of the TRP channel family has been described basically in all tissues studied. Moreover, the pattern of expression and the susceptibility to modulators of each channel subtype in each tissue will shape their influence on the cell/tissue response. With this idea in mind this review aims to give an overall and updated perspective about the TRP expression research focusing mainly on TRPA1, TRPC, TRPM, and TRPL subfamilies, in nervous tissue, summarizing the data available on the presence of TRP channels and the techniques employed on each study. A comment on their putative function is also provided.

Key words: TRP, Transient receptor potential, TRPA1, TRPM, TRPC, TRPV, TRPML, Expression, Nervous system, Neuron

1. Introduction

TRP or transient receptor potential channels were discovered first in Drosophila as light sensitive channels responsible for the transduction of the light stimulus to an electrical response in the photoreceptor (1). Soon after, mammalian homologs were cloned (2–4) and those were followed by different subfamilies of cationic channels with different patterns of expression depending on the animal, age, and tissue.

TRP channels are modulated by a wide panoply of physicochemical agents and contribute to cell depolarization. In the last few years, several works have characterized the presence and function of TRP channels in neuronal and nonneuronal tissue; in the present review, we will focus on the pattern of expression in mammalian nervous system.

Arpad Szallasi and Tamás Bíró (eds.), *TRP Channels in Drug Discovery: Volume II*, Methods in Pharmacology and Toxicology,
DOI 10.1007/978-1-62703-095-3_7,

The TRP channel family is formed by 7 subfamilies, 6 of them present in mammals (TRPC, TRPM, TRPV, TRPA, TRPP, and TRPML) grouping 28 channels. They have 6 transmembrane domains and a pore forming region between segments 5 and 6. Besides, the physiological properties of these channels, their pattern of expression in different tissues, and different parts of the neurons will determine their function.

2. TRPA1

TRPA1 is a channel involved in the transduction of painful thermal, mechanical, and chemical stimuli. Northern blot analysis show expression of mRNA in the human brain among other nonneuronal tissues (5), nevertheless no detailed study has been published. In the peripheral nervous system, TRPA1 channel presence has been shown in DRG, spinal roots, motoneurons, peripheral nerves, and intestinal plexi (myenteric and submucous) by immunohistochemical and western blot techniques (6).

Virtually all the published data about TRPA1 localization in nervous tissue have been carried out in rats and mice. Rat TRPA1 has been found in sensory ganglia using molecular and immunological techniques: DRG (6–8), trigeminal ganglia (8–10) (for a detailed study see: (11)), geniculate ganglion (12), nodose ganglion (13), and in the complex of jugular, nodose, and petrosal ganglia (14). Physiological data, using selective agonists, points out also to the possible expression of the channel in other systems like striatum (15), tractus solitarius nucleus (16), presynaptic terminals to the supraoptic nucleus (17), and astrocytes in rat hippocampal astrocyte–neuron cultures (18).

Mice TRPA1 has a similar distribution to rat nervous system, almost no studies reported the presence of the channel in the central nervous system, being the sensory part of the peripheral nervous system the main body of evidence of the expression of the channel. Northern blot experiments show the expression of the mRNA in nociceptive DRG neurons, where it appears after the first postnatal week (19) and not in whole brain (20, 21); northern and western blot plus immunohistochemistry corroborated the expression of the channel at the sensory terminals in dorsal root trigeminal and nodose ganglia (22). RT-PCR showed mRNA expression in the lung vagal sensory neurons (23). Western blot experiments demonstrated also the appearance of TRPA1 channel in the sciatic nerve and spinal cord (24). It has been detected in tongue nerve terminals, nerves innervating vestibular sensory cells, olfactory neurons, and nerve fibers in the lamina propria by immunohistochemistry (25–27). RT-PCR and immunohistochemistry also reported expression of TRPA1 in enteric neurons and fibers (28).

3. TRPC Subfamily

Transient receptor potential canonical (TRPC) channels were the first discovered in mammals and they have the strongest homology with their Drosophila counterparts. It is formed by seven members, named from TRPC1 to TRPC7. Each channel is formed by two dimers of each subunit being homotetramers or heterotetramers, the possible combinations (besides the homomers) are (1 + 4/5, 2 + 6, 4 + 5, 3 + 6, 3 + 7, 6 + 7; 1 + 3 only in embryo). TRPC1 presence and levels have been studied by mRNA detection methods, by electrophysiological methods (patch clamp), and immunological based methods (immunostaining and western blot) showing a changing pattern with age and species.

3.1. TRPC1

It was the first mammalian homolog discovered and the homomer constitutes a Ca^{2+} permeant cationic channel (29). It is present in human, mouse, and rat. In humans TRPC1 mRNA levels are very high during the embryonic period in telencephalon, diencephalon, and hindbrain; in adults it is present in amygdala, corpus callosum, caudate nucleus, hippocampus, cingulate gyrus, globus pallidus, hypothalamus, locus coeruleus, middle frontal gyrus, medulla oblongata, nucleus accumbens, parahippocampus, putamen, striatum, superior frontal gyrus, thalamus, substantia nigra, subthalamic nucleus, cerebellum, and spinal cord. The mRNA levels in the cerebellum are about twice the levels in other tissues, where it is very similar among them (3, 30). Nevertheless, TRPC1 expression has been characterized more deeply in rat and mice.

Rat TRPC1 mRNA is also expressed in many areas of the nervous system, and the presence of the channel has been reported by several authors (31–33); the mRNA is present in all the areas examined: cortex, olfactory bulb, hippocampus, forebrain, midbrain, brainstem, cerebellum, dorsal raphe, tuberomamillary nucleus, and ventral tegmental area (31, 33–35). The protein has been detected in CA1 and CA3 pyramidal neurons, granule cells in the dentate gyrus, cells in the amygdala, and cerebellar Purkinje cells (36). In the hippocampus the subcellular location comprises dendrites, soma, and axon; nevertheless the presence of the protein in the synapses is negative (36), in cerebellar Purkinje cells and dopaminergic neurons of the substantia nigra association of TRPC1 proteins with the mGluR1 receptor has been reported in the spines of the molecular layer in the cerebellum and in the dendritic arborization of the dopaminergic neurons (37, 38).

Mouse TRPC1 is also ubiquitous in the nervous system with a maximum expression of the mRNA during the embryonic period (39). weak expression of mRNA has been reported in cortex (layer II to IV), putamen, diencephalon, brain stem, and cerebellum (Purkinje cells and granule cells); medium expression appears in

hippocampal pyramidal cells and dentate gyrus granule cells (40). In the medial temporal lobe, strong protein expression has been shown mainly in the dendritic tree of central nucleus amygdala neurons, decreasing the levels in the basolateral, lateral, and central nuclei. This cellular distribution is also present in the pyramidal layers of CA1, CA2, and CA3; granule cells in the dentate gyrus, subicullum, and entorhinal cortex (41). TRPC1 protein is also present in the DRG, spinal cord, and nodose ganglia, increasing mRNA levels from the embryonic stage to adulthood (42).

In the last few years several works have related working memory and spatial navigation phenomena in rodents with the presence of a metabotropic sustained plateau depolarization; this plateau is generated with the contribution of TRPC channels expressed on this area, probably an heteromer of TRPC1 + TRPC4/5 (43, 44).

3.2. TRPC2

In humans, it is a pseudogene that contains several mutations codifying stop codons (45) while in rodents it is expressed in the vomeronasal organ of rodents contributing to the detection of pheromones (46); it is also expressed in large sensory neurons of the dorsal root ganglia (42) and in the aminergic neurons of dorsal raphe and ventral tegmental area (35). It is not present in the tuberomammillary nucleus and locus coeruleus (35).

3.3. TRPC3

TRPC3 channel mRNA expression in humans has been characterized for the first time in 1996 (47). Riccio et al. (30) demonstrate a strong expression in cerebellum, caudate, putamen, and striatum. It is also expressed in the other brain regions studied but 2–4 times less: amygdala, cingulate gyrus, globus pallidus, hippocampus, hypothalamus, locus coeruleus, middle frontal gyrus, medulla oblongata, nucleus accumbens, parahippocampus, substantia nigra, superior frontal gyrus, thalamus, and spinal cord.

TRPC3 expression in the rat has been reported in the brain and cerebellum, where the mRNA levels are the highest compared to the other tissues (33). A more detailed characterization of TRPC3 mRNA expression has shown it in cortex, olfactory bulb, midbrain, brainstem, cerebellum (31), dorsal raphe, and ventral tegmental area (35). In the rat hippocampus, tuberomamillary nucleus and locus coeruleus TRPC3 have been reported as non-present by other authors (31, 35) but immunohistochemical characterization shows TRPC3 protein expression in the soma of CA1 and CA3 pyramidal cells and granule cells of the dentate gyrus (48) also in cholinergic interneurons in the striatum (49). At the cellular level, TRPC3 appears in rat synaptosomes, indicating the presence of the channel at the synaptic level (50). Hippocampal expression of TRPC3 matches with the expression described for TRPC1/4/5 more than TRPC6 raising the possibility of forming heteromers with TRPC1 instead of TRPC6 (48). Nevertheless, protein expression studies show that TRPC3 protein couples to TrkB receptor

and both reaches maximum levels during the fetal and short time after birth in rat (till P20) and human, in adults even if the mRNA is present the protein is not expressed (51). This difference in results could be due to the heteromers formed during the development period (complexes with TRPC1/4/5) different from the ones formed in adulthood (TRPC6/7) or to a modification of TRPC3 protein in adulthood due to post-translational modification or alternative splicing.

Mice TRPC3 expression provides the majority of the data about the localization of this channel. "In situ" hybridization experiments agreed with the data from humans and rats showing the maximum expression levels in cerebellar Purkinje cells without labeling the molecular layers; it has also a high expression in the mitral olfactory cells and periglomerular cells. In the putamen positive labeling has been found in large size cells. Weak expression is also reported in septal and thalamic nuclei and several brain stem nuclei: dorsal cochlear, inferior olive, and locus coeruleus (40, 52). Western blot experiments show the presence of the channel in the mice medullary ventral respiratory group, where it contributes to the respiratory rhythm (53). RT-PCR data complements the previous experiments showing the same pattern of expression and adding the presence of a weak expression at hippocampal level (34). The autonomous nervous system also shows expression of mRNA of this channel in dorsal root and nodose ganglia where the levels of TRPC3 mRNA increase during development matching TRPC1 time course (42).

3.4. TRPC4

TRPC4 in humans is expressed in the nervous system being the higher amount of mRNA located in parahippocampus, nucleus accumbens, amygdala, hippocampus, and cingulate gyrus; a lower but not very different amount of mRNA is located in cerebellum, globus pallidus, hypothalamus, locus coeruleus, middle frontal gyrus, medulla oblongata, putamen, striatum, substantia nigra, superior frontal gyrus, and thalamus. TRPC4 mRNA appears also at the spinal cord but a much lower level (30).

In rat TRPC4 decreases the expression from E18 to adulthood, northern blot plus "in situ" hybridization techniques reported that in young animals the mRNA appears mostly in septum, cortical plate, and hippocampus with a weaker staining in the dentate gyrus; towards the adulthood the expression remains only in neurons from the CA1 and CA2 of the hippocampal formation (54). Nevertheless other authors show a more extensive expression of the mRNA throughout the rat and mice brain and increasing protein levels from E18 to adult animals in hippocampus, prefrontal cortex, subiculum, and entorhinal cortex (55). "In situ" hybridization displays a strong labeling in CA1, CA2, lateral septum, subiculum, and tenia tecta; moderate labeling is found in amygdala, cerebellar Punkinje and granule cells layers, entorhinal cortex, habenula, CA3, dentate gyrus, ventral hypothalamus, motor,

orbitofrontal, piriform, prefrontal and somatosensory cortices (layers 2, 3, 5, and 6). Weak expression is shown in hippocampal hilus, paraventricular hypothalamus, medial septum, and substantia nigra. This study also points out several locations where the mRNA is not expressed: caudate putamen, molecular layer of the cerebellum, corpus callosum, dorsal hypothalamus, islands of Calleja, thalamus, nucleus accumbens, and layer I of motor, prefrontal, and somatosensory cortices (55). This difference in results could be caused by a splice variant (33, 54, 56, 57).

More sensitive techniques such as RT-PCR reported a widespread expression in adult olfactory bulb, hippocampus, dorsolateral geniculate nucleus, cortex and nodose ganglia (31, 33, 58), nonserotoninergic neurons of the dorsal raphe, tuberomamillary nucleus, and ventral tegmental area (35). Immunohistochemical studies reveal the presence of TRPC4 channel in the hippocampal area where CA1-3 pyramidal neurons and granule cells of the dentate gyrus present the protein in their cell bodies and lateral septum (48, 55).

The mice TRPC4 are also distributed in many areas of the nervous system. The first studies in the whole brain reported a strong expression in olfactory mitral and granule cells, septal nuclei, subiculum, and pyramidal and granule cell layers of the hippocampus; weak expression appears in the granule cell later of the cerebellum (40). Expression of mRNA was also found using the same technique in cortical neurons (52); internal granular layer of the olfactory bulb, but not in mitral cells (59). These differences in expression are maybe reflecting again the different expression of TRPC4 isoforms.

Protein expression has been reported by using selective antibodies in basal ganglia, cerebellum, cerebrum, forebrain, and hippocampus (34). A similar pattern of expression to rat TRPC4 was found in mice by using RT-PCR (55).

Finally, TRPC4 is expressed also in rat and mice dorsal root ganglion neurons where its level increases from E12 to adulthood and after nerve injury (60) reflecting their involvement in axonal and dendrite growth.

3.5. TRPC5

It is the closest member to TRPC4; they are almost identical in structure and electrophysiological properties. Moreover, their distribution in mouse and rat CNS has been shown to be similar (55).

In humans TRPC5 mRNA is mainly expressed in the cerebellum, followed by cerebral cortex, entorhinal cortex, occipital and frontal lobe by northern blot analysis (59, 61). Real time RT-PCR reported the highest levels of expression in amygdala, cerebellum, cingulate gyrus, and superior frontal gyrus; intermediate levels were detected in locus coeruleus, nucleus accumbens, and parahippocampal region; the lowest levels of TRPC5 mRNA were detected

in caudate nucleus, globus pallidus, medulla oblongata, thalamus, putamen, striatum, substantia nigra, and spinal cord (30).

The mRNA TRPC5 distribution in rat and mice is similar in the nervous system of both species. "In situ" hybridization showed a strong expression in the hippocampal area and cerebral cortex layers 2–6, but almost all the areas studied show more or less presence; nevertheless mRNA was not detected in caudate putamen, corpus callosum, lateral and medial septum, cortical layer 1, substantia nigra (55), locus coeruleus (62) (but see (35)), dorsal raphe, tuberomamillary nucleus, and ventral tegmental area (35). The DRG ganglia also present mRNA expression of TRPC5 with a peak at E18 during development, followed by a decrease in young animals and a gradual raise in adulthood (42). The contribution of those TRPC5 to sustained depolarizations (plateau potentials) has been exposed by electrophysiological recordings in prefrontal cortex (44), entorhinal cortex (43), hippocampal CA1 pyramidal neurons (63), and locus coeruleus (62).

3.6. TRPC6

In humans the highest levels of TRPC6 mRNA quantified by RT-PCR have been shown in placenta and lung. Inside the nervous system there is relative medium expression in the caudate nucleus and cingulate gyrus; the rest of the areas studied show an homogeneous low expression, those areas are: amygdala, cerebellum, globus pallidus, hippocampus, hypothalamus, locus coeruleus, middle frontal gyrus, medulla oblongata, nucleus accumbens, parahippocampus, putamen, striatum, subtantia nigra, superior frontal gyrus, thalamus, spinal cord, and pituitary (30, 64).

The rat TRPC6 mRNA is expressed in the cerebellar interneurons, Purkinje cells, and granule cells (65). The mRNA is also expressed in the ventral tegmental area, tuberomamilary nucleus, and Raphe nucleus colocalizing with orexin, while it was not detected in the locus coeruleus (35). The channel has been detected by immunohistochemistry in: Petrosal ganglion (66), in the developing hippocampus the TRPC6 channel is found in all regions till P14 (67) while in adulthood only the molecular layer is labeled (48); retinal ganglion cells (68, 69), substantia nigra of the striatum associated to mGluR1 but not in cholinergic interneurons (49) and a small number of hypocretin-orexin neurons in the hypothalamus (70). TRPC6 channel has been also detected in the brain resistance arteries where they play a central role in the regulation of the myogenic tone (71).

Mice TRPC6 channel has also a wide distribution in the nervous system. The protein has been shown in the microvilli of the apical portion of the olfactory epithelium (72); the mRNA was detected by RT-PCR in most of the nervous system, but the higher levels were found in the basal ganglia, cerebrum, forebrain, and hippocampus (C2 area) with some difference in the levels among mouse strains (34) and pituitary cells (64).

3.7. TRPC7

It was the last member of the TRPC subfamily to be cloned (73). TRPC7 mRNA in human nervous tissue has a widespread distribution with higher levels in the cerebellum, medulla, occipital pole, frontal lobe, temporal lobe, amygdala, hippocampus, caudate nucleus, nucleus accumbens, hypothalamus, locus coeruleus, putamen, and striatum (30).

The rat homologous TRPC7 mRNA is expressed in Dorsal raphe (except in the serotoninergic neurons), tuberomamillary nucleus, ventral tegmental area, and it is absent from the locus coeruleus (35). The TRPC7 has been identified in the striatum cholinergic interneurons where it is activated by mGluR1 and mGluR5 (49) and in the soma of nodose ganglion neurons (it is absent in the baroreceptor afferents) (74) and it has also been demonstrated its presence in the hypothalamic hypocretin/orexin neurons (70).

Since the first cloning of TRPC7 in mouse (73) where they described a moderate expression in the brain compared to other tissues (heart, lung, and eye) not many studies explored the expression of the mRNA or the protein in the nervous system. The presence of the mRNA has been shown at very low levels in mice embryonic brain and cortex (39) and in DRG and NG neurons. In the NG, mRNA level increases from E18 to adulthood (42). Western blot experiments show the presence of TRPC7 together with TRPC3 in the medullary ventral respiratory group (53).

4. TRPM Subfamily

It is composed of eight members named from TRPM1 to TRPM8 all of them with a high homology but they can be classified in several groups according to their similarities in sequence: TRPM1/3, TRPM4/5, and TRPM6/7; TRPM2 and TRPM8 are not grouped due to their differences with the other members. They participate in multiple functions due to their sensitivity to physical and chemical stimuli (for a review on their function, see (75, 76)). Their levels of expression varies depending on the tissue, so in the human brain TRPM2 and TRPM3 have the highest mRNA levels followed by TRPM6 and TRPM7; TRPM1, 4, and 5 have a reduced expression and TRPM8 is virtually undetectable (77).

4.1. TRPM1

Besides the general distribution mentioned before, there is only another work, focused in different isoforms of TRPM1 expressed in human melanocytes, reporting again TRPM1 mRNA expression in the brain by (78). To our best knowledge there is no study about fine regional distribution in the nervous system of human or rat.

In the mouse, the study of TRPM1 expression has been investigated in the sensory system reporting the absence of this subunit

in the nodose ganglion and DRG (lumbar and thoracic) (79). There are other reports about the presence of TRPM1 in several sensory cells of the inner ear (26) and the ON bipolar cells of the mouse retina (80–82).

4.2. TRPM2

TRPM2 is one of the most expressed TRPM subunits in human (77). In the human brain has been shown two isoforms, a long version (6.5 kb) expressed ubiquitously and a short one (5.5 kb) present only in the caudate and putamen (83, 84). The regions where the presence of the long isoform as it has been shown by northern blot are: cerebellum, cerebral cortex, medulla, spinal cord, occipital pole, frontal lobe, amygdala, corpus callosum, hippocampus, putamen, caudate nucleus, subthalamic area, thalamus, and substantia nigra (83, 84). RT-PCR experiments showed a very similar pattern with the highest expression in the caudate, putamen, and striatum and the lowest in the spinal cord; intermediate expression is found in amygdala, cerebellum, cingulate gyrus, globus pallidus, hippocampus, hypothalamus, locus coeruleus, medial frontal gyrus, medulla oblongata, nucleus accumbens, parahippocampal gyrus, substantia nigra, superior frontal gyrus, and thalamus (85).

In the rat nervous system, TRPM2 expression has been explored studying mRNA and protein presence in: cortex (86, 87) and CA1—CA3 hippocampal pyramidal neurons but not in interneurons (88, 89). TRPM2 mRNA is present also in striatum (91, 92) and substantia nigra pars compacta but not in the pars reticulata (93, 94). Besides the expression in neurons, TRPM2 is also present in the rat microglial cells but not in astrocytes nor cerebellar granule cells (95). Recently the functional presence of the channel has been also demonstrated in the peripheral nervous system DRG neurons (96).

Mice TRPM2 channels can be found distributed through the whole brain as in human and rat. Northern blot experiments reported localized expression in olfactory bulb, cerebrum, hippocampus, midbrain, and cerebellum (97) and in cortex, striatum, and cerebellum (84). It was also detected in hippocampal pyramidal cells by "in situ" hybridization and immunocytochemical techniques (88) where they contribute to synaptic transmission (98). RT-PCR data reported a medium level expression in cerebrum, cerebellum, forebrain, basal ganglia, and hippocampus (34).

4.3. TRPM3

Together with TRPM2, TRPM3 is one of the most expressed TRPM subunits in the brain, it is also the last member described for the TRPM subfamily (for a review, see (99)). This subunit has been detected in the human brain by northern blot and western blot (100). Some authors (77) reported the highest mRNA levels in the brain but other authors claim that highest expression is detected in kidney (101). These differences could be explained by

the multiple isoforms detected for this channel due to the existence of several alternative splicing sites (102). RT-PCR experiments showed also expression in the human spinal cord (101).

Due to their recent cloning (100) data on localized rat TRPM3 expression in the nervous system is very scarce. It has been shown that the channel is expressed in the four layers of the cerebellar cortex (103).

At the whole brain level TRPM3 expression has been reported by northern blot in mice (102) while "in situ" hybridization showed expression in eye, dentate gyrus, the intermediate lateral septal nuclei, the indusium griseum, and the tenia tecta; an interesting difference with rat and mouse is that no TRPM3 expression has been found in the kidney (34, 102, 104). RT-PCR experiment shows differences among the expression level of three mouse strains in the cerebrum [34]; it has been also reported strong mRNA expression of TRPM3 on basal ganglia, forebrain, cerebellum, hippocampus (34), and in dorsal root and trigeminal ganglia which participates in the detection of noxious thermal stimuli (105). In the eye strong mRNA expression is detected in the retinal pigmented epithelium (80).

4.4. TRPM4

Two isoforms have been reported to be present in human brain using northern blot technique (though bands are very weak): TRPM4a (106) and TRPM4b (107, 108) which differs from each other mainly in their permeability to divalent cations (TRPM4b only allows monovalent cations to pass through the channel pore). RT-PCR experiments show also a weak TRPM4 mRNA expression in the whole brain (77). The main isoform is TRPM4b, while TRPM4a and TRPM4c are alternative splicing isoforms (108, 109).

The main role described for TRPM4 in rat nervous system is its participation in the vascular tone in the cerebral arteries and vascular smooth muscle cells (110). Rat brain express TRPM4a (mainly) and TRPM4b mRNA but the TRPM4a protein is rarely found in the membrane in transfected cells, where TRPM4b is the main subunit (111). A recent work reports TRPM4 protein expression in several hypothalamic nuclei: cell bodies of the magnocelular cells in the supraoptic nucleus, paraventricular nucleus, nucleus circularis, and neurons within the medial forebrain bundle (112, 113).

Mouse TRPM4 mRNA was reported for the first time in mouse brain by northern blot experiments (a very faint band) (108) and RT-PCR (114, 115). Functional and RT-PCR analysis reported also the expression of the channel in pre-Bötzinger neurons together with TRPM5 (116, 117) and microglial cells (118).

4.5. TRPM5

Human TRPM5 distribution was studied for the first time by Prawitt (119) using northern and southern blot and RT-PCR

techniques; they reported a very weak expression of the mRNA in the nervous system compared to other tissues. Some authors (77) reported only a residual expression by RT-PCR of TRPM5 mRNA in human brain.

The expression in rodent brain is also scarce. This channel has been associated mainly to taste and odor transduction since the protein is expressed in taste buds (120, 121) and olfactory epithelium (122, 123), recently their involvement in sensing the chemical composition of the luminal environment in the auditory tube has also been described (124). Nevertheless, localized expression inside the nervous system has been reported by RT-PCR in cerebral arteries but not in vascular smooth cells (110) and preBötzinger neurons (116). RT-PCR experiments in mice also shown that TRPM5 and TRPM4 are expressed in dorsal root and nodose ganglion neurons during the embryonic period but the levels are drastically reduced in the first 2 weeks postnatal (125). It is also present in the supraoptic nucleus, together with TRPM4, but at lower levels (113).

4.6. TRPM6

It is, together with TRPM7, the only known ion channel—kinase protein (126). The main function of those channels is the maintenance of the Mg^{2+}/Ca^{2+} homeostasis (127, 128). Some authors (77) reported a weak expression of TRPM6 mRNA by RT-PCR in human brain. Using the same technique TRPM6 mRNA expression is reported to be present in the vascular tissue inside the human brain (129).

Rodent expression data of TRPM6 in the nervous system is scarce and only RT-PCR in dorsal root and nodose ganglia have shown a gradual increase of the levels from embryo to adulthood (79). To the best of our knowledge no expression studies in the brain have been reported.

4.7. TRPM7

TRPM7 mRNA expression has been described in human brain for the first time by northern blot and RT-PCR (130); nevertheless the number of mRNA copies is small (77).

In rodents, the mouse TRPM7 mRNA has been shown in the whole brain by northern blot (131) and the protein is expressed in rat brain microglia (132). RT-PCR shows mRNA expression in cortex and cerebellum (86) and increasing levels in nodose ganglia as the mouse develops while dorsal root remains low in adult after a peak in the second postnatal week (79). Western blot and immunocytochemical techniques show the protein at the presynaptic level in cultured rat sympathetic neurons (133) where they seem to facilitate vesicle fusion with the plasma membrane (134).

Functional experiments demonstrate TRPM7 currents in CA3 (135) and CA1 neurons (136).

4.8. TRPM8

According to the RT-PCR data obtained by Fonfria et al (77), no copies of TRPM8 are present in the human brain. Nevertheless immunohistochemical methods showed some positive neurons in DRG (137).

Rat TRPM8 is expressed in several areas of the peripheric nervous system: northern-blot and "in situ" hybridization showed the presence of the channel in DRG and trigeminal ganglion small neurons, while no mRNA was detected in spinal cord nor brain (8, 138). RT-PCR and immunohistochemical experiments further demonstrated the presence in DRG neurons (139). Also some vagal afferents show a positive response to antibodies against TRPM8 (140). In the central nervous system hippocampal cultured cells' negative response to menthol was used as a result to prove the nonexpression of this channel (141). Also immunohistochemistry discarded the presence of TRPM8 in ventromedial medulla (142).

The profile of TRPM8 expression in the mouse is very similar to the rat. RT-PCR display a gradual increase in DRG and nodose ganglion TRPM8 mRNA levels during development (79), a similar increase has been reported by using DRG from TRPM8^{GFP} transgenic mice (143). Northern blot experiments also show TRPM8 in DRG but failed to do so in spinal cord, superior cervical ganglion, and brain, and "in situ" hybridization labeled small neurons of the trigeminal neurons (20, 144). Overall, TRPM8 positive neurons contribute to cold sensation together with TRPA1 and TRPV1 in DRG, trigeminal ganglion, geniculate ganglion (7, 9, 12, 145–147) but recent work on trigeminal ganglion neurons show that TRPM8 together with Kv1 potassium channels plays a critical role in thermal sensation even in TRPA$^{-/-}$ mice (148). In the complex formed by jugular, nodose, and petrosal ganglia, TRPM8 is expressed together with TRPA1 and TRPV1 but it does not localize in the same cell with TRPA1 (14) reflecting the different role that each channel could be playing in cold transduction (149).

5. TRPV Subfamily

This group is composed of six channels named from TRPV1 to 6. They can be activated by different mechanism but at least the TRPV1 to 4 have in common their sensitivity to different ranges of temperature. They are commonly associated with sensory systems but accumulating evidence show that they can also play an important role in several processes in the central nervous system.

5.1. TRPV1

The first studies about TRPV1 localization in human nervous system were made using labeled resiniferatoxin ([^{3}H]RTX), those pioneering studies showed positive labeling in preoptic area, locus

coeruleus, medial hypothalamus, reticular formation, and ventral thalamus (150). [^{3}H]RTX binding studies also characterized the presence of TRPV1 channels in Cynomolgus monkeys finding the highest value in the dorsal horn of the spinal cord, the other areas stained were: locus coeruleus, preoptic area, hypothalamus, somatosensory cortex, somatomotor cortex, pontine reticular formation, and midbrain gray matter (151). The first work cloning human TRPV1 reported by RT-PCR experiments expression of mRNA in spinal cord, whole brain, cerebellum, hippocampus, frontal cortex, layers 3 and 5 of the parietal cortex, and the highest expression in DRG (152–154). Immunohistochemical experiments corroborated the presence of the protein in human DRG (155).

Rat expression of TRPV1 is also very similar to the reported for human with DRG levels being the highest compared to spinal cord, whole brain, cerebellum, hippocampus, and frontal cortex (153). Immunohistochemical data also show the presence of the channel in trigeminal ganglia, nodose ganglia, DRG, periaqueductal gray, and rostral ventromedial medulla and throughout the cortex (155–158); the DRG unmyelinated projections to the spinal cord are also labeled by antibodies against TRPV1 as well as lamina I and II (156, 159). Besides the presence in the hippocampus, RT-PCR and immunohistochemistry techniques have shown the presence of the channel in cortex (layers 3 and 5), medial amygdala, medial and lateral habenula, striatum, hypothalamus, centromedian and paraventricular thalamic nuclei, substantia nigra, locus coeruleus, reticular formation, cerebellum, and inferior olive (8, 152, 160). In the substantia nigra, TRPV1 is located also presynaptically in glutamatergic synapses (160). A detailed study using immunohistochemistry techniques and western blot in the rat central nervous system demonstrates TRPV1 channel presence in hippocampus, spinal cord, hindbrain, cerebellum, mesencephalon, cortex, olfactory bulb and DRG staining neurons, astrocytes, and pericytes (161). Functional experiments reported also the presence in the rat hippocampus (162).

The mice TRPV1 distribution is also very similar to human and rat. Two studies provide a very detailed description of the distribution of TRPV1 in the nervous system, and the results were compared to the TRPV1$^{-/-}$ mice as a control. The first study uses [^{3}H]RTX finding labeling in olfactory nuclei, frontal, piriform, parietal and retrosplenial cortices (distributed throughout all layers), hippocampus (pyramidal layer, *stria oriens,* and *radiata*), dentate gyrus, amygdala, lateral and medial septal nuclei, caudate putamen, thalamus (mainly in paracentral and medial habenular nuclei), hypothalamus (arcuate, dorsal medial, periventricular, and ventromedial hypothalamic nuclei), interpeduncular nuclei, periaqueductal gray, raphe nuclei and superior colliculus, locus coeruleus, cerebellar cortex (mainly in cellular layers), dorsal horn of the spinal cord (mainly in the lumbar area), dorsal root, and

trigeminal ganglia (163). The second study consists in a fine immunohistochemical study looking at several areas of the central nervous system which showed positive expression in hippocampus (pyramidal neurons in CA1–CA3 and molecular layer of the dentate gyrus), basal ganglia (caudate putamen, globus pallidus, and substantia nigra) thalamus, hypothalamus, cerebral peduncle, pontine nuclei, periaqueductal gray matter, cerebellar cortex (exterior of the Purkinje cell, basket cells), dentate cerebellar nucleus, and periaqueductal gray (164). RT-PCR experiments detected also mRNA in dorsal root, nodose, and superior cervical ganglia (165).

5.2. TRPV2

A close homolog to TRPV1, they can form heteromers. The data about human expression of this channel in the nervous system show a reduced and localized expression. Immunohistochemistry techniques show a restricted expression to cerebellar Purkinje cells in the whole CNS (166). Using a cynomolgus macaque as an experimental model some authors show also a restricted expression for TRPV2 by immunohistochemistry staining in the hypothalamic-neurohypophisial system, only hypothalamic paraventricular, suprachiasmatic, and supraoptic nuclei were stained and mainly oxytocin and vasopressin releasing neurons (167).

On the other hand, TRPV2 seems widely expressed in rat central nervous system and DRG where it also heteromerizes with TRPV1. Greffrath, Binzen, Schwarz, Saaler-Reinhardt, and Treede (2003) and Liapi and Wood (2005) achieved a positive labeling using immunohistochemistry and observed colocalization with TRPV1 (157, 168). In the same work (157) described the expression of the channel throughout the rat central nervous system mainly in layers IV, V, and VI; also cingulate and insular cortex; no TRPV2 was detected in the piriform cortex. Frederick et al. (8) by a ribonuclease protection assay detected mRNA of TRPV2 in DRG, trigeminal ganglion, spinal cord, cerebellum, hippocampus, and cortex. During the embryonic period mouse TRPV2 is expressed in DRG and motoneurons in the spinal cord where they promote axon outgrowth (169). In the adult rat TRPV2 is expressed throughout the spinal cord mainly in nociceptive areas (laminae I and Iii) (170) and dorsal lateral nucleus, nucleus ambiguus, and motor trigeminal nucleus (171). Immunofluorescence showed that TRPV2 is also expressed in the trigeminal and nodose ganglia (172, 173). RT-PCR detected mRNA of TRPV2 also appears in enteric neurons (174).

Besides in the embryonic spinal cord, mouse mRNA TRPV2 is also expressed in the nodose ganglion (165). RT-PCR detects mRNA mainly in basal ganglia, cerebellum, forebrain, hippocampus, DRG, nodose ganglion, and superior cervical ganglion (34, 165). Immunohistochemistry labels nerves with TRPV2 channels in the olfactory epithelium and the myenteric plexus, mainly

inhibitory motor neurons and primary afferent neurons (27, 175). The same technique also labels neurons in the dorsal root ganglion (176).

5.3. TRPV3

Human expression of TRPV3 was described by two groups independently. The first group reported the expression of the TRPV3 mRNA by RT-PCR: the maximum expression is found in the central nervous system (177), immunohistochemistry experiments showed also the protein at the DRG level. The second group reported the expression of the TRPV3 mRNA by RT-PCR in the brain, spinal cord, and DRG of humans; they also carried out "in situ" hybridization experiments in cynomolgus monkey showing mRNA expression in the central nervous system in cortex, thalamus, and striatum; in the spinal cord they got labeling in the ventral horn and interneurons in the intermediate zone and deep laminae of the dorsal horn; in the peripheral nervous system they found expression in the superior cervical ganglion, dorsal root ganglion, and trigeminal ganglion. No staining was detected in glial cells (178). Immunohistochemistry also show expression of TRPV3 in several human tissues: DRG, peripheral nerves, and ventral spinal cord (137).

Using a ribonuclease protection assay the TRPV3 mRNA in DRG, trigeminal ganglion, spinal cord, cerebellum, and cortex was detected (8). Rat TRPV3 was also found by RT-PCR in the substantia nigra pars compacta (179).

Expression of TRPV3 has also been studied using mouse as a model but surprisingly northern blot data showed a strong expression in keratinocytes but it did not found mRNA in brain, DRG, nor spinal cord (180), which it makes sense with functional data pointing out that only heat sensation through keratinocytes is affected in TRPV3$^{-/-}$ mice (181, 182). Nevertheless, expression of the channel has been found in the nerve terminals of the olfactory epithelium by immunohistochemistry (27). Also recent behavioral experiments showed that an incense compound that activates putative TRPV3 channels induces a behavior change in WT mice vs. TRPV3$^{-/-}$ (183). RT-PCR shows also a very low expression of TRPV3 mRNA in basal ganglia, cerebellum, cerebrum, forebrain, and hippocampus (34).

5.4. TRPV4

The first work where they cloned the human TRPV4 channel reported no mRNA ("in situ" hybridization) expression in the brain, DRG, or sensory nerve fibers, but they got a positive result in peripheral fibers (sympathetic and parasympathetic). Nevertheless, immunohistochemistry in human tissue showed TRPV4 in DRG and peripheral nerves (137).

Some authors reported also no expression in rat TRPV4 DRG (184); in this case northern blot techniques also reported no expression in brain, hypothalamus, nor sensory ganglia (or faint in

trigeminal ganglion (185). Nevertheless, other groups using northern blot and single cell RT-PCR (186) and by immunohistochemical techniques (187) showed mRNA and protein expression in DRG, brain, and dorsal horn of the spinal cord. Immunohistochemical experiments showed also a positive in hypothalamus neuropil (188, 189) and using western blot and immunohistochemistry (190) showed TRPV4 expression in the supraoptic and paraventricular nuclei. The TRPV4 mRNA was detected in DRG and trigeminal ganglion but only obtained a very faint signal in spinal cord, cerebellum, and cortex (8). DRG TRPV4 was also detected by northern blot (191). This channel has also been detected in astrocytes of cortex and hippocampus and surrounding cortices but not in neurons using RT-PCR, western blot, and immunocytochemistry (89, 192).

In mice, TRPV4 have been found by "in situ" hybridization in: vascular organ of the lamina terminalis, subfornical organ, median preoptic area, ependymal cells of the lateral ventricles and scattered neurons in cortex, thalamus, hippocampus, and cerebellum (185). Also "in situ" hybridization and immunoblotting demonstrated TRPV4 expression in hippocampal neurons and astrocytes "in situ" and immunocytochemistry in vitro (193). The expression in nerve fibers in the olfactory epithelium has also been shown (27). Finally, RT-PCR data displayed a strong mRNA expression in basal ganglia and cerebellum and a lower expression in cerebrum, forebrain, and hippocampus (34).

5.5. TRPV5 and TRPV6

Both channels are structurally close and they are related to Ca^{2+} homeostasis and they are not expressed in the nervous system, for a recent review see (194).

6. TRPML Subfamily

The TRPML subfamily is composed by three members (TRPML1, TRPML2, and TRPML3). The data available about expression and function of this family is scarce; they are part of the lysosomal and endosomal mechanisms except TRPML3 which can be present in the membrane and they can form homomers and heteromers among them (195). For a review on each of these channels, see (196–198).

6.1. TRPML1

This member of the TRPML subfamily is expressed ubiquitously in humans (199) and mice (200) and it is involved in the late endocytic pathway (201).

6.2. TRPML2

A detailed study about RT-PCR expression has been published where the expression of the channel is reported in all the tissues studied in mice (202).

6.3. TRPML3

Like TRPML2, TRPML3 mRNA presence was also studied by RT-PCR with a positive result in expression in all the tissues studied (202).

7. Concluding Remarks

In the present review we tried to briefly summarize the widespread distribution of the novel TRP cation channel family in the nervous system; their location, together with their ability to be modulated by very different physical, chemical, and intracellular stimuli, is a reflection of the different roles they can play. Functionally, TRP channels seem involved from high cognitive processes such as spatial navigation and working memory, where they are modulated by neurotransmitters, to the simplest signal transduction such as thermoreception or mechanoreception, where the temperature or a mechanical change is enough to generate a response. Besides the functions directly related to the nervous system they also play a central role in Ca^{2+}/Mg^{2+} homeostasis and intracellular mechanisms.

We are still beginning to understand the importance of the TRP in those processes and we hope this review will help to those interested on their characterization.

References

1. Montell C, Rubin GM (1989) Molecular characterization of the drosophila trp locus: a putative integral membrane protein required for phototransduction. Neuron 2:1313–1323
2. Zhu X, Chu PB, Peyton M, Birnbaumer L (1995) Molecular cloning of a widely expressed human homologue for the Drosophila trp gene. FEBS Lett 373:193–198
3. Wes PD (1995) TRPC1, a human homolog of a Drosophila store-operated channel. Proc Natl Acad Sci USA 92:9652–9656
4. Petersen C, Berridge MJ, Borgese MF, Bennett DL (1995) Putative capacitative calcium entry channels: expression of Drosophila trp and evidence for the existence of vertebrate homologues. Biochem J 311:41
5. Stokes A, Wakano C, Koblan-Huberson M, Adra CN, Fleig A, Turner H (2006) TRPA1 is a substrate for de-ubiquitination by the tumor suppressor CYLD. Cell Signal 18:1584–1594
6. Anand U, Otto WR, Facer P, Zebda N, Selmer I, Gunthorpe MJ, Chessell IP, Sinisi M, Birch R, Anand P (2008) TRPA1 receptor localisation in the human peripheral nervous system and functional studies in cultured human and rat sensory neurons. Neurosci Lett 438: 221–227
7. Obata K, Katsura H, Mizushima T, Yamanaka H, Kobayashi K, Dai Y, Fukuoka T, Tokunaga A, Tominaga M, Noguchi K (2005) TRPA1 induced in sensory neurons contributes to cold hyperalgesia after inflammation and nerve injury. J Clin Invest 115:2393–2401
8. Frederick J, Buck ME, Matson DJ, Cortright DN (2007) Increased TRPA1, TRPM8, and TRPV2 expression in dorsal root ganglia by nerve injury. Biochem Biophys Res Commun 358:1058–1064
9. Kobayashi K, Fukuoka T, Obata K, Yamanaka H, Dai Y, Tokunaga A, Noguchi K (2005)

Distinct expression of TRPM8, TRPA1, and TRPV1 mRNAs in rat primary afferent neurons with adelta/c-fibers and colocalization with trk receptors. J Comp Neurol 493: 596–606

10. Ro JY, Lee J-S, Zhang Y (2009) Activation of TRPV1 and TRPA1 leads to muscle nociception and mechanical hyperalgesia. Pain 144:270–277
11. Kim YS, Son JY, Kim TH, Paik SK, Dai Y, Noguchi K, Ahn DK, Bae YC (2010) Expression of transient receptor potential ankyrin 1 (TRPA1) in the rat trigeminal sensory afferents and spinal dorsal horn. J Comp Neurol 518:687–698
12. Katsura H, Tsuzuki K, Noguchi K, Sakagami M (2006) Differential expression of capsaicin-, menthol-, and mustard oil-sensitive receptors in naive rat geniculate ganglion neurons. Chem Senses 31:681–688
13. Zhao H, Sprunger LK, Simasko SM (2010) Expression of transient receptor potential channels and two-pore potassium channels in subtypes of vagal afferent neurons in rat. Am J Physiol Gastrointest Liver Physiol 298: G212–G221
14. Hondoh A, Ishida Y, Ugawa S, Ueda T, Shibata Y, Yamada T, Shikano M, Murakami S, Shimada S (2010) Distinct expression of cold receptors (TRPM8 and TRPA1) in the rat nodose-petrosal ganglion complex. Brain Res 1319:60–69
15. Werkheiser JL, Rawls SM, Cowan A (2006) Icilin evokes a dose- and time-dependent increase in glutamate within the dorsal striatum of rats. Amino Acids 30:307–309
16. Sun B, Bang S-I, Jin Y-H (2009) Transient receptor potential A1 increase glutamate release on brain stem neurons. Neuroreport 20:1002–1006
17. Yokoyama T, Ohbuchi T, Saito T, Sudo Y, Fujihara H, Minami K, Nagatomo T, Uezono Y, Ueta Y (2011) Allyl isothiocyanates and cinnamaldehyde potentiate miniature excitatory postsynaptic inputs in the supraoptic nucleus in rats. Eur J Pharmacol 655:31–37
18. Shigetomi E, Tong X, Kwan KY, Corey DP, Khakh BS (2011) TRPA1 channels regulate astrocyte resting calcium and inhibitory synapse efficacy through GAT-3. Nat Neurosci 15:70–80
19. Hjerling-Leffler J, Alqatari M, Ernfors P, Koltzenburg M (2007) Emergence of functional sensory subtypes as defined by transient receptor potential channel expression. J Neurosci 27:2435–2443
20. Smith MP, Beacham D, Ensor E, Koltzenburg M (2004) Cold-sensitive, menthol-insensitive neurons in the murine sympathetic nervous system. Neuroreport 15:1399–1403
21. Story GM, Peier AM, Reeve AJ, Eid SR, Mosbacher J, Hricik TR, Earley TJ, Hergarden AC, Andersson DA, Hwang SW, McIntyre P, Jegla T, Bevan S, Patapoutian A (2003) ANKTM1, a TRP-like channel expressed in nociceptive neurons, is activated by cold temperatures. Cell 112:819–829
22. Nagata K, Duggan A, Kumar G, García-Añoveros J (2005) Nociceptor and hair cell transducer properties of TRPA1, a channel for pain and hearing. J Neurosci 25:4052–4061
23. Nassenstein C, Kwong K, Taylor-Clark T, Kollarik M, Macglashan DM, Braun A, Undem BJ (2008) Expression and function of the ion channel TRPA1 in vagal afferent nerves innervating mouse lungs. J Physiol 586:1595–1604
24. Andrade EL, Luiz AP, Ferreira J, Calixto JB (2008) Pronociceptive response elicited by TRPA1 receptor activation in mice. Neuroscience 152:511–520
25. Nagatomo K, Kubo Y (2008) Caffeine activates mouse TRPA1 channels but suppresses human TRPA1 channels. Proc Natl Acad Sci USA 105:17373–17378
26. Takumida M, Ishibashi T, Hamamoto T, Hirakawa K, Anniko M (2009) Expression of transient receptor potential channel melastin (TRPM) 1-8 and TRPA1 (ankyrin) in mouse inner ear. Acta Otolaryngol 129:1050–1060
27. Nakashimo Y, Takumida M, Fukuiri T, Anniko M, Hirakawa K (2010) Expression of transient receptor potential channel vanilloid (TRPV) 1–4, melastin (TRPM) 5 and 8, and ankyrin (TRPA1) in the normal and methimazole-treated mouse olfactory epithelium. Acta Otolaryngol 130:1278–1286
28. Poole DP, Pelayo JC, Cattaruzza F, Kuo Y-M, Gai G, Chiu JV, Bron R, Furness JB, Grady EF, Bunnett NW (2011) Transient receptor potential ankyrin 1 is expressed by inhibitory motoneurons of the mouse intestine. Gastroenterology 141:565–575, 575.e1–4
29. Zitt C, Zobel A, Obukhov AG, Harteneck C, Kalkbrenner F, Lückhoff A, Schultz G (1996) Cloning and functional expression of a human Ca2+-permeable cation channel activated by calcium store depletion. Neuron 16: 1189–1196
30. Riccio A (2002) mRNA distribution analysis of human TRPC family in CNS and peripheral tissues. Mol Brain Res 109:95–104
31. Mizuno N, Kitayama S, Saishin Y, Shimada S, Morita K, Mitsuhata C, Kurihara H, Dohi T (1999) Molecular cloning and characteriza-

tion of rat trp homologues from brain., *Brain research*. Mol Brain Res 64:41–51

32. Wang W, O'Connell B, Dykeman R, Sakai T, Delporte C, Swaim W, Zhu X, Birnbaumer L, Ambudkar IS (1999) Cloning of Trp1beta isoform from rat brain: immunodetection and localization of the endogenous Trp1 protein. Am J Physiol Cell Physiol 276:C969–C979
33. Garcia RL, Schilling WP (1997) Differential expression of mammalian TRP homologues across tissues and cell lines. Biochem Biophys Res Commun 239:279–283
34. Kunert-Keil C, Bisping F, Krüger J, Brinkmeier H (2006) Tissue-specific expression of TRP channel genes in the mouse and its variation in three different mouse strains. BMC Genomics 7:159
35. Sergeeva OA, Korotkova TM, Scherer A, Brown RE, Haas HL (2003) Co-expression of non-selective cation channels of the transient receptor potential canonical family in central aminergic neurones. J Neurochem 85: 1547–1552
36. Strübing C, Krapivinsky G, Krapivinsky L, Clapham DE (2001) TRPC1 and TRPC5 form a novel cation channel in mammalian brain. Neuron 29:645–655
37. Kim SJ, Kim YS, Yuan JP, Petralia RS, Worley PF, Linden DJ (2003) Activation of the TRPC1 cation channel by metabotropic glutamate receptor mGluR1. Nature 426: 285–291
38. Martorana A, Giampà C, DeMarch Z, Viscomi MT, Patassini S, Sancesario G, Bernardi G, Fusco FR (2006) Distribution of TRPC1 receptors in dendrites of rat substantia nigra: a confocal and electron microscopy study. Eur J Neurosci 24:732–738
39. Boisseau S, Kunert-Keil C, Lucke S, Bouron A (2009) Heterogeneous distribution of TRPC proteins in the embryonic cortex. Histochem Cell Biol 131:355–363
40. Otsuka Y, Sakagami H, Owada Y (1998) Differential localization of mRNAs for mammalian trps, presumptive capacitative calcium entry channels, in the adult mouse brain. Tohoku J Exp Med 185:139–146
41. von Bohlen Und Halbach O, Hinz U, Unsicker K, Egorov AV (2005) Distribution of TRPC1 and TRPC5 in medial temporal lobe structures of mice. Cell Tissue Res 322: 201–206
42. Elg S, Marmigere F, Mattsson JP, Ernfors P (2007) Cellular subtype distribution and developmental regulation of TRPC channel members in the mouse dorsal root ganglion. J Comp Neurol 503:35–46
43. Zhang Z, Reboreda A, Alonso A, Barker PA, Séguéla P (2011) TRPC channels underlie cholinergic plateau potentials and persistent activity in entorhinal cortex. Hippocampus 21:386–397
44. Yan H-D, Villalobos C, Andrade R (2009) TRPC channels mediate a muscarinic receptor-induced afterdepolarization in cerebral cortex. J Neurosci 29:10038–10046
45. Liman ER, Innan H (2003) Relaxed selective pressure on an essential component of pheromone transduction in primate evolution. Proc Natl Acad Sci USA 100:3328–3332
46. Lucas P, Ukhanov K, Leinders-Zufall T, Zufall F (2003) A diacylglycerol-gated cation channel in vomeronasal neuron dendrites is impaired in TRPC2 mutant mice: mechanism of pheromone transduction. Neuron 40:551–561
47. Zhu X, Jiang M, Peyton M, Boulay G, Hurst R, Stefani E, Birnbaumer L (1996) trp, a novel mammalian gene family essential for agonist-activated capacitative Ca2+ entry. Cell 85:661–671
48. Chung YH, Sun Ahn H, Kim D, Hoon Shin D, Su Kim S, Yong Kim K, Bok Lee W, Ik Cha C (2006) Immunohistochemical study on the distribution of TRPC channels in the rat hippocampus. Brain Res 1085:132–137
49. Berg AP, Sen N, Bayliss DA (2007) TrpC3/C7 and Slo2.1 are molecular targets for metabotropic glutamate receptor signaling in rat striatal cholinergic interneurons. J Neurosci 27:8845–8856
50. Goel M, Sinkins WG, Schilling WP (2002) Selective association of TRPC channel subunits in rat brain synaptosomes. J Biol Chem 277:48303–48310
51. Li H-S, Xu X-ZS, Montell C (1999) Activation of a TRPC3-dependent cation current through the neurotrophin BDNF. Neuron 24:261–273
52. Mori Y, Takada N, Okada T, Wakamori M, Imoto K, Wanifuchi H, Oka H, Oba A, Ikenaka K, Kurosaki T (1998) Differential distribution of TRP Ca2+ channel isoforms in mouse brain. Neuroreport 9:507–515
53. Ben-Mabrouk F, Tryba AK (2010) Substance P modulation of TRPC3/7 channels improves respiratory rhythm regularity and ICAN-dependent pacemaker activity. Eur J Neurosci 31:1219–1232
54. Funayama M, Goto K, Kondo H (1996) Cloning and expression localization of cDNA for rat homolog of TRP protein, a possible store-operated calcium (Ca2+) channel. Brain Res Mol Brain Res 43:259–266
55. Fowler MA, Sidiropoulou K, Ozkan ED, Phillips CW, Cooper DC (2007) Corticolimbic

expression of TRPC4 and TRPC5 channels in the rodent brain. PLoS One 2:e573

56. Satoh E, Ono K, Xu F, Iijima T (2002) Cloning and functional expression of a novel splice variant of rat TRPC4. Circ J 66: 954–958
57. Schaefer M, Plant TD, Stresow N, Albrecht N, Schultz G (2002) Functional differences between TRPC4 splice variants. J Biol Chem 277:3752–3759
58. Munsch T, Freichel M, Flockerzi V, Pape H-C (2003) Contribution of transient receptor potential channels to the control of GABA release from dendrites. Proc Natl Acad Sci USA 100:16065–16070
59. Philipp S, Hambrecht J, Braslavski L, Schroth G, Freichel M, Murakami M, Cavalié A, Flockerzi V (1998) A novel capacitative calcium entry channel expressed in excitable cells. EMBO J 17:4274–4282
60. Wu D, Huang W, Richardson PM, Priestley JV, Liu M (2008) TRPC4 in rat dorsal root ganglion neurons is increased after nerve injury and is necessary for neurite outgrowth. J Biol Chem 283:416–426
61. Sossey-Alaoui K, Lyon JA, Jones L, Abidi FE, Hartung AJ, Hane B, Schwartz CE, Stevenson RE, Srivastava AK (1999) Molecular cloning and characterization of TRPC5 (HTRP5), the human homologue of a mouse brain receptor-activated capacitative Ca2+ entry channel. Genomics 60:330–340
62. Cui N, Zhang X, Tadepalli JS, Yu L, Gai H, Petit J, Pamulapati RT, Jin X, Jiang C (2011) Involvement of TRP channels in the CO-chemosensitivity of locus coeruleus neurons. J Neurophysiol 105:2791–2801
63. Tai C, Hines DJ, Choi HB, Macvicar BA (2010) Plasma membrane insertion of TRPC5 channels contributes to the cholinergic plateau potential in hippocampal CA1 pyramidal neurons. Hippocampus 967:958–967
64. Tomić M, Kucka M, Kretschmannova K, Li S, Nesterova M, Stratakis CA, Stojilkovic SS (2011) Role of nonselective cation channels in spontaneous and protein kinase A-stimulated calcium signaling in pituitary cells. Am J Physiol Endocrinol Metab 301:E370–E379
65. Huang W-C, Young JS, Glitsch MD (2007) Changes in TRPC channel expression during postnatal development of cerebellar neurons. Cell Calcium 42:1–10
66. Buniel MCF, Schilling WP, Kunze DL (2003) Distribution of transient receptor potential channels in the rat carotid chemosensory pathway. J Comp Neurol 464:404–413
67. Tai Y, Feng S, Ge R, Du W, Zhang X, He Z, Wang Y (2008) TRPC6 channels promote dendritic growth via the CaMKIV-CREB pathway. J Cell Sci 121:2301–2307
68. Wang X, Teng L, Li A, Ge J, Laties AM, Zhang X (2010) TRPC6 channel protects retinal ganglion cells in a rat model of retinal ischemia/reperfusion-induced cell death. Investig Ophthalmol Vis Sci 51:5751–5758
69. Warren EJ, Allen CN, Brown RL, Robinson DW (2006) The light-activated signaling pathway in SCN-projecting rat retinal ganglion cells. Eur J Neurosci 23:2477–2487
70. Cvetkovic-Lopes V, Eggermann E, Uschakov A, Grivel J, Bayer L, Jones BE, Serafin M, Mühlethaler M (2010) Rat hypocretin/orexin neurons are maintained in a depolarized state by TRPC channels. PLoS One 5:e15673
71. Welsh DG, Morielli AD, Nelson MT, Brayden JE (2002) Transient receptor potential channels regulate myogenic tone of resistance arteries. Circ Res 90:248–250
72. Elsaesser R, Montani G, Tirindelli R, Paysan J (2005) Phosphatidyl-inositide signalling proteins in a novel class of sensory cells in the mammalian olfactory epithelium. Eur J Neurosci 21:2692–2700
73. Okada T (1999) Molecular and functional characterization of a novel mouse transient receptor potential protein homologue TRP7. Ca2+-permeable cation channel that is constitutively activated and enhanced by stimulation of G protein-coupled receptor. J Biol Chem 274:27359–27370
74. Glazebrook PA, Schilling WP, Kunze DL (2005) TRPC channels as signal transducers. Pflügers Archiv 451:125–130
75. Ramsey IS, Delling M, Clapham DE (2006) An introduction to TRP channels. Annu Rev Physiol 68:619–647
76. Venkatachalam K, Montell C (2007) TRP channels. Annu Rev Biochem 76:387–417
77. Fonfria E, Murdock PR, Cusdin FS, Benham CD, Kelsell RE, McNulty S (2006) Tissue distribution profiles of the human TRPM cation channel family. J Recept Signal Transduct Res 26:159–178
78. Oancea E, Vriens J, Brauchi S, Jun J, Splawski I, Clapham DE (2009) TRPM1 forms ion channels associated with melanin content in melanocytes. Sci Signal 2:ra21
79. Staaf S, Franck MC, Marmigère F, Mattsson JP, Ernfors P (2010) Dynamic expression of the TRPM subgroup of ion channels in developing mouse sensory neurons. Gene Expr Patterns 10:65–74

80. Gilliam JC, Wensel TG (2011) TRP channel gene expression in the mouse retina. Vision Res 51:2440–2452
81. Shen Y, Heimel JA, Kamermans M, Peachey NS, Gregg RG, Nawy S (2009) A transient receptor potential-like channel mediates synaptic transmission in rod bipolar cells. J Neurosci 29:6088–6093
82. Xu Y, Dhingra A, Fina M, Koike C, Furukawa T, Vardi N (2011) mGluR6 deletion renders the TRPM1 channel in retina inactive. J Neurophysiol 107:948–957
83. Nagamine K, Kudoh J, Minoshima S, Kawasaki K, Asakawa S, Ito F, Shimizu N (1998) Molecular cloning of a novel putative Ca2+ channel protein (TRPC7) highly expressed in brain. Genomics 54:124–131
84. Uemura T, Kudoh J, Noda S, Kanba S, Shimizu N (2005) Characterization of human and mouse TRPM2 genes: identification of a novel N-terminal truncated protein specifically expressed in human striatum. Biochem Biophys Res Commun 328:1232–1243
85. Fonfria E, Mattei C, Hill K, Brown JT, Randall A, Benham CD, Skaper SD, Campbell CA, Crook B, Murdock PR, Wilson JM, Maurio FP, Owen DE, Tilling PL, McNulty S (2006) TRPM2 is elevated in the tMCAO stroke model, transcriptionally regulated, and functionally expressed in C13 microglia. J Recept Signal Transduct Res 26:179–198
86. Aarts M, Iihara K, Wei W-L, Xiong Z-G, Arundine M, Cerwinski W, MacDonald JF, Tymianski M (2003) A key role for TRPM7 channels in anoxic neuronal death. Cell 115:863–877
87. Kaneko S, Kawakami S, Hara Y, Wakamori M, Itoh E, Minami T, Takada Y, Kume T, Katsuki H, Mori Y, Akaike A (2006) A critical role of TRPM2 in neuronal cell death by hydrogen peroxide. J Pharmacol Sci 101:66–76
88. Olah ME, Jackson MF, Li H, Perez Y, Sun H-S, Kiyonaka S, Mori Y, Tymianski M, MacDonald JF (2009) Ca2+-dependent induction of TRPM2 currents in hippocampal neurons. J Physiol 587:965–979
89. Bai J-Z, Lipski J (2010) Differential expression of TRPM2 and TRPV4 channels and their potential role in oxidative stress-induced cell death in organotypic hippocampal culture. Neurotoxicology 31:204–214
90. Cook NL, Vink R, Helps SC, Manavis J, van den Heuvel C (2010) Transient receptor potential melastatin 2 expression is increased following experimental traumatic brain injury in rats. J Mol Neurosci 42:192–199
91. Fonfria E, Marshall IC, Boyfield I, Skaper SD, Hughes JP, Owen DE, Zhang W, Miller BA, Benham CD, McNulty S (2005) Amyloid beta-peptide(1-42) and hydrogen peroxide-induced toxicity are mediated by TRPM2 in rat primary striatal cultures. J Neurochem 95:715–723
92. Hill K, Tigue NJ, Kelsell RE, Benham CD, McNulty S, Schaefer M, Randall AD (2006) Characterisation of recombinant rat TRPM2 and a TRPM2-like conductance in cultured rat striatal neurones. Neuropharmacology 50: 89–97
93. Freestone PS, Chung KKH, Guatteo E, Mercuri NB, Nicholson LFB, Lipski J (2009) Acute action of rotenone on nigral dopaminergic neurons–involvement of reactive oxygen species and disruption of Ca2+ homeostasis. Eur J Neurosci 30:1849–1859
94. Chung KKH, Freestone PS, Lipski J (2011) Expression and functional properties of TRPM2 channels in dopaminergic neurons of the substantia nigra of the rat. J Neurophysiol 106:2865–2875
95. Kraft R, Grimm C, Grosse K, Hoffmann A, Sauerbruch S, Kettenmann H, Schultz G, Harteneck C (2004) Hydrogen peroxide and ADP-ribose induce TRPM2-mediated calcium influx and cation currents in microglia. Am J Physiol Cell Physiol 286:C129–C137
96. Nazıroğlu M, Özgül C, Çiğ B, Doğan S, Uğuz AC (2011) Glutathione modulates Ca(2+) influx and oxidative toxicity through TRPM2 channel in rat dorsal root ganglion neurons. J Membr Biol 242:109–118
97. Hara Y, Wakamori M, Ishii M, Maeno E, Nishida M, Yoshida T, Yamada H, Shimizu S, Mori E, Kudoh J, Shimizu N, Kurose H, Okada Y, Imoto K, Mori Y (2002) LTRPC2 Ca2+-permeable channel activated by changes in redox status confers susceptibility to cell death. Mol Cell 9:163–173
98. Xie Y-F, Belrose JC, Lei G, Tymianski M, Mori Y, Macdonald JF, Jackson MF (2011) Dependence of NMDA/GSK3beta mediated metaplasticity on TRPM2 channels at hippocampal CA3-CA1 synapses. Mol Brain 4:44
99. Oberwinkler J, Phillipp S (2007) TRPM3. In: Flockerzi V, Nilius B (eds) Transient receptor potential (TRP) channels, Handbook of experimental biology. Springer, Berlin, pp 253–267
100. Grimm C, Kraft R, Sauerbruch S, Schultz G, Harteneck C (2003) Molecular and functional characterization of the melastatin-related cation channel TRPM3. J Biol Chem 278: 21493–21501
101. Lee N, Chen J, Sun L, Wu S, Gray KR, Rich A, Huang M, Lin J-H, Feder JN, Janovitz EB,

Levesque PC, Blanar MA (2003) Expression and characterization of human transient receptor potential melastatin 3 (hTRPM3). J Biol Chem 278:20890–20897

102. Oberwinkler J, Lis A, Giehl KM, Flockerzi V, Philipp SE (2005) Alternative splicing switches the divalent cation selectivity of TRPM3 channels. J Biol Chem 280:22540–22548
103. Zamudio-Bulcock PA, Everett J, Harteneck C, Valenzuela CF (2011) Activation of steroid-sensitive TRPM3 channels potentiates glutamatergic transmission at cerebellar Purkinje neurons from developing rats. J Neurochem 119:474–485
104. Deo M, Yu J-Y, Chung K-H, Tippens M, Turner DL (2006) Detection of mammalian microRNA expression by "in situ" hybridization with RNA oligonucleotides. Dev Dyn 235:2538–2548
105. Vriens J, Owsianik G, Hofmann T, Philipp SE, Stab J, Chen X, Benoit M, Xue F, Janssens A, Kerselaers S, Oberwinkler J, Vennekens R, Gudermann T, Nilius B, Voets T (2011) TRPM3 is a nociceptor channel involved in the detection of noxious heat. Neuron 70:482–494
106. Xu XZ, Moebius F, Gill DL, Montell C (2001) Regulation of melastatin, a TRP-related protein, through interaction with a cytoplasmic isoform. Proc Natl Acad Sci USA 98:10692–10697
107. Launay P, Fleig A, Perraud A-L, Scharenberg AM, Penner R, Kinet J-P (2002) TRPM4 is a Ca2+-activated nonselective cation channel mediating cell membrane depolarization. Cell 109:397–407
108. Nilius B, Prenen J, Droogmans G, Voets T, Vennekens R, Freichel M, Wissenbach U, Flockerzi V (2003) Voltage dependence of the Ca2+-activated cation channel TRPM4. J Biol Chem 278:30813–30820
109. Vennekens B, Nilius R (2007) Insights into TRPM4 function, regulation and physiological role. Handb Exp Pharmacol (179):269–285
110. Earley S, Waldron BJ, Brayden JE (2004) Critical role for transient receptor potential channel TRPM4 in myogenic constriction of cerebral arteries. Circ Res 95:922–929
111. Yoo JC, Yarishkin OV, Hwang EM, Kim E, Kim D-G, Park N, Hong S-G, Park J-Y (2010) Cloning and characterization of rat transient receptor potential-melastatin 4 (TRPM4). Biochem Biophys Res Commun 391:806–811
112. Armstrong WE, Wang L, Li C, Teruyama R (2010) Performance, properties and plasticity of identified oxytocin and vasopressin neurones in vitro. J Neuroendocrinol 22: 330–342
113. Teruyama R, Sakuraba M, Kurotaki H, Armstrong WE (2011) Transient receptor potential channel m4 and m5 in magnocellular cells in rat supraoptic and paraventricular nuclei. J Neuroendocrinol 23:1204–1213
114. Murakami M, Xu F, Miyoshi I, Sato E, Ono K, Iijima T (2003) Identification and characterization of the murine TRPM4 channel. Biochem Biophys Res Commun 307:522–528
115. Mathar I, Vennekens R, Meissner M, Kees F, Van der Mieren G, Camacho Londoño JE, Uhl S, Voets T, Hummel B, van den Bergh A, Herijgers P, Nilius B, Flockerzi V, Schweda F, Freichel M (2010) Increased catecholamine secretion contributes to hypertension in TRPM4-deficient mice. J Clin Invest 120:3267–3279
116. Crowder EA, Saha MS, Pace RW, Zhang H, Prestwich GD, Del Negro CA (2007) Phosphatidylinositol 4,5-bisphosphate regulates inspiratory burst activity in the neonatal mouse preBötzinger complex. J Physiol 582:1047–1058
117. Mironov SL (2008) Metabotropic glutamate receptors activate dendritic calcium waves and TRPM channels which drive rhythmic respiratory patterns in mice. J Physiol 586: 2277–2291
118. Beck A, Penner R, Fleig A (2008) Lipopolysaccharide-induced down-regulation of Ca2+ release-activated Ca2+ currents (I CRAC) but not Ca2+-activated TRPM4-like currents (I CAN) in cultured mouse microglial cells. J Physiol 586:427–439
119. Prawitt D (2000) Identification and characterization of MTR1, a novel gene with homology to melastatin (MLSN1) and the trp gene family located in the BWS-WT2 critical region on chromosome 11p15.5 and showing allele-specific expression. Hum Mol Genet 9:203–216
120. Pérez CA, Huang L, Rong M, Kozak JA, Preuss AK, Zhang H, Max M, Margolskee RF (2002) A transient receptor potential channel expressed in taste receptor cells. Nat Neurosci 5:1169–1176
121. Medler KF (2011) Multiple roles for TRPs in the taste system: not your typical TRPs. Adv Exp Med Biol 704:831–846
122. Lin W, Margolskee R, Donnert G, Hell SW, Restrepo D (2007) Olfactory neurons expressing transient receptor potential channel M5 (TRPM5) are involved in sensing semiochemicals. Proc Natl Acad Sci USA 104:2471–2476

123. Gulbransen BD, Clapp TR, Finger TE, Kinnamon SC (2008) Nasal solitary chemoreceptor cell responses to bitter and trigeminal stimulants in vitro. J Neurophysiol 99: 2929–2937

124. Krasteva G, Hartmann P, Papadakis T, Bodenbenner M, Wessels L, Weihe E, Schütz B, Langheinrich AC, Chubanov V, Gudermann T, Ibanez-Tallon I, Kummer W (2012) Cholinergic chemosensory cells in the auditory tube. Histochem Cell Biol 137(4): 483–497

125. Staaf S, Oerther S, Lucas G, Mattsson JP, Ernfors P (2009) Differential regulation of TRP channels in a rat model of neuropathic pain. Pain 144:187–199

126. Schmitz C, Dorovkov MV, Zhao X, Davenport BJ, Ryazanov AG, Perraud A-L (2005) The channel kinases TRPM6 and TRPM7 are functionally nonredundant. J Biol Chem 280: 37763–37771

127. Schlingmann KP, Weber S, Peters M, Niemann Nejsum L, Vitzthum H, Klingel K, Kratz M, Haddad E, Ristoff E, Dinour D, Syrrou M, Nielsen S, Sassen M, Waldegger S, Seyberth HW, Konrad M (2002) Hypomagnesemia with secondary hypocalcemia is caused by mutations in TRPM6, a new member of the TRPM gene family. Nat Genet 31:166–170

128. Voets T, Nilius B, Hoefs S, van der Kemp AWCM, Droogmans G, Bindels RJM, Hoenderop JGJ (2004) TRPM6 forms the Mg2+ influx channel involved in intestinal and renal Mg2+ absorption. J Biol Chem 279:19–25

129. Thilo F, Suess O, Liu Y, Tepel M (2011) Decreased expression of transient receptor potential channels in cerebral vascular tissue from patients after hypertensive intracerebral hemorrhage. Clin Exp Hypertens 33:533–537

130. Nadler MJ, Hermosura MC, Inabe K, Perraud AL, Zhu Q, Stokes AJ, Kurosaki T, Kinet JP, Penner R, Scharenberg AM, Fleig A (2001) LTRPC7 is a Mg.ATP-regulated divalent cation channel required for cell viability. Nature 411:590–595

131. Runnels LW, Yue L, Clapham DE (2001) TRP-PLIK, a bifunctional protein with kinase and ion channel activities. Science 291: 1043–1047

132. Jiang X, Newell EW, Schlichter LC (2003) Regulation of a TRPM7-like current in rat brain microglia. J Biol Chem 278:42867–42876

133. Krapivinsky G, Mochida S, Krapivinsky L, Cibulsky SM, Clapham DE (2006) The TRPM7 ion channel functions in cholinergic synaptic vesicles and affects transmitter release. Neuron 52:485–496

134. Brauchi S, Krapivinsky G, Krapivinsky L, Clapham DE (2008) TRPM7 facilitates cholinergic vesicle fusion with the plasma membrane. Proc Natl Acad Sci USA 105: 8304–8308

135. Gee CE, Benquet P, Gerber U (2002) Group I metabotropic glutamate receptors activate a calcium-sensitive transient receptor potential-like conductance in rat hippocampus. J Physiol 546:655–664

136. Tian S-L, Jiang H, Zeng Y, Li L-L, Shi J (2007) NGF-induced reduction of an outward-rectifying TRPM7-like current in rat CA1 hippocampal neurons. Neurosci Lett 419:93–98

137. Facer P, Casula MA, Smith GD, Benham CD, Chessell IP, Bountra C, Sinisi M, Birch R, Anand P (2007) Differential expression of the capsaicin receptor TRPV1 and related novel receptors TRPV3, TRPV4 and TRPM8 in normal human tissues and changes in traumatic and diabetic neuropathy. BMC Neurol 7:11

138. McKemy DD, Neuhausser WM, Julius D (2002) Identification of a cold receptor reveals a general role for TRP channels in thermosensation. Nature 416:52–58

139. Stein RJ, Santos S, Nagatomi J, Hayashi Y, Minnery BS, Xavier M, Patel AS, Nelson JB, Futrell WJ, Yoshimura N, Chancellor MB, De Miguel F (2004) Cool (TRPM8) and hot (TRPV1) receptors in the bladder and male genital tract. J Urol 172:1175–1178

140. Xing H, Ling JX, Chen M, Johnson RD, Tominaga M, Wang C-Y, Gu J (2008) TRPM8 mechanism of autonomic nerve response to cold in respiratory airway. Mol Pain 4:22

141. Crawford DC, Moulder KL, Gereau RW, Story GM, Mennerick S (2009) Comparative effects of heterologous TRPV1 and TRPM8 expression in rat hippocampal neurons. PLoS One 4:e8166

142. Tani M, Onimaru H, Ikeda K, Kawakami K, Homma I (2010) Menthol inhibits the respiratory rhythm in brainstem preparations of the newborn rats. Neuroreport 21: 1095–1099

143. Takashima Y, Ma L, McKemy DD (2010) The development of peripheral cold neural circuits based on TRPM8 expression. Neuroscience 169:828–842

144. Peier AM, Moqrich A, Hergarden AC, Reeve AJ, Andersson DA, Story GM, Earley TJ, Dragoni I, McIntyre P, Bevan S (2002) A TRP channel that senses cold stimuli and menthol. Cell 108:705–715

145. Weil A, Moore SE, Waite NJ, Randall A, Gunthorpe MJ (2005) Conservation of

functional and pharmacological properties in the distantly related temperature sensors TRVP1 and TRPM8. Mol Pharmacol 68: 518–527

146. Dhaka A, Earley TJ, Watson J, Patapoutian A (2008) Visualizing cold spots: TRPM8-expressing sensory neurons and their projections. J Neurosci 28:566–575
147. Karashima Y, Talavera K, Everaerts W, Janssens A, Kwan KY, Vennekens R, Nilius B, Voets T (2009) TRPA1 acts as a cold sensor in vitro and in vivo. Proc Natl Acad Sci USA 106: 1273–1278
148. Madrid R, de la Peña E, Donovan-Rodriguez T, Belmonte C, Viana F (2009) Variable threshold of trigeminal cold-thermosensitive neurons is determined by a balance between TRPM8 and Kv1 potassium channels. J Neurosci 29:3120–3131
149. Fajardo O, Meseguer V, Belmonte C, Viana F (2008) TRPA1 channels mediate cold temperature sensing in mammalian vagal sensory neurons: pharmacological and genetic evidence. J Neurosci 28:7863–7875
150. Acs G, Palkovits M, Blumberg PM (1996) Specific binding of [3H]resiniferatoxin by human and rat preoptic area, locus ceruleus, medial hypothalamus, reticular formation and ventral thalamus membrane preparations. Life Sci 59:1899–1908
151. Szabo T (2002) Pharmacological characterization of vanilloid receptor located in the brain. Mol Brain Res 98:51–57
152. Mezey E, Tóth ZE, Cortright DN, Arzubi MK, Krause JE, Elde R, Guo A, Blumberg PM, Szallasi A (2000) Distribution of mRNA for vanilloid receptor subtype 1 (VR1), and VR1-like immunoreactivity, in the central nervous system of the rat and human. Proc Natl Acad Sci USA 97:3655–3660
153. Hayes P, Meadows HJ, Gunthorpe MJ, Harries MH, Duckworth DM, Cairns W, Harrison DC, Clarke CE, Ellington K, Prinjha RK, Barton AJ, Medhurst AD, Smith GD, Topp S, Murdock P, Sanger GJ, Terrett J, Jenkins O, Benham CD, Randall AD, Gloger IS, Davis JB (2000) Cloning and functional expression of a human orthologue of rat vanilloid receptor-1. Pain 88:205–215
154. Baumann TK, Chaudhary P, Martenson ME (2004) Background potassium channel block and TRPV1 activation contribute to proton depolarization of sensory neurons from humans with neuropathic pain. Eur J Neurosci 19:1343–1351
155. Karai L, Brown DC, Mannes AJ, Connelly ST, Brown J, Gandal M, Wellisch OM, Neubert JK, Olah Z, Iadarola MJ (2004) Deletion of vanilloid receptor 1-expressing primary afferent neurons for pain control. J Clin Invest 113:1344–1352
156. Guo A, Vulchanova L, Wang J, Li X, Elde R (1999) Immunocytochemical localization of the vanilloid receptor 1 (VR1): relationship to neuropeptides, the P2X 3 purinoceptor and IB4 binding sites. Eur J Neurosci 11: 946–958
157. Liapi A, Wood JN (2005) Extensive co-localization and heteromultimer formation of the vanilloid receptor-like protein TRPV2 and the capsaicin receptor TRPV1 in the adult rat cerebral cortex. Eur J Neurosci 22:825–834
158. Starowicz K, Maione S, Cristino L, Palazzo E, Marabese I, Rossi F, de Novellis V, Di Marzo V (2007) Tonic endovanilloid facilitation of glutamate release in brainstem descending antinociceptive pathways. J Neurosci 27:13739–13749
159. Valtschanoff JG, Rustioni A, Guo A, Hwang SJ (2001) Vanilloid receptor VR1 is both presynaptic and postsynaptic in the superficial laminae of the rat dorsal horn. J Comp Neurol 436:225–235
160. Marinelli S, Di Marzo V, Florenzano F, Fezza F, Viscomi MT, van der Stelt M, Bernardi G, Molinari M, Maccarrone M, Mercuri NB (2007) N-arachidonoyl-dopamine tunes synaptic transmission onto dopaminergic neurons by activating both cannabinoid and vanilloid receptors. Neuropsychopharmacology 32: 298–308
161. Tóth A, Boczán J, Kedei N, Lizanecz E, Bagi Z, Papp Z, Edes I, Csiba L, Blumberg PM (2005) Expression and distribution of vanilloid receptor 1 (TRPV1) in the adult rat brain. Brain Res Mol Brain Res 135:162–168
162. Li H-B, Mao R-R, Zhang J-C, Yang Y, Cao J, Xu L (2008) Antistress effect of TRPV1 channel on synaptic plasticity and spatial memory. Biol Psychiatry 64:286–292
163. Roberts JC, Davis JB, Benham CD (2004) [3H]Resiniferatoxin autoradiography in the CNS of wild-type and TRPV1 null mice defines TRPV1 (VR-1) protein distribution. Brain Res 995:176–183
164. Cristino L, de Petrocellis L, Pryce G, Baker D, Guglielmotti V, Di Marzo V (2006) Immunohistochemical localization of cannabinoid type 1 and vanilloid transient receptor potential vanilloid type 1 receptors in the mouse brain. Neuroscience 139:1405–1415
165. Zhang L, Jones S, Brody K, Costa M, Brookes SJH (2004) Thermosensitive transient receptor potential channels in vagal afferent neurons of the mouse. Am J Physiol Gastrointest Liver Physiol 286:G983–G991

166. Kowase T, Nakazato Y, Yoko-O H, Morikawa A, Kojima I (2002) Immunohistochemical localization of growth factor-regulated channel (GRC) in human tissues. Endocr J 49: 349–355
167. Wainwright A, Rutter AR, Seabrook GR, Reilly K, Oliver KR (2004) Discrete expression of TRPV2 within the hypothalamo-neurohypophysial system: Implications for regulatory activity within the hypothalamic-pituitary-adrenal axis. J Comp Neurol 474: 24–42
168. Greffrath W, Binzen U, Schwarz ST, Saaler-Reinhardt S, Treede R-D (2003) Co-expression of heat sensitive vanilloid receptor subtypes in rat dorsal root ganglion neurons. Neuroreport 14:2251–2255
169. Shibasaki K, Murayama N, Ono K, Ishizaki Y, Tominaga M (2010) TRPV2 enhances axon outgrowth through its activation by membrane stretch in developing sensory and motor neurons. J Neurosci 30:4601–4612
170. Lewinter RD, Skinner K, Julius D, Basbaum AI (2004) Immunoreactive TRPV-2 (VRL-1), a capsaicin receptor homolog, in the spinal cord of the rat. J Comp Neurol 470:400–408
171. Lewinter RD, Scherrer G, Basbaum AI (2008) Dense transient receptor potential cation channel, vanilloid family, type 2 (TRPV2) immunoreactivity defines a subset of motoneurons in the dorsal lateral nucleus of the spinal cord, the nucleus ambiguus and the trigeminal motor nucleus in rat. Neuroscience 151:164–173
172. Ichikawa H, Sugimoto T (2004) The co-expression of P2X3 receptor with VR1 and VRL-1 in the rat trigeminal ganglion. Brain Res 998:130–135
173. Okano H, Koike S, Bamba H, Toyoda K, Uno T, Hisa Y (2006) Participation of TRPV1 and TRPV2 in the rat laryngeal sensory innervation. Neurosci Lett 400:35–38
174. Kashiba H, Uchida Y, Takeda D, Nishigori A, Ueda Y, Kuribayashi K, Ohshima M (2004) TRPV2-immunoreactive intrinsic neurons in the rat intestine. Neurosci Lett 366:193–196
175. Mihara H, Boudaka A, Shibasaki K, Yamanaka A, Sugiyama T, Tominaga M (2010) Involvement of TRPV2 activation in intestinal movement through nitric oxide production in mice. J Neurosci 30:16536–16544
176. Tamura S, Morikawa Y, Senba E (2005) TRPV2, a capsaicin receptor homologue, is expressed predominantly in the neurotrophin-3-dependent subpopulation of primary sensory neurons. Neuroscience 130:223–228
177. Smith GD, Gunthorpe MJ, Kelsell RE, Hayes PD, Reilly P, Facer P, Wright JE, Jerman JC, Walhin J-P, Ooi L, Egerton J, Charles KJ, Smart D, Randall AD, Anand P, Davis JB (2002) TRPV3 is a temperature-sensitive vanilloid receptor-like protein. Nature 418: 186–190
178. Xu H, Ramsey IS, Kotecha SA, Moran MM, Chong JA, Lawson D, Ge P, Lilly J, Silos-Santiago I, Xie Y, DiStefano PS, Curtis R, Clapham DE (2002) TRPV3 is a calcium-permeable temperature-sensitive cation channel. Nature 418:181–186
179. Guatteo E, Chung KKH, Bowala TK, Bernardi G, Mercuri NB, Lipski J (2005) Temperature sensitivity of dopaminergic neurons of the substantia nigra pars compacta: involvement of transient receptor potential channels. J Neurophysiol 94:3069–3080
180. Peier AM, Reeve AJ, Andersson DA, Moqrich A, Earley TJ, Hergarden AC, Story GM, Colley S, Hogenesch JB, McIntyre P, Bevan S, Patapoutian A (2002) A heat-sensitive TRP channel expressed in keratinocytes. Science 296:2046–2049
181. Moqrich A, Hwang SW, Earley TJ, Petrus MJ, Murray AN, Spencer KSR, Andahazy M, Story GM, Patapoutian A (2005) Impaired thermosensation in mice lacking TRPV3, a heat and camphor sensor in the skin. Science 307:1468–1472
182. Huang SM, Li X, Yu Y, Wang J, Caterina MJ (2011) TRPV3 and TRPV4 ion channels are not major contributors to mouse heat sensation. Mol Pain 7:37
183. Moussaieff A, Rimmerman N, Bregman T, Straiker A, Felder CC, Shoham S, Kashman Y, Huang SM, Lee H, Shohami E, Mackie K, Caterina MJ, Walker JM, Fride E, Mechoulam R (2008) Incensole acetate, an incense component, elicits psychoactivity by activating TRPV3 channels in the brain. FASEB J 22: 3024–3034
184. Delany NS, Hurle M, Facer P, Alnadaf T, Plumpton C, Kinghorn I, See CG, Costigan M, Anand P, Woolf CJ, Crowther D, Sanseau P, Tate SN (2001) Identification and characterization of a novel human vanilloid receptor-like protein, VRL-2. Physiol Genomics 4:165–174
185. Liedtke W, Choe Y, Martí-Renom MA, Bell AM, Denis CS, Hudspeth AJ, Friedman JM, Heller S (2000) Vanilloid receptor–related osmotically activated channel (VR-OAC), a candidate vertebrate osmoreceptor. Cell 103: 525–535
186. Alessandri-Haber N, Yeh JJ, Boyd AE, Parada CA, Chen X, Reichling DB, Levine JD (2003) Hypotonicity induces TRPV4-mediated nociception in rat. Neuron 39:497–511

187. Cao D-S, Yu S-Q, Premkumar LS (2009) Modulation of transient receptor potential Vanilloid 4-mediated membrane currents and synaptic transmission by protein kinase C. Mol Pain 5:5
188. Guler AD, Lee H, Iida T, Shimizu I, Tominaga M, Caterina M (2002) Heat-evoked activation of the ion channel, TRPV4. J Neurosci 22:6408–6414
189. Wechselberger M, Wright CL, Bishop GA, Boulant JA (2006) Ionic channels and conductance-based models for hypothalamic neuronal thermosensitivity. Am J Physiol Regul Integr Comp Physiol 291:R518–R529
190. Carreño FR, Ji LL, Cunningham JT (2009) Altered central TRPV4 expression and lipid raft association related to inappropriate vasopressin secretion in cirrhotic rats. Am J Physiol Regul Integr Comp Physiol 296:R454–R466
191. Zhang Y, Wang Y-H, Ge H-Y, Arendt-Nielsen L, Wang R, Yue S-W (2008) A transient receptor potential vanilloid 4 contributes to mechanical allodynia following chronic compression of dorsal root ganglion in rats. Neurosci Lett 432:222–227
192. Benfenati V, Amiry-Moghaddam M, Caprini M, Mylonakou MN, Rapisarda C, Ottersen OP, Ferroni S (2007) Expression and functional characterization of transient receptor potential vanilloid-related channel 4 (TRPV4) in rat cortical astrocytes. Neuroscience 148: 876–892
193. Shibasaki K, Suzuki M, Mizuno A, Tominaga M (2007) Effects of body temperature on neural activity in the hippocampus: regulation of resting membrane potentials by transient receptor potential vanilloid 4. J Neurosci 27: 1566–1575
194. Peng J-B (2011) TRPV5 and TRPV6 in transcellular Ca(2+) transport: regulation, gene duplication, and polymorphisms in African populations. Adv Exp Med Biol 704:239–275
195. Curcio-Morelli C, Zhang P, Venugopal B, Charles FA, Browning MF, Cantiello HF, Slaugenhaupt SA (2010) Functional multimerization of mucolipin channel proteins. J Cell Physiol 222:328–335
196. Colletti GA, Kiselyov K (2011) TRPML1. Adv Exp Med Biol 704:209–219
197. Flores EN, García-Añoveros J (2011) TRPML2 and the evolution of mucolipins. Adv Exp Med Biol 704:221–228
198. Noben-Trauth K (2011) The TRPML3 channel: from gene to function. Adv Exp Med Biol 704:229–237
199. Sun M (2000) Mucolipidosis type IV is caused by mutations in a gene encoding a novel transient receptor potential channel. Hum Mol Genet 9:2471–2478
200. Falardeau J, Kennedy J, Acierno J, Sun M, Stahl S, Goldin E, Slaugenhaupt S (2002) Cloning and characterization of the mouse Mcoln1 gene reveals an alternatively spliced transcript not seen in humans. BMC Genomics 3:3
201. Manzoni M, Monti E, Bresciani R, Bozzato A, Barlati S, Bassi MT, Borsani G (2004) Overexpression of wild-type and mutant mucolipin proteins in mammalian cells: effects on the late endocytic compartment organization. FEBS Lett 567:219–224
202. Samie MA, Grimm C, Evans JA, Curcio-Morelli C, Heller S, Slaugenhaupt SA, Cuajungco MP (2009) The tissue-specific expression of TRPML2 (MCOLN-2) gene is influenced by the presence of TRPML1. Pflügers Archiv 459:79–91

Chapter 8

Investigation of the Possible Role of TRP Channels in Schizophrenia

Loris A. Chahl

Abstract

Schizophrenia is a debilitating psychiatric disorder. The limitations of current treatments for schizophrenia have led to an ongoing search for new drug targets. The observations that subjects with schizophrenia have impaired thermoregulation, are less sensitive to pain than normal subjects, and exhibit reduced niacin flare responses suggested that TRPV1 channels, and possibly also other temperature-sensitive TRPs that are co-expressed with TRPV1 on sensory neurons, might be linked with schizophrenia. In order to model deficit in function of TRP channels in animals, capsaicin treatment of neonatal rats was used to induce lifelong loss of a high proportion of primary afferent neurons that co-express TRPV1 and related TRP channels. The methods used to test the proposal that TRPV1 deficit induces brain and behavioral changes expected in an animal model of schizophrenia are described.

Key words: TRP channels, Schizophrenia, TRPV1, Animal models

1. Introduction

Schizophrenia is a debilitating psychiatric disorder characterized by positive symptoms including hallucinations and delusions, negative symptoms such as anhedonia and social withdrawal, and cognitive deficits in attention and executive function. The etiology of the disorder is not clear, but it is widely accepted that it is a neurodevelopmental disorder involving both genetic and environmental factors (1, 2). The symptoms of the disorder commonly manifest in early adulthood with a higher incidence in males. Several susceptibility genes for schizophrenia have been identified, including neuregulin 1 (NRG1), catechol-O-methyltransferase (COMT), dysbindin, disrupted in schizophrenia 1 (DISC1), and regulator of

Arpad Szallasi and Tamás Bíró (eds.), *TRP Channels in Drug Discovery: Volume II*, Methods in Pharmacology and Toxicology,
DOI 10.1007/978-1-62703-095-3_8,

G-protein signaling (RGS) protein-4 (RGS-4), with the strongest evidence being for NRG1 (3–13).

Studies on postmortem human brain from subjects with schizophrenia have shown that the brains are reduced in volume (14–16), have larger ventricles and thinner cortices compared with those of healthy individuals (17, 18). Selemon et al. (19, 20) also observed that neuronal density was increased in the prefrontal cortex of subjects with schizophrenia and proposed that the symptoms of schizophrenia resulted from reduced cortical connectivity, a proposal that is now known as the "reduced neuropil hypothesis" (21).

Drugs used for the treatment of the symptoms of schizophrenia have a range of pharmacological actions but share the property of dopamine D_2 receptor antagonism. Although the classical dopamine D_2 receptor antagonists are effective in treating the positive symptoms of schizophrenia, they produce serious motor side effects. The newer atypical antipsychotic drugs produce fewer motor side effects than the older drugs but none of the current antipsychotic agents is effective in treating all of the symptoms of schizophrenia, the cognitive deficits being notably resistant to treatment.

The limitations of current treatments for schizophrenia have led to an ongoing search for new drug targets. In recent years transient receptor potential (TRP) channels have emerged as targets worthy of investigation in psychiatric disorders (22, 23). Of particular interest is the TRPV1 channel (previously known as the capsaicin or vanilloid receptor 1 (VR1)), first identified in sensory neurons (24, 25) but now known to be widely distributed in both the central and peripheral nervous systems. The TRPV1 channel is activated by plant substances such as capsaicin, endogenous substances including the endocannabinoid, anandamide, inorganic ions (Ca^{2+} and Mg^{2+}), as well as pH change and physical stimuli such as heat and mechanical stimuli (25–27).

An investigation of the possible role of TRPV1 channels in schizophrenia was prompted by the observations that subjects with schizophrenia have impaired thermoregulation (28–30), are less sensitive to pain than normal subjects (31–35) and exhibit reduced flare responses to niacin (nicotinic acid) and methylnicotinate (36, 37). Injection of capsaicin into the preoptic area of rats produced hypothermia, whereas desensitization of TRPV1 channels by repeated capsaicin administration induced impaired ability to thermoregulate against heat (38) similar to that observed in schizophrenia. The central effects of capsaicin on thermoregulation are mediated by action on TRPV1 channels since they were absent in TRPV1-KO mice (24). Indeed, it has been proposed that TRPV1 channels play a role in body temperature maintenance in nonpathological states (39).

Activation of peripheral TRPV1 channels on sensory neurons by agonists such as capsaicin results in nociception by activation of spinal neurons, and neurogenic flare and inflammation by release from their peripheral terminals of neuropeptides, including substance P and calcitonin gene related peptide (CGRP) (40, 41). These observations raised the possibility that schizophrenia could result from a lifelong deficit in function of TRPV1-expressing, capsaicin-sensitive primary afferent neurons, leading to reduced connectivity in the higher central nervous system such as has been demonstrated in the mouse barrel cortex following reduced somatosensory input following whisker trimming (42). The association between cannabis use and first episode psychosis (43–46), and the complex interactions between TRPV1, cannabinoid and dopaminergic mechanisms in the central nervous system (CNS) (see 23) added further support to the proposal that TRPV1 channels might be linked with schizophrenia.

Schizophrenia in all its complexity may be a uniquely human disorder and thus development and validation of animal models for testing new drug targets presents difficulties. Indeed, it is likely that no single animal model will fully manifests all of the signs considered to be characteristics of schizophrenia. Nevertheless, many animal models have been developed in an attempt to model aspects of schizophrenia. These include neurochemical, neurodevelopmental, and genetic models. Earlier models were neurochemical models that involved manipulations of the dopaminergic system. More recent neurochemical models have focused on other neurotransmitter systems such as the glutamatergic system. Other models include the neonatal ventral hippocampal lesion model, an important neurodevelopmental model (47), several genetic models (7, 8), and animal models of gene–environment interactions (48). In a study of animal models of schizophrenia, it is pertinent to consider those aspects that may be measured in animals. Changes in behavior such as increased locomotor activity, disruption of prepulse inhibition to acoustic startle, and impaired learning may be measured in animals. Brain structural changes such as reduced brain weight, reduced cortical thickness, increased ventricle size, and increased cortical cell density may also be measured. Reversibility of behavioral changes with antipsychotic drugs, despite their limitations in the treatment of schizophrenia, is also commonly considered an important criterion for assessing the validity of an animal model of schizophrenia. Whilst it might not be possible to model in animals aspects of the disorder such as thought disorder, delusions, and cognitive deficits, it has been suggested that research directed at greater understanding of animal cognition might result in discovery of improved drugs for treatment of schizophrenia (49).

In order to model deficit in function of TRPV1 channels, the well-known property of capsaicin of induction of lifelong loss of a

high proportion of TRPV1-expressing primary afferent neurons by treatment of neonatal rats was used (50). Newson et al. (51) used this property of capsaicin to test the proposal that TRPV1 deficit induces brain changes, including increased neuronal density, similar to those found in schizophrenia. The behavior of the rats was also observed since behavior is very commonly measured in putative animal models of schizophrenia.

The results from the investigation of the possible role of TRPV1 channels in schizophrenia described below showed that at 5–7 weeks rats treated as neonates with capsaicin had increased locomotor activity in a novel environment and the male rats had reduced brain weight. The capsaicin-treated rats also had reduced hippocampal and coronal cross-sectional area, reduced cortical thickness, and increased neuronal density in several cortical areas (51). Thus treatment of neonatal rats with the TRPV1 ligand, capsaicin, was found to produce brain structural changes similar to those found in postmortem brain of humans with schizophrenia. More recently it has been found that neonatal capsaicin treatment induced changes in central cholinergic, monoaminergic, and cannabinoid systems in the adult animal (52). It should be noted that capsaicin injection in neonates produces a brief period of hypoxia which may cause long-lasting changes in rat brain. Therefore, it remains to be determined whether the changes observed by Newson et al. (51) and Zavitsanou et al. (52) in rat brain following neonatal capsaicin treatment resulted from loss of TRPV1 channel function in the peripheral or central nervous system or from some other toxic effect.

2. Materials

2.1. Animals

Litters from six time-mated pregnant female Wistar rats were used. The rats were housed in plastic cages (73 × 54 × 24 cm) with shredded paper bedding, and a wire mesh top cover. The animals were kept at a constant temperature of 21°C ± 1°C on a 12–12 h light–dark cycle with lights on at 7:00 A.M. Food and water were freely available.

2.2. Drugs

1. Capsaicin (Sigma-Aldrich Pty Ltd., Australia) stock solution 10^{-2} M made in a vehicle of 10% Tween 80 and 10% ethanol in saline
2. Sodium pentobarbitone (Lethabarb, Virbac (Australia) Pty Ltd., Australia)
3. Salbutamol sulfate aerosol (Ventolin, Allen & Hanburys, Australia)

2.3. Equipment and Solutions

The specific equipment used in the experiment is detailed below. Alternative equipment for behavioral observations and microscopy may be substituted.

1. Syringes and 30 g needles.
2. Perspex observation chamber (height 32 cm × depth 44 cm × length 72 cm) located in the home room and containing two foam objects placed identically for each animal.
3. Guillotine
4. 10% formalin solution
5. Cryostat
6. Gelatin chrom alum-coated slides
7. Coverslips
8. Cresyl violet 5% solution OR 0.003% thionin, 1.7% ethanol, and 0.13% formalin, adjusted to pH 3.5 with glacial acetic acid
9. Ethanol solutions (70%, 95%, 100%)
10. Histolene (Fronine, Riverstone, NSW, Australia)
11. Ultramount (Fronine)
12. Zeiss Axioskop light microscope with a motorized stage and a miniature monitor (Lucivid—Microbrightfield Inc., USA) attached to a camera lucida
13. Neurolucida software (Microbrightfield)
14. Paxinos and Watson (1998) rat brain atlas (53)

3. Methods

3.1. Neonatal Capsaicin Treatment

1. Within 24–36 h of birth, remove dam from the home cage and remove neonatal rats one at a time for treatment.
2. Place neonates in the supine position on a bed of crushed ice. Immediately upon disappearance of the righting reflex (less than 1 min), remove neonates from the ice and inject subcutaneously (s.c.) with either capsaicin, 50 mg/kg (Note 1), or an equivalent volume of vehicle, consisting of 10% alcohol and 10% Tween 80, into the dorsal region of the neck, using a sterile 30-gauge needle and syringe.
3. Following injection, place neonates in a small clear perspex observation chamber with other injected littermates: each animal being placed between the fingers of a latex glove filled with 37°C water and warmed with a heating lamp (Note 2).
4. Spray a measured dose (two 'puffs') of salbutamol aerosol (Ventolin) into the chamber to alleviate respiratory difficulty induced by capsaicin (Note 3).

5. Keep neonates in the observation chamber until all signs of respiratory distress have disappeared and they have regained their righting reflex.
6. Place capsaicin-treated neonates in a small, warm-holding cage until all littermates had been injected and had recovered. Transfer neonates to a clean cage with the dam. Observe the dam's behavior to ensure she accepts the neonates (Note 4).
7. Check and weigh rat pups twice weekly. Wean rats at 21–23 days after birth by placement into new cages, with one or two other animals of the same sex.

3.2. Behavioral Observations

1. On observation days, typically twice weekly, remove rats from the home cage and place them in a perspex observation chamber located in the home room.
2. Commence measurement of behaviors immediately without giving the animals time to become familiar with the observation cage. Observe each animal for 10 min using the same trained observer and strict criteria to manually quantify behaviors including number of circuits of the cage (locomotor activity), number of climbs of an object or sides (climbing), number of rears (rearing), face washing, scratching, and chewing (stereotypy). Validate behavioral observations with a second independent observer who is blind to the treatment of the rats (Note 5). Weigh animals after each session.

3.3. Histology

1. At 5–7 weeks of age, euthanase rats with a lethal dose of sodium pentobarbitone, 100 mg/kg, intraperitoneally, and remove head using a guillotine.
2. Remove brains from the skulls. Weigh and place brains in 10% formalin solution for 2 weeks.
3. Cut serial coronal sections, 50 μm, on a cryostat. Mount every third section on gelatin chrom alum-coated slides, air dry, and Nissl stain with cresyl violet solution for 1 min and wash in running water until the water becomes clear, or with thionin solution for 18 h at room temperature (54). This latter method yielded superior staining for neuronal counting since the cells were stained blue and the white matter pink (Fig. 1).
4. Following staining, dehydrate sections in ascending concentrations of ethanol (70%, 95%, 2 × 100%).
5. Clear sections with histolene and coverslip with Ultramount.

3.4. Microscopy

Select closely matched sections from each brain at several levels with the aid of the rat brain atlas (53). Observe sections under bright-field microscopy using a light microscope with a motorized stage and a miniature monitor attached to a camera lucida. Use neurolucida software to trace outlines of the sections and count neurons.

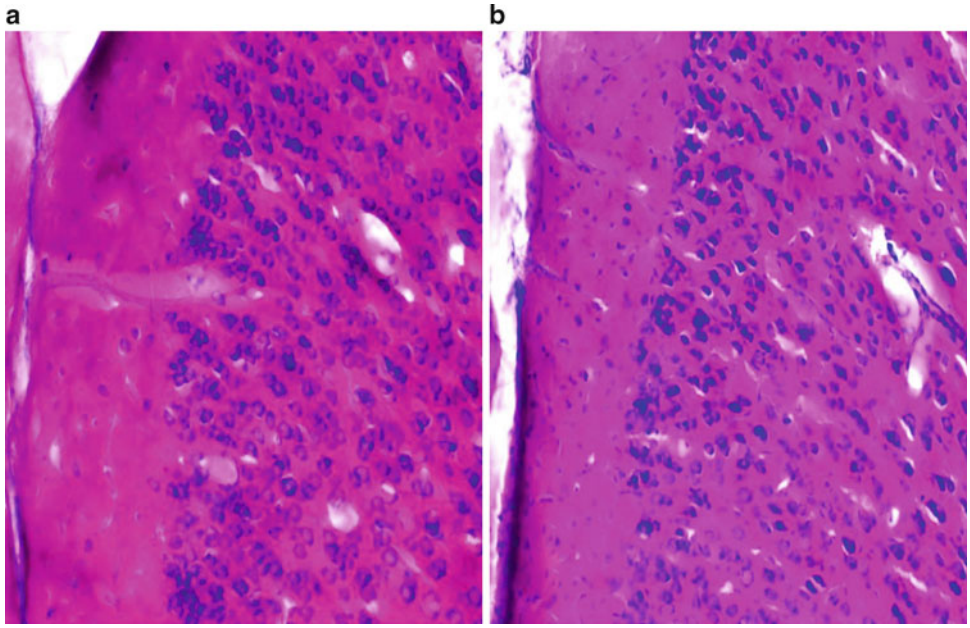

Fig. 1. Photomicrographs of the secondary motor cortex from a capsaicin-treated rat (**a**) and a vehicle control (**b**). Note greater neuronal density and beaded-like columns of cells in the capsaicin-treated rat.

3.4.1. Measurement of Section Areas and Cortical Thickness

1. Measure total area of sections at Bregma 2.70 mm, 1.20 mm, –1.60 mm, –2.56 mm, –3.60 mm, and –5.80 mm, hippocampal area at Bregma –2.56 mm and –3.60 mm, lateral ventricle area at Bregma 1.20 mm, –1.60 mm, and –2.56 mm, and aqueduct area at Bregma –5.80 mm (Fig. 2).
2. Measure cortical thickness at several levels. Measure corpus callosum thickness, and width between the dorsal tips of the left and right cingulum at Bregma 1.20 mm, –1.60 mm and –2.56 mm (Fig. 2).

3.4.2. Neuronal Cell Counting

1. Count neurons using a two-dimensional counting method, in the following regions: anterior cingulate (AC), the primary somatosensory cortex jaw (SIJ), the secondary motor cortex (M2), and caudate putamen (CPu) at Bregma 1.20 mm, the primary auditory cortex (Au1) at Bregma –3.60 mm, and the primary visual cortex monocular (VIM) at Bregma –5.80 mm. For each region use a counting box of appropriate size and count all neurons in the box in which the nucleolus is visible (Note 6).
2. Calculate neuronal density from the total neuronal count divided by the area of the counting box measured by the Neurolucida software. Calculate the neuronal density for each region for each animal as the average results for left and right sides of the brain and express as cells per μm^2.

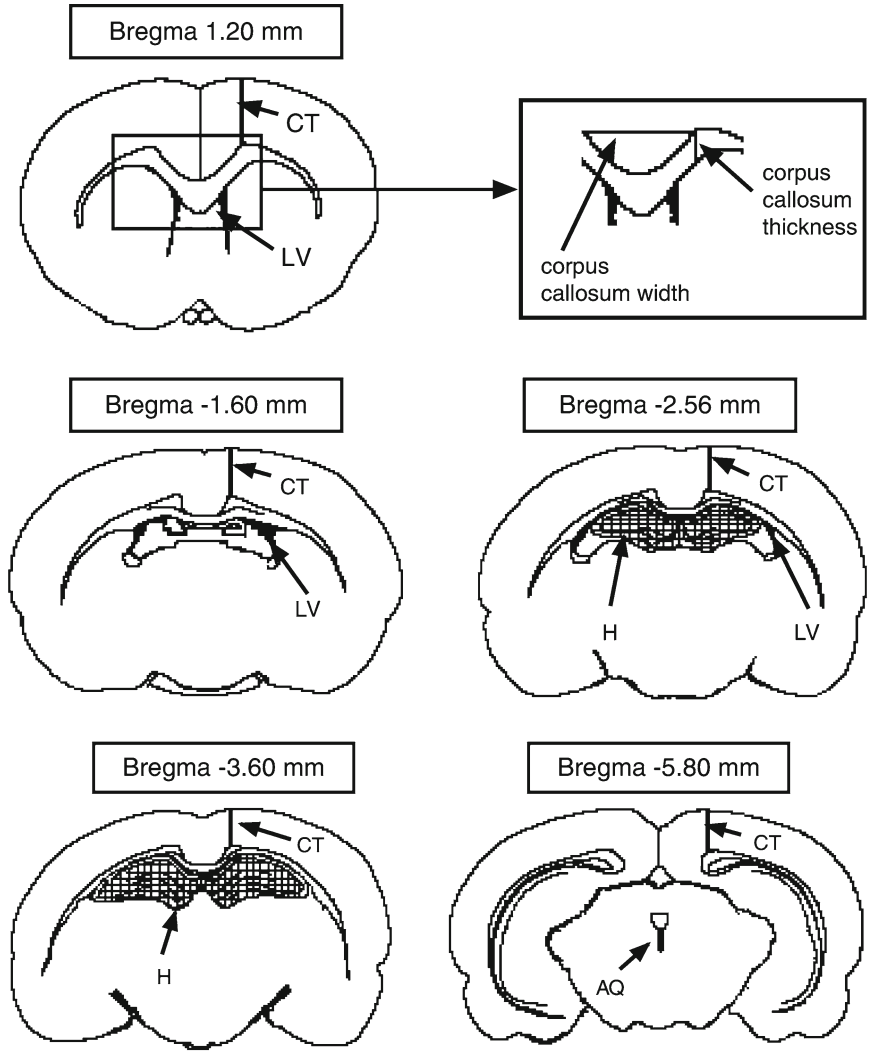

Fig. 2. Diagrams of coronal brain sections at Bregma 1.20 mm, –1.60 mm, –2.56 mm, –3.60 mm, and –5.80 mm showing the location of structures measured in this study. Cross-sectional area was calculated from the area of the entire section. Location of measurements of cortical thickness (CT), and corpus callosum height and width (see insert) are shown as *thick lines*, areas of the lateral ventricles (LV) and aqueduct (AQ) are shown in *black*, and the hippocampus (H) is shown *cross-hatched*. (Bregma 2.70 mm not shown). (Reproduced from Reference 51).

3.5. Statistical Analyses

Analyze data that do not involve repeated measures of the same parameter on the same animals by two-way analysis of variance using a statistical package such as GraphPad Prism 4.0 (GraphPad Software Inc.). Where analysis shows a significant gender effect, analyze data for males and females separately using Bonferroni post-tests. For data where measures on the same animals were repeated (behavioral data), use two-way analysis of variance with repeated measures (Note 7). Express results as means and standard errors of the means (SEM). For all data analyses use $\alpha = 0.05$.

4. Notes

1. The dose of capsaicin, 50 mg/kg, is used since it had been shown in previous studies to produce marked loss of capsaicin-sensitive primary afferent neurons (50).
2. It is important to keep the pups warm since they lose heat rapidly following ice anesthesia and capsaicin treatment.
3. Respiratory difficulty in capsaicin-treated pups is not completely prevented by salbutamol (51) and therefore it is possible that the brief period of hypoxia following capsaicin injection might induce long-lasting changes in rat brain. A study of the effects of hypoxia alone would be a useful extension to the present study.
4. Neonatal rats appear to suffer no ill effects from hypothermia. Also, no local tissue damage occurred at the injection site in any of the animals. Using the method described the survival rate of the animals following capsaicin treatment is high, approximately 90%.
5. Use of strict criteria results in a high level of inter-rater reliability.
6. Stereological counting is not considered necessary. The risk of double counting is avoided by using sections 50 μm thick and counting only cells with the nucleolus visible.
7. For behavioral data with occasional missing data points, two-way analysis of variance with repeated measures should be performed with a statistical package such as SPSS 12.0 for Windows, as missing data points cannot be handled by GraphPad Prism 4.0.

References

1. Prasad KM, Talkowski ME, Chowdari KV, McClain L, Yolken RH, Nimgaonkar VL (2010) Candidate genes and their interactions with other genetic/environmental risk factors in the etiology of schizophrenia. Brain Res Bull 83:86–92
2. Jaaro-Peled H, Hayashi-Takagi A, Seshadri S, Kamiya A, Brandon NJ, Sawa A (2009) Neurodevelopmental mechanisms of schizophrenia: understanding disturbed postnatal brain maturation through neuregulin-1 – ErbB4 and DISC1. Trends Neurosci 32:485–495
3. Bertolino A, Blasi G (2009) The genetics of schizophrenia. Neuroscience 164:288–299
4. Schwab SG, Wildenauer DB (2009) Update on key previously proposed candidate genes for schizophrenia. Curr Opin Psychiatry 22: 147–153
5. Mei L, Xiong WC (2008) Neuregulin 1 in neural development, synaptic plasticity and schizophrenia. Nat Rev Neurosci 9:437–452
6. Harrison PJ (2007) Schizophrenia susceptibility genes and neurodevelopment. Biol Psychiatry 61:1119–1120
7. O'Tuathaigh CMP, Babovic D, O'Meara G, Clifford JJ, Croke DT, Waddington JL (2007) Susceptibility genes for schizophrenia: characterization of mutant mouse models at the level of phenotypic behaviour. Neurosci Biobehav Rev 31:60–78
8. Chen J, Lipska BK, Weinberger DR (2006) Genetic mouse models of schizophrenia: from

hypothesis-based to susceptibility gene-based models. Biol Psychiatry 59:1180–1188

9. Ross CA, Margolis RL, Reading SAJ, Pletnikov M, Coyle JT (2006) Neurobiology of schizophrenia. Neuron 52:139–153
10. Stefansson H, Sigurdsson E, Steinthorsdottir V, Bjornsdottir S, Sigmundsson T, Ghosh S, Brynjolfsson J, Gunnarsdottir S, Ivarsson O, Chou TT, Hjaltason O, Birgisdottir B, Jonsson H, Gudnadottir VG, Gudmundsdottir E, Bjornsson A, Ingvarsson B, Ingason A, Sigfusson S, Hardardottir H, Harvey RP, Lai D, Zhou M, Brunner D, Mutel V, Gonzalo A, Lemke G, Sainz J, Johannesson G, Andresson T, Gudbjartsson D, Manolescu A, Frigge ML, Gurney ME, Kong A, Gulcher JR, Petursson H, Stefansson K (2002) Neuregulin 1 and susceptibility to schizophrenia. Am J Hum Genet 71:877–892
11. Li D, Collier DA, He L (2006) Meta-analysis shows strong positive association of the neuregulin 1 (NRG1) gene with schizophrenia. Hum Mol Genet 15:1995–2002
12. Munafò MR, Thiselton DL, Clark TG, Flint J (2006) Association of the NRG1 gene and schizophrenia: a meta-analysis. Mol Psychiatry 11:539–546
13. Munafò MR, Attwood AS, Flint J (2008) Neuregulin 1 genotype and schizophrenia. Schizophrenia Bull 34:9–12
14. Schlaepfer TE, Harris GJ, Tien AY, Peng LW, Lee S, Federman EB, Chase GA, Barta PE, Pearlson GD (1994) Decreased regional cortical gray matter volume in schizophrenia. Am J Psychiatry 151:842–848
15. Selemon LD, Kleinman JE, Herman MM, Goldman-Rakic PS (2002) Smaller frontal gray matter volume in post-mortem schizophrenic brains. Am J Psychiatry 159:1983–1991
16. McDonald C, Grech A, Toulopoulou T, Schulze K, Chapple B, Sham P, Walshe M, Sharma T, Sigmundsson T, Chintis X, Murray RM (2002) Brain volumes in familial and non-familial schizophrenic probands and their unaffected relatives. Am J Med Genet (Neuropsychiatric Genetics) 114:616–625
17. Shenton ME, Kikinis R, Jolesz FA, Pollak SD, Lemay M, Wible CG, Hokama H, Martin J, Metcalf D, Coleman M, McCarley RW (1992) Abnormalities of the left temporal lobe and thought disorder in schizophrenia. A quantitative magnetic resonance imaging study. N Engl J Med 327:604–612
18. McCarley RW, Wilbe CG, Frumin M, Hirayasu Y, Levitt JJ, Fischer IA, Shenton ME (1999) MRI anatomy of schizophrenia. Biol Psychiatry 45:1099–1119
19. Selemon LD, Rajkowska G, Goldman-Rakic PS (1995) Abnormally high neuronal density in the schizophrenic cortex. A morphometric analysis of prefrontal area 9 and occipital area 17. Arch Gen Psychiatry 52:805–820
20. Selemon LD, Rajkowska G, Goldman-Rakic PS (1998) Elevated neuronal density in prefrontal area 46 in brains from schizophrenic patients: application of a 3-dimensional, stereologic counting method. J Comp Neurol 392: 402–412
21. Selemon LD, Goldman-Rakic PS (1999) The reduced neuropil hypothesis: a circuit based model of schizophrenia. Biol Psychiatry 45: 17–25
22. Kauer JA, Gibson HE (2009) Hot flash: TRPV channels in the brain. Trends Neurosci 32:215–224
23. Chahl LA (2010) TRP Channels in the brain: psychiatric disorders. In: Szallasi A (ed) TRP Channels in Health and Disease: Implications for Diagnosis and Tharapy. Nova Science Publishers Inc., New York, pp 393–413
24. Caterina MJ, Schumacher MA, Tominaga M, Rosen TA, Levine JD, Julius D (1997) The capsaicin receptor: a heat-activated ion channel in the pain pathway. Nature 389:816–824
25. Tominaga M, Caterina MJ, Malmberg AB, Rosen TA, Gilbert H, Skinner K, Raumann BE, Basbaum AI, Julius D (1998) The cloned capsaicin receptor integrates multiple pain-producing stimuli. Neuron 21:531–543
26. Tominaga M, Tominaga T (2005) Structure and function of TRPV1. Pflugers Archiv Eur J Physiol 451:143–150
27. Szallasi A, Cortright DN, Blum CA, Eid SR (2007) The vanilloid receptor TRPV1: 10 years from channel cloning to antagonist proof-of-concept. Nat Rev Drug Discov 6:357–372
28. Hermesh H, Shiloh R, Epstein Y, Manaim H, Weizman A, Munitz H (2000) Heat intolerance in patients with chronic schizophrenia maintained with antipsychotic drugs. Am J Psychiatry 157:1327–1329
29. Chong TWH, Castle DJ (2004) Layer upon layer: thermoregulation in schizophrenia. Schizophrenia Res 69:149–157
30. Shiloh R, Weizman A, Epstein Y, Rosenberg SL, Valevski A, Dorfman-Etrog P, Wiezer N, Katz N, Munitz H, Hermesh H (2001) Abnormal thermoregulation in drug-free male schizophrenia patients. Eur Neuropsychopharmacol 11: 285–288
31. Kudoh A, Ishihara H, Matsuki A (2000) Current perception thresholds and postoperative pain in schizophrenic patients. Regional Anaesth Pain Med 25:475–479

32. Blumensohn R, Ringler D, Eli I (2002) Pain perception in patients with schizophrenia. J Nerv Mental Dis 190:481–483
33. Hooley JM, Delgado ML (2001) Pain insensitivity in the relatives of schizophrenia patients. Schizophrenia Res 47:265–273
34. Bonnot O, Anderson GM, Cohen D, Willer JC, Tordjman S (2009) Are patients with schizophrenia insensitive to pain? A reconsideration of the question. Clin J Pain 25: 244–252
35. Potvin S, Marchand S (2008) Hypoalgesia in schizophrenia is independent of antipsychotic drugs: a systematic quantitative review of experimental studies. Pain 138:70–78
36. Waldo MC (1999) Co-distribution of sensory gating and impaired niacin flush response in the parents of schizophrenics. Schizophrenia Res 40:49–53
37. Messamore E, Hoffman WE, Janowsky A (2003) The niacin skin flush abnormality in schizophrenia: a quantitative dose-response study. Schizophrenia Res 62:251–258
38. Szolcsanyi J (2004) Forty years in capsaicin research for sensory pharmacology and physiology. Neuropeptides 38:377–384
39. Gavva NR (2008) Body-temperature maintenance as the predominant function of the vanilloid receptor TRPV1. Trends Pharmacol Sci 29:550–557
40. Szallasi A, Blumberg PM (1999) Vanilloid (capsaicin) receptors and mechanisms. Pharmacol Rev 51:159–211
41. Holzer P (1991) Capsaicin: cellular targets, mechanisms of action, and selectivity for thin sensory neurons. Pharmacol Rev 43: 143–201
42. Sadaka Y, Weinfeld E, Lev DL, White EL (2003) Changes in mouse barrel synapses consequent to sensory deprivation from birth. J Comp Neurol 457:75–86
43. Degenhardt L, Hall W (2006) Is cannabis use a contributory cause of psychosis? Canad J Psychiatry 51:556–565
44. Laviolette SR, Grace AA (2006) The roles of cannabinoid and dopamine receptor systems in neural emotional learning circuits: implications for schizophrenia and addiction. Cell Mol Life Sci 63:1597–1613
45. Sundram S (2006) Cannabis and neurodevelopment: implications for psychiatric disorders. Hum Psychopharmacol 21:245–254
46. Malone DT, Hill MN, Rubino T (2010) Adolescent cannabis use and psychosis: epidemiology and neurodevelopmental models. Br J Pharmacol 160:511–522
47. Tseng KY, Chambers LA, Lipska BK (2009) Neonatal ventral hippocampal lesion as a heuristic neurodevelopmental model of schizophrenia. Behav Brain Res 204:295–305
48. Ayhan Y, Sawa A, Ross CA, Pletnikov MV (2009) Animal models of gene-environment interactions in schizophrenia. Behav Brain Res 204:274–281
49. Barak S, Weiner I (2011) Putative cognitive enhancers in preclinical models related to schizophrenia: the search for an elusive target. Pharmacol Biochem Behav 99:164–189
50. Jancsó G, Király E, Jancsó-Gábor A (1977) Pharmacologically induced selective degeneration of chemosensitive primary sensory neurons. Nature (London) 270:741–743
51. Newson P, Lynch-Frame A, Roach R, Bennett S, Carr V, Chahl LA (2005) Intrinsic sensory deprivation induced by neonatal capsaicin treatment induces changes in rat brain and behaviour of possible relevance to schizophrenia. Br J Pharmacol 146:408–418
52. Zavitsanou K, Dalton VS, Wang H, Newson P, Chahl LA (2010) Receptor changes in brain tissue of rats treated as neonates with capsaicin. J Chem Neuroanat 39:248–255
53. Paxinos G, Watson C (1998) The rat brain in stereotaxic coordinates, 4th edn. Academic, San Diego, CA
54. Tolivia J, Tolivia D (1985) A new technique for differential and simultaneous staining of nerve cells and fibers. J Neurosci Methods 13:305–311

Chapter 9

Investigating Diseases of Dopaminergic Neurons and Melanocytes Using Zebrafish

Amanda Decker and Robert Cornell

Abstract

Zebrafish offer experimental advantages that have been exploited by developmental biologists and, increasingly, by those interested in disease mechanisms. Parkinson's disease is characterized by the loss of dopaminergic neurons of the substantia nigra and motor symptoms such as slow movement, rigidity, and tremor. Traditionally investigators have used rodents and non-human primates as model animals to study the genetic and environmental causes of Parkinson's diseases. However zebrafish offer an attractive alternative for behavioral studies because the larvae are small enough to fit into multi-well plates and thus are amenable to automated behavioral analysis. While there are significant anatomical differences between the zebrafish and human brains, in the zebrafish diencephalon there is a group of dopaminergic neurons whose projections are analogous to those of neurons in the human substantia nigra. Studies taking advantage of these features have measured the swimming behavior of zebrafish larvae in which expression of genes linked to familial Parkinson's disease have been reduced, or that have been treated with pharmaceutical agents that target dopaminergic neurons. These studies have also included histological analyses of dopaminergic neurons. Zebrafish have also been used to dissect the genetic pathways that govern differentiation and survival of melanocytes. The assumption is that disruption of these pathways underlies diseases of melanocytes, which include vitiligo, a disease of melanocyte degeneration, and metastatic melanoma. It is believed that melanocytes and dopaminergic neurons must share vulnerability to particular mutations or environmental insults because risk for Parkinson's disease and metastatic melanoma are associated with one another. Interestingly a mutagenesis screen in zebrafish may have identified one such shared requirement. In a forward screen, a mutant exhibiting melanocyte cell death was isolated and later shown to harbor a loss-of-function mutation in the gene encoding ion channel Transient Receptor Potential Melastatin-like 7 (TRPM7). TRPM7 was previously identified as possibly conferring risk for a Parkinsonian condition. This example reveals the potential for studies in zebrafish to reveal the genetic requirements of dopaminergic neurons, of melanocytes, and those shared by both cell types. This chapter provides the protocols used by our research group to examine the behavior of zebrafish larvae, and to monitor dopaminergic neurons and melanocytes by histology.

Key words: Zebrafish, Parkinson's disease, Melanocyte, Vitiligo, Dopamine

Arpad Szallasi and Tamás Bíró (eds.), *TRP Channels in Drug Discovery: Volume II*, Methods in Pharmacology and Toxicology,
DOI 10.1007/978-1-62703-095-3_9,

1. Introduction

1.1. Zebrafish as a Model to Investigate Pathways Controlling the Viability of Dopaminergic Neurons

Parkinson's disease (PD) is a common neurodegenerative disorder with a poorly understood etiology. It is characterized by the loss of dopaminergic neurons of the substantia nigra, and consequently motor symptoms such as slow movement, rigidity, and tremor. Although recessive and dominant forms of familial PD exist, most cases are idiopathic, indicating that both genetic and environmental factors contribute to the disease state (1). Research on the genetic underpinnings of PD has been carried out using the mouse as a model system. However, the fact that deleting mouse orthologs of familial PD genes only rarely alters the number of dopaminergic neurons demonstrates the difficulty of modeling PD in the mouse (reviewed in 2). It is thus important to explore new model systems for use in establishing the genetic underpinnings of PD.

The zebrafish (*Danio rerio*) is a versatile model organism that can be used to study the neural basis of behavior and of movement disorders (reviewed in 3). Larval zebrafish exhibit a repertoire of measureable behaviors, and these increase in complexity as the animal ages (4). Advantages of using zebrafish as a model organism to study movement defects include the fact that a large number of animals can be tested in a single experiment, behaviors can be measured in automated fashion, water-soluble pharmacological agents can be administered easily, and the animals are amenable to genetic manipulation. Investigators in this field have quantified locomotor activity of larval zebrafish using custom-built materials (5) or automated behavior recording apparatuses built by Noldus (Wageningen, The Netherlands) (6) and Viewpoint (Montreal, Canada) (7).

The above-described features of zebrafish and the presence in the zebrafish ventral diencephalon of a proposed anatomical correlate of the mammalian substantia nigra (8) have led to the use of zebrafish in investigating the genetic and environmental factors that contribute to the death of dopaminergic neurons in PD and other neurodegenerative diseases. Specifically, many studies have tested the consequences of down-regulating zebrafish orthologs of familial Parkinson's disease genes, including *dj-1* (9, 10), *pink1* (11–13), *lrrk2* (14, 15), and *parkin* (16, 17). Each of these studies included both motility assays and histology-based analysis of dopaminergic neurons. Notably, zebrafish appear to be sensitive to the toxins that destroy DA neurons in humans; both embryos and adult fish treated with pharmacological agents that induce parkinsonism (such as 1-methyl-4-phenyl-1,2,3,6-tetrahydropyridine (MPTP) and 6-hydroxydopamine (6OHDA)) are less motile and have fewer DA neurons than untreated embryos (18–22). The investigations carried out to date suggest that the zebrafish model, with its unique set of experimental advantages, will be extremely useful in investigating the pathogenic mechanisms underlying motor disorders such as PD.

1.2. Zebrafish as a Model to Investigate Pathways Controlling the Viability of Melanocytes

Melanocytes produce melanin through a metabolic pathway that generates toxic intermediates like dihydroxyindole; these metabolites are thought to predispose melanocytes to disease (23, 24). The melanocyte disease vitiligo co-occurs with auto-immune disorders and is associated with polymorphisms in genes that contribute to immune responses (25). However, the pathogenesis of vitiligo may be influenced by the presence of reactive oxygen species (ROS), including those produced during melanin synthesis, as suggested by the elevation of ROS in skin when vitiligo is active (26). Interestingly melanocytes and dopaminergic neurons share risk factors—either genetic or environmental—because people with PD are at increased risk for metastatic melanoma, a deadly skin cancer that originates in either melanocytes or melanocyte stem cells (27). Given the similarity of melanin and dopamine metabolic pathways, mutations in genes encoding enzymes shared by these pathways would seem obvious candidates to confer risk for diseases of both cell types. However, the pathways have no known common enzymes. Of note, single nucleotide polymorphisms near *PLA2G6* are associated with elevated risk both for Parkinsonism (28–31) and for cutaneous melanoma (32). These findings indicate that *PLA2G6,* encoding a phospholipase, is one of the elusive genes that is important for the normal physiology of both cell types. Identifying the shared vulnerabilities of melanocytes and dopaminergic neurons is expected to yield insight into the serious diseases that affect these cell types.

Zebrafish are well established as a model for the study of genetic pathways regulating melanocyte development and survival, and mutagenesis screens have identified over 200 pigmentation mutants (33, 34). Melanophores in fish and amphibians, in contrast to melanoctyes, their mammalian counterparts, do not transfer melanosomes to neighboring keratinocytes. Nevertheless, the genetic pathways involved in the lineage specification and differentiation of mammalian melanocytes appear to be highly conserved in the melanophores of fish. These events are controlled by the presence of growth factors and the expression of a particular combination of transcription factors over time (35, 36). The expression of *mitfa* (microphthalmia-associated transcription factor a) and *dct* (dopachrome tautomerase) defines the melanoblast stage of melanophore development (37, 38), although it should be noted that *mitfa* expression is not limited to melanoblasts (39). Future investigations delineating the mechanisms that govern melanophore differentiation and survival in zebrafish will shed light on the basic aspects of melanophore biology, including the genetic and environmental vulnerabilities they share with dopaminergic neurons.

In our efforts to answer these questions, we conducted a mutagenesis screen in zebrafish for mutants deficient in melanophores (40). We discovered that the ion channel transient receptor potential melastatin-like 7 (TRPM7) is necessary for melanophore

survival in zebrafish (41). Trpm7 is a ubiquitously expressed channel that conducts divalent cations (42, 43). In *trpm7* mutants, melanophore death is dependent on melanin synthesis, implying that Trpm7 is involved in containing the toxic intermediates of melanin synthesis within the melanosome (44). Interestingly, a TRPM7 variant is associated with a parkinsonian disorder called amyotrophic lateral sclerosis-parkinsonism/dementia complex of Guam (45). This implies that TRPM7 may be another of the elusive shared genetic requirements of melanocytes and dopaminergic neurons, although a requirement for TRPM7 in dopaminergic neurons has not yet been demonstrated directly.

Here we provide protocols that we deploy in our investigations of pathways regulating the development and survival of dopaminergic neurons and melanophores.

2. Materials

2.1. Equipment

2.1.1. Equipment for Behavior Analysis

1. Zebrabox (Viewpoint Zebrabox, Viewpoint LifeSciences)
2. Incubator at 28.5°C, fitted with lights on a 14 h on/10 h off cycle
3. 96-well plates (Note 1)

2.1.2. Equipment for Expression Analysis

Water bath set to 70°C.

2.1.3. Equipment for Acridine Orange and TUNEL Assays

Microscope equipped for epifluorescence illumination and with a GFP filter set.

2.2. Reagents and Solutions

2.2.1. Reagents and Solutions for Behavior Analysis

1. Drugs (1-methyl-4-phenylpyridinium, MPP+-iodide available from Sigma) (Note 2)
2. Embryo medium: 5 mM NaCl, 0.017 mM KCl, 0.33 mM $CaCl_2$, 0.033 $MgSO_4$, 0.1% methylene blue in deionized water (dH_20)
3. Ringer's Solution: 116 mM NaCl, 2.9 KCl, 1.8 mM $MgCl_2$, 5 mM HEPES in dH_20

2.2.2. Reagents and Solutions for Histology

1. Four percent PFA (fixing solution): 4% paraformaldehyde in PBS pH 7–7.5 (store at –20°C)
2. Anti-Dig FAB Frag-AP (Roche)
3. Blocking solution: PBST with 2 mg/ml BSA, 5% sheep serum

4. Color buffer: Tris 0.1 M pH 9.5, $MgCl_2$ 50 mM, NaCl 100 mM, 0.1% TWEEN-20, in dH_20 (make on day of use)
5. Hyb1 hybridization mix: 50% formamide, SSC 5×, 0.1% TWEEN-20, 1 M citric acid (plus enough to adjust pH of mixture to 6.0) in dH_20
6. Hyb2: Hyb1 with 50 ug/ml heparin, 0.5 mg/ml yeast tRNA
7. NBT/BCIP (nitro-blue tetrazolium/bromo-4-chloro-3-indolyl phosphate) (Roche)
8. PBS: 0.8% NaCl, 0.02% KCl, and 0.02 M PO_4 buffer in dH_20
9. PBST: PBS, 0.1% Tween-20
10. PBDT: 0.5% DMSO, 1% BSA, 0.5% Triton-X-100, 1% goat serum in PBS
11. PO_4 buffer (0.1 M): 68 mM Na_2HPO_4, 31.6 M NaH_2PO_4 in dH_20
12. Prot K: Proteinase K diluted in PBS from storage solution in 50% glycerol, 10 mM Tris pH 7.5, 20 mM $CaCl_2$ in dH_20
13. Probe: synthesis creates antisense RNA probes (46)
14. SSC (sodium chloride sodium citrate) 20× stock: 3 M NaCl, 300 mM Na citrate, pH to 7.0 with citric acid
15. Tricaine (3-aminobenzoic acid ethyl ester methanesulfonate) (Sigma): working solution is 10 ppm or 25–300 mg/l

2.2.3. Reagents and Solutions for Immunohistochemistry

1. Antibodies: Anti-tyrosine hydroxylase (Millipore) (1:400–1:1,000), Goat anti-mouse IgG (1:200), Mouse perodixase anti-peroxidase (1:200)
2. Bleach solution: 0.1% KOH, 3% H_2O_2 in PBSTX
3. DAB solution: 0.05 M PO_4 buffer, 1% DMSO, 0.05% DAB
4. DAB (3,3′-diaminobenzidine): 1 g DAB in 25 ml dH_20 (can be prepared ahead and frozen in 1 mg/25 µl aliquots)
5. PBSTX: PBS with 0.1% Triton-X-100

2.2.4. Reagents and Solutions for Acridine Orange and TUNEL Assays

1. Acridine Orange (Sigma)
2. Fluorescein dUTP (Roche)
3. TdT (terminal deoxynucleotidyl transferase) (Roche)
4. TTase (thioltransferase) buffer: 2 mM $CoCl_2$ added the day of the experiment to dH_2O
5. TTBST: 25 mM Tris buffer, 0.2 M Na cacodylate, 0.25 mg/ml BSA, 0.2% TWEEN-20, pH to 6.6

3. Methods

3.1. Methods for Locomotion Analysis

This visual assay of motor behavior (adapted from (47)) shows the distance that individual fish swim in a given time period with alternating light and dark conditions. Although we chart movement using a commercial automated system, at least one group has assembled an automated system from the basic components (camera, lens, light box, computer) and written open-source software to run it (5). Manual methods have also been reported, but we have found that these fail to capture subtle differences between groups revealed by large-scale analysis.

3.1.1. Preparation

1. Harvest embryos and raise them in embryo medium, in an incubator at 28°C and with regulated light conditions. Methods for zebrafish care and husbandry have been published elsewhere (48).
2. Manually dechorionate embryos at 2 dpf (days postfertilization).
3. Transfer larvae to wells at 4 dpf. Exclude larvae that do not respond to a light touch and those with gross morphological malformations from movement analysis (49).

   In the absence of drug treatment

   (a) Transfer one larva into each well of a 96 well plate.

   (b) Fill each well with Ringer's solution (just enough to avoid forming a convex surface; total volume should be 370 µl).

   With drug treatment

   (a) Transfer larvae into a small Petri dish.

   (b) Fill the Petri dish to 3 ml with Ringer's solution, and apply drug or vehicle (controls).

   (c) Incubate, applying gentle rocking or agitation.

   (d) Use a 1 ml pipette tip to transfer one larva in a total volume of 370 µl of Ringer's solution including drugs into one well of a 98-well dish.
4. Return plate to incubator O/N (over night).
5. Move the plate loaded with larvae into the measurement apparatus at 5 dpf and allow it to equilibrate for at least 1 h (Note 3).

3.1.2. Motility Test

1. Calibrate the machine according to the manufacturer's suggestions, and empirically determine the optimal conditions for each experiment by checking to make sure that movement is traced without false positives. We routinely use the following settings:

   Format: "Tracking" format

   Integration period: 60 s

Detection threshold: black 19

Movement threshold: small/large, 10.0 cm/s; 'inact'/small, 0.1 cm/s

Light driving: A repeated cycle of light for 30 min followed by darkness for 30 min (Note 4)

2. Perform analysis in a quiet, dark, and secluded room without variation in ambient temperatures or olfactory stimuli.
3. Monitor behavior for 7 h in alternating light/dark conditions using the tracking feature.
4. At end of the assay, examine fish individually for touch response and exclude dead or unresponsive individuals from further analyses.

3.1.3. Data Analysis

1. Viewpoint provides tracking data for distance moved, duration of movement, and the number of movements for the defined categories of large, small and "inact" along with movement tracings.
2. Compute the variable total distance for each fish = smldist + lardist (note that with these settings there will be very little lardist-categorized movement).
3. Assign each fish to a category and find descriptive statistics over desired time period (Fig. 1).

3.2. Methods for Histology

This whole-mount immunohistochemistry protocol was adapted from one published elsewhere (48).

3.2.1. Whole-Mount Immunohistochemistry for Anti-tyrosine Hydroxylase in 5-Day Postfertilization Larvae

1. Place fish anesthetized with tricaine into 4% PFA and incubate with gentle rocking for 7 h at room temperature (21–22°C, RT), or O/N to 24 h at 4°C.
2. Wash in dH_2O one time and then incubate in dH_2O O/N or for up to 24 h at RT, to permeabilize the tissue through osmotic shock.
3. Pre-incubate fish for 0.5–1 h in PBDT + 2.5% GS.
4. Incubate fish in primary antibody diluted in PBDT + 2.5% GS, for 4–5 h at RT or O/N at 4°C.
5. Wash on rotator with PBSTX, four times for 15 min (4 × 15).
6. Incubate in secondary antibody in PBDT + 2.5% GS 4–5 h at RT, or O/N at 4°C.
7. Wash in PBSTX 4 × 15 min.
8. Incubate in tertiary antibody in PBDT + 2.5% GS for 4–5 h at RT, or O/N at 4°C.
9. Wash in PBSTX 2 × 15 min, and then in 0.1 M PO_4 buffer (pH 7.3) 2 × 15 min (Note 5).

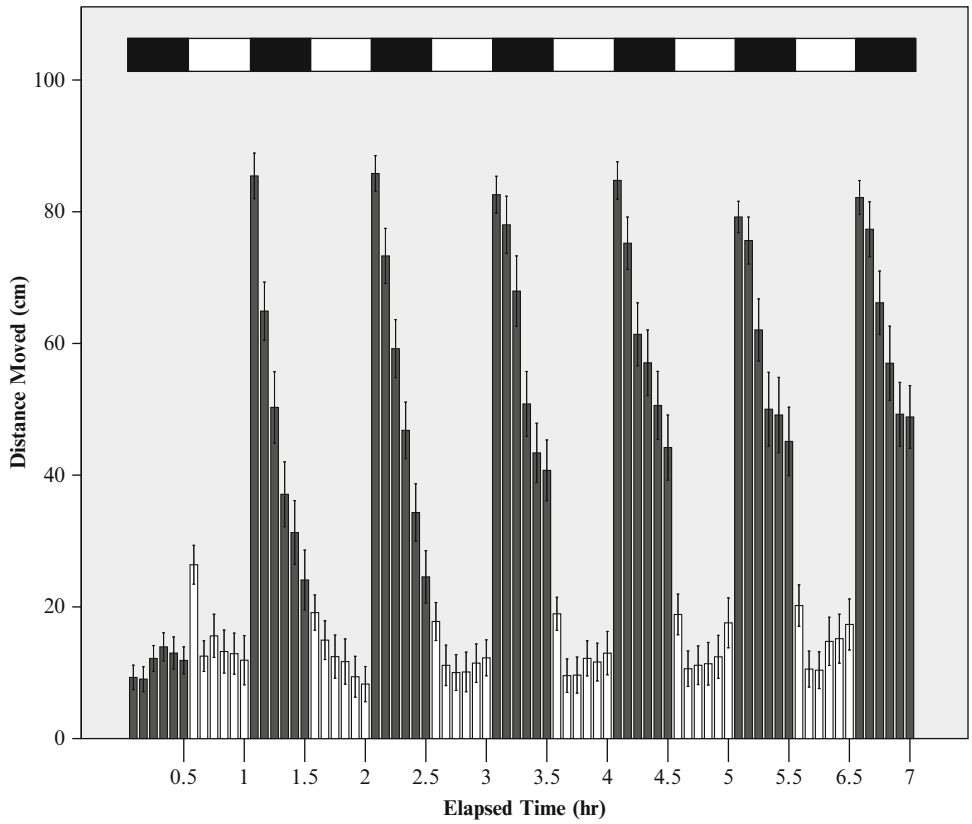

Fig. 1. Average distance moved by 48 zebrafish larvae at 5 dpf, over a total of 7 h during which the larvae are subjected to a cycle of 30 min of darkness followed by 30 min light (indicated by *line* above the *bars*). Error bars are equal to one standard error. Note that behavior in the first cycle usually does not match that in subsequent cycles. The reason for this difference is unclear but may reflect stress invoked by the transition from the acclimation period.

10. Pre-incubate fish in 0.75–1 ml of DAB solution for 20 min while mixing.
11. Add 10 µl of 0.1% H_2O_2. Monitor the reaction until the desired signal intensity is achieved (4–10 min).
12. Stop the reaction by removing the DAB mixture and rinsing in PBS 3×.
13. To visualize internal staining in pigmented larvae, rinse once in PBS and add bleach solution for up to 1 h.
14. Place fish in 50% PBS/50% Glycerol for documentation. Embryos are stable for several months stored at 4°C.

3.2.2. In Situ Hybridization (for mitfa or dct in the Presence of Melanoblasts)

This protocol for in situ hybridization is abbreviated and adapted from a previously published one (46).

Whole-Animal In Situ Hybridization

Day 1

Performed at RT in approximately 500 µl volumes, for up to 30 larvae per microcentrifuge tube.

1. Place fish anesthetized with tricaine into 500 µl of 4% PFA in a 1.5 ml microcentrifuge tube, and incubate for 6 h at RT, or O/N at 4°C.
2. Rinse in PBST 3×5 min.
3. For long-term storage, place in 100% methanol (MeOH) and store at –20°C. Before use, re-hydrate at RT in sequential 10-min washes: 66% MeOH/33% PBST, 33% MeOH/66% PBST, 100% PBST.
4. Incubate 24-hpf embryos for 10 min in 10 µg/ml Prot K in PBST at RT, with gentle rocking.
5. Stop the Prot K reaction by fixing in 4% PFA for 30 min at RT.
6. Wash 4×5 min in PBST.
7. Wash in Hyb1 for 1–2 h at 70°C.
8. Add warm Hyb2 with probe (1×) and incubate O/N at 70°C.

Day 2

1. Pre-warm wash solutions to 70°C.
2. Remove probe Hyb mix and save (it can be re-used many times).
3. Perform three 10-min washes at 70°C in the following sequence: 66% Hyb2 and 33% 2× SSC, 33% Hyb2 and 66% 2× SSC, 100% 2× SSC.
4. Follow with 3×20 min washes at 70°C, with 0.2× SSC.
5. Wash 5 min at RT in PBST.
6. Incubate in blocking solution for 1 h at RT.
7. Incubate in 1:5,000 dilution of sheep-anti-DIG-Alkaline Phosphatase (AP Fab fragments) in blocking solution, or 1:20,000 of sheep-anti-FITC-AP at 4°C O/N (Note 6).

Day 3

1. Wash 6×20 min at RT in PBST.
2. Wash 3×5 min in color buffer.
3. Develop in a dark container with 20 µl/ml NBT/BCIP solution, for about 1 h at RT (Note 7).

4. Wash 3 × 10 min in PBST (Note 8 for double in situ).
5. Visualize under bright field and store in PBST at 4°C for several weeks.

Acridine Orange Staining

Acridine orange (AO) is a fluorescent vital dye that stains apoptotic cells (50).

1. Place live embryos or larvae in 1× AO at RT for 30 min.
2. Wash 3 × 10 min in Ringer's solution.
3. Anesthetize in tricaine.
4. Mount live embryos in 3% methylcellulose for several minutes.
5. Visualize with GFP filter (signal will appear green rather than orange).

TUNEL Assay

Terminal dUTP nick end labeling (TUNEL) labels the fragmented DNA observed in apoptotic cells (51). This protocol is based on (52).

Day 1

1. Re-hydrate dechorionated embryos stored in 100% methanol at RT in sequential 10-min washes: 66% MeOH/33% TTBST, 33% MeOH/66% TTBST, 100% TTBST.
2. Digest in Prot K for 30 min with 1 μg/ml at 37°C.
3. Wash in 2 mg/ml glycine 2 × 5 min.
4. Wash 3.5 min in TTBST 1×.
5. Wash 2 × 5 min in 1× TTase buffer.
6. Add 0.5 μl TdT enzyme (100 U) and Fluorescein dUTP to 400 μl TTase buffer for a final concentration of 0.05 μM Fluorescein dUTP.
7. Pre-incubate 45 min at 4°C in the dark.
8. Incubate for 1 h at 37°C in the dark.
9. Rinse twice in TTBST in the dark.
10. Wash with TTBST 4°C O/N in the dark.

Day 2

1. Incubate at 70°C for 30 min.
2. Incubate in blocking solution for 2 h at RT.
3. Add sheep-anti-FITC-AP at 1:20,000 dilution.
4. Incubate 4°C O/N.

Day 3

1. Wash in TTBST 6 × 20 min RT.
2. Rinse in color buffer 2 × 5 min.
3. Develop in dark at RT, in 20 μg/ml NBT/BCIP solution with 5% polyvinyl alcohol diluted in color buffer.

4. Rinse in TTBST 3 × 10 min.
5. Visualize with GFP filter.

4. Notes

1. Plates with 96 or 48 wells produce similar results, whereas we detect greater amounts of movement in plates with 24 wells (49). For 96-well plates, the following styles have worked well: ELISA, flat-bottom, and round bottom.
2. As MPP + degrades quickly in solution, for longer assays it should be replaced daily.
3. Even after O/N acclimation within the zebrabox, movement is erratic for up to an hour. Differences can be obscured by this noise, a point that is especially relevant for motor assays, as most studies have not used a positive control.
4. We use 0 power light for 180,000 ms, followed by a transition from 0 to 100-power over the course of 1 s, and 100 power light for 18,0000 ms. Over long periods, light produces more spontaneous swimming behavior, but a light to dark transition triggers a strong, short-term bout of swimming (53).
5. If background signal is excessive, carry out additional washes (2 × 5 min in PBS).
6. If background signal is excessive, add 0.3 M levamisole along with either anti-DIG or anti-FITC in blocking solution.
7. If signaling is weak, development can be continued on the next day. In this case, remove the NBT/BCIP, place embryos into PBST and store at 4°C O/N. Continue the reaction in the morning. If signal is too strong, place embryos in 100% MeOH at –20°C O/N, and then continue with wash steps.
8. For a double in situ with both DIG and FITC, add one secondary antibody at a time (usually FITC first). Develop, inactivate alkaline phosphatase by incubating in 100 mM glycine-hydrochloride, pH 2.2, for 30 min., rinse in PBST, re-fix the specimen in 4% PFA, incubate in blocking solution, and then proceed with the other secondary antibody.

References

1. Tanner CM (2003) Is the cause of Parkinson's disease environmental or hereditary? Evidence from twin studies. Parkinsons Dis 91: 133–142
2. Kitada T, Tong YR, Gautier CA, Shen J (2009) Absence of nigral degeneration in aged parkin/DJ-1/PINK1 triple knockout mice. J Neurochem 111(3):696–702
3. Flinn L, Bretaud S, Lo C, Ingham PW, Bandmann O (2008) Zebrafish as a new animal model for movement disorders. J Neurochem 106(5):1991–1997

4. Drapeau P, Saint-Amant L, Buss RR, Chong M, McDearmid JR, Brustein E (2002) Development of the locomotor network in zebrafish. Prog Neurobiol 68(2):85–111
5. Cario CL, Farrell TC, Milanese C, Burton EA (2011) Automated measurement of zebrafish larval movement. J Physiol (Lond) 589(15):3703–3708
6. Panula P, Sallinen V, Sundvik M, Kolehmainen J, Torkko V, Tiittula A, Moshnyakov M, Podlasz P (2006) Modulatory neurotransmitter systems and behavior: towards zebrafish models of neurodegenerative diseases. Zebrafish 3(2):235–247
7. Rihel J, Prober DA, Arvanites A, Lam K, Zimmerman S, Jang S, Haggarty SJ, Kokel D, Rubin LL, Peterson RT, Schier AF (2010) Zebrafish behavioral profiling links drugs to biological targets and rest/wake regulation. Science 327(5963):348–351
8. Rink E, Wullimann MF (2001) The teleostean (zebrafish) dopaminergic system ascending to the subpallium (striatum) is located in the basal diencephalon (posterior tuberculum). Brain Res 889(1–2):316–330
9. Bretaud S, Allen C, Ingham PW, Bandmann O (2007) p53-dependent neuronal cell death in a DJ-1-deficient zebrafish model of Parkinson's disease. J Neurochem 100(6):1626–1635
10. Baulac S, Lu H, Strahle J, Yang T, Goldberg MS, Shen J, Schlossmacher MG, Lemere CA, Lu Q, Xia WM (2009) Increased DJ-1 expression under oxidative stress and in Alzheimer's disease brains. Mol Neurodegener 4:12
11. Sallinen V, Kolehmainen J, Priyadarshini M, Toleikyte G, Chen YC, Panula P (2010) Dopaminergic cell damage and vulnerability to MPTP in Pink1 knockdown zebrafish. Neurobiol Dis 40(1):93–101
12. Xi YW, Ryan J, Noble S, Yu M, Yilbas AE, Ekker M (2010) Impaired dopaminergic neuron development and locomotor function in zebrafish with loss of pink1 function. Eur J Neurosci 31(4):623–633
13. Anichtchik O, Diekmann H, Fleming A, Roach A, Goldsmith P, Rubinsztein DC (2008) Loss of PINK1 function affects development and results in neurodegeneration in zebrafish. J Neurosci 28(33):8199–8207
14. Sheng D, Qu D, Kwok KH, Ng SS, Lim AY, Aw SS, Lee CW, Sung WK, Tan EK, Lufkin T, Jesuthasan S, Sinnakaruppan M, Liu J (2010) Deletion of the WD40 domain of LRRK2 in Zebrafish causes Parkinsonism-like loss of neurons and locomotive defect. Plos Genet 6(4):e1000914
15. Ren GQ, Xin SC, Li S, Zhong HB, Lin S (2011) Disruption of LRRK2 does not cause specific loss of dopaminergic neurons in zebrafish. Plos One 6(6):e20630
16. Fett ME, Pilsl A, Paquet D, van Bebber F, Haass C, Tatzelt J, Schmid B, Winklhofer KF (2010) Parkin is protective against proteotoxic stress in a transgenic zebrafish model. Plos One 5(7):e11783
17. Flinn L, Mortiboys H, Volkmann K, Koester RW, Ingham PW, Bandmann O (2009) Complex I deficiency and dopaminergic neuronal cell loss in parkin-deficient zebrafish (Danio rerio). Mov Disord 24:S135–S135
18. Lam CS, Korzh V, Strahle U (2005) Zebrafish embryos are susceptible to the dopaminergic neurotoxin MPTP. Eur J Neurosci 21(6):1758–1762
19. Anichtchik OV, Kaslin J, Peitsaro N, Scheinin M, Panula P (2004) Neurochemical and behavioural changes in zebrafish Danio rerio after systemic administration of 6-hydroxydopamine and 1-methyl-4-phenyl-1,2,3,6-tetrahydropyridine. J Neurochem 88(2):443–453
20. Bretaud S, Lee S, Guo S (2004) Sensitivity of zebrafish to environmental toxins implicated in Parkinson's disease. Neurotoxicol Teratol 26(6):857–864
21. Wen L, Wei W, Gu WC, Huang P, Ren X, Zhang Z, Zhu ZY, Lin S, Zhang B (2008) Visualization of monoaminergic neurons and neurotoxicity of MPTP in live transgenic zebrafish. Dev Biol 314(1):84–92
22. McKinley ET, Baranowski TC, Blavo DO, Cato C, Doan TN, Rubinstein AL (2005) Neuroprotection of MPTP-induced toxicity in zebrafish dopaminergic neurons. Mol Brain Res 141(2):128–137
23. Pan TH, Li XQ, Jankovic J (2011) The association between Parkinson's disease and melanoma. Int J Cancer 128(10):2251–2260
24. Fiala KH, Whetteckey J, Manyam BV (2003) Malignant melanoma and levodopa in Parkinson's disease: causality or coincidence? Parkinsonism Relat Disord 9(6):321–327
25. Boissy RE, Nordlund JJ (2011) Vitiligo: current medical and scientific understanding. Giornale italiano di dermatologia e venereologia: organo ufficiale. Societa italiana di dermatologia e sifilografia 146(1):69–75
26. Glassman SJ (2011) Vitiligo, reactive oxygen species and T-cells. Clin Sci 120(3):99–120
27. Liu R, Gao X, Lu Y, Chen HL (2011) Meta-analysis of the relationship between Parkinson disease and melanoma. Neurology 76(23):2002–2009
28. Shi CH, Tang BS, Wang L, Lv ZY, Wang J, Luo LZ, Shen L, Jiang H, Yan XX, Pan Q, Xia K, Guo JF (2011) PLA2G6 gene mutation in

autosomal recessive early-onset parkinsonism in a Chinese cohort. Neurology 77(1):75–81

29. Paisan-Ruiz C, Guevara R, Federoff M, Hanagasi H, Sina F, Elahi E, Schneider SA, Schwingenschuh P, Bajaj N, Emre M, Singleton AB, Hardy J, Bhatia KP, Brandner S, Lees AJ, Houlden H (2010) Early-onset L-dopa-responsive parkinsonism with pyramidal signs due to ATP13A2, PLA2G6, FBXO7 and spatacsin mutations. Move Disord: Off J Move Disord Soc 25(12):1791–1800
30. Sina F, Shojaee S, Elahi E, Paisan-Ruiz C (2009) R632W mutation in PLA2G6 segregates with dystonia-parkinsonism in a consanguineous Iranian family. Eur J Neurol: Off J Eur Feder Neurol Soc 16(1):101–104
31. Paisan-Ruiz C, Bhatia KP, Li A, Hernandez D, Davis M, Wood NW, Hardy J, Houlden H, Singleton A, Schneider SA (2009) Characterization of PLA2G6 as a locus for dystonia-parkinsonism. Ann Neurol 65(1):19–23
32. Kvaskoff M, Whiteman DC, Zhao ZZ, Montgomery GW, Martin NG, Hayward NK, Duffy DL (2011) Polymorphisms in nevus-associated genes MTAP, PLA2G6, and IRF4 and the risk of invasive cutaneous melanoma. Twin Res Hum Genet: Off J Int Soc Twin Stud 14(5):422–432
33. Haffter P, Granato M, Brand M, Mullins MC, Hammerschmidt M, Kane DA, Odenthal J, vanEeden FJM, Jiang YJ, Heisenberg CP, Kelsh RN, FurutaniSeiki M, Vogelsang E, Beuchle D, Schach U, Fabian C, NussleinVolhard C (1996) The identification of genes with unique and essential functions in the development of the zebrafish, Danio rerio. Development 123:1–36
34. Amsterdam A, Burgess S, Golling G, Chen WB, Sun ZX, Townsend K, Farrington S, Haldi M, Hopkins N (1999) A large-scale insertional mutagenesis screen in zebrafish. Genes Dev 13(20):2713–2724
35. Dorsky RI, Moon RT, Raible DW (1998) Control of neural crest cell fate by the Wnt signalling pathway. Nature 396(6709):370–373
36. Quigley IK, Parichy DM (2002) Pigment pattern formation in zebrafish: a model for developmental genetics and the evolution of form. Microsc Res Tech 58(6):442–455
37. Kelsh RN, Eisen JS (2000) The zebrafish colourless gene regulates development of non-ectomesenchymal neural crest derivatives. Development 127(3):515–525
38. Lister JA, Robertson CP, Lepage T, Johnson SL, Raible DW (1999) nacre encodes a zebrafish microphthalmia-related protein that regulates neural-crest-derived pigment cell fate. Development 126(17):3757–3767
39. Curran K, Raible DW, Lister JA (2009) Foxd3 controls melanophore specification in the zebrafish neural crest by regulation of Mitf. Dev Biol 332(2):408–417
40. Cornell RA, Yemm E, Bonde G, Li W, D'Alencon C, Wegman L, Eisen J, Zahs A (2004) Touchtone promotes survival of embryonic melanophores in zebrafish. Mech Dev 121(11):1365–1376
41. McNeill MS, Paulsen J, Bonde G, Burnight E, Hsu MY, Cornell RA (2007) Cell death of melanophores in zebrafish trpm7 mutant embryos depends on melanin synthesis. J Invest Dermatol 127(8):2020–2030
42. Nadler MJ, Hermosura MC, Inabe K, Perraud AL, Zhu Q, Stokes AJ, Kurosaki T, Kinet JP, Penner R, Scharenberg AM, Fleig A (2001) LTRPC7 is a Mg.ATP-regulated divalent cation channel required for cell viability. Nature 411(6837):590–595
43. Runnels LW, Yue L, Clapham DE (2001) TRP-PLIK, a bifunctional protein with kinase and ion channel activities. Science 291(5506):1043–1047
44. McNeill MS, Paulsen J, Bonde G, Burnight E, Hsu MY, Cornell RA (2007) Cell death of melanophores in zebrafish trpm7 mutant embryos depends on melanin synthesis. J Invest Dermatol 127(8):2020–2030
45. Hermosura MC, Nayakanti H, Dorovkov MV, Calderon FR, Ryazanov AG, Haymer DS, Garruto RM (2005) A TRPM7 variant shows altered sensitivity to magnesium that may contribute to the pathogenesis of two Guamanian neurodegenerative disorders. Proc Natl Acad Sci USA 102(32):11510–11515
46. Thisse C, Thisse B (2008) High-resolution in situ hybridization to whole-mount zebrafish embryos. Nat Protoc 3(1):59–69
47. Emran F, Rihel J, Dowling JE (2008) A behavioral assay to measure responsiveness of zebrafish to changes in light intensities. J Vis Exp: JoVE 20:923
48. Westerfield M (2000) The zebrafish book a guide for the laboratory use of zebrafish Danio (Brachydanio) rerio. ZFIN. University of Oregon, Eugene
49. Padilla S, Hunter DL, Padnos B, Frady S, Macphail RC (2011) Assessing locomotor activity in larval zebrafish: influence of extrinsic and intrinsic variables. Neurotoxicol Teratol 33(6):674–679
50. Furutani-Seiki M, Jiang YJ, Brand M, Heisenberg CP, Houart C, Beuchle D, van Eeden FJ, Granato M, Haffter P, Hammerschmidt M, Kane DA, Kelsh RN, Mullins MC, Odenthal J,

Nusslein-Volhard C (1996) Neural degeneration mutants in the zebrafish, Danio rerio. Development 123:229–239

51. Gavrieli Y, Sherman Y, Ben-Sasson SA (1992) Identification of programmed cell death in situ via specific labeling of nuclear DNA fragmentation. J Cell Biol 119(3):493–501
52. Cole LK, Ross LS (2001) Apoptosis in the developing zebrafish embryo. Dev Biol 240(1): 123–142
53. Burgess HA, Granato M (2007) Modulation of locomotor activity in larval zebrafish during light adaptation. J Exp Biol 210(14): 2526–2539

Chapter 10

A Practical Guide to Evaluating Anxiety-Related Behavior in Rodents

Caitlin J. Riebe and Carsten T. Wotjak

Abstract

Tests of innate fear and anxiety take advantage of the natural anxieties and interests of mice and rats. They often rely on the animals' motivation to explore their environment as well as their apprehension towards novelty or exposure. Here we describe the technical and experimental details of five classical tests of anxiety-like behavior which are frequently applied for experiments in rats and mice. The open field test is a simple open arena, which can be used to assess anxiety as well as general locomotor activity. The light–dark box and elevated-plus maze (EMP) offer the animals a choice between nonaversive and aversive areas of an apparatus and the novelty-induced hypophagia (NIH) and social interaction tests rely on novelty-induced suppression of natural behaviors in mice and rats. Our practical guide ends with a discussion of advantages and limitations of each test. We hope that our recommendations enable an easy establishment of the behavioral paradigms and allow for a better comparability of the results between different labs.

Key words: Mice, Rats, Anxiety, Fear, Behavior, Innate, Rodent

1. Introduction

Behavioral tests have been used to assess anxiety for decades and stem back to 1934 when Calvin Hall (1) pioneered the use of the open field to analyze emotional behavior in rats. Since then many complex behavioral paradigms for gauging animal emotionality have been developed; however, the key to assessing *innate* anxiety is engineering the paradigms in such a way as to be able to observe and quantify the natural behavior of the animals. These tests do not rely on any learning or conditioning processes and instead seek to mimic certain aspects of the animals' natural environment which may induce fear or anxiety.

Rodents, such as mice and rats, are naturally exploratory creatures and spend much of their lives foraging for food and shelter.

Arpad Szallasi and Tamás Bíró (eds.), *TRP Channels in Drug Discovery: Volume II*, Methods in Pharmacology and Toxicology,
DOI 10.1007/978-1-62703-095-3_10,

However, being so vulnerable to predation, they are also wary of novel, unprotected or brightly lit environments. Tests of innate anxiety in rats and mice take advantage of their natural curiosity as well as their fears of novel, exposed environments. Parameters are defined and calibrated to create a conflict between the motivation to explore and their innate anxiety; finding the appropriate balance allows for detection of both increases as well as decreases in anxiety-like behavior in comparison to control groups or baseline measures.

This chapter will provide practical guidelines for five of the major behavioral tests used to assess innate anxiety in mice and rats. The open field test is one of the most widely used behavioral tests in rodents and is based on exploratory behavior in a brightly lit open area. The elevated-plus maze (EPM) and the light–dark box are based on exploration in an environment with relatively protected vs. relatively bright, exposed areas. These tests create distinct situations where the animals' fears and drive to explore are in direct conflict. Novelty-induced hypophagia (NIH; aka novelty-induced suppression of feeding; NSF) evaluates feeding behavior in an anxiety-producing novel environment and takes advantage of the fact that anxious animals tend to be less motivated to eat. Lastly, the social interaction test assesses mutual investigation between two conspecifics and relies on anxiety-induced changes in social behavior.

2. Materials

2.1. Subjects

1. The strain, sex, and housing conditions of the animals must be carefully considered and reported for each experiment. Regarding the strain, it should be noted that rodent (and especially mouse) strains are very specific and that even closely related strains may display very different behavioral characteristics (2). Therefore, it is mandatory to strictly adhere to the exact mouse strain nomenclature.
2. When considering sex, not only can anxiety-related characteristics differ between the sexes, but such behavior can vary across the estrus cycle of the female. Estrus stage must be controlled with ovariectomization and hormone replacement or determined by vaginal swabs.
3. It is recommended that animals are singly housed to avoid being disturbed by the testing of cage mates, and kept on a reverse light–dark cycle so that animals are tested during their active phase. Housing conditions must be constant and clearly defined for each experiment. In general, each experimental group should include 10–12 mice or 6–8 rats.

4. Mice can be picked up by the first 1/3 of their tail, whereas rats can either be picked up at the very base of the tail or, preferably, grasped under the shoulders. Handling of the animals can affect anxiety-related behavior and should be minimized and kept constant for all animals. Usually when placed in a testing apparatus, animals should be facing a wall or closed arm of the apparatus. This is done to ensure that the animal does not automatically run into the open or out of the closed arm when released from the experimenter.

2.2. Testing Apparatus

The testing areas should always be isolated from the area where the animals are housed. If a completely separate room is not available then the testing area may be segregated from the rest of the room with an opaque curtain. It is important that all sides of the area are similar in color and appearance to avoid creating any preference or aversion to one section or another.

2.2.1. Open Field Test

1. The open field is a large square arena surrounded by walls where a variety of anxiety related and exploratory behaviors can be measured (Notes 1 and 2). The arena should be at least 60 cm × 60 cm for mice and about 120 cm × 120 cm for rats (Note 3). The walls should be about 50–60 cm high, i.e., high enough that the animals cannot escape (Fig. 1).
2. A video camera connected to a recording device is mounted above the open field at a sufficient distance to be able to detect the animal at all locations within the apparatus (Note 4).

2.2.2. Light–Dark Box

1. The light–dark box is an enclosed square divided into a brightly lit and a dimly lit compartment connected by a short tunnel (Note 5). The entire box is 52 cm × 20 cm with 25 cm high walls all around. There is a 7 cm thick double wall dividing the

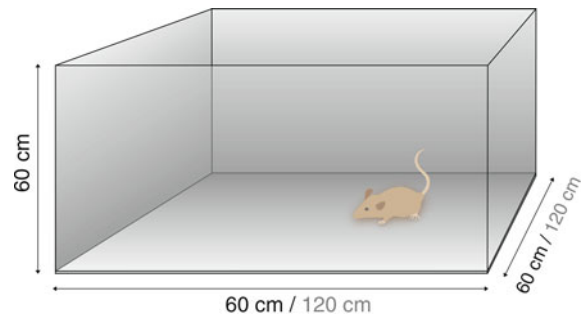

Fig. 1. The open field test is a simple square open arena. The dimensions for mice are shown in *black* and the dimensions for rats are shown in *gray*. The apparatus should be at least 60 cm × 60 cm for mice and 120 cm × 120 cm for rats. The walls should be about 60 cm high or high enough that animals cannot escape. The entire box is illuminated between 150 and 700 lux.

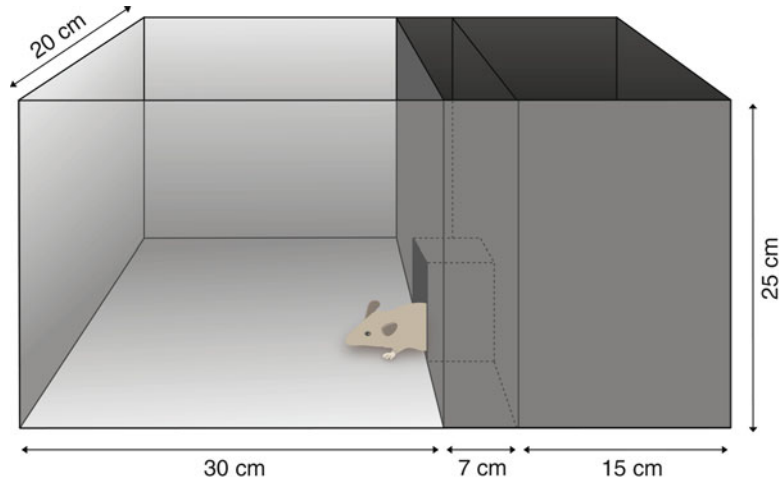

Fig. 2. The light–dark box is a 52 cm × 25 cm square arena with 25 cm high walls, which can be utilized for both mice and rats. The box is divided into a 30 cm and 15 cm compartment linked by a 7 cm wide double wall. A 7 cm × 7 cm tunnel is cut out of the wall to create a tunnel between the two compartments. The smaller compartment is lit at 15–20 lux with a *red light* and the large compartment is lit at 150–700 lux with a *white light*.

length of the box into a 30 cm and a 15 cm compartment. Both sides of the double wall have a 7 cm × 7 cm door cutout in the bottom center. The doors of either side of the double wall are connected by a tunnel, which spans the distance between the walls and is the same height and width as the doors (Fig. 2). The same apparatus dimensions can be used for both mice and rats (Note 6).

2. The entire floor and inner walls of the dark compartment are painted black with waterproof paint and the light compartment is left light gray. A white light is mounted above the light compartment at a sufficient height to create illumination on the floor of the compartment between 150 and 700 lux. A red light is mounted above the dark compartment to illuminate it at 15–20 lux. A camera should be mounted above the apparatus, so that the entire apparatus including both sides of the tunnel is fully visible.

2.2.3. Elevated Maze

1. The elevated-plus maze consists of an elevated "+" shaped platform with walls surrounding two adjacent arms (the *closed* arms). The other two arms have no walls and are considered the *open* arms. For mice, the dimensions are as follows: 30 cm arm length, 5 cm arm width, 15 cm wall height and raised 40–75 cm from the floor. For rats, the platform dimensions are slightly larger: 50 cm arm length, 10 cm arm width, 40 cm wall and raised 70–120 cm from the floor (Fig. 3). The open arms may have a small (~3–5 mm) rim running along the edge of the floor to prevent animals from sliding off.

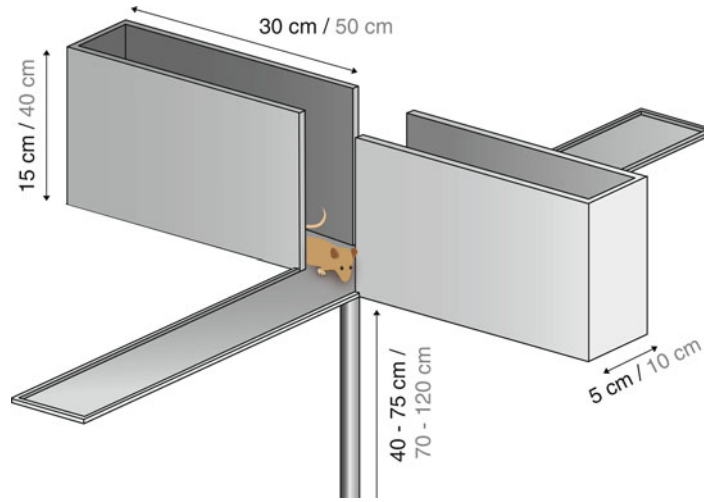

Fig. 3. The elevated-plus maze is a "+" shaped apparatus with walls surrounding two adjacent arms. The dimensions for mice are shown in *black* and the dimensions for rats are shown in *gray*. For mice the arms is 30 cm × 5 cm with 15 cm walls for the closed arms and for rats the arms are 50 cm × 10 cm with 40 cm walls around the closed ones. The entire apparatus is raised off the floor by 40–75 cm for mice and 70–120 cm for rats. The closed arms are illuminated at 15–20 lux and the open arms are illuminated at about 300 lux.

2. Four separate light fixtures are used for the EPM—one mounted above each arm. White light of approximately 300 lux is used over the open arms and red light (15–20 lux) over the closed arms (Note 7). A camera should be mounted above the apparatus in a position that allows visibility of the animal everywhere within the maze. The camera can also be tilted at a slight angle to the maze to allow for better differentiation among behaviors such as freezing, sniffing, head dipping, and grooming, especially in the middle area of the maze and on the open arms.

2.2.4. Novelty-Induced Hypophagia/Suppression of Feeding

Testing for the novelty-induced hypophagia (aka novelty-induced suppression of feeding; NSF) test is done in a clean standard housing chamber without bedding (Fig. 4) or in an open field apparatus. The chamber is illuminated with up to 700 lux with overhead lighting. A camera is mounted either beside or behind the chamber so that the entire inner chamber is visible. In preparation, oat flakes are soaked with a 30% sucrose solution either by spraying the flakes with the solution or pipetting a couple drops of solution onto the flakes and then allowing them to dry. Several of the sucrose-soaked oat flakes (2–3 for mice, 5–10 for rats) are weighed and placed in the center of the testing cage or arena.

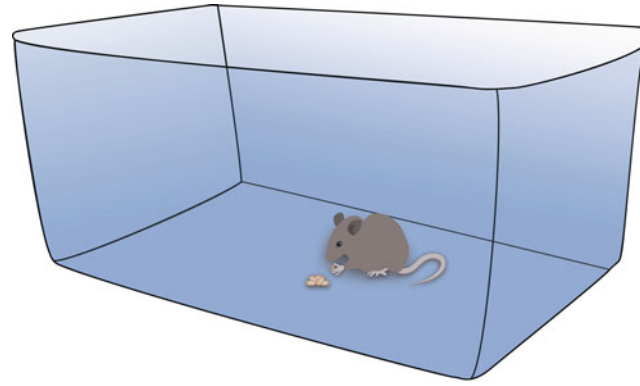

Fig. 4. The novelty-induced hypophagia test is done either in an empty housing cage or in an open field apparatus illuminated up to 700 lux from an overhead white light source. Sucrose-soaked oat flakes are placed in the center of the apparatus.

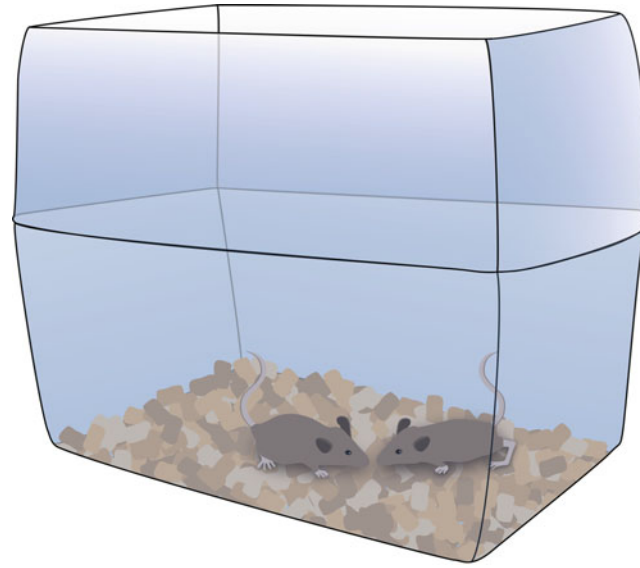

Fig. 5. The social interaction test takes place in a clean housing chamber with fresh bedding on the floor and illuminated up to 700 lux with overhead white lights. A second housing cage with the bottom cutoff is placed upside down on top of the first cage to serve as a wall extension preventing the animals from escaping.

2.2.5. Social Interaction Test

The social interaction test is performed in a clean standard housing chamber with fresh bedding in the bottom. A second empty housing chamber is used as a lid by cutting off the bottom and placing it upside down on top of the test chamber (Fig. 5). The cage is illuminated with up to 700 lux from overhead white light. A video camera is positioned beside the cage so that the entire inner area is visible.

3. Methods

3.1. Open Field Test

3.1.1. Procedure

1. Remove an animal from their home cage and place it gently in the open field facing a corner. The animal is allowed to freely explore for 5 min, during which behavior is recorded (Note 8).
2. Remove the animal from the apparatus and return it to their home cage.
3. Clean the apparatus before testing the next animal (Note 9).

3.1.2. Data Analysis

1. A characteristic anxiety-like behavior of rodents is *thigmotaxis*, which, in the open field, is maintaining contact with the walls when walking around the apparatus (Note 10).
2. Thigmotaxis can be measured as time spent in contact with the walls or the distance covered while in contact with the walls. Many video tracking programs can score thigmotaxis, where it can be defined as the animal being within 2–4 cm of the walls—the exact distance will depend on how the program defines and tracks the animal as well as the size of the animal (Note 11). Additionally, the "center" of the open field can be defined as distinct from the periphery. Ideally, this is a square shape in the middle of the apparatus that covers the same area as the perimeter. However, some tracking programs will automatically define the center. The following measures are scored for the open field: total distance traveled, immobility time (or total time minus time spent moving), thigmotaxis time, thigmotaxis distance, time in the center, distance traveled in the center. Measures of thigmotaxis distance and center distance are normalized to the total distance traveled. This is done by dividing each measure by the total distance measure (e.g., center distance % = center distance/total distance traveled).
3. Total distance traveled and immobility time give a sense of the general activity level of the animal. Observer-based analysis will not include distance measures; instead a score of how often an animal rears (i.e., raises up onto its hindpaws) can be used to indicate general activity level. Anxiety level is inferred from time spent or distance traveled while engaging in thigmotaxis vs. time spent or distance traveled in the center (observer-based analysis will only include a time score for either behavior). More anxious animals will spend more time engaging in thigmotaxis and less time venturing out to the center, whereas less anxious ones will spend more time exploring the center and less time on the walls.

3.2. Light–Dark Box

3.2.1. Procedure

The light–dark box can be performed one of two ways, which differ in the starting position of the animal. In option 1, the animals begin in the light box and in option 2 they begin in the dark box. Both options will be outlined here.

Option 1: An animal is taken from their home cage and placed in the center of the light compartment facing the doorway. As soon as the animal enters the dark compartment the 5-min testing session begins. The animal is allowed to freely explore during this time and returned to their home cage afterwards.

Option 2: An animal is taken from their home cage and placed in the center of the dark compartment facing the doorway. A 5-min testing session begins immediately, where the animal is allowed to freely explore before being returned to their home cage (Note 12).

3.2.2. Analysis

Option 1: A timer is started as soon as an animal is placed in the apparatus and the latency to enter the dark compartment is observed and recorded. Once the animal first enters the dark compartment a new timer is set for the 5-min test session, within which time in each compartment, latency to re-enter the light compartment and number of entries into each compartment are scored.

Option 2: The 5-min testing session begins as soon as the animal is placed in the dark compartment. Time in each compartment, latency to enter the light compartment, and number of entries into each compartment are scored.

The time in the light and dark compartments are used to calculate a proportional score for each measure (see below). Time in the tunnel area is not scored and not included in analysis and calculations:

Light time = time in light/(time in light + time in dark)

Dark time = time in dark/(time in light + time in dark)

Transition scores (i.e., the total number of entries into either compartment) are used to control for general locomotor activity. The latency to enter the dark box (option 1) is a measure of anxiety with a lower latency associated with high anxiety. Conversely, higher latency to (re-)enter the light box is associated with high anxiety. Higher scores for *dark time* as well as lower scores for *light time* both indicate higher anxiety.

3.3. Elevated-Plus Maze

3.3.1. Procedure

1. The animal is taken from their home cage and gently placed into the neutral center area facing a closed arm.
2. The animal is allowed to freely explore the maze for 5 min and then removed from the maze and returned to their home cage.

3.3.2. Analysis

1. For analysis, the EPM is divided into three distinct areas: the closed arm areas, the open arm areas, and the neutral or center area between the four arms of the maze. Entries into and time spent in central area are not included in the analyses. Behavior is scored for the following measurements: number of open arm entries, number of close arm entries, time in open arms, and time in closed arms. An entry into a closed or open arm occurs when the animal has left the center area onto the arm and not when the animal has entered the center region (Note 13).

2. The total number of closed arm entries is a measure of general activity. Entries into the open arms and time spent in the open arms give a measure of anxiety, with decreased time and entries related to increased anxiety.

$$\text{Open arm entries} = \text{number of open arm entries} / (\text{open arm} + \text{closed arm entries})$$

$$\text{Open arm time} = \text{time on open arm} / (\text{total time in open} + \text{closed arms})$$

3.4. Novelty-Induced Hypophagia

3.4.1. Procedure

1. Several days prior to testing animals must be familiarized with the food to be used during testing (Notes 14 and 15). This is to eliminate the effect of taste novelty and put emphasis on environmental neophobia. In order to familiarize them, each animal is given 1–2 sucrose-soaked oat flakes on 3 separate days before the test day. The latency to eat the oat flakes (scoring details provided below) is recorded each day and can be used as a baseline score as well as to assess the overall motivational state of the animals.
2. For testing, an animal is removed from their home cage and placed facing a corner in the novel test area. The animal is allowed to freely explore the environment and food for 10 min and then returned to their home cage. The leftover food is removed and weighed before the used test cage is set aside and a new cage is prepared for the next animal.

3.4.2. Analysis

The measures taken include the latency to begin eating the provided food as well as the amount of food consumed. The latency to eat does not include mere physical contact with the food or the carrying of food around the cage, but only the time at which the animal first puts the food in their mouth to eat.

3.5. Social Interaction

3.5.1. Procedure

Two animals from the same experimental group are both placed into the test cage at the same time. They are allowed to freely explore for 5 min after which they are both returned to their respective home cages (Note 16). The used test cage is set aside and a new cage is prepared for the next animals; however, the same lid cage may be used repeatedly.

3.5.2. Analysis

The duration of investigative behavior between the two animals is scored and one score is recorded for each pair of animals. Investigative behaviors include sniffing of the anogential region, ears, trunk, tail, and mouth as well as grooming or closely following one another. The duration of aggressive behaviors, such as biting, boxing, or mounting as well as sexual behaviors are also recorded (if present). Lower time spent on social investigation as well as more time spent on aggressive behaviors is indicative of higher anxiety (Note 17).

4. Notes

1. Testing apparatuses can be constructed out of opaque or painted plexiglass, acrylic or polyethylene plastic. If wood is used, all the inner edges and corners must be sealed and the inner walls painted with waterproof paint to allow for thorough cleaning of the apparatus. In cases where video analysis is to be used it is advisable to use a light gray material or paint for the apparatus. Thus, both black and white strains of mice and rats can be detected by the video analysis software allowing the same setup to be used with all strains tested. The testing area should always be isolated from the area where the animals are housed. If a completely separate room is not available, the testing area may be segregated from the rest of the room with an opaque curtain. It is important that all sides of the area are similar in color and appearance to avoid creating any preference or aversion to one section or another.
2. The open field can also be constructed in a circular shape, using all the same procedures and analyses as with the square box. However, as with any circular apparatus, animals can be prone to stereotypies in that they may begin to continuously run in circles because there is no edge or barrier to stop them.
3. The actual size of the open field box makes a significant difference in the ability to assess anxiety-related behavior with the test. The test can, and often is, used as a general control measure for locomotion within a test battery.[1] In this case smaller dimensions (e.g., 30 cm × 30 cm for mice and 60 cm × 60 cm for rats) are sufficient. However, in order to be able to measure anxiety-related behavior larger areas are needed. The bigger the box, the more open and exposed the center area is, which creates a sharper contrast to the relatively protected wall areas and allows for a better distinction between anxious and nonanxious animals.
4. Whether behavior is scored online or offline, all behavioral testing should be recorded with a camera. Before an animal is placed in an apparatus the video recorder is turned on and the animal number is indicated orally or visually to the camera. As soon as an animal is placed in a testing situation the experimenter moves away from the setup as quickly and quietly as possible and remains as quiet as possible throughout duration of the test. In cases where online scoring is done, the observer does not watch the animal directly, but rather remotely, from a monitor hooked up to the recording camera, where the experimenter can be out of view of the animal.

[1]When used as a test for locomotion, the open field should be illuminated with only 0–20 lux.

5. Lighting is especially important because it allows the experimenter to control the aversiveness of the testing environment. The testing room should be evenly illuminated with an overhead white light source. Lighting should be adjustable between 20 and 600 lux. It must be ensured that the lighting is stable and does not flicker as this can be quite aversive for the animals.
6. An alternate construction of the light–dark box excludes the tunnel area between the light and dark compartments. In this case there is just a door between the two sides of the box. However, this apparatus may provide a less sensitive measure of anxiety behavior.
7. Not only the total illumination, but also the difference in illumination between the open and closed arms must be considered in the EPM. This difference in illumination creates a kind of light–dark box effect within the EPM and can be adjusted to obtain appropriate baseline scores. For example, if animals tend to be too anxious, the lighting above the open arms can be lowered. It is recommended that untreated animals spend 15–20% of the time on the open arms to allow for a bidirectional modulation of anxiety-like behavior.
8. Testing in the open field may take place for up to 30 min in order to evaluate locomotor activity or cognitive abilities such as learning and memory. However, only the first 5 min of testing is used to analyze anxiety behavior. Confounding factors, such as immobility (i.e., freezing or resting) are not likely to take place within this time. After the initial 5 min significant habituation takes place and anxiety measures would reach floor values. Therefore, analysis of anxiety behavior becomes confounded by the fact that decreases in anxiety are undetectable.
9. Any testing apparatus must be thoroughly cleaned or replaced after each animal. The entire floor and inner walls of the apparatus are wiped down with a mixture of soap and water, followed by clean water and then completely dried with a towel. However, excessively rigorous cleaning and drying procedures should be avoided as they can create static (particularly if the setup is made of plexiglass or plastic), which can be particularly disturbing for the animals.
10. Observers must be trained to score behavior for any test and demonstrate satisfactory inter- and intra-rater consistency in their scoring before analyzing test results. Each observer scores behavior slightly differently, but it is most important to have consistency within one scorer. Ideally, a training DVD of about 20 trails should be established. Trainees repeatedly score this DVD and compare their scores among themselves as well as with those of previous observers. The inter-rater correlation must be at least 90% and the intra-rater correlation must be at least 85%.

For scoring purposes it should be noted that an *entry* into any area or compartment is defined as the animal having *all four* paws within that area or compartment. Unless otherwise noted, a *latency* score is the amount of time it takes for an animal to first engage in a given behavior starting from the test onset. Although behavioral definitions may vary, consistency in the analysis must be maintained. When scoring test results observers must always be blind to the experimental condition of the animal.

11. Analysis of video recordings can be done with various computer tracking programs. Such software is set to automatically detect the rat or mouse as a distinct object, separate from the background and track its progress within a defined area or areas. In this way total distance traveled, as well as entries into, latency to enter, and time in defined areas can be analyzed. The sampling rate of any tracking program should be set to 4 Hz (higher rates do not provide additional information).

    Alternatively, automatic analysis can be done via infrared beams. The beams are part of the apparatus setup and linked to a recording program that automatically detects and records each time the animals breaks a beam. Infrared beams are most useful in tests where immobility and entries are scored, such as the open field, light–dark box, and EPM. Infrared beams can also be used to automatically evaluate vertical exploration, such as rearing (i.e. upward exploration).[2]

12. Although both procedural options for the light-dark box have been included, there are some notable advantages to option 2. First of all, placing animals directly in an exposed and bright environment (as is done in option 1) could lead to freezing behavior before the animal enters the dark box—this is an indication of fear, however the resulting high latency would be analyzed as low anxiety. With option 2, only the latency to enter the light compartment is scored where high latency indicates fearfulness. This measurement is unconfounded by freezing, since freezing in the dark box and the resulting increased latency would both be indicative of increased anxiety.

    Secondly, placing animals first into the light compartment may serve to reduce the animals' curiosity about the light compartment. With their curiosity satiated and their fear of exposure still effective they may be unmotivated to re-enter the light compartment once they leave it. The results then reflect a reduced exploratory drive, rather than increased anxiety.

[2] One disadvantage of using infrared beams is that the dimensions of the setup are often limited by commercially available supplies. Another disadvantage is the lack of video protocols that can be used in conjunction with infrared beams and as a consequence, the procedure operates in a so-called black-box.

It may even be for these reasons that these two methods are not directly comparable and can produce different results with the same treatments (3).

13. The elevated-zero maze is a variation of the EPM also consisting of open and closed areas; however, the platform is a continuous ring rather than a cross shape. Two adjacent quarters of the ring are surrounded by walls on either side and the other two quarters are left open. This setup serves to eliminate the neutral zone of the EPM and animals are forced to be in either an open or closed area. However, time spent in this neutral zone seems to be an important indicator of exploratory motivation and should therefore not be eliminated from the apparatus or analyses (4). Additionally, animals prone to stereotypic behavior may continuously run in circular areas and fail to properly explore the apparatus.
14. One caveat to remember when employing food-related tests, such as the NIH test, is that the appetitive value of food may not always be constant across groups. Pharmacological and genetic manipulations can both increase or decrease appetite or the rewarding properties of food independently of anxiety. Therefore, differences in behavior in the NIH test may not necessarily reflect changes in anxiety, but rather changes in the motivation for food. For example, knockout of a specific gene may dampen the value of food rewards leading to a longer latency to start feeding. Although the gene may have no effect on anxiety per se this would be interpreted as increased anxiety. Additionally, sedation or hyperactivity caused by some drug treatments may affect feeding behavior (*for review see* 5).
15. It has been recommended here to use a highly palatable food in the NIH test. However, another alternative is to food deprive animals and offer normal chow food during the test. In this case, animals are food deprived for 24 h before testing; they are still allowed normal access to water. Testing continues in the same manner as previously described except several grams of normal chow are offered instead of sucrose-soaked oat flakes. However, caution must be exercised when employing food deprivation because it is a significant stressor for the animals, which can have long-lasting effects on behavior (6).
16. There are actually two options for interaction partners in the social interaction test—either a second animal from the same experimental group, as described above, or a separate stimulus animal. The disadvantage of using an animal from the same group is that the N of each group is cut in half and statistical power is reduced. This can, of course, be overcome by increasing the number of animals in the experiment; however, due to limitations with certain treatments or animal strains, this is not always possible. The disadvantage of using a separate stimulus

animal is that its behavior can confound the results. For example, if its behavior changes over time as a result of being repeatedly exposed to different test animals.

17. The results of the social interaction test alone are not necessarily enough to draw conclusions on the anxiety state of animals. This is due to the fact that reduced social investigation is also a hallmark of other psychiatric disorders, such as schizophrenia and autism, and may not be a pure measure of anxiety (7). Especially when characterizing different strains of animals (from breeding or genetic modification), it would be advisable to use other behavioral measures of anxiety along with the social interaction test.

5. Concluding Remarks

Although all of the behavioral tests outlined here can be used to evaluate innate anxiety, some would be recommended above others. For instance, the social interaction test is confounded by the fact that reduced social investigation can be a symptom of schizophrenia- or autism-related behavior rather than just anxiety. Additionally, the NIH test can be confounded by changes in the appetitive value of the food reward independently of changes in anxiety. Therefore, these tests should not be employed without validation with other, more "pure" tests for assessing anxiety.

For mice, the light–dark box would be the first choice for evaluating innate anxiety; it has relatively few practical problems and confounding factors and has been well tested and consistently validated in mice. The EPM comes in second place as a test for innate anxiety in mice. Although it is a relatively pure measure of anxiety and a well validated test the EPM can have highly variable results. This is due to animals that fail to enter the open arms at all or, conversely, get "stuck" on the open arms if they freeze up in extreme fear or even hang on the edges or fall off altogether. The NIH test is a good choice for mice when looking at stress-induced changes in anxiety because it combines stress-induced anhedonia as well as novelty fear. In these circumstances, the differences between groups are amplified making the test more sensitive than normal. However, one must remain aware of the effects of stress and the fact that this is no longer a pure measure of anxiety. To date, the use of the open field as a test for innate anxiety in mice may be questioned, as it lacks significant pharmacological validation. This may be because the test is confounded by the high overall locomotor activity of mice.

In rats the EPM would be a first choice for measuring innate anxiety; it is not prone to the same variability as with the mouse EPM and is a well-validated behavioral test in rats. The open field tends to also be a reliable measure of anxiety in rats, which are relatively calm in nature compared to mice.

When using the open field to control for locomotor activity behavior should be analyzed using either a video tracking program or infrared beams. Video tracking has the advantage of allowing for reanalysis of the recording in case of mistakes or in order to assess additional behaviors, such as rearing or immobility. Infrared beams have the advantage of being able to be used in complete darkness; however, this will not allow for any video recording, and therefore no re-analysis. Rearing and immobility can be difficult to define and score by an observer, but are often automatically assessed using infrared beam tracking. When establishing video or infrared tracking protocols they should always first be validated with observational data.

Light is one of the parameters used to induce fear and anxiety in rodents and must therefore be carefully considered in all behavioral tests. Additionally, lighting in the housing room(s) must be taken into account in conjunction with behavioral testing. If strong overhead lights are used in the housing room, animals situated at the top of a rack may encounter much brighter conditions than those housed lower down. Upon testing these animals may show less avoidance of brightly lit areas, which would confound or complicate the results. Therefore, lighting conditions in the housing areas should be kept as uniform as possible or all animals to be used in an experiment should be kept in areas of fairly uniform lighting conditions. For example, animals may not be kept on the top level of housing racks, but rather just empty cages with bedding.

Lighting is the simplest way to increase or decrease the aversiveness of testing situations and can be used to easily adjust the baseline anxiety profile of any behavioral test. Illumination levels have been suggested for many of the tests; however, no standard procedure can be given as lighting must be adjusted to reach an intermediate baseline behavioral readout of 15–20% for open arm/light compartment/center time. It is noteworthy that too high light intensities may render the entire setup aversive (i.e., no areas of relative safety) as well as the fact that there is an interaction between the state of the animal (e.g., modified by prior stress exposure) and light condition (8).

Although a regular procedure, cage changing is a significant stressor to both rats and mice. Therefore, it should be avoided for 1– 2 days before testing. For tests that use novel cages, such as NIH and social interaction, the home cages should not be changed for at least 4 days prior to testing. This is to ensure that there is a significant difference in odor between the home cage environment and the novel cage environment.

Interpretation of the results of the behavioral tests described must always be made with caution. Since they rely on both anxiety- as well as exploratory-based behaviors, these tests generally fail to distinguish between decreased anxiety and increased novelty seeking or between increased anxiety and decreased curiosity. To help resolve

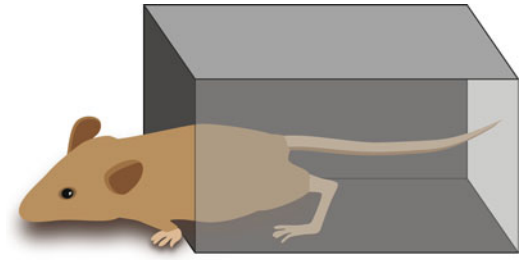

Fig. 6. The stretch-attend posture is a typical risk assessment behavior seen in rodents. It occurs when an animal, in a more protected area of an apparatus, stretches its body towards a less protected area while remaining close to the floor and sniffing the air or ground in front of it. Such behaviors can give insight into the animals' exploratory drive and can be sensitive measures for evaluating changes in anxiety.

such issues, many behavioral tests of innate fear and anxiety can include an analysis of risk-assessment behaviors, such as a stretched attend posture (Fig. 6), scanning, or sniffing. The stretch attend posture is when an animal, in a more protected area of an apparatus, stretches its body towards a less protected area while remaining close to the floor and sniffing the air or ground in front of it. Risk-assessment behaviors give an indication of the animal's motivation to explore and can be more sensitive measures for detecting changes in anxiety in relation to exploratory motivation.

Although video tracking systems can give very precise analysis of time, location, and distance, a lot of potentially valuable data cannot be detected with such programs. For example, vertical motions such as rearing or jumping are difficult, if not impossible, to define in most video tracking programs. Immobility and freezing, which can be important indices of anxiety, are also often not differentiated from stationary grooming. Most importantly, risk assessment behaviors can often not be analyzed using tracking systems and in some tests, such as the EPM, it has been found that the risk assessment behaviors and not open arm time or entries correlate with corticosterone levels (9). Therefore, whenever possible offline video analysis should be done by an experimenter to score ethological behaviors in addition to automatic tracking analysis.

All behavioral tests should include some measure of activity, such as with the open field under nonaversive light conditions (0–20 lux), and it is important to compare activity levels across groups in addition to measures of anxiety. For example, many pharmacological compounds can cause hyperactivity or lethargy. In these cases latency scores between groups cannot be compared, as they depend just as much on activity level as on anxiety level. In general, there should be similar changes in entry counts and time for any given area and divergent changes (i.e., one measure increases while the other decreases) indicate changes in activity.

Despite the widespread use of the behavioral tests outlined in this chapter, each one must be pharmacologically validated when newly established in a research group. This is done in order to

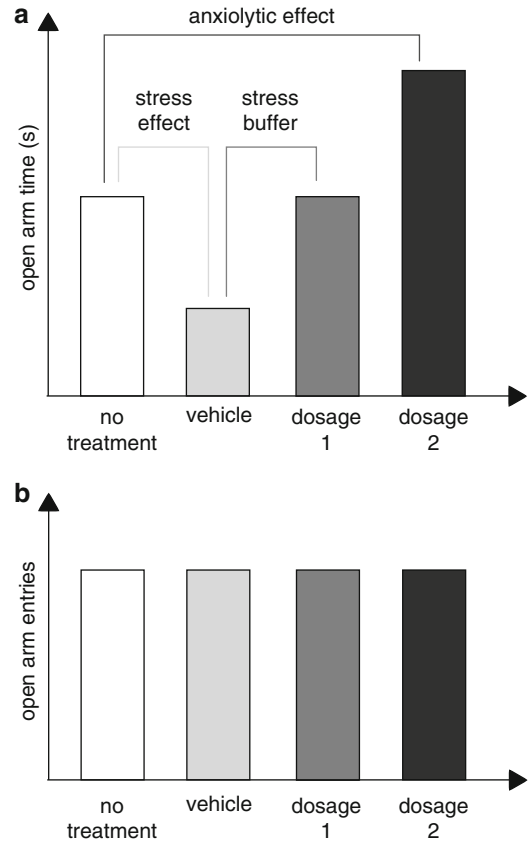

Fig. 7. All behavioral tests must be pharmacologically validated when they are established to ensure the setup is suited for invoking anxiety and evaluating changes in anxiety-like behavior. This validation is done with IP injections of anxiolytic compounds such as benzodiazepines (e.g., diazepam, 0.5–2 mg/kg). Ideally, more than one dosage is tested and compared against a vehicle treated and a nontreated control group. (**a**) As shown exemplarily for a prototype plus-maze experiment, injection stress can lead to increased anxiety-related behavior and lower doses of the anxiolytic compound may only buffer the effect of the stress bringing behavioral measures back to untreated levels. In order to properly evaluate the setup, the treatment must be able to decrease anxiety-related behaviors (which may be seen as an increase or decrease in a specific measure, depending on the test and behavior being evaluated) beyond that of the nontreated control group. (**b**) At the same time, one must control for effects on locomotor activity, since an unspecific increase in arousal/exploratory behavior might be mistaken for a specific anxiolytic effect.

ensure that the test has been setup in a way that enables analysis of anxiety. This validation is done with an anxiolytic compound, such as diazepam (at a dosage of 0.5–2 mg/kg IP). Several dosages may need to be tested and should all be compared against a vehicle treated and a nontreated control group. Often injection stress can lead to increased anxiety-related behavior, which is then only buffered by diazepam treatment. In order to properly evaluate the anxiety dependence of the setup, diazepam treatment must be able to decrease anxiety-related behaviors beyond that of the nontreated control group (see Fig. 7). Additionally, when testing

novel potentially anxiolytic drugs a positive control (i.e., diazepam treatment) group should always be included.

When first characterizing the anxiety profile of a group of animals it is common to do a battery of several different anxiety tests. Utilizing more than one test reduces the impact of confounding variables from any one test and increases the likelihood of finding a significant effect. On one hand, there may be interactions between the various tests, whereby a prior test affects anxiety behavior per se (e.g., due to repeated handling of the animals), which is then recorded in subsequent tests. On the other hand, this method is an efficient use of animals where genetic manipulations or treatment may be time consuming or costly. Regardless, it must be taken into consideration that the overall chance of a Type I error increases as an increasing number of measurements are utilized. Therefore, it is highly recommended that the key significant findings from a test battery be repeated with an independent sample of animals. This will also control for any anxiety-related effects of the test battery itself.

One of the major disadvantages of most behavioral tests is that they cannot be used for repeated testing within animals. The reason for this can often be explained by a decreased motivation to explore. Although rodents are very curious about new places, they do not want to unnecessarily expose themselves to anxiogenic environments. Therefore, once animals have been exposed to unprotected or bright environments they will have a reduced need to explore it upon being re-exposed to the test setup. This phenomenon is also known as *one trial sensitization*, where avoidance of aversive components of a test is induced upon repeated testing, and is characterized by a loss of anxiolytic response to benzodiazepine treatment (10). This is especially true for the EPM and light–dark box. However, it can also apply to novel objects and social interaction, where curiosity may also become satiated leading to a decrease in exploration.

References

1. Hall C (1934) Emotional behavior in the rat 1. Defecation and urination as measures of individual differences in emotionality. J Comp Psychol 18:385–403
2. Griebel G et al (2000) Differences in anxiety-related behaviours and in sensitivity to diazepam in inbred and outbred strains of mice. Psychopharmacology 148:164–170
3. Chaouloff F, Durand M, Mormède P (1997) Anxiety- and activity-related effects of diazepam and chlordiazepoxide in the rat light/dark and dark/light tests. Behav Brain Res 85:27–35
4. Hogg S (1996) A review of the validity and variability of the elevated plus-maze as an animal model of anxiety. Pharmacol Biochem Behav 54:21–30
5. Dulawa S, Hen R (2005) Recent advances in animal models of chronic antidepressant effects: the novelty-induced hypophagia test. Neurosci Biobehav Rev 29:771–783
6. Cabib S et al (2000) Abolition and reversal of strain differences in behavioral responses to drugs of abuse after a brief experience. Science 289:463–465
7. Chadman KK, Yang M, Crawley JN (2009) Criteria for validating mouse models of psychiatric diseases. Am J Med Genet Part B 150B: 1–11

8. Strekalova T et al (2005) Stress-induced hyperlocomotion as a confounding factor in anxiety and depression models in mice. Behav Phamacol 16:171–180
9. Rodgers RJ et al (1999) Corticosterone response to the plus-maze: high correlation with risk assessment in rats and mice. Physiol Behav 68:47–53
10. Carobrez AP, Bertoglio LJ (2005) Ethological and temporal analysis of anxiety-like behavior: the elevated plus-maze model 20 years on. Neurosci Biobehav Rev 29:1193–1205

Chapter 11

Rodent Models of Conditioned Fear: Behavioral Measures of Fear and Memory

Jennifer L. McGuire, Jennifer L. Coyner, and Luke R. Johnson

Abstract

Pavlovian fear conditioning is a robust technique for examining behavioral and cellular components of fear learning and memory. In fear conditioning, the subject learns to associate a previously neutral stimulus with an inherently noxious co-stimulus. The learned association is reflected in the subjects' behavior upon subsequent re-exposure to the previously neutral stimulus or the training environment. Using fear conditioning, investigators can obtain a large amount of data that describe multiple aspects of learning and memory. In a single test, researchers can evaluate functional integrity in fear circuitry, which is both well characterized and highly conserved across species. Additionally, the availability of sensitive and reliable automated scoring software makes fear conditioning amenable to high-throughput experimentation in the rodent model; thus, this model of learning and memory is particularly useful for pharmacological and toxicological screening. Due to the conserved nature of fear circuitry across species, data from Pavlovian fear conditioning are highly translatable to human models. We describe equipment and techniques needed to perform and analyze conditioned fear data. We provide two examples of fear conditioning experiments, one in rats and one in mice, and the types of data that can be collected in a single experiment.

Key words: Amygdala, Associative learning, Memory, Stress, Fear, Pavlov, Autoscoring, Freezing, Conditioned stimulus, Unconditioned stimulus, Conditioned response

1. Introduction

Classical fear conditioning, also known as Pavlovian fear conditioning, is a robust procedure for evaluating associative learning and memory. As such it is a key behavioral model for testing pharmacologic agents regulating learning and memory. During fear conditioning, the subject learns to associate a previously non-threatening stimulus (designated the conditioned stimulus or CS), with an innately noxious stimulus (designated the unconditioned

Arpad Szallasi and Tamás Bíró (eds.), *TRP Channels in Drug Discovery: Volume II*, Methods in Pharmacology and Toxicology,
DOI 10.1007/978-1-62703-095-3_11,

stimulus or US). If this association is successfully learned and remembered, the previously neutral CS will by itself elicit a fear response (designated the conditioned response or CR) appropriate to the original noxious US. Normally, the CS–US association is readily acquired and the memory and subsequent CR can persist for years without further reinforcement. Disruption of learning and memory by pharmacological agents can occur at the acquisition, consolidation, reconsolidation, and extinction phases of classical fear conditioning.

Associative learning is a critical survival tool and as such the underlying mechanism for classical fear conditioning is highly conserved across species. Animals as diverse as fruit flies and humans can be conditioned using similar procedures (1). In experimental classical fear conditioning, the CS can be almost any discrete non-threatening cue such as a tone, light, or scent; the US is noxious or mildly painful. Generally, in vertebrates, the US can be as simple as a puff of air into the face or a brief electric shock. Auditory conditioning, where the CS–US is a tone–shock pairing is most frequently used in rodents (mice and rats) and is described in this chapter.

The neural circuitry underlying auditory fear conditioning is the most studied and best understood of the fear conditioning paradigms. In auditory fear conditioning, a commonly used CS is a neutral non-noxious sound using a single frequency tone (1–3). Auditory signals reach the lateral amygdala via two routes: a direct thalamoamygdala route and indirectly via the auditory cortex (2). Evidence indicates that synaptic plasticity at these synapses underlies the formation of an auditory conditioned fear memory (2, 4, 5). Behavioral expression of conditioned fear memory requires an intact central nucleus of the amygdala (6–9). Learned associations of the CS with the training context require synaptic input from the hippocampus (1, 3). Thus, intact hippocampal function is essential for contextual components of fear conditioning (10–12). Synaptic input from the prefrontal cortex is required both for the extinction of conditioned fear memories (13–15) and for the behavioral expression of conditioned fear (15–17). Behavioral changes in the components of fear conditioning can therefore be indicative of function in the areas of the brain from which they originate.

Following classical fear conditioning, physiological and behavioral indicators of fear are expressed upon presentation of the CS. Physiologic changes include activation of the hypothalamic pituitary adrenal (HPA) axis and the autonomic nervous system (ANS) (18–20). A key behavioral response to the CS is freezing behavior. Freezing is an innate defensive behavior leading to the cessation of all movement except as required for breathing (21, 22). This is a well-validated indicator of fear in rodents (23, 24). Freezing behavior is an ideal behavior to measure because it is quantifiable, easy to obtain through direct observation,

and measurement can be automated. Below we describe common rodent subjects, apparatus, and methods to perform and analyze fear conditioning experiments.

2. Materials

2.1. Rodents as Subjects

1. All strains of rats and mice can be used for classical fear conditioning. An important consideration for fear conditioning and behavioral testing in general, is the age of the rodent at the time of experimentation. Most experiments and pharmacological manipulations are carried out in adult animals. Fear conditioning can be performed on animals of any age and learning can occur. However, in very young and adolescent animals the learning and memory phenotype is quite different from adult animals (21, 25). For general phenotyping of learning and memory deficits or enhancement, adult animals (generally between 8 and 16 weeks of age) are used.
2. Rodent subjects should be housed under uniform conditions with respect to lighting, temperature, and potential stressors, such as cage changes, housing room traffic, or other disturbances (26).
3. Animals ordered into the facility from a laboratory animal supplier should be allowed to habituate to their new housing conditions for a week or more.
4. Unless circumstances dictate single housing (such as postsurgical animals or highly aggressive animals) rodents should not be singly housed as this may have adverse effects on behavioral results (27, 28). Rats are generally housed two or three per cage while mice may be housed up to five per cage. With aggressive strains of mice, such as C57BL/6 housing male animals fewer than five to a cage may be optimal.
5. Enrichment items such as pressed cotton nesting material or rodent chew toys may also be provided and should meet institutional guidelines. It should be pointed out however, that enrichment facilitates coping and resilience to stress (29, 30) and may be problematic in studies attempting to evaluate consequences of stress on behavior and brain function or in studies along similar lines.
6. All experiments conducted on animals must be reviewed and approved by an Institutional Animal Care and Use Committee.
7. The numbers of animals required per experimental group should be determined by power analysis. Generally 7–10 rats per condition and 10–15 mice per condition provide sufficient

statistical power. The example experiments described here were conducted on adult male (8–10 weeks old) Sprague–Dawley rats and adult (8–12 weeks old) C57Bl/6xDBA/2J hybrid male and female mice.

2.2. Equipment Needed for Laboratory-Based Pavlovian Fear Conditioning

The primary and essential components for fear conditioning are:

1. A conditioning chamber with an electrical conduction rod floor.
2. An electrical shock generator.
3. A tone generator.
4. Cameras and recording equipment.
5. A sound attenuation box to isolate sounds, especially an auditory CS, within the conditioning chamber.
6. Additional components include alternate flooring and wall panels to change the appearance of the testing environment (Fig. 1) and software for automated scoring of freezing behavior if desired. Fear conditioning chambers are available from many companies who manufacture behavioral testing apparatus. In the example experiments, fear conditioning apparatus for rats were manufactured by Coulbourn Instruments (Whitehall, PA).

2.3. Equipment Needed for Measurement of Freezing Behavior

1. Pavlovian fear conditioning allows the investigator to obtain quantitative measures of conditioned fear memory. A well-characterized response to conditioned fear in rodents is "freezing." Freezing is an innate defensive behavior leading to the cessation of all movement, excluding respiration. Freezing behavior is an ideal behavior to measure because it is quantifiable, easy to obtain, and measurement can be automated.
2. Measures of freezing are obtained for each subject by visual observation and/or automated scoring of freezing. Scoring of freezing by a human observer should be consistent and reproducible. Variability between human scorers can occur, thus ideally only one person should score each data set. If this is not possible, or the data set is large, internal controls for consistency should be used.
3. For high-throughput analysis, freezing behavior can be scored using automated scoring programs. Commercially available automatic freeze scoring software include FreezeFrame® available through Coulbourn Instruments (Whitehall, PA) and AnyMaze® software available through Stoelting (Wood Dale, IL). Mousemove (described in (31)) is a free program for scoring freezing behavior available for download from the Malinow group at Cold Spring Harbor Laboratories (http://malinowlab.cshl.edu/downloads/). Computerized systems combine

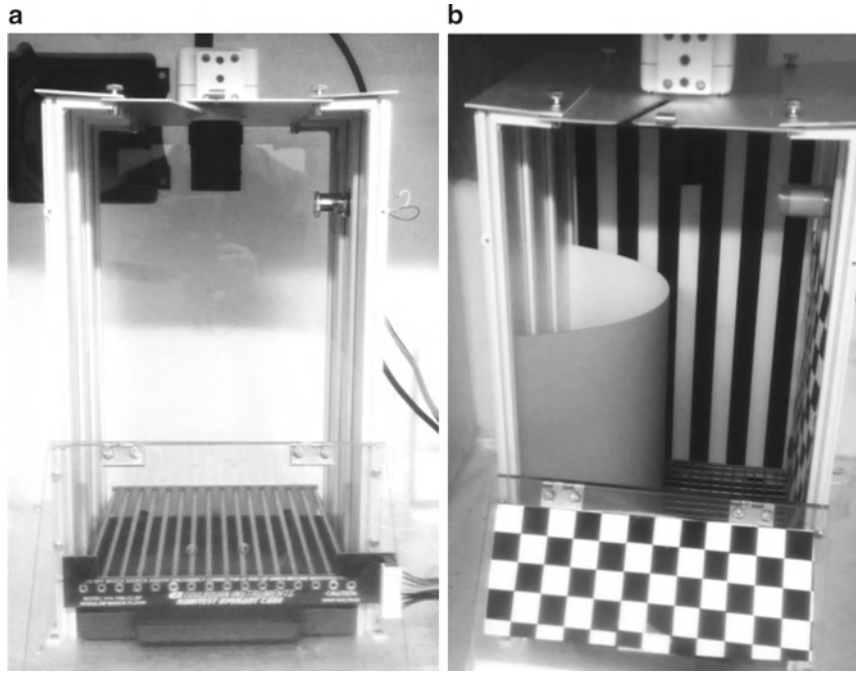

Fig. 1. Examples of training and testing environments in classical fear conditioning. *Panel A* depicts the fear conditioning chamber used for habituation, training, and context testing. The chamber is enclosed by a sound-attenuating outer box (not visible in this figure) aimed at reducing extraneous noise. The chamber is equipped with a camera, speaker (attached to the sound generator), and a small house light. *Panel B* depicts the chamber used for cue testing. Investigators must ensure that this chamber looks, feels, and smells differently from the original chamber so as to isolate the fear response exclusively to the CS. The chamber dimensions and appearance of the walls have been altered, and the flooring is a mesh grid rather than the conducting rods. Light conditions have been changed (a yellow film has been placed over the fixture) and the cleaning solution used between animals is changed from 70% alcohol (used in the learning and context association phases) to either 1% acetic acid or a commercially available disinfectant.

the sensitivity and objectivity desired for unbiased data. FreezeFrame®, and most automated scoring software for freezing, is not a tracking system, but rather, a motion detection system that is capable of detecting movements as small as 1 mm. This is accomplished by calculating motion in a given digital image detected over a period of time and given a score based on pixels. Then, two successive images are subtracted and if the pixel score equals zero (0), no motion occurred. In contrast, if a nonzero score is calculated between two successive images, it is due to motion. The animal is monitored several times each second and so the ability to reliably detect fine movements of the head and limbs is possible and consistent between animals. Additionally, FreezeFrame® is capable of scoring freezing in low-light levels and will filter shadows or artifact from electronic equipment.

4. Measures of freezing calculated by any automated system should be compared to values determined by the human

investigator in pilot trials. Whatever method of scoring is chosen, it is critical that the investigator ensures consistency across groups of subjects. It is highly advisable to video record each aspect of the experiment so that the investigator has the ability to verify freezing scores and analyze multiple aspects of behavior (Note 1).

5. In the experiments described below, using rats as subjects, freezing behavior was manually scored from recorded video, by an observer blind to the training conditions. Data from experiments using mouse subjects were scored using Freezeframe automated scoring software available from Coulbourn Instruments (Whitehall, PA). Freezeframe allows the user to define freezing. This is done by setting the threshold of maximum movement (number of pixels changing) and the minimum duration for which the number of pixels changing must remain below threshold, a temporal parameter termed "bout." The freezing threshold was determined by a trained researcher from digital playback of recorded training sessions in the Freezeframe program and the minimum bout duration was set at 0.25 s.

3. Methods

A "classical" fear conditioning protocol involves four components: *habituation, training, context memory test, and cue* (*CS*) *memory test* (see Fig. 1 and data in Figs. 2 and 3). An additional component of extinction of the conditioned response can be included as well (Note 2). Extinction is a new learning process in which upon repeated presentation of the CS in the absence of the US the subject learns that the CS no longer predicts the US. Subsequent to this new learning, the CS no longer generates the conditioned response. For each phase of fear conditioning, pertinent data should be collected. Baseline measurements of movement and anxiety can be obtained prior to training, either over a number of days during habituation or on the training day prior to the first CS–US presentation (Note 3). Some automated scoring programs include a tracking component, which will measure actual distance traveled during the test or segments of the test, but determining baseline freezing is sufficient to indicate potential confounding differences in pretraining activity. This is particularly important under circumstances where experimental manipulations may be sedating, cause hyperactivity, impair locomotor function and balance (which may make movement on the grid floor more difficult), and for obtaining a complete phenotype of genetically modified animals.

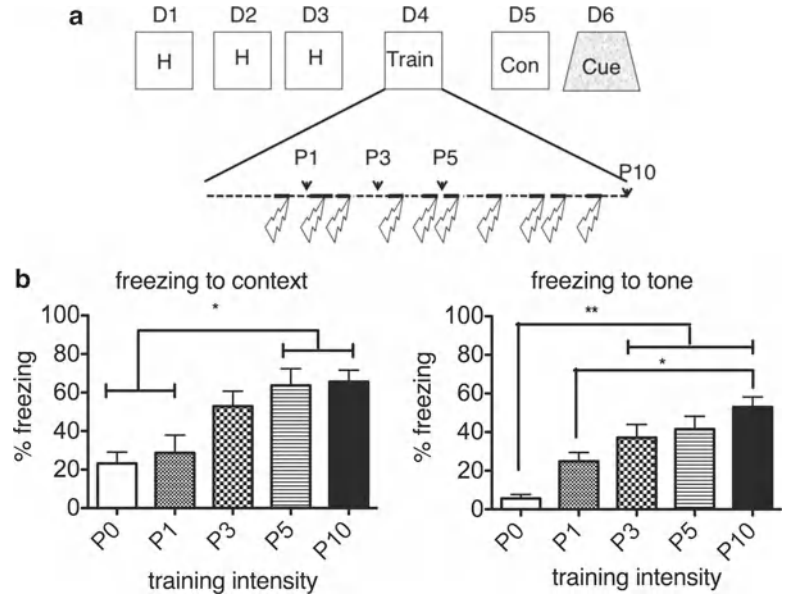

Fig. 2. Classical fear conditioning example data from rats. Data from memory test to both cued stimulus (tone) and to the contextual environment. Data shows effect of increased number of CS + US pairings during training on the subsequent memory test. (**a**) Schematic of experimental design—male Sprague–Dawley rats were habituated to the training context for 20 min for 3 days prior to fear conditioning. On the training day, individual cohorts received 0, 1, 3, 5, or 10, 30 s 5 kHz pure tone auditory cues co-terminating with a 0.6 mA. 5 s foot shock. 24 h after training, animals were tested for fearful contextual association and 24 h after the context test the same animals were tested for fear to the training cue in a novel context. (**b**) Increasing the number of CS–US pairings from 0 (control animals receiving no tones or shocks) to 10 increased the strength of memory consolidation creating a stepwise increase in the amount of both context-driven and cue-driven fear behavior. Animals receiving 5 and 10 CS–US pairings froze significantly more to the training context 24 h later than animals receiving 0 or 1 CS–US pair. P10 animals that received 10 CS–US pairings froze more to the auditory cue than either P0 or P1 animals while P3 and P5 froze significantly more than the P0 controls. Data expressed as mean +/− SEM, * and ** indicate $p < 0.05$.

3.1. Habituation

1. Move animals out of the housing room to a holding room near to the rooms housing the fear conditioning chambers. Allow the animals a minimum of 20–30 min to calm down after transport. Habituating animals to the conditioning chambers as well as to human handling, transport, and other aspects of the experimental procedures is important for minimizing unconditioned freezing (Note 4). In the example experiments, rats were handled daily for a total of 5 days in an effort to reduce the stress of human contact.
2. Put the animals into the training/testing chamber and allow the animal to explore the environment. To reduce baseline freezing (32), rats were habituated to the conditioning chamber each day for 20 min for three consecutive days (Fig. 2a).

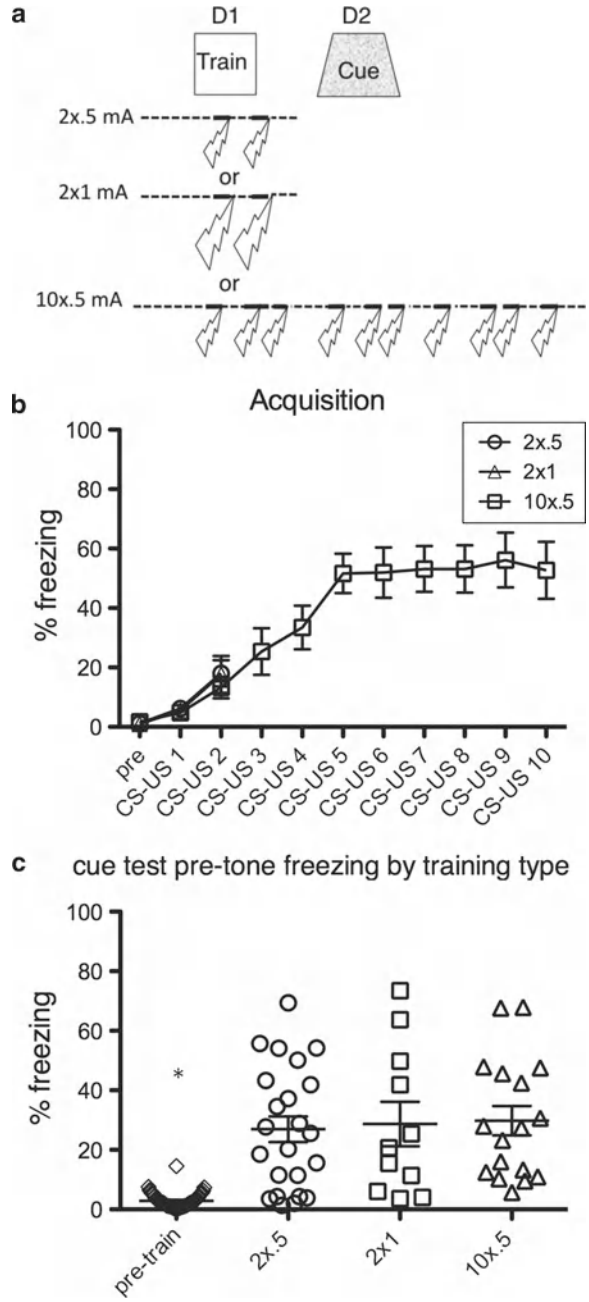

Fig. 3. Classical fear conditioning example data from mice. Data from memory acquisition and test to cued stimulus (tone). Data shows effect of increased number of CS + US pairings and increase in US intensity (amperage) during training on the subsequent memory test. (**a**) Schematic of experimental design. After a 3-min habituation period, C57BL/6 x DBA/2J mice underwent fear conditioning in one of three training conditions as indicated. For all three training protocols, the conditioned stimulus was a 30 s 5 kHz pure tone that co-terminated with either a 0.5 mA or 1.0 mA 2 s foot shock. (**b**) All three training groups showed equivalent freezing to tone. Notice that freezing increases significantly to the second tone as no learning occurs prior to the completion of the first CS–US pair. Notice also that the group receiving ten CS–US presentations reaches a ceiling for freezing behavior around CS–US 5. (**c**) The 3-min habituation period in both the training and cue tests is informative as to baseline anxiety state in the animals. Prior to any training mice showed very little freezing. 24 h later in a novel environment, all three training groups showed significantly higher baseline freezing than their pretraining baselines, although none of the groups differed from each other. Data is expressed as mean +/– SEM, * = $p < 0.05$.

3. Return the animals to housing room.
4. Rats readily adjust to being handled whereas mice do not. Therefore, mice were not handled prior to the habituation-training day (Fig. 3a). With repeated handling, mice may begin to show signs of chronic stress (33).
5. Habituation of mice consisted of 3 min in the chamber on the training day before the onset of the first tone.

3.2. Training

1. All the training and testing protocol should be programmed in advance. It is generally a good idea to run a pilot experiment to determine a protocol which gives an appropriate level of freezing in the memory tests for the control condition. When there is no a priori hypothesis as to whether the experimental treatment will facilitate or impair memory formation, freezing in the control condition should fall into a median range of 50–60%. If the treatment is expected to facilitate memory formation, a less rigorous training protocol will allow more sensitive detection of increases in freezing behavior. In the reverse condition when treatment impairs fear memory, a more rigorous training protocol may be desirable.
2. Move the animals out of the housing room to the holding room.
3. While the animals are recovering from transport, check the chambers. Make sure the volume of the conditioned stimulus is set as desired, check the voltage of the grid floor, and make sure the cameras are working. Make sure there are available supplies for cleaning the chambers between animals.
4. In delay conditioning, the conditioned stimulus is contingent in time with the unconditioned stimulus. In the example experiments, a 30 s 5 kHz, 75 dB pure tone conditioned stimulus co-terminates with a brief foot-shock delivered through the conducting rod floor. Schematics of the timeline for each experiment are provided in Figs. 2 and 3 (Note 5).
5. In both experiments, subjects were allowed 3 min in the chamber prior to the first CS–US presentation (Figs. 2a and 3a).
6. In experiments with three or more CS–US presentations, the interval between CS–US presentations was variable to prevent the subject from anticipating CS onset. In the experiments described in Fig. 2, the interval varied between 90 and 180 s with a mean of 120 s. In the 10×0.5 mA condition described in Fig. 3, the inter-trial interval varied between 15 and 50 s with a mean of 30 s.
7. Within an experiment, each subject received the same pattern of CS–US presentations. In the rat experiments (Figs. 2 and 4) the US was delivered for 0.5 s at 0.6 mA current. In the mouse

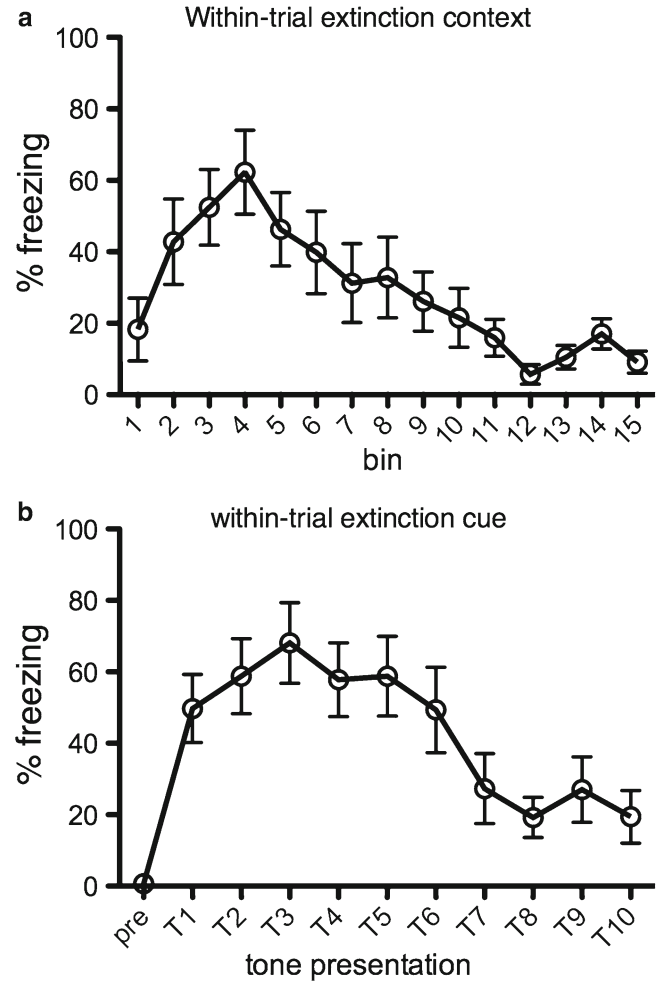

Fig. 4. Examples of within-trial extinction of context and cued fear. (**a**) Context extinction: 24 h after fear conditioning male Sprague–Dawley rats were returned to the training chamber for 15 min. 20 s of each minute was scored for freezing behavior. Percent of time freezing in each 20 s bin was graphed across the 15 min. (**b**) Cue extinction: 24 h after context testing, the same animals introduced to a second, novel chamber. After a 3-min habituation period, the same 30 s 5 kHz tone used in the training procedure was presented in the new chamber. The tone was presented ten times over 15 min with a variable inter-tone interval. Pretone freezing and percent freezing to each cue was plotted over the course of the test.

experiments (Fig. 3) the US was delivered for 2 s at either 0.5 mA or 1.0 mA current as described.

8. Place the animal into the chamber and run the training protocol.
9. Return the animal to the holding room and thoroughly clean the chamber (Note 4).
10. Training can be compared between experimental and control conditions for rate of acquisition and maximal freezing

(Fig. 3b). When using mild shock as the unconditioned stimulus, differences in pain threshold, which will affect the rate of acquisition, extent of freezing, and subsequent memory test should be accounted for. Again this is particularly important when experimental manipulations may have analgesic (or hyperalgesic) effects and in transgenic animals.

11. The strength of learning and the resultant memory can be easily manipulated by varying the training intensity either through the number of CS–US presentations or the intensity of the US (Fig. 2b).

3.3. Context Memory

1. Testing context memory involves simply returning the subject to the training environment and measuring fear behavior. In this test, rats were returned to the training chamber for 15 min 1 day after fear conditioning training (Fig. 2). Freezing can be scored over the duration of the test or in smaller bins of time across the test. In this example, freezing was scored for the first 20 s of each minute (Fig. 2b).
2. In longer tests, particularly those that are being manually scored, scoring shorter bins of time may be more time efficient. In our experience, scoring 20 s of each minute is representative of freezing across the entire test. Furthermore, by breaking up longer context tests into bins of time, the reduction of fear (context extinction) over time, when no CS or US is presented, can be determined (Fig. 4a).

3.4. Cue Memory

1. Move the animals from the housing area to the holding room.
2. To test learning and memory to the CS component of conditioned fear (tone in the example experiments), testing must be conducted in an environment free (to the greatest practical extent) of contextual reminders of the training (34). The goal is to have a pure measure of the strength of the tone–shock association. Ideally, testing could occur in completely novel chambers; however, this is not usually practical and the training chambers are used for the cue test. In this case, as many features of the testing environment are changed as possible. Changes include the chamber dimensions or geometry, flooring, lighting, cleaning solution, and other olfactory cues, adding patterns to the chamber walls and if possible changing the lighting conditions and visual cues in the testing room itself (Fig. 1).
3. While the animals are recovering, check the testing chambers and make sure the sound generator is set to produce an identical conditioned stimulus to the training stimulus in frequency (KHz) and volume (dB). Alter the contextual cues in the chamber if the training chamber is also the testing chamber.

4. In the mouse experiments, the testing chambers were altered to provide the new environment for the cue test (Fig. 1). The conducting rod floors were replaced with a mesh grid floor and white paper used to line the catch pan underneath. Graphic black and white patterns were applied to the walls of the conditioning chambers. Strips of acetate were slotted into the interior of the chamber to further change the visual appearance. Yellow acetate filters were placed over the house lights to change the lighting effect. A 1% acetic acid solution was used to mask the previous cleaning solution and provide new olfactory cues. Lights in the testing room were dimmed from the training day to change the appearance of the testing room.
5. In the rat experiments, testing for cued fear memory was conducted in a second chamber novel to the rat subjects. Lighting conditions, box geometry, flooring surface (smooth surface with sawdust bedding as opposed to the conducting rod floor), wall color, and olfactory cues differed from the training chamber.
6. Place subjects into the chamber and start the protocol.
7. Subjects were allowed a 3-min exploration period in the novel environment prior to the first CS presentation. Freezing behavior was scored for the initial 3-min exploration period and for each CS presentation.
8. After 3 min, a CS identical 30 s 5 kHz tone used in the fear conditioning training was presented to the animals. Over the course of the test (20 min), the CS was presented ten times with a variable inter-trial interval. The inter-trial interval was between 90 s and 180 s with a 120 s mean but was a different pattern from that used in fear conditioning training.
9. Once the test is completed, return the animal to the holding room and thoroughly clean the chamber.
10. Freezing to the first CS presentation is the purest indicator of the conditioned response to the auditory stimulus, without the influence of preceding stimuli. Frequently however, multiple tones are presented during the course of the test and total cue-associated freezing is reported. Data presented in Fig. 2b is the mean freezing across all tone presentations for each training condition. Additionally, in tests where the CS is presented many times, within-trial extinction to the un-reinforced conditioned stimulus can be evaluated (Fig. 4b.)
11. Comparisons of pretraining freezing with posttraining freezing in a novel environment (Fig. 3c) may indicate fear generalization or stress-induced neophobia. However, in situations where the training environment is masked to produce the alternate context for cue testing, context bleed-through due to inadequate masking of the training environment should be considered.

4. Notes

1. Videos of the testing were digitally recorded for manual scoring. Mouse experiments were conducted in Coulbourn Habitest chambers and scored using Coulbourn's FreezeFrame® software. The mouse chambers are 7 in. wide by 7 in. deep by 12 in. high with ¼ in. conducting rods spaced ½ in. apart. Rat chamber dimensions are 12 in. wide by 10 in. deep by 12 in. high with ¼ in. conducting rods spaced ¾ in. apart. Specific chamber dimensions can vary; however, they must be appropriate for the animal (e.g., grid floor spacing is wider for rats) and allow for the ability to move and explore.
2. Careful and thorough planning and preparation are the key to successful execution of behavioral experiments. Determine in advance the duration of each stage of the fear conditioning experiment and timing for other experimental manipulations such as drug administration. Also, verify availability of the chambers, holding areas, and manpower to complete the experiment well in advance.
3. Within a given experiment, make every effort to test subjects at the same time of the day. While fear conditioning is an exceptionally robust behavioral paradigm, circadian rhythms in hormonal and molecular systems influencing learning and memory may introduce subtle phenotypic changes and variability (35–37). The majority of researchers train and test animals housed on a standard 12:12 light cycle (lights on during the day) with good results.
4. Researchers conducting behavioral experiments must make an effort to control as many variables as possible and no amount of attention to detail is too much. Subtle factors such as odors (e.g., perfumes, fear pheromones, the smell of other animals) or extraneous noise (mechanical equipment, construction, nearby vocalization) in the housing, holding, or testing rooms potentially impact the results. To that end, it is important to thoroughly clean the chambers (particularly the grid flooring) between subjects with an appropriate cleaning solution (e.g., 70% ethanol, 1% acetic acid) and testing rooms should be clean and away from high-traffic locations.
5. The experiments described above are tests of long-term memory (LTM), that is, the animals are tested after the period of time required for new protein synthesis and stabilization of learning and short-term memory (STM) into enduring memory (38). Pavlovian fear conditioning of the rodent has revealed a discrete time course for such changes believed to be 4–6 h for the consolidation of training into long-term memory (39, 40).

The mechanisms of STM and LTM are distinct. Short-term memory involves activation of cAMP second messenger systems and short-term synaptic remodeling independent of new protein synthesis (41). Long-term memory formation is dependent on new protein synthesis in the amygdala (39, 42, 43). It should be noted that experimental treatments frequently have differential effects on short- and long-term memory (39, 41). Pavlovian fear conditioning can be used to test either STM or LTM based upon whether conditioning training and subsequent context and cue testing occur within the 4–6 h consolidation window or beyond it. Caution should be used when testing both short- and long-term memory in the same cohort of animals. Behavior is influenced by previous experience and as a result, tests for STM may influence behaviors on any subsequent behavioral tests such as those for LTM.

6. Having low volume (around 60 dB) background noise in the training/testing chamber may help obscure unavoidable noise outside and is frequently either a ventilation fan in the sound attenuation box or a scrambled frequency white noise produced from the sound generator. The holding room should be in close proximity to the testing room, but situated where the animals cannot hear the auditory cue prior to training or to testing. Preexposure to the CS will adversely affect the learning of the CS–US association through a process called latent inhibition (44).
7. Ideally, stressors such as cage changes should not coincide with a testing day. Likewise, if animals were without water during a prolonged period of time (e.g., overnight due to water bottle leakage) and/or were subjected to wet bedding, the resulting stress to the animal may adversely affect behavioral results.
8. Maintaining a detailed lab notebook with anticipated and unanticipated aspects or occurrences of an experiment will aid the investigator in data analysis and alert the research group to factors that potentially played a role in their results.

References

1. LeDoux JE (2000) Emotion circuits in the brain. Ann Rev Neurosci 23:155–184
2. Johnson LR et al (2008) A recurrent network in the lateral amygdala: a mechanism for coincidence detection. Front Neural Circuits 2:3
3. Maren SQ, Quirk GJ (2004) Neuronal signaling of fear and memory. Neuroscience 5: 844–852
4. Blair H et al (2001) Synaptic plasticity in the lateral amygdala: a cellular hypothesis. Learn Mem 8:229–242
5. Johansen JP et al (2011) Molecular mechanisms of fear learning and memory. Cell 147(3):509–524
6. Choi JS, Brown TH (2003) Central amygdala lesions block ultrasonic vocalization and freezing as conditional but not unconditional responses. J Neurosci 23(25):8713–8721
7. Ciocchi S et al (2010) Encoding of conditioned fear in central amygdala inhibitory circuits. Nature 468(7321):277–282
8. Wilensky AE et al (2006) Rethinking the fear circuit: the central nucleus of the amygdala is

required for the acquisition, consolidation, and expression of Pavlovian fear conditioning. J Neurosci 26(48):12387–12396
9. Pare D, Quirk GJ, Ledoux JE (2004) New vistas on amygdala networks in conditioned fear. J Neurophysiol 92(1):1–9
10. Fanselow MS, LeDoux JE (1999) Why we think plasticity underlying Pavlovian fear conditioning occurs in the basolateral amygdala. Neuron 23(2):229–232
11. Maren S, Aharonov G, Fanselow MS (1997) Neurotoxic lesions of the dorsal hippocampus and Pavlovian fear conditioning in rats. Behav Brain Res 88(2):261–274
12. Phillips RG, LeDoux JE (1992) Differential contribution of amygdala and hippocampus to cued and contextual fear conditioning. Behav Neurosci 106(2):274–285
13. Vidal-Gonzalez I et al (2006) Microstimulation reveals opposing influences of prelimbic and infralimbic cortex on the expression of conditioned fear. Learn Mem 13(6):728–733
14. Milad MR, Quirk GJ (2002) Neurons in medial prefrontal cortex signal memory for fear extinction. Nature 420(6911):70–74
15. Morgan MA, LeDoux JE (1995) Differential contribution of dorsal and ventral medial prefrontal cortex to the acquisition and extinction of conditioned fear in rats. Behav Neurosci 109(4):681–688
16. Sotres-Bayon F, Quirk GJ (2010) Prefrontal control of fear: more than just extinction. Curr Opin Neurobiol 20(2):231–235
17. Corcoran KA, Quirk GJ (2007) Activity in prelimbic cortex is necessary for the expression of learned, but not innate, fears. J Neurosci 27(4):840–844
18. Stiedl O et al (2004) Behavioral and autonomic dynamics during contextual fear conditioning in mice. Auton Neurosci 115(1–2): 15–27
19. Brinks V, de Kloet ER, Oitzl MS (2008) Strain specific fear behaviour and glucocorticoid response to aversive events: modeling PTSD in mice. Prog Brain Res 167:257–261
20. Rodrigues SL (2009) JE; Sapolsky, RM, The influence of stress hormones on fear circuitry. Ann Rev Neurosci 32:289–313
21. Bronstein PM, Hirsch SM (1976) Ontogeny of defensive reactions in Norway rats. J Comp Physiol Psychol 90(7):620–629
22. Clinchy M et al (2010) The neurological ecology of fear: insights neuroscientists and ecologists have to offer one another. Front Behav Neurosci 4:21
23. Blanchard RJ, Blanchard DC (1969) Passive and active reactions to fear-eliciting stimuli. J Comp Physiol Psychol 68(1):6
24. Blanchard RJ, Flannelly KJ, Blanchard DC (1986) Defensive behavior of laboratory and wild Rattus norvegicus. J Comp Physiol Psychol 100(2):6
25. Stanton ME (2000) Multiple memory systems, development and conditioning. Behav Brain Res 110(1–2):25–37
26. Prager EM et al (2011) The importance of reporting housing and husbandry in rat research. Front Behav Neurosci 5:38
27. Sharp JL et al (2002) Stress-like responses to common procedures in male rats housed alone or with other rats. Contemp Top Lab Anim Sci 41(4):8–14
28. Voikar V et al (2005) Long-term individual housing in C57BL/6J and DBA/2 mice: assessment of behavioral consequences. Genes Brain Behav 4(4):240–252
29. Mitra RA, Adamec R, Sapolsky R (2009) Resilience against predator stress and dendritic morphology of amygdala neurons. Behav Brain Res 205:535–543
30. Barbelivien A et al (2006) Environmental enrichment increases responding to contextual cues but decreases overall conditioned fear in the rat. Behav Brain Res 169(2):231–238
31. Kopec CD et al (2007) A robust automated method to analyze rodent motion during fear conditioning. Neuropharmacology 52(1): 228–233
32. Schmitt U, Hiemke C (1998) Strain differences in open-field and elevated plus-maze behavior of rats without and with pretest handling. Pharmacol Biochem Behav 59(4): 807–811
33. Longordo F et al (2011) Do mice habituate to "gentle handling?" A comparison of resting behavior, corticosterone levels and synaptic function in handled and undisturbed C57BL/6J mice. Sleep 34(5):679–681
34. Bolles C, Collier A (1976) Effect of predictive cues on freezing in rats. Anim Learn Behav 4:2
35. Chaudhury D, Colwell CS (2002) Circadian modulation of learning and memory in fear-conditioned mice. Behav Brain Res 133(1): 95–108
36. Eckel-Mahan KL et al (2008) Circadian oscillation of hippocampal MAPK activity and cAmp: implications for memory persistence. Nat Neurosci 11(9):1074–1082
37. Gerstner JR et al (2009) Cycling behavior and memory formation. J Neurosci 29(41): 12824–12830
38. Kandel ER (2001) The molecular biology of memory storage: a dialogue between genes and synapses. Science 294(5544): 1030–1038

39. Schafe GE, LeDoux JE (2000) Memory consolidation of auditory Pavlovian fear conditioning requires Protein synthesis and protein kinase A in the amygdala. J Neurosci 20(18):Rc96
40. Schafe GE et al (2001) Memory consolidation of Pavlovian fear conditioning: a cellular and molecular perspective. Trends Neurosci 24(9):540–546
41. Izquierdo I et al (1999) Separate mechanisms for short- and long-term memory. Behav Brain Res 103(1):1–11
42. Schafe GE et al (1999) Memory consolidation for contextual and auditory fear conditioning is dependent on protein synthesis, PKA, and MAP kinase. Learn Mem 6(2):97–110
43. Barondes SH, Cohen HD (1967) Delayed and sustained effect of acetoxycycloheximide on memory in mice. Proc Natl Acad Sci USA 58(1):157–164
44. Lubow RE, Moore AU (1959) Latent inhibition: the effect of nonreinforced pre-exposure to the conditional stimulus. J Comp Physiol Psychol 52:415–419

Chapter 12

Chick Anxiety–Depression Screening Model

Stephen W. White and Kenneth J. Sufka

Abstract

The chick anxiety–depression model is a hybrid, dual pharmacological screening assay in which both anxiety and depression present sequentially over a 2 h isolation period. This separation stress paradigm utilizes socially raised domestic fowl chicks, aged 4–6 days posthatch, that are isolated from conspecifics during which distress vocalizations (DVocs) are recorded. DVoc rates during the first 5 min are high and represent the anxiety-like phase; DVoc rates decline over the next 20–30 min to about 50% the initial rate and then stabilize for the remainder of the test session. This last 90 min represents the depression-like phase. These two phases are pharmacologically dissociable in that anxiolytics reduce the rate of DVocs during the anxiety-like phase and antidepressants delay the onset of the depression-like phase by attenuating the decline of DVoc rates.

Key words: Chick, Anxiety–depression, Social separation, Domestic fowl, Anxiolytic screen, Antidepressant screen, Separation stress, Hybrid-model

1. Introduction

Rodent-based models remain the mainstay for pharmacological screening of anxiolytics and antidepressants. The open-field test and the elevated plus maze are common models used to screen anxiolytics. Exposure to open spaces acts as an anxiogenic stimulus inducing decreased exploratory behavior that serves as a measure of anxiety. Anxiolytic drugs have been shown to increase the amount of exploratory behavior in these models. The tail suspension and forced-swim tests are common models used to screen antidepressants. Exposure to an inescapable stressor leads to immobility (i.e., behavioral despair). Antidepressants have been shown to delay the onset of immobility in these models. While these models are widely utilized in drug discovery research, they are not without limitations.

Arpad Szallasi and Tamás Bíró (eds.), *TRP Channels in Drug Discovery: Volume II*, Methods in Pharmacology and Toxicology,
DOI 10.1007/978-1-62703-095-3_12,

A major validity issue in efficacy screening models is the degree of their pharmacological sensitivity; in some instances, a model may be vulnerable to false positives where a drug shows efficacy in the animal model yet fails in clinical trials and/or it may be vulnerable to false negatives where a drug screens ineffective in the model yet would have benefited individuals with syndrome (for review see (1)). This lowers the predictive validity of the screening model and leads to two problems. First, models prone to false positives push ineffective drugs into Phase I and II of clinical trials exposing human subjects to possible harmful compounds and costing millions of dollars thus using valuable investment resources. Second, models prone to false negatives keep effective compounds from clinical use and, as such, fail to provide adequate treatment for those who suffer. This latter problem also affects corporate/shareholder profitability.

An additional concern is whether rodent screening models meet the National Institute of Health's (NIH) and United Kingdom's "3R" policy of Replacement, Reduction, and Refinement. Replacement refers to replacement of animal models with non-animal models or models that use less sentient species; Reduction refers to reducing the number of purpose-bred animals for use in research; Refinement refers to developing procedures which minimize the pain and suffering and/or improve overall animal welfare.

As an alternative that addresses many of the concerns detailed above, we have developed an anxiety–depression simulation/screening paradigm using an avian model. This chick paradigm seems to provide a more clinically relevant non-rodent-based model of a neuropsychiatric syndrome and appears useful as a high-utility, dual-drug screen for anxiolytic and antidepressant compounds. Below we provide an overview of the procedure and detail studies demonstrating the chick anxiety–depression model possesses face, construct, and predictive validity (2–4).

The chick anxiety–depression model utilizes socially raised chicks isolated at 4–6 days posthatch. Chicks tested with conspecifics show low rates of vocalization throughout a 2 h test session whereas chicks tested in isolation show high rates of distress vocalizations (DVocs) during the first 5 min (i.e., the anxiety-like phase) which decline over the next 20 min by 40–50% of the initial rate and remain steady throughout the remaining isolation period (i.e., depression-like phase). The reduced DVoc rates during this latter phase mirror the pattern seen in traditional behavioral despair depression models. Evidence for an anxiety-like phase is provided by the ability of the benzodiazepine agonist chlordiazepoxide to lower DVoc rates during the first 5 min of isolation. Evidence that the 30–120 min interval of isolation represents a depression-like phase comes from the ability of the tricyclic antidepressant imipramine to attenuate the decline in DVocs during this period (2).

Further research by this lab has demonstrated that all current FDA approved drugs for the treatment of anxiety, specifically panic disorder, which this portion of the model simulates, and depression have proven efficacious in the paradigm (4, 5). Anxiolytic drugs that have screened positive include meprobamate, pentobarbital, clonidine, chlordiazepoxide, phenelzine, and alprazolam (3, 5, 6). Antidepressant drugs that have screened positive include phenelzine, imipramine, citalopram, and maprotiline (3, 7). Another interesting parallel with clinical findings is that certain classes of antidepressant drugs possess anxiolytic effects and this model has accurately screened them as well. For example, the antidepressants phenelzine, imipramine, and maprotiline, attenuate DVoc rates in the anxiety-like phase (3, 7).

A more recent pharmacological validation study (4) of putative antidepressant compounds acting at novel targets has provided interesting results that also parallel human clinical data. Separate dose response studies were conducted with seven compounds that screened positive for antidepressant effects in rodent depression models and included the androgen precursor prasterone, the *N*-Methyl-d-aspartate receptor antagonists memantine and ketamine, the progesterone receptor antagonist mifepristone, the balanced monoamine triple reuptake inhibitor DOV216,303, the γ-Aminobutyric acid receptor antagonist CGP36742, and the corticotropin receptor 1 antagonist antalarmin. Prasterone, memantine, ketamine, and DOV216,303 attenuated and CPG36742 enhanced the pattern of vocalizations in the anxiety-like phase. Prasterone, ketamine, mifepristone, DOV216,303, and CPG36742 attenuated behavioral despair, whereas memantine and antalarmin did not. This pattern of drug effects parallels what clinical data exists and highlights two important characteristics of this dual screening assay. First, the model better predicts Phase II and III clinical failures (e.g., antalarmin and memantine). Second, the model has the potential to reveal contraindications of compounds where anxiety and depression are comorbid. For example, the chick anxiety–depression model demonstrated CPG36742 attenuated the depression-like phase but exacerbated the anxiety-like phase. Given that a significant number of individuals are comorbid (8, 9) with anxiety and depression, this GABA-B antagonist would unlikely pass clinical trials (4).

When compared to the rodent models, the chick anxiety–depression model more closely meets the NIH and UK's "3R" policy of Reduction, Refinement, and Replacement. The model reduces the number of purpose-bred research animals as male chicks are a by-product of the commercial egg-laying industry and are typically discarded at hatch. Their use in drug screening adds no purpose bred research animals and decreases use of rodents. The model also possesses a refined methodology as it minimizes the stress-provoking stimuli to a single test session in which two

clinical syndromes are presented. Typical rodent models either simulate anxiety or depression, thus subjecting more animals to stressors. Finally, the chick model replaces the standard rodent-based models of anxiety and depression with a phylogenetically lower and, perhaps, less sentient species.

One final issue in drug screening models is the matter of utility. Utility refers to how simple and cost effective a paradigm is to employ. While rodent models are simple to use, requiring little in special equipment and measure spontaneous behaviors, they are expensive in purchase costs and per diem provisions. Typically, the purchase price of an individual mouse costs in the \$5.00–\$6.00 range and an individual rat costs in the \$20.00–\$25.00 range. Comparatively, our vendor charges \$0.60 per chick. On an animal cost basis alone, a chick model runs about 10% of a mouse model and 2.5% of a rat model. In addition to the lower purchase price of animals, the per diem costs are less for the chick model than for the rodent models. Rodent per diem cages charges are over \$1 per day in which rats are typically housed 1/cage and mice 3–5/cage. Rodents are typically quarantined for 3–7 days prior to being used in any screening trial. Our chick model is conducted within a week from hatch and has a total vivarium charge of under \$40. As a comparison the chick per diem costs run about 3% of a rodent model.

2. Materials

2.1. Animals

Cockerels are received into the laboratory at 1–2 days posthatch and housed in $34 \times 57 \times 40$ cm cages with 9–15 chicks per cage ($n = 12$ is typical). Food and water are available ad libitium via gravity feeders (Fig. 1). Daily maintenance that entails the replacement of tray liners and filling food and water gravity feeders is conducted during the hour that precedes the animal's dark cycle. Lights are operated on a 12:12 light dark cycle. Supplemental heating sources are provided to maintain appropriate housing temperatures in the range of 32 ± 1°C.

2.2. Testing Equipment

1. A six unit testing apparatus containing Plexiglas chambers ($25 \times 25 \times 22$ cm) surrounded by sound-attenuating media is used to record separation-induced vocalizations aimed at modeling anxiety-like (0–5 min of social separation) and depression-like (30–120 min of social separation) patterns of responses (Figs. 1 and 2). Each unit is lined with acoustical fiber media, illuminated by a 25-W light bulb, and ventilated by an 8-cm-diameter rotary fan (Model FP-108AX S1, Commonwealth Industrial Corp., Taipei, Taiwan).

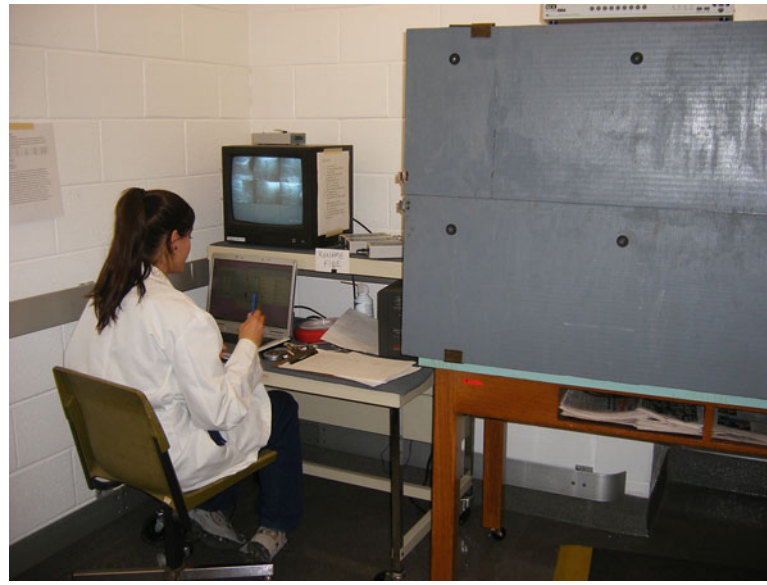

Fig. 1. Animal housing unit.

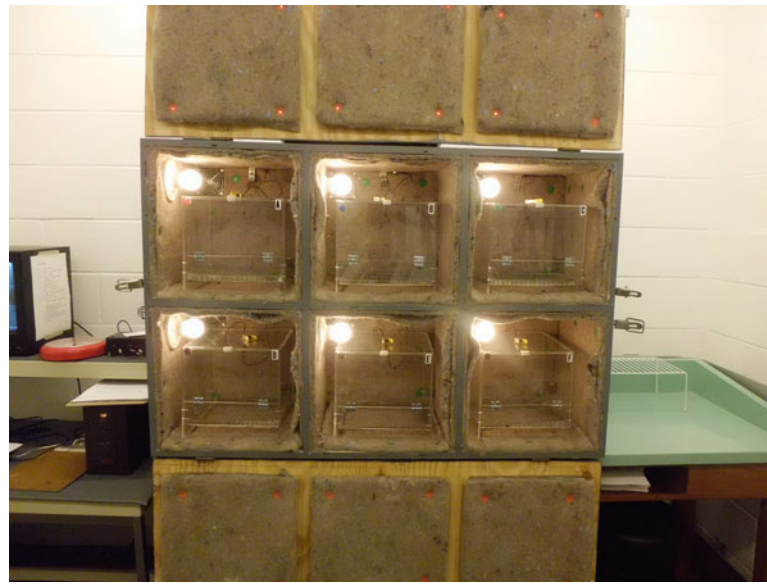

Fig. 2. Six-unit isolation test apparatus and data acquisition hardware.

2. Miniature video cameras (Model PC60XP, SuperCircuits, Inc., Liberty Hill, TX) mounted in the sound-attenuating enclosures at floor level and routed through a multiplexor (Model PC47MC, SuperCircuits, Inc.) provided televised display of the chicks for behavioral observation.
3. To record DVocs, microphones (Radio Shack Omnidirectional Model 33-3013 (modified for AC current)) are mounted at

the top of the Plexiglas chamber. These vocalizations are routed to a computer equipped with custom designed software for data collection.

3. Methods

1. Squads of six chicks are taken from their home cage and placed within a lidded plastic transport container.
2. To track subject assignment to various treatment conditions, chicks are marked using colored felt pens (i.e., six colors at two different body locations).
3. Body weight is determined for each chick to determine dosing and identify outliers (i.e., low body weight).
4. Drugs can be administered through various routes. Routes of administration include intracerebroventricular (ICV), intramuscular (IM), intraperitoneal (IP), and oral (gavage is not necessary as chicks reflexively swallow when fluid is placed into beak).

   Injection to test interval varies from 0 min to 24 h depending upon route of administration and pharmacokinetic properties of test articles. Our typical procedure uses IM injection and a 15 min interval.
5. Chicks are group transported inside the lidded container to an adjacent testing room.
6. Each chick is placed into an individual testing unit.
7. Doors for the testing chamber are then closed and secured.
8. The program for recording vocalizations is started and allowed to run for time intervals ranging from 3 min (for anxiety modeling only) up to 120 min (for anxiety–depression modeling).
9. Following the completion of the test session chicks are removed from the testing apparatus and returned to the home cage.
10. Records of the electronic files from the data collection program recording vocalizations are stored on the hard drive and backed up on a flash drive for data analysis.
11. The dependent measure of DVocs can be expressed in a number of different ways. In our initial examination, we present the data as means (±SEM) in 1–5 min blocks across the entire test period. This gives us a fine-grained evaluation to ensure (a) replication of anxiety–depression patterns of responses and (b) what blocks to submit to statistical analyses. For such analyses prefer to use rate/minute as the dependent measure for describing the anxiety-like (0–5 min test period) and depression-like (30–120 min test period) phases. The depression-like phase

may also be sequentially presented in smaller time units if highlighting differences in onset of action of test articles.

12. Our experimental designs (isolated vs. non-isolated X vehicle and several drug doses across the test session) require 3-, 2- and 1-way Analysis of Variance (ANOVAs). Factors include: stress treatment condition (between), drug dose (between), and time (within). Given that drug effects are typically not seen under non-isolated test conditions, separate 1-way ANOVAs across drug dose for each of the anxiety-like and depression-like phases are used to test for significant drug effects. We typically use Fisher's LSD tests for post-hoc analyses.

4. Notes

1. Our custom designed data collection software was developed in-house. Mechanical counters have been used in previous experiments. Both work sufficiently; and any means to reliably record vocalizations can be utilized. It is worth mentioning that chicks produce two distinct types of vocalizations. One is an attempt to re-establish contact with conspecifics, or DVocs. These chirps are the target behavior to be recorded and occur when placed in isolation. The other type of vocalization is referred to as a pleasure call and occurs when foraging for food and/or with conspecifics; these calls have a lower spectrographic frequency signal and lower decibel level. Adjustments to the volume levels on the microphones or software application is necessary in order to obtain all of the DVocs as they do tend to vary in intensity (loudness).
2. Consideration of the welfare of the animals during shipment should be made. Shipment mortality rates of chicks can be affected by the seasonal changes in temperature and general climate without special shipping cartons. Our supplier provides insulated shipping containers in order to protect animals delivered in the colder winter months.
3. The isolation apparatus we use is custom manufactured. Any apparatus that isolates chicks while providing proper sound attenuation, ventilation, and light would suffice. Our apparatus is designed with six isolation chambers to maximize data collection. While we find this number to be convenient, we see no reason why a larger or smaller apparatus would not work.
4. We have previously used battery-operated microphones and found them unreliable in that it was difficult to know when a battery was running low. We modified our microphones to

operate on an AC circuit and we suggest that battery-operated microphones should not be used.

5. Some pharmacological agents cause sedation. Monitoring the animals with mini-cameras allows us to detect drug induced sedation that may confound DVoc rates.
6. During our research, we have found subtle experimenter differences in behavioral data collected. Such data variability can be minimized by assigning single roles to each component in the experiment from weighing/coding to injection protocol to data collection procedures.
7. It is paramount to keep chicks in a social environment during all procedures up to the isolation manipulation. When a procedure must be conducted on an individual chick (e.g., weighing), this should be done as quickly and efficiently as possible to ensure that they are returned to the group to minimize social separation stress.
8. During housing we monitor chicks for low growth rates under the assumption this may reflect poor health and delayed maturation. These animals are routinely removed and replaced with animals that were to serve as conspecifics during testing. Where our standard housing for experimental test animals is 12 per cage, we recommend conspecific housing at 15–18 per cage.
9. Given chicks engage in robust feeding/drinking behavior at the onset of the 12-h light cycle, we control for this potential confound by initiating testing 1–2 h into the light cycle.

References

1. Willner P (1991) Behavioural models in psychopharmacology. In: Willner P (ed) Behavioral models in psychopharmacology: theoretical, industrial and clinical perspectives. Cambridge University Press, Cambridge, pp 3–18
2. Sufka K et al (2006) Modeling the anxiety-depression continuum hypothesis in domestic fowl chicks. Behav Pharmacol 17:681–689
3. Warnick J et al (2009) Modeling the anxiety-depression continuum in chicks. J Psychopharmacol 23:143–156
4. Sufka K et al (2009) Antidepressant efficacy screening of novel targets in the chick anxiety-depression model. Behav Pharmacol 20:146–154
5. Warnick J, Wicks W, Sufka K (2006) Modeling anxiety-like states: pharmacological characterization of the chick separation stress paradigm. Behav Pharmacol 17:581–587
6. Feltenstein M et al (2004) The chick separation stress paradigm: a validation study. Pharmacol Biochem Behav 77:221–226
7. Feltenstein M, Sufka K (2005) Screening antidepressants in the chick separation stress paradigm. Psychopharmacology 181:153–159
8. Kessler R et al (1994) Lifetime and 12-month prevalence of DSM-III-R psychiatric disorders in the United States. Results from the national comorbidity survey. Arch Gen Psychiatry 51:8–19
9. Kessler R et al (2005) Lifetime prevalence and age-of-onset distributions of DSM-IV disorders in the national comorbidity survey replication. Arch Gen Psychiatry 62:593–602

Chapter 13

A Clinically Relevant Thromboembolic Stroke Model in the Aged Rat

Ryan C. Turner, Alisa S. Elliott, Jason D. Huber, and Charles L. Rosen

Abstract

Animal models have been an integral component of scientific discovery concerning ischemic stroke pathophysiology and the accompanying therapeutic targets. Unfortunately, the knowledge gleaned from these studies has failed to translate to enhanced therapeutics in the clinical environment [O'Collins VE, Macleod MR, Donnan Ga, Horky LL, van der Worp BH, Howells DW, Ann Neurol 59: 467–477, 2006]. We argue that this failed translation is a direct result of inadequate animal models that fail to address the greatest risk factor for stroke, age [Rosen CL, Dinapoli VA, Nagamine T, Crocco T, J Neurosurg 103:687–694, 2005]. Herein we provide comprehensive step-by-step instructions for a clinically relevant thromboembolic stroke model in aged rats [Dinapoli VA, Rosen CL, Nagamine T, Crocco T, J Neurosci Methods 154: 233–238, 2006]. This technique, utilizing the only FDA-approved therapeutic agent for the treatment of stroke, tissue plasminogen activator (tPA), allows for pathophysiologic studies in addition to testing potential therapeutic agents in combination with the currently approved treatment regimen.

Key words: Stroke, Middle cerebral artery occlusion, Rat model of ischemia, Selective embolization, TPA

1. Introduction

The desire to model stroke in the preclinical environment remains relevant due to the immense societal impact of stroke. Stroke remains the world's second leading cause of mortality, resulting in ~6,000,000 deaths annually (1). Worse yet, survivors often experience significant morbidity. These factors necessitate the development of improved therapeutic agents that can be applied to a greater percentage of those afflicted with stroke.

Arpad Szallasi and Tamás Bíró (eds.), *TRP Channels in Drug Discovery: Volume II*, Methods in Pharmacology and Toxicology,
DOI 10.1007/978-1-62703-095-3_13,

In spite of more than 100 agents that have progressed from what appeared to be successful preclinical studies to clinical trials, tissue plasminogen activator remains the only FDA-approved treatment and can be used in a relatively small number of patients due to contraindications and a limited window of opportunity (2). The question of why so many agents have failed to translate successfully remains largely unanswered. Assessing this failed translation, it is clear that one key difference exists between the animal models and the clinical realm—the consideration of age.

The average stroke patient is elderly—approximately 72% of patients are over the age of 65 yet the vast majority of preclinical studies are completed in 3-month-old rats which equates to essentially a young adult (3). Additionally, 52% of stroke victims are female but most preclinical studies utilize male animals. Furthermore, 87% of strokes are ischemic and caused by a thrombus or embolus occluding a vessel, most often being the middle cerebral artery. Despite this fact, many preclinical studies utilize other methods of occlusion ranging from a suture to endothelin-1 to photothrombosis.

The stroke model described in this work seeks to model the clinical scenario as closely as possible by utilizing aged, female rats and a thrombus to occlude the middle cerebral artery (4). While this is but one model of ischemia in terms of technique and animal type used, we believe it is the most clinically relevant for studying the pathophysiology of stroke and assessing various proposed pharmacologic agents.

2. Materials

2.1. Equipment

Equipment described below is used in our laboratory. Alternatives are available and may be substituted where appropriate.

1. VetEquip RC^2 (Rodent Circuit Controller) anesthesia machine
2. Harvard Apparatus Homeothermic Blanket Control Unit with Probe
3. Harvard Apparatus Homeothermic Blanket
4. Oster GOLDEN A5 with #10 clip for hair removal
5. Leica M400-E Operative Microscope
6. Moor Instruments DRT4 Laser Doppler Perfusion Monitor
7. Aitecs SEP-215 Plus syringe pump for administering saline
8. Harvard Apparatus Pump 11 for administering tissue plasminogen activator
9. Integra 2.7 mm twist drill bit with adjustable safety stop
10. Integra Camino Bolt (cranial bolt for insertion of Doppler probe)

11. ISMATEC Reglo Peristaltic Pump for cardiac perfusion of the animal
12. –80°C freezer
13. Autoclave (for sterilizing surgical equipment)
14. Incubator (for thrombus preparation)

2.2. Supplies for Thrombus Preparation

1. Intramedic Clay Adams brand Nonradiopaque polyethylene tubing
   (a) PE 50—I.D. 0.58 mm and O.D. 0.965 mm
   (b) PE 10—I.D. 0.28 mm and O.D. 0.61 mm
2. Petri dish
3. 1 ml syringe
4. Bunsen Burner
5. 0.9% Physiologic Saline

2.3. Surgical Instruments and Supplies

1. Kendall Curity Gauze Sponges (for making gauze pillow)
2. VWR Laboratory Labeling Tape (for making gauze pillow)
3. Puritan Cotton Tipped Applicators
4. Kendall MonoJect 20 ml syringe
5. Ethicon 3-0 Coated Vicryl Suture
6. Syneture 5-0 Sofsilk Suture
7. Forceps (sharp and dull; different sizes)
8. Surgical scissors (large and small sizes)
9. Surgical scalpel
10. Bard-Parker Stainless Steel Surgical Blade #15
11. Microscissors
12. Microvascular clips (x 2)
13. Microvascular clip holder
14. Hemostat
15. Needle Driver
16. Bone Rongeur for craniotomy
17. 2 mm brain block
18. Razor blades
19. Sterile surgical gowns
20. Sterile surgical gloves
21. Sterile surgical drapes
22. Instrument pouch for autoclave
23. Microsyringe for thrombus injection

2.4. Drugs/Chemicals

1. Baxter 0.9% Sodium Chloride Injection USP 1,000 ml
2. 2,3,5-Triphenyl tetrazolium chloride, Sigma-Aldrich
3. Activase (tissue plasminogen activator), Genentech
4. Phosphate-buffered Saline (PBS)
5. Scrub Care® Providone Iodine Cleansing Solution, Scrub
6. Dechra VETROPOLYCIN veterinary ophthalmic ointment
7. Isoflurane

3. Methods

The following sections describe all steps of the thromboembolic stroke model beginning with chemical and surgical preparation through achieving reperfusion.

3.1. Chemical Preparation

3.1.1. Activase (Tissue Plasminogen Activator)

1. Add 100 ml of physiologic saline to 100 mg bottle of Activase, creating a concentration of 1 mg/ml.
2. Dissolve the mixture by gentle shaking.
3. Aliquot 1.5 ml in 2 ml Eppendorf tubes and store at −80°C until needed. To achieve the final dose of 5 mg/kg, 5 ml/kg is given. For example, a 300 g rat receives 1.5 ml of the 1 mg/ml mixture.

3.1.2. 2% Triphenyl Tetrazolium Chloride

1. Weigh 2 g of 2,3,5-Triphenyl tetrazolium chloride.
2. Place in a 100 ml Pyrex round media storage bottle with screw cap.
3. Fill to 100 ml with phosphate-buffered saline.

3.2. Surgical Preparation

3.2.1. Preparation of Sterile Surgical Instruments

1. Place clean instruments in autoclave pouch. Instruments should be in the open position when applicable to ensure proper sterilization.
2. Place autoclave pouch containing instruments in the autoclave.
3. Ensure autoclave is filled with deionized water.
4. Run autoclave (most cycles are at least 20 min).
5. After cycle is complete and pressure reduced, crack the autoclave door slightly.
6. Run drying cycle (per manufacturer instructions).
7. Allow temperature to normalize with room temperature.
8. Remove pack.

3.2.2. Anesthesia Induction

1. Place rat in the anesthesia induction chamber.
2. Induce anesthesia for 10 min with the gas valve set at 4.0%.

3. Remove rat from induction chamber and place the nose of the rat in the nose cone.
4. Maintain anesthesia via nose cone with the gas valve set at 2.0% for remainder of procedure.

3.2.3. Aseptic Surgical Preparation

1. Shave the hair of the rat in the proper position (see below).
2. Apply sterile surgical drapes around the surgical site.
3. Ready these areas for surgery using a surgical preparation solution such as betadine.
4. Place a drop of eye ointment in each eye to prevent postsurgical ophthalmic infections.

3.2.4. Preparation of Gauze Pillow

1. Roll gauze pads together creating a 2.5 cm diameter by 5 cm long cylinder.
2. Secure with laboratory labeling tape.

3.3. Creation of Thrombus

1. Position the young-adult donor rat on the homeothermic heating pad in a supine position while placing the lower limbs in the down position, exposing the groin region.
2. Prepare the right groin area for aseptic surgery (see above).
3. Using a surgical scalpel, make a 4 cm incision parallel to the midline in the groin.
4. Using blunt dissection techniques, dissect down to the femoral artery and vein. Passing through the layers of fat and connective tissue, the inferior epigastric artery will become visible, arising from the femoral artery and coursing towards the superficial layers of the lower abdomen.
5. Using a 3-0 suture, retract the external oblique muscle overlying the femoral artery using a hemostat in order to widen the field of view.
6. Isolate the femoral artery from the surrounding femoral vein and nerve.
7. Using a 5-0 suture, ligate distal portion of femoral artery.
8. Place microvascular clip (aneurysm clip) proximally to ligated portion of the femoral artery. Leave sufficient space (approximately 2 cm) between suture and clip. This process is visualized in Fig. 1.
9. Once microvascular clip and suture are in place, effectively ceasing blood flow through this portion of the femoral artery, use microscissors to make a small cut in the top portion of the femoral artery. Use caution to not sever the entire vessel so that the base of the artery remains intact despite an opening in the top portion.
10. Cut a 15 cm long segment of PE50 tubing. Bevel one end of the cut segment at approximately 45°.

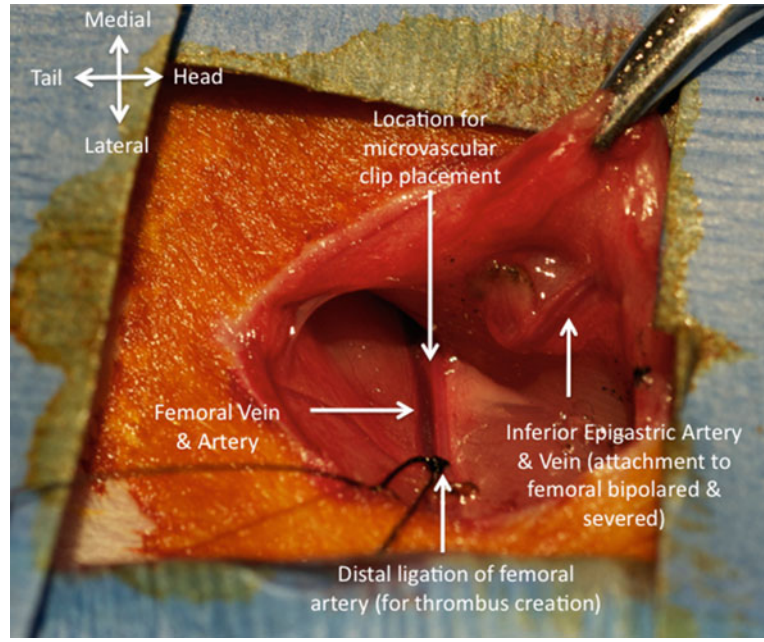

Fig. 1. Femoral artery dissection in preparation for blood draw to create thrombus. Note space between suture and microvascular clip—this is where femoral artery lumen will be exposed to insert PE50 tubing.

11. Insert beveled end of PE50 tubing into opening of the femoral artery. With application of light pressure, artery circumference will stretch to accommodate the tubing.
12. Once beveled end of PE50 tubing is entirely inside the artery lumen (0.5 cm inside), release the microvascular clip briefly.
13. PE50 tubing should rapidly fill with blood. Upon filling, the microvascular clip is replaced.
14. Remove blood-filled PE50 tubing and bipolar coagulate the femoral artery proximal to incision, in order to prevent bleeding.
15. Remove microvascular clip and remove traction on overlying muscles.
16. Suture wound with 3-0 suture.
17. Place blood-filled PE50 tubing in an incubator at 37°C for 120 min.
18. Store thrombus in refrigerator overnight.

3.4. Preparation of Thrombus for MCAO

1. Remove thrombus from refrigerator.
2. Add saline to petri dish to wash thrombus.
3. Affix a 20 cm segment of PE10 tubing to a 1 ml syringe via a sharp 27 gauge needle.

4. Insert free end of PE10 tubing into lumen of thrombus-filled PE50 tubing.
5. With slow but constant pressure, eject thrombus into saline-filled petri dish.
6. Visually assess thrombus diameter and appearance for uniformity using the microscope. A well-formed thrombus should appear consistent throughout (a smooth exterior with no missing pieces).
7. Wash clot by drawing into PE10 tubing attached to a syringe and expelling repeatedly back into saline. Upon initial expulsion, red cells will become detached from thrombus resulting in a cloudy appearance within saline. When clot is washed thoroughly it should appear ~25% narrower and no additional cloudiness produced.
8. Prepare modified PE50 tubing for injection of the thrombus. This is done by heating the PE50 tubing over a bunsen burner, removing from the heat, and then stretching the heated portion quickly, reducing the diameter.
9. You should now have a piece of PE50 tubing that is regular in diameter on the left and right end and much thinner in the middle. Cut tubing in the middle of the thin portion creating two pieces of the modified PE50 tubing.
10. Set a micrometer to 0.3 mm. Pull the modified PE tube between the jaw blades, starting at the thinnest portion and progressing to the thicker segment. Where blades "catch" the tubing is where the tubing is then cut. This creates a modified PE50 segment of tubing with an outer diameter of 0.3 mm.
11. When ready to inject thrombus, draw clot into modified PE50 tubing either directly or indirectly (via PE10 tubing).

3.5. Measurement of Cerebral Blood Flow

When performing middle cerebral artery occlusion, confirmation of proper thrombus (or suture in other models) placement is essential for verifying the induction of ischemia as well as for monitoring tissue plasminogen activator-induced reperfusion. Briefly, a cranial bolt with accompanying laser Doppler cerebral blood flow (CBF) probe is inserted into the cranium above the area corresponding to the vascular region supplied by the middle cerebral artery (MCA). This provides continual readings to document CBF at baseline as well as during and after insertion of thrombus and during reperfusion.

1. Position rat on homeothermic heating pad such that it is on its left side, with the right side exposed.
2. Prepare region between ear and eye for aseptic surgery (see above).
3. Using a surgical scalpel, make an incision that is 2 cm medial and cephalic to right ear to 2 cm lateral and cephalic to right ear.

4. Temporalis muscle should now be exposed. Using scalpel, make a 1 cm incision along right edge at the point where temporalis muscle inserts into skull. Make another 1 cm incision parallel to the first incision in cephalic direction. Now to complete temporalis flap, cut along medial insertion. Use the bipolar at low setting (i.e., 15–20 Malis units) to control bleeding.
5. Reflect temporalis flap using 3-0 suture and a hemostat to expose Bregma.
6. After removing excess tissue to clearly expose sutures, use tip of scalpel blade to start a small burr hole approximately 3 mm caudal to Bregma and 3 mm medial to the linea temporalis (twirl the scalpel with attached blade in your fingers, similar to a drill bit).
7. Once a starting groove has been made in skull with scalpel blade, switch to drill bit (approximately 7/64 of an inch) and continue making burr hole. Do this part slowly and remove bone fragments frequently, particularly once dural surface is exposed.
8. When the burr hole is finished, it should be a perfect circle and dura mater should be exposed such that you can see vasculature (Fig. 2).

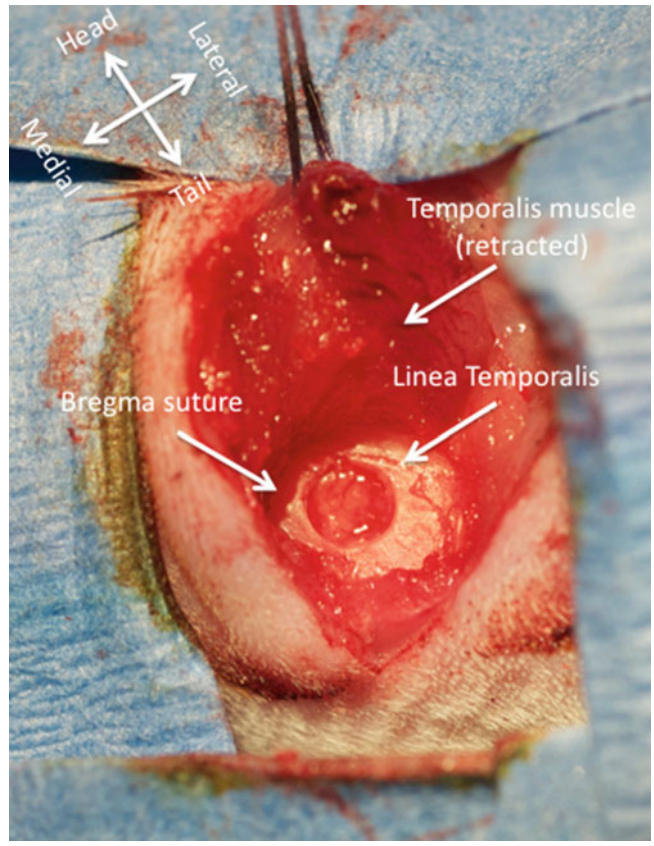

Fig. 2. Burr hole ready for insertion of cranial bolt and laser Doppler probe for cerebral blood flow measurement.

9. Affix cranial bolt over middle cerebral artery by carefully screwing it into parietal bone surrounding burr hole.
10. Insert laser Doppler probe into cranial bolt opening for monitoring cerebral blood flow.
11. Remove hemostat providing traction and withdraw suture from temporalis muscle.
12. Rat is now ready to be positioned for middle cerebral artery occlusion procedure.

3.6. Middle Cerebral Artery Occlusion

The thromboembolic model described herein is advantageous in that it most closely mimics the clinical scenario. This is accomplished by administering a thrombus created from a young-adult donor rat into the middle cerebral artery, the vessel most frequently occluded in the human population. Additionally, proper placement can be verified through the use of the laser Doppler cerebral blood flow recording discussed previously.

1. Place rat in supine position on homeothermic heating pad being careful not to disrupt laser Doppler probe that has been inserted previously for monitoring purposes.
2. Place a small pillow (see above) under head of rat such that anterior portion of head and neck are parallel to operating table. This is important as it brings anatomical structures of interest (carotid artery and its branches) more superficial. This allows increased access to the bifurcation of the carotid artery and visualization of the internal carotid artery.
3. Place forelimbs of rat in traction such that chest is fully exposed, enhancing visualization during dissection.
4. Using surgical scalpel, make a midline cervical incision running from near the mandible to the sternum.
5. Dissect through superficial connective tissue to visualize mandibular glands and muscles overlying the trachea.
6. Focusing to right (the rat's right side) of the midline, a triangle formed by three different muscles should be apparent (Fig. 3). The medial border of this triangle is created by the sternohyoid, the inferior lateral border by the sternomastoid, and the superior lateral by the inferior portion of the digastric.
7. Separate these muscles by dissecting through connective tissue between the muscles. Use care to avoid damaging muscles as this can result in unnecessary trauma and excessive bleeding.
8. Retract superior lateral border of triangle (inferior portion of digastric) by encircling muscle with 3-0 suture and providing traction using a hemostat. Common carotid artery should now be visible in center of the triangle.

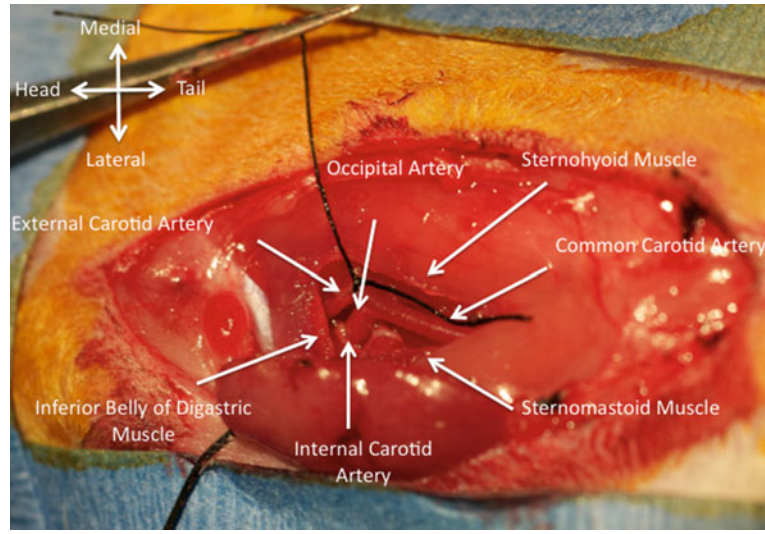

Fig. 3. Vessels prepared for insertion of thrombus. The external carotid artery stump, seen ligated by the suture, is the site of insertion. This stump can be manipulated such that it is in line with the internal carotid artery, allowing for a straight shot from the ECA stump into the ICA and subsequently the MCA.

9. Carefully isolate common carotid artery from surrounding connective tissue.
10. Follow common carotid artery superiorly to its bifurcation into external and internal carotid arteries.
11. Carefully isolate external carotid artery, the more superficial of the branches from the common carotid artery. The other branch from bifurcation is the internal carotid artery.
12. Follow external carotid artery cephalically until the superior thyroid artery (first anterior-oriented branch off of external carotid) comes into view (Fig. 4). The superior thyroid artery may be attached underneath the superior angle of the triangle, between the digastric muscle and sternohyoid muscle.
13. Bipolar coagulate superior thyroid artery and cut in the center of bipolared portion, separating superior thyroid artery from external carotid artery.
14. Ligate external carotid artery near origin from common carotid artery. Use a single tie that can be untied easily as this is a temporary ligation.
15. Bipolar coagulate external carotid artery in the most distal region possible, above where the superior thyroid artery branched off.
16. Cut external carotid artery in middle of the bipolared segment, creating the external carotid artery stump at the bifurcation of

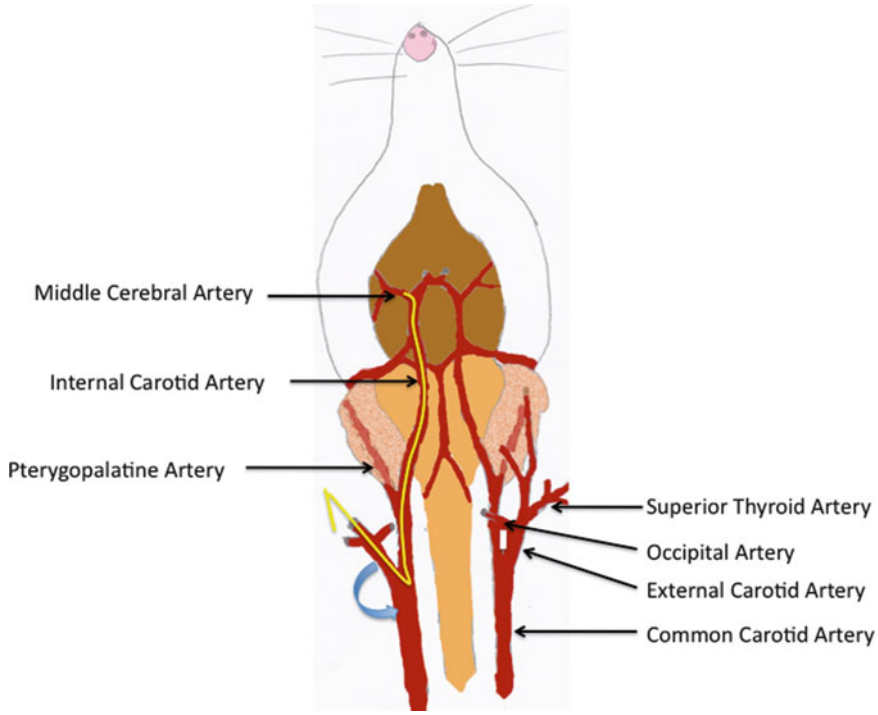

Fig. 4. Diagrammatic representation of vasculature in the neck and brain relevant for middle cerebral artery occlusion (MCAO). It is important to note the location of the superior thyroid artery and the occipital artery as these must be dissected and bipolared prior to thrombus insertion. When inserting the thrombus, ensure the modified tubing is placed from the external carotid artery stump into the internal carotid and then the middle cerebral, avoiding the pterygopalatine artery.

the common carotid artery. This stump should move freely while attached to the common carotid artery at this point—if not, dissect more thoroughly such that the stump can be moved such that it is inline with the internal carotid artery.

17. Isolate internal carotid artery. While isolating, a branch originating near the ECA–ICA bifurcation becomes apparent called the occipital artery.
18. Isolate the portion of the occipital artery nearest the internal carotid artery and bipolar this vessel. Once the vessel is bipolared sufficiently, cut this vessel in the bipolared segment. The external carotid artery stump can be seen in Fig. 3. Also visible in this figure is the common carotid artery and the internal carotid artery.
19. Finish isolating the internal carotid artery down to the next branch (pterygopalatine artery). Ensure that both the ICA and the pterygopalatine artery can be seen at this bifurcation (Fig. 4) as it is essential that the tubing can be visualized in the proper vessel when inserted in subsequent steps.
20. Apply two microvascular clips—one on the common carotid artery and one on the internal carotid artery. These are to occlude

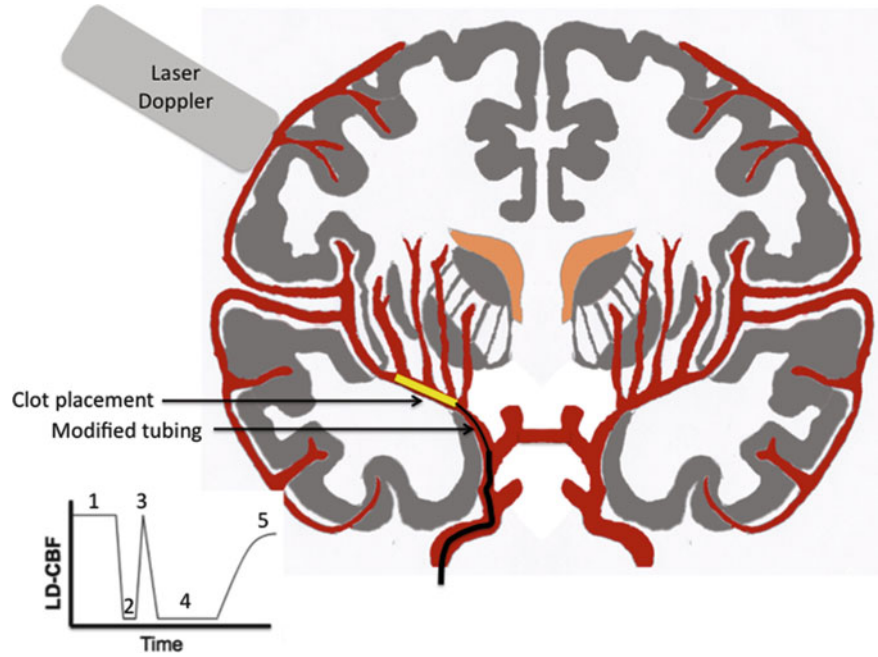

Fig. 5. Laser Doppler recording of CBF during MCAO procedure. (1) Baseline CBF recording, (2) occlusion with modified tubing prior to clot injection, (3) verification by withdrawing catheter approximately 1 mm, (4) injection of clot and CBF reduction to 20% or less of baseline, (5) reperfusion from tPA administration.

blood flow temporarily while inserting the thrombus. A drop in CBF in the MCA territory, as measured with the laser Doppler monitoring system, should be observed at this point (Fig. 5).

21. Mark the modified PE50 tubing prepared previously with a permanent marker at 18 mm from the modified end. This mark will allow for visualization through the artery as the clot is inserted in subsequent steps.
22. Draw the clot into the modified PE50 tubing using the microsyringe. If the clot cannot be drawn into the modified tubing, wash the clot more in the saline until small enough to be drawn into the modified tubing.
23. Position the microsyringe with attached modified PE50 tubing filled with the clot such that the modified tubing is in line with the external carotid artery stump. To do this, use modeling clay positioned in the groin of the rat as the mounting point for the microsyringe and adjust this superiorly or inferiorly such that the modified tubing and clot are in the proper location.
24. Cut the bipolared segment off of the external carotid artery stump so that the lumen can be visualized.
25. Loosen the suture placed around the external carotid artery and begin to insert the modified tubing containing the clot while bending the external carotid artery stump towards the syringe, inline with the internal carotid artery. Once the tubing

is inserted beyond the suture, tighten the suture once again around the tubing.

26. Remove the microvascular clip from the internal carotid artery but leave the other microvascular clip on the common carotid artery at this time.
27. Continue inserting the modified tubing containing the clot into the internal carotid artery. Ensure that the tubing remains in the internal carotid artery and does not enter the pterygopalatine artery by observing the tubing inside the vessel.
28. When the 18 mm mark approaches the bifurcation, slow the insertion process and watch the laser Doppler monitor for changes in cerebral blood flow.
29. When the laser Doppler number drops, indicating blood flow to the MCA is disrupted, the tubing is in the correct place (Fig. 5). Pull back approximately 1 mm on the modified tubing and watch the cerebral blood flow be restored, as indicated by the laser Doppler recording (Fig. 5). This is a confirmatory step for ensuring no hemorrhage was caused.
30. When the cerebral blood flow is restored, inject 5 μl of saline to eject the blood clot from the modified tubing.
31. Once the clot is injected, the cerebral blood flow should drop again to a value similar to that seen previously when occluding with the tubing only (Fig. 5).
32. After injecting the clot, wait 5 min to ensure clot stability prior to slowly removing the modified tubing.
33. When removing the modified tubing, a microvascular clip will need to be placed on the internal carotid artery prior to withdrawing the modified tubing entirely.
34. Once the clip is placed, remove the modified tubing the rest of the way and use the remaining suture around the external carotid artery stump to ligate the stump permanently. The stump can also be bipolar coagulated to ensure proper closure and prevent bleeding.
35. Remove both microvascular clips at this time. The CBF in the MCA territory should remain decreased at 20% or less of baseline (Fig. 5).
36. Cover the exposed tissues with a saline-soaked gauze pad while the animal remains under anesthesia prior to closing the wound using a 3-0 suture.

3.7. Achieving Reperfusion

In this thromboembolic model, reperfusion is obtained via administration of tissue plasminogen activator, the same compound that is utilized clinically. This allows for the study of new therapeutics in conjunction with the presently approved agent—a combination therapy approach. Briefly, tissue plasminogen activator can be given intravenously via the same catheter used to administer saline in the femoral vein.

1. Follow the procedure for "Creation of Thrombus," found above.
2. Isolate the femoral vein from the artery and nerve.
3. Using a 5-0 suture, ligate the distal end of the exposed femoral vein.
4. Using a 5-0 suture, prepare a loose ligation more proximally. This will be to hold the intravenous catheter in place but cannot be tightened until the catheter is inserted.
5. Insert the 22-gauge catheter proximal to the total ligation of the femoral vein but distal to the loose suture.
6. Secure the intravenous catheter with the previously prepared 5-0 suture.
7. Connect the intravenous catheter to a syringe pump loaded with saline.
8. Administer saline at a rate of 1 ml/h to maintain proper fluid balance.
9. At 2 h after induction of ischemia by injecting the clot, administer tissue plasminogen activator via a syringe pump at a dose of 5 mg/kg. A 30% bolus should be given and the remaining administered over a period of 30 min. This is done via the same intravenous catheter used for saline administration and is done simultaneously.
10. While administering tissue plasminogen activator, closely observe the rat for bleeding from open wounds and stop via bipolar.
11. Observe the cerebral blood flow measurement, as blood flow should be restored following tissue plasminogen activator administration (Fig. 5).
12. Once complete, carefully remove the intravenous catheter and either suture or bipolar this open segment of the femoral vein.
13. Remove the laser Doppler probe and cranial bolt.
14. Suture all wounds using a 3-0 suture.

3.8. Poststroke Assessment

Assessment of animals poststroke in the past has largely focused on volumetric measurements and the ability of the compound being tested to alter infarct volume. In recent years the focus has begun to shift towards behavioral outcomes to increase clinical relevancy (5). This shift has been largely predicated on the failure of compounds to translate from preclinical models to clinical trials. Despite the hundreds of clinical trials initiated for pharmacologic agents to treat ischemic stroke, tissue plasminogen activator remains the only FDA-approved compound.

As such, we will discuss briefly both aspects of assessment poststroke: functional and volumetric.

3.8.1. Functional Assessment

Modified Neurological Severity Score

The Modified Neurological Severity Score (MNSS) has long been utilized as a functional assessment for stroke as it is proposed to assess both motor and sensory deficits after ischemia (6). This scale, while simple when applied to the young animal, is fraught with challenges when applied to the aged animal. The aged animal is fundamentally unique in that motor activity, even prior to injury, is greatly reduced as well as balance and sensory perception. Therefore, the utility of this scale in the aged population may simply be more of a qualifier for whether or not stroke occurred rather than an accurate assessment of stroke severity.

Raising rat by tail (normal = 0; maximum = 3)	(3)
Flexion of forelimb	1
Flexion of hindlmb	1
Head movement >10° to vertical axis within 30 s	1
Placing rat on floor (normal = 0; maximum = 3)	(3)
Normal walk	0
Inability to walk straight	1
Circling toward the paretic side	2
Falls down to paretic side	3
Sensory tests (normal = 0; maximum = 2)	(2)
Placing test (visual and tactile test)	1
Proprioceptive test (deep sensation, pushing paw against table edge to stimulate limb muscles)	1
Beam balance tests (normal = 0; maximum = 6)	(6)
Balances with steady posture	0
Grasps side of beam	1
Hugs beam and one limb falls down from beam	2
Hugs beam and two limbs fall down from beam, or spins on beam (>60 s)	3
Attempts to balance on beam but falls off (>40 s)	4
Attempts to balance on beam but falls off (>20 s)	5
Falls off; no attempt to balance or hang on the beam (<20 s)	6
Reflex absence and abnormal movements (normal = 0; maximum = 4)	(4)
Pinna reflex (head shake when auditory meatus is stimulated)	1
Corneal reflex (eye blink when cornea is lightly touched with cotton)	1
Startle reflex (motor response to a brief auditory stimulus)	1
Seizures, monoclonus, and myodystony	1
Maximum points	(18)

Points are assessed for inability to perform specified task or for absence of reflex, resulting in more severely impaired animals receiving a higher score. The following ranges have been used to categorize injury severity: 1–6 mild injury, 7–12 moderate injury, and 13–18 severe injury.

Sensorimotor Assessment

Assessment of sensorimotor activity can be done as part of scoring systems such as the aforementioned MNSS but can also be done using other techniques such as open-field/locomotor activity, rotarod, staircase test, the cylinder test, grip-strength, adhesive label test, and others (7). While the intent of this work is not to review all functional tests, it is important to consider the variety of factors that impact the assessment of motor ability. Perhaps most important are the inherent differences seen from animal to animal at baseline. Therefore, it is important to either normalize to baseline or provide adequate training to meet a preset criterion. Additionally, age must be considered. Young adult animals behave differently than aged animals and have significantly more mobility before and after ischemia. Furthermore, alterations in the methodology used to induce MCAO produces highly variable results depending on occlusion type, location, duration, and strain of animals used.

Cognitive Assessment

Cognitive assessment of rodents poststroke remains a widely debated topic, similar to other behavioral assessments. There is little agreement as to the most appropriate measures or expected results as past work has been highly variable. Some commonly utilized techniques include the Morris Water Maze, radial maze, passive avoidance, and active avoidance (8). Each of these tests has been designed to assess some aspect of learning or memory but requires significant motor ability and baseline ability may vary from strain to strain and with age.

3.8.2. Volumetric Assessment

1. At time of sacrifice, anesthetize the rat as described previously.
2. Once anesthetized, place the rat in a supine position.
3. Make a horizontal incision, approximately 2 in. wide, in the upper abdomen of the rat.
4. Cut vertically at each end of this incision, cutting through the diaphragm and rib cage.
5. A flap has now been created consisting of the sternum and the anterior portion of the rib cage that can be retracted using a large hemostat.
6. Quickly remove any fascia remaining around the heart and aorta so that both structures can be visualized clearly.
7. Insert the peristaltic pump needle into the left ventricle and into the aorta. Visualize the needle in the aorta to confirm proper placement.

8. Start the pump and set to a rate of approximately 10 ml/min for 10 min using physiologic saline to perfuse the animal.
9. Cut the right atrium to allow for the blood to drain out of the animal. Over time the fluid should become clear and the tissues/organs should become pale (particularly liver and eyes), indicating a successful perfusion.
10. After 10 min (and 100 ml of saline), turn off the pump and remove the needle from the aorta.
11. Decapitate the animal.
12. Extract the brain, being careful not to damage the cortex.
13. Place the brain in the 2 mm brain block.
14. Place in −80°C freezer for approximately 5 min.
15. Remove from freezer and slice using razor blades.
16. Place each slice in a separate well in a 12 well plate.
17. Add 2 ml of 2% TTC in PBS to each slice.
18. Place in incubator for 20 min.
19. Remove plate from incubator and scan into an image file (jpg, tif, etc.).
20. Calculate lesion volume using previously described techniques (Photoshop, ImageJ, etc.) (9).

4. Notes

1. If the instrument pouch is wet upon removal from the autoclave, it is likely that the door was not opened/cracked appropriately and/or the drying cycle did not run properly. Do NOT open the door to the maximum extent immediately as this allows colder room air to rush in and create condensation on the instruments.
2. We strongly recommend relying on CBF measurements throughout the procedure. CBF changes can be seen with each step, ranging from the initial brief reduction seen when placing microvascular clip on the CCA to those corresponding to duration of ischemic episode.
3. Creating a high quality burr hole without damaging the brain is vital for confirming ischemia and reperfusion but is often challenging, even for the experienced surgeon. After initiating the hole with the scalpel and switching to the drill bit, be sure to frequently remove bone fragments to prevent forcing them into the brain. Also, try applying enough downward force to engage the drill bit in the cranium but then apply slight upward

force to prevent the bit from entering the dura and brain. This upward force also assists in directing bone fragments out of the cranium rather than inside.

4. Our group, as well as others in the field, has experimented with different methods of recording cerebral blood flow such as extracranial measurements from the cranium surface. While it is possible to obtain readings from this position, we have not found consistent success at ensuring proper occlusion and reperfusion. One of the primary obstacles encountered is the ability to achieve preset criteria for assessing ischemia/reperfusion. We define ischemia as a drop of 80% or more from baseline laser Doppler recording and define reperfusion as a return to 80% or greater of the baseline value or visual absence of thrombus upon craniotomy.
5. Prior to inserting the cranial bolt, verify the position of the Doppler probe within the bolt. Depending on the supplies/equipment used, the probe may be longer than the bolt. In this case, it may be helpful to apply a moldable but somewhat rigid material (such as bone wax) to the probe to prevent the probe from extending beyond the bolt.
6. Washing the clot properly is one of the most critical steps of the process. Wash too little and reperfusion becomes unreliable, wash too much and spontaneous reperfusion occurs. The proper amount of washing requires practice and a trained eye—this can be acquired with attention to detail and some basic experience.
7. We have found significant variance in the PE 50 tubing used to form the clot when purchased from various manufacturers. In addition to slight variances in size, lumen texture is also variable with some appearing smoother while others are slightly ribbed. For this reason, we utilize the INTRAMEDIC listed in the materials section. We have found the most success with this tubing as it conforms to rigid tolerances and as such is consistent from reel to reel.
8. We have also found that the method of anesthesia used influences volume of the clot. Isoflurane may result in smaller diameter clots than using Ketaject. For this reason, it may be advantageous to utilize Ketaject for blood draws from the donor animal.
9. When perfusing the animal, it may be desirable to use a dulled needle. Often a sharp needle may penetrate the aorta leading to poor quality perfusions. If you experience this problem, file the tip of the needle to create a dulled tip.

References

1. Woodruff TM, Thundyil J, chun Tang S, Sobey CG, Taylor SM, Arumugam TV (2011) Pathophysiology, treatment, and animal and cellular models of human ischemic stroke. Mol Neurodegener 6:1–19
2. O'Collins VE, Macleod MR, Donnan GA, Horky LL, van der Worp BH, Howells DW (2006) 1,026 experimental treatments in acute stroke. Ann Neurol 59:467–477
3. Rosen CL, Dinapoli VA, Nagamine T, Crocco T (2005) Influence of age on stroke outcome following transient focal ischemia. J Neurosurg 103:687–694
4. Dinapoli VA, Rosen CL, Nagamine T, Crocco T (2006) Selective MCA occlusion: a precise embolic stroke model. J Neurosci Methods 154:233–238
5. Roof RL, Schielke GP, Ren X, Hall ED (2001) A comparison of long-term functional outcome after 2 middle cerebral artery occlusion models in rats. Stroke 32:2648–2657
6. Chen J, Li Y, Wang L, Zhang Z, Lu D, Lu M, Chopp M (2001) Therapeutic benefit of intravenous administration of bone marrow stromal cells after cerebral ischemia in rats. Stroke 32:1005–1011
7. Boltze J, Kowalski I, Förschler A, Schmidt U, Wagner D, Lobsien D, Emmrich J, Egger D, Kamprad M, Blunk J, Emmrich F (2006) The stairway: a novel behavioral test detecting sensomotoric stroke deficits in rats. Artif Organs 30:756–763
8. DeVries AC, Nelson RJ, Traystman RJ, Hurn PD (2001) Cognitive and behavioral assessment in experimental stroke research: will it prove useful? Neurosci Biobehav Rev 25:325–342
9. Yang Y, Shuaib A, Li Q (1998) Quantification of infarct size on focal cerebral ischemia model of rats using a simple and economical method. J Neurosci Methods 84:9–16

Chapter 14

Use of Cell-Stretch System to Examine the Characteristics of Mechanosensor Channels: Axonal Growth/ Neuroregeneration Studies

Koji Shibasaki

Abstract

Temperature-sensitive TRP (so-called "thermoTRP") channels are well recognized for their contributions to sensory transduction, responding to a wide variety of stimuli including temperature, nociceptive stimuli, touch, and osmolarity. However, the precise roles for the thermoTRP channels during development have not been determined. To explore the functional importance of thermoTRP channels during neural development, the temporal expression was determined in embryonic mice. Interestingly, TRPV2 expression was detected in spinal motor neurons in addition to the DRG from E10.5, and was localized in axon shafts and growth cones, suggesting that the channel is important for axon outgrowth regulation. We revealed that endogenous TRPV2 was activated in a membrane-stretch-dependent manner in developing neurons by knocking down the TRPV2 function with dominant negative TRPV2 and TRPV2-specific shRNA, and significantly promoted axon outgrowth. In this section, the author introduces experimental methods to investigate the mehcanosensor functions of TRPV2 in axonal outgrowth or regeneration.

Key words: Mechanosensor, TRPV2, Electroporation, In ovo, DRG, Motor neuron, Culture

1. Introduction

Mechanisms of axonal outgrowth still have many mysteries, although many chemoattractive and chemorepulsive molecules related to axonal outgrowth were identified, and their intracellular signaling was examined. It is a specific characteristic that neurons can grow to the length of more than 1 m in humans (1, 2). This mechanism of elongation has been called "passive stretching" (2). From embryonic stages, the passive stretching-dependent axonal outgrowth begins. As our body grows, the distances between

Arpad Szallasi and Tamás Bíró (eds.), *TRP Channels in Drug Discovery: Volume II*, Methods in Pharmacology and Toxicology, DOI 10.1007/978-1-62703-095-3_14,

neuronal cell bodies and growth cones gradually increase, thereby exerting tensile forces on the axons.

In some of in vitro studies, the growth cones of cultured sensory axons were attached to glass needles to examine their response to forces (3, 4). Axons could be stretched up to approximately 100 μm over a few hours (2). Moreover, artificial external forces induce axonal outgrowth. A group developed a unique chamber system in which neurons are cultured on two initially contiguous platforms that are pulled apart by a stepped motor (5, 6) in order to improve axonal regeneration following injury. The axons plated onto the platforms can be elongated by this system. This system provides ten times faster speed than typical growth-cone-mediated axonal outgrowth rates (7). In addition to the above observations, using orthopedic leg-lengthening procedures in adult rats, it was found that applied forces *in vivo* could double inter-nodal distances. Notably, acute stretching resulting in high tension, as it occurs clinically when large nerve gaps are directly joined, impairs axonal regeneration (8, 9).

Recently, we reported that TRPV2 was a mechanosensor channel which contributed to axonal outgrowth in a membrane stretch-dependent manner (10), consistent with previous report described the sensor function of TRPV2 against hypotonic stimulus (11). Taken together, these results indicate that forces are powerful stimulators of axonal outgrowth through TRPV2 activation. In addition to those reports, we also recently reported that activation of TRPV2 through mechanical stimulus by intestinal movement regulated intestinal motility (12). In this section, the author introduces good systems to investigate the mehcanosensor functions in axonal outgrowth or regeneration.

2. Materials

2.1. Animals

1. ICR strain mice were utilized. Embryos were considered as E0.5 at noon on the day at which vaginal plugs were observed.
2. Fertilized chicken eggs were purchased from Gen Corporation (Gifu, Japan), and the eggs were cultured for 3 days at 38.5°C until they become embryos at the Hamburger and Hamilton stage (HH) 10–14.
3. All animal care and procedures were performed according to NIH, NIPS (National Institute for Physiological Sciences) and Gunma University guidelines.

2.2. Equipment

1. Membrane stretch was applied by a computer-controlled stepping motor machine (STB-150, STREX, Japan) as previously described (13). *In vitro* and *in ovo* electroporations were performed by a pulse generator, ECM830 (BTX).

2.3. Solutions

1. A standard bath solution containing 140 mM NaCl, 5 mM KCl, 2 mM $MgCl_2$, 2 mM $CaCl_2$, 10 mM HEPES, and 10 mM glucose, pH 7.4, was used for whole cell patch-clamp recordings. The standard bath solution for the patch-clamp experiments was the same as that used in fluorescence measurements.
2. Pipette solution for whole-cell recordings contained 140 mM CsCl, 0.5 mM EGTA, 2 mM Mg-ATP, 2 mM K_2-GTP, and 10 mM HEPES, pH 7.4.

3. Methods

3.1. Cultivation of Dissociated Embryonic DRG/Motor Neuron Cells and Embryonic DRG Explants

Embryonic mouse DRG or motor neurons were prepared using a modified protocol originally designed for cultivation of the mouse hippocampus (14).

1. DRGs or the ventral half of spinal cords was dissected from E12.5 embryos and dissociated using mechanical trituration.
2. Cells were plated on poly-d-lysine-coated coverslips (15 mm round, Assistant, Germany) at a final density of $3–5 \times 10^5$ cells/coverslip in Neurobasal Medium (Invitrogen, Carlsbad, CA) with B27 supplement (Invitrogen), NGF (10 ng/mL, Sigma, St. Louis, MO), NT-3 (10 ng/mL, Calbiochem, La Jolla, CA), and penicillin/streptomycin (1:250, Invitrogen, Carlsbad, CA).
3. After 12 h, coverslips were immersed in fresh Neurobasal Medium with B27 supplement, NGF and NT-3. To prevent overgrowth of glia and fibroblasts, cultures were treated with cytosine arabinoside (5 μM; Calbiochem). Embryonic DRG explant cultures were also performed from E12.5 embryos. Dissected DRGs were put on poly-d-lysine-coated coverslips in Neurobasal Medium with B27 supplement, NGF and NT-3. After 12 h, coverslips were immersed in fresh Neurobasal Medium with B27 supplement, NGF and NT-3 (with cytosine arabinoside (5 μM)). To examine the effect of low calcium on TRPV2-dependent axon outgrowth, we utilized low Ca^{2+} DMEM (0.15 mM low Ca^{2+}) or regular DMEM (2 mM normal Ca^{2+}) with 10% fetal bovine serum, NGF, NT-3, and penicillin/streptomycin instead of above culture medium.

3.2. Application of Cyclic Stretch

1. Membrane stretch was applied by a machine (STB-150) as described above.
2. Dissociated DRG or ventral spinal cord cells were transferred onto a 4-cm^2 silicon chamber (Fig. 1a, b) coated with 50 μg/mL fibronectin at a density of 3×10^4 cells/cm^2.

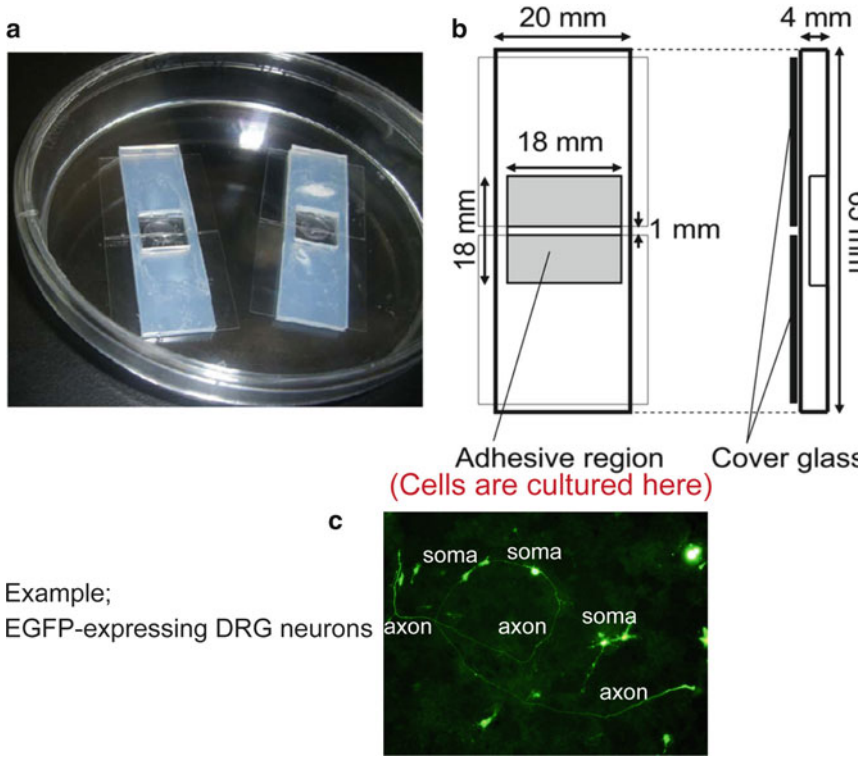

Fig. 1. *In vitro* cell-stretch system. (**a**, **b**) Elastic silicone chambers and their dimensions. Two pieces of cover glass (*rectangle*) are attached to the bottom of the silicone chamber with an adhesive agent and a 1 mm width slit (from glass edge to edge) is made in the center of the chamber so that only the slit area can be elongated upon extension. (**c**) DRG neurons were cultured on the silicone chamber (the gray 18 mm × 18 mm square place in (**b**)) after EGFP cDNA was electroporated. Many soma and axons were visualized by EGFP expression.

3. After 2 days, the silicon chamber was attached to a stretching apparatus that was driven by a computer-controlled stepping motor (Fig. 2a). Using this system, quantitative and uniform stretch (+2.8% length for 15 s) was applied to the cells upon Ca^{2+}-imaging experiments by Fura-2 (Fig. 2b, c).

3.3. In Vitro and In Ovo Electroporation

In vitro electroporation was performed by a modified protocol as previously described (15, 16).

3.3.1. In Vitro Electroporation

1. Embryonic DRGs or the ventral half of spinal cords (at E12.5) were dissociated using mechanical trituration from anesthetized embryos by chilling on ice. DRGs and spinal cords were transferred into DNA solutions (5 μg/μL) in PBS containing 0.1% fast green as a tracer were transferred to the electroporation chamber with dissociated DRG cells.
2. Five square pulses (33 mV) of 50-ms duration with 950-ms intervals were applied by a pulse generator, ECM830 (BTX).

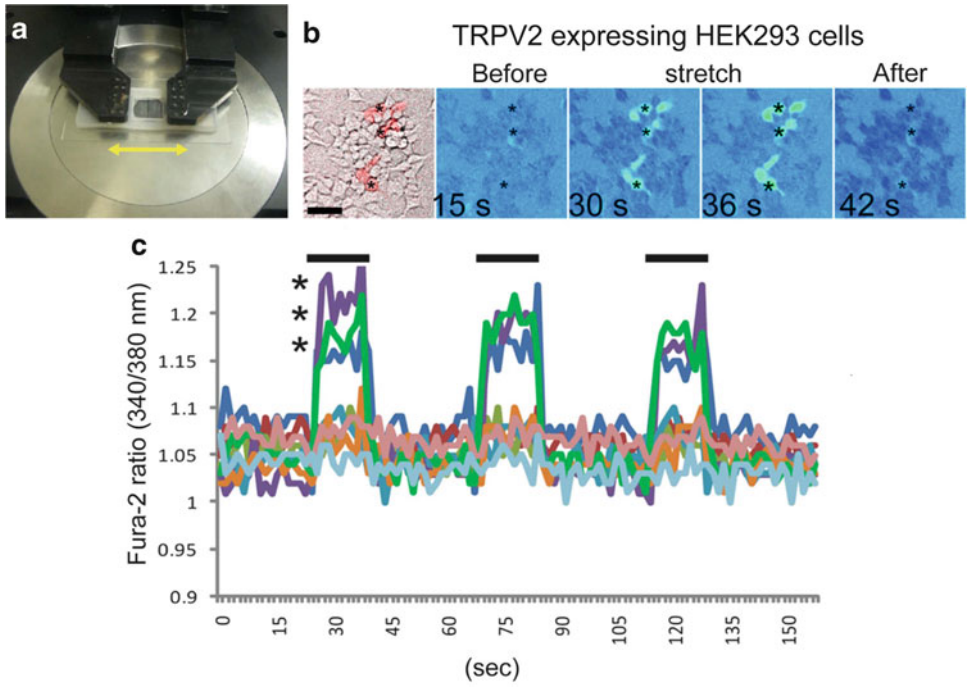

Fig. 2. *In vitro* cell-stretch system. (**a**) After 48 h of cell culture, the silicone chamber is set in two arms of the extension device on the Ca^{2+}-imaging microscope. An *arrow* in (**c**) indicates the direction of extension. (**b**) HEK293 cells expressing TRPV2 were exposed to membrane stretch (102.8% extension) for 15 s by the STREX machine during Ca^{2+}-imaging. The red signals in the most left picture represent the TRPV2 transfected cells revealed by Ds-Red co-expression. Fura-2 ratio traces by symbols are from the cells indicated by the same symbols in the pseudocolor image. Ca^{2+} influx was observed only in the trasfected cells (*red cells*) by 102.8% stretch. (**c**) The representative traces are shown in the graph (both transfected and non-transfetced cells). These figures are cited and modified by a previous report (10).

3.3.2. In Ovo Electroporation

In ovo electroporation was performed as described previously (17).

1. Chicken eggs were windowed, small amounts of EGFP-reporter plasmids were injected in the neural tube lumen in chick embryos at the HH 10–14 with 0.05% fast green (Fig. 3a), and the injected DNA was unilaterally pulse-electroporated (35 mV, 5 times, 50 ms duration with 950 ms intervals).
2. The window was sealed with adhesive tape and the eggs were returned to the incubator (38.5°C) for further incubation. The bodies of embryos were dissected after 1 day, and the EGFP-leveled axon length was measured and quantified (Fig. 3b).

3.4. Fluorescent Measurements and Electrophysiology

Fura2 fluorescence was measured by Fura2-AM (Molecular Probes, Carlsbad, CA) in a standard bath solution as described above. The 340:380 nm ratio was recorded. Whole-cell recording data were sampled at 10 kHz and filtered at 5 kHz for analysis (Axon 200B amplifier with pCLAMP software, Axon Instruments, Foster City, CA).

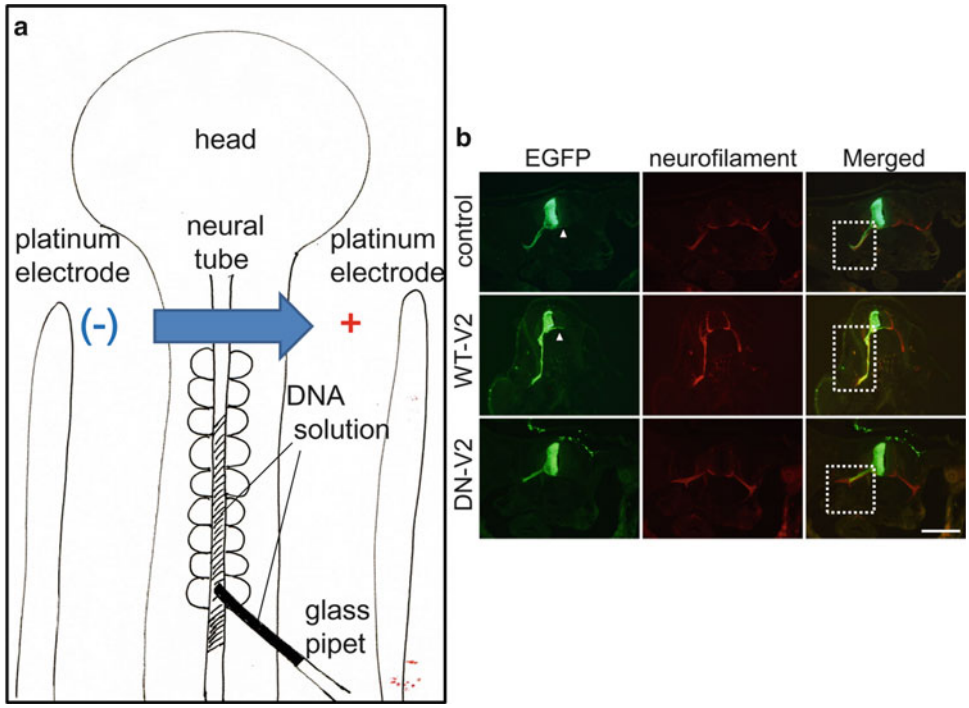

Fig. 3. *In ovo* electroporation revealed that TRPV2 was involved in axonal outgrowth through its activation by membrane stretch. (**a**) Schematic drawing of in ovo electroporation method. Egg shells were broken by scissors, and the chick embryos were visualized. DNA solution (5 mg/mL) was injected into the neural tube by glass pipette (the author used mouth glass pipet-like ES cell injection for KO mice generation). After DNA injection (you can check by the color of Fastgreen), platinum electrodes were placed both sides of the embryo. Then, five square pulses (33 mV) of 50-ms duration with 950-ms intervals were applied by a pulse generator, ECM830 (BTX). The egg shells were sealed by tapes, and the eggs were incubated for 24 h at 38.5°C. (**b**) Representative images of motor neurons, which were identified by neurofilament expression (*red*) in chick embryos; a control spinal cord tissue expressing EGFP, a tissue expressing wild type TRPV2 **(**WT-V2) and a tissue expressing dominant negative TRPV2 (DN-V2). *Arrowheads* indicate commissure axons. All plasmid DNAs were incorporated by electroporation in ovo at HH 10–14 stages. After 1 day, chick embryos were fixed and tissue sections were prepared. WT-V2 expression significantly enhanced axon outgrowth compared with EGFP (*dashed square*), but DN-TRPV2 expression significantly reduced axon outgrowth compared with EGFP (*dashed square*). Scale bar, 1 mm. These figures are cited and modified by a previous report (10).

4. Notes

1. The silicon chambers, which were used for membrane stretch experiments, must be coated by fibronectin.
2. The silicon chambers can be used repeatedly after wash and pasteurized.
3. Power of uniform stretch was determined by distance of each slide glass (see Fig. 2a) in bottom of the silicon chamber.
4. For *in ovo* electroporation, you must make fine glass pipettes. The pipette resistance should be over 15 Mohm (if you can check by patch-clamp).

5. After you purchased the fertilized chicken eggs, you have to keep those at 38.5°C for 3 days. The embryos located to top of the eggs. So you must carefully consider where you would like to make windows for the manupuration.
6. If you need long culture for in ovo electroporation, you have to transfer the embryos to the other egg shells.
7. If the response is too small in Ca^{2+}-imaging experiments, you should add 0.02% (v/v) pluronic F-127 (in 140 mM NaCl, 5 mM KCl, 2 mM $CaCl_2$, 2 mM MgCl2, 10 mM HEPES, and 10 mM glucose, pH 7.4, adjusted with NaOH). This manupuration greatly enhances the response.

References

1. Smith DH (2009) Stretch growth of integrated axon tracts: extremes and exploitations. Prog Neurobiol 89:231–239
2. Suter DM, Miller KE (2011) The emerging role of forces in axonal elongation. Prog Neurobiol 94:91–101
3. Bray D (1984) Axonal growth in response to experimentally applied mechanical tension. Dev Biol 102:379–389
4. Lamoureux P, Buxbaum RE, Heidemann SR (1989) Direct evidence that growth cones pull. Nature 340:159–162
5. Pfister BJ, Iwata A, Meaney DF, Smith DH (2004) Extreme stretch growth of integrated axons. J Neurosci 24:7978–7983
6. Pfister BJ, Bonislawski DP, Smith DH, Cohen AS (2006) Stretch-grown axons retain the ability to transmit active electrical signals. FEBS Lett 580:3525–3531
7. Gordon-Weeks PR (ed) (2000) Neuronal growth cones. Cambridge University Press, Cambridge
8. Sunderland IR, Brenner MJ, Singham J, Rickman SR, Hunter DA, Mackinnon SE (2004) Effect of tension on nerve regeneration in rat sciatic nerve transection model. Ann Plast Surg 53:382–387
9. Yi C, Dahlin LB (2010) Impaired nerve regeneration and Schwann cell activation after repair with tension. Neuroreport 21:958–962
10. Shibasaki K, Murayama N, Ono K, Ishizaki Y, Tominaga M (2010) TRPV2 enhances axon outgrowth through its activation by membrane stretch in developing sensory and motor neurons. J Neurosci 30:4601–4612
11. Muraki K, Iwata Y, Katanosaka Y, Ito T, Ohya S, Shigekawa M, Imaizumi Y (2003) TRPV2 is a component of osmotically sensitive cation channels in murine aortic myocytes. Circ Res 93:829–838
12. Mihara H, Boudaka A, Shibasaki K, Yamanaka A, Sugiyama T, Tominaga M (2010) Involvement of TRPV2 activation in intestinal movement through nitric oxide production in mice. J Neurosci 30:16536–16544
13. Naruse K, Yamada T, Sokabe M (1998) Involvement of SA channels in orienting response of cultured endothelial cells to cyclic stretch. Am J Physiol 274:H1532–H1538
14. Shibasaki K, Suzuki M, Mizuno A, Tominaga M (2007) Effects of body temperature on neural activity in the hippocampus: regulation of resting membrane potentials by transient receptor potential vanilloid 4. J Neurosci 27:1566–1575
15. Matsuda T, Cepko CL (2004) Electroporation and RNA interference in the rodent retina in vivo and in vitro. Proc Natl Acad Sci USA 101:16–22
16. Nakahira E, Kagawa T, Shimizu T, Goulding MD, Ikenaka K (2006) Direct evidence that ventral forebrain cells migrate to the cortex and contribute to the generation of cortical myelinating oligodendrocytes. Dev Biol 291:123–131
17. Itasaki N, Bel-Vialar S, Krumlauf R (1999) 'Shocking' developments in chick embryology: electroporation and in ovo gene expression. Nat Cell Biol 1:E203–E207

Chapter 15

Methods in Neuronal Growth Cone Biology

Robert J. Gasperini and Lisa Foa

Abstract

Axon guidance is a crucial component of normal nervous system development. Errors in axon guidance can result in disorders such as autism and schizophrenia. In order to understand the pathogenesis of these disorders, we need to understand the fundamental mechanisms of growth cone motility, which ultimately direct axon guidance. In this chapter, we describe protocols and methods that our laboratory uses to study normal growth cone physiology and biochemistry. We describe the "pipette" turning assay [Lohof AM, Quillan M, Dan Y, Poo MM, J Neurosci 12(4): 1253–1261, 1992] that we have adapted for primary cultures of rodent dorsal root ganglia. We also describe methods for calcium imaging of growth cones and provide data to demonstrate the absolute requirement of TRP channels for growth cone navigation. These techniques provide researchers with considerable scope and flexibility in experimental design and can be adapted to provide high-throughput biochemical data for the elucidation of mechanisms governing the action of guidance molecules.

Key words: Growth cones, Axon guidance, Turning assay, Neuronal development, TRPC

1. Introduction

During embryonic development, the process of connecting the millions of neurons that comprise the precise network of our nervous system begins. Axon guidance is crucial to this process. Each developing neuron extends an axon that is tipped with a highly specialized navigational organ, the growth cone. This membranous structure responds to repulsive and attractive chemotactic guidance cues that may be substrate bound or gradients of soluble, diffusible molecules. Growth cones are physiologically relevant cell structures that allow researchers a high level of microscopic access to many important membrane-associated channels and signaling domains. Understanding the cellular signaling mechanisms that regulate growth cone responses to these cues is vital if we are to understand the mechanisms of development that underpin

Arpad Szallasi and Tamás Bíró (eds.), *TRP Channels in Drug Discovery: Volume II*, Methods in Pharmacology and Toxicology,
DOI 10.1007/978-1-62703-095-3_15,

neurodevelopmental diseases such as autism, mental retardation, and schizophrenia.

Most guidance cues alter growth cone motility by eliciting an asymmetric rise in calcium and subsequent second messenger signals across the growth cone (1), with growth cone motility biased towards the side of high intracellular calcium (2–4). Determining the source and molecular basis of spatial and temporal regulation of calcium signals is key to understanding growth cone navigation and axon guidance. It is now clear that activation of transient receptor potential (TRP) channels is important in the early signaling events that transduce the guidance cue signal to changes in growth cone motility.

Calcium entry through TRP channels in growth cone navigation has been clearly demonstrated in a variety of neurons, including Xenopus spinal neurons, rat cerebellar neurons, and sensory neurons from dorsal root ganglia (5–7). Exactly which TRP channels are required for growth cone navigation is likely to depend on neuronal subtype and temporal gradients during development. In cerebellar granule cells, TRPC3 and TRPC6 are necessary for growth cone turning towards brain-derived neurotrophic factor (BDNF) (5). In dorsal root ganglion neurons, TRPM8 channels mediate calcium responses induced by transthyretin protein in growth cones (8). However, most studies on TRP function in growth cones have used relatively nonspecific inhibitors, such as SKF96365 (9), and hence the full extent of TRP requirement for growth cone motility remains to be determined. Although TRPs have been shown to be necessary for growth cone navigation, the exact molecular transduction of guidance cue receptor to TRPC gating is still unclear (1, 5, 6). Recent evidence suggests that BDNF activation of the tyrosine kinase type B (TrkB) receptors and calcium influx via TRPCs requires phospho-inositide 3-kinase (Pi3K) activation of phosphatidylinositol-(3,4,5)-trisphosphate (PIP_3) and Akt (10).

TRP channel activation is thought to be important in the regulation of basal, or resting calcium, which is buffered at extremely low concentrations in growth cones. This buffering ensures a dynamic signal-to-noise ratio of growth cone calcium, so that small changes in calcium are instructive (1, 11). The postsynaptic calcium-regulatory protein, Homer1b/c, contributes to basal cytosolic calcium by gating the activity of TRPC channels (7). In HEK293 cells, Homer couples TRPC channels with the inositol triphosphate receptor (IP_3R) on the endoplasmic reticulum membrane (12). When bound in this conformation, spontaneous activity of TRPC channels is reduced, contributing to the low basal cytosolic calcium levels in resting cells. Upon receptor activation or internal calcium store depletion, the Homer-TRPC-IP_3R complex dissociates, promoting calcium influx via TRPC channels and IP_3R activation

(12). Similarly in neurons, reducing Homer expression results in growth cones being repelled from a gradient source of BDNF, a molecule which is normally chemoattractive (7). Calcium imaging of growth cones has demonstrated that reduced expression of Homer1b/c results in the spontaneous activity of SKF96365-sensitive channels, likely TRPC channels (7). This evidence confirms that TRP channels are important in the maintenance of basal cytosolic calcium in growth cones and hence vital to growth cone navigation.

The study of growth cone motiltiy is not only important for an understanding of axon guidance, but growth cones are also an excellent model for understanding the dynamics of protein interactions in neuronal membranes. Growth cone guidance in vitro has been studied extensively since the 1970s. Many studies focused on growth cone contact with bound substrates or other cell types (13–18). However as noted above, growth cones in vivo respond not only to contact with the extracellular matrix and other cells, but they also respond to gradients of soluble guidance cues. Early chemotactic assays demonstrated that growth cones would turn towards a source of soluble nerve growth factor (19). While early assays were relatively crude, they clearly demonstrated that growth cones would re-orient towards soluble sources of guidance cues such as NGF. The "pipette" turning assay was refined by the Poo laboratory in 1992 (20) and that paper has formed the basis of "pipette" assays that we use today. The gradients produced by the "pipette" assay are likely to be substantially steeper than the gradients found in vivo (21). Consequently, there have been several attempts to develop assays that better represent the 3-dimensional, shallow gradients that growth cones are more likely exposed to in vivo (21, 22). Steepness of molecular gradients notwithstanding, the original assay described by Lohoff et al. (20) has proven invaluable in deciphering many of the cell signaling mechanisms that are necessary for growth cone guidance, findings which have subsequently been extended in vivo to spinal cord regeneration (23, 24).

2. Materials

2.1. Equipment

1. Micropipettes are pulled using microprocessor-controlled puller, P-87 (Sutter Instrument Co., USA) from borosilicate glass capillaries with an internal filament, an outer diameter of 1.0 mm and internal diameter of 0.58 mm (Harvard Instruments, USA).
2. Micropipettes are polished to nominal tip openings of 1.5–2.5 μm using a microforge, MF-830 (Narashige, Japan).

3. Imaging dishes: Using a bench-top lathe, A 10 mm hole is bored through the base of 35 mm plastic petri dishes (Iwaki, Asahi, Japan). 13 mm, acid washed #1 coverslips are glued to the underside of dishes using an acid-cure silicone glue (3 M). Alternatively, dishes can be purchased in a variety of formats from MatTek Corporation, USA.
4. Micropipettes are positioned in dishes using a micromanipulator (M3, Narashige, Japan).
5. Pressure pulses to micropipettes are controlled by a pressure delivery system (Picospritzer, Parker-Hanniffin Corp., USA).
6. Tissue culture incubator conditions should be controlled to 37°C and 5% CO_2.
7. Growth cone turning experiments are performed using phase contrast optics on an inverted microscope (Optiphot, Nikon). Images are acquired using a monochrome video camera (PCO, Switzerland) and custom software (MatLab, MathWorks, USA).
8. Calcium imaging experiments are performed using an attenuated (33% transmission) 340 and 380 nm wavelength illumination source (Lambda DG-4, Sutter). Images are acquired sequentially at 510 nm using an EMCCD camera (Evolve, Photometrics) and inverted microscope (Eclipse TiE; Nikon Instruments) using a 40× Fluor-S oil-immersion objective (Nikon).

2.2. Reagents and Solutions

1. Coverslips are coated with poly-ornithine (1 mg/ml, Sigma) and laminin (100 μg/ml, Gibco).
2. Dissociated neurons from dorsal root ganglia are cultured in sensory neuron medium (SNM) which consists of Dulbecco's Modified Eagle Medium / Ham's F-12 medium 1:1 (SAFC Biosciences), fetal calf serum (5%v/v), penicillin G (100 U/ml), streptomycin (100 μg/ml), nerve growth factor (NGF, 50 ng/ml, Sigma-Aldrich), and N2 neural medium supplement (Gibco).
3. A variety of guidance cues can be used to establish chemotactic gradients. Here, we use BDNF (10 μg/ml, Alomone Laboratories), netrin-1 (5 μg/ml, R+D Systems), phorbol 12-myristate 13-acetate (PMA, 100 nM, Sigma Aldrich), sema-3a (20 ng/ml, R+D Systems), glutamate (1 mM, Sigma Aldrich).
4. Calcium indicator: Fura-2 AM (Molecular Probes, Invitrogen).
5. Calcium imaging buffer is prepared from Hanks Balanced Salt Solution (HBSS, Gibco) supplemented with calcium chloride (2 mM), magnesium chloride (1.2 mM), HEPES (10 mM), glucose (5 mM), nerve growth factor (NGF, 50 ng/ml), and N2 supplement (Invitrogen).

3. Methods

3.1. Preparation of Imaging Dishes

Growth cones are thin membranous structures, and hence it is necessary to maximize imaging resolution in order to view growth cone filopodia and lamellipodia. To do this we use custom-made imaging dishes.

1. Wash dishes in ethanol and rinse in sterile water and UV sterilize. Coat the coverslip glass at the base of the well in poly-ornithine overnight, rinse and allow to dry.
2. The dishes at this point can be stored for several days prior to use.
3. On the day of imaging, coat the coverslip wells with laminin and incubate at 37°C and 5% CO_2 for 1–2 h. Wash laminin immediately prior to cell plating.

3.2. Cell Culture

Primary cultures of dissociated sensory neurons from thoracic dorsal root ganglia are derived from embryonic day 16–18 (E16–18) Hooded Wistar or Sprague–Dawley rat embryos.

1. Dissect ganglia from decapitated embryos (Note 1). Pin into dissection dishes, bathed in DMEM-F12 tissue culture medium or HBSS.
2. Remove the skin and meninges overlying the spinal column and remove the spinal cord, exposing the ganglia.
3. Extract the ganglia, picking them from the nerve roots.
4. Place whole ganglia into 200 µl of SNM, in a microcentrifuge tube. Mechanically dissociate ganglia by trituration through 200 µl pipette tip.
5. Plate cells at low density onto poly-ornithine and laminin-coated glass coverslips within imaging dishes (100 µl per dish).
6. Incubate cells for 1 h in a 5% CO_2/95% room air incubator at 37°C then supplement with an additional 2 ml of media and incubate for a further 2–3 h.
7. Transfer cultures to microscope for imaging. Maintain cultures at 37°C throughout the imaging session.
8. Image only isolated growth cones from actively protruding axons.

3.3. Micropipettes

Micropipettes are used to develop microgradients of guidance cues and are made from borosilicate glass capillaries with an internal filament. Capillary glass of various dimensions can be used; however, consistent pipettes are pulled from 1.0 mm OD × 0.58 mm ID glass.

1. Pull micropipettes using the microprocessor-controlled puller.
2. Fire-polish the pipette orifice to an opening of 1.0–2.0 µm with a microforge (Fig. 1).

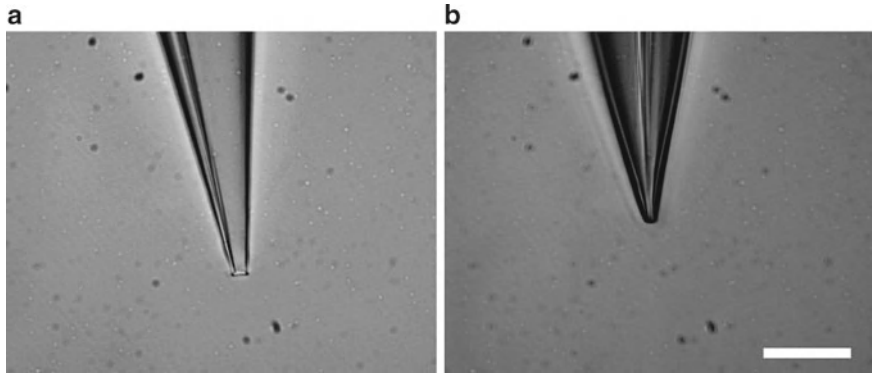

Fig. 1. Manufacture of pipettes used in microgradient preparation. The dimensions and tip opening profiles of typical micropipettes manufactured for the growth cone turning assay. (**a**) Bright field image representing a typical micropipette pulled with the microprocessor controlled puller. (**b**) shows the same pipette after the tip had been fire-polished and shaped in a microforge. Scale bar is 10 μm.

3.4. Growth Cone Turning Assay

Growth cone turning assays are performed as previously described (20), modified slightly for neurons derived from dorsal root ganglia. The assay can be set up using any known or novel guidance cue. Experimental parameters that should be controlled to ensure consistency of microgradients include air pressure supplied to the micropipette, pulse duration, and pulse frequency. Concentrations of guidance cue molecules at the growth cone are estimated to be 10^{-3} of micropipette concentrations (20). To illustrate the gradient of guidance cue, we have used the dye, trypan blue, in an aqueous phosphate-buffer. Using previously published ejection parameters of 10 ms pulses and 5 psi pressure (20), a circular bolus of dye was ejected and was observed to rapidly disperse into the surrounding medium (Fig. 2a). In order to determine the precision of the ejections, 8-bit grayscale images were captured at 140 ms intervals and a circular area, 25 μm in radius approximating the visible dye bolus, was quantitated. Analysis of the average pixel intensities showed slight variability in the maximal dye concentration of each repetitively ejected bolus. However, the area of each response over time appeared consistent, suggesting the total mass of dye ejected was similar (Fig. 2b).

To more fully explore the characteristics of microgradients, especially at the outer margins where growth cones would be predicted to encounter guidance cue molecules, the gradient profile of the plume was assessed as a line scan, originating radially from the pipette tip to the visible plume margins, rather than the integrated pixel intensity of the visible dye bolus area. The line scan approach would be predicted to more closely approximate the concentration profile or gradient of dye concentration. Analysis of the dye concentration close to the tip (<10 μm) shows a linear decay profile over time but a more nonlinear decay profile at greater (>25 μm)

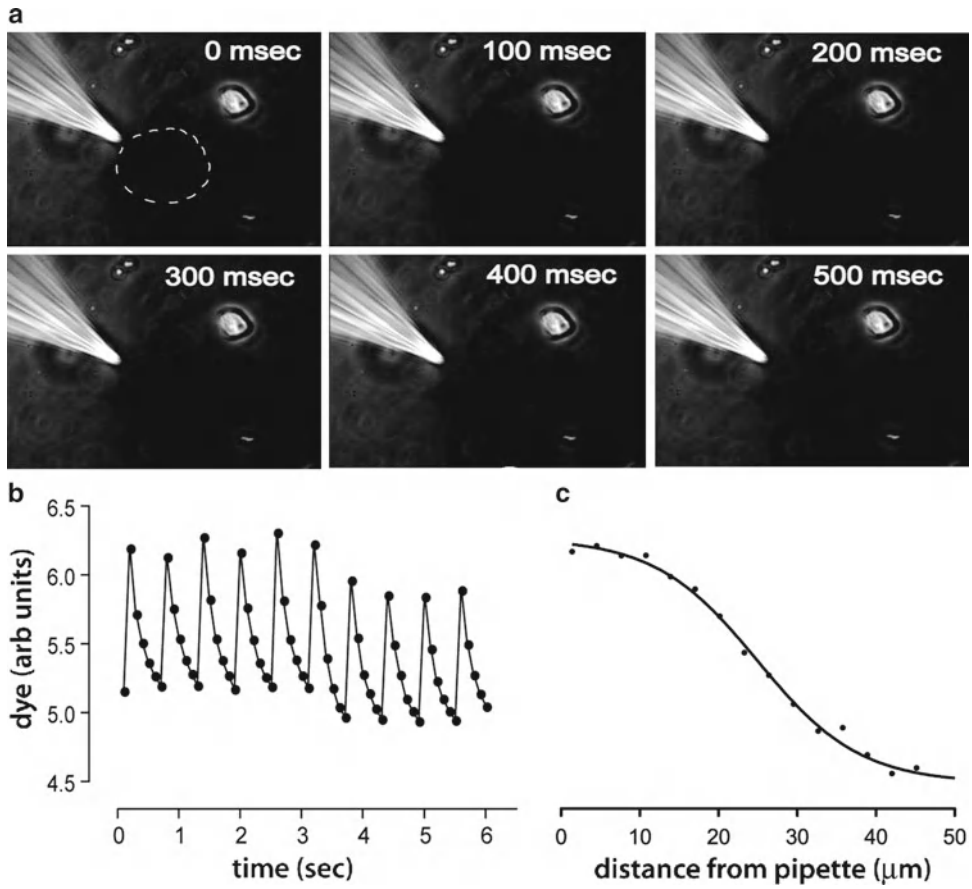

Fig. 2. Pulsatile ejection of dye with a micropipette in vitro. (**a**) A sequence of images taken at 100 ms intervals and demonstrating the decay of a dye plume concentration after pulsatile ejection from a micropipette. Pulse occurred at 0 ms. Decay of dye plume concentration is visually apparent by 400 ms after ejection. *Dotted line* represents circular area used to quantify dye concentration. Scale bar is 10 μm. (**b**) Figure demonstrating the variation in dye concentration in multiple, repetitive dye injection. The *circular area* defined in Fig. 1a was used as a measure of the visible dye bolus and its mean pixel value was calculated following ten successive pulsatile ejections. Time interval is 140 ms. (**c**) Figure shows an estimation of dye concentration as a function of distance from micropipette tip. Decay of concentration close to the pipette proceeds in a linear manner, although the linearity of decay decreased with increasing distance from pipette tip.

distances from the tip (Fig. 2c). These observations are in good agreement with work previously done using fluorescent dextrans, confirming the microgradient profile of the proposed assay (20). The method for setting up the turning assay is:

1. As described in Sect. 3.2, place culture dish, containing cells on the microscope, using a heated stage to maintain 37°C.
2. Load the micropipette with 2–5 μl of the desired chemotactic agent or known guidance cue and attach the micropipette to the micromanipulator and picospritzer.

3. Lower the micropipette so that is clearly within the visible field of view, but outside the focal plane, while a suitable growth cone is identified (Note 2).
4. Position the selected growth cone in the center of the screen and lower the micropipette into position. Position micropipette tips 80–100 μm from growth cones and within 5–10 μm of the culture substrate, at a 45° angle to initial axon trajectory.
5. Set the stimulator to deliver 10 ms pulses and the picospritzer pressure at 5 psi. This will produce the microgradient of guidance cues.
6. Acquire images every 7 s for 30 min using image acquisition software. Maintain focus on the growth cone throughout the imaging period. Light intensity should be adjusted using neutral density filters to achieve low levels of illumination thereby avoiding nonspecific phototoxic damage and aberrant turning of growth cones.
7. Analyze data using ImageJ (NIH), measuring turning angles, axon extensions. Only analyze growth cones that extend at least 10 μm within the 30 min imaging period. Turning angles are defined as the change in axon trajectory of the distal 10 μm of axon compared to the initial starting trajectory. Attraction and repulsion are designated positive and negative angles, respectively.
8. Use an appropriate test of statistical significance, such the Mann–Whitney U-test (Prism 4, GraphPad Software) to analyze turning angles, comparing each treatment to the control.

Here, we show an example in which DRG growth cones turn in response to microgradients of BDNF, netrin-1, PMA, sema-3a, and glutamate, compared to a control exposure of SNM (Fig. 3). Embryonic rat sensory neurons from wild-type thoracic DRG were prepared as described. After plating, cells extended lengthy axons with effusive growth cones exhibiting highly motile fillopodial and lamellapodial behaviors within the 30 min assay period. DRG growth cones showed robust chemoattraction towards BDNF, netrin-1, and glutamate, when compared to a control gradient of SNM, and robust chemo-repulsion in gradients of sema-3a and PMA (Fig. 1a). Graphical representations of growth cone responses in this turning assay were represented as histograms showing mean turning angles (Fig. 1b) and axon extension (Fig. 1c). Turning angles were calculated 30 min after initiation of a microgradient. Axon extension rates were not significantly different between treatments, indicating that the general cellular health of DRGs was not compromised during the assay. Both average turning angles and axon extension rates were similar to responses seen in other cells such as rat cerebellar granule cells and *Xenopus* spinal neurons (5, 6, 25), confirming that DRG are an excellent model for studying

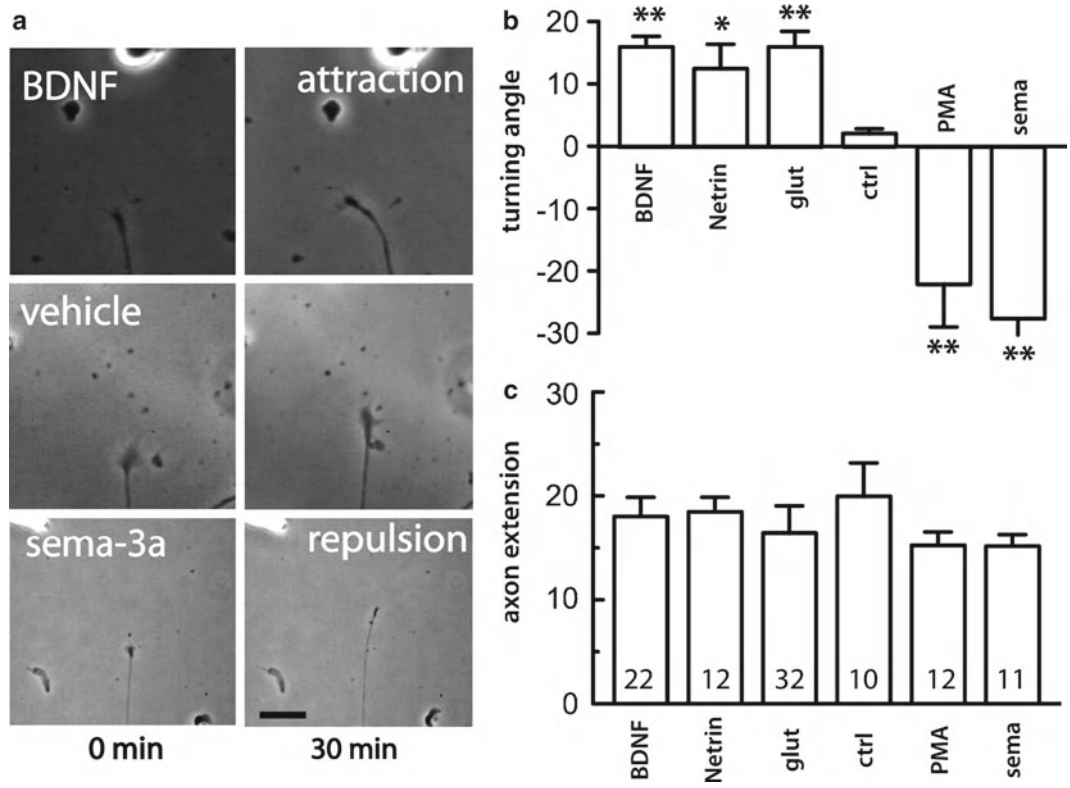

Fig. 3. Motile responses of DRG sensory neurons in the turning assay. Motile turning responses of wild-type DRG neurons to netrin-1, BDNF, glutamate, sema-3a, PMA, and vehicle microgradients in the growth cone turning assay. BDNF, netrin, and glutamate caused attraction while sema-3A and PMA induced repulsion of DRG growth cones. Vehicle control gradient induced random turning responses. Positive angles represent attraction and negative angles represent repulsion. (**a**) Phase contrast images at the initiation of microgradient (0 min) and at the termination of the assay (30 min). (**b**–**c**) Histograms depicting DRG neuron turning (**b**) and extension responses (**c**) (mean, SEM and number of observations, *n*). Axon extension rates did not differ significantly between any of the guidance molecules tested after 30 min. Significant differences from control values are marked as: $*p<0.05$; $**p<0.005$; Mann–Whitney U-test. *Error bars* indicate SEM. Scale bar for (**a**) is 10 μm.

the mechanisms that govern axon path finding. Furthermore, the speed at which DRG neurons extend processes suggests that 30 min is a suitable imaging period, rather than the usual 1 h originally described for Xenopus spinal neurons (20).

3.5. Pharmacological or Molecular Modification of the Turning Assay

The turning assay can be modified by bath application of pharmacological agents, or by introducing genetic constructs, such as targeted morpholinos (Gene Tools) or siRNA into the cells during the trituration process. We typically use morpholinos to manipulate protein expression (Note 3). Morpholino oligonucleotides were originally developed to achieve stable protein knockdown in zebrafish and have now been used extensively in many vertebrate systems to effectively reduce protein expression without the

reported off-target effects observed with RNA interference (26). We find that 4–6 h of growth in the presence of a targeted morpholino reliably results in 50% reduction of protein expression (7).

1. For pharmacological manipulation of proteins, for example membrane ion channels, add agonists or antagonists to the bath prior to the start of the turning assay. Addition of large volumes during the assay will disrupt the guidance cue gradient.
2. For reduction in protein expression using morpholinos, add morpholinos (5–10 μM) to whole ganglia prior to trituration. Proceed with ganglia dissociation and plating as described above. Allow cells to grow for at least 4–6 h prior to the turning assay.

We show here an example of bath application of SKF96365 in a turning assay. This experiment demonstrates the necessity of TRP-like channels in growth cone turning. SKF96365 is a nonselective antagonist of TRPC channels and other store-operated channels (27). The addition of SKF96365 to the bath abolished attractive turning of DRG growth cones towards a microgradient of BDNF (Fig. 4). This data suggests that DRG growth cones rely on calcium influx through store-operated calcium channels. These results are consistent with known function of TRPC in motile growth cones. Calcium dependent turning of *Xenopus* spinal neurons requires

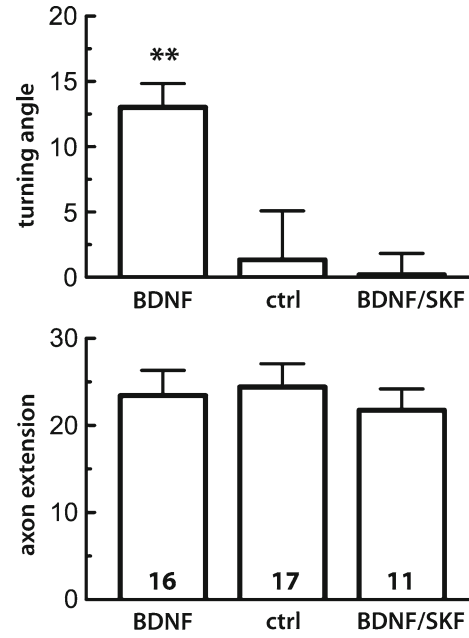

Fig. 4. SKF96365-sensitive calcium channels are necessary for BDNF-mediated growth cone motility. (**a**) Growth cone turning towards BDNF is abolished when SKF96365-sensitive channels are inactivated. (**b**) SKF treatment is specific to turning since axon extension rates do not differ significantly from BDNF only or control experiments. Significant differences are marked as: $*p<0.005$; Mann–Whitney U-test. *Error bars* indicate SEM.

xTRPC1 signaling (6, 25). In cerebellar granule cells, the calcium-dependent guidance cue BDNF signals through TRPC3 and TRPC6 channels (5). These studies concluded that BDNF and netrin-1, via respective TrkB and DCC receptors, either directly or indirectly activate TRPC, which in turn activate calcium signaling in the growth cone (5, 6, 25). More recent work suggests the activation of TRPCs by BDNF is likely indirect, via PI3K and Akt (10). It is likely that the cellular context will determine which TRP channels are required for growth cone motility.

3.6. Calcium Imaging

Most guidance cues alter growth cone motility by eliciting an asymmetric rise in calcium and subsequent second messenger signals across the growth cone (reviewed in (1)). Growth cone direction is biased towards the high calcium side of the growth cone (2–4). Determining the source of calcium and molecular basis of the spatial and temporal regulation of calcium signals is key to understanding growth cone navigation and axon guidance. The example shown in Fig. 5 was prepared as described below. It demonstrates a global rise in intracellular calcium in response to a microgradient of BDNF.

1. Transfer plated DRG neurons to a room temperature solution of Fura-2 AM (5 μM, Invitrogen) in serum-free SNM and incubate for 20 min at 37°C.
2. Wash cells once with fresh SNM and incubate for a further 30 min at 37°C to allow complete de-esterification.
3. Mount onto an imaging chamber and exchange SNM for Imaging buffer, which is used for all calcium imaging experiments. All experiments are carried out at 37°C.
4. Move culture in imaging chamber to the inverted microscope (Eclipse TiE; Nikon Instruments) equipped with heated stage or an environment-controlled chamber (Clear State Solutions, Australia).
5. Image growth cones with alternate excitation using an attenuated (33% transmission) 340 and 380 nm wavelength illumination source (Lambda DG-4, Sutter).
6. Acquire images (5–25 ms) at 510 nm using an EMCCD digital camera (Evolve, Photometrics) using a 40xFluor-S oil-immersion objective (Nikon) equipped with DIC optics. To acquire images, use a frame rate of 1 Hz and define regions of interest (ROIs) using NIS Elements 6D software (Nikon).
7. Using appropriate software, perform background subtraction. Calculate fluorescence ratio (R) for each ROI as the intensity of emission during 340 nm excitation divided by intensity of emission during 380 nm, on a pixel-by-pixel basis.
8. Estimate calcium concentrations using the formula:

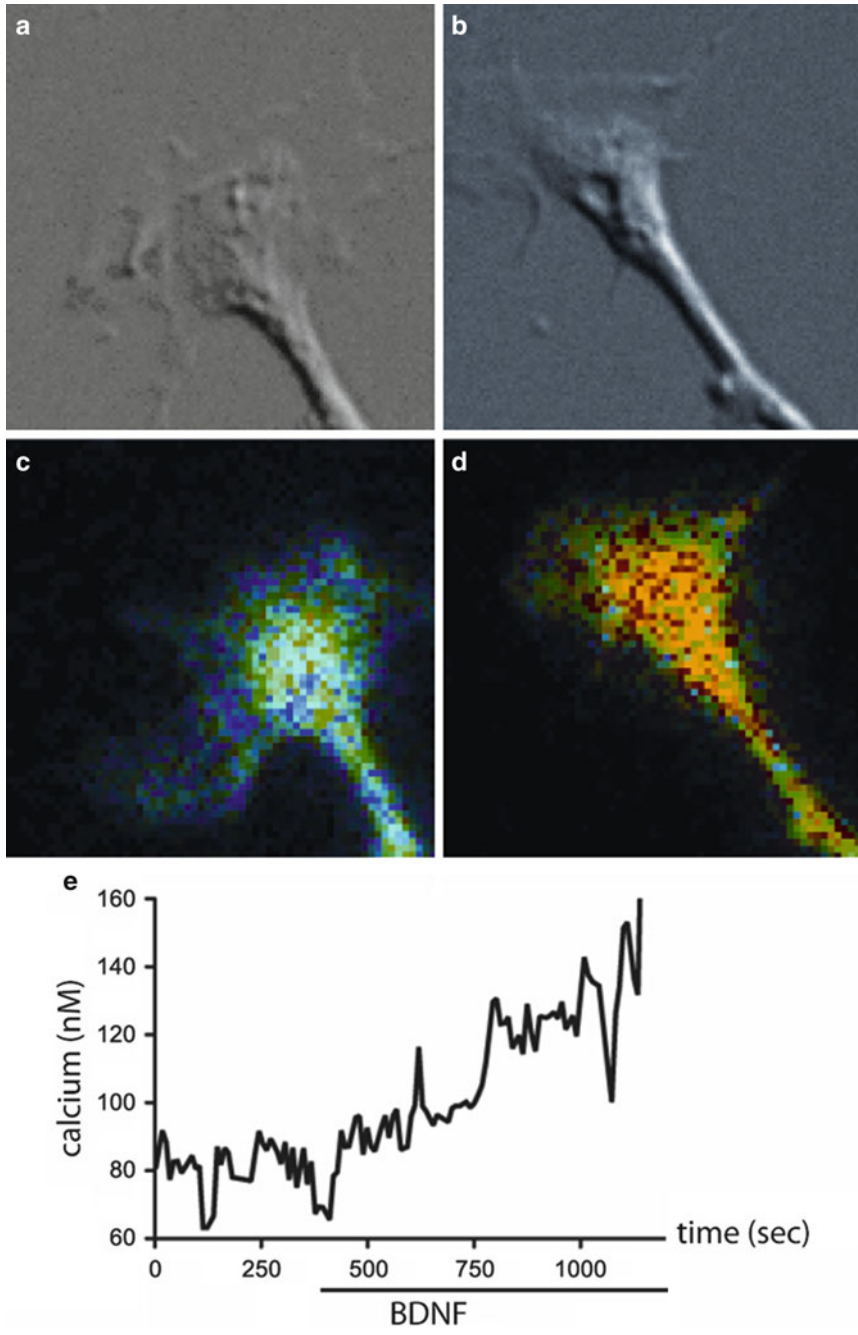

Fig. 5. BDNF induces a global rise in intracellular calcium in growth cones. (**a**–**b**) DIC images of a growth cone before and after initiation of a BDNF microgradient. (**c**–**d**) Pseudo-colored images depicting global increase in growth cone calcium concentration following BDNF gradient initiation. (**e**) Estimation of intracellular calcium concentration over time after initiation of BDNF gradient.

$$[\text{Calcium}] = K_{(\text{eff})} \times \frac{R - R_{\min}}{R_{\max} - R}$$

where $K_{(\text{eff})}$ describes an effective binding constant Kd (224 nM at 37°C) × (F380 at saturable calcium/F380 at low calcium), R is the ratio at 340/380 nm at the current time point, $R_{\min}$ and $R_{\max}$ are the calculated ratios at 340/380 nm of cells at saturable and minimal cytosolic calcium concentrations.

9. Use statistical software such as Prism 5 (Graph-Pad Software) for graphical and statistical analysis of data.

4. Notes

1. When dissecting ganglia, remove all possible traces of meninges and nerve roots.
2. When selecting growth cones for imaging, ensure that they are in the center of the camera field of view. Ensure that the growth cone is not caught up on any cellular debris on the substrate.
3. When using morpholinos to reduce protein expression within cells, a targeted morpholino should be used in the treatment group and a mispaired morpholino for the control group. Protein knockdown should always be verified with immunocytochemistry and western analysis. Similarly if using siRNA, a control siRNA should always be included and knockdown should be verified and demonstrated.
4. Perform calcium-free experiments in calcium-free imaging buffer supplemented with 300 μm EGTA.

Acknowledgments

This work was supported by the NHMRC grant # 512801 and a grant from the Ian Potter Foundation to LF. RJG was supported by an Australian Government Postgraduate Award.

References

1. Tojima T, Hines JH, Henley JR, Kamiguchi H (2011) Second messengers and membrane trafficking direct and organize growth cone steering. Nat Rev Neurosci 12(4): 191–203
2. Gomez TM, Robles E, Poo M, Spitzer NC (2001) Filopodial calcium transients promote substrate-dependent growth cone turning. Science 291(5510):1983–1987
3. Gomez TM, Zheng JQ (2006) The molecular basis for calcium-dependent axon pathfinding. Nat Rev Neurosci 7(2):115–125
4. Zheng JQ (2000) Turning of nerve growth cones induced by localized increases in

intracellular calcium ions. Nature 403(6765): 89–93

5. Li Y, Jia Y-C, Cui K, Li N, Zheng Z-Y, Wang Y-Z et al (2005) Essential role of TRPC channels in the guidance of nerve growth cones by brain-derived neurotrophic factor. Nature 434(7035):894–898
6. Wang GX, Poo M-M (2005) Requirement of TRPC channels in netrin-1-induced chemotropic turning of nerve growth cones. Nature 434(7035):898–904
7. Gasperini R, Choi-Lundberg D, Thompson MJW, Mitchell CB, Foa L (2009) Homer regulates calcium signalling in growth cone turning. Neural Dev 4:29
8. Gasperini RJ, Hou X, Parkington H, Coleman H, Klaver DW, Vincent AJ et al (2011) TRPM8 and Nav1.8 sodium channels are required for transthyretin-induced calcium influx in growth cones of small-diameter TrkA-positive sensory neurons. Mol Neurodegener 6(1):19
9. Zhu X, Jiang M, Birnbaumer L (1998) Receptor-activated Ca^{2+} influx via human Trp3 stably expressed in human embryonic kidney (HEK)293 cells. Evidence for a non-capacitative Ca^{2+} entry. J Biol Chem 273(1):133–142
10. Henle SJ, Wang G, Liang E, Wu M, Poo M-M, Henley JR (2011) Asymmetric PI(3,4,5)P3 and Akt signaling mediates chemotaxis of axonal growth cones. J Neurosci 31(19):7016–7027
11. Gomez TM, Snow DM, Letourneau PC (1995) Characterization of spontaneous calcium transients in nerve growth cones and their effect on growth cone migration. Neuron 14(6):1233–1246
12. Yuan JP, Kiselyov K, Shin DM, Chen J, Shcheynikov N, Kang SH et al (2003) Homer binds TRPC family channels and is required for gating of TRPC1 by IP3 receptors. Cell 114(6):777–789
13. Challacombe JF, Snow DM, Letourneau PC (1996) Actin filament bundles are required for microtubule reorientation during growth cone turning to avoid an inhibitory guidance cue. J Cell Sci 109(Pt 8):2031–2040
14. Challacombe JF, Snow DM, Letourneau PC (1997) Dynamic microtubule ends are required for growth cone turning to avoid an inhibitory guidance cue. J Neurosci 17(9):3085–3095
15. Letourneau PC (1978) Chemotactic response of nerve fiber elongation to nerve growth factor. Dev Biol 66(1):183–196
16. Gomez T, Letourneau P (1994) Filopodia initiate choices made by sensory neuron growth cones at laminin/fibronectin borders in vitro. J Neurosci 14(10):5959–5972
17. Burden-Gulley SM, Lemmon V (1996) L1, N-cadherin, and laminin induce distinct distribution patterns of cytoskeletal elements in growth cones. Cell Motil Cytoskeleton 35(1): 1–23
18. Brittis PA, Lemmon V, Rutishauser U, Silver J (1995) Unique changes of ganglion cell growth cone behavior following cell adhesion molecule perturbations: a time-lapse study of the living retina. Mol Cell Neurosci 6(5):433–449
19. Gundersen R, Barrett J (1979) Neuronal chemotaxis: chick dorsal-root axons turn toward high concentrations of nerve growth factor. Science 206:1079
20. Lohof AM, Quillan M, Dan Y, Poo MM (1992) Asymmetric modulation of cytosolic cAMP activity induces growth cone turning. J Neurosci 12(4):1253–1261
21. Rosoff WJ, Urbach JS, Esrick MA, McAllister RG, Richards LJ, Goodhill GJ (2004) A new chemotaxis assay shows the extreme sensitivity of axons to molecular gradients. Nat Neurosci 7(6):678–682
22. Mai J, Fok L, Gao H, Zhang X, Poo M-M (2009) Axon initiation and growth cone turning on bound protein gradients. J Neurosci 29(23):7450–7458
23. Ming GL, Song HJ, Berninger B, Holt CE, Tessier-Lavigne L, Poo MM (1997) cAMP-dependent growth cone guidance by netrin-1. Neuron 19(6):1225–1235
24. Qiu J, Cai D, Dai H, McAtee M, Hoffman PN, Bregman BS et al (2002) Spinal axon regeneration induced by elevation of cyclic AMP. Neuron 34(6):895–903
25. Shim S, Goh EL, Ge S, Sailor K, Yuan JP, Roderick HL et al (2005) XTRPC1-dependent chemotropic guidance of neuronal growth cones. Nat Neurosci 8(6):730–735
26. Alvarez VA, Ridenour DA, Sabatini BL (2006) Retraction of synapses and dendritic spines induced by off-target effects of RNA interference. J Neurosci 26(30):7820–7825
27. Merritt JE, Armstrong W, Benham C, Hallam TJ, Jacob R, Jaxa-Chamiec A et al (1990) SK&F 96365, a novel inhibitor of receptor-mediated calcium entry. Biochem J 271(2): 515–522

Part III

TRPs and Skin

Chapter 16

Transient Receptor Potential Channels and Pruritus

Heike Benecke, Janine Wäring, Tobias Lotts, and Sonja Ständer

Abstract

Itch induction and allergy development are regulated by highly complex pathways that involve dynamic cross-talk events between cells within the skin. These include the transient receptor potential (TRP) ion channels. For example, the intensity, quality, and the clinical characteristics of itch, pain, and inflammatory sensations can be influenced by thermal stimuli within the activation range of thermo-sensitive TRP cannels. The thermo-TRP channel TRPV1 contributes to the regulation of the skin surface temperature which has a major impact on the epidermal permeability barrier. TRPV1 has an important role in the induction of histamine-mediated pruritus in sensory neurons while TRPV4 has a role to play in histamine-independent itch induction. The stimulation of TRPV2 on mast cells provokes pro-inflammatory degranulation events and subsequent release of histamine, thus directly promoting the induction of itch. TRPV3 is likely to have a crucial function in epidermal barrier formation and hair morphogenesis. TRPM8 and TRPA1 interfere with the induction of sensory sensations. Cutaneously expressed temperature sensors of the TRP channel family thus became an attractive target for pharmacological treatment of pruritic, inflammatory, and nociceptive processes.

Key words: Itch, Pruritus, Pain, Histamine, Capsaicin, Therapy

1. Introduction

Itch induction and allergy development are regulated by highly complex pathways that involve dynamic cross-talk events between cells within the skin. These include immunological and non-immunological cells such as keratinocytes which express and release pruritogenic mediators of allergy-evoked itch in humans and mice (reviewed in (1–5)). The transient receptor potential (TRP) ion channels have an important role in induction as well as relief of pain and itch. In humans, it was shown that the intensity, quality, and the clinical characteristics of itch, pain, and inflammatory sensations can be influenced by thermal stimuli within the activation

Arpad Szallasi and Tamás Bíró (eds.), *TRP Channels in Drug Discovery: Volume II*, Methods in Pharmacology and Toxicology,
DOI 10.1007/978-1-62703-095-3_16,

range of thermo-sensitive TRP cannels. Moreover, thermo-TRP channels contribute to the regulation of the skin surface temperature which has a major impact on the epidermal permeability barrier (6). Impaired formation and dysregulation of the epidermal barrier is an important trigger of pruritic skin. In addition, an important role of TRPV1 in the induction of histamine-mediated pruritus has been discovered (7). Cutaneously expressed temperature sensors of the TRP channel family thus became an attractive target for pharmacological treatment of pruritic, inflammatory, and nociceptive processes (8–10). For example, the TRPV1 agonist capsaicin has been used to treat chronic pruritus of different origins since a long time. However, the underlying molecular mechanisms responsible for the beneficial effects of TRP channel modulation in diseased skin have not been sufficiently elucidated yet.

Mammalian thermo-TRP channel physiology was largely studied in mice and rats which represent an appropriate model system of man. Most TRP channels expressed in rodents are conserved in humans (reviewed in (11–13)). Studies on their functional characterization in the recombinant system revealed comparable activation patterns and modulation or sensitization by similar physical and chemical stimuli. For example, topical application of the TRPV1 agonist capsaicin leads to nocifensive behavior when applied to human, mouse, or rat skin (reviewed in (13)). Thus, many recent studies focused on the creation of knockout and transgenic animals to study the physiological relevance of TRP channels for itch and allergy development and the contribution of specific pruriceptor-expressing cell populations. Several mouse models have already been described that appropriately fit the physiological data. However, a recent review provides a comprehensive summary of the model systems used so far in itch research that additionally refers to species-dependent similarities and differences in itch pathways between various systems (14).

Although some TRPs were already shown to exhibit distinct characteristics with regard to ligands or activating stimuli such as temperature, the overall mechanisms underlying their physiological role seem to be the same.

In the next section, we focus on functional thermo-TRP channel expression in the mouse and rat skin and discuss their potential implications in pruritus and allergy development.

2. Heat Receptors

The role of thermal TRP channel sensors with moderate (TRPV4: >25°C, TRPV3: >33) and high heat thresholds (TRPV1: >43°C; TRPV2: >50°C) has been the focus of many studies in the past. Their overall potential not only in mediating the perception of

high temperatures but also in nociceptive signaling became more and more important for therapeutic treatment of certain skin diseases. There is compelling evidence for the role of TRPV1 as a key player in itch and allergy development (reviewed in (1, 8, 15) and references therein), while TRPV3 and TRPV4 have come more recently into focus as potential mediators and modulators of itch (1, 16).

2.1. TRPV1

TRPV1 is by far the most important player in the development as well as therapy of pruritus. Like most TRP proteins, it forms a non-selective channel that comprises diverse stimulation mechanisms: the first identified ligand was capsaicin, but it can also be activated by natural substances like piperine, camphor, eugenol, synthetic capsaicin, and the plant-derived resiniferatoxin (17). Endogenously, it is activated by cannabinoid anandamide (18–20) and endovanniloid N-arachidonoyl dopamine (NADA) (21, 22). Other physiologically relevant activators are temperatures above 42°C and protons (pH < 5.9) (23, 24). It was initially described to be expressed on C- and Aδ-type nociceptive sensory neurons (23, 25); later it was also found in non-neuronal cells including dendritic cells, dermal mast cells, epidermal and hair follicle keratinocytes, and other epithelial cells (26–31).

Besides the long-known role of TRPV1 in pain pathways (23–25), there is broad agreement on the involvement of TRPV1 in itch and allergy via multiple mechanisms. Clinically, many reports support an important role of TRPV1 in the induction of itch and allergy as in allergic rhinitis (32). Very early it was shown that the activation of TRPV1 resulted in the release of certain neuropeptides, e.g., substance P (SP) and calcitonin gene-related peptide (CGRP), and other itch mediators like interleukins, prostaglandins, and also growth factors (33, 34), and each of them was found to be participating in pruritic pathways ((35), reviewed in (36)) after they were initially detected in pain pathways. Some of them can lead to the release of additional pruritogens and many can in turn affect TRPV1 activity (27, 35, 37, 38). Most of these effects were observed in capsaicin-sensitive nerve fibers, even before it was known that TRPV1 was the molecular candidate (39).

The first itch-mediator identified in relation to TRPV1 was histamine, until today the best analyzed pruritogen in this context. Kim et al. showed that calcium influx into rat DRG neurons upon histamine stimulation could be inhibited by TRPV1 antagonists (40). With the help of further suitable blockers, they could identify phospholipase A2 and lipoxygenase as the pathways responsible for TRPV1 activation; this was confirmed later in mice (7, 40). Later, PLCβ3 was identified as the mediator of histamine-induced itch via TRPV1 (41, 42). To date it is assumed that in sensory neurons, histamine binds to the histamine H1 receptor, which subsequently induces the synthesis of the TRPV1 activator 12-hydroperoxyeicosatetraenoic

acid (12-HPETE) by lipoxygenases (43). This substance can also induce scratching when injected intradermally, but interestingly this cannot be blocked by the application of the TRPV1 blocker capsazepine, but by the TRPV1 agonist capsaicin (44, 45). At the same time, histamine-induced scratching is significantly reduced in TRPV1 gene-deficient mice or when TRPV1, histamine receptor H1R, PLA2, or 12-lipoxygenase blockers are applied (42). The mechanisms behind these paradoxical findings are yet to be elucidated.

A similar paradoxical observation is that rats lacking the TRPV1-positive neurons by chemical ablation develop severe skin lesions due to intense scratching (46). On the other hand, mice in which TRPV1-expressing sensory neurons were ablated did not show any symptoms of itch, either spontaneously or after subcutaneous injection of major pruritogens such as histamine, serotonin, and agonists of the proteinase-activated receptor PAR-2 (47). It seems there are more pathways involved in these phenomena than currently known.

As mentioned above, SP, commonly known in pain pathways, is an important itch mediator, although it does not seem to mediate all scratching behaviors, as the deletion of the gene-encoding SP does not prevent serotonin-evoked scratching (48). In a rather unusual animal model, the naked mole rat, a recent study revealed a link between SP and histamine-induced itch (49). In this species, there is expression of SP in the small diameter DRG neurons (50). These animals did not display any pruritic symptoms like scratching when histamine was applied, but exhibited marked scratching behavior after SP was injected intrathecally. At the same time, nocifensive behavior was absent after capsaicin application, but could also be "rescued" by intrathecal SP administration. As an explanation, the authors point out that in the naked mole-rat, capsaicin-sensitive fibers terminate in the deeper laminae of the dorsal horn in addition to the superficial layers. This might enable SP to act via superficially expressed neurokinin1 receptors and overcome possible inhibitory action by the deep dorsal horn projections. This study supports the idea that TRPV1-positive fibers mediate histamine-induced itch. In addition to histamine, there are other substances known to activate and sensitize TRPV1, e.g., bradykinin, eicosanoids, neurotrophins, and prostaglandins, leading to a sensitization of the peripheral nerve fibers that thus become more susceptible to pruritic stimuli (reviewed in (15)).

In 2007, it was shown that TRPV1, like its relative TRPV3, is involved in skin barrier homeostasis in the sense that capsaicin delayed dermal barrier recovery after tape-stripping-induced barrier disruption in both mice and humans. The additional application of capsazepine stopped this delay (6). More recent publications underline these findings: a potent TRPV1 antagonist, PAC-14028, could significantly suppress scratching behavior and was capable of

alleviating other symptoms of atopic dermatitis by accelerating skin barrier recovery (51). Later, the same group was able to confirm this in a mouse model, the blocker stopped allergen- and resiniferatoxin-induced scratching and the degranulation of mast cells (51), making PAC-14028 a promising antipruritic therapeutic candidate.

Capsaicin is widely applied as a topical therapeutic against itch (52, 53) because prolonged application leads to the desensitization of TRPV1 and subsequent non-responsiveness of the respective fibers. Nevertheless, a recent review doubts that there is scientific proof for this effect after analyzing six studies on this issue (54). There are other substances with antipruritic effects, namely tacrolimus and pimecrolimus; while their targets are not known to date, TRPV1 might be one of them (55–57). Besides, there are other studies than those reviewed in Gooding and coworkers that could show the relieving effect of TRPV1 agonists on itch on a cellular level (44, 45). The same is true for noxious heat, another TRPV1 activator. Yosipovitch et al. have shown that this stimulus was capable of reducing scratching behavior, while a TRPV1 antagonist was not able to do so (58). These additional findings would favor a general role for TRPV1 agonists and other stimuli in antipruritic therapy.

Two recently identified players in pruritus are vesicular glutamate transporter 2 (VGLUT2) and Pirt. It has been suggested that VGLUT2 might contribute to itch sensations (59, 60) via interaction with TRPV1. Both worked with conditional knock-out mice with deleted VGLUT2 expression in various subpopulations of DRG neurons, namely, Nav1.8-, TRPV1-, and tyrosine hydroxylase- (Th) expressing cells. These conditional knock-out mice showed drastically increased scratching behavior to the point when there was formation of overt skin lesions. This affected the conditional knockout in TRPV1-expressing cells as well as VGLUT2 deletion in combination with the other proteins. At the same time, in both groups there was a huge overlap of TRPV1 and VGLUT2 expression, giving rise to the assumption that glutamatergic transmission might interact with TRPV1 on some level. Interestingly, the deletion of VGLUT2 in the Nav1.8 conditional knock-out mice led to distinct results in the two studies: While Liu et al. found those mice to exhibit spontaneous itch, Lagerström and coworkers could not observe such effects in their corresponding Nav1.8-Cre mice. The discrepancies found in the two studies might be explained by differences in the specificity of the conditional knock-out mice, but still there is more effort needed to clarify the underlying processes.

Another newly identified member of the group of itch-related proteins is the membrane protein Pirt, a regulatory subunit of TRPV1 expressed in DRG neurons that was, as many of the players in itch, initially identified as the one involved in pain pathways (61). Very recently it was shown to play a role also in histamine-dependent as

well as -independent itch using Pirt gene-deficient mice (62). Patel et al. showed that the knock-out mice showed significantly reduced scratching behavior upon histamine application as well as chloroquine and 5-HT. Additionally, in measurements of DRG neurons prepared from Pirt knock-out mice, a significantly smaller proportion responded to the aforementioned substances in comparison to wild-type DRG neurons. In an allergy model it was shown that, like injection of the mast cell degranulator 48/80, Pirt also seems to contribute to mast cell-dependent itch.

Most likely there will be more TRPV1-related players discovered in the future, and new pathways concerning the known players will be unraveled.

2.2. Thermo Channel TRPV1 as Target for Antipruritic Therapy

Given the increasing evidence that cold and heat receptors are involved in the modulation of itch, they represent an interesting treatment target. However, there are hardly any studies to date in the field of the antipruritic potency of potential ligands.

The best known substance in the treatment of chronic pruritus is the TRPV1 agonist capsaicin, which is used for decades in itchy patients. Some double blind studies have been performed that have convincingly demonstrated its antipruritic effects (Table 1). A large number of papers describe cases and case series with effective capsaicin therapy in various diseases (Table 2). A recent systematic review focused on the efficacy of capsaicin in chronic pruritus. Among the 500 publications, they selected six studies only, which fulfilled the current criteria of valid study designs (54). The studies covered hemodialysis-related pruritus (63, 64), pruritus ani (65), notalgia paresthetica (53), and brachioradial pruritus (66). Though a statistically significant difference in responder rates was observed in all except hemodialysis-related pruritus, the authors conclude that there is no convincing evidence for the use of capsaicin to treat pruritus in any medical condition (54). This discrepancy arises from the fact that the validity of the included scores and second outcome measure has not been demonstrated. In sum, though there is clinical evidence for an antipruritic effect of capsaicin for decades, new studies which include valid instruments have to be performed.

2.3. TRPV2

Like its human counterpart, the capsaicin-receptor homolog TRPV2 is activated by noxious heat (>52°C) (23, 67) and expressed in the rodent skin (reviewed in (1, 13)). TRPV2 expression was detected in afferent cell bodies of rat trigeminal sensory neurons and DRG (67–69).

In peripheral inflammation, TRPV2 was found to be up-regulated in rat DRG neurons (70). The suggestion that impaired TRPV2 expression may therefore contribute to the progression of certain skin diseases makes this receptor important as a potential therapeutic target. In humans, for example, histamine-induced itch

Table 1
Randomized, placebo-controlled, double blind trials: capsaicin in chronic pruritus.

Diagnosis	Capsaicin treatment	References
Brachioradial pruritus	0.025%, 3–5x/d, 4 wks	Wallengren 1998 (66)
Hemodialysis-related pruritus	0.025–0.03%, 4 x/d, 4–6 wks	Breneman et al. 1992, (63); Tarng et al. 1996, (64) Cho et al. 1996 (154) Makhlough et al. 2010, (182)
Lichen simplex	0.075%, 4 x/d, 6 wks	Kantor et al. 1996 (183)
Notalgia paresthetica	0.025%, 3–5 x/d, 4 wks	Wallengren et al. 1995 (53)
Prurigo nodularis	0.025% or 0.075%, 3 x/d, 2 wks	Munn et al. 1997 (184)
Pruritus ani	0.006%, 3x/d, 4 wks	Lysy et al. 2003 (65)
Psoriasis vulgaris	0.025%, 4-6 x/d, 6 wks	Bernstein et al. 1986 (185), Ellis et al. 1993 (186)

x/d, times per day; wks, weeks; mo, months

is inhibited by the activation of TRPV2 on sensory neurons via noxious temperature stimuli above 50°C (58). However, the physiological role of the channel as a nociceptor remains unclear. The predominant expression in a neurotrophin-3-dependent subpopulation in developing and adult mouse DRG substantiates its contribution to the development of noxious heat-sensitive DRG neurons in rodents (71).

In addition, non-neuronal cells in the rodent skin have been reported to express the TRPV2 channel. While mouse keratinocytes show rare immunoreactivity to TRPV2- specific antibodies (72), murine mast cells, which exhibit a key impact on the initiation of itch, significantly express TRPV2 channels (26, 27, 73). The stimulation of TRPV2 on mast cells including thermal, mechanical, and osmotic cues provokes pro-inflammatory degranulation events and subsequent release of histamine, thus directly promoting the induction of itch (73). This further supports the potential regulatory impact of TRPV2 on itch development.

2.4. TRPV3

TRPV3 expression has been extensively documented in the literature in both human and rodent skin, with a predominant appearance in epidermal keratinocytes (74–78). Although, also detectable in the human and primate DRG, its presence in the rat and mouse DRG system could not be confirmed at first, and was therefore controversial (74, 75, 77–79). TRPV3 expression is sensitive to environmental conditions and seems to be down-regulated in cultured keratinocytes and epidermal cell lines (74, 75). However, changes in the expression profile in vivo can occur in human disease states.

Table 2
Case reports and case series: capsaicin in chronic pruritus.

Diagnosis	Capsaicin treatment	Authors
Aquagenic pruritus, aquagenic urticaria	0.025–1.0%, 3 x/d, 3–4 wks	Lotti et al. 1994, (187) Hautmann et al. 1994, (188); Reimann et al. 2000, (189); Cappugi et al. 1989, (190)
Atopic dermatitis	0.025%, 3 x/d, 10 days	Reimann et al. 2000, (189); Cappugi et al. 1989, (190); Tupker et al. 1992, (191)
Brachioradial pruritus	0.025%, 0.075%, 4–5 x/d, 2–6 wks	Goodless et al. 1993, (192); Knight et al. 1994, (193);
Contact dermatitis	0.025%, 3 x/d, 10 days	Cappugi et al. 1989, (190)
Hydroxyethyl starch-induced pruritus	0.025–0.05%, 2x/d, 5 wks–6 mo	Reimann et al. 2000, (189); Szeimies et al. 1994, (194)
Lichen planus	0.025%, 3 x/d, 10 days	Cappugi et al. 1989, (190)
Lichen simplex	0.025–0.075%, 4–5 x/d, 2 wks–2 mo	Kantor et al. 1996, (183); Reimann et al. 2000, (189); Reimann et al. 1995, (195)
Notalgia paresthetica	0.025–0.5%, 2 mo 8% capsaicin patch once	Reimann et al. 2000, (189); Metz et al. 2011, (200)
Prurigo nodularis	0.025%, 5 x/d, 2 wks–2 mo	Ständer et al. 2001, (52); Reimann et al. 2000, (189); Tupker et al. 1992, (191); Reimann et al. 1995, (195)
Pruritus in Hodgkin´s lymphoma	0.05%, 2 mo	Reimann et al. 2000, (189)
Pruritus in T-cell lymphoma	0.3%, 4 wks	Reimann et al. 2000, (189)
Pruritus of unknown origin	0.025%, 3 x/d, 10 days	Cappugi et al. 1989, (190)
Psoriasis vulgaris	0.025–0.1%, 4 wks, 10 mo	Reimann et al. 2000, (189); Cappugi et al. 1989, (190); Neess et al. 2000, (196)
PUVA-induced itch/pain	0.025–0.075%, 4 x/d, 1 wk	Kirby et al. 1997, (197) Burrows et al. 1994, (198)
Hemodialysis-related pruritus	0.05%, 3x/d, 5 d	Weisshaar et al. 2003, (199)

x/d, times per day; wks, weeks; mo, months

The TRPV3 channel is a sensor of temperatures in the range above 33°C (74, 75, 79, 80). Withdrawal responses of TRPV3-deficient mice are significantly decelerated under acute noxious heating, indicating that, in addition to heat perception, the

channel also functions in pain pathways (79). In agreement with this, TRPV3 overexpression in mouse keratinocytes essentially modulates pain sensitivity by participation in thermal hyperalgesia (81).

Recent studies indicate an important role of TRPV3 in thermal information processing in the skin. Mandadi and coworkers described the heat-induced ATP secretion from mouse keratinocytes which further acts as a transmitter on adjacent sensory neurons (82). ATP-induced signal transmission in mammalian epithelial cells is well known (83). Mouse keratinocytes show the ability to secrete additional transmitters such as nerve growth factor (NGF), prostaglandin E2 (PGE2), and interleukin-1α (IL-1α) (81, 82, 84–88) in response to certain types of stimulation. Application of the clove-oil component eugenol induces secretion of the inflammatory cytokine IL-1α from TRPV3-expressing mouse keratinocytes, leading to the sensitization of the skin (85, 89). Studies with murine mast cell/fibroblast co-culture systems revealed that IL-1α triggers mast cell proliferation and may thus contribute to mast cell hyperplasia in skin diseases (90). IL-1α and other transmitting molecules have a pro-inflammatory character and act as pruritogens by the subsequent activation of sensory nerve fibers (1, 8, 27, 91, 92). TRP activity-dependent transmitter release from skin cells may therefore have an essential impact on pain and pruritus development in sensory neurons (81, 82). In the case of neuropeptide-dependent signal transmission, stimulation of one keratinocyte is sufficient to activate neighboring cells and finally to depolarize nerve endings in the skin (93). Keratinocytes thus act as an interfacial sensor connecting the sensory system to the external environment.

As the outermost barrier of the body, the skin is exposed to various skin sensitizers and potential allergens. The TRPV3 channel is speculated to be a receptor for such effectors (85, 94) and is thought to be involved in inflammatory, nociceptive, and pruritic processes (1, 10, 16, 77, 95). Supported by the existence of common regulatory molecules and activating substances, the channel is suggested to operate synergistically with other TRP channels to mediate these processes. In this context, Pirt, a modulator of TRPV1 which is involved in histaminergic itch induction, is discussed to additionally modulate TRPV3 activity (14). TRPV3 shares similar expression patterns with TRPV1 and colocalizes with the vanilloid receptor homolog to form functional heterodimers in the skin (80). Moreover, both channels are similarly modulated by agonists such as citral (96). This also functionally links TRPV3 to TRPV1 as a key mediator of pain and itch. Furthermore, both TRPV1 and TRPV3 are involved in epidermal barrier formation and regulate the proliferation/differentiation balance (97) dysregulated in certain skin diseases with pruritic symptoms.

For treatment of inflamed and pruritic skin, substances including monoterpenoids like camphor and menthol are topically applied

(98–101) that modulate the activity of TRPV3 and other thermo-TRPs in a multifunctional way. Camphor, for example, activates TRPV3 (79, 102, 103), TRPV1 (104), and TRPA1 (105) in a concentration-dependent manner and skin treatment induces a very complex spectrum of warm and painful burning sensations followed by algesia (reviewed in (1)). The analgesic and antipruritic effects (106) induced by the drug are therefore believed to result from cross-talk mechanisms between certain TRP-dependent activation pathways. Menthol, a nonselective agonist of thermo-TRPs (105), is suggested to cause burning and itching effects in humans (107).

Several known TRPV3-activating, naturally occurring skin sensitizers and allergens derive from the spices oregano, thyme, and clove (85, 94, 108, 109). The oregano-ingredient carvacrol (103) is described as a multimodal inducer of pain, itch, and burning sensations which induces mixed warm and painful burning sensations when applied to the skin (reviewed in (1, 85)). Additionally, physiological substances in the body such as arachidonic acid and related unsaturated fatty acids have been identified that are thought to potentiate TRPV3 activity. In the plasma of patients with chronic renal failure, these substances have been shown to be significantly decreased (110). The observation that these patients often develop pruritic symptoms characterized by severe itching and dry skin may support a potential link between TRPV3 activity and the progression of itch (95).

The role of TRPV3 in certain skin diseases, in particular dermatitis, has been demonstrated by several studies using transgenic mice and rats that are deficient in TRPV3 or express mutant proteins with impaired functionality. These rodent strains often have defective hair growth, severe spontaneous dermatitis with inflammatory reactions comparable to human atopic dermatitis and/or allergic and pruritic phenotypes as indicated by their scratching behavior (16, 94, 111–113). These studies indicate a crucial function of the channel for epidermal barrier formation and hair morphogenesis (79, 114). TRPV3 may therefore represent an appropriate novel target for therapy of alopecia and inflammatory signaling in distinct skin diseases.

2.5. TRPV4

The innocuous heat-activated TRPV4 ion channel is expressed in the mouse and rat DRG and on free nerve endings of small-diameter neurons (115–118). Additionally, TRPV4 is expressed by non-neuronal and transiently by inflammatory cells of the mouse and rat skin including keratinocytes (72, 77, 116) and mast cells (73, 119). The channel is activated by thermal cues close to the range of the physiological skin temperature (>25°C) (115, 120). However, the role of TRPV4 in thermosensation is still controversial. Behavioral studies performed with TRPV4/V3 double knockout mice showed normal thermal preference and rather normal heat nociception and

hyperalgesia, indicating that heat sensation may not be the major role of either TRPV4 or TRPV3 (121). This is in contrast with a previous study using the same mouse strain which provides evidence for the involvement of the channel in thermal hyperalgesia (122).

Due to its expression in epidermal keratinocytes and mechanosensory nerve endings, TRPV4 is thought to contribute to mechanosensation of the skin (115, 116, 120). Dry skin and osmotic pressure lead to the activation of the cutaneously expressed channel (123, 124) subsequently inducing release of ATP in murine keratinocytes (82). Together with TRPV3, TRPV4 thus is involved in the processing of thermal information between keratinocytes and sensory neurons in the skin. In agreement with this, mice lacking TRPV4 display decreased cutaneous pain and increased thresholds for somatic mechanical nociception (116, 117, 125).

Along with the other thermo-TRP channels, TRPV4 is also thought to be involved in the neurophysiology of itch (1, 16, 77). This hypothesis, for instance, is favored by the finding that recombinant TRPV4 is sensitive to eicosanoids which represent lipid peroxidation products of endocannabinoids and arachidonic acid (126) and exhibit known puritogenic potential (127). Eicosanoids, including prostaglandins, leukotrienes, thromboxanes, and hyrdoxyeicosatetraenoic acids, are generated in the skin and contribute as mediators or modulators to physiological and pathophysiological processes (128, 129). In psoriatric skin, which is often accompanied by pruritic symptoms, significantly increased levels of aracidonic acid have been detected (130, 131).

As already mentioned above, dysregulation of the epidermal barrier is a major stimulus of itch induction (15). TRPV4 is an important player in the regulation of epidermal barrier integrity and homeostasis within the skin (6). TRPV4-deficient mice show severe defects in cell–cell contacts and impaired stratification and maturation of intercellular junctions (132, 133). Thus, TRPV4 is thought to be a temperature-dependent regulatory component of the skin with a junction-dependent barrier function. Treatment with the TRPV4 agonist 4a-Phorbol 12,13-didecanone accelerates epidermal barrier recovery, and thermal stimulation of the skin within the activation range of TRPV4 had the same effect on mouse and human skin (6). TRPV4 shares this essential role in the epidermal barrier with TRPV1, which is co-expressed in the bodies of DRG neurons and, furthermore, potentiates the activity of TRPV4 (134). The finding that TRPV1 activation by capsaicin delays barrier recovery (6), therefore, hints at a potential cross-talk of pathways involving both channels and supports their importance in the regulation of epidermal barrier formation. The hypothesis of interactive channel-dependent pathways is further emphasized by the idea of shared regulatory molecules like Pirt (135). Knockout studies performed with Pirt, the regulator of TRPV1 (136),

revealed an essential role for Pirt in both histaminergic and histamine-independent itch and in proper itch sensation, further supporting a functional cross-talk between TRPV1 and TRPV4 in epidermal barrier formation.

TRPV4 was reported to be co-expressed with PAR2 on afferent neurons of mouse DRG (137). PAR2 stimulates the release of SP and CGRP from these neurons upon activation (125, 138). Scratching behavior in mice provoked by stimulation of the skin with the PAR2-specific ligand SLIGRL-NH2 emphasizes the involvement of PAR2 in the initiation of pruritic processes (139). Through second messenger molecules, PAR2 sensitizes TRPV4 further, leading to an enhanced release of SP and CGRP in the DRG (125). There is evidence for the involvement of both SP and CGRP in itchy skin diseases in mice (140, 141). The fact that TRPV4 and PAR2 are coexpressed in the skin on sensory neurons and keratinocytes ((142) and references therein) suggests that, apart from its impact in neuropathic pain and in mechanical hyperalgesia of the intestine, TRPV4 has a role to play in histamine-independent itch induction (143). However, in the intestine it was shown that TRPV4 and PAR2 pathways are not coupled on the level of sensory neurons. Here, PAR4 activation, which also induces scratching behavior in mice (144), affects PAR2 and TRPV4-dependent signaling.

3. Cold Receptors

Moderate cooling is used as a therapeutic tool to reduce itch and alleviate painful sensations in skin diseases (8). The cold receptors TRPM8 and TRPA1 have been shown to be functionally expressed in the human and rodent skin. Naturally occurring agonists of TRPM8 like menthol, icilin, and eucalyptol (145–147) mimic cooling sensations and are therefore used as therapeutic agents to reduce the sensation of itch.

3.1. TRPM8

The cold receptor TRPM8 is activated by innocuous cold temperatures and natural cooling compounds like menthol and eucalyptol, or synthetic substances like icilin or WS-12 (74, 75, 148–150).

It was first identified in prostate-derived cDNA and is up-regulated in prostate cancer and other carcinomas (151). Later it was shown that it is expressed in a subpopulation of small diameter sensory neurons; remarkably, there is almost no overlap of TRPM8- with CGRP- and TRPV1-expressing cells (74, 75, 148), perhaps accounting for their distinct roles in thermosensation and indicating that TRPM8 proteins might not be involved in pain pathways.

For a long time, participation of TRPM8 proteins in itch was suspected because cooling and the effect of cooling agents reliably relieve pruritus (152). In the last 2 years, there is growing evidence for a role of TRPM8 in pruritus or allergy as more and more publications reported a connection between TRPM8 and certain allergic or pruritic pathways. For example, there are indications that TRPM8, like some TRPVs, could be involved in epidermal barrier homeostasis (153).

In 2010, it was also postulated that TRPM8 might play a role in cold-induced urticaria (154). TRPM8 was shown to be expressed in a rat basophilic mast cell line (RBL-2H3) and the application of menthol as well as cooling induced a calcium influx into the cells, leading to a subsequent histamine release. This was not the case when TRPM8 was blocked or down-regulated by blockers or siRNAs, respectively. Additionally, menthol injections led to intense scratching, which was significantly reduced by additional injection of a TRPM8 blocker. Another study 1 year later was not able to confirm these findings (155). While the first attempt worked with a carcinoma cell line, the latter used mast cells, thereby most likely providing the more physiological approach. No response could be detected in either human or mouse mast cells derived from blood progenitor cells or bone marrow, respectively. In the latter, they were at least able to detect TRPM8 transcripts, which was not the case in the human mast cells. They also did not detect any up-regulation of TRPM8 in cold urticaria patients or relevant SNPs in their genomic sequences. Finally, over-expression of TRPM8 did not lead to any alteration in mast cell activation or mast cell-driven allergic responses and TRPM8−/− mice did not show alterations in the antigen-induced anaphylactic responses.

According to a very recent case report, topical application of the potent TRPM8 agonist icilin over several days could relieve vulval itch caused by lichen sclerosus et atrophicus; these findings have not been extended, using for example, a mouse model or controlled double-blind studies (156). Additionally the question has to be raised if TRPM8 is the only candidate protein in this case report. It is known that TRPA1 can be activated by icilin, too; therefore it needs to be clarified whether TRPA1 could also be a molecular target involved in the antipruritic effect of icilin (157).

Consistent with this finding, a hairless rat model tested by Wei in 2005 revealed an antipruritic effect of icilin (158). The basis for this approach was other case reports about topically applied icilin. Generalized pruritus and subsequent skin lesions by intense scratching were induced by a low magnesium diet. Topically applied icilin powder significantly reduced scratching and bite marks after 5 days; the first effects could already be observed after the first application. Here again, the observed effect might also be based upon TRPA1 interaction.

In future, there might be other proofs for a role of TRPM8 in itch and/or allergy. Additionally, other TRP channels might be involved via multiple mechanisms which are yet to be determined.

3.2. TRPA1

TRPA1 is the only protein of the ankyrin subfamily that is found in mammals to date. Known agonists are allyle isothiocyanate (AITC), allicin, carvacrol, gingerol, eugenol, and cinnamaldehyde (159–162), many of them eliciting an irritating sensation when applied to the skin, suggesting a possible role for them in pain and itch. It can also be activated by acrolein, bradykinin, and even cannabinoids, i.e., Δ(9)-tetrahydrocannabinol (THC) (160, 161, 163), which gives rise to the assumption of its participation in itch and inflammation pathways (164). Additionally, it could be confirmed that TRPA1 also responds to known TRPM8 agonists like menthol and icilin, indicating its contribution to cold sensation (157, 165). It is still under discussion whether TRPA1 channels are activated by low temperatures below 18°C or not (124, 157, 165, 166).

Besides neuronal tissues like DRG, trigeminal ganglia, and neurons of the small intestine (156, 167, 168), it is also expressed in non-neuronal tissues such as skeletal muscles, colon, lung, and keratinocytes (157, 169–171). Interestingly, TRPA1 and TRPV1 proteins are co-expressed in several tissues and it could already be shown that there is some interaction between the two (157, 172–174), leading to the assumption that TRPA1 might be involved in itch via those interactions.

Although it is commonly accepted that TRPA1 is involved in the pain pathway, in the past there was no evidence for its role in itch or allergy. Nevertheless, in 2009 it was already assumed that TRPA1 might play a role in allergic asthma (175). TRPA1 gene-deficient mice displayed strongly reduced airway hyperreactivity and other asthma-related symptoms such as cytokine and mucus production. These effects could be reversed by the application of the TRPA1-blocker HC-030031, making TRPA1 a promising target for the treatment of asthma.

The group around Bautista reported that by interaction with Mas-related G protein-coupled receptors, TRPA1 is strongly involved in histamine-independent itch (176). Mrgprs were already known to be involved in the development of pruritus (177, 178), but the above-mentioned paper could additionally show in vivo and in vitro that TRPA1 acts downstream of MrgprC11 as well as MrgprA3. In their approach, they used primary cells and transfected cell lines as well as TRPV1- and TRPA1 gene-deficient mice. Chloroquine and BAM-22 could activate a subset of sensory neurons that co-express TRPV1 and A1; subsequent experiments showed that TRPA1 is interacting with both receptors, as all responses to chloroquine and BAM-22 were drastically impaired when TRPA1 was knocked down pharmacologically or

genetically. Activation of MrgprA3- and MrgprC11-transfected NG108 cells by chloroquine and BAM-22, respectively, could elicit exclusive or much stronger calcium signals when TRPA1 was co-transfected. Finally, TRPA1 gene-deficient mice showed significantly attenuated scratching behavior after injection of Bam-22 or chloroquine. It could even be confirmed by pharmacological approaches that the activation of TRPA1 by MrgprA3 happens via Gßγ-signaling, while the interaction with MrgprC11 uses a PLC pathway.

Another recent study reported a contribution of TRPA1 in endothelin-1(ET-1)-induced pruritus (179). ET-1-induced pruritus does not rely on the presence of PLCβ3, but requires TRPV1-expressing nociceptors. The non-selective TRP channel blocker ruthenium red (RR) and the TRPA1-specific inhibitor AP18, but not the TRPV1-specific blocker capsazepine, could increase the number of scratches after injection of the tested substances into the neck of BL6-mice. In contrast, only capsazepine and ruthenium red were able to reduce histamine-induced scratching. Morphine could not evoke any changes in scratching after ET-1 application, demonstrating that the reason for the scratching was itch, not pain. The fact that TRPA1-blockers resulted in an increased number of scratches leads to the assumption that TRPA1-activity is actually relieving pruritus. The authors assume that the channel might interact with the adenylyl cyclase/protein kinase C pathway or it might act via non-neuronal cells such as keratinocytes, thereby inhibiting ET-1 induced itch. TRPV1 might also be involved, as it could be shown that TRPA1 desensitization is regulated by TRPV1 (174), but the actual mechanisms behind this still have to be elucidated.

The recently reported relief of vulval pruritus after topical application of icilin (156) might also be an important finding in terms of TRP-related itch. The authors suggest that the observed efficacy of topical icilin, a TRPM8 agonist, is due to its ability to activate TRPM8. Since icilin is also an activator of TRPA1 channels (157), it has to be considered that the observed effect is due to the activation of TRPA1. Also an earlier report of the antipruritic effect of topical icilin on hairless rats (158) might be based upon the activation of the TRPA1. Finally, TRPA1 can be sensitized by PAR2 (144), a member of the proteinase-activated receptor family. Different receptors of this family have been shown to be involved in pruritus (reviewed in (180)). The fact that PAR2 is involved in non-histaminergic itch (181) together with the mentioned sensitization of TRPA1 suggests another possible pathway by whichTRPA1 might contribute to the modulation of pruritus.

Taken together, there is growing evidence that TRPA1 is an important player in itch and most likely there will be several studies following these initial findings.

References

1. Bíró T, Tóth BI, Marincsák R et al (2007) TRP channels as novel players in the pathogenesis and therapy of itch. Biochim Biophys Acta 1772:1004–1021
2. Metz M, Grundmann S, Ständer S (2011) Pruritus: an overview of current concepts. Vet Dermatol 22:121–131
3. Dillon SR, Sprecher C, Hammond A (2004) Interleukin 31, a cytokine produced by activated T cells, induces dermatitis in mice. Nat Immunol 5:752–760
4. Takaoka A, Arai I, Sugimoto M et al (2006) Involvement of IL-31 on scratching behavior in NC/Nga mice with atopic-like dermatitis. Exp Dermatol 15:161–167
5. Takaoka A, Arai I, Sugimoto M et al (2007) Role of scratch-induced cutaneous prostaglandin D production on atopic-like scratching behaviour in mice. Exp Dermatol 16:331–339
6. Denda M, Sokabe T, Fukumi-Tominaga T et al (2007) Effects of skin surface temperature on epidermal permeability barrier homeostasis. J Invest Dermatol 127:654–659
7. Imamachi N, Park GH, Lee H et al (2009) TRPV1-expressing primary afferents generate behavioral responses to pruritogens via multiple mechanisms. Proc Natl Acad Sci USA 106:11330–11335
8. Paus R, Schmelz M, Bíró T et al (2006) Frontiers in pruritus research: scratching the brain for more effective itch therapy. J Clin Invest 116:1174–1186
9. Levine JD, Alessandri-Haber N (2007) TRP channels: targets for the relief of pain. Biochim Biophys Acta 1772:989–1003
10. Steinhoff M, Bíró T (2009) A TR(I)P to pruritus research: role of TRPV3 in inflammation and itch. J Invest Dermatol 129:531–535
11. Minke B, Cook B (2002) TRP channel proteins and signal transduction. Physiol Rev 82:429–472
12. Saito S, Shingai R (2006) Evolution of thermoTRP ion channel homologs in vertebrates. Physiol Genomics 27:219–230
13. Moran MM, McAlexander MA, Bíró T et al (2011) Transient receptor potential channels as therapeutic targets. Nat Rev Drug Discov 10:601–620
14. Patel KN, Dong X (2011) Itch: cells, molecules, and circuits. ACS Chem Neurosci 2:17–25
15. Steinhoff M, Bienenstock J, Schmelz M et al (2006) Neurophysiological, neuroimmunological, and neuroendocrine basis of pruritus. J Invest Dermatol 126:1705–1718
16. Yoshioka T, Imura K, Asakawa M et al (2009) Impact of the Gly573Ser substitution in TRPV3 on the development of allergic and pruritic dermatitis in mice. J Invest Dermatol 129:714–722
17. Szallasi A, Blumberg P (1989) Resiniferatoxin, a phorbol-related diterpene, acts as an ultrapotent analog of capsaicin, the irritant constituent in red pepper. Neuroscience 30:1515–1520
18. Zygmunt PM, Petersson J, Andersson DA et al (1999) Vanilloid receptors on sensory nerves mediate the vasodilator action of anandamide. Nature 400:452–457
19. Smart D, Gunthorpe MJ, Jerman JC et al (2000) The endogenous lipid anandamid is a full agonist at the human vanilloid receptor (hVR1). Br J Pharmacol 129:227–230
20. Di Marzo V, Bisogno T, De Petrocellis L (2001) Anandamide: some like it hot. Trends Pharmacol Sci 22:346–349
21. Huang SM, Bisogno T, Trevisani M et al (2002) An endogenous capsaicin-like substance with high potency at recombinant and native vanilloid VR1 receptors. Proc Natl Acad Sci USA 99:8400–8405
22. Sagar DR, Smith PA, Millns PJ et al (2004) TRPV1 and CB[1] receptor-mediated effects of the endovanilloid/endocannabinoid N-arachidonoyl-dopamine on primary afferent fibre and spinal cord neuronal responses in the rat. Eur J Neurosci 20:175–184
23. Caterina MJ, Schumacher MA, Tominaga M et al (1997) The capsaicin receptor: a heat-activated ion channel in the pain pathway. Nature 389:816–824
24. Tominaga M, Caterina MJ, Malmberg AB et al (1998) The cloned capsaicin receptor integrates multiple pain-producing stimuli. Neuron 21:531–543
25. Caterina MJ (2000) Impaired nociception and pain sensation in mice lacking the capsaicin receptor. Science 288:306–313
26. Bodó E, Kovács I, Telek A et al (2004) Vanilloid receptor-1 (VR1) is widely expressed on various epithelial and mesenchymal cell types of human skin. J Invest Dermatol 123:410–413
27. Bíró T, Maurer M, Modarres S et al (1998) Chracterization of functional vanilloid receptors expressed by mast cells. Blood 91:1332–1340
28. Ständer S, Moormann C, Schumacher M et al (2004) Expression of vanilloid receptor subtype 1 in cutaneous sensory nerve fibers, mast cells, and epithelial cells of appendage structures. Exp Dermatol 13:129–139

29. Inoue K, Koizumi S, Fuziwara S et al (2002) Functional vanilloid receptors in cultured normal human epidermal keratinocytes. Biochem Biophys Res Commun 291: 124–129
30. Basu S, Srivastava P (2005) Immunological role of neuronal receptor vanilloid receptor 1 expressed on dendritic cells. Proc Natl Acad Sci USA 102:5120–5125
31. Denda M, Fuziwara S, Inoue K et al (2001) Immunoreactivity of VR 1 on epidermal keratinocyte of human skin. Biochem Biophys Res Commun 285:1250–1252
32. Alenmyr L, Högestätt ED, Zygmunt PM et al (2009) TRPV1-mediated itch in seasonal allergic rhinitis. Allergy 64:807–810
33. Dallos A, Kiss M, Polyánka H et al (2006) Effects of the neuropeptides substance P, calcitonin gene-related peptide, vasoactive intestinal polypeptide and galanin on the production of nerve growth factor and inflammatory cytokines in cultured human keratinocytes. Neuropeptides 40:251–263
34. Jessell TM, Iversen LL, Cuello AC (1978) Capsaicin-induced depletion of substance P from primary sensory neurones. Brain Res 152:183–188
35. Kim S-J, Park GH, Kim D et al (2011) Analysis of cellular and behavioral responses to imiquimod reveals a unique itch pathway in transient receptor potential vanilloid 1 (TRPV1)-expressing neurons. Proc Natl Acad Sci USA 108:3371–3376
36. Raap U, Ständer S, Metz M (2011) Pathophysiology of itch and new treatments. Curr Opin Allerg Clin Immunol 11:420–427
37. Chuang HH, Prescott ED, Kong H et al (2001) Bradykinin and nerve growth factor release the capsaicin receptor from PtdIns (4,5) P2-mediated inhibition. Nature 411:957–962
38. Southall MD, Li T, Gharibova LS et al (2003) Activation of epidermal vanilloid receptor-1 induces release of proinflammatory mediators in human keratinocytes. Pharmacology 304:217–222
39. Caterina MJ, Julius D (2001) The vanilloid receptor: a molecular gateway to the pain pathway. Annu Rev Neurosci 24:487–517
40. Kim BM, Lee SH, Shim WS et al (2004) Histamine-induced Ca(2+) influx via the PLA(2)/lipoxygenase/TRPV1 pathway in rat sensory neurons. Neurosci Lett 361:159–162
41. Han S-K, Mancino V, Simon MI (2006) Phospholipase Cbeta 3 mediates the scratching response activated by the histamine H1 receptor on C-fiber nociceptive neurons. Neuron 52:691–703
42. Shim W-S, Tak MH, Lee MH et al (2007) TRPV1 mediates histamine-induced itchingvia the activation of phospholipase A2 and 12-lipoxygenase. J Neurosci: Off J Soc Neurosci 27:2331–2337
43. Hwang SW, Cho H, Kwak J et al (2000) Direct activation of capsaicin receptors by products of lipoxygenases: endogenous capsaicin-like substances. Proc Natl Acad Sci USA 97:6155–6160
44. Kim HJ, Kim DK, Kim H et al (2008) Involvement of the BLT2 receptor in the itch-associated scratching induced by 12-(S)-lipoxygenase products in ICR mice. Br J Pharmacol 154:1073–1078
45. Kim D-K, Kim HJ, Sung KS et al (2007) 12(S)-HPETE induces itch-associated scratchings in mice. Eur J Pharmacol 554:30–33
46. Carrillo P, Camacho M, Manzo J (1998) Cutaneous wounds produced by capsaicin treatment of newborn rats are due to trophic disturbances. Neurotoxicol Teratol 20:75–81
47. Mishra SK, Tisel SM, Orestes P et al (2011) TRPV1-lineage neurons are required for thermal sensation. EMBO J 30:582–593
48. Cuellar JM, Jinks SL, Simons CT et al (2003) Deletion of the preprotachykinin A gene in mice does not reduce scratching behavior elicited by intradermal serotonin. Neurosci Lett 339:72–76
49. Smith ESJ, Blass GR, Lewin GR et al (2010) Absence of histamine-induced itch in the African naked mole-rat and "rescue" by Substance P. Mol Pain 6:29
50. Park TJ, Comer C, Carol A et al (2003) Somatosensory organization and behavior in naked mole-rats: II. Peripheral structures, innervation, and selective lack of neuropeptides associated with thermoregulation and pain. J Compar Neurol 465:104–120
51. Yun J-W, Seo JA, Jang WH et al (2011) Antipruritic effects of TRPV1 antagonist in murine atopic dermatitis and itching models. J Invest Dermatol 131:1576–1579
52. Ständer S, Luger T, Metze D (2001) Treatment of prurigo nodularis with topical capsaicin. J Am Acad Dermatol 44:471–478
53. Wallengren J, Klinker M (1995) Successful treatment of notalgia paresthetica with topical capsaicin: vehicle-controlled, double-blind, crossover study. J Am Acad Dermatol 32:287–289
54. Gooding SMD, Canter PH, Coelho HF et al (2010) Systematic review of topical capsaicin

in the treatment of pruritus. Int J Dermatol 49:858–865

55. Ständer S, Ständer H, Seeliger S et al (2007) Topical pimecrolimus and tacrolimus transiently induce neuropeptide release and mast cell degranulation in murine skin. Br J Dermatol 156:1020–1026
56. Pereira U, Boulais N, Lebonvallet N et al (2010) Mechanisms of the sensory effects of tacrolimus on the skin. Br J Dermatol 163:70–77
57. Nakano T, Andoh T, Tayama M et al (2008) Effects of topical application of tacrolimus on acute itch-associated responses in mice. Biol Pharm Bullet 31:752–754
58. Yosipovitch G, Fast K, Bernhard JD (2005) Noxious heat and scratching decrease histamine-induced itch and skin blood flow. J Invest Dermatol 125:1268–1272
59. Liu Y, Abdel SO, Zhang L et al (2010) VGLUT2-dependent glutamate release from nociceptors is required to sense pain and suppress itch. Neuron 68:543–556
60. Lagerström MC, Rogoz K, Abrahamsen B et al (2010) VGLUT2-dependent sensory neurons in the TRPV1 population regulate pain and itch. Neuron 68:529–542
61. Kim AY, Tang Z, Liu Q et al (2008) Pirt, a phosphoinositide-binding protein, functions as a regulatory subunit of TRPV1. Cell 133:475–485
62. Patel KN, Liu Q, Meeker S et al (2011) Pirt, a TRPV1 modulator, is required for histamine-dependent and -independent itch. PloS one 6:p.e.20559
63. Breneman DL, Cardone JS, Blumsack RF et al (1992) Topical capsaicin for treatment of hemodialysis-related pruritus. J Am Acad Dermatol 26:91–94
64. Tarng DC, Cho YL, Liu HN et al (1996) Hemodialysis-related pruritus: a double-blind, placebo-controlled, crossover study of capsaicin 0.025% cream. Nephron 72:617–622
65. Lysy J, Sistiery-Ittah M, Israelit Y (2003) Topical capsaicin–a novel and effective treatment for idiopathic intractable pruritus ani: a randomised, placebo controlled, crossover study. Gut 52:1323–1326
66. Wallengren J (1998) Brachioradial pruritus: a recurrent solar dermopathy. J Am Acad Dermatol 39:803–806
67. Caterina MJ, Rosen TA, Tominaga M et al (1999) A capsaicin-receptor homologue with a high threshold for noxious heat. Nature 398:436–441
68. Ichikawa H, Sugimoto T (2000) Vanilloid receptor 1-like receptor-immunoreactive primary sensory neurons in the rat trigeminal nervous system. Neuroscience 101:719–725
69. Lewinter RD, Skinner K, Julius D et al (2004) Immunoreactive TRPV-2 (VRL-1), a capsaicin receptor homolog, in the spinal cord of the rat. J Comp Neurol 470:400–408
70. Shimosato G, Amaya F, Ueda M et al (2005) Peripheral inflammation induces up-regulation of TRPV2 expression in rat DRG. Pain 119:225–232
71. Tamura S, Morikawa Y, Senba E (2005) TrpV2, a capsaicin receptor homologue, is expressed predominantly in the neurotrohpin-3-dependent subpopulation of primary sensory neurons. Neuoscience 130:223–228
72. Chung MK, Lee H, Caterina MJ (2003) Warm temperatures activate TRPV4 in mouse 308 keratinocytes. J Biol Chem 278: 32037–32046
73. Stokes AJ, Shimoda LMN, Koblan-Hoberson M et al (2004) A TrpV2-PKA signaling module for transduction of physical stimuli in mast cells. J Exp Med 200:137–144
74. Peier AM, Reeve AJ, Andersson DA (2002) A heat-sensitive TRP channel expressed in keratinocytes. Science 296:2046–2049
75. Peier AM, Moqrich A, Hergarden AC (2002) A TRP channel that senses cold stimuli and menthol. Cell 108:705–715
76. Xu H, Ramsey IS, Kotecha SA (2002) TRPV3 is a calcium-permeable temperature-sensitive cation channel. Nature 418:181–186
77. Chung MK, Lee H, Mizuno A (2004) 2-Aminoethoxydiphenyl borate activates and sensitizes the heat-gated ion channel TRPV3. J Neurosci 24:5177–5182
78. Chung MK, Lee H, Mizuno A (2004) TRPV3 and TRPV4 mediate warmth-evoked currents in primary mouse keratinocytes. J Biol Chem 279:21569–21575
79. Moqrich A, Hwang SW, Earley TJ (2005) Impaired thermosensation in mice lacking TRPV3, a heat and camphor sensor in the skin. Science 307:1468–1472
80. Smith GD, Gunthorpe MJ, Kelsell RE (2002) TRPV3 is a temperature-sensitive vanilloid receptor-like protein. Nature 418:186–190
81. Huang SM, Lee H, Chung MK (2008) Overexpressed transient receptor potential vanilloid 3 ion channels in skin keratinocytes modulate pain sensitivity via prostaglandin E2. J Neurosci 28:13727–13737
82. Mandadi S, Sokabe T, Shibasaki K (2009) TRPV3 in keratinocytes transmits temperature information to sensory neurons via ATP. Pflugers Arch 458:1093–1102

83. Enomoto K, Furuya K, Yamagishi S (1994) The increase in the intracellular Ca2+ concentration induced by mechanical stimulation is propagated via release of pyrophosphorylated nucleotides in mammary epithelial cells. Pflugers Arch 427:533–542
84. Koizumi S, Fujishita K, Inoue K et al (2004) Ca2+ waves in keratinocytes are transmitted to sensory neurons: the involvement of extracellular ATP and P2Y2 receptor activation. Biochem J 380:329–338
85. Xu H, Delling M, Jun JC (2006) Oregano, thyme and clove-derived flavors and skin sensitizers activate specific TRP channels. Nat Neurosci 9:628–635
86. Tsutsumi M, Denda S, Inoue K (2009) Calcium ion gradients and dynamics in cultured skin slices of rat hindpaw in response to stimulation with ATP. J Invest Dermatol 129:584–589
87. Dallos A, Kiss M, Polyanka H et al (2006) Effects of the neuropeptides substance P, calcitonin gene-related peptide, vasoactive intestinal polypeptide and galanin on the production of nerve growth factor and inflammatory cytokines in cultured human keratinocytes. Neuropeptides 40:251–263
88. Chun KS, Lao HC, Langenbach R (2010) The prostaglandin E2 receptor, EP2, stimulates keratinocyte proliferation in mouse skin by G protein-dependent and {beta}-arrestin1-dependent signaling pathways. J Biol Chem 285:39672–39681
89. Corsini E, Primavera A, Marinovich M (1998) Selective induction of cellassociated interleukin-1alpha in murine keratinocytes by chemical allergens. Toxicology 129:193–200
90. Kameyoshi Y, Morita E, Tanaka T (2000) Interleukin-1 alpha enhances mast cell growth by a fibroblast-dependent mechanism. Arch Dermatol Res 292:240–247
91. Paus R, Cotsarelis G (1999) The biology of hair follicles. N Engl J Med 341:491–497
92. Stenn KS, Paus R (2001) Controls of hair follicle cycling. Physiol Rev 81:449–494
93. Boulais N, Misery L (2008) The epidermis: a sensory tissue. Eur J Dermatol 18:119–127
94. Asakawa M, Yoshioka T, Matsutani T (2006) Association of a mutation in TRPV3 with defective hair growth in rodents. J Invest Dermatol 126:2664–2672
95. Hu HZ, Xiao R, Wang C et al (2006) Potentiation of TRPV3 channel function by unsaturated fatty acids. J Cell Physiol 208:201–212
96. Stotz SC, Vriens J, Martyn D et al (2008) Citral sensing by transient receptor potential channels in dorsal root ganglion neurons. PLoS One 3(5):e2082
97. Cheng X, Jin J, Hu L et al (2010) TRP channel regulates EGFR signaling in hair morphogenesis and skin barrier formation. Cell 141:331–343
98. Burkhart CG, Burkhart HR (2003) Contact irritant dermatitis and anti-pruritic agents: the need to address the itch. J Drugs Dermatol 2:143–146
99. Santos FA, Rao VS (2001) Possible role of mast cells in cineole-induced scratching behavior in mice. Food Chem Toxicol 40:1453–1457
100. Umezu T, Sakata A, Ito H (2001) Ambulation-promoting effect of peppermint oil and identification of its active constituents. Pharmacol Beiochem Behav 69:383–890
101. Anand P (2003) Capsaicin and menthol in the treatment of itch and pain: recently cloned receptors provide the key. Gut 52:1233–1235
102. Vogt-Eisele AK, Weber K, Sherkheli MA et al (2007) Monoterpenoid agonists of TRPV3. Br J Pharmacol 151:530–540
103. Sherkheli MA, Benecke H, Doerner JF et al (2009) Monoterpenoids induce agonist-specific desensitization of transient receptor potential vanilloid-3 (TRPV3) ion channels. J Pharm Pharm Sci 12:116–128
104. Xu H, Blair NT, Clapham DE (2005) Camphor activates and strongly desensitizes the transient receptor potential vanilloid subtype 1 channel in a vanilloid-independent mechanism. J Neurosci 25:8924–8937
105. Macpherson LJ, Hwang SW, Miyamoto T et al (2006) More than cool: promiscuous relationships of menthol and other sensory compounds. Mol Cell Neurosci 32:335–343
106. Green BG (1990) Spatial summation of chemical irritation and itch produced by topical application of capsaicin. Percept Psychophys 48:12–18
107. Wasner G, Schwarz K, Schattschneider J et al (2004) Interaction between histamine-induced itch and experimental muscle pain. Eur J Pain 8:179–185
108. Bryant B, Silver WL (2000) Receptors and transduction in taste. In: Finger TE, Silver WL, Restrepo D (eds) The Neurobiology of Taste and Smell. Wiley-Liss, New York, pp 287–314
109. Schöll I, Jensen-Jarolim E (2004) Allergenic potency of spices: hot, medium hot, or very hot. Int Arch Allergy Immunol 135:247–261
110. Peck LW, Monsen ER, Ahmad S (1996) Effect of three sources of long-chain fatty

acids on the plasma fatty acid profile, plasma prostaglandin E2 concentrations, and pruritus symptoms in hemodialysis patients. Am J Clin Nutr 64:210–214

111. Kochukov MY, McNearney TA, Fu Y et al (2006) Thermosensitive TRP ion channels mediate cytosolic calcium response in human synoviocytes. Am J Physiol Cell Physiol 291:C424–C432
112. Imura K, Yoshioka T, Hikita I et al (2007) Influence of TRPV3 mutation on hair growth cycle in mice. Biochem Biophys Res Commun 363:479–483
113. Xiao R, Tang J, Wang C et al (2008) Calcium plays a central role in the sensitization of TRPV3 channel to repetitive stimulations. J Biol Chem 283:6162–6174
114. Chung MK, Jung SJ, Oh SB (2011) Role of TRP channels in pain sensation. Adv Exp Med Biol 704:615–636
115. Liedtke W, Coe Y, Marti-Renom MA (2000) Vanilloid-receptor related osmotically activated channel (VR-OAC), a candidate vertebrate osmoreceptor. Cell 103:525–535
116. Suzuki M, Watanabe Y, Oyama Y (2003) Localization of mechanosensitive channel TRPV4 in mouse skin. Neurosci Lett 353:189–192
117. Suzuki M, Mizuno A, Kodaira K et al (2003) Impaired pressure sensation in mice lacking TRPV4. J Biol Chem 278:22664–22668
118. Güler AD, Lee H, Iida T et al (2002) Heat-evoked activation of the ion channel, TRPV4. J Neurosci 22:6408–6414
119. Yang WZ, Chen JY, Yu JT (2007) Effects of low power laser irradiation on intracellular calcium and histamine release in RBL-2H3 mast cells. Photochem Photobiol 83:979–984
120. Strotmann R, Hartenek C, Nunnenmacher K (2000) OTRPC4, a nonselective cation channel that confers sensitivity to extracellular osmolarity. Nat Cell Biol 2:695–702
121. Huang SM, Li X, Yu Y (2011) TRPV3 and TRPV4 ion channels are not major contributors to mouse heat sensation. Mol Pain 7:37
122. Todaka H, Taniguchi J, Satoh J (2004) Warm temperature-sensitive transient receptor potential vanilloid 4 (TRPV4) plays an essential role in thermal hyperalgesia. J Biol Chem 279:35133–35138
123. Denda M, Sato J, Masuda Y (1998) Exposure to a dry environment enhances epidermal permeability barrier function. J Invest Dermatol 111:858–863
124. Dhaka A, Viswanath V, Patapoutian A (2006) Trp ion channels and temperature sensation. Annu Rev Neurosci 29:135–161
125. Grant AD, Cottrell GS, Amadesi S (2007) Protease-activated receptor 2 sensitizes the transient receptor potential vanilloid 4 ion channel to cause mechanical hyperalgesia in mice. J Physiol 578:715–733
126. Needleman P, Turk J, Jakschik BA (1986) Arachidonic acid metabolism. Annu Rev Biochem 55:69–102
127. Watanabe H, Vriens J, Prenen J (2003) Anandamide and arachidonic acid use epoxyeicosatrienoic acids to activate TRPV4 channels. Nature 424:434–438
128. Ruzicka T, Burg G (1987) Effects of chronic intracutaneous administration of arachidonic acid and its metabolites. Induction of leukocytoclastic vasculitis by leukotriene B4 and 12-hydroxyeicosatetraenoic acid and its prevention by prostaglandin E2. J Invest Dermatol 88:120–123
129. Ikai K (1999) Psoriasis and the arachidonic acid cascade. J Dermatol Sci 21:135–146
130. Christophers E, Sterry W (1993) Psoriasis. In: Fitzpatrick Th, Eisen AZ, Wolff K (eds) Dermatology in General Medicine. McGraw Hill, New York, NY, pp 489–515
131. Grimminger F, Mayser P (1995) Lipid mediators, free fatty acids and psoriasis. A review. Prostaglandins Leukot Essent Fatty Acids 52:1–15
132. Sokabe T, Tominaga M (2010) The TRPV4 cation channel: a molecule linking skin temperature and barrier function. Commun Integr Biol 3:619–621
133. Sokabe T, Fukumi-Tominaga T, Yonemura S et al (2010) The TRPV4 channel contributes to intercellular junction formation in keratinocytes. J Biol Chem 285:18749–18758
134. Cao DS, Yu SQ, Premkumar LS (2009) Modulation of transient receptor potential Vanilloid 4-mediated membrane currents and synaptic transmission by protein kinase C. Mol Pain 5:5
135. Patel KN, Liu Q, Meeker S et al (2011) Pirt, a TRPV1 modulator, is required for histamine-dependent and -independent itch. PLoS One 6:e20559
136. Kim AY, Tang Z, Liu Q et al (2008) Pirt, a phosphoinositide-binding protein, functions as a regulatory subunit of TRPV1. Cell 133:475–485
137. Augé C, Balz-Hara D, Steinhoff M et al (2009) Protease-activated receptor-4 (PAR 4): a role as inhibitor of visceral pain and hypersensitivity. Neurogastroenterol Motil 21:1189–e107
138. Frateschi S, Camerer E, Crisante G et al (2011) PAR2 absence completely rescues inflammation and ichthyosis caused by altered CAP1/Prss8 expression in mouse skin. Nat Commun Jan 2:161

139. Shimada SG, Shimada KA, Collins JG (2006) Scratching behavior in mice induced by the proteinase-activated receptor-2 agonist, SLIGRL-NH2. Eur J Pharmacol 530:281–293
140. Andoh T, Katsube N, Maruyama M et al (2001) Involvement of leukotriene B(4) in substance P-induced itch-associated response in mice. J Invest Dermatol 117:1621–1626
141. Yamaoka J, Di ZH, Sun W (2007) Changes in cutaneous sensory nerve fibers induced by skin-scratching in mice. J Dermatol Sci 46:41–51
142. Chen Y, Yang C, Wang ZJ (2011) Proteinase-activated receptor 2 sensitizes transient receptor potential vanilloid 1, transient receptor potential vanilloid 4, and transient receptor potential ankyrin 1 in paclitaxel-induced neuropathic pain. Neuroscience 193:440–451
143. Sipe WE, Brierley SM, Martin CM et al (2008) Transient receptor potential vanilloid 4 mediates protease activated receptor 2-induced sensitization of colonic afferent nerves and visceral hyperalgesia. J Physiol Gastrointest Liver Physiol 294:G1288–G1298
144. Tsujii K, Andoh T, Lee JB et al (2008) Activation of proteinase-activated receptors induces itch-associated response through histamine-dependent and -independent pathways in mice. J Pharmacol Sci 108:385–388
145. Chuang HH, Neuhausser WM, Julius D (2004) The super-cooling agent icilin reveals a mechanism of coincidence detection by a temperature-sensitive TRP channel. Neuron 43:859–869
146. Voets T, Owsianik G, Janssens A et al (2007) TRPM8 voltage sensor mutants reveal a mechanism for integrating thermal and chemical stimuli. Nat Chem Biol 3:174–182
147. Xing H, Chen M, Ling J et al (2007) TRPM8 mechanism of cold allodynia after chronic nerve injury. J Neurosci 27:13680–13690
148. McKemy DD, Neuhausser WM, Julius D (2002) Identification of a cold receptor reveals a general role for TRP channels in thermosensation. Nature 416:52–58
149. Bödding M, Wissenbach U, Flockerzi V (2007) Characterisation of TRPM8 as a pharmacophore receptor. Cell calcium 42:618–628
150. Beck B, Bidaux G, Bavencoffe A et al (2007) Prospects for prostate cancer imaging and therapy using high-affinity TRPM8 activators. Cell calcium 41:285–294
151. Tsavaler L, Shapero MH, Morkowski S et al (2001) Trp-p8, a novel prostate-specific gene, is up-regulated in prostate cancer and other malignancies and shares high homology with transient receptor potential calcium channel proteins Trp-p8, a novel prostate-specific gene, is up-regulated in prostate C. Cancer Res 61:3760–3769
152. Carstens E, Jinks SL (1998) Skin cooling attenuates rat dorsal horn neuronal responses to intracutaneous histamine. Neuroreport 9:4145–4149
153. Denda M, Tsutsumi M, Denda S (2010) Topical application of TRPM8 agonists accelerates skin permeability barrier recovery and reduces epidermal proliferation induced by barrier insult: role of cold-sensitive TRP receptors in epidermal permeability barrier homoeostasis. Exp Dermatol 19:791–795
154. Cho Y, Jang Y, Yang YD et al (2010) TRPM8 mediates cold and menthol allergies associated with mast cell activation. Cell calcium 48:202–208
155. Medic N, Desai A, Komarow H et al (2011) Examination of the role of TRPM8 in human mast cell activation and its relevance to the etiology of cold-induced urticaria. Cell calcium 50:473–480
156. Han JH, Choi H-K, Kim SJ (2011) Topical TRPM8 agonist (Icilin) relieved vulva pruritus originating from lichen sclerosus et atrophicus. Acta dermato-venereologica: 8–9
157. Story GM, Peier AM, Reeve AJ et al (2003) ANKTM1, a TRP-like channel expressed in nociceptive neurons, is activated by cold temperatures. Cell 112:819–829
158. Biró T, Ko MC, Bromm B et al (2005) Controversies in experimental dermatology How best to fight that nasty itch—from new insights into the neuroimmunological, neuroendocrine, and neurophysiological bases of pruritus to novel therapeutic approaches. Exp Dermatol 14:225–240
159. Macpherson LJ, Geierstanger BH, Viswanath V et al (2005) The pungency of garlic: activation of TRPA1 and TRPV1 in response to allicin. Curr Biol 15:929–934
160. Bandell M, Story GM, Hwang SW et al (2004) Noxious cold ion channel TRPA1 is activated by pungent compounds and bradykinin. Neuron 41:849–857
161. Bautista DM, Jordt SE, Nikai T et al (2006) TRPA1 mediates the inflammatory actions of environmental irritants and proalgesic agents. Cell 124:1269–1282
162. Bautista DM, Movahed P, Hinman A et al (2005) Pungent products from garlic activate the sensory ion channel TRPA1. Proc Natl Acad Sci USA 102:12248–12252
163. Jordt SE, Bautista DM, Chuang HH et al (2004) Mustard oils and cannabinoids excite

sensory nerve fibres through the TRP channel ANKTM1. Nature 427:260–265

164. Akopian AN, Ruparel NB, Patwardhan A et al (2008) Cannabinoids desensitize capsaicin and mustard oil responses in sensory neurons via TRPA1 activation. J Neurosci: Off J Soc Neurosci 28:1064–1075
165. Karashima Y, Damann N, Prenen J et al (2007) Bimodal action of menthol on the transient receptor potential channel TRPA1. J Neurosci: Off J Soc Neurosci 27:9874–9884
166. Karashima Y, Talavera K, Everaerts W et al (2009) TRPA1 acts as a cold sensor in vitro and in vivo. Proc Natl Acad Sci USA 106: 1273–1278
167. Nagata K, Duggan A, Kumar G (2005) Nociceptor and hair cell transducer properties of TRPA1, a channel for pain and hearing. J Neurosci 25:4052–4061
168. Poole DP, Pelayo JC, Cattaruzza F (2011) Transient receptor potential ankyrin 1 is expressed by inhibitory motoneurons of the mouse intestine. Gastroenterology 141:565–575
169. Jaquemar D, Schenker T, Trueb B (1999) An ankyrin-like protein with transmembrane domains is specifically lost after oncogenic transformation of human fibroblasts * lacking in SV40 transformed cells as well as in many. Biochemistry 274:7325–7333
170. Atoyan R, Shander D, Botchkareva NV (2009) Non-neuronal expression of transient receptor potential type A1 (TRPA1) in human skin. J Invest Dermatol 129:2312–2315
171. Stokes A, Wakano C, Koblan-Huberson M et al (2006) TRPA1 is a substrate for de-ubiquitination by the tumor suppressor CYLD. Cell signal 18:1584–1594
172. Salas MM, Hargreaves KM, Akopian AN (2009) TRPA1-mediated responses in trigeminal sensory neurons: interaction between TRPA1 and TRPV1. Eur J Neurosci 29:1568–1578
173. Staruschenko A, Jeske NA, Akopian AN (2010) Contribution of TRPV1-TRPA1 interaction to the single channel properties of the TRPA1 channel. J Biol Chem 285:15167–15177
174. Akopian AN, Ruparel NB, Jeske NA et al (2007) Transient receptor potential TRPA1 channel desensitization in sensory neurons is agonist dependent and regulated by TRPV1-directed internalization. J Physiol 583:175–193
175. Caceres AI, Brackmann M, Elia MD et al (2009) A sensory neuronal ion channel essential for airway inflammation and hyperreactivity in asthma. Proc Natl Acad Sci USA 106:9099–9104
176. Wilson SR, Gerhold KA, Bifolck-Fisher A et al (2011) TRPA1 is required for histamine-independent, Mas-related G protein-coupled receptor-mediated itch. Nat Neurosci 14:595–602
177. Liu Q, Tang Z, Surdenikova L et al (2009) Sensory neuron-specific GPCR Mrgprs are itch receptors mediating chloroquine-induced pruritus. Cell 139:1353–1365
178. Liu Q, Weng HJ, Patel KN et al (2011) The distinct roles of two GPCRs, MrgprC11 and PAR2, in itch and hyperalgesia. Sci Signal 4:ra45-ra45
179. Liang J, Ji Q, Ji W (2011) Role of transient receptor potential ankyrin subfamily member 1 in pruritus induced by endothelin-1. Neurosci Lett 492:175–178
180. Davidson S, Giesler GJ (2010) The multiple pathways for itch and their interactions with pain. Trends Neurosci 33:550–558
181. Dai Y, Wang S, Tominaga M et al (2007) Sensitization of TRPA1 by PAR2 contributes to the sensation of inflammatory pain. J Clin Invest 117:1979–1987
182. Makhlough A, Ala S, Haj-Heydari Z (2010) Topical capsaicin therapy for uremic pruritus in patients on hemodialysis. Iran J Kidney Dis 4:137–140
183. Kantor GR, Resnik KS (1996) Treatment of lichen simplex with topical capsaicin cream. Acta Derm Venereol 76:161
184. Munn SE, Burrows NP, Abadia-Molina F et al (1997) The effect of topical capsaicin on substance P immunoreactivity: a clinical trial and immuno-histochemical analysis. Acta Derm Venereol 77:158–159
185. Bernstein JE, Parish LC, Rapaport M et al (1986) Effects of topically applied capsaicin on moderate and severe psoriasis vulgaris. J Am Acad Dermatol 15:504–507
186. Ellis CN, Berberian B, Sulica VI et al (1993) A double-blind evaluation of topical capsaicin in pruritic psoriasis. J Am Acad Dermatol 29:438–442
187. Lotti T, Teofoli P, Tsampau D (1994) Treatment of aquagenic pruritus with topical capsaicin cream. J Am Acad Dermatol 30:232–235
188. Hautmann G, Teofoli P, Lotti T (1994) Aquagenic pruritus, PUVA and capsaicin treatments. Br J Dermatol 131:920–921
189. Reimann S, Luger T, Metze D (2000) Topische Anwendung von Capsaicin in der Dermatologie zur Therapie von Juckreiz und Schmerz. Hautarzt 51:164–172
190. Cappugi P, Lotti T, Tsampau D et al (1989) Capsaicin treatment of different dermatological affection with itching. Skin Pharmacol 2:230

191. Tupker RA, Coenraads PJ, van der Meer JB (1992) Treatment of prurigo nodularis, chronic prurigo and neurodermatitis circumscripta with topical capsaicin. Acta Derm Venereol 72:463–465
192. Goodless DR, Eaglstein WH (1993) Brachioradial pruritus: treatment with topical capsaicin. J Am Acad Dermatol 29:783–784
193. Knight TE, Hayashi T (1994) Solar (brachioradial) pruritus—response to capsaicin cream. Int J Dermatol 33:206–209
194. Szeimies RM, Stolz W, Wlotzke U et al (1994) Successful treatment of hydroxyethyl starch-induced pruritus with topical capsaicin. Br J Dermatol 131:380–382
195. Reimann S, Metze D (1995) Topische Capsaicin-Therapie bei Lichen simplex und Prurigo nodularis. Z Hautkr 70:586–588
196. Neess CM, Dissemond J, Herrmann G et al (2000) Treatment of pruritus by capsaicin in a patient with pityriasis rubra pilaris receiving RE-PUVA therapy. Clin Exp Dermatol 25:209–211
197. Kirby B, Rogers S (1997) Treatment of PUVA itch with capsaicin. Br J Dermatol 137:152
198. Burrows NP, Norris PG (1994) Treatment of PUVA-induced skin pain with capsaicin. Br J Dermatol 131:584–585
199. Weisshaar E, Dunker N, Gollnick H (2003) Topical capsaicin therapy in humans with hemodialysis-related pruritus. Neurosci Lett 345(3):192–194
200. Metz M, Krause K, Maurer M et al (2011) Treatment of notalgia paraesthetica with an 8% capsaicin patch. Br J Dermatol 165: 1359–1361

Chapter 17

Skin Sensitivity Studies

Laurent Misery

Abstract

Sensitive skin is defined as the occurrence of erythema and/or abnormal stinging, burning, and tingling sensations (and sometimes as pain or pruritus) in response to multiple factors that may be physical (UV, heat, cold, wind), chemical (cosmetics, soaps, water, pollutants), psychological (stress), or hormonal (menstrual cycle). Because sensitive skins are defined as a response to multiple factors that may be physical and/or chemical, an abnormal activation of TRP channels appears probable. They can be studied using questionnaires or clinical tests with different stimuli. In vitro studies are also possible with co-cultures of neurons and skin cells mimicking neurogenic inflammation.

Key words: Sensitive skin, Reactive skin, Capsaicin, Lactic acid, Neurogenic inflammation

1. Introduction

Although the existence of sensitive skin has been challenged in the past and remains somewhat controversial, there is now a near-consensus that sensitive skin can be defined clinically (1) as abnormal stinging, burning, and tingling sensations (and sometimes as pain or pruritus) in response to multiple factors that may be physical (UV, heat, cold, wind), chemical (cosmetics, soaps, water, pollutants), psychological (stress), or hormonal (menstrual cycle). Erythema is often, but not always, a feature. Tests that may help to establish the diagnosis include the stinging test, heat sensitivity test, and capsaicin test. However, the diagnosis relies on history-taking, which is obviously the most reliable method given that, by definition, skin sensitivity occurs in response to a variety of factors.

Sensitive skin is also known as reactive or overreactive skin, intolerant skin, and irritable skin. The term "reactive skin" seems preferable over "sensitive skin," which may induce confusion with sensitized skin due to an allergic disorder. Although the pathophysiology

Arpad Szallasi and Tamás Bíró (eds.), *TRP Channels in Drug Discovery: Volume II*, Methods in Pharmacology and Toxicology,
DOI 10.1007/978-1-62703-095-3_17,

of sensitive skin is unclear (2), the underlying mechanism is not immunological or allergic. Histological examination only rarely shows vasodilation with an inflammatory infiltrate. In general, there are no histological abnormalities. The "skin tolerance threshold" is abnormally low. Skin barrier function is altered in some patients, leading to transepidermal water loss that may promote contact with irritants. The abnormal sensations and vasodilation reflect the involvement of the cutaneous nervous system (2). Neuromediators such as substance P, calcitonin gene-related peptide, and vasoactive intestinal peptide may induce neurogenic inflammation with vasodilation and mast cell degranulation. In addition, nonspecific inflammation may result from the release of interleukins 1 and 8, prostaglandins E2 and F2, and tumor necrosis factor alpha.

Although it has never been demonstrated, the role of TRP channels in skin reactivity is obvious. Because sensitive skins are defined as a response to multiple factors that may be physical and/or chemical, an abnormal activation of TRP channels appears probable (2). In the skin, TRP channels are known to be expressed on nerve endings, Merkel cells and keratinocytes (3). TRPV1 is activated by capsaicin, phorbol esters, heat, and H^+ ions. TRPV3 is activated by heat and camphor. TRPV4 activation is due to heat, mechanical stresses, hypo-osmotic stress, and phorbol ester derivatives. Cold and menthol activate TRPM8. TRPA1 is activated by cold, wasabi, mustard, horseradish, or bradykinin. TRP channels are probably activated by other substances that are included in cosmetic products. The activation of TRP channels is followed by Ca^{2+} influx into cells then depolarization.

Reactive skin is extremely common. In France, about 50% of individuals (59% of women and 41% of men) report having reactive skin (4). This patient-reported prevalence varies little across countries (5) and reactive skin is clearly an extremely common cosmetic problem. Racial factors have been suggested but none has been identified, and the prevalence of reactive skin seems chiefly related to environmental factors. This prevalence increases in the summer (6), suggesting a role for UV exposure, but there is no association with the skin phototype (7). Although the appearance of the skin is normal in the vast majority of cases, reactive skin may occur in individuals who have another skin disorder (e.g., atopic dermatitis, seborrheic dermatitis, or rosacea) (4).

Skin reactivity is not confined to the face. Among patients reporting reactive skin, 70% have involvement of extrafacial sites such as the hands (58%), scalp (36%), feet (34%), neck (27%), torso (23%), or back (21%) (8). On the scalp, the semiology is somewhat different, and we recently developed a new assessment scale (9, 10).

The best methods for exploring sensitive skin are those which use questionnaires. However, some clinical tests are commonly used and in vitro studies are possible.

2. Materials

2.1. Clinical Studies

2.1.1. Questionnaires

Because symptoms of skin sensitivity are mainly subjective and transient, their description by subjects with sensitive skin is the best method. However, standardized questionnaires are useful because they allow the obtention of scores.

We participate in the definition of two scores: Sensitive Scale for skin sensitivity of the face and the 3S Questionnaire for skin sensitivity of the scalp (10). We will focus on the 3S Questionnaire because the Sensitive Scale is not yet published.

2.1.2. Clinical Tests

Several tests are available to study sensitive skins: stinging tests with capsaicin or lactic acid, irritation test with sodium laurylsulfate, study of subclinical erythema with cross-polarized light, infrared thermographic scanner, quantitation of cutaneous thermal sensation, nicotinate test, laser Doppler velocimetry, colorimetry, etc. (1, 11).

We will focus on stinging tests because they are the most commonly used and are more specific of TRPV1 activation. They are performed by using lactic acid (5 or 10%) (12) or capsaicin.

2.2. In Vitro Studies

Skin reactivity could be considered as a clinical model of neurogenic inflammation (2). Following the activation of TRP channels by various factors, neuronal membrane is depolarized and there is a release of neuropeptides. These neuropeptides induce inflammation, with erythema and discomfortable sensations. By using a coculture of neurons and keratinocytes and measuring neuronal activation in response to TRPV1 activation, we propose an in vitro model of neurogenic inflammation (13).

2.2.1. Animals

1. Kantor male piglets

2.2.2. Reagents

1. Dulbecco's modified Eagle medium (DMEM) (Invitrogen, Paisley, UK)
2. 50× B-27 Supplement (Invitrogen)
3. Dispase® (Invitrogen)
4. Phosphate buffered saline (PBS) without calcium and magnesium (Invitrogen)
5. Dimethyl sulfoxide (DMSO) (Sigma-Aldrich, St. Louis, MO)
6. Collagenase IV (Sigma-Aldrich)
7. Capsaicin (Sigma-Aldrich)
8. Brain-derived neurotrophic factor (BDNF) (Sigma-Aldrich)
9. Nerve growth factor (NGF) (Sigma-Aldrich)
10. Keratinocyte growth media 2 (KGM2 Bullet Kit) (Lonza, Levallois, France)
11. Trypsin (1/250 with EDTA) (Lonza)

12. Normocin® (Invivogen, Toulouse, France)
13. Substance P (SP) enzyme immunoassay (R&D Systems, Lille, France)

3. Methods

3.1. Clinical Studies

3.1.1. Questionnaires

For the occurrence of tightness, burning, prickling, itching or pain sensations, each of these five symptoms are graded in terms of their impact on quality of life (Table 1). The grades are attributed as follows: 0—sensation absent, 1—sensation present but not troublesome, 2—sensation somewhat troublesome, 3—sensation sufficiently troublesome to make me change my lifestyle, 4—sensation unbearable. A score that we named 3S (Sensitive Scalp Score) is obtained from the sum of the grades given to each type of sensation, the maximum possible score being 20 (Notes 1 and 2).
The 3S score is effective for discrimination between slightly sensitive or sensitive scalp and very sensitive scalp and for distinction between sensitive or not sensitive scalp. However, no cut-off points have been defined until now.

3.1.2. Clinical Tests

Capsaicin or lactic acid is applied on a nasogenien groove. Vehicle is applied on the other groove as a control. Stingings are evaluated (from 0 to 3) each minute for 5 min (Notes 1–4).

3.2. In Vitro Studies

3.2.1. Cell Cultures

1. To obtain sensory neurons, dorsal root ganglia (DRG) were removed from the pigs, and neuronal cells were isolated (Note 1).
2. Ganglia were incubated at 37°C for 30 min in DMEM supplemented with 0.40 U/mL of collagenase IV and incubated for 15 min with trypsin.
3. Individual cells were mechanically dissociated by repeated pipetting.

Table 1
The 3S questionnaire

For each of the five following symptoms (Do you feel itching, prickling, tightness, pain or burning on your scalp?), which of the statements below does best describe how it affects you?
No, I do not feel it
Yes, but it is not troublesome
Yes, and it is slightly troublesome
Yes, and it is sufficiently troublesome to alter my lifestyle
Yes, and it is unbearable

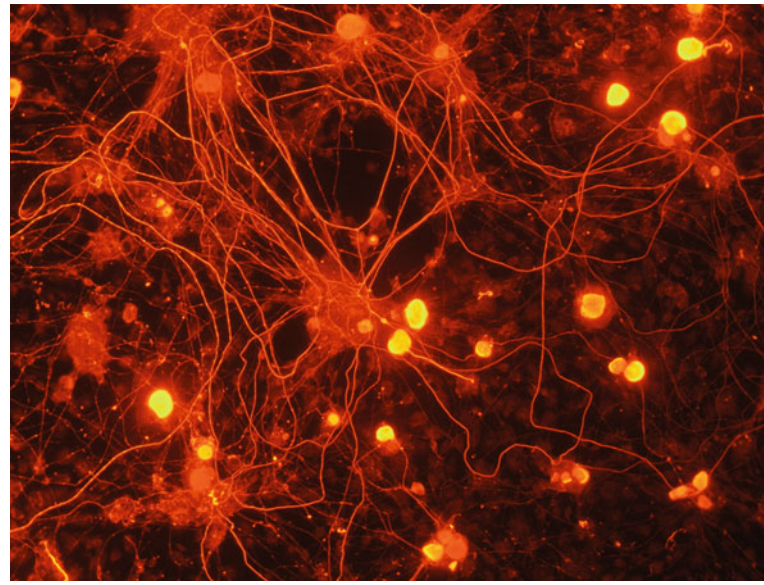

Fig. 1. Immunostaining of sensory neurons with anti-PGP9.5 antibodies after 7 days of a coculture with keratinocytes.

4. They were resuspended in KGM2 supplemented with 10% B-27, 100 ng/mL mouse NGF, 10 ng/mL human BDNF and 1× Normocin® (referred to hereafter as coculture media).
5. To isolate keratinocytes, the abdominal skin was rapidly excised, and hypodermis and reticular dermis were removed using a scalpel.
6. The thin layers of skin were incubated overnight at 4°C in Ham F12 supplemented with 20 U/mL Dispase®.
7. The following day, the epidermis was removed, incubated three times for 15 min each in trypsin solution, and the cell suspension was resuspended in coculture media. Cocultures were performed for 7 days (Fig. 1).

3.2.2. Measurement of SP Secretion (Notes 2 and3)

1. Neuronal cells were seeded in 96-well cell culture microplates with 50,000 cells per well.
2. Keratinocytes were then added to the wells 12 h later at a density of 10,000 cells per well.
3. Cells were cultured in coculture medium at 37°C in an atmosphere of 5% CO_2. The medium was removed and fresh medium was added every 2 days.
4. After 1 week of coculture, we measured the basal levels of substance P and these levels after a 10-min, 1-h or 72-h exposure to 10 µM capsaicin.

4. Notes

4.1. Clinical Studies

4.1.1. Questionnaires

1. This questionnaire is very useful for studies on scalp sensitivity because objective measurements are difficult due to the fact that hairs hide erythema.
2. It allows qualitative studies according to each symptom.

4.1.2. Clinical Tests

1. This is not a diagnostic test. It only brings a new element in favor of skin sensitivity.
2. It is useful to make comparisons.
3. It has to be interpreted cautiously because it can vary from 1 day to another.
4. It is very easy.

4.2. In Vitro Studies

1. Dissection of DRG and cell isolations require experienced operator.
2. Because results are very variable from one experiment to another and from one donor to another, results must be converted into a percentage of inhibition SP release.
3. By the addition of different substances, it is possible to evaluate the inhibitory or targeting effects of these substances on skin reactivity (14, 15).

References

1. Berardesca E, Fluhr JW, Maibach HI (2006) Sensitive skin syndrome. Taylor & Francis, New York
2. Ständer S, Schneider SW, Weishaupt C, Luger TA, Misery L (2009) Putative neuronal mechanisms of sensitive skin. Exp Dermatol 18:417–423
3. Boulais N, Misery L (2008) The epidermis: a sensory tissue. Eur J Dermatol 18:119–127
4. Misery L, Myon E, Martin N, Verrière F, Nocera T, Taieb C (2005) Peaux sensibles en France: approche epidemiologique [In French]. Ann Dermatol Venereol 132:425–429
5. Misery L, Boussetta S, Nocera T, Perez-Cullell N, Taieb C (2009) Sensitive skin in Europe. J Eur Acad Dermatol Venereol 23:376–381
6. Misery L, Myon E, Martin N, Consoli S, Boussetta S, Nocera T et al (2007) Sensitive skin: psychological effects and seasonal changes. J Eur Acad Dermatol Venereol 21:620–628
7. Misery L, Sibaud V, Merial-Keny C (2011) Sensitive skin in the American population: prevalence, clinical data and the role of dermatologist. Int J Dermatol 50:961–967
8. Saint-Martory C, Roguedas-Contios AM, Sibaud V, Degouy A, Schmitt AM, Misery L (2008) Sensitive skin is not limited to the face. Br J Dermatol 158:130–133
9. Misery L, Sibaud V, Ambronati M, Macy G, Boussetta S, Taieb C (2008) Sensitive scalp: does this condition exist? An epidemiological study. Contact Dermatitis 58:234–238
10. Misery L, Rahhali N, Ambonati M, Black D, Saint-Martory C, Schmitt AM et al (2011) Evaluation of sensitive scalp severity and symptomatology by using a new score. J Eur Acad Dermatol Venereol 25:1295–1298
11. Farage MA, Maibach HI (2010) Sensitive skin: closing in on a physiological cause. Contact Dermatitis 62:137–149
12. Frosch PJ, Kligman AM (1977) A method of apraising the stinging capacity of topically applied substances. J Soc Cosmet Chem 28:197–209

13. Pereira U, Boulais N, Lebonvallet N, Lefeuvre L, Gouegerot A, Misery L (2010) Development of an in vitro culture of primary sensitive pig neurons and keratinocytes for the study of cutaneous neurogenic inflammation. Exp Dermatol 19:931–935
14. Pereira U, Boulais N, Lebonvallet N, Pennec JP, Dorange G, Misery L (2010) Mechanisms of the sensory effects of tacrolimus on the skin. Br J Dermatol 163:70–77
15. Pereira U, Garcia-Le Gal C, Le Gal G, Boulais N, Lebonvallet N, Dorange G, Lefeuvre L, Gougerot A, Misery L (2010) Effects of sangre de drago on an in vitro model of cutaneous neurogenic inflammation. Exp Dermatol 19:796–799

Chapter 18

Hair Follicle Culture

Michael P. Philpott

Abstract

Hair follicle organ culture allows individual hair follicles from many species to be maintained in culture during which time hair fiber is produced. Cultured hair follicles can be used to investigate the role of hair growth regulatory factors especially with regards hair growth stimulation and anagen to catagen transition, metabolism and the process of hair fiber synthesis. They are also responsive to drugs and small molecules and as such can be used to dissect the role of signal transduction pathways in the regulation of hair biology. Although a number of papers have reported the use of cultured hair follicles to investigate regulation of the hair cycle with the exception of anagen to catagen transition, we have still to model the entire hair cycle in vitro and this is one major limitation of the model. We also have to accept that despite the best efforts it is still difficult to keep follicles in culture much beyond 10 days. However, the model should prove an excellent system with which to use siRNA and this may open up an ever greater understanding of the factors that regulate hair biology.

Key words: Hair, Follicle, Culture, Anagen, Catagen

1. Introduction

In order to understand the mechanisms involved in the regulation of hair follicle development, growth, differentiation and cycling, it is important to have available as many model systems as possible including in vivo animal models, cell, and organ culture. Each of these model systems has its advantages and disadvantages. In vivo models allow follicles to be studied in situ and detailed observations can be made using morphological criteria, immunohistochemistry, in situ hybridization, and RT-PCR. However, it is difficult to quantify molecular or biochemical parameters of individual follicles and in vivo models do not allow follicles to be studied in a fully defined environment. Cell culture involves the isolation and culture of individual cell populations from which

Arpad Szallasi and Tamás Bíró (eds.), *TRP Channels in Drug Discovery: Volume II*, Methods in Pharmacology and Toxicology,
DOI 10.1007/978-1-62703-095-3_18,

many morphological, biochemical, and molecular parameters can be measured. However, cell culture results in the loss of the normal three-dimensional architecture of the organ and as such, it is sometimes difficult to translate observations from cell culture to the whole organ. Histiotypic culture, in which different cell types may be co-cultured goes some way towards addressing some of the disadvantages of cell culture but still do not fully mimic the in vivo environment.

Organ culture involves the in vitro culture of either an intact organ in the case of embryonic tissue or, in the case of neonatal or adult tissue, usually small pieces of an organ (1). The advantage of organ culture is that the component cells of the organ are maintained in their in vivo three-dimensional environment and that often the external environment in which the organ maintained is fully defined. However, disadvantages include lack of blood supply, associated systemic factors and innervation. Perhaps the most obvious of these is blood supply. For an organ-maintained tissue to survive gases, nutrients, growth regulatory factors, and waste products must be freely diffusible through the tissue. Therefore, if the organ to be maintained is too large, then the cells in its center will not be sufficiently perfused, as a result they will become necrotic and die, resulting in loss of integrity of the cultured organ. Because of these size restrictions, organ culture is frequently used for embryonic tissues and less so for adult organs. However, the hair follicle is an ideal size for organ culture.

1.1. Culture Medium

Prior to the development of culture systems for human hair follicles, methods had been described for the maintenance of human sebaceous glands as well as apocrine and eccrine sweat glands using supplemented Williams E medium (2); originally developed for the culture of hepatocytes (3). In our hands Williams E medium supports optimum growth of follicles when compared to other types of tissue culture medium although a wide range of tissue culture medium and supplements have been used by researchers. Low calcium keratinocyte growth medium (KGM) does not support in vitro hair follicle growth although the ORS remains viable. Histology of hair follicles cultured in KGM suggests that low calcium-induced changes in cell adhesion are primarily responsible for the inhibition of hair growth. Likewise culture of hair follicles in Williams E medium lacking phenol red is also inhibitory, although whether this inhibition is a direct result of removing the estrogenic effects of phenol red is not known. Other media have been used by other workers including DMEM (4), Hams F12 (5), RPMI 1640 (6, 7), and Eagles MEM (8). However, in all instances lower rates of in vitro hair follicle growth were reported by these workers, when compared to those reported for Williams E.

As well as selecting a suitable tissue culture medium for hair follicle culture, it is also essential to add additional supplements.

In our hands we have found that 2 mM l-glutamine, insulin (10 μg/ml), and hydrocortisone (10–100 ng/ml) are important for successful hair follicle culture. In addition, we also add penicillin (100 U/ml) and streptomycin (100 μg/ml). Insulin and glutamine are essential for successful in vitro follicle culture and without their inclusion in tissue culture medium very slow rates of follicle growth will be achieved; moreover, in the absence of insulin some follicles will enter catagen (9). Penicillin and streptomycin are our choice of antibiotics although other workers have also used gentamicin. Fungizone is inhibitory and should not be used. In our laboratories (10, 11), we have found that serum inhibits hair follicle growth at levels as low as 1% (v/v). However, other workers report stimulation of follicle growth by serum (4). This is difficult to interpret however, it is worth noting that rates of in vitro growth achieved in these studies are lower than those achieved by us using serum-free medium (11). Therefore, in suboptimal conditions serum may indeed have a stimulatory action.

As well as a variety of different culture mediums and supplements having been used for follicle culture, a number of different support systems have also been used. In our laboratory, we traditionally place hair follicles in individual wells of 24-well plates. Imai et al. (5, 6) have used traditional methods of organ maintenance in which follicles were maintained at the air–liquid interface on lens tissue paper placed on a stainless steel mesh, whilst Kondo et al. (4) used siliconized glass tubes containing 1.5 ml of medium, gassed with 95% O_2/5% CO_2. Most tissue culture mediums are buffered by bicarbonate and therefore, require gassing with between 5 and 10% CO_2. In our hands, HEPES is inhibitory and to be avoided if possible. Imai et al. (5) have investigated a number of other different environments including 95% air/5% CO_2 and 95% O_2/5% CO_2 and at different temperatures 25°C, 31°C and 37°C of which they reported that 95% O_2/5% CO_2 and a temperature of 31°C were optimum. However, these observations were based on hair follicle morphology and rates of tritiated thymidine uptake and hair follicle length measurements were not made. In our hands, gassing follicles with oxygen instead of air is toxic. Gelatin sponges have also been used to support human hair growth in vitro (8). We routinely use such sponges for maintenance of isolated PSU (12) and murine vibrissae follicles (13). However, we find that for isolated follicle bulbs they do not offer any significant growth advantage.

1.2. Hair Follicle Isolation

For the successful culture of hair follicles, it is essential to ensure that the hair follicles are not damaged on isolation. If follicles are even slightly damaged, then they will either fail to grow or more often grow at much reduced rates. Several methods have been used to isolate intact hair follicles. These include plucking, collagenase digestion, shearing, and micro-dissection.

1.2.1. Plucking

This is the oldest technique for isolating hair follicles and has been used as a source of ORS for primary and explant keratinocyte culture (14–16) and for metabolic and cytotoxic experiments (17–19). However as a source of hair follicles for organ maintenance, plucking has a number of drawbacks namely: plucking usually results in considerable physical damage to the hair follicle and usually the dermal papilla and sebaceous gland are torn from the follicle and left in the skin (19–22). Because of this physical damage, plucked hair follicles are not viable for organ maintenance.

1.2.2. Collagenase Digestion

The use of enzymes such as collagenase to isolate skin glands and appendages has been used by a number of workers (23–25). The major problem with any enzymatic form of isolation is that they can either cause tissue disaggregation or promote primary explant, neither of which is desirable in organ culture. Collagenase digestion has however been very useful for isolating large numbers of follicles for biochemical or cell culture (24, 25).

1.2.3. Shearing

Shearing was first reported for the successful isolation of human eccrine sweat glands (2) and later for the isolation of human apocrine and sebaceous glands (26, 27). The success of this method is due to the periglandular capsule of collagen that surrounds skin glands and appendages in situ. Repeated chopping of skin with a sharp pair of scissors causes this collagen capsule to shear and the glands pop out. Shearing can be used to isolate intact human hair follicles (28) although the yield is variable and because of the elongated nature of the hair follicle as opposed to the globular structure of the skin glands shearing tends to cut hair follicles into small segments one of which usually includes an intact hair follicle bulb. Shearing has however proved very useful for the isolation of large numbers of intact, murine, pelage follicles for biochemical analysis (29).

1.2.4. Micro-dissection

Traditionally micro-dissection is the most reliable method of isolating intact hair follicles, although great care must be taken not to damage the follicle. At present, micro-dissection is the only accurate method for isolating intact pilosebaceous units consisting of the hair follicle and sebaceous gland. Sanders et al. (12) have described the isolation of human pilosebaceous units from female facelift skin. It is obvious that whilst micro-dissection is a useful method for isolating intact pilosebaceous units, the number of follicles that can be obtained severely restricts the number of experiments that can be carried out. In 1990, we reported on a modified method of micro-dissection that was able to yield much larger numbers of intact hair follicle bulbs (10). Isolation of hair follicles using this method is achieved by cutting human skin into thin strips approximately 3–5 mm × 10 mm and then by using a scalpel blade to cut through the skin at the dermal–subcutaneous fat interface. Then by placing the fat layer under a stereo-dissecting microscope (cut side uppermost), it is possible to identify the cut ends of the hair follicle protruding

from the fat. Using watchmakers forceps the outer root sheath can be grasped and the intact follicle bulb removed from the fat. Care must be taken when removing the follicles not to grasp the hair fiber as this will damage the follicle and this will dramatically influence the ability of these follicles to grow in culture.

Using this method, it is routinely possible to isolate in excess of 100 human anagen hair follicles in 1–2 h from a piece of skin 4 cm × 2 cm. Hair follicles in the catagen stage of their growth cycle are occasionally seen isolated by this method although their yield is small, usually 2–5 catagen follicles for every 100 anagen hair follicles isolated. These catagen hair follicles can be cultured and appear to progress into a telogen-like state however, their small number preclude any serious functional experiments. The method described above works very well for scalp hair follicles. Other workers have also reported isolation and in vitro culture of follicles from different areas of the body including the beard, axilla and pubis, although no significant differences in growth rate were observed (30).

The methods described above yield large numbers of hair follicle bulbs. However, by isolating follicles by cutting at the dermal–subcutaneous fat interface we leave behind in the discarded epidermis and dermis most of the permanent portion of the hair follicle including the sebaceous gland, infundibulum, and isthmus. To isolate intact pilosebaceous units (PSU), we use careful microdissection (12). These techniques are slow, as care must be taken not to damage the hair follicle. However, using such methods it is possible to isolate several dozen PSU in a couple of hours.

2. Materials

2.1. Equipment

For the isolation of human hair follicles, it is essential to have a good dissecting microscope and sharp watchmakers forceps. Forceps and other instruments were sterilized by autoclaving. For culture, any CO_2 humidified incubator will do. For hair follicle measurement, we use an inverted microscope with either eye piece measuring graticule or a digital camera.

1. Binocular Dissecting microscope Nikon SMZ-1B (Nikon Instruments Europe BV, http://www.nikoninstruments.com) with a Photonic PL3000 light source (Nikon Instruments Europe BV, http://www.nikoninstruments.com)
2. Scalpel blades Swann Morton No 22 and No 24 (Swann-Morton, Sheffield, UK)
3. Watchmakers Forceps No 5 (Ideal-Tek, Switzerland)
4. Thermo Scientific; Shandon Dissecting Board (1.9 × 40.6 × 30.5 cm) (Thermo Fisher Scientific Inc., http://www.thermoscientific.com)

5. Plastic petri dishes 60 mm diameter (Sterilin Ltd, Newport Wales now part of Thermo Fisher)
6. Multiwell plates Falcon 24-well plates (Beckton Dickinson, Oxford, UK)
7. Humidified CO_2 Incubator
8. Nikon Eclipse Inverted Light microscope (TE2000-S with epi-fluorescent attachment) (Nikon Instruments Europe BV, http://www.nikoninstruments.com)

2.2. Reagents

1. Williams E Medium bought as liquid media (1×) (Sigma-Aldrich, Poole, UK). In our experience, medium made up from powder sustains suboptimal growth of hair follicles.
2. Penicillin and Streptomycin (Sigma-Aldrich, Poole, UK). Bought as a single solution with both antibiotics at 100× concentration. Keep frozen as 1 ml aliquots at −20°C. When required aliquots are defrosted and 1 ml added to 100 ml of Williams E medium.
3. l-glutamine (Sigma-Aldrich, Poole, UK). Bought as liquid at 200 mM (100×). Store at −20°C as 10 ml aliquots. 1 ml is added to 100 ml of Williams E medium immediately prior to use to make a final concentration of 2 mM.
4. Hydrocortisone (Sigma-Aldrich, Poole, UK). Bought in vials containing 1 mg powder. Reconstitute with 1 ml 100% (v/v) Ethanol, followed by 19 ml tissue culture medium (Williams E). Store at −20°C as 1 ml aliquots. Add 100 µl to 100 ml of tissue culture medium to make a final concentration of 50 ng/ml.
5. Insulin (Sigma-Aldrich, Poole, UK). Bought as vials of 100 mg powder to which 10 ml of sterile distilled water is added followed by 100 µl of glacial acetic acid. Store as 100 µl aliquots at −20°C and add 100 µl to 100 ml of tissue culture medium to give a final concentration of 10 µg/ml.
6. Earls Balanced Salts Solution (EBSS) and Phosphate Buffered Saline with 2 mM Ca^{2+} and 2 mM Mg^{2+} (PBS+) (Sigma-Aldrich, Poole, UK).
7. Gelfoam® expandable gelatin sponge (Pfizer, USA).

3. Methods

3.1. Isolation of Human Hair Follicles

1. Skin from facelifts should be kept wrapped in sterile gauze moistened with PBS until required (Note 1).
2. Using a sharp scalpel blade Swann Morten No 22 or No 24 skin is cut into small pieces of approx. 10 mm × 5 mm.

3. Place these pieces in EBSS:PBS (1:1) in 60 mm plastic petri dishes during the dissection process and keep at room temperature (RT). We use EBSS:PBS as the EBSS provides glucose for the biopsy and PBS acts as a buffer allowing the isolation medium to be carried out on an open bench if required.
4. Take one 10 mm × 5 mm piece of skin and lay on its side and with a sharp scalpel blade cut at the interface between the subcutaneous fat and dermis using a dissecting board as this helps reduce blunting of scalpel blades. Cutting between the interface of the dermis and subcutaneous fat cuts the hair follicle just below the sebaceous gland resulting in the lower portion of the hair follicle including the follicle bulb being left in the subcutaneous fat from which it can be easily isolated. Note we use micro-dissection (see below) if we require an intact pilosebaceous unit with sebaceous gland and isthmus and infundibulum.
5. Place subcutaneous fat which contains the follicle bulb in EBSS:PBS (1:1) in a 60 mm plastic petri dish until required for follicle isolation. These can be kept at room temperature (RT) for several hours.
6. Repeat for other skin pieces and keep in EBSS:PBS (1:1) at RT.
7. Hair follicles are easily isolated by placing the subcutaneous fat on the upturned lid of a 60 mm plastic petri dish and under a dissecting microscope with the cut surface facing upward gently grasp the protruding cut portion (outer root sheath and hair fiber) of the follicle and gently pull the follicle bulb from the fat.
8. Place isolated follicle in 60 mm petri dish containing EBSS. We would normally expect to isolate at least 100 hair follicles using this method over 2–3 h from a facelift of approximately 1 cm × 4 cm in dimension. However, in recent years less invasive facelifts are carried out and increasingly this results in much smaller pieces of skin and often containing fewer hair follicles.
9. Once follicles have been isolated, we routinely place them into culture immediately (see below). However, follicles can be kept overnight in William E culture medium (below) at 37°C in a humidified CO_2 incubator.

3.2. Hair Follicle Organ Culture

1. Hair follicles are cultured individually in 24-well multiwall plates (Falcon 3047) containing 500 µl of Williams E medium supplemented with 2 mM l-glutamine, 10 mg/ml insulin, 10–50 ng/ml hydrocortisone, 100 U/ml penicillin, and 100 mg/ml streptomycin (Notes 2–5).
2. By placing hair follicles in individual wells of 24-well plates individual growth rates are measured using either an eye piece graticule in an inverted microscope or more routinely using a digital camera attached to the microscope.
3. Medium is changed every 3–4 days by using a 5 ml syringe with a small needle attached to aspirate the medium (Notes 6–8).

3.3. In Vitro Hair Growth Measurements

1. The standard approach when culturing human hair follicles in vitro is to measure the initial length of the follicle on day zero of the experiment and then to make daily measurement of the entire length at 24 h intervals. Daily rates of hair growth can then be calculated (9).
2. Another very powerful application of the in vitro hair growth model is its use to investigate factors that initiate anagen–catagen transition by either observing the hair follicles under an inverted microscope while in culture or following routine histology (9, 31–38).
3. However, in addition to measuring hair follicle growth rates it is also important to analyze whether follicles are in their active growth phase or show signs of catagen as demonstrated by rounding of the dermal papilla. The reason for such observations is important since many actives under investigation may not work via stimulation of anagen; in fact it is highly likely that regulation of anagen–catagen transition is going to be a more productive area of hair biology research. Two excellent examples of this method of analysis being applied include the study by Andrew Messengers group (39) by investigating the effects of cyclosporine A on hair follicle growth. They showed that 18 of 42 cyclosporine-treated follicles (43%) were still growing after 15 days compared with one of 42 control follicles (2%). This suggests that the hypertrichotic action of cyclosporin A may be due to prolongation of the anagen phase of the hair growth cycle.

3.4. Isolation and Culture of the Human Pilosebaceous Unit

In addition to isolation and culture of intact hair follicle bulbs, methods have also been devised for the isolation of intact pilosebaceous units which include the follicle bulb, isthmus, sebaceous gland, and infundibulum (12). Isolated pilosebaceous units are maintained in the same culture medium as isolated follicle bulbs however, rather than leave the follicles free floating we use gelatin sponge (Gelfoam) supports (40). To dissect human pilosebaceous units the following protocol is employed.

1. Skin should be kept wrapped in sterile gauze moistened with PBS until required.
2. Using a sharp scalpel blade Swann Morten No 22 or No 24 skin is cut into small pieces of approx. 10 mm × 5 mm.
3. Place these pieces in EBSS:PBS (1:1) in 60 mm plastic petri dishes during the dissection process and keep at room temperature (RT). We use EBSS:PBS as the EBSS provides glucose for the biopsy and PBS acts as a buffer allowing the isolation medium to be carried out on an open bench if required.
4. Under a dissection microscope further cut the small pieces of skin into thin slithers approximately 1–2 mm wide.

5. When viewed under a dissecting microscope, individual pilosebaceous units can be seen and can be carefully dissected (Note 9).
6. Intact pilosebaceous units are cultured on Gelfoam supports in individual wells of 24-well plated in 500 µl of Williams E medium as described above (Note 10).

3.5. Isolation and Culture of Hair Follicles from Other Species

In addition, hair follicles from human skin follicles can also be cultured from a wide range of other species including rats and mice (13, 41–48), sheep (49–52), goats (53), and red deer (54).

1. Generally because of the size of these follicles they have to be isolated using micro-dissection and the steps outlined above for isolation and culture of the human pilosebaceous unit are appropriate.
2. In our hands rat pelage follicles can be maintained free floating in Williams E medium (47) as described for human hair follicles (10).
3. Mouse and rat vibrissae follicles are best maintained on Gelfoam (13). Although their small size can make dissection difficult mouse and rat vibrissae follicles are larger than pelage follicles and easy to isolate by dissection. Vibrissae follicles also have an advantage in that their hair cycle is relatively short and predictable compared to human hair follicles and as such hair follicles from different stages of the cycle can be studies in vitro, something that cannot be done with human hair follicles (48) and can also be used to partially model the hair cycle in vitro (13).
4. The red deer model developed by Julie Thornton and Valerie Randall (54) is also very elegant as these follicles are androgen responsive and so provide a nice model to study the effects of androgens on hair follicle growth.

4. Notes

1. Skin specimens are normally brought to our laboratory wrapped in sterile gauze moistened with saline and placed in plastic pots. Ideally follicles should be isolated on the same day as the skin is obtained. We would routinely isolate hair follicles within several hours of the skin being removed from the patient. In our hands this gives optimum follicle growth. However, ourselves, and others have kept skin overnight both in a fridge but also in a humidified incubator at 37°C. In our experience if storing in an incubator it is preferable to cut the skin into small pieces (see step 2 under Sect. 3.1) and place four or five of these pieces in a 5 cm plastic petri dish containing 5 ml of hair follicle culture medium.

2. When culturing hair follicles, it is important to select only good healthy follicles and to exclude any that show signs of damage being sustained during isolation. Key signs of damage include distorted follicle bulbs, signs that the hair fiber has been fully or partially separated from the hair matrix. More subtle signs are blebbing of pigment into the follicle bulb or dermal papilla. If follicles with any of these characteristics are used for culture, it is very likely they will have reduced rates of growth and or undergo premature entry into catagen. The reason for this premature catagen may well be linked to the well characterized "alarm response" of hair follicles in which they quickly cycle through catagen and into telogen in response to physical or chemical insult (55). When handling hair follicles, they should be held using watchmakers forceps and gently grasped at the extreme end of the outer root sheath. They should not be picked up at the follicle bulb region as this will damage the matrix/dermal papilla and affect follicle growth.
3. Traditionally we have used bovine insulin but recently deliveries from this source have been disrupted and so we now use human insulin without any adverse effects.
4. Historically we have used hydrocortisone at 10 ng/ml; however, unpublished data from our group have suggested that higher doses of hydrocortisone may result in improved growth rates and better hair follicle morphology.
5. Serum should be avoided.
6. If the active being screened is labile this may requires its daily administration.
7. We have found that hair follicles will grow for up to 10 days in Williams E medium without medium change and that daily medium changes have no effect on growth rate.
8. If commercial aspirators used to aspirate medium from flasks is used, the suction is too great and follicles are frequently sucked up with the medium and lost.
9. Care must be taken to ensure that the follicle bulb and in particular the sebaceous gland is not damaged. Normally, a compromise has to be reached between dissecting an intact pilosebaceous unit and the amount of collagen that can be removed and usually it is better not to attempt to clean the units too much otherwise they may be damaged.
10. Because of the opaque nature of Gelfoam, it is difficult to make detailed measurements of hair follicle growth although follicles can be measured at the start of the experiment and at the end enabling total hair growth over the course of the experiment to be analyzed. We have routinely used our standard Williams E

hair follicle medium to maintain pilosebaceous units, although this is at the expense of the sebaceous gland (12) which required a richer tissue culture medium. However, this sebaceous gland medium is inhibitory to hair follicle growth (12).

References

1. Trowell OA (1959) The culture of mature organs in a synthetic medium. Exp Cell Res 16(1):118–147
2. Lee CM, Jones CJ, Kealey T (1984) Biochemical and ultrastructural studies of human eccrine sweat glands isolated by shearing and maintained for seven days. J Cell Sci 72:259–274
3. Williams GM, Weisberger EK, Weisberger JH (1971) Isolation and long-term culture of epithelial like cells from rat liver. J Exp Cell Res 69:106–112
4. Kondo S, Hozumi Y, Aso K (1990) Organ culture of human scalp hair follicles: effect of testosterone and oestrogen on hair growth. Arch Dermatol Res 282:442–445
5. Imai R, Miura Y, Mochida K, Jindo T, Takamori K, Ogawa H (1992) Organ culture conditions of human hair follicles. J Dermatol Sci 3:163–171
6. Imai R, Jindo T, Miura Y, Mochida K, Takamori K, Ogawa H (1993) Organ culture of human hair follicles in serum-free medium. Arch Dermatol Res 284:466–471
7. Jindo T, Tsuboi R, Imai R, Takamori K, Rubin JS, Ogawa H (1994) Hepatocyte growth fator/scatter factor stimulates hair growth of mouse vibrissae in organ culture. J Invest Dermatol 103:306–309
8. Li L, Paus R, Margolis LB, Hoffman RM (1992) Hair growth *in vitro* from histocultured mouse skin. In Vitro Cell Dev Biol 28A:479–481
9. Philpott MP, Sanders DA, Kealey T (1994) Effects of insulin and insulin-like growth factors on cultured human hair follicles; IGF-I at physiologic concentrations is an important regulator of hair follicle growth *in vitro*. J Invest Dermatol 102:857–861
10. Philpott MP, Green MR, Kealey T (1990) Human hair growth *in vitro*. J Cell Sci 97:463–471
11. Westgate GE, Gibson WT, Kealey T, Philpott MP (1993) Prolonged maintenance of human hair follicles *in vitro* in a serum-free defined medium. Br J Dermatol 129:372–379
12. Sanders DA, Philpott MP, Kealey T (1994) The isolation and maintenance of the human pilosebaceous unit. Br J Dermatol 131:166–176
13. Philpott MP, Kealey T (2000) Cyclical changes in rat vibrissa follicles maintained *in vitro*. J Invest Dermatol 115:1152–1155
14. Wells J (1982) A simple technique for establishing cultures of epithelial cells. Br J Dermatol 107:669–675
15. Limat A, Noser FK (1986) Serial cultivation of single keratinocytes from the outer root sheath of human scalp hair follicles. J Invest Dermatol 87:485–488
16. Lenoir MC, Bernard BB, Pautrat G, Darmon M, Shroot B (1988) Outer root sheath cells of human hair follicle are able to regenerate a fully differentiated epidermis *in vitro*. Dev Biol 130:610–620
17. Vermorken AJM, Spierenburg RP, van Bennekom CA (1979) Heterozygote detection in glucose-6-phosphate dehydrogenase defficiency: limitations of hair follicle analysis. Clin Genet 16:353–356
18. Wells J (1981) Plucked hairs as cytogenetic monitors of exposure to radiation or mutagenic chemicals. Radiat Prot Dosim 1:305
19. Mahe YF, Buan B, Billoni N, Loussouarn G, Michelet J-F, Gautier B, Bernard BA (1996) Pro-inflammatory cytokine cascade in human plucked hair. Skin Pharmacol 9:366–375
20. Van Scott EJ, Reinertson RP, Steinmuller RJ (1957) The growing hair root of the human scalp and morphological changes therein following amethopetrin therapy. J Invest Dermatol 29:197–204
21. Ludwig E (1967) Separation of the hair from its papilla and connective tissue sheath. In: Montagna W, Dobson RI (eds) Advances in the biology of the skin, vol 9. Pergamon Press, New York, pp 177–182
22. Bassukas ID, Hornstein OP (1989) Effects of plucking on the anatomy of the anagen hair bulb. Arch Dermatol Res 281:188–192
23. Kealey T (1983) The metabolism and hormonal responses of human eccrine sweat glands

isolated by collagenase digestion. Biochem J 212:143–148

24. Martinet N, Kim HC, Girard JE et al (1988) Epidermal hair follicle transglutaminase; partial characterisation of soluble enzymes in newborn mouse skin. J Biol Chem 263: 4236–4241
25. Weinberg WC, Brown PD, Stetler-Stevenson WG, Yuspa SH (1991) Modulation of hair follicle cell proliferation and collagenolytic activity by specific growth factors. Ann N Y Acad Sci 642:281–290
26. Kealey T, Lee CM, Thody AJ, Coaker T (1986) The isolation of human sebaceous glands and apocrine sweat glands by shearing. Br J Dermatol 114:181–188
27. Barth JH, Ridden J, Philpott MP, Kealey T (1989) Lipogenesis by isolated human apocrine sweat glands: testosterone has no effect during long term organ maintenance. J Invest Dermatol 92:333–336
28. Kealey T, Philpott MP (1994) Human pilosebaceous culture: the background. In: Lane B, Leigh IM, Watt F (eds) The Keratinocyte Handbook. Cambridge University Press, Cambridge, pp 109–129
29. Green MR, Clay CS, Gibson WT, Hughes TC, Smith CG, Westgate GE, Kealey T (1986) Rapid isolation in large numbers of intact, viable individual hair follicles from the skin: biochemical and ultrastructural characterisation. J Invest Dermatol 87:768–770
30. Kondo S, Hozumi Y, Sato N, Aso K (1992) Organ culture of human hair follicles derived from different areas of the body. J Dermatol 19:348–352
31. Soma T, Tsuji Y, Hibino T (2002) Involvement of transforming growth factor-beta2 in catagen induction during the human hair cycle. J Invest Dermatol 118(6):993–997
32. Foitzik K, Spexard T, Nakamura M, Halsner U, Paus R (2005) Towards dissecting the pathogenesis of retinoid-induced hair loss: all-trans retinoic acid induces premature hair follicle regression (catagen) by upregulation of transforming growth factor-beta2 in the dermal papilla. J Invest Dermatol 124(6):1119–1126
33. Foitzik K, Krause K, Conrad F, Nakamura M, Funk W, Paus R (2006) Human scalp hair follicles are both a target and a source of prolactin, which serves as an autocrine and/or paracrine promoter of apoptosis-driven hair follicle regression. Am J Pathol 168(3):748–756
34. Bodó E, Tobin DJ, Kamenisch Y, Bíró T, Berneburg M, Funk W, Paus R (2007) Dissecting the impact of chemotherapy on the human hair follicle: a pragmatic in vitro assay for studying the pathogenesis and potential management of hair follicle dystrophy. Am J Pathol 171(4):1153–1167
35. Roosen GF, Westgate GE, Philpott M, Berretty PJ, Nuijs TA, Bjerring P (2008) Temporary hair removal by low fluence photoepilation: histological study on biopsies and cultured human hair follicles. Lasers Surg Med 40(8):520–528
36. Lu Z, Fischer TW, Hasse S, Sugawara K, Kamenisch Y, Krengel S, Funk W, Berneburg M, Paus R (2009) Profiling the response of human hair follicles to ultraviolet radiation. J Invest Dermatol 129(7):1790–1804
37. Kloepper JE, Sugawara K, Al-Nuaimi Y, Gáspár E, van Beek N, Paus R (2010) Methods in hair research: how to objectively distinguish between anagen and catagen in human hair follicle organ culture. Exp Dermatol 19(3):305–312
38. Borbíró I, Lisztes E, Tóth BI, Czifra G, Oláh A, Szöllosi AG, Szentandrássy N, Nánási PP, Péter Z, Paus R, Kovács L, Bíró T (2011) Activation of transient receptor potential vanilloid-3 inhibits human hair growth. J Invest Dermatol 131(8):1605–1614
39. Taylor M, Ashcroft ATT, Messenger AG (1993) Cyclosporin A prolongs human hair growth in vitro. J Invest Dermatol 100:237–239
40. Li L, Margolis LB, Paus R, Hoffman RM (1994) Hair shaft elongation, follicle growth, and spontaneous regression in long term, gelatin sponge-supported histoculture of human scalp skin. Proc Natl Acad Sci USA 89:8764–8768
41. Strangeways DH (1931) The growth of hair *in vitro*. Arch Exp Zellforsch 11:344
42. Davidson P, Hardy MH (1952) The development of the mouse vibrissae *in vivo* and *in vitro*. J Anat 86:342–356
43. Bartosova L, Rebora A, Moretti G, Cipriani C (1971) Studies on rat hair culture. I. A reevaluation of technique. Arch Derm Forsch 240:95–106
44. Frater R, Whitmore PG (1973) In vitro growth of postembryonic hair. J Invest Dermatol 61:72–81
45. Frater R (1980) The effect of rat serum on the morphology of rat hair follicles in tissue culture. Arch Dermatol Res 269:13–20
46. Buhl AE, Waldon BS, Kawabe TT, Holland DVM (1989) Minoxidil stimulates mouse vibrissae follicles in organ culture. J Invest Dermatol 92:315–320

47. Philpott MP, Green MR, Kealey T (1992) Rat hair follicle growth *in vitro*. Br J Dermatol 127:600–607
48. Robinson M, Reynolds AJ, Jahoda CAB (1997) Hair cycle stage of the mouse vibrissa follicle determines subsequent fibre growth and follicle behaviour *in vitro*. J Invest Dermatol 108:495–500
49. Bates EJ, Hynd PI, Penn NM, Nancarrow MJ (1997) Serum free culture of wool follicles: effects of nutrients, growth factors and hormones. Br J Dermatol 137:498–505
50. Hynd PI, Winder LM, Jahoda CAB, Bickerstaffe R (1992) Preliminary investigations of Romney wool growth *in vitro*. Wool Technol Sheep Breed 40:102–105
51. Hynd PI, Nancarrow M (1996) Inhibition of polyamine synthesis alters hair follicle function and fibre composition. J Invest Dermatol 106:249–253
52. Winder LM (1999) Specific components of adult sheep serum inhibit wool growth in tissue culture. Exp Dermatol 8: 320–322
53. Ibraheem M, Galbraith H, Scaife J, Ewen S (1993) Growth and viability of secondary hair follicles in the Angora goat cultured in vitro. J Anat 182:231–238
54. Thornton MJ, Thomas DJ, Brinklow BR, Loudon ASI, Randall VA (1994) Only androgen dependant hairs of red deer are stimulated by testosterone and IGF-I *in vitro*. Br J Dermatol 131:427A
55. Mehregan AH (1979) Alarm reaction of pilosebaceous apparatus. J Am Acad Dermatol 1:55–58

Part IV

TRPs and Metabolic Disorders

Chapter 19

Animal Models for Type 1 Diabetes

Anish Suri and Matteo Levisetti

Abstract

The incidence of autoimmune diabetes has been steadily increasing in the developed world. A complex interplay between genetic factors and dysregulated immune cells ultimately results in breakdown of self-tolerance against islet beta cell antigens and loss of beta cell mass, which leads to insulin deficiency and persistent hyperglycemia. Much progress in our understanding of immunological mechanisms that underlie autoimmune diabetes has been made in recent years. A significant portion of the experimental investigations have been performed in rodent models of autoimmune diabetes that are reviewed in this chapter. In addition, an understanding of the biochemical characteristics of class II MHC molecules that predispose to autoimmune diabetes and their relationship to selection of the autoimmune T-cell repertoire are discussed. Finally, data supporting insulin as a dominant autoantigen are reviewed along with various effector pathways and cell types that induce islet beta cell death.

Key words: Autoimmune diabetes, T-cells, NOD, MHC, Islet beta cells

1. Introduction

Type 1 diabetes mellitus (T1DM), formerly known as insulin-dependent diabetes mellitus (IDDM), is an autoimmune disease characterized by T-cell-mediated destruction of the insulin-secreting pancreatic islet beta cells (1). Much progress in understanding the clinical disease has been accomplished in the past 20+ years due to extensive experimental investigations in animal models that recapitulate many salient features of the human disease. In this report, we will review the different animal models that can be utilized to evaluate various facets of autoimmune diabetogenesis, including genetic susceptibility, T-cell autoreactivity, target autoantigens, and effector mechanisms of islet beta cell inflammation and death. An understanding of the available experimental tools may allow the investigator to select the optimal model system to answer focused scientific questions.

Arpad Szallasi and Tamás Bíró (eds.), *TRP Channels in Drug Discovery: Volume II*, Methods in Pharmacology and Toxicology, DOI 10.1007/978-1-62703-095-3_19,

The autoimmune destruction of the pancreatic beta cells in T1DM causes insulin deficiency and hyperglycemia. The peak onset occurs between ages 10 and 12 years; however, it can occur from a few months of age into late adulthood. Males and females are equally affected. The overall prevalence of T1DM in the United States is 0.25–0.5% of the population, or 1 of 400 children and 1 of 200 adults. The incidence of T1DM is increasing in developing countries. T1DM accounts for 5–10% of all cases of diabetes and needs to be accurately diagnosed so that appropriate therapy with insulin is not delayed. Insulin deficiency can lead to diabetic ketoacidosis (DKA), a life-threatening acute metabolic condition. Chronic hyperglycemia is the primary contributor to the disabling microvascular complications and contributes to macrovascular disease.

Antibodies to beta cell antigens can be found in the majority of patients before diagnosis, and persist for some time after the onset of clinical diabetes. These disease markers are antibodies to insulin (IAA), to beta cell-specific tyrosine phosphatases IA-2 and IA-2 beta, and to glutamic acid decarboxylase (GAD65). The presence of two or three antibodies has high sensitivity and specificity for rapid progression to insulin dependency and may help clarify the diagnosis in some patients.

The genetic susceptibility to T1DM is manifested by linkage with several gene loci and association with HLA-DR and DQ (2). The IDDM1 gene located in the HLA region of chromosome 6, and the IDDM2 gene in the region 5-prime upstream of the insulin gene on chromosome 11 contribute 42% and 10%, respectively, to the observed familial clustering of the disease. In the family of a patient with T1DM, the risk of an identical twin developing the disease is 30–50%, an offspring is 6%, and a sibling is 5%. The striking familial discordance supports the importance of environmental factors in disease pathogenesis.

A majority of experimental work in autoimmune diabetes has been focused on two preclinical rodent models: the Bio-Breeding/Worcester diabetes-prone (BB/W-DP) rat and the nonobese diabetic (NOD) mouse model (3–5). A unique advantage of using the BB rat or NOD mouse is that the disease in these animals mimics many features of human T1DM, including spontaneous onset, expression of disease-associated major histocompatibility complex (MHC) molecules, and involvement of diabetogenic T-cells that ultimately destroy the pancreatic islet beta cells. Although the BB rat model was identified several years before the NOD mouse, a majority of the recent work has been conducted in NOD mice due to availability of transgenic and knock-out animals that have facilitated in depth immunological investigations into pathophysiological mechanisms underlying autoimmunity. In both BB rats and NOD mice, autoreactive T-cells play an obligatory role in the induction of diabetes, and disease transfer into naive recipients is readily accomplished by adoptive transfer of CD4+ and CD8+

T-cells (6–9). Furthermore, in both rodent models, an important role for regulatory T-cells in controlling the diabetogenic process has been identified (10–12). The presence of serum antibodies against islet beta cell proteins has also been demonstrated in BB rats and NOD mice prior to the onset of hyperglycemia (13).

2. A Unique Role for T1DM-Associated Class II MHC Molecules

The class II MHC molecules are heterodimeric proteins present on professional antigen-presenting cells (APCs) such as dendritic cells (DCs), B cells and macrophages, and are composed of an alpha and beta chain that associate noncovalently to present antigenic peptides to CD4+ T-cells. The peptide-binding groove of class II MHC molecules consists of four major distinct pockets (P1, P4, P6, and P9), which bind to specific amino acids or "anchor" residues from the displayed antigenic peptide. Most of the polymorphism in MHC molecules is located in the peptide-binding groove, including the composition of amino acids that form the four binding pockets, which define allele-specific binding motifs. The peptide binding affinity for MHC molecules is significantly influenced by the interactions of specific anchor residues (derived from the antigenic peptide) with the binding pockets of the MHC molecules (14, 15).

In the case of T1DM, the class II MHC locus is the single-most important genetic factor that predisposes to disease. In both rodents and man, the diabetogenic class II MHC molecules share the unique feature of the presence of a non-Asp amino acid at position 57 of the beta chain; this position in all other class II MHC molecules is a conserved Asp residue (16). Specifically, the NOD class II MHC, I-Ag7, expresses a Ser at beta57 while the human HLA-DQ2 or 8 express an Ala at the same position. The beta57 residue forms an integral part of the P9 pocket of the peptide-binding groove of class II MHC molecules (17). The protein crystal structures of I-Ag7 and HLA-DQ8 revealed that presence of a non-Asp beta57 residue generated a P9 pocket that was wider and more open towards the c-terminus of the bound peptide (18–20). In most other class II MHC alleles, the conserved beta57 Asp residue forms an ion pair with an opposing alpha76 Arg amino acid that defines the rim of the P9 pocket; the absence of this salt–bridge interaction in diabetogenic class II MHC molecules influences the unique structural features of the P9 pocket, as described above.

The unique biochemical and structural features of diabetogenic class II MHC molecules have a marked impact on the nature of peptides that are selected for display to CD4+ T-cells. Numerous earlier studies had suggested that diabetogenic class II MHC

molecules bound peptides with little or no specificity, which supported the idea that this may allow for inadequate negative selection of developing T-cells in the thymus resulting in escape of autoreactive T-cells (21, 22). However, much of the data for these observations came from biochemical binding analysis of diabetogenic class II MHC molecules with synthetic peptides with little to no understanding of the naturally selected repertoire of peptides displayed by APCs. This issue was addressed in subsequent studies that utilized mass spectrometry to identify peptides directly isolated from diabetogenic class II MHC molecules present on the surface of APCs. Several key findings emerged from these detailed analyses: (1) contrary to previous observations, both human and murine diabetogenic class II MHC molecules selected for peptides with a well-defined binding motif that was characterized by a biased presence of multiple acidic amino acids (either Glu or Asp) towards the c-terminus; (2) the acidic amino acids interacted with the P9 pocket and contributed significantly towards the peptide binding affinity for the class II MHC molecule; (3) the specificity of the P9 pocket, composed of non-Asp beta57 residue, was key in determining the final repertoire of peptides selected by APCs—this was best supported by the finding that APCs expressing a modified I-Ag7 with beta57 Ser Asp change selected for an entirely different set of peptides that did not exhibit any bias for the c-termini acidic residues; and (4) APCs expressing either the murine (I-Ag7) or human (HLA-DQ8) diabetogenic class II MHC molecules selected for identical peptides (23–26). The importance of this last observation is key when evaluating antigenic epitopes that activate diabetogenic T-cells, as there is likely to be a direct corollary between NOD T-cell epitopes and those found in human T1DM patients. To this end, an excellent example is the identification of insulin peptide spanning residues 9–23 of the beta chain as being a dominant autoantigenic epitope in both NOD mice and human T1DM subjects (27). This and other autoantigens are discussed in more detail in the following section.

The important role for class II MHC molecules in T1DM is highlighted by several key findings in NOD mice: (1) transgenic NOD mice expressing a modified I-Ag7 molecule wherein the beta57 Ser is mutated to an Asp are protected from diabetes (28, 29); (2) NOD mice heterozygous for the expression of a beta57 Asp-expressing class II MHC molecule exhibit a markedly lower incidence of disease (30); (3) class II MHC k.o. mice are protected from diabetes (31); and (4) the expression of I-Ag7 correlates with the presence of higher numbers of autoreactive T-cells in the periphery of NOD mice or congenic B6 mice expressing I-Ag7 (32, 33). Experimentally, the frequencies of autoreactive T-cells can be determined using limiting dilution analysis (32), or more specifically by utilizing MHC-peptide tetramers to track antigen-specific T-cells by FACS analysis (33).

What are the various facets of the autoreactive T-cell response that are influenced by diabetogenic class II MHC alleles? An obvious role for class II MHC molecules may relate to their ability to effectively select and display islet beta cell antigenic peptides that conform to the unique binding motif (34, 35). Indeed, in NOD mice several reports have identified target epitopes of autoreactive T-cells that exhibit the preferred peptide-binding motif for I-Ag7 (reviewed in (36)). A related role for class II MHC molecules may also involve the effects on the thymic selection milieu, which has marked effect on the repertoire of T-cells in the periphery. In this instance, the skewed selection of peptides characterized by the presence of multiple c-termini acidic residues may narrow the breadth of the repertoire of peptides presented by the thymic epithelia and APCs. This may subsequently allow for inefficient negative selection of autoreactive T-cells. Indeed, the expression of I-Ag7 alone has been correlated with the presence of higher numbers of self-reactive T-cells in the periphery (32), and in the report by Schmidt et al., heterozygosity for class II MHC alleles resulted in the thymic deletion of an I-Ag7-restricted CD4+ diabetogenic T-cell (37). Yet other reports have suggested that the Tregs in NOD mice are quantitatively and/or functionally reduced, which may be another aspect related to the expression of T1DM-associated class II MHC alleles (38–41). In support of this argument, expression of other class II MHC molecules in addition to I-Ag7 resulted in higher numbers of regulatory T-cells in the periphery and reduced incidence of disease (42–44).

3. T-cells and T1DM

Previous studies in both the NOD and BB/W-DP rat models have demonstrated that both CD4+ and CD8+ T-cells play an important role in islet beta cell autoimmunity. Targeted gene knock-out NOD mice lacking either class I MHC (CD8+ T-cells) or class II MHC (CD4+ T-cells) molecules are protected from diabetes (31, 45–48). CD4+ and CD8+ T-cells have been shown to have direct effects on the function and survival of islet beta cells, albeit utilizing distinct effector mechanisms. In this section, we will summarize various experimental approaches that can be employed to evaluate diabetogenic T-cells.

3.1. Adoptive Transfer of Disease

The earliest studies in rodent models demonstrated that diabetes could be readily transferred into neonatal or immuno-deficient recipients (on the SCID or RAG$^{-/-}$ background) using unfractionated whole lymphocytes (usually spleen cells) from diabetic animals. In such cases, the incidence of disease was highest when both CD4+ and CD8+ T-cells were present, which again pointed to

a cooperative role between the two subsets (9). In other experiments, adoptive transfer of diabetes could be inhibited by co-transfer of CD4+ T-cells from disease-free mice; these data supported a regulatory role for CD4+ T-cells (10). Subsequent studies have confirmed and extended the role of regulatory T-cells (Tregs) in controlling diabetogenic T-cells (41). A defective role for T regs in NOD mice, and possibly human subjects, has been suggested as a possible mechanism underlying the breakdown of tolerance (49). It remains to be determined the extent to which the unique peptide-binding motif of diabetogenic class II MHC molecules influences the development and function of Tregs in NOD mice and human subjects.

3.2. Isolating and Cloning of Islet-Reactive T-cells

This approach has high value when evaluating the natural islet-reactive CD4+ and CD8+ T-cell repertoires in NOD mice developing diabetes. The elegant studies by Haskins et al. demonstrated that primary diabetogenic T-cells could be isolated from infiltrated islets of NOD mice, and these T-cells could be propagated under in vitro conditions using islet beta cells as the source of antigen in conjunction with NOD APCs (50, 51). Although technically challenging, such efforts eventually identified a panel of diabetogenic T-cell clones that could readily transfer disease into neonatal or SCID recipients, which confirmed the obligatory role for T-cells in induction of T1DM. Cloning of spontaneously occurring islet-reactive T-cells has several important implications: one, the biological relevance is high since this represents the natural T-cell population that penetrates and destroys the islet beta cells; two, such analysis allows for the temporal evaluation of the autoreactive T-cell repertoire in relation to events leading to destruction of islet beta cells; three, primary islet-reactive T-cells could be used as probes to identify their cognate antigens derived from the islet beta cells; and four, based on the shared class II MHC homology between NOD mice and human T1DM patients, there is high probability that similar T-cell populations and target antigens are likely represented in human patients. A significant caveat with isolating and cloning islet cells pertains to success with adoptive transfer of disease. Often in vitro culture alters the phenotype of the T-cell such that it is unable to induce diabetes when transferred into recipient animals. This limitation may likely be due to altered expression of adhesion molecules and/or chemokine receptors that may affect T-cell trafficking, or could be due to the requirement that T-cells of additional specificities are needed to initiate the assault against islet beta cells. Indeed, in some instances in vitro cloned T-cells may induce insulitis without any signs of overt hyperglycemia (52, 53). Hence, in light of these challenges, a stringent requirement for induction of disease by islet-reactive T-cells should not be an absolute condition for classification of pathogenic T-cells in T1DM.

3.3. T-Cell Receptor Transgenic Mice

Several groups have now successfully cloned the T-cell receptor (TCR) alpha and beta chain genes from diabetogenic CD4+ and CD8+ T-cells to generate transgenic NOD mice to aid in various experimental studies (54, 55). Generation of TCR transgenic mice has several advantages: (1) the onset of diabetes is synchronous in terms of kinetics and incidence, which is in contrast to wild-type NOD mice where the timing of maximal diabetes incidence varies between 12 and 24 weeks and longer; (2) the presence of a monoclonal diabetogenic T-cell population allows one to answer mechanistic questions related to T-cell selection and peripheral activation, which are likely difficult to track and address in a polyclonal repertoire of T-cells; (3) provides a rich source of pathogenic T-cells that can be used in adoptive transfer experiments; and (4) allows for identification of various effector mechanisms that could be utilized by CD4+ and CD8+ T-cells to kill the insulin-producing islet beta cells (56, 57). Lessons learned from evaluation of TCR transgenic mice need to be eventually confirmed in wild-type NOD mice.

3.4. T-cells Against Model Antigens

Another permutation to studying autoimmune diabetes is utilizing model antigens implanted in islet beta cell as neo-self antigens. The advantage to this approach pertains to the ready availability of reagents and tools that facilitate detailed analysis of disease biology. To this end, two notable model antigens, chicken ovalbumin (Ova) and hen egg-white lysozyme (HEL) have been expressed in the pancreatic islets under the insulin promoter in transgenic mice. The T-cell responses to both Ova and HEL have been well studied on different MHC background: H-2b for Ova and H-2k for HEL (58, 59). Autoimmune diabetes can be induced in either antigen-transgenic mice via crossing on to TCR transgenic mice that bear either CD4+ or CD8+ T-cells reactive against Ova or HEL (e.g., OT-I and OT-II TCR transgenic mice that express Ova-specific CD8+ or CD4+ T-cells, respectively, or 3A9 TCR transgenic mice that bear HEL-specific CD4+ T-cells); or via adoptive transfer of antigen-specific T-cells (60–63). Another related model system has utilized viral proteins expressed selectively in islet beta cells along with CD8+ TCR transgenic T-cells directed to a viral epitope (64). The expression of a viral protein as a "neo" diabetogenic antigen offers the advantage of evaluating the relationship between viral infection and onset of autoimmunity (64, 65). Previous studies in mice and humans have pointed to a possible correlation between Coxsackie virus infections and the subsequent onset of autoimmune diabetes (66–68). The utility of these various transgenic mouse models has also enabled studies focused on understanding the relationship between levels of self-antigen and central selection in thymus; identification of professional APCs (DCs) that mediate priming and activation of autoreactive T-cells in the draining lymph nodes of the pancreas; control of autoreactive T-cells by Tregs; and effector mechanisms of islet beta cell inflammation. But despite

these advantages there are several caveats to using transgenic models that should be considered based on the experimental questions: (1) most of the transgenic mice expressing neo-islet model antigens are not on the NOD background which limits evaluations related to T1DM-susceptibility genes including the class II MHC; (2) the temporal expression and levels of the model antigen may be very different from the natural islet beta cell antigens that are targeted in disease; and (3) the hierarchy and cascade of multiple autoantigens that are targeted during various stages of diabetogenesis are likely not represented in transgenic models.

4. Role of the B Cell

Although T1DM is caused by the T-cell-mediated destruction of pancreatic beta cells, B cells also contribute significantly to disease development. Early studies demonstrated that T1DM could be completely inhibited or significantly suppressed in NOD mice rendered B-cell-deficient through genetic manipulation (69). More recent studies have demonstrated that T1DM development in NOD mice can be suppressed by targeting B cells with monoclonal antibodies or by blocking the survival factor BAFF (BLyS) (70–72).

T1DM development in NOD mice, as well as in humans, is preceded by the appearance of autoantibodies targeting beta cell antigens, like insulin (73). Whether these beta cell autoantibodies contribute to the pathogenesis of T1DM in humans and NOD mice remains an open question. A more pathogenic role for NOD B cells is serving as an APC subset that efficiently supports the expansion of pathogenic effector CD4 T-cells (74, 75). This role as an important APC population was further supported by studies in which NOD mice with B cells deficient in MHC class II molecules had reduced disease development (76).

5. NOD Autoantigens

Autoantibodies to beta cell antigens are detected before the onset of T1DM in both humans and the NOD mouse model of the disease. Spontaneously occurring antibodies have led to the identification of multiple beta cell autoantigens, including insulin, glutamic acid decarboxylase, IA-2 and others, including the recently identified ZnT8 transporter. Various reviews have provided a comprehensive list of the autoantigenic targets of B and T-cells in both humans and the NOD mouse (36, 77, 78).

5.1. Insulin

There is extensive evidence that autoimmunity directed at insulin, and its precursors, is central to the pathogenesis of T1DM in the NOD mouse. The initial major advance in defining a role for T-cells targeting insulin was the cloning of T-cells directly from islets of NOD mice by Daniel and colleagues (79). They discovered that the majority of CD4+ T-cell clones isolated from the islet infiltrates reacted with insulin, and of those reactive with whole insulin protein, more than 90% were stimulated by the 9–23 peptide of the beta chain (B:9–23). These primary T-cell clones were shown to accelerate the onset of diabetes in young NOD mice and to cause diabetes in NOD.scid recipient mice (80). Additional investigations confirmed the important role of insulin as an autoantigen in the pathogenesis of autoimmune diabetes. First, NOD mice rendered tolerant to insulin by transgenic overexpression of the preproinsulin molecule in APCs had a significantly reduced incidence of diabetes (81, 82). Second, NOD mice in which the dominant epitope of insulin was mutated by genetic manipulation exhibited diminished disease (27). Third, an anti-insulin anti-B:9–23 TCR-transgenic mouse developed disease when crossed onto a RAG-deficient background (83).

Recent studies have extended our understanding of interactions between insulin and MHC and the complexities of the T-cell response to insulin and its peptides. These studies not only confirm an important role for insulin in T1DM pathogenesis but offer additional perspectives to our understanding of the role played by the MHC proteins that confer the greatest risk for the disease. For example, why is the 9–23 segment of the insulin beta chain the central focus of the T-cell response? The B:9–23 peptide interacts weakly with the I-Ag7 molecule and binds in at least two different registers (84). These features of the B:9–23 peptide–MHC interaction may result in defective negative selection and escape of autoreactive T-cell clones. There is also recent evidence that B:9–23 peptides are generated within islet beta cell secretory granules and that a subset of B:9–23-reactive T-cells recognize unique peptide–MHC complexes formed with these peptides but do not recognize the peptide when insulin is processed by APCs (85). The identification of C-peptide-reactive T-cells also demonstrates the lack of tolerance to insulin (and its precursors) present in the NOD mouse and highlights the role that secreted beta cell peptides may play in the formation of unique peptide–MHC complexes (86). It may be that peptide–MHC complexes formed in the thymus do not recapitulate the complexes that are formed in the inflammatory interface between beta cells and APCs, indeed a recent report by Mohan et al. evaluating insulin-specific T-cells lends support to these conclusions (87). The deleting complexes are presumably formed by the traditional processing and presentation of proinsulin peptides in thymic medullary epithelial cells. Here, peptides are selected by the biological and physical forces that govern peptide

selection by I-Ag7 molecules in thymic cells and are not the same as events that might occur in the periphery. Although proinsulin is clearly expressed in the thymus (88, 89), perhaps largely under the control of the autoimmune regulator transcription factor (90), there is no evidence of the expression of the prohormone processing machinery, such as the prohormone convertases 1 and 2, which would be required to generate the actual C-peptide fragment that is secreted by the beta cell.

6. Toxin-Induced Diabetes and Insulitis

NOD mice and BB rats provide models of spontaneous autoimmune diabetes. Additional models of T1DM are based on exposures to toxins, such as streptozotocin (STZ). STZ is used as chemotherapy for insulinomas. STZ is a toxic glucose analog that accumulates in the pancreatic beta cell via the GLUT2 transporter. When mice receive multiple small sub-diabetogenic doses of STZ, pancreatic insulitis, selective beta cell destruction, and diabetes ensue after a delay of several days (91). Islet autoantibodies appear after STZ treatment, but there is no evidence for an etiologic role for autoantibodies in this model. Low-dose STZ appears to induce autoimmunity in susceptible hosts by altering beta cells and inducing auto-immunogenicity.

7. Effector Mechanisms of Islet Beta Cell Death

An active area of research has focused on understanding the molecular mechanisms underlying the immune-mediated destruction of islet beta cells in T1DM. Due to the pleiotrophic nature of inflammatory cell types involved in T1DM, numerous molecular mechanisms have been shown to play a role in islet beta cell death. In experimental models, the Fas/FasL, perforin/granzyme and TNF-receptor pathway have all been implicated in the apoptotic death of islet beta cells. NOD *lpr/lpr* mice (Fas-deficient) are protected by spontaneous diabetes and are resistant to challenge by diabetogenic T-cells (92). More specifically, transgenic NOD mice bearing islet beta cells with a mutated Fas molecule lacking a functional death domain exhibit delayed disease (93). Similarly, perforin-deficient NOD mice exhibit significantly reduced and delayed incidence of diabetes, even though insulitis was still evident in these animals (94, 95). The deficiency of TNF-R1 (p55 subunit) on the NOD background also leads to protection from diabetes despite the presence of insulitis. However, disease could be induced in NOD-p55$^{-/-}$ mice upon adoptive transfer of CD8+ TCR transgenic

T-cells, which suggests that the TNF-R1 is likely not the dominant pathway for cytotoxic T-cell-mediated killing of islet beta cells (96). Other studies by Pakala et al. also demonstrated a key role for TNF-R1 on islet beta cells and their susceptibility to diabetes induced by CD4+ TCR transgenic T-cells (56). Besides T-cells, a role for macrophages in killing of islet beta cells has also been noted in autoimmune diabetes; in vivo depletion of macrophages leads to protection from disease, and under in vitro conditions activated macrophages can directly kill primary islet beta cells (57, 97, 98). Lastly, an important role for soluble mediators, especially cytokines, has been recognized in driving islet inflammation. Some of the notable features of cytokine-driven inflammatory processes include: direct killing of islet beta cells (e.g., TNF-alpha); generation of nitric oxide and oxygen-free radicals (induced by IL-1, TNF-alpha, interferon-gamma) that are toxic to the function and survival of islet beta cells; increasing the sensitivity of islet beta cells to CD8+ T-cell-mediated killing via up-regulation of class I MHC or expression of co-stimulatory molecules (via interferon-gamma); and enhancing migration of leukocytes by changes to the expression of vasculature adhesion molecules and chemotactic gradients (reviewed in detail by Rabinovitch (99)).

8. Concluding Remarks

Our understanding of the immunological basis for T1DM has been facilitated by extensive investigations in animal models, particularly NOD mice. Several key shared features including the presence of disease-susceptible MHC molecules, obligatory role for islet-reactive T-cells and expression of various pro-inflammatory molecules underscore the importance of NOD mice as an excellent model for the human disease. Recent investigations have begun to dissect the complex interplay between effector and regulatory T-cells, an area that continues to grow with much vigor. Although numerous experimental manipulations have halted the autoimmune process and reversed the disease in NOD mice, the interventions tested to date in clinical trials have not produced sustained, clinically meaningful results (100). The relative failure of single-agent therapies in the clinic, chosen largely based on their efficacy in animal models, may point to the need for rationally designed combination therapies with agents targeting immuno-suppression, immunomodulation and islet regeneration as the future for successful intervention and prevention trials. An in depth understanding into the identity and nature of islet antigens that initiate and sustain diabetogenic T-cells is important for future therapeutic manipulations. Parallel development of robust biomarkers that can identify at-risk individuals early during the autoimmune process will be important for clinical

intervention. Lastly, a concerted effort in understanding the regenerative potential of pancreatic islet beta cells may be crucial to restore normoglycemia in individuals wherein the autoreactive T-cells are controlled by strategies targeting key immune pathways and/or cells.

References

1. Bluestone JA, Herold K, Eisenbarth G (2010) Genetics, pathogenesis and clinical interventions in type 1 diabetes. Nature 464:1293–1300
2. McDevitt H (2001) The role of MHC class II molecules in the pathogenesis and prevention of type I diabetes. Adv Exp Med Biol 490:59–66
3. Lam-Tse WK, Lernmark A, Drexhage HA (2002) Animal models of endocrine/organ-specific autoimmune diseases: do they really help us to understand human autoimmunity? Springer Semin Immunopathol 24:297–321
4. Rossini AA, Mordes JP, Greiner DL (1989) The pathogenesis of autoimmune diabetes mellitus. Curr Opin Immunol 2:598–603
5. Anderson MS, Bluestone JA (2005) The NOD mouse: a model of immune dysregulation. Annu Rev Immunol 23:447–485
6. Like AA, Weringer EJ, Holdash A, McGill P, Atkinson D, Rossini AA (1985) Adoptive transfer of autoimmune diabetes mellitus in biobreeding/Worcester (BB/W) inbred and hybrid rats. J Immunol 134:1583–1587
7. Whalen BJ, Greiner DL, Mordes JP, Rossini AA (1994) Adoptive transfer of autoimmune diabetes mellitus to athymic rats: synergy of CD4+ and CD8+ T cells and prevention by RT6+ T cells. J Autoimmun 7:819–831
8. Wicker LS, Miller BJ, Mullen Y (1986) Transfer of autoimmune diabetes mellitus with splenocytes from nonobese diabetic (NOD) mice. Diabetes 35:855–860
9. Bendelac A, Carnaud C, Boitard C, Bach JF (1987) Syngeneic transfer of autoimmune diabetes from diabetic NOD mice to healthy neonates. Requirement for both L3T4+ and Lyt-2+ T cells. J Exp Med 166:823–832
10. Boitard C, Bendelac A, Richard MF, Carnaud C, Bach JF (1988) Prevention of diabetes in nonobese diabetic mice by anti-I-A monoclonal antibodies: transfer of protection by splenic T cells. Proc Natl Acad Sci USA 85:9719–9723
11. Greiner DL, Handler ES, Nakano K, Mordes JP, Rossini AA (1986) Absence of the RT-6 T cell subset in diabetes-prone BB/W rats. J Immunol 136:148–151
12. Zhou X, Bailey-Bucktrout S, Jeker LT, Bluestone JA (2009) Plasticity of CD4(+) FoxP3(+) T cells. Curr Opin Immunol 21:281–285
13. Liu E, Eisenbarth GS (2002) Type 1A diabetes mellitus-associated autoimmunity. Endocrinol Metab Clin North Am 31:391–410, vii-viii
14. Latek RR, Unanue ER (1999) Mechanisms and consequences of peptide selection by the I-Ak class II molecule. Immunol Rev 172:209–228
15. Allen PM, Babbitt BP, Unanue ER (1987) T-cell recognition of lysozyme: the biochemical basis of presentation. Immunol Rev 98:171–187
16. Todd JA, Bell JI, McDevitt HO (1987) HLA-DQ beta gene contributes to susceptibility and resistance to insulin-dependent diabetes mellitus. Nature 329:599–604
17. Fremont DH, Monnaie D, Nelson CA, Hendrickson WA, Unanue ER (1998) Crystal structure of I-Ak in complex with a dominant epitope of lysozyme. Immunity 8:305–317
18. Corper AL, Stratmann T, Apostolopoulos V, Scott CA, Garcia KC, Kang AS, Wilson IA, Teyton L (2000) A structural framework for deciphering the link between I-Ag7 and autoimmune diabetes. Science 288:505–511
19. Latek RR, Suri A, Petzold SJ, Nelson CA, Kanagawa O, Unanue ER, Fremont DH (2000) Structural basis of peptide binding and presentation by the type I diabetes-associated MHC class II molecule of NOD mice. Immunity 12:699–710
20. Lee KH, Wucherpfennig KW, Wiley DC (2001) Structure of a human insulin peptide-HLA-DQ8 complex and susceptibility to type 1 diabetes. Nat Immunol 2:501–507
21. Stratmann T, Apostolopoulos V, Mallet-Designe V, Corper AL, Scott CA, Wilson IA, Kang AS, Teyton L (2000) The I-Ag7 MHC class II molecule linked to murine diabetes is a promiscuous peptide binder. J Immunol 165:3214–3225
22. Carrasco-Marin E, Shimizu J, Kanagawa O, Unanue ER (1996) The class II MHC I-Ag7

molecules from non-obese diabetic mice are poor peptide binders. J Immunol 156:450–458

23. Suri A, Vidavsky I, van der Drift K, Kanagawa O, Gross ML, Unanue ER (2002) In APCs, the autologous peptides selected by the diabetogenic I-Ag7 molecule are unique and determined by the amino acid changes in the P9 pocket. J Immunol 168:1235–1243
24. Suri A, Walters JJ, Gross ML, Unanue ER (2005) Natural peptides selected by diabetogenic DQ8 and murine I-A(g7) molecules show common sequence specificity. J Clin Invest 115:2268–2276
25. Suri A, Walters JJ, Kanagawa O, Gross ML, Unanue ER (2003) Specificity of peptide selection by antigen-presenting cells homozygous or heterozygous for expression of class II MHC molecules: the lack of competition. Proc Natl Acad Sci USA 100:5330–5335
26. Muixi L, Gay M, Munoz-Torres PM, Guitart C, Cedano J, Abian J, Alvarez I, Jaraquemada D (2011) The peptide-binding motif of HLA-DR8 shares important structural features with other type 1 diabetes-associated alleles. Genes Immun 12:504–512
27. Nakayama M, Abiru N, Moriyama H, Babaya N, Liu E, Miao D, Yu L, Wegmann DR, Hutton JC, Elliott JF, Eisenbarth GS (2005) Prime role for an insulin epitope in the development of type 1 diabetes in NOD mice. Nature 435:220–223
28. Quartey-Papafio R, Lund T, Chandler P, Picard J, Ozegbe P, Day S, Hutchings PR, O'Reilly L, Kioussis D, Simpson E et al (1995) Aspartate at position 57 of nonobese diabetic I-Ag7 beta-chain diminishes the spontaneous incidence of insulin-dependent diabetes mellitus. J Immunol 154:5567–5575
29. Singer SM, Tisch R, Yang XD, Sytwu HK, Liblau R, McDevitt HO (1998) Prevention of diabetes in NOD mice by a mutated I-Ab transgene. Diabetes 47:1570–1577
30. Hattori M, Buse JB, Jackson RA, Glimcher L, Dorf ME, Minami M, Makino S, Moriwaki K, Kuzuya H, Imura H et al (1986) The NOD mouse: recessive diabetogenic gene in the major histocompatibility complex. Science 231:733–735
31. Mora C, Wong FS, Chang CH, Flavell RA (1999) Pancreatic infiltration but not diabetes occurs in the relative absence of MHC class II-restricted CD4 T cells: studies using NOD/CIITA-deficient mice. J Immunol 162:4576–4588
32. Kanagawa O, Martin SM, Vaupel BA, Carrasco-Marin E, Unanue ER (1998) Autoreactivity of T cells from nonobese diabetic mice: an I-Ag7-dependent reaction. Proc Natl Acad Sci USA 95:1721–1724
33. Stratmann T, Martin-Orozco N, Mallet-Designe V, Poirot L, McGavern D, Losyev G, Dobbs CM, Oldstone MB, Yoshida K, Kikutani H, Mathis D, Benoist C, Haskins K, Teyton L (2003) Susceptible MHC alleles, not background genes, select an autoimmune T cell reactivity. J Clin Invest 112:902–914
34. Suri A, Walters JJ, Rohrs HW, Gross ML, Unanue ER (2008) First signature of islet beta-cell-derived naturally processed peptides selected by diabetogenic class II MHC molecules. J Immunol 180:3849–3856
35. Suri A, Levisetti MG, Unanue ER (2008) Do the peptide-binding properties of diabetogenic class II molecules explain autoreactivity? Curr Opin Immunol 20:105–110
36. Lieberman SM, DiLorenzo TP (2003) A comprehensive guide to antibody and T-cell responses in type 1 diabetes. Tissue Antigens 62:359–377
37. Schmidt D, Amrani A, Verdaguer J, Bou S, Santamaria P (1999) Autoantigen-independent deletion of diabetogenic CD4+ thymocytes by protective MHC class II molecules. J Immunol 162:4627–4636
38. Serreze DV, Leiter EH (1988) Defective activation of T suppressor cell function in nonobese diabetic mice. Potential relation to cytokine deficiencies. J Immunol 140:3801–3807
39. Kukreja A, Cost G, Marker J, Zhang C, Sun Z, Lin-Su K, Ten S, Sanz M, Exley M, Wilson B, Porcelli S, Maclaren N (2002) Multiple immuno-regulatory defects in type-1 diabetes. J Clin Invest 109:131–140
40. D'Alise AM, Ergun A, Hill JA, Mathis D, Benoist C (2011) A cluster of coregulated genes determines TGF-beta-induced regulatory T-cell (Treg) dysfunction in NOD mice. Proc Natl Acad Sci USA 108:8737–8742
41. Bluestone JA, Tang Q, Sedwick CE (2008) T regulatory cells in autoimmune diabetes: past challenges, future prospects. J Clin Immunol 28:677–684
42. Luhder F, Katz J, Benoist C, Mathis D (1998) Major histocompatibility complex class II molecules can protect from diabetes by positively selecting T cells with additional specificities. J Exp Med 187:379–387
43. Ferreira C, Singh Y, Furmanski AL, Wong FS, Garden OA, Dyson J (2009) Non-obese diabetic mice select a low-diversity repertoire of natural regulatory T cells. Proc Natl Acad Sci USA 106:8320–8325
44. Singer SM, Tisch R, Yang XD, McDevitt HO (1993) An Abd transgene prevents diabetes in nonobese diabetic mice by inducing regulatory T cells. Proc Natl Acad Sci USA 90:9566–9570

45. Sumida T, Furukawa M, Sakamoto A, Namekawa T, Maeda T, Zijlstra M, Iwamoto I, Koike T, Yoshida S, Tomioka H et al (1994) Prevention of insulitis and diabetes in beta 2-microglobulin-deficient non-obese diabetic mice. Int Immunol 6:1445–1449
46. Serreze DV, Leiter EH, Christianson GJ, Greiner D, Roopenian DC (1994) Major histocompatibility complex class I-deficient NOD-B2mnull mice are diabetes and insulitis resistant. Diabetes 43:505–509
47. Katz J, Benoist C, Mathis D (1993) Major histocompatibility complex class I molecules are required for the development of insulitis in non-obese diabetic mice. Eur J Immunol 23:3358–3360
48. Wicker LS, Leiter EH, Todd JA, Renjilian RJ, Peterson E, Fischer PA, Podolin PL, Zijlstra M, Jaenisch R, Peterson LB (1994) Beta 2-microglobulin-deficient NOD mice do not develop insulitis or diabetes. Diabetes 43:500–504
49. Bluestone JA, Tang Q (2005) How do CD4+CD25+ regulatory T cells control autoimmunity? Curr Opin Immunol 17:638–642
50. Peterson JD, Pike B, McDuffie M, Haskins K (1994) Islet-specific T cell clones transfer diabetes to nonobese diabetic (NOD) F1 mice. J Immunol 153:2800–2806
51. Haskins K, McDuffie M (1990) Acceleration of diabetes in young NOD mice with a CD4+ islet-specific T cell clone. Science 249:1433–1436
52. Peterson JD, Haskins K (1996) Transfer of diabetes in the NOD-scid mouse by CD4 T-cell clones. Differential requirement for CD8 T-cells. Diabetes 45:328–336
53. Haskins K, Wegmann D (1996) Diabetogenic T-cell clones. Diabetes 45:1299–1305
54. Katz JD, Wang B, Haskins K, Benoist C, Mathis D (1993) Following a diabetogenic T cell from genesis through pathogenesis. Cell 74:1089–1100
55. Verdaguer J, Schmidt D, Amrani A, Anderson B, Averill N, Santamaria P (1997) Spontaneous autoimmune diabetes in monoclonal T cell nonobese diabetic mice. J Exp Med 186:1663–1676
56. Pakala SV, Chivetta M, Kelly CB, Katz JD (1999) In autoimmune diabetes the transition from benign to pernicious insulitis requires an islet cell response to tumor necrosis factor alpha. J Exp Med 189:1053–1062
57. Jun HS, Santamaria P, Lim HW, Zhang ML, Yoon JW (1999) Absolute requirement of macrophages for the development and activation of beta-cell cytotoxic CD8+ T-cells in T-cell receptor transgenic NOD mice. Diabetes 48:34–42
58. Lesage S, Hartley SB, Akkaraju S, Wilson J, Townsend M, Goodnow CC (2002) Failure to censor forbidden clones of CD4 T cells in autoimmune diabetes. J Exp Med 196:1175–1188
59. Kurts C, Carbone FR, Barnden M, Blanas E, Allison J, Heath WR, Miller JF (1997) CD4+ T cell help impairs CD8+ T cell deletion induced by cross-presentation of self-antigens and favors autoimmunity. J Exp Med 186:2057–2062
60. Martin-Orozco N, Wang YH, Yagita H, Dong C (2006) Cutting Edge: Programmed death (PD) ligand-1/PD-1 interaction is required for CD8+ T cell tolerance to tissue antigens. J Immunol 177:8291–8295
61. Camacho SA, Heath WR, Carbone FR, Sarvetnick N, LeBon A, Karlsson L, Peterson PA, Webb SR (2001) A key role for ICAM-1 in generating effector cells mediating inflammatory responses. Nat Immunol 2:523–529
62. Byersdorfer CA, Schweitzer GG, Unanue ER (2005) Diabetes is predicted by the beta cell level of autoantigen. J Immunol 175:4347–4354
63. DiPaolo RJ, Unanue ER (2001) The level of peptide-MHC complex determines the susceptibility to autoimmune diabetes: studies in HEL transgenic mice. Eur J Immunol 31:3453–3459
64. Ohashi PS, Oehen S, Aichele P, Pircher H, Odermatt B, Herrera P, Higuchi Y, Buerki K, Hengartner H, Zinkernagel RM (1993) Induction of diabetes is influenced by the infectious virus and local expression of MHC class I and tumor necrosis factor-alpha. J Immunol 150:5185–5194
65. Ohashi PS, Oehen S, Buerki K, Pircher H, Ohashi CT, Odermatt B, Malissen B, Zinkernagel RM, Hengartner H (1991) Ablation of "tolerance" and induction of diabetes by virus infection in viral antigen transgenic mice. Cell 65:305–317
66. Horwitz MS, Ilic A, Fine C, Balasa B, Sarvetnick N (2004) Coxsackieviral-mediated diabetes: induction requires antigen-presenting cells and is accompanied by phagocytosis of beta cells. Clin Immunol 110:134–144
67. Horwitz MS, Bradley LM, Harbertson J, Krahl T, Lee J, Sarvetnick N (1998) Diabetes induced by Coxsackie virus: initiation by bystander damage and not molecular mimicry. Nat Med 4:781–785
68. Bach JF (2005) Infections and autoimmune diseases. J Autoimmun 25(Suppl):74–80
69. Serreze DV, Chapman HD, Varnum DS, Hanson MS, Reifsnyder PC, Richard SD,

Fleming SA, Leiter EH, Shultz LD (1996) B lymphocytes are essential for the initiation of T cell-mediated autoimmune diabetes: analysis of a new "speed congenic" stock of NOD.Ig mu null mice. J Exp Med 184:2049–2053

70. Hu CY, Rodriguez-Pinto D, Du W, Ahuja A, Henegariu O, Wong FS, Shlomchik MJ, Wen L (2007) Treatment with CD20-specific antibody prevents and reverses autoimmune diabetes in mice. J Clin Invest 117:3857–3867
71. Fiorina P, Vergani A, Dada S, Jurewicz M, Wong M, Law K, Wu E, Tian Z, Abdi R, Guleria I, Rodig S, Dunussi-Joannopoulos K, Bluestone J, Sayegh MH (2008) Targeting CD22 reprograms B-cells and reverses autoimmune diabetes. Diabetes 57:3013–3024
72. Zekavat G, Rostami SY, Badkerhanian A, Parsons RF, Koeberlein B, Yu M, Ward CD, Migone TS, Yu L, Eisenbarth GS, Cancro MP, Naji A, Noorchashm H (2008) In vivo BLyS/BAFF neutralization ameliorates islet-directed autoimmunity in nonobese diabetic mice. J Immunol 181:8133–8144
73. Melanitou E, Devendra D, Liu E, Miao D, Eisenbarth GS (2004) Early and quantal (by litter) expression of insulin autoantibodies in the nonobese diabetic mice predict early diabetes onset. J Immunol 173:6603–6610
74. Serreze DV, Fleming SA, Chapman HD, Richard SD, Leiter EH, Tisch RM (1998) B lymphocytes are critical antigen-presenting cells for the initiation of T cell-mediated autoimmune diabetes in nonobese diabetic mice. J Immunol 161:3912–3918
75. Falcone M, Lee J, Patstone G, Yeung B, Sarvetnick N (1998) B lymphocytes are crucial antigen-presenting cells in the pathogenic autoimmune response to GAD65 antigen in nonobese diabetic mice. J Immunol 161:1163–1168
76. Noorchashm H, Lieu YK, Noorchashm N, Rostami SY, Greeley SA, Schlachterman A, Song HK, Noto LE, Jevnikar AM, Barker CF, Naji A (1999) I-Ag7-mediated antigen presentation by B lymphocytes is critical in overcoming a checkpoint in T cell tolerance to islet beta cells of nonobese diabetic mice. J Immunol 163:743–750
77. Babad J, Geliebter A, DiLorenzo TP (2010) T-cell autoantigens in the non-obese diabetic mouse model of autoimmune diabetes. Immunology 131:459–465
78. Moser A, Hsu HT, van Endert P (2010) Beta cell antigens in type 1 diabetes: triggers in pathogenesis and therapeutic targets. F1000 Biol Rep 2:75
79. Wegmann DR, Norbury-Glaser M, Daniel D (1994) Insulin-specific T cells are a predominant component of islet infiltrates in pre-diabetic NOD mice. Eur J Immunol 24:1853–1857
80. Daniel D, Gill RG, Schloot N, Wegmann D (1995) Epitope specificity, cytokine production profile and diabetogenic activity of insulin-specific T cell clones isolated from NOD mice. Eur J Immunol 25:1056–1062
81. French MB, Allison J, Cram DS, Thomas HE, Dempsey-Collier M, Silva A, Georgiou HM, Kay TW, Harrison LC, Lew AM (1997) Transgenic expression of mouse proinsulin II prevents diabetes in nonobese diabetic mice. Diabetes 46:34–39
82. Jaeckel E, Lipes MA, von Boehmer H (2004) Recessive tolerance to preproinsulin 2 reduces but does not abolish type 1 diabetes. Nat Immunol 5:1028–1035
83. Jasinski JM, Yu L, Nakayama M, Li MM, Lipes MA, Eisenbarth GS, Liu E (2006) Transgenic insulin (B:9-23) T-cell receptor mice develop autoimmune diabetes dependent upon RAG genotype, H-2g7 homozygosity, and insulin 2 gene knockout. Diabetes 55:1978–1984
84. Levisetti MG, Suri A, Petzold SJ, Unanue ER (2007) The insulin-specific T cells of nonobese diabetic mice recognize a weak MHC-binding segment in more than one form. J Immunol 178:6051–6057
85. Mohan JF, Levisetti MG, Calderon B, Herzog JW, Petzold SJ, Unanue ER (2010) Unique autoreactive T cells recognize insulin peptides generated within the islets of Langerhans in autoimmune diabetes. Nat Immunol 11:350–354
86. Levisetti MG, Lewis DM, Suri A, Unanue ER (2008) Weak proinsulin peptide-major histocompatibility complexes are targeted in autoimmune diabetes in mice. Diabetes 57:1852–1860
87. Mohan JF, Petzold SJ, Unanue ER (2011) Register shifting of an insulin peptide-MHC complex allows diabetogenic T cells to escape thymic deletion. J Exp Med 208:2375–2383
88. Jolicoeur C, Hanahan D, Smith KM (1994) T-cell tolerance toward a transgenic beta-cell antigen and transcription of endogenous pancreatic genes in thymus. Proc Natl Acad Sci USA 91:6707–6711
89. Chentoufi AA, Palumbo M, Polychronakos C (2004) Proinsulin expression by Hassall's corpuscles in the mouse thymus. Diabetes 53:354–359
90. Anderson MS, Venanzi ES, Klein L, Chen Z, Berzins SP, Turley SJ, von Boehmer H, Bronson R, Dierich A, Benoist C, Mathis D (2002) Projection of an immunological self shadow within the thymus by the aire protein. Science 298:1395–1401

91. Like AA, Rossini AA (1976) Streptozotocin-induced pancreatic insulitis: new model of diabetes mellitus. Science 193:415–417
92. Chervonsky AV, Wang Y, Wong FS, Visintin I, Flavell RA, Janeway CA Jr, Matis LA (1997) The role of Fas in autoimmune diabetes. Cell 89:17–24
93. Savinov AY, Tcherepanov A, Green EA, Flavell RA, Chervonsky AV (2003) Contribution of Fas to diabetes development. Proc Natl Acad Sci USA 100:628–632
94. Kagi D, Odermatt B, Ohashi PS, Zinkernagel RM, Hengartner H (1996) Development of insulitis without diabetes in transgenic mice lacking perforin-dependent cytotoxicity. J Exp Med 183:2143–2152
95. Kagi D, Odermatt B, Seiler P, Zinkernagel RM, Mak TW, Hengartner H (1997) Reduced incidence and delayed onset of diabetes in perforin-deficient nonobese diabetic mice. J Exp Med 186:989–997
96. Kagi D, Ho A, Odermatt B, Zakarian A, Ohashi PS, Mak TW (1999) TNF receptor 1-dependent beta cell toxicity as an effector pathway in autoimmune diabetes. J Immunol 162:4598–4605
97. Calderon B, Suri A, Unanue ER (2006) In CD4+ T-cell-induced diabetes, macrophages are the final effector cells that mediate islet beta-cell killing: studies from an acute model. Am J Pathol 169:2137–2147
98. Jun HS, Yoon CS, Zbytnuik L, van Rooijen N, Yoon JW (1999) The role of macrophages in T cell-mediated autoimmune diabetes in nonobese diabetic mice. J Exp Med 189:347–358
99. Rabinovitch A (1998) An update on cytokines in the pathogenesis of insulin-dependent diabetes mellitus. Diabetes Metab Rev 14:129–151
100. Shoda LK, Young DL, Ramanujan S, Whiting CC, Atkinson MA, Bluestone JA, Eisenbarth GS, Mathis D, Rossini AA, Campbell SE, Kahn R, Kreuwel HT (2005) A comprehensive review of interventions in the NOD mouse and implications for translation. Immunity 23:115–126

Chapter 20

Type 2 Diabetes Models

Dorte X. Gram

Abstract

This chapter deals with type 2 diabetes in vivo models and techniques suitable for testing new anti-diabetic compounds. In particular, the testing of TRP antagonist for beneficial effects against type 2 diabetes is considered. There are many choices of both in vitro techniques and in vivo models and in principle they can be combined in various ways. The comprehensive listing of all relevant tests and models is too long to be discussed and described in detail here. Therefore, a few selected in vivo experiments (author's models of choice) are described. These are acute experiments after single dose of the TRP antagonist in rodents and could/should be repeated after chronic dosing. Non-rodent models are briefly discussed, and a single model and test are suggested but not described in detail. The experiments are aiming at demonstrating that the TRP antagonists are effective in treating hyperglycemia, impaired glucose tolerance, impaired insulin secretion, and insulin resistance in vivo and should, thus, be sufficient to demonstrate preclinical proof of concept of a TRP antagonist in type 2 diabetes in rodents. The experiments are suggestions and could be replaced or supplemented by others.

Key words: Type 2 diabetes models, Preclinical pharmacology, OGTT, Hyperglycemia, IGT, Impaired insulin secretion, Insulin resistance

1. Introduction

Type 2 diabetes is in epidemic rise around the world. Recently the International Diabetes Federation (IDF) released new and alarming figures on the numbers of diagnosed diabetes patients in the world: *"Data from global studies demonstrates that the number of people with diabetes in 2011 has reached a staggering 366 million, 4.6 million deaths are due to diabetes and health care spending on diabetes has reached 465 billion USD"* (1). This is alarming and a real threat to the healthcare systems around the world. Therefore, the development of novel efficacious diabetes therapeutics that can potentially address diabetes as well as the diabetes complications

Arpad Szallasi and Tamás Bíró (eds.), *TRP Channels in Drug Discovery: Volume II*, Methods in Pharmacology and Toxicology,
DOI 10.1007/978-1-62703-095-3_20,

are highly needed. TRP antagonists could be a new and promising approach, for instance the TRPV1 antagonists as suggested by us in our patent application (2) and recently by Astellas Pharma Inc., Japan (3).

According to the World Health Organization (WHO), human type 2 diabetes is currently recommended to be diagnosed as follows: Demonstration of fasting plasma glucose≥7.0 mmol/L (126 mg/dl) or 2-h plasma glucose≥11.1 mmol/L (200 mg/dl) 2 h after 75 g anhydrous glucose in an oral glucose tolerance test (OGTT). Impaired glucose regulation [impaired glucose tolerance (IGT) and impaired fasting glycemia (IFG)] refers to a metabolic state intermediate between normal glucose homeostasis and diabetes. This symptom stems from impairments in the stimulated insulin secretion possibly accompanied by reduced insulin sensitivity. Abnormal glucose tolerance (IGT or diabetes) is a condition that belongs to the so-called Metabolic Syndrome. The Metabolic Syndrome is a cluster of diseases that are all linked to each other (with increased risk of developing the others). It comprises impaired glucose regulation (IGT or diabetes), insulin resistance, raised arterial pressure, raised plasma triglycerides, central (truncal) obesity, and microalbuminuria (4). These are all cardiovascular disease (CVD) risk factors. Often a person with abnormal glucose regulation will have one or more of the other CVD risk factors (5). Diabetics do not die from hyperglycemia itself but from the resulting CVD, such as ischemic heart disease. A tight control of glycemic levels in patients has been associated with a reduction in mortality as well as complications.

When developing new anti-diabetics, the primary endpoint is the effect on hyperglycemia. Important secondary endpoints are IGT, impaired insulin secretion and insulin resistance. In the following, these endpoints are in focus in terms of demonstrating preclinical efficacy of a TRP antagonist in models of type 2 diabetes. However, as noted above, human type 2 diabetes is associated with insulin resistance, arterial hypertension, hyperlipidemia, central obesity, and microalbuminuria as well as CVD. These endpoints are also relevant to test for, when developing new anti-diabetic agents but are not reviewed in this chapter.

The role of TRP antagonists in type 2 diabetes mellitus has—to our knowledge—previously been investigated only in very few in vivo studies. As published in our own patent application (2) and later at the 2007 European Neuropeptide Club Meeting (6) we have, ourselves, investigated the role of TRPV1 in glucose homeostasis. We did this by (a) studying high-fat-fed TRPV1 mice and (b) the effect of the TRPV1 antagonist BCTC in glucose intolerant rats. The TRPV1 antagonist BCTC had been described both in vitro (7) and in vivo (8) prior to our studies with information on the pharmacokinetics of the compound in rats. In models of pain, BCTC had been described to be orally available and to have an effect on rodent models of pain. We used this information to design our own experiment in obese rats.

In experiment (a) The TRPV1 knock out and control mice were given a high-fat diet (HFD) for several weeks to induce glucose intolerance as previously described in normal mice (9). We found that TRPV1-deficient mice were resistant to the development of impaired glucose tolerance and that this was associated with an increased glucose-stimulated insulin secretion (2). In experiment (b) we further found that BCTC in Zucker obese fatty rats improved oral glucose tolerance after a single dose of 15 mg/kg p.o. and that this was associated with increased levels of insulin. We also did a chronic dosing study in these rats and found that following 2 weeks of bi-daily doses of BCTC p.o. (7,5 or 15 mg/kg) the glucose tolerance was improved. Recently, Astellas Pharmaceuticals, Japan, has published results on the effect of BCTC on hyperglycemia, lipidemia, insulin resistance and insulin resistance in *ob/ob* mice (3). To our knowledge, no publications exist on the effect of a TRPV1 antagonist on impaired glucose regulation either in non-rodent animals or in man.

In order to demonstrate a beneficial effect of TRP antagonists in type 2 diabetes, a vast variety of in vivo models and applicable techniques exists that have all been used to study parts of the symptoms of type 2 diabetes. It is beyond the scope of this chapter to review all of these. In the following, therefore, the focus is on animal models and applicable methods that can elucidate a possible effect on the primary endpoint, namely the anti-hyperglycemic effect. In principle, all of the in vivo models can be combined with all of the techniques. The described models and techniques are a selection of models chosen for the following reasons: (1) it should yield a clear answer with regard to the effect of a TRP antagonist as anti-hyperglycemic agent and (2) it should be relatively easy to handle for persons not otherwise dealing with experimental diabetes research.

Effective treatment of hyperglycemia is a must for new anti-diabetics. This can be tested in any animal model that has an elevated blood glucose level (both fasting and fed). These models might also have an impaired glucose tolerance, a defective insulin secretion and may be accompanied by insulin resistance. Ideally, a diabetes drug designed to reduce hyperglycemia should not work in a normal individual due to the risk of inducing hypoglycemia. Risk of hypoglycemic events is a common safety parameter when developing new diabetes drugs. Insulins do exert a hypoglycemic effect even at normo-glycemia—the new GLP-1 analogs do not—and this is considered a safety benefit. Therefore, it is important to deselect compounds that are effective at normo-glycemic levels. This can be tested in a normal mouse or rat. We have previously used standard black C57Bl/J6 mice and Wistar or Sprague–Dawley rats. Since the primary endpoint for novel anti-diabetics is the effect on hyperglycemia, a pure hyper-glycemic (type 1 diabetes like) model can be chosen. Experimental induction of hyperglycemia can be accomplished by use of drugs such as streptozotocin (STZ) (10, 11) or alloxan (12) to normal animals. The two compounds

both destroy the insulin-producing β-cells of the islets of Langerhans in the pancreas in a dose-dependent manner. The treatment can be combined with nicotinamide for β-cell protection to obtain only a partial depletion of the insulin-producing cells (13), or it can be accompanied by a partial pancreatectomy in order to reduce the dose of STZ or alloxan needed to deplete the β-cells. These STZ/alloxan diabetic models are basically normal animals (without obesity or insulin resistance) that develop hyperglycemia, and are therefore more type 1 diabetes-like models. They can however be employed to study the effect of a TRP antagonist on hyperglycemia in a traditional drug candidate screening program for antihyperglycemic effect. No spontaneous type 2 diabetes models exist without the involvement of a high-energy diet and/or age and eventually "sedentary lifestyle" (lack of exercise).

The "usual suspects" are divided into pre-diabetes, early diabetes, and diabetes/late diabetes models.

There are a number of rodent animal models of type diabetes available including the obese diabetic mice (*ob/ob* and *db/db*), the new zealand obese mouse (NZO), the Goto Kakizaki (GK) rat, the obese Zucker rat, Zucker Diabetic Fatty rat (ZDF), and the Israeli sand rat (psammosys obesus) (14). We have primarily worked with the *ob/ob* mouse, the *db/db* mouse, the obese Zucker rat, and the ZDF rat and will focus on these. They all have a genetic mutation in the leptin receptor system. This results in a lack of satiety and therefore continuously eating and rapidly developing obesity associated with glucose intolerance, hypertrophy of β-cell-mass, progressive hyperinsulinemia and insulin resistance. Lean littermates can be used for the comparison. The *ob/ob* mice and obese Zucker rats are considered pre-diabetes models or models of IGT. In the *ob/ob* mice hyperglycemia develops with hyperinsulinemia, whereas in *db/db* mice and in the ZDF rat, hyperglycemia is associated with a progressive loss of β-cell mass. The two latter models are therefore considered models of later stages of diabetes, whereas the *ob/ob* mouse is a model of early diabetes (and pre-diabetes).

Non-rodent animal models usually comprise cats, dogs, pigs, and monkeys. Cats can develop a type 2-like diabetes (15) in association with increased age and body weight. Dogs can develop obesity and a state of pre-diabetes with insulin resistance in association with increased age and overweight (15, 16) and can develop a type 1-like diabetic state (15). So far no standardized cat or dog type 2 diabetes models are available for the study of anti-diabetic effects. In pigs, obesity with its associated features can be induced by diet (17–19). In monkeys, both pre-diabetes and diabetes can occur, often in the older more obese individuals (20).

STZ induction of diabetes in combination with a high-fat diet will result in a type 2 diabetes-like state in rats (21), dogs (22), and pigs (23, 24). Also available are a number of knock-out animals and humanized models. Such models are not reviewed here.

The choice of laboratory animals and specific techniques are many and there are "pro's and con's" related to all of them. As published in our patent application (2) and at a scientific meeting (6), we have ourselves chosen to test a TRPV1 antagonist, BCTC, in pre-diabetic obese Zucker rats evaluating the effect using the oral glucose tolerance test (OGTT) and demonstrating an effect on IGT associated with potentiated insulin secretion. Astellas Pharmaceuticals used the early-diabetic *ob/ob* mice to demonstrate efficacy of chronic BCTC on fasting plasma glucose, insulin and triglycerides and the OGTT to demonstrate efficacy of BCTC on impaired oral glucose tolerance, impaired glucose stimulated insulin secretion, and insulin sensitivity. Previously, we have used fed *db/db* mice to demonstrate efficacy of GLP-1 agonists on hyperglycemia (25). Further we have used the *db/db* mice to demonstrate the induction of acute (potentiated) hyperglycemia following a single dose of resiniferatoxin s.c. (26) indicating that these mice are responsive to stimulation by a TRPV1-receptor modulator. The pig, the dog, or the monkey could be used as non-rodent proof-of-concept models. It needs to be demonstrated which of these models is best in terms of evaluating a potential anti-hyperglycemic effect of TRP antagonists.

Various techniques can be employed to demonstrate the effect on hyperglycemia: measurement of the non-fasting and fasting blood glucose levels, measurement of HbA_{1c} and lactate, measurement of blood glucose, and plasma insulin following an OGTT to demonstrate effect on fasting blood and plasma insulin as well as on oral glucose tolerance and glucose stimulated insulin secretion. To study the stimulated insulin secretion, glucose can also be injected either i.v. or i.p. (rodents), also called IVGTT or IPGTT. To study the insulin sensitivity, an indirect measure can be obtained from the OGTT blood glucose and plasma insulin data, as we have previously described (27). To be more accurate, it is desirable to use either the IVGTT used in combination with a mathematical method, the minimal modeling (28), or the golden standard technique to assess insulin sensitivity, the (eu)glycemic glucose clamp (29). These procedures along with studies in pigs are not trivial and do require a high level of both training and expertise. Therefore, such experiments are not described in the following. Recommendations on such studies can however be made on an ad hoc basis by direct contact to the author.

To demonstrate efficacy of a TRP antagonists for their possible anti-diabetic efficacy, the following tests could be suggested as a minimum:

1. *Effect on hyperglycemia*: Measurement of the blood glucose levels during a defined time-frame in hyperglycemic animals.
2. *Effect on impaired glucose tolerance*: Measure the fasting blood glucose levels and the 2-h blood glucose level following a standard OGTT.

3. *Effect on insulin secretion*: Measure the plasma insulin in response to an OGTT to assess the immediate insulin response to glucose.
4. *Effect on insulin sensitivity*: Use the blood glucose and plasma insulin data to calculate the indirect measure of insulin sensitivity during the OGTT: the inverse relationship between the incremental area under the plasma insulin profiles and the incremental area under the blood glucose profiles during the OGTT.

Obviously, some of these assessments can occur in the same animals during an experiment. Thus, it is suggested to perform the following in vivo experiments to obtain preclinical proof of concept:

1. Screening of several analgesic and orally available TRP antagonists:
   (a) Acute effect on hyperglycemia in *db/db* mice, single-dose and dose–response (potency) studies.
2. Detailed profiling of selected potent anti-diabetic TRP antagonists:
   (a) Effect on IGT, impaired insulin secretion and insulin resistance in the obese Zucker rat, assessment after acute and chronic exposure.
3. Detailed profiling of the lead compound(s) in a non-rodent model (not described in detail in the following):
   (a) Acute and chronic effect on hyperglycemia, IGT, insulin secretion, and insulin resistance in the STZ-HFD pig.

2. Materials

In principle, the suggested in vivo experiments can be conducted by anyone with experience in handling and blood sampling the particular laboratory animal and with the permission to perform the sort of suggested experiments. The associated in vitro analysis can be performed by anyone familiar with standard laboratory techniques as RIA or ELISAs. The laboratory animals need to be housed in a standard animal facility with ambient controlled conditions as change of air and temperature.

2.1. Acute Effect on Hyperglycemia in db/db Mice

1. Gloves
2. Prepared sampling scheme with space for noting the blood glucose values
3. Male *db/db* mice (The Jackson Laboratory, Sacramento, CA) to be arriving at the age of 6 weeks, 8–10 mice per group

4. Glucometer, hand held (or other apparatus), for instance the Accu-Chek Compact used by many diabetics (Roche)
5. Glucometer strips (Roche)
6. Scalpels
7. 1 and 2 ml syringes
8. Gavages for mice, size small (Feeding Needles, Sweden, http://www.feeding-needles.com)
9. Test compound in solution for oral delivery, dosing volume max 2 ml/ mouse

2.2. Effect on IGT and Impaired Insulin Secretion in the Zucker Obese Rats

1. Make sure to have enough test compound and have it prepared in solution for oral delivery, dosing volume max. 5 ml/ rat
2. Male Zucker obese rats to be arriving at the age of 6 weeks, 8–10 mice per group (Charles River Laboratories International, Inc., Wilmington, MA)
3. Special Altromin chow (Altromin Spezialfutter GmbH & Co. KG, Lage, Germany)
4. Scale for measurement of the body weight of rats (up to 2,000 g)
5. Glucometer, hand held, or other apparatus, for instance the Accu-Chek Compact used by diabetics for regular glucose monitoring (Roche)
6. Glucometer strips (Roche)
7. Scalpels
8. 1 and 5 ml syringes
9. Heparinised hematocrite capillary tubes, min 100 µl
10. Wax for hematocrite capillary tubes
11. Cooled hematocrite centrifuge
12. Racks for 5 ml tubes
13. 5 ml tubes
14. Rat insulin assays, for instance the Mercodia rat insulin ELISA and sample dilution buffer (Mercodia, Uppsala, Sweden)
15. Pipettes and tips for sampling 10, 50, 70, 200, and 1,000 µl
16. Ice and container for ice
17. Dry ice and container for dry ice (for insulin ELISA racks)
18. Gavages for rats, size: medium–large (Feeding Needles, Sweden)
19. Glucose solution for oral delivery (500 mg/ml)
20. Test compound in solution for oral drug delivery

3. Methods

It is important that relevant in vitro analysis, as well as pharmacokinetic studies of the TRP antagonists, has been made prior to these experiments. The dose levels chosen for the diabetes experiments should stem from such studies and from efficacy studies regarding analgesic effect of the TRP antagonists to avoid excessive use of diseased animals.

3.1. Acute Effect on Hyperglycemia in db/db Mice

1. Male *db/db* should be ordered to arrive at the age of 6 weeks (Notes 1–5).
2. Mark the mice permanently (Note 6).
3. Prepare a scheme for noting 3 blood sample measures for each mouse and bring it with the hand-held glucometer (Note 7) including strips, gloves, and scalpels to the animal facility.
4. After at 1-week acclimatization period, the fed blood glucose level is measured three times in each mouse. This serves as acclimatization to the blood sampling procedure. The samples for the measurement of blood glucose (Note 8) are obtained as follows: Gently take the mouse from the box and place it on the top of the cage lid-grid by holding the tail with your thumb and fore finger. Gently fix the tail between your fingers and with the other hand use the point of a scalpel to create a small, fresh, clean wound at the tail-tip through which the blood can be obtained. Start the hand-held glucose analyzer. Gently squeeze the lateral sides of the tail (from root to bottom) to stimulate blood extravasation of a blood droplet. Use a 1 ml syringe to aspire the droplet and confer it to the hand-held glucose analyzer. Note the blood glucose value on a prepared scheme.
5. The mean value of these measurements is calculated and used to allocate the mice into groups with matching mean blood glucose levels (Note 9).
6. The mice should be re-grouped so that each group is housed together for convenience when dosing.
7. The mice are left for another week of acclimatization.
8. Before the experiment: Prepare a scheme for body weight and calculation of oral dose and for blood glucose measurements, gather all items on the materials list and bring it to the animal facility.
9. On the test day: The mice are bled from the tail tip capillary several times for the measurement of blood glucose and are dosed orally once. Blood samples are obtained at time 0, 30, 60, 90, 120, 180 min (Note 10). The duration and frequency

can vary depending on your test compound. Start by assessing the blood glucose levels as described above.

10. Dose the TRP antagonist orally by gavage shortly after the 0 min blood sample. Aspire the calculated dosing volume into a syringe and mount the disposable gavage. The mouse is then taken from the cage, the tail is fixed with your little-finger and the scruff of the neck is fixed by your thumb and fore finger. Lift the mouse to a vertical position (holding it in the air) and try to stretch the neck. Gently insert the gavage into the mouth and further down into the stomach. Slowly inject the volume from the syringe through the gavage and retract the gavage gently (Notes 11 and 12). Put the mouse back in the cage and start the clock!
11. Obtain the rest of the blood samples as accurately as possible on the given time points as described above. Mark the scheme if the samples are delayed.
12. Plot the blood glucose data and evaluate efficacy. This could be done by determining (a) if the blood glucose reaches a target level within a defined time frame, (b) the time of onset of action, (c) the duration of action and (d) the area under the curve (AUC) of the blood glucose curves as compared to vehicle.
13. Select some potent TRP antagonists to proceed to similar dose–response experiments in *db/db* mice, 4 dose-levels and a vehicle/control group is suggested to be able to calculate the ED_{50} of the effect on hyperglycemia.
14. Select potent compounds to proceed to tests in the obese Zucker rat.

3.2. Effect on IGT, Impaired Insulin Secretion, and Insulin Sensitivity in the Obese Zucker Rats

1. Order special diet and 6 weeks old male Zucker obese rats, 8–10 rats per group (Notes 3, 5, 13, and 14).
2. Prepare schemes for notification of the rat body weight during the experiment.
3. Mark the rats permanently (Note 6).
4. After the acclimatization period (1–2 weeks) assess the body weight of the rats and allocate them into groups with matching mean body weights (Note 9).
5. Prepare for the OGTT: insulin ELISA rack schemes, schemes for noting the blood glucose values and for assessing the rat body weights (+ calculated oral doses of TRP antagonist and glucose).
6. Fast the rats for minimum 6 h (Note 15).
7. Prepare labeled 5 ml tubes (rat no, time) and place them in racks kept on ice, 1 rack per time point. Bring them to the animal facility with pen, gloves, scalpels, capillary tubes, schemes for bodyweight, glucose and insulin, insulin ELISA racks on dry-ice, pipettes and tips for 10 and 70 µl sampling, 1

and 5 ml syringes, hand-held glucometer (Note 7), glucose and test compound for oral dosing gavages.

8. Organize a place where to do the oral dosing, blood sampling, and glucose analysis and a place where to prepare the plasma insulin samples.
9. Prepare the vehicle (control) and test compound solutions.
10. The overall OGTT procedure: Sample for the measurement of basal blood glucose (Note 8) and plasma insulin values. Dose the TRP-antagonist orally at a predefined time point prior to test start (Note 16). Shortly prior to test start, obtain samples for blood glucose and plasma insulin measurements in all rats. Immediately thereafter dose the rats with oral glucose (2 g/kg). Start the clock!—Make sure that the time spend dosing corresponds to the time spend blood sampling. After the oral glucose collect blood samples again for the measurement of blood glucose and plasma insulin values at time 30, 60, and 120 min after oral glucose (Note 10).
11. Perform the oral dosing as described here: Aspire the predefined dosing volume of either the test compound or the oral glucose solution and mount the gavage. Take the rat from the cage and place it on top of the lid grid. Pick up the rat with one hand, by fixing at the scruff of the neck. Keep it in a vertical position (holding it in the air) and try to stretch the neck. Gently insert the gavage into the mouth and further down into the stomach. Slowly inject the volume from the syringe through the gavage and retract the gavage gently (Note 11). Put the rat back to the cage.
12. Obtain the blood samples for the measurement of blood glucose and plasma insulin in the following way: Gently take the rat from the box and place it on the top of the cage lid-grid. Gently fix the tail between your fingers and with the other hand use the point of a scalpel to create a small, fresh, clean wound at the tail-tip through which the blood can be obtained from the tail tip capillary. Gently squeeze the lateral sides of the tail (from root to bottom) to stimulate blood extravasation of a blood droplet. Start the glucometer. With the 1 ml syringe aspire a droplet of blood from the tail tip capillary and add it to the glucometer. Note the value on the blood glucose scheme. Then use a 100 µl capillary tube to aspire app. 70 µl blood from the rat tail tip, keep the forefinger over one of the opposite opening and stick the blood filled opening into wax to seal the capillary tube. Then place the capillary tube vertically (wax down) into the labeled 5 ml tubes in racks placed on ice. Put the rat back to the cage. After sampling all rats, take the filled capillary tubes and spin them at 4°C to separate the plasma. When the time permits, bring the tubes to the table where you have your cooled ELISA racks and rack schemes. Split each capillary tube exactly at the transition from plasma to white blood cells.

This can be done by holding each end of the tube and gently rubbing the tube against a slightly pointed, elongated, rough metal surface. When you can feel that the glass grips the metal surface, then try to break the tube in two, thus exposing the plasma. Aspire 10 µl plasma from the capillary tube and transfer it directly into the cooled ELISA rack in the predefined well according to the ELISA rack scheme. Mark the scheme if needed (hemolysis, lipidemia). Store on dry ice during the experiment and transfer to a −20°C freezer, until analysis (only for uncoated ELISA racks).

13. Supplement the plasma sample with sample dilution buffer to obtain the required volume for assaying. Assay the plasma insulin samples according to the instructions of the provider of the rat insulin ELISA analysis kit.
14. Plot the blood glucose and the plasma insulin data.
15. Evaluate the data with use of statistical analysis; IGT: Assess the 2-h blood glucose data and compare to controls. If basal levels are not equal, try to subtract the baseline values from the rest of the dataset and compare the δ-2-h blood glucose levels again; Insulin secretion: Assess the 30 min insulin level and compare to control. Calculate the incremental area and compare to control—try different time-intervals (e.g., 0–30 min, 0–120 min), calculate inverse relationship between $AUC_{0-30\ min\ insulin}$ and $AUC_{0-30\ min\ blood\ glucose}$ as a measure of insulin secretion; Insulin sensitivity: Calculate the $AUC_{0-120\ min\ insulin}$ and $AUC_{0-120\ min\ blood\ glucose}$, and calculate the inverse product as an indirect measure. The AUCs are calculated by the trapezoidal method (Note 2).

4. Notes

1. Be aware to use young *db/db* mice no older than 8 weeks of age, if you want to demonstrate a diabetes-preventive effect.
2. It is easier to demonstrate efficacy on hyperglycemia if the blood glucose levels are high as in the *db/db* mouse.
3. When ordering the animals, make sure to get them from a provider close to your own time-zone. Otherwise an acclimatization period of minimum 2 weeks is needed for the blood glucose circadian rhythm to restore.
4. *db/db* mice are sensitive to low temperature (can disturb the development of frank diabetes), the housing room needs to be slightly above room temperature.
5. After the acute experiment in *db/db* mice, the mice can be reused for single dose experiments up to 8 times with a washout period of 1 week (for compounds with a half-life of less than 12 h) or for chronic dosing experiments.

6. Be aware to permanently mark the animals used in the chronic studies. Even though you keep the animals housed in groups, it has been seen that the animals (especially rodents) escape from the cages. If you do not have a clear marking of the individuals you may need to take them out of the experiment with less power of the tests as a consequence.
7. The hand-held glucometers are less precise than validated, calibrated devices (CV of the measurements is app. 20%) and often not validated for use in laboratory animals, but in practice it is a cheap and easy way to assess continuous samples of blood glucose. Some scientific groups use the glucometers for the assessment of glucose during prolonged periods of repetitive glucose assessment, as the clamp procedure. For more precise assessment of blood glucose, validated and calibrated instruments should be used (in parallel). We have experience with the glucose-oxidase method that was used in the EBIO plus auto analyzer (Eppendorf, Germany), but a variety of systems are available. Reference laboratories as well as contract research organisations offer the assessment of blood glucose in validated assays on an ad hoc basis. If the blood glucose samples are to be shipped for later analyses, we recommend that plasma is separated, stored at –20°C and assessed for the level of plasma glucose.
8. We usually measure blood glucose but plasma glucose can also be used. Be aware that the levels of glucose are higher in plasma as compared to whole blood. This difference can vary from species to species. Be aware to be consistent in your own measurements—choose one or always note if you measure blood or plasma glucose.
9. Make sure to allocate the animals into the groups so that the test groups have matching mean levels of the primary endpoint. We usually allocate *db/db* mice and pigs based on their blood glucose levels, the obese rats based on their fasting insulin levels or body weight.
10. Blood volume—be aware of not exceeding limitations!
11. Be aware to train the animals to the dosing procedure and to dose in a standardized and reproducible manner. If s.c. injection is used, note the site of injection, needle size, and length.
12. For the oral dosing of rodents, be aware to ensure the correct placement of the gavage: if the gavage is misplaced in the trachea the expiration can be felt on your cheek if you hold the rat up against it. If you dose the amount of glucose into the lungs, the animal will die.
13. To demonstrate efficacy on insulin secretion use in vivo models that still have insulin secretory capacity as the *ob/ob* mouse.
14. The development of obesity and thus the IGT in the obese rodents is very dependent on free access to food. With group

housing you can experience that one rat dominates the others and prevents them from ad libitum eating. This will result in variability in food intake between the rats. Since the rodents are very social animals and suffer from being individually housed, we have tried to house the obese Zucker rats in cages with 2 rats in each cage, separated by a fenestrated plexi-glass wall. This permits them to see and smell each other, but gives each rat individual access to food. This further allows you to do a detailed registration of individual food intake during an experiment.

15. Fasting of animals prior to the OGTT or other tests should occur in a standardized manner. We have used 18 h overnight fast. Be aware that for the rodents with deficiency in their leptin system, this long fast could be very very stressful. Therefore, we have used fasting of shorter duration for these rodents, but minimum for 6 h.
16. The time of dosing of the test compound prior to the OGTT should be assessed in advance. It could be based on previous pharmacokinetic studies, to ensure that a suitable plasma concentration of the compound is present in the circulation at the beginning of the OGTT. The suitable concentration should be defined and could for instance be the ED_{50} for the anti-analgesic effect of the TRP antagonist.

References

1. International Diabetes Federation (2011) New IDF data reveals diabetes epidemic continues to escalate. http://www.idf.org/new-idf-data-reveals-diabetes-epidemic-continues-escalate?utm_medium=email&utm_campaign=IDF+Quarterly+News+October&utm_content=IDF+Quarterly+News+October+CID_8d91ef357e60aaf9e21f6f2d4e7976ba&utm_source=campaignmonitor&utm_term=more. Accessed 13 Sept 2011
2. Gram DX, Hansen AJ (2006) Inhibition of the activity of the capsaicin receptor in the treatment of obesity or obesity-related diseases and disorders. Patent application, PCT/DK2005/000502
3. Tanaka H, Shimaya A, Kiso T et al (2011) Enhanced insulin secretion and sensitization in diabetic mice on chronic treatment with a transient receptor potential vanilloid 1 antagonist. Life Sci 88:559–563
4. World Health Organization (1999) Definition, diagnosis and classification of diabetes mellitus and its complications. Report of a WHO consultation. Part 1. Diagnosis and classification of diabetes mellitus
5. Reaven GM (1988) Role of insulin resistance in human disease. Diabetes 37:1595–1607
6. Gram DX, Hansen AJ (2007) The role of TRPV1 in impaired glucose tolerance in mice. Oral communication. The European neuropeptide club meeting, Santorini, Greece
7. Valenzano K, Grant E, Wu G et al (2003) N-(4-tertiarybutylphenyl)-4-(3-chloropyridin-2-Yl) tetrahydropyrazine-1(2H)-carbox-amide (BCTC), a novel, orally effective vanilloid receptor 1 antagonist with analgesic properties: I. In vitro characterization and pharmacokinetic properties. J Pharmacol Exp Ther 306:377–386
8. Pomonis J, Harrison J, Mark L et al (2003) N-(4-tertiarybutylphenyl)-4-(3-cholorphyridin-2-Yl) tetrahydropyrazine-1-(2H)-carbox-amide (BCTC), a novel, orally effective vanilloid receptor 1 antagonist with analgesic properties: II. In vivo characterization in rat models of inflammatory and neuropathic pain. J Pharmacol Exp Ther 306:387–393
9. Winzell MS, Ahrén B (2004) The high-fat diet-fed mouse: a model for studying mechanisms and treatment of impaired glucose tolerance and type 2 diabetes. Diabetes 53: S215–S219
10. Hara H, Lin YJ, Zhu X et al (2008) Safe induction of diabetes by high-dose streptozotocin in pigs. Pancreas 36:31–38

11. Ozaki K, Monnai M, Onoma M et al (2008) Effects of mitemcinal (GM-611), an orally active erythromycin-derived prokinetic agent, on delayed gastric emptying and postprandial glucose in a new minipig model of diabetes. J Diabetes Complications 22:339–347
12. Dahech I, Belghith KS, Hamden K et al (2011) Antidiabetic activity of levan polysaccharide in alloxan-induced diabetic rats. Int J Biol Macromol 49:742–746
13. Larsen MO, Rolin B, Sturis J et al (2006) Measurements of insulin responses as predictive markers of pancreatic beta-cell mass in normal and beta-cell-reduced lean and obese Gottingen minipigs in vivo. Am J Physiol Endocrinol Metab 290:E670–E677
14. Buschard K, Thon R (2003) Diabetic animal models, chapter 9. In: Hau J, Van Hoosier GL (eds) Handbook of laboratory animal science, vol 2, Animal models. CRC, Boca Raton, FL
15. Reusch C (2011) Diabetes mellitus in dogs and cats. Kleintierpraxis 56:204–218
16. Verkest KR, Fleeman LM, Morton JM et al (2011) Compensation for obesity-induced insulin resistance in dogs: assessment of the effects of leptin, adiponectin, and glucagon-like peptide-1 using path analysis. Domest Anim Endocrinol 41:24–34
17. Raun K, Von Voss P, Knudsen LB (2007) Liraglutide, a once-daily human glucagon-like peptide-1 analog, minimizes food intake in severely obese minipigs. Obesity 15:1710–1716
18. Litten-Brown JC, Corson AM, Clarke L (2010) Porcine models for the metabolic syndrome, digestive and bone disorders: a general overview. Animal 4:899–920
19. Kreutz RP, Alloosh M, Mansour K et al (2011) Morbid obesity and metabolic syndrome in ossabaw miniature swine are associated with increased platelet reactivity. Diabetes Metab Syndr Obes 4:99–105
20. Wagner JD, Kavanagh K, Ward GM et al (2006) Old world nonhuman primate models of type 2 diabetes mellitus. ILAR J 47:259–271
21. Reed MJ, Meszaros K, Entes LJ et al (2000) A new rat model of type 2 diabetes: the fat-fed, streptozotocin-treated rat. Metab Clin Exp 49:1390–1394
22. Ionut V, Liu H, Mooradian V, Castro AVB et al (2010) Novel canine models of obese prediabetes and mild type 2 diabetes. Am J Physiol Endocrinol Metab 298:E38–E48
23. Koopmans SJ, Dekker R, Ackermans MT et al (2011) Dietary saturated fat/cholesterol, but not unsaturated fat or starch, induces C-reactive protein associated early atherosclerosis and ectopic fat deposition in diabetic pigs. Cardiovasc Diabetol 10:64
24. Koopmans SJ, VanderMeulen J, Wijdenes J et al (2011) The existence of an insulin-stimulated glucose and non-essential but not essential amino acid substrate interaction in diabetic pigs. BMC Biochem 12:25
25. Skovgaard M, Kodra JT, Gram DX et al (2006) Using evolutionary information and ancestral sequences to understand the sequence-function relationship in GLP-1 agonists. J Mol Biol 363:977–988
26. Andersen LB (2005) The acute effect of resiniferatoxin on blood glucose levels in C57BLKS (db/db) mice. Master thesis in veterinary medicine, The royal veterinary and agricultural university, Denmark
27. Gram DX, Hansen AJ, Wilken M et al (2005) Plasma calcitonin gene-related peptide is increased prior to obesity, and sensory nerve desensitization by capsaicin improves oral glucose tolerance in Obese Zucker rats. Eur J Endocrinol 153:963–969
28. Bergman RN (1989) Toward physiological understanding of glucose tolerance. Minimal-model approach. Diabetes 38:1512–1527
29. DeFronzo RA, Tobin JD, Andres R (1979) Glucose clamp technique: a method for quantifying insulin secretion and resistance. Am J Physiol 237:E214–E223

Chapter 21

Using Diet to Induce Metabolic Disease in Rodents

Angela M. Gajda, Michael A. Pellizzon, and Matthew R. Ricci

Abstract

Animal models of disease are important tools that allow us to model human conditions and test therapies. Metabolic disease, also called the Metabolic Syndrome (MS), is characterized by obesity, insulin resistance (IR), dyslipidemia and hypertension, the simultaneous occurrence of which increases the risk for developing coronary artery disease, type II diabetes and stroke. While genetic (spontaneous) animal models exist, many researchers prefer diet-induced models of the MS, since it is generally thought that the environment (and particularly the diet) plays a large role in the growing incidence of this disease in humans. This chapter will briefly outline some of the diet-induced approaches for animal models of the MS.

Key words: Rodent diets, Metabolic syndrome, High-fat diets, High-fructose diets, High-sodium diets, MCD diets

1. High-Fat Diets for Diet-Induced Obesity Models

Rats and mice are commonly used as models of human obesity as they will readily gain weight and develop other MS perturbations in response to high-fat feeding. Numerous high-fat diets have been reported in the literature to promote diet-induced obesity (DIO) in rodents, but not all share the same formula; it is important to describe the diet being used so that others can interpret or replicate the findings.

In the past, typically a high-fat diet (HFD) was formulated by adding fat to grain-based chow, and commonly these diets also contained other components such as cholesterol and cholic acid to create high-fat "Western diets" to induce obesity and atherosclerosis in rodents (1–3). These diets were among the first to be used for obesity research studies since the chow was readily available from

Arpad Szallasi and Tamás Bíró (eds.), *TRP Channels in Drug Discovery: Volume II*, Methods in Pharmacology and Toxicology, DOI 10.1007/978-1-62703-095-3_21,

most animal facilities and it could be made relatively easily in the laboratory. However, such diets can lead to nutritional inadequacies since the added fat will dilute other nutrients (protein, vitamins, minerals and fiber), potentially rendering the final diet nutrient deficient. In addition, chows contain non-nutrients such as phytoestrogens which can vary from lot to lot or chow to chow (4) and can reduce adiposity and improve insulin sensitivity in mice relative to diets with low phytoestrogens (5, 6). As such, it is difficult to determine whether these dietary factors can induce changes to the MS phenotype independent of the level of fat.

In recent years, diets which contain purified ingredients have been more commonly used for designing HFDs. These diets are made from highly refined ingredients which typically contain one main nutrient (i.e. corn starch is 100% carbohydrate) allowing for simple modifications to macronutrient contents while at the same time remaining nutritionally balanced. For example, calories from corn starch can be replaced with the same number of calories from a fat source without any changes to other nutrients in the diet. In addition, the ingredients have a greater consistency between batches relative to those from grain-based chows, thus providing for better reproducibility between studies.

When choosing a HFD, the level of fat in the diet should be taken into consideration. Most low-fat chow and purified diets that support normal growth contain 10–15% of the calories from fat while high-fat diets commonly used for DIO typically contain 32–60% of calories from fat. Investigators will change the level of dietary fat depending upon the study objective. For example, one study may require an animal diet with fat content similar to that of a human diet. Americans typically consume about 33% of calories from fats (7), so in this case, choosing an animal diet which is moderately high in fat (i.e., 32% fat) would be important to help meet the study objectives. Also, one must consider that it may be more difficult to reverse the drive to obesity on a very high-fat diet (i.e., 60% fat), whereas something like compound efficacy may be more detectable when used in conjunction with a moderately high-fat diet.

However, there are also advantages to using higher fat (50–60 kcal%) diets. Typically, there is a dose–response for body weight as a function of dietary fat (8). Thus animals fed a higher fat diet tend to gain more weight in a shorter period of time which can save time and costs to the investigators. Hence the popularity of using diets containing 60% of calories from fat has grown as a standard method of promoting DIO in rodent models.

The type of fat is also an important consideration. As one scientist has said, “Oils ain’t oils” (9), meaning all fats are not equal in terms of inducing disease. For example, when rodents were fed purified ingredient diets with similar amounts of fat, those fed diets with fish oil, which contain a high concentration of

polyunsaturated fatty acids as omega-3 fatty acids, did not gain as much weight and were more insulin sensitive compared to those fed saturated fatty acids (SF) (10–12). However, not all studies support this and it may depend on dietary fat level and gender (12, 13). In addition, the chain length can also play a role in the phenotype. Traditionally, fat sources used in high-fat rodent diets for DIO contain more SF and as such are more solid at room temperature. The use of hydrogenated coconut oil in a HFD is common because it forms a solid which allows for producing high-fat pelleted diets. This particular fat source contains a very high percentage of SF (~99%), with 66% being medium chain fatty acids. Lard, on the other hand, has been more commonly used in high-fat diets and contains longer chain fatty acids such as palmitate and stearate. Though lard contains more than 30% SF, it has been shown to promote greater adiposity in mice than coconut oil (10, 14).

Most rodents tend to become obese on a HFD, but there can be variable responses in glucose tolerance, IR, triglycerides (TG) and other parameters depending on the strain, gender (1, 15) and type of dietary fat (10–12). Outbred Sprague–Dawley and Wistar rats have a variable response to a high-fat diet (32 or 45 kcal% fat) such that some animals rapidly gain excess weight (i.e. beyond those fed a low-fat diet) while others gain only as much weight as those on a low-fat diet (16). Researchers commonly separate these groups into DIO and diet-resistant (DR) groups (16–18). Therefore, the use of this model allows for a means to study human obesity development and related phenotypes (i.e., IR, glucose intolerance). Furthermore, DIO and DR rats have been selectively bred over time, allowing the researcher to look early in life (prior to the onset of obesity) for genetic traits that may later predispose them to their DIO or DR phenotypes (1, 19).

Several wild-type mouse models are generally available and each may have a different tendency to gain weight on a HFD (~60% by energy) (3). Some inbred strains such as C57BL/6 or AKR mice are quite susceptible to obesity on HFDs (15), while mice of the A/J and SWR/J strains tend to be resistant to DIO (20, 21). However, even strains that may exhibit similar levels of obesity may have varied metabolic responses. For example, when fed a 60 kcal% fat (mostly coconut oil), C57BL/6 mice are more glucose intolerant, compared to obese AKR mice which are more insulin resistant (15).

While mice and rats may become obese and insulin resistant on a HFD, it is difficult to promote a diabetic state as beta cells of the pancreas are capable of increasing production and secretion of insulin. Streptozotocin (STZ) has been administered to rats and mice to produce necrosis in the pancreatic β-cells resulting in ablation of insulin production (22), and recent work has shown that low-dose STZ (i.p. at 90–100 mg/kg) administration in combination

with high-fat feeding (60 kcal% fat) can promote increases in blood glucose in ICR mice relative to similarly treated low-fat fed or high-fat fed animals without STZ (23, 24). Similar studies have also been conducted with C57BL/6 mice (25). Diabetic obese rats have also been developed using similar techniques (26–28). Hence, these models may be useful to promote development of diabetes simultaneously with obesity.

2. Diet-Induced Atherosclerosis/ Hypercholesterolemia in Rodent Models

Atherosclerosis is a complex chronic disease characterized by the accumulation of lipids within arterial walls, which can cause narrowing, hardening and/or complete blockage of arteries. Hypercholesterolemia (i.e., elevated total cholesterol (TC) and low-density lipoprotein cholesterol (LDL-C)) is a well-known risk factor (29), and other important contributors include inflammation, oxidative stress, and IR (30, 31). Foods high in dietary SF and cholesterol (i.e., "Western-type diets") have been associated with increased LDL-C in humans (32), and similar responses have been found in certain animal models used in research. Therefore, in order to better understand the etiology of atherosclerosis and available therapies to reduce it, Western-type diets containing high levels of SF and cholesterol are commonly used to "push" the atherosclerosis risk factors in certain rodent models such as mice, hamsters and guinea pigs. However, certain dietary manipulations are required depending on the rodent model.

2.1. Mice

Normal mice and rats are not ideal models of cardiovascular disease research since they typically have very low levels of LDL-C and high levels of high-density lipoprotein cholesterol (high HDL-C) when fed a low-fat/low-cholesterol diet. This is in contrast to humans where the reverse is true. While diets containing high levels of cholesterol and SF (~0.5% cholesterol, ~40 kcal% fat as hydrogenated coconut oil) can increase TC, both HDL-C and non-HDL-C (LDL) (33–35) contribute to this increase, limiting atherosclerosis development (36). In order to induce mild atherosclerosis, addition of cholic acid to the diet, a bile acid (0.1–1%) is required (37–41) as this increases LDL-C by both facilitating fat and cholesterol absorption and reducing conversion of cholesterol to bile acids (42, 43). While cholic acid allows for some atherosclerosis development, it may have an independent effect, given that it can influence genes that regulate lipoprotein metabolism and inflammation as well as reduce plasma TG and HDL-C (36, 37, 42).

The ability to change the genetic make-up of mice and produce "transgenic" or "knockout" mice has allowed for the development of many interesting and useful disease models. Genetically modified mice such as those with mutations that slow the removal of cholesterol from the blood have led to more "human-like" models which can show significant elevations in circulating LDL-C and atherosclerotic lesions. Some of these knockout mouse models (such as the LDL receptor knockout [LDLr KO] and the Apolipoprotein E knockout [apoE KO]) can be very responsive after 12 weeks on a high cholesterol diet (0.15–1.25% cholesterol) (44–46). Lesion development is very dramatic in apoE KO mice fed a Western-type diet and beginning stages of atherosclerosis (i.e. fatty streak lesions) can be found at 6 weeks (47). Even plaque rupture has been reported in these mice fed a high-fat, lard-based diet with cholesterol (0.15%) after only 8 weeks (48). With these mouse models, the main influence on atherosclerosis is dietary cholesterol rather than the level of fat (49–51), but certain threshold levels of dietary cholesterol may exist, at least within the context of a low-fat purified diet (52). Very high fat diets (i.e., 60 kcal% fat) are capable of inducing some atherosclerosis (53, 54), and the fatty acid profile and carbohydrate type (i.e. fructose, sucrose) can be manipulated to modify the atherosclerosis phenotype to the researcher's advantage (46, 49, 55).

2.2. Hamsters

A well-known model in atherosclerosis research is the Golden Syrian Hamster. Like mice and rats, hamsters typically have a high percentage of HDL-C when fed a low-fat/low-cholesterol diet. In contrast to other rodent models, hamsters can also show significant elevations in LDL-C when challenged with dietary cholesterol (~0.1–0.5%) (but without cholic acid), and like humans, SF sources (butter fat, 15–20% fat w/w) can increase these levels further (56, 57). With such diets, the beginning stages of atherosclerosis (i.e. fatty streaks, foam cells) can be found in as little as 6 weeks (58, 59). In fact, a diet containing a source of SF (hydrogenated coconut oil) but without cholesterol can promote more aortic cholesterol accumulation compared to a diet with both cocoa butter and 0.15% cholesterol (57). Mechanisms related to cholesterol processing by the liver allow for the hamster's increased susceptibility compared to mice and rats (43, 60, 61). Additionally, it is important to consider the protein source when studying lipoprotein metabolism and atherosclerosis in this model as hamsters fed casein and lactalbumin had higher levels of LDL-C and atherosclerosis than those fed an equal amount of soy protein, and like humans, males may be more susceptible than females (62).

2.3. Guinea Pigs

Unlike other wild-type rodents, guinea pigs have a cholesterol profile similar to humans with most circulating cholesterol trans-

ported in LDL when maintained on a low-fat/low-cholesterol diet and exhibit many features of lipoprotein metabolism that are found in humans (63). Like hamsters, they can elevate TC and LDL-C levels when fed a diet high in SF (i.e., palm kernel oil, ~80% SF) and a diet with added cholesterol (at least up to 0.3%, w/w) can cause further elevations in LDL-C and induce atherosclerotic lesions (i.e., fatty streaks) after 12 weeks (64–66). The increased sensitivity of LDL-C with dietary manipulation with minimal change to HDL-C increases the value of the guinea pig for studies examining the influence of drug therapies on lowering LDL-C (67, 68). While increasing dietary cholesterol is very important to atherosclerosis development, one study found that high cholesterol diets (0.25%), which are high in carbohydrate and moderately high in fat, are more capable of promoting atherosclerosis than those low in carbohydrate but very high in fat. This was thought to be due to an increased number of small LDL particles, which are considered more atherogenic in humans (69). Furthermore, the type of protein (i.e. high casein-to-soy protein ratio) (70) or carbohydrate (i.e. high sucrose) (71) can exacerbate the condition.

3. Effect of High Fructose/Sucrose Diets on Plasma Lipid Levels and IR in Rodents

Refined carbohydrate sources such as high-fructose corn syrup (HFCS) are used in many processed foods and surveys in the US have suggested that the intake of this sweetener has increased dramatically since the 1970s (72) . As we have learned over the past few decades, an excess intake of refined carbohydrates is associated with increased weight gain, hypertriglyceridemia (hyper-TG), and IR in humans and animal models (73, 74). In order to understand more about the impact of refined carbohydrates on health and therapies to reduce these MS phenotypes, certain rodent models have been useful. Purified diets containing around 60–70% (by energy) fructose or sucrose (which is a 50:50 molar mixture of fructose and glucose) are capable of elevating TG and glucose production in the liver, ultimately leading to IR and hyper-TG relative to diets containing mainly glucose carbohydrate sources (i.e. dextrose, corn starch) (73, 74). Typically, rodent chow diets contain only 4% sucrose and <0.5% free fructose with most carbohydrates as both digestible starch and non-digestible fiber from grain sources (i.e. wheat, corn, soy). In contrast, low-fat purified diets can contain higher levels of sucrose and this will depend heavily on the formula being used. If desired, it is easy to modify purified diets by manipulating the carbohydrate sources to promote MS while maintaining essential nutrients at the recommended levels. However, each rodent model responds differently to high levels of sucrose and fructose.

Sprague–Dawley and Wistar rats are both established models of sucrose-induced IR and hyper-TG (75, 76). Both of these phenotypes can develop as quickly as 2 weeks when these animals are fed a diet containing 68% sucrose (by energy) relative to one with the same level of carbohydrate as corn starch (75). It appears that the fructose component of sucrose is largely responsible for the hyper-TG and IR produced by high sucrose diets (77–79). While a very high concentration of sucrose or fructose induces this phenotype quickly in male rats, a lower level of sucrose (17% of energy) can also induce IR when fed to rats for 30 weeks relative to a diet containing mainly corn starch (80). Furthermore, gender is important in the development of sucrose-induced IR and hyper-TG in rats as females (unlike males) are typically not responsive to elevations in dietary sucrose (81). Other than IR and hyper-TG, high sucrose or fructose diets can promote marginal weight gain in rats, but this typically requires a prolonged period of time and a significantly greater energy intake (82).

Similar to rats, hamsters fed high-fructose diets (~60% of energy) may develop IR and elevations in circulating TG levels after only 2 weeks compared to those fed low-fructose diets (83, 84). However, unlike rats, hamsters fed high-sucrose diets (60% by energy) may not elevate TG and develop only mild IR (83). Since sucrose is half fructose, it appears that the level of dietary fructose is quite important in the rapid development of IR and hyper-TG in hamsters. Other factors, including the addition of cholesterol (0.25%), may also allow the researcher to induce a combination of hypercholesterolemia, greater IR, and hyper-TG in this model compared to fructose alone (85), further improving the fructose-fed hamster as a model of dyslipidemia.

In contrast to rats and hamsters, the mouse is used less frequently as a model for sucrose/fructose-induced IR and hyper-TG as the commonly used C57BL/6 mouse either does not develop IR or develops the phenotype more slowly (86, 87). Despite not developing IR, glucose tolerance can be reduced in C57BL/6 mice fed a high sucrose diet (50% sucrose) relative to those fed a similar diet high in corn starch from 10 to 55 weeks, and this has been attributed as a reduced pancreatic insulin secretion (87). However, the mouse genome is much easier to manipulate than that of the rat allowing for several knockout models, including the LDLr KO mouse, which show responses to high dietary fructose (49).

4. Nonalcoholic Fatty Liver Disease

Nonalcoholic fatty liver disease (NAFLD) encompasses a spectrum of disease states, from steatosis (fatty liver) to non-alcoholic

steatohepatitis (also called NASH; steatosis with inflammatory changes) followed by progression to fibrosis, cirrhosis, and hepatocellular carcinoma (88). Excess liver fat is believed to be a manifestation of the MS (89) and not surprisingly NASH is associated with obesity, IR, dyslipidemia and type II diabetes in humans (90). Most obese adults have hepatic steatosis and at least one-third of these individuals will eventually develop worsening NAFLD (91, 92). Therefore, the prevalence of NAFLD will likely rise with obesity rates.

Diet-inducible animal models of NAFLD exist and include feeding a methionine- and choline-deficient (MCD) diet, a choline-deficient diet (CD) or a HFD. There is of course overlap in these diet types. These different dietary approaches produce different severities of the disease and likely work by different mechanisms.

4.1. MCD Diets

Of the dietary approaches discussed here, MCD diets produce the most severe phenotype in the shortest timeframe. Used for over 40 years, MCD diets will quickly induce measurable hepatic steatosis (mainly macrovesicular) in rodents by 2–4 weeks and this progresses to inflammation and fibrosis shortly thereafter (93, 94). Fat levels in MCD diets can vary, though typically they contain about 20% fat by energy. The mechanism for steatosis includes impaired VLDL secretion due to lack of phosphatidyl choline synthesis (95). MCD diet-induced NASH is reversible in rats by switching to a diet with sufficient methionine and choline (96).

Importantly, unlike human or other diet-induced rodent models of NAFLD, rodents fed with MCD diets lose weight (due to a vastly lower caloric intake) and do not become insulin resistant (97, 98). Since most humans with NASH are obese and insulin resistant, this represents an important difference in how MCD diets model human NASH.

Within the context of an MCD diet, other dietary components affect the NASH phenotype. Sucrose is an important component of the MCD diet, since replacing it with corn starch greatly reduces liver fat accumulation, inflammation and injury, likely through reductions in sucrose-induced de novo lipogenesis and triglyceride synthesis (99). In a follow-up study, Pickens et al. showed that despite inducing the same overall level of hepatic fat accumulation, fructose was more effective than glucose at inducing hepatocellular injury in mice fed with MCD diets for 21 days (100). Not surprisingly, the source of dietary fat can also alter the phenotype. For example, relative to SF, polyunsaturated fats increase liver fat oxidation and induce expression of proinflammatory genes leading to inflammation though this does not necessarily correlate with increased liver damage (101). Also, relative to butter fat, olive oil reduced liver triglyceride accumulation while fish oil reduced liver cholesterol levels (102).

4.2. CD Diets

Like MCD diets, CD diets also tend to contain higher levels of fat, though it is often difficult to know the specifics since unfortunately authors rarely publish the details of the diet formulas. CD diets induce steatosis, inflammation and fibrosis over 10 weeks without any difference in body weight compared to the control group (103). This lack of weight loss makes CD diets more appealing to some researchers. When both CD and MCD diets were fed to rats for 7 weeks, the MCD diet group had higher scores of liver inflammation and steatosis than the CD group. However, the CD fed rats gained weight, were insulin resistant and had higher plasma lipids than the MCD group (104).

The mechanisms involved with liver fat accumulation may be different from those at work during MCD diet feeding (95). Interestingly, choline deficiency in the context of a lard-based HFD (45% of calories) was shown to improve glucose tolerance compared to the choline sufficient group in mice (105).

4.3. High-Fat Diets

As discussed earlier, HFDs are well-known to increase body weight, body fat and induce IR in rodent models. HFD can also increase liver fat levels quite rapidly (within days) as well as hepatic IR before significant increases in peripheral fat deposition occur (106). Chronically, HFD-induced liver fat accumulation may not follow a linear progression and liver fat levels may actually decrease, then increase again during prolonged HFD feeding (107). When fed for equal lengths of time, HFD feeding results in tenfold lower liver fat levels compared to what accumulates on an MCD diet (108). In general, HFD feeding does not produce liver fibrosis and only mild steatosis as compared to MCD diets (90), thus highlighting an important difference between these dietary regimes. It is important to remember that the term "HFD" encompasses a wide variety of diet formulas and diets of different composition can be expected to alter the liver phenotype in various ways.

Cong et al. (109) took an interesting approach by modifying a very HFD (60% of calories) to simultaneously contain low levels (but not zero) of methionine and choline. C57BL/6 mice were fed the diet for 23 weeks and developed obesity, IR, dyslipidemia as well as liver steatosis, inflammation and fibrosis. While the study design is weakened by the lack of a high-fat, choline and methionine replete control group, it seems plausible that longer term feeding of HFDs containing lower than normal levels of methionine and choline allow for the development of NASH without the issues of weight loss.

The idea of modifying so-called "standard" HFDs is powerful since it allows the researcher to "fine-tune" the phenotype to meet their needs. Along these lines, in the LDLr KO mouse, adding cholesterol to a HFD increases liver fat levels, signs of liver damage and produces macro- and microvesicular steatosis similar to that seen in human NASH, compared to HFD alone (110). Vitamin D

deficiency within a HFD worsened NAFLD versus HFD with adequate vitamin D in Sprague–Dawley rats (111). When medium chain triglycerides replaced long chain triglycerides in a 35 kcal% fat diet, steatosis was prevented in rats (112). In C57BL/6 mice, animals consuming both HFD and fructose/sucrose enriched drinking water developed hepatic fibrosis while a group consuming HFD alone did not (113).

As with other diet-induced diseases, it appears possible to influence liver disease using a HFD while mice are still in utero. Bruce et al. found that feeding a HFD to dams during gestation and lactation made offspring more susceptible to developing NASH when fed a HFD from weaning (114).

5. Diets High in Sodium (and Fructose) For Hypertension

While researchers use both rats and mice to study diet-induced hypertension, there are more published papers using rats, perhaps because of their larger size, the amount of physiological data available, and robust blood pressure response that some strains present.

The main dietary contributor to diet-induced hypertension is the level of NaCl. Purified ingredient diets generally contain about 0.1% Na, while chow diets contain about 0.3–0.4% Na. The Dahl salt-sensitive (SS) rat shows a significant rise in blood pressure within 2–4 weeks after being fed a purified diet containing 8% NaCl (115, 116), though lower levels of NaCl (4%) will still raise blood pressure (117) albeit more slowly (118). This rise in blood pressure can be attenuated by the addition of extra vitamin E to the diet (119) or by supplementing the diet with extra potassium (116).

The effect of the background diet on NaCl-induced hypertension was demonstrated by the work of Mattson et al. When 4% NaCl was added to both a grain-based chow diet and a purified ingredient diet, Dahl SS rats fed with the purified diet had higher blood pressure and more renal damage compared to chow-fed rats (120). Given the many differences between grain-based and purified ingredient diets, it is difficult to know exactly which component(s) were responsible for the difference. For example, there is evidence that the source of protein (121), carbohydrate (122), fat (123), fiber (124) and/or the level of minerals such as potassium may be responsible (116), all of which can greatly differ between grain-based and purified ingredient diets.

Mattson et al. also found that that offspring from parents who were fed a 4% NaCl purified diet had higher blood pressures regardless of the diet they were fed after weaning, suggesting that the diet fed to the mother during pregnancy can promote or "program" hypertension in the offspring (120).

Aside from salt-sensitive rats, outbred rat strains such as the Sprague–Dawley (which are in widespread use for obesity research) can develop hypertension. When fed an 8% NaCl diet, hypertension develops but this usually occurs over a longer time period and to a lesser magnitude compared to Dahl SS rats (125). Sprague–Dawley rats can also develop hypertension as they become obese on a HFD (126). Diets high in fructose (around 60% of calories) but with normal levels of NaCl (0.1%) can induce metabolic abnormalities, including increased blood pressure (127, 128) and kidney damage in both Sprague–Dawley and Wistar rats (127–129). The IR induced by such high fructose diets (129) is believed to play a causal role in the development of hypertension (130).

Even in a spontaneous rat model of hypertension (such as the spontaneously hypertensive rat (SHR) which will develop hypertension on a variety of diets), diet can be used to modify the onset or degree of this disease. For example, dietary supplementation with antioxidants (such as vitamins E and C) can lower blood pressure in stroke-prone SHR (131), as can dietary calcium supplementation (132). As mentioned earlier, the mouse is not as widely used for the study of diet-induced hypertension. Inbred mice such as the C57BL/6 can develop elevated blood pressure on purified diets high in NaCl (8%), though the time frame for this appears to be on the order of several months (133).

6. Summary

It is clear from the examples given in this chapter that diet is a strong influence on phenotype and that diet-induced rodent models are valuable tools for researchers to study the causes of and therapies for metabolic disease. It is important for researchers to remember that controlling the diet is key to controlling phenotype. While diets made from purified ingredients allow for finer control over diet formulation while also limiting batch-to-batch variability, grain-based diets are less easily manipulated and more prone to change over time, as well as contain non-nutritive components that can affect phenotype. Therefore, choice of diet (in any experimental situation) should be made carefully so as to give both the highest probability of inducing the desired phenotype while limiting variability.

References

1. Levin B, Dunn-Meynell A, Balkan B, Keesey RE (1997) Selective breeding diet-induced obesity obesity Selective breeding for for diet-induced and resistance in Sprague-Dawley rats and resistance in rats. Am J Physiol 273(2):R725–R730
2. Paigen B, Mitchell D, Reue K, Morrow A, Lusis AJ, LeBoeuf RC (1987) Ath-1, a gene determining atherosclerosis susceptibility and high density lipoprotein levels in mice. Proc Natl Acad Sci USA 84(11): 3763

3. West DB, Boozer CN, Moody DL, Atkinson RL, Sakaguchi M, Koya D, Haneda M, Kashiwagi A, Uzu T, Rossmeisl M, Jilkova Z, Stefl B, Pastalkova E, Drahota Z, Houstek J, Physiol AJ, Metab E, Joost H, Churchill GA, Peters LL, Physiol JA, B D, West B, N C, Boozer N, L D, Moody L, L R, Atkinson L, L D (2012) Dietary obesity in nine inbred mouse strains dietary strains. Am J Physiol Regul Integr Comp Physiol 262(6): R1025–R1032
4. Jensen MN, Ritskes-Hoitinga M (2007) How isoflavone levels in common rodent diets can interfere with the value of animal models and with experimental results. Lab Animal 41(1): 1–18.
5. Cederroth CR, Vinciguerra M, Gjinovci A, Klein M, Suter M, Neumann D, James RW, Cederroth M, Doerge DR, Wallimann T, Meda P, Foti M (2008) Dietary phytoestrogens activate AMP-activated protein kinase with improvement in lipid and glucose metabolism. Diabetes 57(5):1176–1185
6. Cederroth CR, Vinciguerra M, Kühne F, Madani R, Doerge DR, Visser TJ, Foti M, Rohner-Jeanrenaud F, Vassalli JD, Nef S (2007) A phytoestrogen-rich diet increases energy expenditure and decreases adiposity in mice. Environ Health Perspect 115(10): 1467–1473
7. Bialostosky K (2002) Dietary intake of micronutrients, and other dietary constituents: United States, 1988–1994. Vital Health Stat 11 (245):1–158
8. Ghibaudi L, Cook J, Farley C, Heek MV, Hwa JJ, Heek MVAN, J J (2002) Fat intake affects adiposity, comorbidity factors, and energy metabolism of Sprague-Dawley rats. Obes Res 10(9):956–963
9. Storlien LH, Higgins J, Thomas T, Brown M, Wang H, Huang X, Else P (2000) Diet composition and insulin action in animal models. Br J Nutr 83(1):85
10. Buettner R, Parhofer K, Woenckhaus M, Wrede C, Kunz-Schughart L, Schölmerich J, Bollheimer L (2006) Defining high-fat-diet rat models: metabolic and molecular effects of different fat types. J Mol Endocrinol 36(3):485
11. Wang H, Storlien LH, Huang XF (2002) Effects of dietary fat types on body fatness, leptin, and ARC leptin receptor, NPY, and AgRP mRNA expression. Am J Physiol Endocrinol Metab 282(6):E1352
12. Ikemoto S, Takahashi M, Tsunoda N, Maruyama K, Itakura H, Ezaki O (1996) High-fat diet-induced hyperglycemia and obesity in mice: differential effects of dietary oils. Metabolism 45(12):1539–1546
13. Pellizzon M, Buison A, Ordiz F, Santa Ana L, Jen K-LC (2002) Effects of dietary fatty acids and exercise on body-weight regulation and metabolism in rats. Obes Res 10(9):947–955
14. Dulloo AG, Mensi N, Seydoux J, Girardier L (1995) Differential effects of high-fat diets varying in fatty acid composition on the efficiency of lean and fat tissue deposition during weight recovery after low food intake 1. Metabolism 44(2):273–279
15. Rossmeisl M, Rim JS, Koza RA, Kozak LP (2003) Variation in type 2 diabetes-related traits in mouse strains susceptible to diet-induced obesity. Diabetes 52(8):1958
16. Farley C, Cook JA, Spar BD, Austin TM, Kowalski TJ (2003) Meal pattern analysis of diet-induced obesity in susceptible and resistant rats. Obesity 11(7):845–851
17. Chang SAM, Lin D, Peters JC (1990) Metabolic differences between obesity-prone and obesity-resistant rats. Am J Physiol 259(6):R1103–R1110
18. Levin BE, Dunn-Meynell AA (2006) Differential effects of exercise on body weight gain and adiposity in obesity-prone and -resistant rats. Int J Obes 30(4):722–727
19. Ricci MR, Levin BE (2003) Ontogeny of diet-induced obesity in selectively bred Sprague-Dawley rats. Am J Physiol Regul Integr Comp Physiol 285(3):R610
20. Surwit R, Feinglos M, Rodin J, Sutherland A, Petro A, Opara E, Kuhn C, Rebuffe-Scrive M (1995) Differential effects of fat and sucrose on the development of obesity and diabetes in C57BL/6J and A/J mice 1. Metabolism 44(5):645–651
21. Prpic V, Watson PM, Frampton IC, Sabol MA, Jezek GE, Gettys TW (2003) Differential mechanisms and development of leptin resistance in A/J versus C57BL/6J mice during diet-induced obesity. Endocrinology 144(4):1155
22. Junod A, Lambert AE, Stauffacher W, Renold AE (1969) Diabetogenic action of streptozotocin: relationship of dose to metabolic response. J Clin Invest 48(11):2129–2139
23. Mu J, Woods J, Zhou YP, Roy RS, Li Z, Zycband E, Feng Y, Zhu L, Li C, Howard AD et al (2006) Chronic inhibition of dipeptidyl peptidase-4 with a sitagliptin analog preserves pancreatic \β-cell mass and function in a rodent model of type 2 diabetes. Diabetes 55(6):1695–1704
24. Mu J, Petrov A, Eiermann GJ, Woods J, Zhou YP, Li Z, Zycband E, Feng Y, Zhu L, Roy RS (2009) Inhibition of DPP-4 with sitagliptin improves glycemic control and restores islet cell mass and function in a rodent model of

type 2 diabetes. Eur J Pharmacol 623(1–3):148–154

25. Kusakabe T, Tanioka H, Ebihara K, Hirata M, Miyamoto L, Miyanaga F, Hige H, Aotani D, Fujisawa T, Masuzaki H et al (2009) Beneficial effects of leptin on glycaemic and lipid control in a mouse model of type 2 diabetes with increased adiposity induced by streptozotocin and a high-fat diet. Diabetologia 52(4):675–683
26. Samuel VT, Beddow SA, Iwasaki T, Zhang XM, Chu X, Still CD, Gerhard GS, Shulman GI (2009) Fasting hyperglycemia is not associated with increased expression of PEPCK or G6Pc in patients with type 2 Diabetes. Proc Natl Acad Sci USA 106(29):12121–12126
27. Srinivasan K, Viswanad B, Asrat L, Kaul C, Ramarao P (2005) Combination of high-fat diet-fed and low-dose streptozotocin-treated rat: a model for type 2 diabetes and pharmacological screening. Pharmacol Res 52(4): 313–320
28. Thackeray JT, Radziuk J, Harper M-E, Suuronen EJ, Ascah KJ, Beanlands RS, Dasilva JN (2011) Sympathetic nervous dysregulation in the absence of systolic left ventricular dysfunction in a rat model of insulin resistance with hyperglycemia. Cardiovasc Diabetol 10:75
29. Pearson TA, Blair SN, Daniels SR, Eckel RH, Fair JM, Fortmann SP, Franklin BA, Goldstein LB, Greenland P, Grundy SM, Hong Y, Miller NH, Lauer RM, Ockene IS, Sacco RL, Sallis JF, Smith SC, Stone NJ, Taubert KA (2002) AHA Guidelines for Primary Prevention of Cardiovascular Disease and Stroke: 2002 Update: Consensus Panel Guide to Comprehensive Risk Reduction for Adult Patients Without Coronary or Other Atherosclerotic Vascular Diseases. American Heart Association Science Advisory and Coordinating Committee. Circulation 106(3):388–391
30. Libby P, Ridker PM, Maseri A (2002) Inflammation and atherosclerosis. Circulation 105(9):1135–1143
31. Van Gaal LF, Mertens IL, De Block CE (2006) Mechanisms linking obesity with cardiovascular disease. Nature 444(7121): 875–880
32. Hegsted DM, McGandy RB, Myers ML, Stare FJ (1965) Quantitative effects of dietary fat on serum cholesterol in man. Am J Clin Nutr 17(5):281–295
33. Srivastava RA (1994) Saturated fatty acid, but not cholesterol, regulates apolipoprotein AI gene expression by posttranscriptional mechanism. Biochem Mol Biol Int 34(2):393–402
34. Srivastava RA, Jiao S, Tang JJ, Pfleger BA, Kitchens RT, Schonfeld G (1991) In vivo regulation of low-density lipoprotein receptor and apolipoprotein B gene expressions by dietary fat and cholesterol in inbred strains of mice. Biochim Biophys Acta 1086(1):29–43
35. Srivastava RA, Tang J, Krul ES, Pfleger B, Kitchens RT, Schonfeld G (1992) Dietary fatty acids and dietary cholesterol differ in their effect on the in vivo regulation of apolipoprotein A-I and A-II gene expression in inbred strains of mice. Biochim Biophys Acta 1125(3):251–261
36. Getz GS, Reardon CA (2006) Diet and murine atherosclerosis. Arterioscler Thromb Vasc Biol 26(2):242–249
37. Nishina PM, Verstuyft J, Paigen B (1990) Synthetic low and high fat diets for the study of atherosclerosis in the mouse. J Lipid Res 31(5):859–869
38. Nishina PM, Lowe S, Verstuyft J, Naggert JK, Kuypers FA, Paigen B (1993) Effects of dietary fats from animal and plant sources on diet-induced fatty streak lesions in C57BL/6J mice. J Lipid Res 34(8):1413–1422
39. Jeong W-I, Jeong D-H, Do S-H, Kim Y-K, Park H-Y, Kwon O-D, Kim T-H, Jeong K-S (2005) Mild hepatic fibrosis in cholesterol and sodium cholate diet-fed rats. J Vet Med Sci 67(3):235–242
40. Yokozawa T, Cho EJ, Sasaki S, Satoh A, Okamoto T, Sei Y (2006) The protective role of Chinese prescription Kangen-karyu extract on diet-induced hypercholesterolemia in rats. Biol Pharm Bull 29(4):760–765
41. Zulet MA, Barber A, Garcin H, Higueret P, Martínez JA (1999) Alterations in carbohydrate and lipid metabolism induced by a diet rich in coconut oil and cholesterol in a rat model. J Am Coll Nutr 18(1):36–42
42. Ando H, Tsuruoka S, Yamamoto H, Takamura T, Kaneko S, Fujimura A (2005) Regulation of cholesterol 7alpha-hydroxylase mRNA expression in C57BL/6 mice fed an atherogenic diet. Atherosclerosis 178(2): 265–269
43. Horton JD, Cuthbert JA, Spady DK (1995) Regulation of hepatic 7 alpha-hydroxylase expression and response to dietary cholesterol in the rat and hamster. J Biol Chem 270(10): 5381–5387
44. Lichtman AH, Clinton SK, Iiyama K, Connelly PW, Libby P, Cybulsky MI (1999) Hyperlipidemia and atherosclerotic lesion development in LDL receptor-deficient mice fed defined semipurified diets with and without cholate. Arterioscler Thromb Vasc Biol 19(8):1938–1944

45. Joseph SB, McKilligin E, Pei L, Watson MA, Collins AR, Laffitte BA, Chen M, Noh G, Goodman J, Hagger GN, Tran J, Tippin TK, Wang X, Lusis AJ, Hsueh WA, Law RE, Collins JL, Willson TM, Tontonoz P (2002) Synthetic LXR ligand inhibits the development of atherosclerosis in mice. Proc Natl Acad Sci USA 99(11):7604–7609
46. Collins AR, Meehan WP, Kintscher U, Jackson S, Wakino S, Noh G, Palinski W, Hsueh WA, Law RE (2001) Troglitazone inhibits formation of early atherosclerotic lesions in diabetic and nondiabetic low density lipoprotein receptor-deficient mice. Arterioscler Thromb Vasc Biol 21(3):365–371
47. Nakashima Y, Plump AS, Raines EW, Breslow JL, Ross R (1994) ApoE-deficient mice develop lesions of all phases of atherosclerosis throughout the arterial tree. Arterioscler Thromb 14(1):133–140
48. Johnson JL, George SJ, Newby AC, Jackson CL (2005) Divergent effects of matrix metalloproteinases 3, 7, 9, and 12 on atherosclerotic plaque stability in mouse brachiocephalic arteries. Proc Natl Acad Sci USA 102(43):15575–15580
49. Merat S, Casanada F, Sutphin M, Palinski W, Reaven PD (1999) Western-type diets induce insulin resistance and hyperinsulinemia in LDL receptor-deficient mice but do not increase aortic atherosclerosis compared with normoinsulinemic mice in which similar plasma cholesterol levels are achieved by a fructose-rich diet. Arterioscler Thromb Vasc Biol 19(5):1223–1230
50. Wu L, Vikramadithyan R, Yu S, Pau C, Hu Y, Goldberg IJ, Dansky HM (2006) Addition of dietary fat to cholesterol in the diets of LDL receptor knockout mice: effects on plasma insulin, lipoproteins, and atherosclerosis. J Lipid Res 47(10):2215–2222
51. Davis HR, Compton DS, Hoos L, Tetzloff G (2001) Ezetimibe, a potent cholesterol absorption inhibitor, inhibits the development of atherosclerosis in ApoE knockout mice. Arterioscler Thromb Vasc Biol 21(12): 2032–2038
52. Teupser D, Persky AD, Breslow JL (2003) Induction of atherosclerosis by low-fat, semisynthetic diets in LDL receptor-deficient C57BL/6J and FVB/NJ mice: comparison of lesions of the aortic root, brachiocephalic artery, and whole aorta (en face measurement). Arterioscler Thromb Vasc Biol 23(10):1907–1913
53. Subramanian S, Han CY, Chiba T, McMillen TS, Wang SA, Haw A, Kirk EA, O'Brien KD, Chait A (2008) Dietary cholesterol worsens adipose tissue macrophage accumulation and atherosclerosis in obese LDL receptor-deficient mice. Arterioscler Thromb Vasc Biol 28(4):685–691
54. King VL, Hatch NW, Chan HW, de Beer MC, de Beer FC, Tannock LR (2009) A murine model of obesity with accelerated atherosclerosis. Obesity 18(1):35–41
55. Merkel M, Velez-Carrasco W, Hudgins LC, Breslow JL (2001) Compared with saturated fatty acids, dietary monounsaturated fatty acids and carbohydrates increase atherosclerosis and VLDL cholesterol levels in LDL receptor-deficient, but not apolipoprotein E-deficient, mice. Proc Natl Acad Sci USA 98(23):13294–13299
56. Otto J, Ordovas JM, Smith D, van Dongen D, Nicolosi RJ, Schaefer EJ (1995) Lovastatin inhibits diet induced atherosclerosis in F1B golden Syrian hamsters. Atherosclerosis 114(1):19–28
57. Alexaki A, Wilson TA, Atallah MT, Handelman G, Nicolosi RJ (2004) Hamsters fed diets high in saturated fat have increased cholesterol accumulation and cytokine production in the aortic arch compared with cholesterol-fed hamsters with moderately elevated plasma non-HDL cholesterol concentrations. J Nutr 134(2):410–415
58. Kahlon T (1996) Cholesterol response and foam cell formation in hamsters fed two levels of saturated fat and various levels of cholesterol. Nutr Res 16(8):1353–1368
59. Castro-Perez J, Briand F, Gagen K, Wang S-P, Chen Y, McLaren DG, Shah V, Vreeken RJ, Hankemeier T, Sulpice T, Roddy TP, Hubbard BK, Johns DG (2011) Anacetrapib promotes reverse cholesterol transport and bulk cholesterol excretion in Syrian golden hamsters. J Lipid Res 52(11):1965–1973
60. Khosla P, Sundram K (1996) Effects of dietary fatty acid composition on plasma cholesterol. Prog Lipid Res 35(2):93–132
61. Dietschy JM, Turley SD, Spady DK (1993) Role of liver in the maintenance of cholesterol and low density lipoprotein homeostasis in different animal species, including humans. J Lipid Res 34(10):1637–1659
62. Blair RM, Appt SE, Bennetau-Pelissero C, Clarkson TB, Anthony MS, Lamothe V, Potter SM (2002) Dietary soy and soy isoflavones have gender-specific effects on plasma lipids and isoflavones in golden Syrian f(1)b hybrid hamsters. J Nutr 132(12):3585–3591
63. Fernandez ML, Volek JS (2006) Guinea pigs: a suitable animal model to study lipoprotein metabolism, atherosclerosis and inflammation. Nutr Metab 3:17

64. Lin EC, Fernandez ML, Tosca MA, McNamara DJ (1994) Regulation of hepatic LDL metabolism in the guinea pig by dietary fat and cholesterol. J Lipid Res 35(3): 446–457
65. Cos E, Ramjiganesh T, Roy S, Yoganathan S, Nicolosi RJ, Fernandez ML (2001) Soluble fiber and soybean protein reduce atherosclerotic lesions in guinea pigs. Sex and hormonal status determine lesion extension. Lipids 36(11):1209–1216
66. Zern TL, West KL, Fernandez ML (2003) Grape polyphenols decrease plasma triglycerides and cholesterol accumulation in the aorta of ovariectomized guinea pigs. J Nutr 133(7):2268–2272
67. Aggarwal D, West KL, Zern TL, Shrestha S, Vergara-Jimenez M, Fernandez ML (2005) JTT-130, a microsomal triglyceride transfer protein (MTP) inhibitor lowers plasma triglycerides and LDL cholesterol concentrations without increasing hepatic triglycerides in guinea pigs. BMC Cardiovasc Disord 5:30
68. Conde K, Vergara-Jimenez M, Krause BR, Newton RS, Fernandez ML (1996) Hypocholesterolemic actions of atorvastatin are associated with alterations on hepatic cholesterol metabolism and lipoprotein composition in the guinea pig. J Lipid Res 37(11): 2372–2382
69. Torres-Gonzalez M, Volek JS, Sharman M, Contois JH, Fernandez ML (2006) Dietary carbohydrate and cholesterol influence the number of particles and distributions of lipoprotein subfractions in guinea pigs. J Nutr Biochem 17(11):773–779
70. Fernandez ML, Wilson TA, Conde K, Vergara-Jimenez M, Nicolosi RJ (1999) Hamsters and guinea pigs differ in their plasma lipoprotein cholesterol distribution when fed diets varying in animal protein, soluble fiber, or cholesterol content. J Nutr 129(7):1323–1332
71. Fernandez ML, Vergara-Jimenez M, Conde K, Abdel-Fattah G (1996) Dietary carbohydrate type and fat amount alter VLDL and LDL metabolism in guinea pigs. J Nutr 126(10):2494–2504
72. Bray GA, Nielsen SJ, Popkin BM (2004) Consumption of high-fructose corn syrup in beverages may play a role in the epidemic of obesity. Am J Clin Nutr 79(4):537–543
73. Daly ME, Vale C, Walker M, Alberti KG, Mathers JC (1997) Dietary carbohydrates and insulin sensitivity: a review of the evidence and clinical implications. Am J Clin Nutr 66(5):1072–1085
74. Basciano H, Federico L, Adeli K (2005) Fructose, insulin resistance, and metabolic dyslipidemia. Nutr Metab 2(1):5
75. Pagliassotti MJ, Prach PA, Koppenhafer TA, Pan DA (1996) Changes in insulin action, triglycerides, and lipid composition during sucrose feeding in rats. Am J Physiol 271(5 Pt 2):R1319–R1326
76. Pagliassotti MJ, Gayles EC, Podolin DA, Wei Y, Morin CL (2000) Developmental stage modifies diet-induced peripheral insulin resistance in rats. Am J Physiol Regul Integr Comp Physiol 278(1):R66–R73
77. Sleder J, Chen YD, Cully MD, Reaven GM (1980) Hyperinsulinemia in fructose-induced hypertriglyceridemia in the rat. Metabolism 29(4):303–305
78. Thresher JS, Podolin DA, Wei Y, Mazzeo RS, Pagliassotti MJ (2000) Comparison of the effects of sucrose and fructose on insulin action and glucose tolerance. Am J Physiol Regul Integr Comp Physiol 279(4):R1334–R1340
79. Thorburn AW, Storlien LH, Jenkins AB, Khouri S, Kraegen E (1989) Fructose-induced in vivo insulin resistance and elevated plasma triglyceride levels in rats. Am J Clin Nutr 49(6):1155– 1163
80. Pagliassotti MJ, Prach PA (1995) Quantity of sucrose alters the tissue pattern and time course of insulin resistance in young rats. Am J Physiol 269(3 Pt 2):R641–R646
81. Horton TJ, Gayles EC, Prach PA, Koppenhafer TA, Pagliassotti MJ (1997) Female rats do not develop sucrose-induced insulin resistance. Am J Physiol 272(5 Pt 2):R1571–R1576
82. Chicco A, D'Alessandro ME, Karabatas L, Pastorale C, Basabe JC, Lombardo YB (2003) Muscle lipid metabolism and insulin secretion are altered in insulin-resistant rats fed a high sucrose diet. J Nutr 133(1): 127–133
83. Kasim-Karakas SE, Vriend H, Almario R, Chow LC, Goodman MN (1996) Effects of dietary carbohydrates on glucose and lipid metabolism in golden Syrian hamsters. J Lab Clin Med 128(2):208–213
84. Taghibiglou C, Carpentier A, Van Iderstine SC, Chen B, Rudy D, Aiton A, Lewis GF, Adeli K (2000) Mechanisms of hepatic very low density lipoprotein overproduction in insulin resistance. Evidence for enhanced lipoprotein assembly, reduced intracellular ApoB degradation, and increased microsomal triglyceride transfer protein in a fructose-fed hamster model. J Biol Chem 275(12): 8416–8425

85. Basciano H, Miller AE, Naples M, Baker C, Kohen R, Xu E, Su Q, Allister EM, Wheeler MB, Adeli K (2009) Metabolic effects of dietary cholesterol in an animal model of insulin resistance and hepatic steatosis. Am J Physiol Endocrinol Metab 297(2): E462–E473
86. Nagata R, Nishio Y, Sekine O, Nagai Y, Maeno Y, Ugi S, Maegawa H, Kashiwagi A (2004) Single nucleotide polymorphism (-468 Gly to A) at the promoter region of SREBP-1c associates with genetic defect of fructose-induced hepatic lipogenesis [corrected]. J Biol Chem 279(28): 29031–29042
87. Sumiyoshi M, Sakanaka M, Kimura Y (2006) Chronic intake of high-fat and high-sucrose diets differentially affects glucose intolerance in mice. J Nutr 136(3):582–587
88. Zafrani ES (2004) Non-alcoholic fatty liver disease: an emerging pathological spectrum. Virchows Arch 444(1):3–12
89. Marchesini G, Babini M (2006) Nonalcoholic fatty liver disease and the metabolic syndrome. Minerva Cardioangiol 54(2):229–239
90. Anstee QM, Goldin RD (2006) Mouse models in non-alcoholic fatty liver disease and steatohepatitis research. Int J Exp Pathol 87(1):1–16
91. Adams LA, Lymp JF, St Sauver J, Sanderson SO, Lindor KD, Feldstein A, Angulo P (2005) The natural history of nonalcoholic fatty liver disease: a population-based cohort study. Gastroenterology 129(1):113–121
92. Browning JD, Szczepaniak LS, Dobbins R, Nuremberg P, Horton JD, Cohen JC, Grundy SM, Hobbs HH (2004) Prevalence of hepatic steatosis in an urban population in the United States: impact of ethnicity. Hepatology 40(6):1387–1395
93. Sahai A, Malladi P, Melin-Aldana H, Green RM, Whitington PF (2004) Upregulation of osteopontin expression is involved in the development of nonalcoholic steatohepatitis in a dietary murine model. Am J Physiol Gastrointest Liver Physiol 287(1): G264–G273
94. Weltman MD, Farrell GC, Liddle C (1996) Increased hepatocyte CYP2E1 expression in a rat nutritional model of hepatic steatosis with inflammation. Gastroenterology 111(6): 1645–1653
95. Kulinski A, Vance DE, Vance JE (2004) A choline-deficient diet in mice inhibits neither the CDP-choline pathway for phosphatidylcholine synthesis in hepatocytes nor apolipoprotein B secretion. J Biol Chem 279(23):23916–23924
96. Mu YP, Ogawa T, Kawada N (2010) Reversibility of fibrosis, inflammation, and endoplasmic reticulum stress in the liver of rats fed a methionine-choline-deficient diet. Lab Invest 90(2):245–256
97. Kirsch R, Clarkson V, Shephard EG, Marais DA, Jaffer MA, Woodburne VE, Kirsch RE, Hall P de la M (2003) Rodent nutritional model of non-alcoholic steatohepatitis: species, strain and sex difference studies. J Gastroenterol Hepatol 18(11):1272–1282
98. Rinella ME, Green RM (2004) The methionine-choline deficient dietary model of steatohepatitis does not exhibit insulin resistance. J Hepatol 40(1):47–51
99. Pickens MK, Yan JS, Ng RK, Ogata H, Grenert JP, Beysen C, Turner SM, Maher JJ (2009) Dietary sucrose is essential to the development of liver injury in the methionine-choline-deficient model of steatohepatitis. J Lipid Res 50(10):2072–2082
100. Pickens MK, Ogata H, Soon RK, Grenert JP, Maher JJ (2010) Dietary fructose exacerbates hepatocellular injury when incorporated into a methionine-choline-deficient diet. Liver Int 30(8):1229–1239
101. Lee GS, Yan JS, Ng RK, Kakar S, Maher JJ (2007) Polyunsaturated fat in the methionine-choline-deficient diet influences hepatic inflammation but not hepatocellular injury. J Lipid Res 48(8):1885–1896
102. Hussein O, Grosovski M, Lasri E, Svalb S, Ravid U, Assy N (2007) Monounsaturated fat decreases hepatic lipid content in non-alcoholic fatty liver disease in rats. World J Gastroenterol 13(3):361–368
103. Fujita K, Nozaki Y, Yoneda M, Wada K, Takahashi H, Kirikoshi H, Inamori M, Saito S, Iwasaki T, Terauchi Y, Maeyama S, Nakajima A (2010) Nitric oxide plays a crucial role in the development/progression of nonalcoholic steatohepatitis in the choline-deficient, l-amino acid-defined diet-fed rat model. Alcohol Clin Exp Res 34(Suppl 1): S18–S24
104. Veteläinen R, van Vliet A, van Gulik TM (2007) Essential pathogenic and metabolic differences in steatosis induced by choline or methione-choline deficient diets in a rat model. J Gastroenterol Hepatol 22(9): 1526–1533
105. Raubenheimer PJ, Nyirenda MJ, Walker BR (2006) A choline-deficient diet exacerbates fatty liver but attenuates insulin resistance and glucose intolerance in mice fed a high-fat diet. Diabetes 55(7):2015–2020
106. Samuel VT, Liu Z-X, Qu X, Elder BD, Bilz S, Befroy D, Romanelli AJ, Shulman GI (2004)

Mechanism of hepatic insulin resistance in non-alcoholic fatty liver disease. J Biol Chem 279(31):32345–32353

107. Gauthier M-S, Favier R, Lavoie J-M (2006) Time course of the development of non-alcoholic hepatic steatosis in response to high-fat diet-induced obesity in rats. Br J Nutr 95(2):273–281
108. Romestaing C, Piquet M-A, Bedu E, Rouleau V, Dautresme M, Hourmand-Ollivier I, Filippi C, Duchamp C, Sibille B (2007) Long term highly saturated fat diet does not induce NASH in Wistar rats. Nutr Metab 4:4
109. Cong W-N, Tao R-Y, Tian J-Y, Liu G-T, Ye F (2008) The establishment of a novel non-alcoholic steatohepatitis model accompanied with obesity and insulin resistance in mice. Life Sci 82(19–20):983–990
110. Subramanian S, Goodspeed L, Wang S, Kim J, Zeng L, Ioannou GN, Haigh WG, Yeh MM, Kowdley KV, O'Brien KD, Pennathur S, Chait A (2011) Dietary cholesterol exacerbates hepatic steatosis and inflammation in obese LDL receptor-deficient mice. J Lipid Res 52(9):1626–1635
111. Roth CL, Elfers CT, Figlewicz DP, Melhorn SJ, Morton GJ, Hoofnagle A, Yeh MM, Nelson JE, Kowdley KV (2012) Vitamin D deficiency in obese rats exacerbates NAFLD and increases hepatic resistin and toll-like receptor activation. Hepatology 55(4):1103–1111
112. Lieber CS, DeCarli LM, Leo MA, Mak KM, Ponomarenko A, Ren C, Wang X (2008) Beneficial effects versus toxicity of medium-chain triacylglycerols in rats with NASH. J Hepatol 48(2):318–326
113. Kohli R, Kirby M, Xanthakos SA, Softic S, Feldstein AE, Saxena V, Tang PH, Miles L, Miles MV, Balistreri WF, Woods SC, Seeley RJ (2010) High-fructose, medium chain trans fat diet induces liver fibrosis and elevates plasma coenzyme Q9 in a novel murine model of obesity and nonalcoholic steatohepatitis. Hepatology 52(3):934–944
114. Bruce KD, Cagampang FR, Argenton M, Zhang J, Ethirajan PL, Burdge GC, Bateman AC, Clough GF, Poston L, Hanson MA, McConnell JM, Byrne CD (2009) Maternal high-fat feeding primes steatohepatitis in adult mice offspring, involving mitochondrial dysfunction and altered lipogenesis gene expression. Hepatology 50(6):1796–1808
115. Karmakar S, Das D, Maiti A, Majumdar S, Mukherjee P, Das AS, Mitra C (2011) Black tea prevents high fat diet-induced non-alcoholic steatohepatitis. Phytother Res 25(7): 1073–1081
116. Ogihara T, Asano T, Ando K, Sakoda H, Anai M, Shojima N, Ono H, Onishi Y, Fujishiro M, Abe M, Fukushima Y, Kikuchi M, Fujita T (2002) High-salt diet enhances insulin signaling and induces insulin resistance in Dahl salt-sensitive rats. Hypertension 40(1):83–89
117. Konda T, Enomoto A, Takahara A, Yamamoto H (2006) Effects of L/N-type calcium channel antagonist, cilnidipine on progressive renal injuries in Dahl salt-sensitive rats. Biol Pharm Bull 29(5):933–937
118. Owens D (2006) Surgically and chemically induced models of disease. In: Suckow MA, Weisbroth SH, Franklin CL (eds) The laboratory rat. Elsevier Academic, Boston, MA, pp 711–732
119. Vasdev S, Gill V, Parai S, Gadag V (2005) Dietary vitamin e supplementation attenuates hypertension in Dahl salt-sensitive rats. J Cardiovasc Pharmacol Ther 10(2):103–111
120. Mattson DL, Kunert MP, Kaldunski ML, Greene AS, Roman RJ, Jacob HJ, Cowley AW (2004) Influence of diet and genetics on hypertension and renal disease in Dahl salt-sensitive rats. Physiological genomics 16(2):194–203
121. Nevala R, Vaskonen T, Vehniäinen J, Korpela R, Vapaatalo H (2000) Soy based diet attenuates the development of hypertension when compared to casein based diet in spontaneously hypertensive rat. Life Sci 66(2):115–124
122. Buñag RD, Tomita T, Sasaki S (1983) Chronic sucrose ingestion induces mild hypertension and tachycardia in rats. Hypertension 5(2):218–225
123. Zhang HY, Reddy S, Kotchen TA (1999) A high sucrose, high linoleic acid diet potentiates hypertension in the Dahl salt sensitive rat. Am J Hypertens 12(2 Pt 1):183–187
124. Preuss HG, Gondal JA, Bustos E, Bushehri N, Lieberman S, Bryden NA, Polansky MM, Anderson RA (1995) Effects of chromium and guar on sugar-induced hypertension in rats. Clin Nephrol 44(3):170–177
125. Thierry-Palmer M, Tewolde TK, Emmett NL, Bayorh MA (2010) High dietary salt does not significantly affect plasma 25-hydroxyvitamin D concentrations of Sprague Dawley rats. BMC Res Notes 3:332
126. Dobrian AD, Davies MJ, Prewitt RL, Lauterio TJ (2000) Development of hypertension in a rat model of diet-induced obesity. Hypertension 35(4):1009–1015
127. Sánchez-Lozada LG, Tapia E, Jiménez A, Bautista P, Cristóbal M, Nepomuceno T, Soto V, Avila-Casado C, Nakagawa T, Johnson

RJ, Herrera-Acosta J, Franco M (2007) Fructose-induced metabolic syndrome is associated with glomerular hypertension and renal microvascular damage in rats. Am J Physiol Renal Physiol 292(1):F423–F429

128. Vasudevan H, Xiang H, McNeill JH (2005) Differential regulation of insulin resistance and hypertension by sex hormones in fructose-fed male rats. Am J Physiol Heart Circ Physiol 289(4):H1335–H1342
129. Hwang IS, Ho H, Hoffman BB, Reaven GM (1987) Fructose-induced insulin resistance and hypertension in rats. Hypertension 10(5):512–516
130. DeFronzo RA (1981) The effect of insulin on renal sodium metabolism. A review with clinical implications. Diabetologia 21(3):165–171
131. Noguchi T, Ikeda K, Sasaki Y, Yamamoto J, Yamori Y (2004) Effects of vitamin E and sesamin on hypertension and cerebral thrombogenesis in stroke-prone spontaneously hypertensive rats. Clin Exp Pharmacol Physiol 31(Suppl 2):S24–S26
132. Sallinen K, Arvola P, Wuorela H, Ruskoaho H, Vapaatalo H, Pörsti I (1996) High calcium diet reduces blood pressure in exercised and nonexercised hypertensive rats. Am J Hypertens 9(2):144–156
133. Yu Q, Larson DF, Slayback D, Lundeen TF, Baxter JH, Watson RR (2004) Characterization of high-salt and high-fat diets on cardiac and vascular function in mice. Cardiovasc Toxicol 4(1):37–46

Chapter 22

Rodent Models to Evaluate Anti-obesity Drugs

Sharon C. Cheetham and Helen C. Jackson

Abstract

This article describes the use of rodent models to evaluate the anti-obesity potential of novel drugs. Although drugs can reduce body weight by altering energy input or energy output, we have focused on the discovery of compounds reducing food intake as this is the most common pharmacological approach for anti-obesity drugs. Methods are described for assessing and interpreting the specificity of the effects of acute and chronic administration of novel compounds on food intake, water intake, and body weight in mice and rats including animal models of overweight and obesity. Genetically obese mice and rats with spontaneously occurring single gene mutations in genes encoding leptin or its receptors have been characterized. However, monogenic obesity in humans is extremely rare and it is now widely accepted that polygenic dietary-induced obese rats and mice are the most appropriate models for predicting the therapeutic potential of novel drugs in common human obesity.

Key words: Obesity, Anti-obesity drug, Animal models, Dietary-induced obesity, Body weight, Food intake

1. Introduction

Over recent years the incidence of obesity and overweight (defined as an excessive accumulation of body fat that impairs health) has been increasing at an alarming rate, not only in developed countries but also in developing countries, where hunger may also occur (1). In 2008, it was estimated that 1.5 billion adults were overweight. Of these, over 200 million men and nearly 300 million women were obese, representing more than one in ten of the world's adult population (1). The health and economic consequences of the escalating obesity epidemic are enormous. Obesity is a major risk factor for cardiovascular and cerebrovascular diseases (heart attack and stroke), type 2 diabetes, musculoskeletal disorders and certain

Arpad Szallasi and Tamás Bíró (eds.), *TRP Channels in Drug Discovery: Volume II*, Methods in Pharmacology and Toxicology,
DOI 10.1007/978-1-62703-095-3_22,

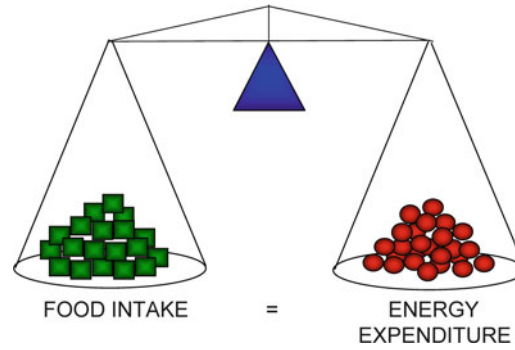

Fig. 1. The energy balance equation. Obesity occurs when energy input is greater than energy output over a prolonged period of time.

cancers, and it is now estimated that at least 2.8 million adults die each year as a result of being overweight or obese (1).

Body weight is a balance between food intake (energy intake) and energy expenditure (energy output) as shown in Fig. 1. Obesity occurs when energy input is greater than energy output over a prolonged period of time. This is typically the case in common human obesity where easy access to cheap, tasty food high in fat, salt, and sugar has led to an increase in energy intake which is often accompanied by a sedentary lifestyle. Strategies for producing weight loss in obese individuals include diet and exercise to reduce energy input and increase energy output. However, dieting often increases food craving and the amount of exercise required is not practical for most obese patients; therefore, such lifestyle interventions are rarely successful and weight regain often occurs (2). It is now widely accepted that more rigorous interventions than diet and exercise alone are required to manage obesity. Bariatric surgery (gastric banding or bypass) produces dramatic and sustained weight loss but has not been without its health risks. Although normally restricted to morbidly obese patients or obese patients with comorbidities such as type 2 diabetes, techniques are constantly improving, and it may be more widely used in the future (3, 4). The alternative approach is to produce weight loss by pharmacological manipulation (in combination with diet and exercise).

In mammals, body weight is maintained by homeostatic mechanisms regulating food intake and energy output which involve complex interactions between the central nervous system and peripheral neurohormonal signals from the pancreas, adipose tissue, and the gastrointestinal tract (5). Due to the complex mechanisms involved in the control of energy balance, a wide variety of central and peripheral targets have been employed in the search for new anti-obesity drugs (6–9). Using these different approaches a vast number of potential anti-obesity drugs have been synthesized and tested in animals. The majority of these drugs reduce energy

input. Examples of treatments for obesity with central action include 5-hydroxytryptamine (5-HT) and noradrenaline reuptake inhibitors, e.g., sibutramine; 5-HT_{2C} receptor agonists, e.g., lorcaserin; 5-HT_6 receptors antagonists; cannabinoid CB_1 receptor antagonists/inverse agonists, e.g., rimonabant; histamine H_3-antagonists and peptide agonists and antagonists, e.g., glucagon-like peptide-1 (GLP-1), leptin and amylin analogues, and melanin-concentrating hormone MCH_1 receptor antagonists. Peripherally acting compounds include lipase inhibitors such as orlistat which reduce the absorption of fat by the gastrointestinal tract.

Despite the amount of work by the pharmaceutical industry in this area, orlistat (Xenical) is the only drug currently on the market for the long-term management of obesity in the USA and Europe. This is because in recent years a number of anti-obesity drugs have been withdrawn from clinical use or not given marketing approval because of concerns that the benefits (efficacy) of giving them do not outweigh the risks (incidence of side-effects). For example, in 2010 sibutramine (Meridia, Reductil) was withdrawn from the market in Europe (by the EMEA (10)) and the USA (voluntarily) due to increased risk of cardiovascular events and rimonabant was not approved in the States, and subsequently withdrawn in Europe (11), due to the emergence of severe psychiatric adverse events. The regulatory hurdles for the development of novel anti-obesity drugs remain exceptionally high and there is still an immense and unmet clinical need for the development of more efficacious and safer drugs to treat obesity.

This article reviews the use of rats and mice to evaluate the anti-obesity potential of novel drugs. We have focused on methods that can be used to measure the efficacy of compounds to produce weight loss as the potential side-effects and safety issues will depend on the specific pharmacological profile of each drug. Moreover, while some safety issues such as abuse potential can be readily assessed in animals, others may not emerge until the drug have been in clinical use for a prolonged period and cannot always be predicted from pre-clinical studies.

2. Methodology

The initial screen for anti-obesity potential will vary depending on the pharmacological target, but as the majority of drugs act by reducing energy input, a typical primary in vivo screen would be to measure the effects of the drug on food intake in rats or mice following acute administration before progressing active compounds to sub-chronic and chronic studies in rodent models of overweight and obesity. After discussing some general considerations regarding the models employed, we have given details of specific protocols

used for acute, sub-chronic, and chronic feeding studies in rats and mice and described a typical screening strategy for identifying anti-obesity action. Finally, we suggest some additional studies that can be used to confirm that the drugs are altering food intake/energy homeostasis in a specific manner and to investigate the effects of drugs on energy output—the other side of the energy balance equation.

2.1. General Considerations

2.1.1. Choice of Species

Rats and mice are the predominant species used to evaluate the effects of drugs on food intake and energy balance. They are small, readily available, economical to use, easy to handle, and body weights and food and water intakes can be measured easily. They are also omnivores with complex digestive systems and many of the central and peripheral mechanisms controlling food intake appear to be similar to those in man. There are some notable physiological differences, for example, rodents do not have gall bladders or a vomit reflex. They also tend to eat their food in a large number of smaller meals each day compared to man and are nocturnal. Furthermore, food intake in rodents is not influenced by some of the complex social, emotional, and psychological factors that can drive food intake in humans. Despite these limitations, the use of rodents in drug discovery to screen for potential anti-obesity action has been validated as many of the drugs found to reduce body weight in the clinic reduce body weight and food intake when given to rats and mice as mentioned below.

Acute and chronic feeding studies can be performed in either rats or mice. The choice of species depends on factors such as cost of the experiment (normally cheaper in mice), cost and availability of the test drug (mice use less), the desire to compare results with historical company data or data in the literature, and the requirement to perform studies in transgenic or knock-out animals. Mice are the species of choice for genetic manipulation. However, animals which develop obesity following overexpression or elimination of particular genes are more useful for studying the biology underlying obesity and for proof-of-concept for novel anti-obesity approaches than general screening purposes as they do not mimic the aetiology of normal human obesity. In general, drugs will be active in both mice and rats though sensitivity to the effects of the drug may vary between the species. Occasionally, however, more prominent species differences may be observed and influence the choice of species employed. For example, rats are normally used in preference to mice in screening strategies for 5-HT_6 receptor antagonists, due to differences in the central distribution and pharmacological profiles of 5-HT_6 receptors in rats, mice, and man (12).

2.1.2. Choice of Strain

Strain differences can occur in both the pharmacological responses to drugs and in the susceptibility to develop obesity when maintained on different experimental diets. The strains employed for both

acute and chronic feeding studies therefore need to be chosen carefully and used consistently for each particular assay. Both inbred and outbred strains can be used for screening purposes. The advantage of using pure inbred strains is that results obtained with them may be less variable as they have the same genetic background. On the other hand, it could be argued that results obtained in inbred animals may be skewed as the human population is not inbred. In contrast, outbred animals are bred to maintain maximum heterozygosity. Outbred animals from the same colony are similar, however, individual animals are genetically unique. Although inter-animal variation may be greater in outbred strains, they are generally more robust and more economical than inbred strains.

The most commonly used mouse strain to evaluate anti-obesity drugs is C57BL/6J. This pure inbred strain is used as the key endpoints, e.g., weight gain and food intake can be very variable in mice. In contrast, strains of rats commonly used in feeding studies are Sprague–Dawley, Wistar, and Long-Evans rats (outbred strains). All of these animals can be used in acute feeding studies (normal, growing animals on standard rodent diet) but will put on weight when given free access to high-fat or cafeteria diets (see below).

2.1.3. Choice of Gender

Acute feeding studies are normally conducted in male rats to circumvent the variation in food intake caused by the oestrus cycle in females (13), however, as obesity occurs in both men and women, chronic feeding studies would ideally be performed in both male and female rodents at some point in the drug discovery process to check that the pharmacological responses to drugs were not gender-specific. In this context, there are clear differences in the distribution of subcutaneous and visceral fat and circulating levels of the adiposity hormones, leptin, and insulin, in men and women which are also seen in laboratory animals (14). Furthermore, male and female rats have been shown to be more sensitive to the inhibitory effects of centrally administered insulin and leptin on food intake, respectively, confirming the existence of gender differences in the control of energy homeostasis. Indeed, it has been suggested that different strategies may be required to reduce body weight in men and women (14).

2.2. Acute Feeding Studies

The aim of acute feeding studies is to provide a quick, reproducible screen for evaluating the ability of novel drugs to reduce food intake and they are normally performed in lean, growing animals maintained on standard rodent diet as they are readily available and relatively inexpensive compared to more specific animal models of overweight/obesity (see below). In these animals, food intake is stimulated by a variety of methods to enable inhibitory effects of drugs on food intake to be detected compared to vehicle-treated control animals. For instance, as rodents are nocturnal, dosing may take place at the onset of the dark period when the food intake of

the control group will normally be high. Alternatively, animals may be deprived of food before the test. While this produces a more robust increase in food intake, it does not reflect the physiological situation, for example, an overnight fast would be a major stressor in mice due to their high metabolic rate. Finally, food intake can be stimulated by training the animals to eat wet mash (or sweetened wet mash) at certain times of the day. The animals find the wet mash palatable and readily consume it even when not food-deprived; therefore, the model reflects the overeating that can occur in man, as food intake is driven by palatability rather than metabolic need. Regardless of the exact methodology employed, the use of acute feeding studies as an initial screen for anti-obesity action for centrally acting drugs has been validated as compounds producing effective weight loss in the clinic (e.g., sibutramine, rimonabant, and locaserin) reduce food intake following acute administration to rats and mice (15–17).

Typical methods used to measure the food intake of mice or rats following acute administration of drugs and examples of data obtained using these procedures are given in Tables 1 and 2 and Figs. 2 and 3.

Food intake is easy to measure and clearly defined; therefore, the relative efficacy of different compounds to reduce food intake can be easily compared. A commonly used measure in acute feeding studies is to determine the dose of drug required to reduce food intake to 50% of control levels over a specific time after dosing (ED_{50} values). Test compounds reducing food intake by 50% (or more) over 24 h are likely to produce significant weight loss 24 h after dosing. Occasionally, the effects of drugs on food intake and body weight may be recorded for longer periods (up to 72 h) following a single treatment or the acute screen may involve giving drugs for up to 7 days, particularly if the compounds are thought to have a delayed onset of action (e.g., MCH_1 receptor antagonists).

Water intake should be measured throughout all feeding studies. The effects of drugs on this parameter will vary depending on the mode of action but drinking behavior can be altered independently of feeding behavior and this information can be used to interpret the results of feeding studies. Animals should be closely observed before and after dosing and at all readings and any relevant observations should be recorded. Furthermore, if animals are housed in cages with wire-grid floors, the cage pads beneath each cage should be regularly examined for changes in urine or fecal output. These observations can give an early indication of whether the drugs are reducing food intake in a specific manner (see below).

2.3. Animal Models of Obesity

Compounds that are active in reducing food intake (and body weight) in the acute screen are likely to be evaluated further in sub-chronic or chronic feeding studies. These can be conducted in lean animals but because the studies are labor-intensive and require

Table 1
Acute feeding studies in normal mice

Animals: • Male C57BL/6 J mice, weight range on arrival 20–25 g
Environmental conditions: • Individually housed in polypropylene cages with solid floors • Normal lighting (lights off from 19.00 to 07.00 h); 21 ± 4°C; 55% ± 20% humidity • Free access to standard pelleted rodent diet and tap water except for 4 h each day when pelleted food replaced by palatable wet mash (1 part powdered standard rodent chow : 1.5 parts tap water) placed in a petri-dish on the cage floor • Mice customized to these conditions for 2 weeks before the test
Experimental procedures: • On the day before the test, mice weighed (to 0.1 g). Intake of wet mash measured for 2 h (to 0.1 g). Data used to allocate the mice into balanced groups ($n = 8$) before drug administration • On day of test, mice weighed and dosed by a suitable route (e.g., po, ip, or sc) with vehicle and test drug (e.g. several doses of the same compound or one dose of several different drugs). One dose of a suitable reference compound may be used for comparison. Pelleted food removed and 1 h later, mice given wet mash. Dish of wet mash and water bottles weighed at 0, 1, 2, and 4 h. At 4 h wet mash replaced by pelleted food. Mice, pelleted food, and water bottles weighed again 24 h after dosing. All measurements made concurrently • Parameters measured: Body weights (g) at 0 and 24 h; change in body weight (g) over 24 h; food (g) and water (g) intake over 1, 2, 4, and 24 h and between 1–2, 2–4, and 4–24 h. In some studies, mice may be weighed again at 48 and 72 h and food and water intakes measured over 48 and 72 h and between 24–48 h and 48–72 h • Animals examined before and after dosing and at each reading and any relevant observations on their appearance and behavior recorded
Data and statistical analysis: • Data expressed as means (adjusted for differences at baseline) and SEM. Data analysis by analysis of covariance (using baseline data as covariate) followed by suitable multiple comparisons tests to compare each drug treatment with the control group
Activity criteria: • Significant reduction in body weight and food intake compared to the control group with comparable efficacy to a suitable reference compound (and no evidence that these effects may be non-specific)
References and examples of data: • Vickers et al. (16) and Fig. 2

large amounts of drug, they are normally performed in animal models of overweight or obesity. These models should mirror the human condition as closely as possible in terms of the causes of the disorder (construct validity); the aetiology, symptoms, and prognosis of the disorder (face validity) and the effects of pharmacological manipulation in the model (predictive validity). It is now generally considered that there are two main types of rodent models of obesity: genetically obese and dietary-induced obese rats and mice (Fig. 4).

Table 2
Acute feeding studies in normal rats

Animals: • Male Sprague–Dawley rats, weight range on arrival 250–300 g
Environmental conditions: • Individually housed in polypropylene cages with wire grid floors. Cage trays with cage pads placed below each cage to detect spilt food and water. Rats given paper bedding to provide environmental enrichment, warmth and an area for them to escape the grid floor • Reverse-phase lighting (lights off from 09.30 to 17.30 h during which time red light used for illumination); 21 ± 4°C; 55% ± 20% humidity • Free access to standard powdered rodent diet and tap water • Diet presented in glass jars with aluminum lids with holes cut in the lids to allow access to the food • Rat acclimatized to these conditions for 2 weeks before the test
Experimental procedures: • On the day before the test, rats weighed (to 0.1 g) at 0 h (onset of the 8 h dark period) and dosed with vehicle by an appropriate route (e.g., po, ip, or sc). Feeding jars and water bottles weighed (to 0.1 g) at 0 h and 6 h later. Any spilt food returned to the appropriate jar before weighing. Body weights and 6 h food and water intakes used to allocate the rats into balanced groups ($n = 8$) before drug administration • On day of test, rats weighed and dosed with vehicle and test drug (e.g., several doses of the same compound or one dose of several different drugs). One dose of a suitable reference compound may be used for comparison. Feeding jars and water bottles weighed at 0 h and 1, 2, 4, 8 and 24 h later. Rats weighed again at 24 h. All measurements made concurrently • Parameters measured: Body weights (g) at 0 and 24 h; change in body weight (g) over 24 h; food (g) and water (g) intake over 1, 2, 4, 8, and 24 h and between 1–2, 2–4, 4–8, and 8–24 h. In some studies, rats may be weighed at 48 and 72 h and food and water intakes measured over 48 and 72 h and between 24–48 h and 48–72 h or rats may be dosed every day and daily food and water intakes measured for up to 7 days • Animals examined before and after dosing and at each reading and any relevant observations on their appearance and behavior recorded. Cage pads examined at each reading for changes in urine/feces
Data and statistical analysis: • Data expressed as means (adjusted for differences at baseline) and SEM. Data analysis by analysis of covariance (using baseline data as covariate) followed by suitable multiple comparisons tests to compare each drug treatment with the control group • ED_{50} values for inhibition of food intake determined if suitable data obtained
Activity criteria: • Significant reduction body weight and food intake compared to the control group with comparable efficacy to a suitable reference compound (and no evidence that these effects may be non-specific)
References and examples of data: • Jackson et al. (17) and Fig. 3

2.3.1. Genetically Obese Animals

A number of different models of genetically obese animals are now available for obesity research (18–20). The most commonly used examples include *ob/ob* mice, *db/db* mice, and Zucker *fa/fa* rats. These animals have been well-characterized and widely used as models of obesity. However, it is now generally accepted that these genetic models do not mimic human obesity as well as animals

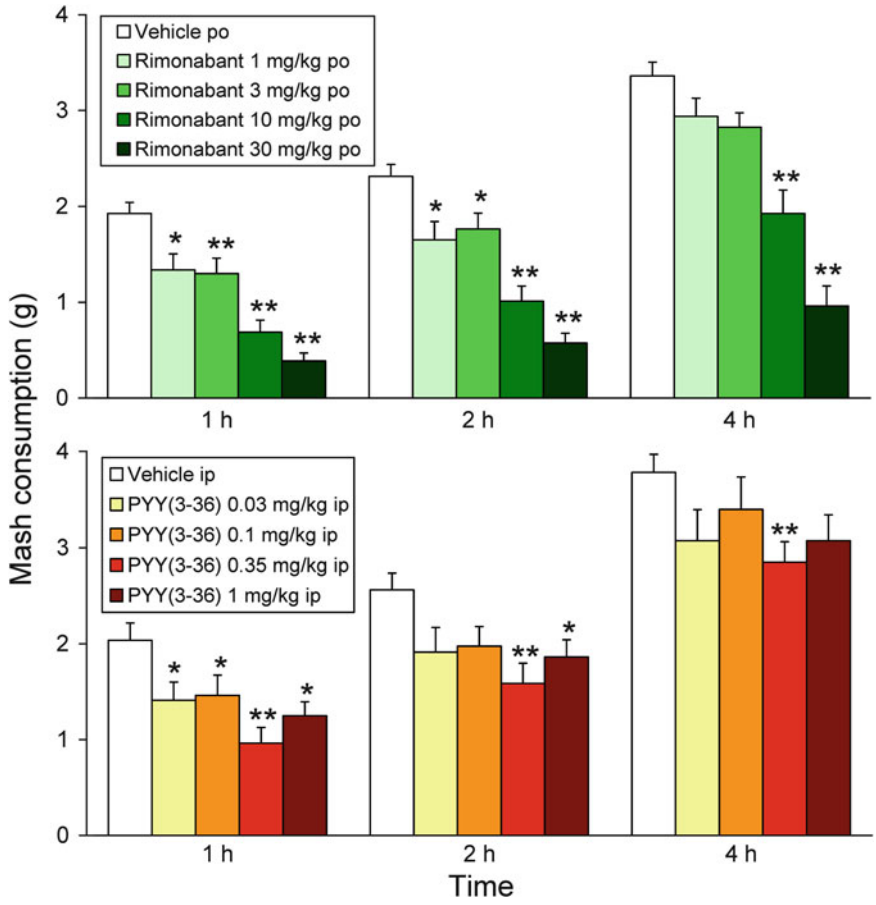

Fig. 2. Effect of acute administration of the CB_1 receptor antagonist, rimonabant, and the peptide, PYY (3–36), on wet mash intake in male C57BL/6J mice. Data obtained using similar methods to those described in Table 1. Results are means and SEM; $n=8$. Data analyzed by analysis of variance followed by Dunnett's test. Significant differences from the vehicle-treated control group are denoted by $^*p<0.05$ and $^{**}p<0.01$. Data on file RenaSci Ltd.

made obese by exposure to high-fat or cafeteria diets. The main reason for this is that genetically obese animals are monogenic (the obesity has arisen following spontaneously occurring single gene mutations which prevent the production of the adipose hormone, leptin (*ob/ob* mice) or result in deficient leptin receptors (*db/db* mice and Zucker *fa/fa* rats)). In contrast, the genetic predisposition to obesity in most human individuals has a polygenic basis. A small number of monogenic forms of obesity have been reported in man including those due to leptin or leptin-receptor deficiency but they are extremely rare (21, 22). Furthermore, although leptin produces dramatic weight loss in leptin-deficient *ob/ob* mice and humans (21, 22), these effects do not appear to translate to common polygenic human obesity which is normally associated with high circulating levels of leptin and leptin resistance (23). The key role played by leptin in the control of energy homeostasis in rodents

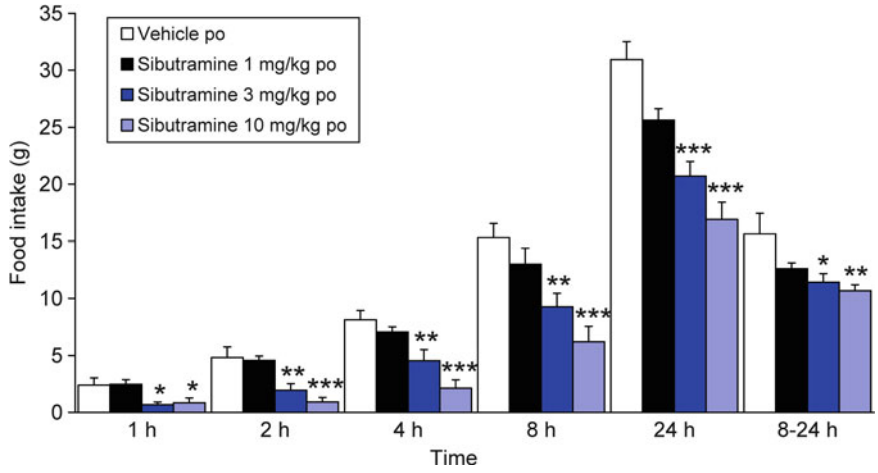

Fig. 3. Effect of acute administration of the 5-HT and noradrenaline reuptake inhibitor, sibutramine, on food intake in male Sprague–Dawley rats with free access to normal powdered rat chow. Animals were maintained on reverse-phase lighting. Sibutramine was dosed at the onset of the 8 h dark period. Data obtained using similar methods to those described in Table 2. Results are means (adjusted for differences at baseline) and SEM; $n=6$–7. Data analyzed by analysis of covariance (used baseline data as covariate) followed by Williams' test. Significant differences from the vehicle-treated control group are denoted by $^{*}p<0.05$, $^{**}p<0.01$ and $^{***}p<0.001$. Data on file RenaSci Ltd.

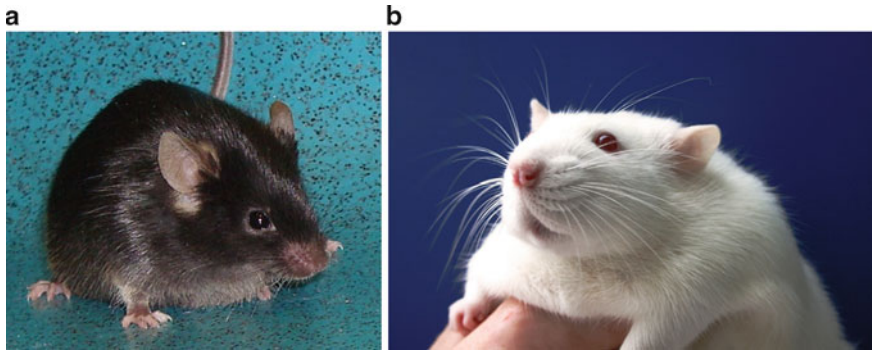

Fig. 4. Examples of animal models of obesity. (**a**) A genetically obese male *db/db* mouse. (**b**) A cafeteria-diet fed dietary-induced obese, female Wistar rat.

and man and concerns that these genetic models do not reflect the aetiology and metabolic signs that characterize common human obesity explains why these models are now rarely used as screens for novel anti-obesity drugs.

2.3.2. Dietary-Induced Obesity

The main advantage of models in which obesity is induced in normal animals by exposure to palatable high-fat or cafeteria diets is that the obesity is likely to be mediated by multiple genes and is therefore closer to the human situation. A number of differences in the exact methodology used by different laboratories exist, but on the whole, the increase in body weight appears to be largely due to increased body fat and the metabolic complications produced by

dietary-induced obesity in laboratory animals mirror those seen in common human obesity. Thus, although dietary-induced obese animal are not typically hyperglycemic, they display increased circulating levels of insulin and leptin, insulin resistance, and mild dyslipidaemia compared to lean controls on normal diet (15, 19, 24). The hypothesis that dietary-induced obese animals can be used as an appropriate model of common human obesity has been largely confirmed by functional genomics, although differences in expression of genes involved with fatty acid metabolism and oxidation in obese human adipocytes and epidydimal fat from dietary-induced obese rats have been detected (24).

The different types of diet used to induce obesity in rodents have been reviewed by other workers (19, 25). In this article we have given specific examples of animal models using overweight or obese rodents maintained on high-fat or cafeteria diets rich in both carbohydrate and fat and described how they can be used together in a screening strategy to evaluate novel drugs to treat obesity.

High Fat-Fed Overweight Rat Model

High-fat diets are now commercially available and are attractive to the experimenter as they can be supplied in either pelleted or powdered form as a single source. This means that measurement of food intake is relatively straightforward and can be performed quickly. These methods are therefore ideal for screening purposes in rats or mice and have been used extensively in drug discovery (for examples, see the literature references cited on http://www.researchdiets.com).

A range of high-fat diets are available supplying between 32 and 60% energy as fat. Control diets supplying only 10% energy as fat are also available. The advantage of the diet supplying 60% energy as fat is that the animals rapidly put on weight reducing the time before they can be used. However, this degree of fat does not reflect the typical human "junk food" diet where dietary fat represents 35–40% of total energy intake (26). In addition, human obesity tends to develop slowly over time. Furthermore, the obesity produced in animals maintained on very high fat diets can be more difficult to reverse by pharmacological manipulation than the obesity induced by more moderate high-fat diets. For these reasons, diets supplying 32% or 45% energy as fat are often preferred.

Most animal models of obesity involve maintaining the animals on the high-fat or cafeteria diets for several months until they become obese. The animals are therefore expensive and, unless a colony is constantly maintained, are not readily available. Acute or sub-chronic studies in rats maintained on a high-fat diet for 2 weeks before the start of the experiment can be used to bridge the gap between acute feeding studies in normal rats or mice and chronic studies in dietary-induced obese animals.

The model described in Table 3 employs young male Sprague–Dawley rats and a high-fat diet supplying 32% energy as fat. The animals are still in an active growth phase during the test and rapidly put on weight when exposed to the diet but are not obese (Fig. 5). The paradigm typically measures the ability of drugs to reduce weight gain compared to the control group rather than to decrease body weight per se. This model of overweight can be used to check the efficacy and tolerability of novel anti-obesity agents

Table 3
Sub-chronic studies in overweight rats

Animals: • Male Sprague–Dawley rats, weight range on arrival 250–300 g
Environmental conditions: • Individually housed in polypropylene cages with wire grid floors. Cage trays with cage pads placed below each cage to detect spilt food and water. Rats given paper bedding to provide environmental enrichment, warmth, and an area for them to escape the grid floor • Reverse-phase lighting (lights off from 09.30 to 17.30 h during which time red light used for illumination); 21 ± 4°C; 55% ± 20% humidity • Free access to high-fat powdered rodent diet (D12266B, 32% energy as fat, Research Diets Inc) and tap water • Diet presented in glass jars with aluminum lids with holes cut in the lids to allow access to the food • Rat acclimatized to these conditions for 2 weeks before the test
Experimental procedures: • During a 3-day run-in period, rats weighed (to 0.1 g) at 0 h (onset of the 8 h dark period) and dosed with vehicle by an appropriate route (e.g., po, ip, or sc). Feeding jars and water bottles weighed (to 0.1 g) every day at 0 h. Any spilt food returned to the appropriate jar before weighing. Toward the end of the baseline period, body weight and available food and water intake data used to allocate the rats into balanced groups ($n = 10$) before drug administration • During drug treatment (e.g., 14 days), rats weighed and dosed with vehicle, test drug (e.g., one of three doses) and reference compound (e.g., sibutramine 7.5 mg/kg po) every day at 0 h (or bi-daily at 0 and 8 h). Feeding jars and water bottles weighed at 0 h every day. All measurements made concurrently • Parameters measured: Body weights (g) at 0 h; change in body weight per week and over the entire drug treatment period (g); daily food and water intakes (g); average daily food and water intakes per week and overall (g/day); cumulative food intake on each day (g) • Animals examined before and after dosing on each day and any relevant observations on their appearance and behavior recorded. Cage pads examined daily (0 h) for changes in urine/feces
Data and statistical analysis: • Data expressed as means (adjusted for differences at baseline) and SEM. Data analysis by analysis of covariance (using baseline data as covariate) followed by suitable multiple comparisons tests to compare each drug treatment with the control group
Activity criteria: • Significant reduction in body weight or body weight and food intake compared to the control group with comparable efficacy to a suitable reference compound (and no evidence that these effects may be non-specific)
References and examples of data: • Heal et al. (27); Henderson et al. (28) and Fig. 5

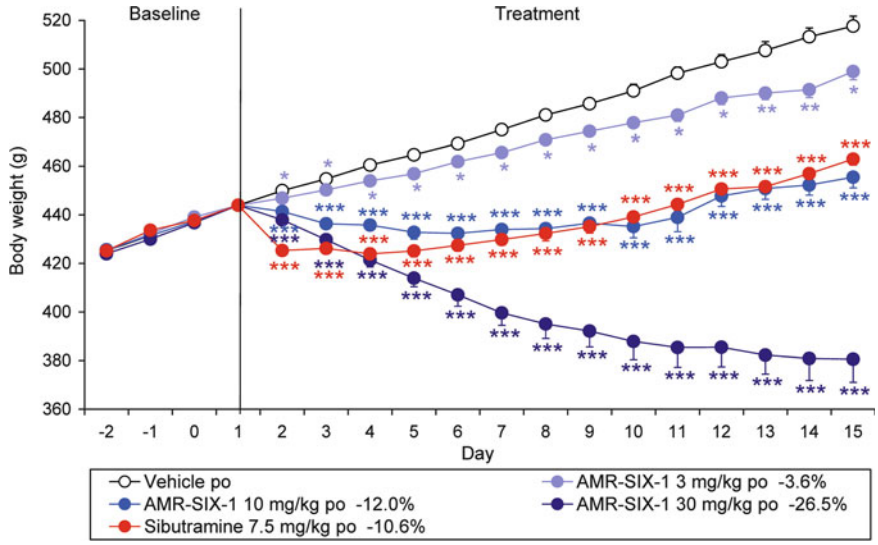

Fig. 5. Effect of sub-chronic administration of the 5-HT_6 receptor antagonist, AMR-SIX-1, on body weight in overweight male Sprague–Dawley rats. Animals were maintained on reverse-phase lighting and a high-fat diet supplying 32% energy as fat. Drugs were dosed at the onset of the 8 h dark period. Sibutramine was used for comparison. Data obtained using similar methods to those described in Table 3. Results are means (adjusted for differences in body weight before drug treatment began on Day 1) and SEM; $n=9$–10. Percentages refer to the % reduction in body weight compared to the control group on Day 15. Data analyzed by analysis of covariance (using Day 1 body weights as covariate) followed by Williams' test (AMR-SIX-1) or the multiple t test (sibutramine). Significant differences from the vehicle-treated control group are denoted by $^*p<0.05$, $^{**}p<0.01$ and $^{***}p<0.001$. Data previously published in abstract form (Henderson et al. (28)).

before proceeding to more rigorous studies in dietary-induced obese rats maintained on more complex diets. It has been validated using the clinically proven anti-obesity agents, sibutramine and rimonabant, which have been shown to significantly reduce body weight and food intake in high-fat fed rats, and also used to evaluate novel pharmacological targets for the treatment of obesity such as 5-HT_6 receptor antagonists (Fig. 5; (27) and (28)).

Dietary-Induced Obese Mice

Mouse models of dietary-induced obesity are popular because they normally require less compound than studies in dietary-induced obese rats as mentioned above. Most mouse models of obesity employ single-source high-fat diets as it can be difficult to measure intake of a cafeteria diet in mice. An example of a protocol which can be used to study the effects of drugs on body weight and food and water intake in dietary-induced obese mice is given in Table 4. In this model, C57BL/6J mice are given a diet containing 45% energy as fat for 16 weeks to induce obesity. During this period, the mice typically develop insulin resistance and elevated leptin levels. Chronic administration of sibutramine, rimonabant, and orlistat for 4 weeks significantly reduces body weight in dietary-induced obese

Table 4
Chronic feeding studies in dietary-induced obese mice

Animals: • Male C57BL/6 J mice, weight range on arrival 20–25 g
Environmental conditions: • Group-housed in polypropylene cages with solid floors, sawdust bedding, a pulped cotton fiber nesting mat, and a cardboard tube (to provide environmental enrichment) for 14 weeks for the induction of obesity. During this period, maintained on normal lighting (lights off from 19.00 to 07.00 h); 21 ± 4°C; 55% ± 20% humidity • Free access to pelleted high-fat diet (D12451, 45% of energy from fat; Research Diets Inc), for the induction of obesity and during the study • Two weeks before the start of the study, mice individually housed and placed on reverse-phase lighting (lights off from 10.00 to 18.00 h during which time red light used for illumination)
Experimental procedures: • During a 7-day run-in period, mice weighed (to 0.1 g) at 0 h (onset of the 8 h dark period) and dosed with vehicle by an appropriate route (e.g., po, ip, or sc). Food (in hopper) and water bottles weighed (to 0.1 g) every day at 0 h. Toward the end of the baseline period, body weight and available food and water intake data used to allocate the mice into balanced groups ($n = 10$) before drug administration • During drug treatment (e.g., 28 days), mice weighed and dosed with vehicle, test drug (e.g., one of three doses) and reference compound (e.g., sibutramine 20 mg/kg po) every day at 0 h (or bi-daily at 0 and 8 h). Food and water bottles weighed at 0 h every day. All measurements made concurrently • Parameters measured: Body weights (g) at 0 h; change in body weight per week and over the entire drug treatment period (g); daily food and water intakes (g); average daily food and water intakes per week and overall (g/day); cumulative food intake on each day (g) • Animals examined before and after dosing each day and any relevant observations on their appearance and behavior recorded
Data and statistical analysis: • Data expressed as means (adjusted for differences at baseline) and SEM. Data analysis by analysis of covariance using baseline data as covariate followed by suitable multiple comparisons tests to compare each drug treatment with the control group
Activity criteria: • Significant reduction in body weight or body weight and food intake compared to the control group with comparable efficacy to a suitable reference compound (and no evidence that these effects may be non-specific)
References and examples of data: • Vickers et al. (16), Cheetham et al. (29) and Fig. 6

mice confirming that this model can be used to screen for centrally and peripherally acting anti-obesity agents as these drugs produce effective weight loss in man (16). For example, this screen has been used to identify novel MCH_1 receptor antagonists which are currently being developed for the treatment of obesity. The weight-loss produced by the MCH_1 receptor antagonist, GW803430, in dietary-induced obese mice is shown in Fig. 6 (29).

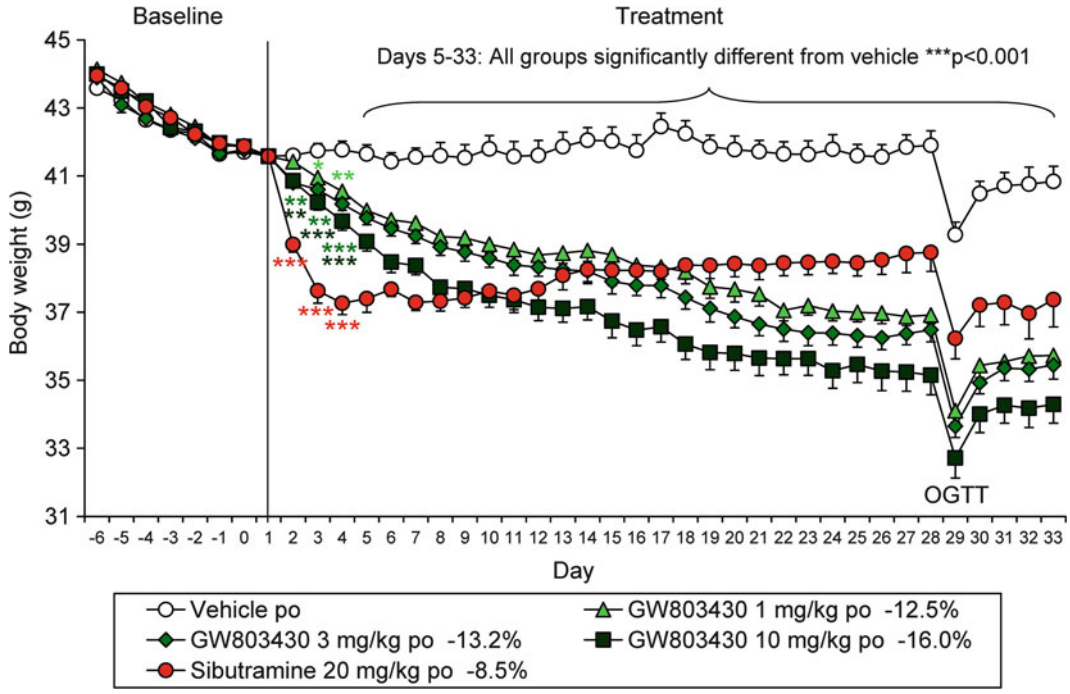

Fig. 6. Effect of chronic administration of the MCH_1 receptor antagonist, GW803430, on body weight in dietary-induced obese, male C57BL/6J mice. Animals were maintained on reverse-phase lighting and a high-fat diet supplying 45% energy as fat. Drugs were dosed at the onset of an 8 h dark period. Sibutramine was used for comparison. Data obtained using similar methods to those described in Table 4. At the end of the 4 week feeding study, animals were deprived of food and an oral glucose tolerance test (OGTT) was performed to investigate the effects of the different drugs on glycaemic control (data not given). Results are means (adjusted for differences in body weight before drug treatment began on Day 1) and SEM; $n = 9–10$. Percentages refer to the % reduction in body weight compared to the control group on Day 33. Data analyzed by analysis of covariance (using Day 1 body weights as covariate) followed by Williams' test (GW803430) or the multiple t test (sibutramine). Significant differences from the vehicle-treated control group are denoted by $^*p < 0.05$, $^{**}p < 0.01$ and $^{***}p < 0.001$. Data previously published in abstract form (Cheetham et al. (29)).

Dietary-Induced Obese Rats

An alternative model, which was used in the registration of the anti-obesity drug, sibutramine, employs female Wistar rats which are made obese by exposure to a simplified cafeteria diet of powdered high-fat diet (containing 20% lard), ground chocolate, and ground salted peanuts for 16 weeks (Table 5). The three different types of food are given in individual pots. The advantage of this strategy is that the different textures and tastes of the different foods encourage the animals to eat. This simplified cafeteria diet is high in both fat and carbohydrate and therefore more closely mirrors a typical "junk food" diet than high-fat diets supplied as a single source in pelleted or powdered form. However, the three different feeding jars have to be weighed at each time-point and therefore studies in dietary-induced obese, female Wistar rats are more labor-intensive and expensive compared to those using a simple high-fat diet. For this reason, studies in dietary-induced obese rats are normally reserved for compounds more advanced in development.

Table 5
Chronic studies in dietary-induced obese rats

Animals:
- Female Wistar rats, weight range on arrival 250–300 g

Environmental conditions:
- Housed in groups of 2–3 in polypropylene cages with solid floors and sawdust bedding for 14 weeks for the induction of obesity
- Reverse-phase lighting (lights off from 09.30 to 17.30 h during which time red light used for illumination); 21 ± 4°C; 55% ± 20% humidity
- Free access to high-fat powdered rodent diet (Special Diet Services, Dietex International Ltd), ground chocolate (Cadburys Dairy Milk), ground salted peanuts (Big D salted peanuts) and tap water for the induction of obesity and during the study
- Diet presented in three separate glass jars with aluminum lids with holes cut in the lids to allow access to the food
- Individually housed in polypropylene cages with wire grid floors for 2 weeks before the start of the study. Cage trays with cage pads placed below each cage to detect spilt food and water. Rats given paper bedding to provide environmental enrichment, warmth and an area for them to escape the grid floor

Experimental procedures:
- During a 7 day run-in period, rats weighed (to 0.1 g) at 0 h (onset of the 8 h dark period) and dosed with vehicle by an appropriate route (e.g., po, ip or sc). Feeding jars and water bottles weighed (to 0.1 g) every day at 0 h. Any spilt food returned to the appropriate jar before weighing. Toward the end of the baseline period, body weight and available food and water intake data used to allocate the rats into balanced groups ($n = 10$) before drug administration
- During drug treatment (e.g., 28 days), rats weighed and dosed with vehicle, test drug (e.g., one of three doses) and reference compound (e.g., sibutramine 5 mg/kg po) every day at 0 h (or bi-daily at 0 and 8 h). Feeding jars and water bottles weighed at 0 h every day. All measurements made concurrently
- Parameters measured: Body weights (g) at 0 h; change in body weight per week and over the entire drug treatment period (g); daily food (kJ) and water (g) intakes; average daily food and water intakes per week and overall (kJ or g/day); cumulative food intake on each day (kJ)
- Animals examined before and after dosing on each day and any relevant observations on their appearance and behavior recorded. Cage pads examined daily (0 h) for changes in urine/feces

Data and statistical analysis:
- Data expressed as means (adjusted for differences at baseline) and SEM. Data analysis by analysis of covariance using baseline data as covariate followed by suitable multiple comparisons tests to compare each drug treatment with the control group

Activity criteria:
- Significant reduction in body weight or body weight and food intake compared to the control group with comparable efficacy to a suitable reference compound (and no evidence that these effects may be non-specific)

References and examples of data:
- Vickers et al. (15), Heal et al. (27), Dickinson et al. (31), Jackson et al. (32–34), Grempler et al. (38) and Fig. 7

Female rats are used in this paradigm as it is important to test novel anti-obesity drugs in both male and female animals as mentioned above. Furthermore, the global incidence of obesity tends to be slightly higher in females than in males (reported to be 7.7%

in men and 11.9% in women in 2005 (30)) and females form the majority of patients entering clinical trials for novel anti-obesity drugs. An additional reason for using female rats in this model is that female rats have flatter growth curves than males that continue to gain weight over their life-cycle. Thus, after several months on the simplified cafeteria diet, the "middle-aged" female rats become weight-stable and the ability of drugs to reduce body weight (as opposed to weight gain) can be assessed.

The obesity induced in the female Wistar rats by exposure to the simplified cafeteria diet is associated with a moderate degree of hyperphagia, impaired glucose tolerance and significantly elevated basal leptin and insulin levels (31). Thus, the syndrome displayed by dietary-induced obese rats is similar in aetiology and its main characteristics to human obesity with insulin resistance (15, 27) confirming that it has construct and face validity. It has also been shown to have excellent predictive validity for the clinic. A wide range of anti-obesity drugs and drug candidates have now been tested in dietary-induced obese, female Wistar rats (e.g., sibutramine, rimonabant, orlistat, topiramate, phentermine, and the combination of topiramate and phentermine (Qnexa) (15, 27, 32–34)) and found to produce a magnitude of weight-loss that correlates very highly with that found in man (15, 27). Examples of the effects of sibutramine, rimonabant, orlistat and the GLP-1 agonist, exenatide, on body weight in dietary-induced obese, female Wistar rats are shown in Fig. 7. This figure also gives examples of the different ways that food intake data can be expressed in sub-chronic or chronic feeding studies.

3. Interpretation of Results

A clinically acceptable anti-obesity drug would decrease food intake in a physiological manner by increasing satiety or reducing hunger. However, drugs can reduce food intake in a number of other ways, e.g., by producing non-specific behavioral effects such as sedation, hyperactivity, and stereotypy that can interfere with the ability of the animal to eat or by simply making the animals feel ill (drug-induced malaise).

Observations made during acute and chronic feeding studies can give an early indication of whether novel compounds are reducing food intake (and body weight) in a specific manner. The specificity of a drugs effect on food intake can be investigated more closely by coupling rigorous behavioral observations with measurement of food intake. In these experiments, which can be performed following acute or chronic administration of drugs, the effects of the test compound on the behavioral satiety sequence are examined, i.e., the normal sequence of events (feeding followed by activity, grooming, and resting) that occurs when an animal eats until it is

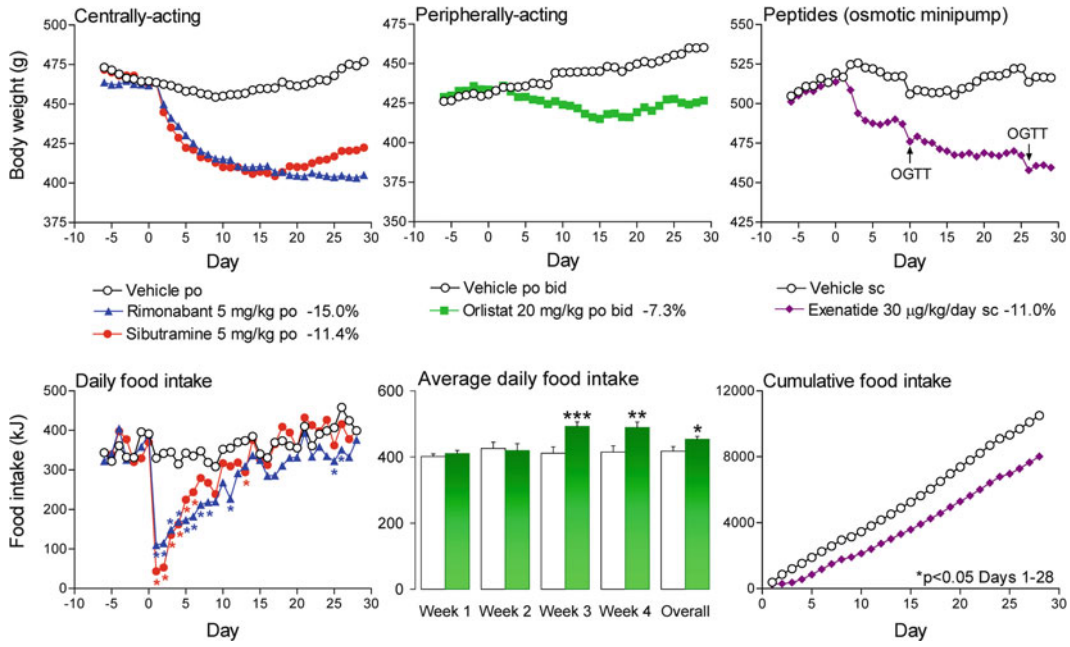

Fig. 7. Effect of a variety of drugs on body weight and food intake in dietary-induced obese, female Wistar rats fed a simplified cafeteria diet. Animals were maintained on reverse-phase lighting. The 5-HT and noradrenaline reuptake inhibitor, sibutramine, and the CB_1 receptor antagonist, rimonabant, were given once daily at the onset of the 8 h dark period (0 h). The lipase inhibitor, orlistat, was given bid at 0 and 4 h and the GLP-1 agonist, exenatide, was given by infusion from subcutaneously implanted osmotic minipumps. The exenatide study included oral glucose tolerance tests (OGTT) as indicated. Other details of the model are as described in Table 5. Results are means (adjusted for differences at baseline), $n = 8$–10. SEMs have been omitted from some of the figures for clarity. Percentages refer to the % reduction in body weight compared to the control group on Day 29. Data analyzed by analysis of covariance (using baseline data as covariate) followed by suitable multiple comparisons tests. Body weights of drug-treated rats were significantly lower ($p < 0.05$) than controls on Days 4–29 (orlistat) or 2–29 (all other drugs). Food intakes of the drug-treated animals were significantly different to the controls as specified. *$p < 0.05$, **$p < 0.01$ and ***$p < 0.001$. Data held on file at RenaSci Ltd. Some of this data has previously been published in abstract form (Jackson et al. (32, 33)).

full (35). An example of a protocol for measuring the effects of a drug on the behavioral satiety sequence in mice is given in Table 6. Similar methodology can be employed in rats. These techniques have been used to show that sibutramine reduces food intake in a physiological manner by enhancing natural satiety (35, 36), whereas the reduction in food intake produced by rimonabant in rats and mice appears to be due to response competition from other behaviors (Fig. 8 and (37)).

The possibility that drugs reduce food intake by making animals feel ill can be quite difficult to evaluate as rodents lack an emetic response and following acute drug administration, may look behaviorally normal. A number of preclinical assays have been developed to try to predict whether drugs are likely to produce nausea in man (15). These include measurement of kaolin intake (as it has been suggested that rats and mice will persistently eat inert material to

Table 6
Behavioral satiety sequencing in mice

Animals: • Male C57BL/6 J mice, weight range on arrival 20–25 g
Environmental conditions: • Individually housed in polypropylene cages with solid floors • Normal lighting (lights off from 19.00 to 07.00 h); 21 ± 4°C; 55% ± 20% humidity • Free access to standard pelleted rodent diet and tap water except for 4 h each day when pelleted food replaced by palatable wet mash (1 part powdered standard rodent chow : 1.5 parts tap water) placed in a petri-dish on the cage floor • Mice customized to these conditions for 2 weeks before the test
Experimental procedures: • On the day before the test, mice weighed (to 0.1 g). Intake of wet mash measured for 1 h (to 0.1 g). Data used to allocate the mice into one of four balanced groups. Two mice from each group tested on each day and results pooled to give a group size of at least 8 • On day of test, mice weighed and dosed by a suitable route (e.g., po, ip or sc) with vehicle or test drug (e.g., one of three doses of the same compound). Pelleted food removed and 1 h later, mice given a weighed amount of wet mash. Behaviors associated with the satiety sequence (feeding, activity, grooming and resting) scored for each animal using a time-sampling procedure (twice a min in 5 min time-bins for 1 h). Animals also examined for any other behaviors which may interfere with food intake. At 1 h, wet mash re-weighed • Parameters measured: total score for each animal for each of the four mutually exclusive behaviors (feeding, activity, grooming and resting) for each 5 min time-bin (maximum of 10). Wet mash intake over 1 h
Data and statistical analysis: • Behavioral data (in 5 min time-bins) analyzed by analysis of variance followed by Dunnett's test. Wet mash intake analyzed as described in Table 1
Interpretation of results: • The effects of different doses of the drug on food intake and the four different components of the satiety sequence are compared to the controls. The test evaluates whether drugs decrease food intake by enhancing natural satiety (expressed as decreased feeding and enhanced resting) or by disrupting normal feeding behavior in a non-specific manner (e.g., decreased feeding accompanied by increased activity/grooming)
References and examples of data: • Jackson et al. (36) and Fig. 8

try to ease gastrointestinal discomfort), the conditioned taste aversion assay (which measures whether drugs produce aversion), and conditioned gaping (which is based on the characteristic gaping exhibited by rats when intraorally infused with a flavored solution previously paired with an emetic drug). These methods have their limitations, for example, exenatide had no effect on kaolin intake in animals but appears to increase the incidence of nausea in man and the conditioned taste aversion assay has been criticized for detecting false positives as the source of the aversion may be unrelated

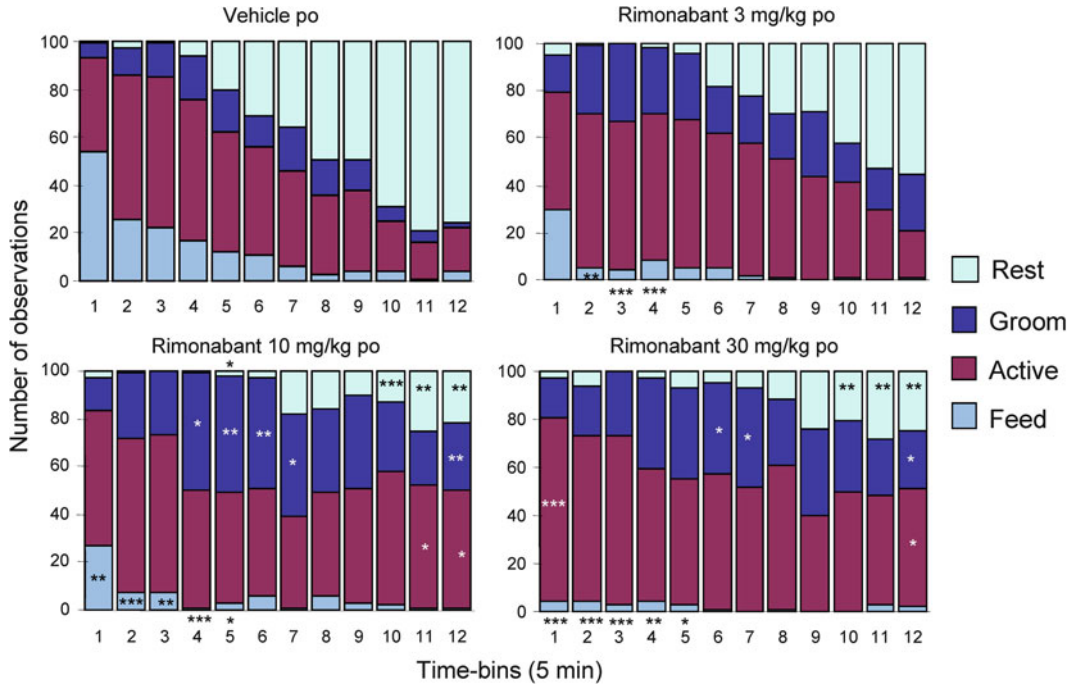

Fig. 8. Behavioral satiety profiling in mice. The natural satiety sequence is feeding following by activity, grooming and resting (control animals). Behavioral observations (twice a min in 5 min time-bins for 1 h) show that the decreased feeding produced by the CB_1 receptor antagonist, rimonabant, at doses of 10 and 30 mg/kg po, may reflect response competition from increased grooming and activity rather than a specific reduction in food intake. Data obtained using similar methods to those described in Table 6. Data analyzed by analysis of variance followed by Dunnett's test, $n=10$. Significant differences from the vehicle-treated control group are denoted by $^{*}p<0.05$, $^{**}p<0.01$ and $^{***}p<0.001$. Data held on file at RenaSci Ltd.

to nausea and malaise (15). However, they can be used in conjunction with the results of behavioral satiety sequencing or other observations made during the study to assess whether drug-induced decreases in food intake are likely to be specific. For example, the persistent appearance of paper bedding in the feces following repeated treatment could indicate that the animals were eating the paper in an attempt to relieve drug-induced gastrointestinal discomfort. This could be examined further by removing and examining the gastrointestinal tract and its contents at the end of the study. Stomach content weights can also be used to indicate whether drugs inhibit gastric motility.

The main endpoint in chronic feeding studies is a reduction in body weight but it is important to know how this has been achieved. Close examination of the time course of the body weight and food and water intake data can be used to assess whether the weight loss was due to reduced food intake. Furthermore, the relative contribution of reduced food intake to the overall weight loss can be assessed using pair-feeding studies in which a group of

vehicle-treated animals is given the same amount of food as eaten by the appropriate drug-treated group.

Compounds reducing body weight without decreasing food intake may be altering energy input indirectly, e.g., by preventing the absorption of fat by the intestine or the uptake of glucose by the kidney (32, 38). Alternatively, the drugs may produce weight loss by increasing energy output by producing non-specific increases in physical activity or by increasing basal metabolic rate and/or thermogenesis. Changes in activity can be examined using automated activity boxes, whereas the effects of drugs on basal metabolic rate and thermogenesis can be measured using closed circuit calorimeters (indirect calorimetry). This specialized technique typically involves placing animals in individual sealed chambers at thermoneutral temperature and measuring their resting oxygen consumption. For example, the anti-obesity drug, sibutramine, has been shown to produce thermogenesis in both animals (39, 40) and man (41) confirming that rodents can be used to explore both parts of the energy balance equation. The thermogenic effects of sibutramine are thought to be due to selective activation of brown adipose tissue. It was originally believed that only vestigial amounts of brown adipose tissue were present in human adults; however, recent findings indicating that it is more common than previously appreciated, have led to increased interest in modulating energy expenditure as a new target for the treatment of obesity (42).

Measurement of water intake and examination of the cage pads below each cage each day can also help in interpretation of the results of feeding studies. Drugs producing marked, persistent reductions in daily water intake are likely to produce loss of condition, whereas increased drinking can be secondary to diuresis/diarrhoea or increased activation. Body composition analysis of the carcasses at the end of chronic studies can be used to investigate the effects of drugs on water content. Clinically acceptable anti-obesity agents would be expected to produce a selective reduction in body fat without loss of water (dehydration) or protein (muscle wasting or cachexia).

4. Conclusions

This article describes the use of mice and rats to evaluate the anti-obesity actions of novel compounds. These models can be used to assess whether drugs are likely to reduce food intake and body weight in the clinic and even to predict the degree of weight loss achievable compared to drugs which have been previously tested in man (15, 27). They are ideally suited for measuring the ability

of combinations of different drugs to reduce body weight—an approach which is becoming increasingly popular in an attempt to improve efficacy (9). The requirements of regulatory authorities regarding the development of novel anti-obesity drugs are extremely strict. In addition to producing weight loss by selectively reducing visceral adiposity, the drugs should be able to improve obesity-related comorbid conditions such as type 2 diabetes, hyperlipidaemia, and hypertension. The fact that dietary-induced obese rodents display similar metabolic disturbances to human obesity and are hypertensive means that they can also be used to examine the effects of drugs on cardio-metabolic risk factors (15, 27). Chronic feeding studies in dietary-induced obese rats and mice can easily be used for this purpose as the effects of drugs on glycaemic control can be determined by performing oral glucose tolerance tests and/or taking blood samples for plasma analysis of metabolic parameters at key points during the study. It is also relatively easy to measure blood pressure in rodents using a tail-cuff method. Novel rodent models for investigating obesity-related human conditions such as cancer and sleep apnea are still being established (20). Finally, it should be remembered that despite the advantages in using rodents to evaluate the efficacy of novel anti-obesity drugs, safety issues are less easy to predict from the animal data and there is no real substitute to progressing promising drug candidates rapidly into clinical trials so that they can be thoroughly assessed in man.

5. Screening Strategy

Following in vitro and ex vivo screens to confirm the activity and selectivity of the drug at its pharmacological target, an ideal screening strategy for a novel anti-obesity agent would involve testing the compound in both mice and rats and include studies in both male and female animals as shown in Fig. 9.

6. Notes

1. Good data are obtained using animals within a small body weight range (and of similar age) at the start of the experiment. In studies which involve habituating animals to high-fat or cafeteria diet for several months, it is worth including a few spare animals so that body weight outliers can be excluded before the start of drug treatment.

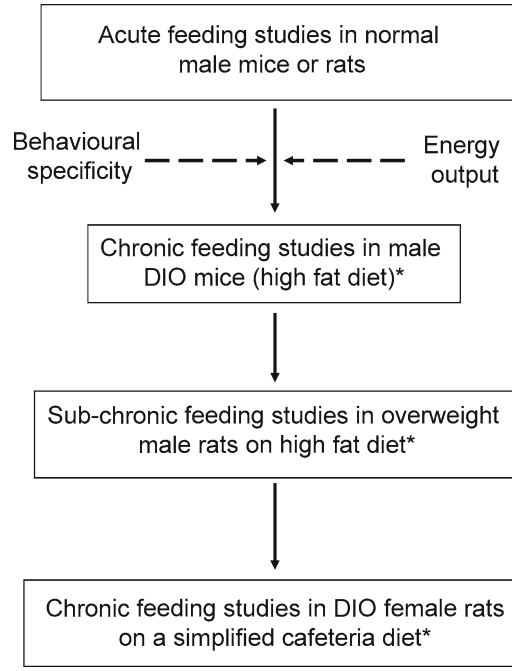

Fig. 9. Example of a screening strategy for a typical anti-obesity agent. The exact assays included in the screening strategy and the order in which the studies are conducted will depend, to some extent, on the known mode of action of the drug. *Sub-chronic and chronic studies in overweight or dietary-induced obese (DIO) animals may include examination of the effects of drugs on other relevant parameters such as glycaemic control, plasma lipids, blood pressure, fat pad weights and body composition analysis.

2. The feeding patterns of animals can easily be disrupted; therefore, all experimental conditions should be standardized and the animals should be disturbed as little as possible while studies are in progress. It is particularly important to prevent exposure to light in animals on reverse-phase lighting and to ensure that temperature and humidity are kept as constant as possible as temperature can effect food intake and body weight if the animals have to expend more energy to keep warm and humidity can alter water intake. Animals also need to be handled regularly, ideally by the same experimenter and given vehicle via appropriate routes during baseline/run-in periods to acclimatize them to the dosing procedures. Animals should also be weighed and food and water intake measured during baseline to accustom them to the methods involved and provide data that can be used to allocate the animals into balanced groups before the start of drug treatment. This data can also be used as covariate in the statistic analysis so that mean values are adjusted for differences between the treatment groups at baseline.

3. Daily and diurnal variation in food intake can occur therefore the food intake of all vehicle and drug-treated animals should be measured at the same time and on the same day. Care should be taken to ensure that the placement of animals in the rack of cages (which can influence environmental conditions such as light levels and the degree of disturbance when the laboratory door is opened) is standardized across the different treatment groups. One animal from each group should be dosed in turn to control for small differences in the time of dosing.

References

1. World Health Organisation (2011) Obesity and overweight: Fact sheet No 311. http://www.who.int/mediacentre/factsheets/fs311/en/index.html. Mar 2011
2. Wu T, Gao X, Chen M, van Dam RM (2009) Long term effectiveness of diet-plus-exercise interventions vs. diet-only interventions for weight-loss: a meta-analysis. Obes Rev 10(3):313–323
3. Dayyeh BK, Thompson CC (2011) Obesity and bariatrics for the endoscopist: new techniques. Therap Adv Gastroenterol 4(6):433–442
4. Dixon JB, Zimmet P, Alberti KG, Rubino F (2011) Bariatric surgery: an IDF statement for obese Type 2 diabetes. Arq Bras Endocrinol Metabol 55(6):367–382
5. Zac-Varghese S, Tan T, Bloom SR (2010) Hormonal interactions between gut and brain. Discov Med 10(55):543–552
6. Vickers SP, Cheetham SC (2007) Preclinical developments in anti-obesity drugs. In: Kirkham T, Cooper S (eds) Appetite and body weight: integrative systems and the development of anti-obesity drugs. Academic Press, Burlington, MA, pp 323–336
7. Sargent BJ, Moore NA (2009) New central targets for the treatment of obesity. Br J Clin Pharmacol 68(6):852–860
8. Valentino MA, Lin JE, Waldman SA (2010) Central and peripheral molecular targets for anti-obesity pharmacotherapy. Clin Pharmacol Ther 87(6):652–662
9. Kennett GA, Clifton PG (2010) New approaches to the pharmacological treatment of obesity: can they break through the efficacy barrier? Pharmacol Biochem Behav 97:63–83
10. EMEA (2010) European Medicines Agency recommends suspension of marketing authorisation for sibutramine. http://www.ema.europa.eu/ema/index.jsp?curl=pages/news_and_events/news/2010/01/news_detail_000985.jsp
11. EMEA (2008) The European Medicines Agency recommends suspension of the marketing authorisation of Acomplia. htttp://www.ema.europa.eu/ema/index.jsp?curl=pages/news_and_events/news/2009/11/news_detail_000244.jsp&murl=menus/news_and_events/news_and_events.jsp&mid=WC0b01ac058004d5c1
12. Hirst WD, Abrahamsen B, Blaney FE, Calver AR, Aloj L, Price GW, Medhurst AD (2003) Differences in the central nervous system distribution and pharmacology of the mouse 5-hydroxytryptamine-6 receptor compared with rat and human receptors investigated by radioligand binding, site-directed mutagenesis, and molecular modelling. Mol Pharmacol 64(6):1295–1308
13. Asarian L, Geary N (2006) Modulation of appetite by gonadal steroid hormones. Philos Trans R Soc Lond B Biol Sci 361(1471):1251–1263
14. Woods SC, Gotoh K, Clegg DJ (2003) Gender differences in the control of energy homeostasis. Exp Biol Med 228:1175–1180
15. Vickers SP, Jackson HC, Cheetham SC (2011) The utility of animal models to evaluate novel anti-obesity agents. Br J Pharmacol 164:1248–1262
16. Vickers SP, Sills S, Dickinson K, Gregory PC, Antel J, Cheetham SC (2005) Comparison of the effects of rimonabant, sibutramine and orlistat on acute food intake and in a model of dietary induced obesity in the mouse. Program No. 532.12. 2005 Neuroscience Meeting Planner, Washington, DC: Society for Neuroscience, Online
17. Jackson HC, Needham AM, Hutchins LJ, Mazurkiewicz SE, Heal DJ (1997) Comparison of the effects of sibutramine and other monoamine reuptake inhibitors on food intake in the rat. Br J Pharmacol 121:1758–1762
18. Kennedy AJ, Ellacott KLJ, King VL, Hasty AH (2010) Mouse models of the metabolic syndrome. Dis Model Mech 3:156–166

19. Panchal SK, Brown L (2011) Rodent models for metabolic syndrome research. J Biomed Biotech. doi: 10.1155/2011/351982
20. Kanasaki K, Koya D (2011) Biology of obesity: lessons from animal models of obesity. doi: 10.1155/2011/197636
21. Farooqi IS, O'Rahilly S (2009) Leptin: a pivotal regulator of human energy homeostasis. Am J Clin Nutr 89:980S–984S
22. Ramachandrappa S, Farooqi IS (2011) Genetic approaches to understanding human obesity. J Clin Invest 121(6):2080–2086
23. Correia ML, Haynes WG (2007) Lessons from leptin's molecular biology: potential therapeutic actions of recombinant leptin and leptin-related compounds. Mini Rev Med Chem 7:31–38
24. Li S, Zhang HY, Hu CC, Lawrence F, Gallagher KE, Surapaneni A, Estrem ST, Calley JN, Varga G, Dow ER, Chen Y (2008) Assessment of diet-induced obese rats as an obesity model by comparative functional genomics. Obesity 16(4):811–818
25. Coskun T, Chen Y, Sindelar D, Heiman M (2007) Animal models to study obesity and type 2 diabetes induced by diet. In: Shafrir E (ed) Animals models of diabetes: frontiers in research, 2nd edn. CRC, Boca Raton, FL, pp 349–357
26. Goor R, Hosking JD, Dennis BH, Graves KL, Waldman GT, Haynes SG (1985) Nutrient intakes among selected North American populations in the Lipid Research Clinic Prevalence Study; composition of fat intake. Am J Clin Nutr 41:299–311
27. Heal DJ, Gosden J, Smith SL (2011) The 5-HT_6 receptor as a target for developing anti-obesity drugs. In: Borsini F (ed) International review of neurobiology, vol 96, Pharmacology of 5-HT_6 receptors, Part II. Academic, Oxford, pp 73–109
28. Henderson AJ, Isherwood ML, Guzzo PR, Moore N, Luche M, Khmelnitsky Y, Rowley H, Viggers J, Cheetham S, Wierschke J (2011) Identification of the 5-HT6 antagonist AMR-SIX-1 for the treatment of obesity. Abstract No. 212. Keystone Symposium, Obesity, Keystone, 12–17 Jan 2011
29. Cheetham SC, Dickinson K, Goddard S, Guzzo P, Surman M, Tiong S, Xie D, Vickers S (2008) Effect of the MCH_1 antagonist, GW803430, on body weight, food and water intake, glucose tolerance, fat pad weight, *ex vivo* binding and various plasma parameters in dietary-induced obese C57BL/6J mice. Program No. 584.24. 2008 Neuroscience Meeting Planner, Washington, DC: Society for Neuroscience, Online
30. Kelly T, Yang W, Chen CS, Reynolds K, He J (2008) Global burden of obesity in 2005 and projections to 2030. Int J Obesity 32(9):1431–1437
31. Dickinson K, North TJ, Anthony DM, Jones RB, Heal DJ (1998) Evaluation of a simplified cafeteria model for the induction of insulin resistant obesity in rats. Int J Obesity 22(Suppl 3):S179
32. Jackson HC, Dickinson K, Jones RB, Schumacher C, Jensen C (2004) Comparison of the effects of sibutramine and orlistat on body weight, food and water intake and body composition in dietary-induced obese rats. Program No. 75.3. 2004 Neuroscience Meeting Planner, San Diego, CA: Society for Neuroscience, Online
33. Jackson HC, Cheetham SC, Dickinson K, Jones RB, Heal DJ, Gregory P, Antel J, McCreary A (2005) Comparison of the effects of rimonabant and sibutramine in a rat model of dietary-induced obesity. Program No. 532.13. 2005 Neuroscience Meeting Planner, Washington, DC: Society for Neuroscience, Online
34. Jackson HC, Cheetham SC, Gregory PC, Antel J (2007) Effect of chronic administration of topiramate and phentermine, alone and in combination, in an animal model of dietary-induced obesity. Program No 629.15. 2007 Neuroscience Meeting Planner, San Diego, CA: Society for Neuroscience, Online
35. Rodgers RJ, Holch P, Tallett AJ (2010) Behavioural satiety sequence (BSS): separating wheat from chaff in the behavioural pharmacology of appetite. Pharmacol Biochem Behav 97(1):3–14
36. Jackson HC, Pleasance IM, Mitchell JM, Heal DJ (2000) Observational analysis of the effects of sibutramine, phentermine and aminorex on food intake in rats. Obes Res 8(Suppl 1):95S
37. Tallett AJ, Blundell JE, Rodgers RJ (2007) Grooming, scratching and feeding: role of response competition in acute anorectic response to rimonabant in male rats. Psychopharmacology 195(1):27–39
38. Grempler R, Thomas L, Klein T, Mark M, Jackson H, Cheetham S, Eickelmann P (2010) Weight loss induced by the potent and selective SGLT-2 inhibitor, BI 10773, is due to body fat reduction: Studies in dietary-induced obese rats. Poster No: 1793-P, American Diabetes Association 70th Scientific Sessions, Orlando, FL, 25–29 June 2010, Online
39. Connoley IP, Liu YL, Frost I, Reckless IP, Heal DJ, Stock MJ (1999) Thermogenic effects of sibutramine and its metabolites. Br J Pharmacol 126(6):1487–1495

40. Skill MJ, Dickinson K, Jones RB, Heal DJ (2000) Thermogenic effect of repeated sibutramine treatment in female Wistar rats. Int J Obesity 24(Suppl 1):S135
41. Saraç F, Pehlivan M, Celebi G, Saygili F, Yilmaz C, Kabalak T (2006) Effects of sibutramine on thermogenesis in obese patients assessed via immersion calorimetry. Adv Ther 23(6):1016–1029
42. Stephens M, Ludgate M, Rees DA (2011) Brown fat and obesity: the next big thing? Clin Endocrinol 74(6):661–670

Part V

TRPs: Colitis, Cancer, Thermosensation, and Musculoskeletal Disorders

Chapter 23

Experimental Colitis Models

Patrick A. Hughes, Stuart M. Brierley, Joel Castro, Andrea M. Harrington, and L. Ashley Blackshaw

Abstract

Inflammatory Bowel Diseases (IBD) are life-threatening chronic and relapsing disorders of the immune system affecting the lower gastrointestinal tract. Despite the considerable efforts of many researchers, much remains to be learnt of their causes and appropriate treatment options. Crohn's disease and ulcerative colitis comprise the majority of clinical IBD cases but differ considerably in terms of clinical representation and likely underlying mechanisms. As such, different animal models have been developed over the last 20 years to best characterize these diseases. It is widely accepted that DSS-induced colitis models ulcerative colitis, while TNBS induced colitis models Crohn's disease. More recently, these models have been extended to investigate the mechanisms underlying the reciprocal regulation of the neuro-immune axis, both in times of acute inflammation and post-inflammation, with the latter modeling aspects of Irritable Bowel Syndrome. We describe the methodology involved in setting up, maintenance and evaluation of these two models of colitis, both of which are simply and economically achieved in a standard laboratory environment.

Key words: Inflammatory Bowel Disease, Irritable Bowel Syndrome, TNBS, DSS, Inflammation, Sensory nerves

1. Introduction

Inflammatory Bowel Diseases (IBD), incorporating Crohn's disease and ulcerative colitis, are chronic relapsing inflammatory conditions with an as-yet undetermined etiology. While some aspects of the clinical characteristics are shared, there are important differences and it is most likely that the underlying mechanisms differ significantly (1, 2). Ulcerative colitis is restricted to the colorectum, and while Crohn's disease may affect any part of the gastrointestinal tract it is generally restricted to distal regions such as the terminal ileum, cecum, colon and peri-anal region. The nature

Arpad Szallasi and Tamás Bíró (eds.), *TRP Channels in Drug Discovery: Volume II*, Methods in Pharmacology and Toxicology,
DOI 10.1007/978-1-62703-095-3_23,

of the damage caused also differs, with ulcerative colitis resulting in a superficial inflammatory response typically restricted to the mucosal layer, while a dense transmural inflammatory infiltrate is observed in Crohn's disease. Further, the pattern of cytokines involved is also different with Crohn's disease typifying a Th1/Th17 mediated disease, while ulcerative colitis demonstrates more of a Th2 phenotype with the caveat that increases in interleukin (IL)-4, the signature Th2 interleukin, are not observed (1, 3). Inflammation or infection may also play a role in the etiology of Functional Gastrointestinal Diseases such as Irritable Bowel Syndrome (4, 5). By definition, the gross anatomy of patients with functional illness is unremarkable, a clear differential from IBD patients; however, a strong correlation exists between sufferers of these diseases and prior gastrointestinal infection (6).

Animal models of colitis have been used for decades to investigate the initiation and maintenance of the immunological aspects of these diseases (7–9). More recently, these models have been used to investigate the effects of inflammation on the nervous supply of the gastrointestinal tract, incorporating the enteric, sensory and descending sympathetic nervous systems both in active inflammation and in post-inflammatory states (4, 10–17). Trinitrobenzene sulfonic acid (TNBS) and Dextran sodium sulfate (DSS) are two of the most commonly used agents used to induce colonic inflammation. Both are relatively simple and economical to develop in a standard laboratory, and both result in a wasting type disease with the associated clinical signs of weight loss, diarrhea, and bloody stools. Importantly, these models are relatively instantaneous and display aspects of dose-dependency making it possible to induce either a strong non-recoverable colitis, or a mild colitis from which the animal makes a full recovery from the clinical aspects. This is a marked difference from genetic models of IBD, which are rarely observed in the human population. While both models have provided insights into the pathogenesis of IBD, much remains to be determined concerning the mechanisms underlying the colitis induced by these models and by IBD in humans.

The TNBS model of colitis has been used to investigate colonic inflammation since the late 1980s (8). TNBS is a haptenizing substance; it does not cause an inflammatory response on its own right, but instead binds microbiotal or autologous proteins and inflammatory responses are then generated against the bound complex. TNBS is typically delivered intra-rectally with ethanol which acts to breakdown the mucosal barrier. Rectal instillation of TNBS typically results in a type I inflammatory (Th1 predominant) response with increased levels of the cytokines IL-12, IFN-γ and TNF-α amongst others (10). Histological features include ulceration, goblet cell destruction, edema and transmural infiltration of the colonic wall. As such, it is generally regarded as modeling aspects of Crohn's diseases. With a mild TNBS colitis these features

are most apparent 2–3 days following treatment after which the animal starts to recover. This recoverable model of TNBS-induced colitis is the best characterized model of post-inflammatory visceral hypersensitivity, whereby extrinsic sensory nerves are sensitized to colonic distension long after the histological resolution of the inflammatory damage (11–13). Marked differences in the susceptibility of animals to TNBS-induced colitis, which are apparent even within strains of the same species, make it essential to perform pilot dose–response experiments prior to the commencement of *bona fide* studies. It is therefore important to note the level of inflammatory damage rather than the dose of TNBS or percentage of ethanol used when comparing data between different groups.

The DSS model of colitis was developed around the same time as the initial reports of the TNBS model, but differs in delivery method and type of inflammatory reaction caused. DSS with a molecular weight of between 36,000 and 50,000 is dissolved in water to make a 2% solution, which the animals then drink in weekly cycles alternating with water. DSS is thought to be directly toxic rather than a hapten, acting to disrupt the epithelial barrier and therefore increase access of pathogens to the colon wall. Histologically, this model has more in common with ulcerative colitis, with damage restricted to the superficial mucosal layer. However, the cytokine pattern is more complicated, with an initial Th1/Th17 mediated response that switches to a Th2 phenotype in chronic models (18). The effects on gastrointestinal nerves also differ from TNBS, with marked changes in sensitivity to chemical stimuli such as serotonin but no reported alterations in visceral sensitivity in either acute or post-inflammatory DSS models (14, 15).

Described below is the specific equipment used in our laboratory to induce an acute TNBS colitis in C57BL/6 mice and DSS colitis in Sprague–Dawley rats. In our hands, treated animals make a full clinical recovery from the colitis in both models, with low mortality. However, it should be noted that C57BL/6 mice are relatively less susceptible to colitis. This equipment can easily be substituted with that of comparable quality/capability and scaled up in the case of larger animals. If a more severe or chronic colitis model is required, the dose of TNBS can be increased or the number of cycles of DSS drinking water can be increased.

2. Materials

2.1. Equipment

1. Animal cages + Wire racks for fasting.
2. Bottles of 5% glucose solution in water.
3. Anesthetic—inhalant preferred, i.e., isoflurane vaporizer (Cyprane—Gas Control Services, SA, Australia). If using

inhalant, an induction box and enough tubing to connect vaporizer to induction box and a 50 mL syringe are required.

4. Animal care scoring sheet.
5. Scoring sheet for scoring histology.
6. Perfusion pump (Masterflex, John Morris Scientific, NSW, Australia) for trans-cardial perfusion.

2.2. Reagents

1. Clear vinyl tubing (PVC) inner diameter 0.75 mm, outer diameter 1.45 (Dural Plastics and Engineering, NSW, Australia).
2. Blunt plastic cannula (BD, NJ, USA).
3. Tetrahydrofuran (THF) (BDH Chemicals, VWR Chemicals, IL, USA).
4. TNBS (2,4,6 Trinitrobenzenesulfonic acid) (also called picrylsulfonic acid (Sigma-Aldrich NSW, Australia)) (Note 1).
5. Hamilton syringe if injecting TNBS into the lumen (Hamilton, NV, USA).
6. DSS (dextran sodium sulfate), molecular weight 40,000 (ICN Biochemicals, OH, USA).
7. Isofluorane (Delvet, NSW, Australia).
8. Surgical lubricant.
9. Formalin or 4% phosphate-buffered paraformaldehyde (pH 7.5).
10. Paraffin embedding equipment.

3. Methods

3.1. TNBS Colitis Model

3.1.1. Cannula Production

The below protocol is optimized for C57BL/6 mice. The cannulae are made for rectal enema of TNBS and are thin enough to fit into the colon and long enough to flood the descending colon to rectum. Cannula are robust enough for multiple use; however, spares should be kept on standby should a cannula fail during experimentation. We generally make ten cannulae at any one time, expecting that a number of them will fail testing due to leaks.

1. Cut enough 10 cm lengths of PVC tubing to make the number of cannula required, plus 30% more for cannula failure.
2. Chop small pieces of PVC tubing into a beaker containing tetrahydrofuran (THF) to make a slurry.
3. Dip one end of each cannula into the slurry to seal it and let it set. Care should be taken to make sure this seal is no wider than the tubing used, and only the end of the tubing is sealed. We typically let cannula seal overnight.

4. Once the cannula is sealed, leak holes can be made. Using a thin metal stent (or equivalent) pierce through both sides of the cannula wall starting 5 mm the bottom seal to create holes for TNBS to leak out. Repeat 5 mm above the first hole, and again 5 mm above that hole for a total of six holes.
5. Using a permanent marker, mark a line on the cannula 3 cm from the sealed end.
6. Attach a blunt plastic cannula attachment (BD) to the unsealed end of the cannula so that it can be fitted to a 1ml syringe.
7. Test each cannula with water to ensure there are no leaks, and the solution dribbles out of the horizontal holes. Discard cannula that fail (i.e., leak from cannula attachment, did not properly seal at bottom or seal is wider than cannula).

3.1.2. TNBS Administration

Rectal Enema

1. Fast mice overnight by lining bottom of cage with wire and removing food (Note 3). This ensures mice will not eat feces, and the colon will be empty. Provide 5% glucose drinking water. Record weight before fasting. We do not use mice if they weigh 20 g or less after fasting, as they are unlikely to recover from TNBS insult.
2. Ready anesthetic requirements. If using inhalant anesthetic, ensure tubing is fitted that will be able to deliver anesthetic to a 50 mL syringe.
3. In the morning of the experiment, make the desired amount of TNBS/ethanol/water mixture and mix well so that TNBS is soluble. Vortex if necessary. TNBS is toxic, and safety equipment should be used at all times when using it.
4. Load a 1 mL syringe with enough TNBS mixture to treat each mouse with 0.1 mL. Attach cannula and remove dead space.
5. Induce anesthesia. We use an induction box with 5% isoflurane, 2% oxygen. Once the mouse is fully anesthetized lower anesthetic to 1.5% for maintenance.
6. Place animal head down into a 50 mL syringe or equivalent that receives anesthetic so that its lower trunk is accessible while it remains anesthetized.
7. Lubricate the end of the cannula and slowly insert it into the rectum. Slowly advance the cannula until it is 3 cm past the mouse anus. Take care not to puncture the colon wall. Some residual feces may remain in the colon even though the mouse has been fasted overnight, which may make it difficult to move the whole 3 cm. If so stop advancing and take note of distance advanced.
8. Very slowly inject 100 μL of TNBS solution into the mouse. The TNBS should leak out of the holes on the side of the

cannula, and care should be taken to inject slowly so that TNBS does not shoot past the targeted area.

9. Once finished, remove cannula and hold mouse vertically upside down for 1 min to allow uniform mixing before placing back in it in its cage and monitor until anesthetic wears off and mouse is ambulatory.
10. Take note of the weight of the mouse, house individually and place cage on a heat pad. Provide the mouse with 5% glucose drinking water for 4–5 days or until it shows signs of recovery from inflammation as indicated by reduced clinical record scores.
11. Control mice should receive the same volume and percentage of ethanol.

Luminal Injection

This method of delivery has been used in mice, rats and guinea pigs to investigate regeneration of epithelia, effects of inflammation on enteric neurons and visceral hypersensitivity (16–19).

1. Sterilize all instruments before use.
2. Induce anesthesia as above.
3. Once anesthetized, place the animal on back and tape arms and legs, so that the peritoneal cavity is accessible.
4. Shave lower trunk and wipe with ethanol to sterilize area.
5. Using a large scalpel blade, slice through skin in one quick movement. A clean single slice is preferred for neater stitching.
6. Open peritoneal cavity longitudinally with fine scissors, preferably along the same line as the cut through the skin. The abdominal cavity is now open and intestines should be visible.
7. Locate area of lower gastrointestinal tract of interest. If intestines need to be moved, care should be taken and moist (saline) q-tips used. Once area of interest is located, inject TNBS mixture into the lumen using a needle gauge appropriate for the animal used.
8. Remove needle, move intestines back to original position and stitch. We prefer stitching the inner peritoneal cavity separately to the skin. Stitching in two layers provides some protection against the mouse opening the peritoneal cavity should a stitch open in its skin.
9. Sterilize outer area with iodine solution/alcohol solution.
10. Remove anesthetic and allow mouse to recover.
11. Give pain relief as required (i.e., butorphenol). If using an opioid, ensure the anesthetic is worn off before giving it to prevent respiratory failure.

12. Weigh the animal and place in cage on a heat pad with free access to 5% glucose drinking water and soaked food for 4–5 days or until it shows signs of recovery from inflammation.
13. Control animal should have surgery and be injected with same percentage of ethanol.

3.2. DSS Colitis Model

The below protocol is optimized Sprague–Dawley rats.

1. Weigh rat.
2. Add DSS to drinking water (we use 2% w/v). We use a 7-day cycle of DSS drinking water to induce colitis. Change the DSS solution every 2 days. To induce a chronic colitis with this model follow the above cycle with normal water for 2 weeks, and repeat DSS cycle again.
3. Control rats will be housed in the same fashion with access to clean drinking water.
4. Monitor the rat's health at least once per day for clinical signs of inflammation.

3.3. Animal Care

1. Animals should have access to 5% glucose solution and soaked food, and should be placed on a heat pad until signs of clinical recovery. In our hands, this takes 4–6 days with TNBS.
2. Animals should be clinically scored at least twice daily from the initial dose. We have a clinical scoring sheet whereby a score of 0 or 1 is given for the following:
   (a) Dull/ruffled coat
   (b) Reluctance to move
   (c) Reduced food intake
   (d) Diarrhea
   (e) Blood in feces
   (f) Weight loss
3. With TNBS-treated mice, once they are putting on weight the glucose solution can be replaced with normal water, soaked food replaced with dry food and the heat pad removed.
4. The animal is now able to be left until the appropriate time for experiments. We have developed both "acute" and "recovery" models of TNBS and DSS whereby we use a 7-day period from the initial TNBS dose, or a 7-day cycle of DSS as "acute" cohort with residual inflammation present, and a 28-day post initial TNBS treatment or 21 days after 7-day DSS cycle as "recovery" cohort. Using these models, we have demonstrated that an acute inflammation occurs from which the animal makes a full histological recovery in both models, but only TNBS treatment induces long-term changes in the sensitivity of extrinsic afferent mechanical sensitivity.

3.4. Scoring of Inflammation

3.4.1. Macroscopic Scoring

The colo-rectum does not have to be fixed for this assessment. At the required time, humanely kill the animal and remove colon. Cut colo-rectum from animal and score blindly using the following sheet:

Score	Observation
0 or 1	Absence or presence of diarrhea in three days previous
0 or 1	Absence or presence of stricture (abnormal narrowing)
0, 1 or 2	Absence or presence (mild or severe) of adhesions

Maximum score is 5.

Then cut colon longitudinally and pin flat under a light microscope (10× magnification).

Score	Observation
0	No damage
1	Hyperemia without ulcers
2	Hyperemia and bowel wall thickening without ulcers
3	One site of ulceration without bowel wall thickening
4	Two or more sites of ulceration or inflammation
5	0.5 cm of major damage
6–10	1 cm of major damage. Score is increased by 1 for every 0.5 cm of major damage to a maximum of 10

Maximum score is 13.

3.4.2. Histological Scoring

Histology is typically assessed using standard hematoxylin and eosin stains. Tissues are typically fixed with formalin, but paraformaldehyde fixation may also be used.

Formalin Fixation

1. Kill the animal with non-recoverable anesthetic or cervical dislocation.
2. Remove colon and gently flush contents out with ice-cold PBS using a 5 mL syringe.
3. Cut into 0.5 cm rings and immerse immediately in neutral buffered 10% formalin and incubate overnight at 4°C.
4. Embed in paraffin and cut 4–6 μm sections on a microtome.

Paraformaldehyde Fixation

1. Deeply anesthetize the animal with non-recoverable anesthetic and place on its back with hands and legs pinned.

2. Open peritoneal cavity below the lowest rib. Open chest by cutting ribs longitudinally along each side to expose the heart.
3. Pierce left ventricle with syringe attached via tubing to a pump that has pre-warmed saline running through it. Take care not to pierce the atrium, or damage other parts of the heart. The needle must stay in place for the entire fixation step.
4. The heart will rapidly begin to swell. Use fine scissors to snick the left atria so that blood can flow out.
5. Once all blood has been removed from the animal, replace saline solution with ice cold 4% paraformaldehyde.
6. A sign of good fixation is rigidity of the neck and movement of the legs inward or head upwards as nerves become fixed.
7. After about 3–5 min, remove fixative filled syringe and place the animal on a dissecting pad.
8. Cut peritoneal cavity longitudinally to expose colo-rectum and remove it.
9. Cut it into 0.5 cm rings.
10. Embed in paraffin, cut 4–6 μm from proximal and distal sections on a microtome and stain with hematoxylin and eosin.

Examine under a microscope (200× magnification) using the following scoring sheet. See Fig. 1 for examples of histological sections of healthy and inflamed colons.

Score	Observation
0, 1, 2, 3	Extent of destruction of normal mucosal architecture (normal, mild, moderate or extensive damage)
0, 1, 2, 3	Presence and degree of cellular infiltration (normal, mild, moderate or transmural inflammation)
0, 1, 2, 3	Extent of muscle thickening (normal, mild, moderate or extensive thickening)
0 or 1	Presence or absence of crypt abscesses
0 or 1	Presence or absence of goblet cell depletion

Maximum score is 11.

3.5. Expected Outcomes

Colitis induced by TNBS or DSS causes a wasting disease in the acute phase with associated clinical signs of weight loss and hunched posture and histological signs of inflammation. The protocols outlined above produce a mild colitis, from which the animal recovers with no readily observable clinical or histological signs of inflammation. However, increased concentrations result in a more severe colitis, from which the animals are unlikely to recover.

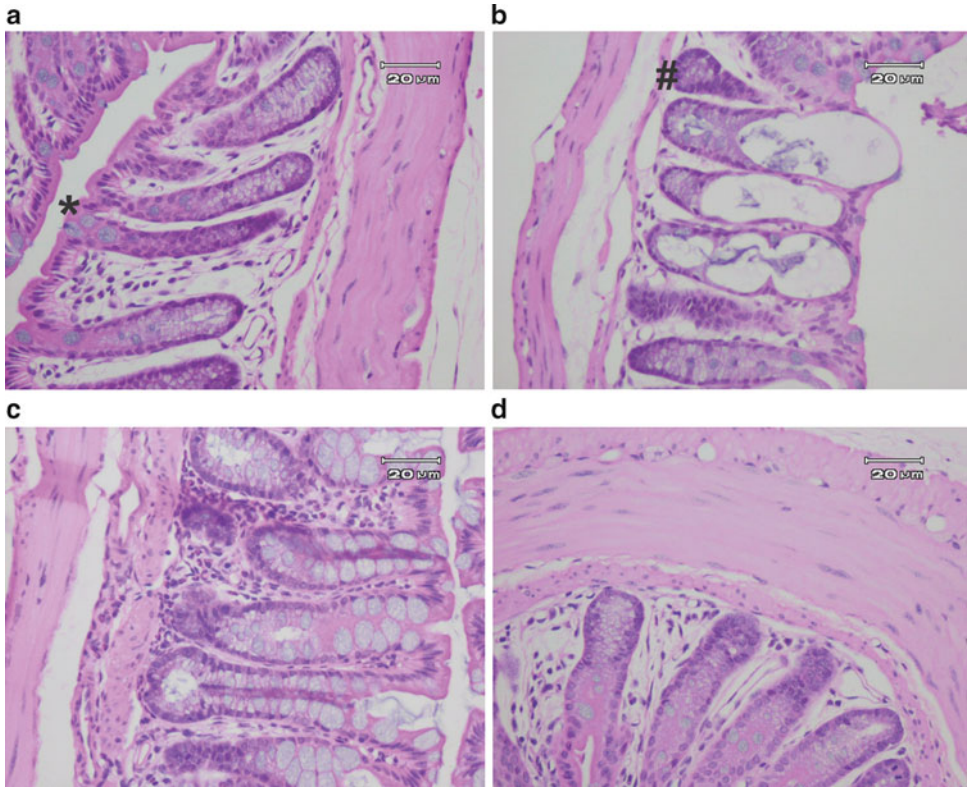

Fig. 1. Hematoxylin and eosin stained sections of colon from healthy and colitic mice. (**a**) Typical section of mouse colon from a healthy mouse. Note intact mucosa, thickness of muscle layer, degree of cellular infiltrate, lack of crypt abscess and number of goblet cells (indicated by *asterisk*). (**b**) Example of severe mucosal damage induced by TNBS colitis. Crypt abscess labeled by *hash*. (**c**) Example of increased inflammatory infiltrate. Note transmural invasion by infiltrate. (**d**) Example of increased muscle thickening.

4. Notes

1. TNBS is toxic and highly volatile and the appropriate safety equipment should be used. TNBS is light sensitive and volatile at room temperature and should be stored in a dark environment, and only enough quantities for daily use should be made at any one time.
2. There are significant sources of variation inherent in these models which can greatly affect the outcomes. The steps taken to minimize this variation are listed below:
   (a) Variation between different batches of TNBS. Buy in bulk, aliquot and store at −20°C.

(b) Variation in susceptibility of animals, particularly with TNBS, both between species but also within species and between strains of the same species.

(c) TNBS has a narrow pharmacological window for the induction of mild colitis from which the animal recovers, whereby a low concentration has no effect, while a high concentration results in a non-recoverable colitis.

(d) Ethanol is used to disrupt the mucosal barrier so that the TNBS can not only access the colon wall, but can also cause an inflammatory reaction if used excessively. The amount of ethanol used should be minimized to ensure barrier disruption only, and not colitis in its own right. We have found 30% is optimal in our mice.

(e) The weight of the mouse also influences the observed effects. In our hands, mice with a post-fasting weight of less than 20 g do not recover well and should not be used.

(f) Pilot dose–response experiments are therefore essential for new users, or users moving within strains of mouse, with the appropriate vehicle control sham experiments. A minimum of five animals should be used for each dose.

(g) Clinical scoring is subjective, and new users should be trained by someone experienced with animal handling. In the above TNBS protocols, the mouse is likely to score between 2 and 4 on the clinical record sheets 2–3 days after TNBS is instilled, but should start to make a recovery by day 4. We have minimal deaths using the above concentration in our strain of C57/Bl6 mice.

(h) The rectal enema method of TNBS instillation is relatively simple, and should take under 5 min per animal. Only light anesthesia is required, and the time spent under the anesthetic should be minimized to reduce variability. An inhalant anesthetic such as isoflurane is preferred, dosing is easily adjusted and recovery is rapid.

(i) Ensure the entire TNBS solution remains in the colon. This is achieved by slowly injecting, and holding the mouse upside down by the tail for 1 min.

(j) Macroscopic and histological scoring should be performed blindly, preferably by someone experienced in colon pathology, across multiple sections of the colon, including proximal, mid and distal regions. A user is unlikely to see all the signs of inflammation in one or two sections, and therefore multiple sections (at least 20) should be scored and averaged.

3. Wire racks are used for fasting to ensure animals cannot eat their droppings when fasting.

Acknowledgments

Supported by National Health and Medical Research Council of Australia (NHMRC) grant number 626960 and NHMRC Australian Biomedical Research Fellowships (P.A.H and S.M.B) and a NHMRC Principal Research Fellowship (L.A.B).

References

1. Bouma G, Strober W (2003) The immunological and genetic basis of inflammatory bowel disease. Nat Rev Immunol 3(7):521–533
2. Xavier RJ, Podolsky DK (2007) Unravelling the pathogenesis of inflammatory bowel disease. Nature 448(7152):427–434
3. Strober W, Fuss IJ (2011) Proinflammatory cytokines in the pathogenesis of inflammatory bowel diseases. Gastroenterology 140(6): 1756–1767
4. Hughes PA, Brierley SM, Blackshaw LA (2009) Post-inflammatory modification of colonic afferent mechanosensitivity. Clin Exp Pharmacol Physiol 36(10):1034–1040
5. Ohman L, Simren M (2010) Pathogenesis of IBS: role of inflammation, immunity and neuroimmune interactions. Nat Rev Gastroenterol Hepatol 7(3):163–173
6. Spiller R, Garsed K (2009) Postinfectious irritable bowel syndrome. Gastroenterology 136(6):1979–1988
7. Strober W, Fuss IJ, Blumberg RS (2002) The immunology of mucosal models of inflammation. Annu Rev Immunol 20:495–549
8. Morris GP et al (1989) Hapten-induced model of chronic inflammation and ulceration in the rat colon. Gastroenterology 96(3):795–803
9. Okayasu I et al (1990) A novel method in the induction of reliable experimental acute and chronic ulcerative colitis in mice. Gastroenterology 98(3):694–702
10. Alex P et al (2009) Distinct cytokine patterns identified from multiplex profiles of murine DSS and TNBS-induced colitis. Inflamm Bowel Dis 15(3):341–352
11. Gschossmann JM et al (2004) Long-term effects of transient chemically induced colitis on the visceromotor response to mechanical colorectal distension. Dig Dis Sci 49(1): 96–101
12. Hughes PA et al (2009) Post-inflammatory colonic afferent sensitisation: different subtypes, different pathways and different time courses. Gut 58(10):1333–1341
13. Brierley SM et al (2009) The ion channel TRPA1 is required for normal mechanosensation and is modulated by algesic stimuli. Gastroenterology 137(6):2084–2095 e3
14. Coldwell JR et al (2007) Increased responsiveness of rat colonic splanchnic afferents to 5-HT after inflammation and recovery. J Physiol 579(Pt 1):203–213
15. Larsson MH, Rapp L, Lindstrom E (2006) Effect of DSS-induced colitis on visceral sensitivity to colorectal distension in mice. Neurogastroenterol Motil 18(2):144–152
16. Ohashi K et al (2007) Colonic mast cell infiltration in rats with TNBS-induced visceral hypersensitivity. J Vet Med Sci 69(12): 1223–1228
17. Ohashi-Doi K et al (2010) A selective, high affinity 5-HT 2B receptor antagonist inhibits visceral hypersensitivity in rats. Neurogastroenterol Motil 22(2):e69–e76
18. Pontell L et al (2009) Structural changes in the epithelium of the small intestine and immune cell infiltration of enteric ganglia following acute mucosal damage and local inflammation. Virchows Arch 455(1):55–65
19. Nurgali K et al (2011) Morphological and functional changes in guinea-pig neurons projecting to the ileal mucosa at early stages after inflammatory damage. J Physiol 589(Pt 2): 325–339

Chapter 24

Tumor Xenograft Models to Study the Role of TRP Channels in Tumorigenesis

V'yacheslav Lehen'kyi, Sergii Khalimonchyk, Albin Pourtier, Maylis Raphaël, and Natalia Prevarskaya

Abstract

This chapter is devoted to the study of the role of TRP channels in tumorigenesis in vivo using a tumor xenograft model in immunodeficient mice. Either cancerous cells naturally expressing TRP channels, or TRP channel stably expressing cancerous or normal cells, could be injected into immunodeficient mice. After grafting cells may grow in mice and form the solid tumors which can be measured and photographed. On reaching the critical allowed size the tumors are excised and consequently mice have to be sacrificed. Once excised, the tumors are photographed, weighted, and volume is measured. In addition, tumors may be subjected to further analysis as immunocytochemistry, western-blotting, PCR, etc. To confirm the role of a particular channel on tumorigenesis in vivo, some tumors could alternatively be treated in vivo with TRP channel-specific siRNA. Hence, tumor xenograft model using immunodeficient mice represents a valuable tool for the study of the role of TRP channels in carcinogenesis in vivo.

Key words: TRP channels, Cancer, Protocol, Xenograft, Swiss nude mice

1. Introduction

The ability of cells to initiate and promote the development of a tumor is called tumorigenesis leading to a more general process called carcinogenesis (1). Tumorigenesis in humans is thought to be a multistep process where certain mutations confer a selective advantage, allowing lineages derived from the mutated cell to outcompete other cells. Although molecular cell biology has substantially advanced cancer research, our understanding of the evolutionary dynamics that govern tumorigenesis is still limited (2). The study of TRP-channel patho/physiology at a molecular level could contribute to highlight their role in early cancer.

Arpad Szallasi and Tamás Bíró (eds.), *TRP Channels in Drug Discovery: Volume II*, Methods in Pharmacology and Toxicology, DOI 10.1007/978-1-62703-095-3_24,

We and others established the role of some TRP channels in epithelial cell cancerigenesis and notably tumorigenesis (3–5). For instance, a role of TRPC6 channel has been demonstrated in the development of human glioma (6) and human esophageal cancer (7), a role of TRPC1 channel has been confirmed in human glioma tumorigenesis (8), as for TRPC3 in human ovarian cancer (9), TRPV2 in prostate cancer (10), and others. In all the above studies the role of TRP channels in tumorigenesis in vivo has been studied using a tumor xenograft model in immunodeficient mice. This approach allows to study the role of a particular TRP channel on the ability of tumor cells or stable clones overexpressing this channel to induce tumor formation in vivo.

Animal models are critical for the study of cancer molecular mechanisms and for the development of new antitumor agents. Immunodeficient mouse models are very useful models for immunology, infectious disease, stem cell biology, cancer, and other research (11). Nude mice are among the most commonly used animal models of immunodeficient mice. The discovery of nude athymic (nu/nu) mice that were T-cell-deficient (12), and later B-cell-deficient and T-cell-deficient severe combined immunodeficient (scid/scid) mice (13), allowed the routine and efficient transplantation and propagation of human tumor tissues (xenografts) in mice.

Although viability and fertility of nude mice are severely reduced, they can be improved under specific pathogen-free conditions. Homozygotes are naturally thymectomized animals, are hairless from birth and completely lack a thymus due to a failure of development of the thymic anlage. The thymic rudiment of homozygous nude mice fails to attract lymphoid cells but their lymphocytes are normal in their ability to populate implanted normal thymuses. The lack of the thymus leads to many defects of the immune system, including depletion of lymphocytes in thymus-dependent regions of lymph nodes and spleen, a greatly reduced population of lymphocytes composed almost entirely of B cells, very poor response to thymus-dependent antigens. Nude mice were proved useful tools for investigations of the role of the thymus in immune reactions (14), can easily accept xenografts and be used in tumorigenicity.

The relevance of each particular animal model depends on how close it replicates the histology, physiological effects, biochemical pathways, and metastatic pattern observed in the same human tumor type. Metastases are especially important because they are the main determinants of the clinical course of the disease and patient survival, and are the target of systemic therapy. Among existing models, orthotopic xenografts of human tumors, or tumor cell lines, in nude mice reproduce the histology and metastatic pattern of most human tumors especially at advanced stage. Despite the fact that orthotopic xenograft models are more promising

than the most commonly used subcutaneous xenografts in preclinical drug development, their capacity to predict clinical response to antitumor agents remains to be studied (15).

The studies of the role of TRP channels in tumorigenesis in vivo have been performed using a tumor xenograft model in immunodeficient mice as a mean for the study of the role of a particular TRP channel on the ability of tumor cells or stable clones overexpressing this channel to induce tumor formation in vivo.

In this chapter we describe how the role of a specific TRP channel can be monitored in vivo, and how its expression can be manipulated by siRNA injections along tumor development.

2. Materials

2.1. Equipment

The equipment needed for tumor xenograft models is precise and need a proper animal facility as close as possible to your laboratory, and where immunodeficient animals can be specifically housed (usually under suppression of air). Animals are maintained in cages covered with air filters at appropriate temperature, humidity, and a day/night cycle, and manipulated under sterile hood. The housing is highly restricted and subject to numerous policies and regulations, such as those from ethical and veterinary committees. The director of the study as each researcher should have specific skills/education and the legal authorization to work with immunodeficient/transgenic animals.

1. Immunodeficient mice 5–6 weeks old, males, of strains such as: swiss nude mice, RjOrl:SWISS (souris CD-1); mice NMRI, RjHan:NMRI; or Rj:NMRI-nu (nu/nu).
2. Sterile syringes 1 ml.
3. Needles of 20–23 G and 26 G in size.
4. Surgical instruments to excise tumors following euthanasia.

2.2. Reagents and Solutions

1 BD Matrigel™ Matrix Growth Factor Complete medium.

2 Standard sterile PBS solution.

3 Solutions for anesthesia: Ketamine (Verbac, France) 50 mg/ml, and Domitor (Janssen Cilag) 0.85 mg/ml. For 1 ml of sterile solution (filtered via 0.22 µm filter) take 0.2 ml of Ketamine solution, add Domitor 0.12 ml and 0.68 ml of saline solution (NaCl 0.9%).

4 Solution for anti-anesthesia: Antisedan (Atipamézole) 5 mg/ml. For 1 ml of sterile solution (filtered via 0.22 µm filter) take 0.1 ml of Antisedan and add 0.9 ml of saline solution (NaCl 0.9%).

5 Pentobarbital (stock solution 200 mg/ml kept at +4°C).

3. Methods

3.1. Preparation of Cells for Injection and Grafting Cells to Immunodeficient Mice

Before starting your experiments, it is strongly recommended to design a proper strategy to study the role of a particular TRP channel on tumorigenesis in vivo. In fact, you have to perform all necessary experiments in vitro prior to experiments in vivo. As an example, if your data in vitro show that your TRP channel is involved either in proliferation or apoptosis resistance, or in migration or invasion, then you can design your studies in vivo. As a general concept, the initial point is whether your channel of interest is expressed in your cell model or not (Scheme 1). If your channel is present in your cell model you can use them directly, and if they are able to create tumors you can use siRNA strategy to prove its role in tumorigenesis. Though you have to think over the appropriate controls before! If your channel is not present it is worth to create stable clones of this channel in your cell line, especially if your channel is known to be present in vivo and disappears during cell culture in vitro. In this case you have to be cautious while interpreting data with stable clones by using multiple clones with different levels of expression. Finally, if your clones give tumors in vivo, the use of a siRNA strategy could confirm the data you have obtained.

Once your cell model is ready together with the respective control (e.g., control clones for stable clones or the cell line which does not express your TRP channel), you can start grafting as below:

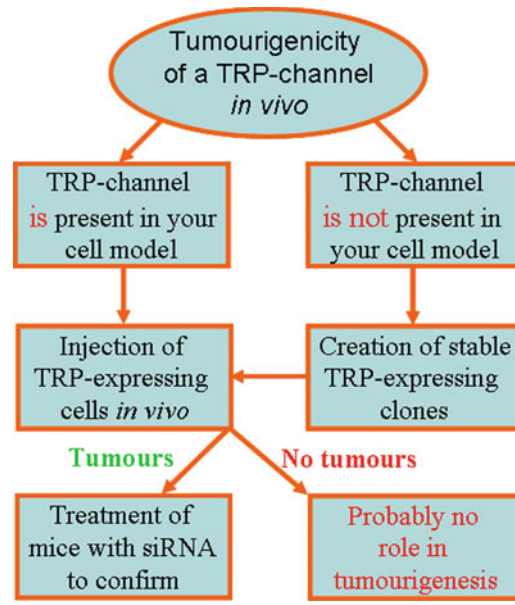

Scheme 1. The general concept of experiments in vivo to study the role of TRP channels in tumorigenesis.

1. Culture cell as usual taking into consideration that you will need 2×10^6 cells per mouse on the day of injections (Note 1).
2. Detach cells very gently using either with Trypsin-EDTA or PBS-EDTA solution. You will need to count the cells and to pellet them again to assure the required quantity of cells (2×10^6) per mouse in each tube.
3. Re-suspend the cells in 100 µl of PBS and transfer the suspension to 0.5 ml tubes containing one volume of Matrigel™ solution (Note 2), so that the total volume is 200 µl per mouse consisting of 1 to 1 v/v of PBS and Matrigel™ (Note 3). Mix thoroughly and leave on ice.
4. Perform anesthesia of mice intraperitoneally with e.g., mix of Ketamine and Domitor at the dose of 10 ml/kg (cf. preparation above) using 1 ml syringes and 26 G needles.
5. Do subcutaneous injections of cells preferably to the back right behind the neck (Note 4) using 1 ml syringes and, e.g., 21 G needles (Note 4 and 5). Use at least 6–10 animals per experimental condition to assure significant statistical data and mark each animal in the cage to easily recognize them (Note 6). Reserve animals for the PBS/Matrigel™ only injections to provide an additional control.
6. Inject Antisedan (Atipamézole) at the dose of 10 ml/kg (cf. preparation above) subcutaneously using 1 ml syringes and 26 G needles to wake up the animal to avoid morbidity due to hypothermia.

3.2. Measuring and Sacrificing Animals

Following injections, daily and careful examination of each animal should be performed. Depending on the cell type, and for the most aggressive cancer cells as PC3 or DU145 (for the prostate cancer) 2–3 weeks is enough to start seeing tumors on their back.

1. Measure tumors as soon as they are visible every 2–3 days using a ruler and avoid stressing much the animals (Note 7).
2. Weigh animals regularly and take pictures; an example is shown in Fig. 1 (Note 8).
3. As soon as one of the tumors within the experimental group reaches its maximal allowed size you have to sacrifice all animals in this group by administering 150 mg/kg of pentobarbital intraperitoneally using 1 ml syringes and 26 G needles.
4. Excise the tumors, document all data from each individually marked mouse. Photograph tumors, weight on the balances, and measure volume (Note 9).
5. Cut the tumors into pieces and freeze them for the further mRNA extraction, protein extraction, and/or put to formaline (3.75%) to further paraffinize them to be analyzed by immunohistochemistry.

Fig. 1. A photo depicting the standard daily procedure of tumor size measurements. You can see a cage placed in a hood where nude mice bearing tumors are measured. Black arrow points out a tumor situated at the back of the mouse.

3.3. siRNA Treatment of Tumors

It is preferable to know the dynamics of the tumor growth before starting experiments with siRNA treatment against TRP channel of interest. It is needed to assure that you begin the treatment when tumor is in the exponential growth phase (to be defined experimentally).

1. Normalize your quantity of siRNA since the total volume injected will be up to 200 μl of siRNA diluted in a sterile PBS (Note 3). For the control group, as in vitro, use a non-coding siRNA, such as siRNA against firefly luciferase.
2. Start daily injections of siRNA intraperitoneally for the period which lasts usually from 2 to 3 weeks. The quantity of siRNA injection is around 120 μg of siRNA per 1 kg intraperitoneally.
3. Continue measuring tumors every 2–3 days using a ruler and avoid stressing much the animals (Note 7).
4. Weigh animals regularly and take pictures; an example is shown in Fig. 1 (Note 8).
5. Sacrifice all your animals at the end of the treatment from both experimental and control group using 150 mg/kg of pentobarbital intraperitoneally using 1 ml syringe and 26 G needles.
6. Excise the tumors, document all data from each individually marked mouse. Photograph tumors, weight on the balances, and measure volume (Note 9).

7. Cut the tumors into pieces and freeze for the further mRNA extraction, protein extraction, and/or put to formaline (3.75%) to further paraffinize them to be analyzed by immunohistochemistry (Note 10).

3.3.1. Notes

There are some important details to follow to assure that you will succeed:

1. Prepare your cells for injections so that they are in the exponential growth phase, i.e., for the majority of cell types around 50–70% of confluence. It will assure their increased vitality during first days of grafting.
2. One day before your experiment, get out of the freezer your Matrigel™ solution and to put it into the fridge at +4°C for 24 h. The day of grafting put all syringes, needles, PBS solution, and Matrigel™ on ice before and during experiment. Transfer the cells in PBS to Matrigel™ as fast as possible, do not allow more than one experimental group at a time since the viability of even cancer cells is rather diminished at +4°C.
3. Be aware of the dead space in the needle while injecting. You can increase the volume up to 30% to assure the desired dose of cells or siRNA.
4. The size/internal diameter of the needle is crucial. The size 21–23 G is optimal. The reticulation of the Matrigel™ components could lead to accumulate fibers and create a filter in case of a too small needle diameter. In addition, cells are damaged while passing through the small needles and therefore not viable.
5. Following injections transfer the resting liquid containing cells from each syringe to one well of a, e.g., 6-well plate. You will see tomorrow if you have injected viable cells and at what rate.
6. Mark your mice properly since you will associate each mice to the result obtained. Even water-resistible marker is erasing from the skin of mice in 2–3 days. Preferably use ear tags and try not to mix the mice from different groups in the same cage.
7. While doing measurements multiply length by width (it is not really possible to measure the depth), even if these are approximate measurements they reflect the relative tumor growth. An example graph you can build from these data is shown in Fig. 2.
8. You can keep the tumors growing till they approach certain limits, and depending on the country, the tumor size generally should not exceed 1,000 mm^3 in volume and 10% of the mouse mass.
9. Keep tumors on ice while measuring them. The volume is usually measured by placing the tumor in the graduated cylinder

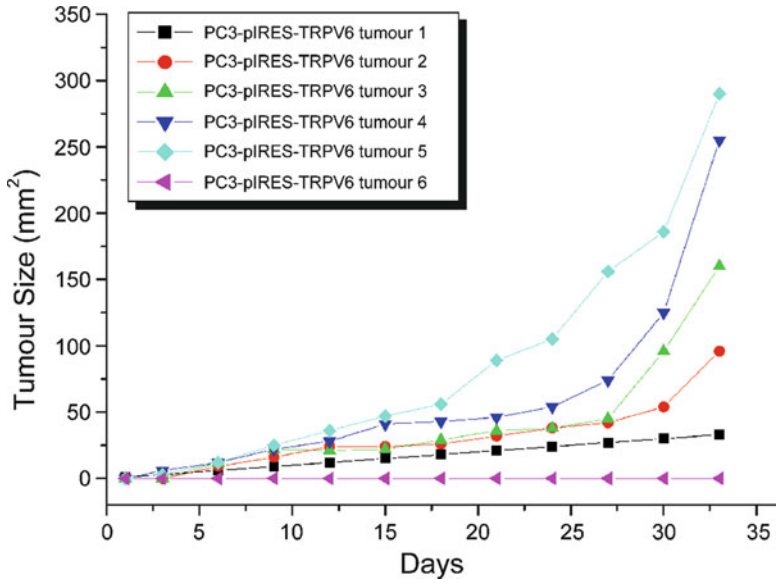

Fig. 2. An example graph of daily measurements of the size of the tumors (length × width) derived from the stable clones overexpressing TRPV6 channels injected into swiss nude mice.

of the appropriate diameter filled with PBS solution till one of the ticks. The tumor will replace PBS and this change you can measure visually or by pipetting the PBS off till the initial tick. In the case of the small tumors you can use 1 ml syringe and a pipette to take off water till the initial tick. Alternatively volume (mm^3) can be estimated according to the formula $(L \times W^2)1/2$ (16).

10. If your siRNA seems to have no effect it does not imply your channel has nothing to do with the tumorigenesis. Extract mRNA or protein first to prove a selective knockdown in tumors formed prior to making any conclusions.

References

1. Frank SA. Somatic mutation: early cancer steps depend on tissue architecture. Curr Biol. 2003 Apr 1;13(7):R261-3. Review. PubMed PMID: 12676101.
2. Spencer SL, Gerety RA, Pienta KJ, Forrest S (2006) Modeling somatic evolution in tumorigenesis. PLoS Comput Biol 2(8):e108
3. Lehen'kyi V, Prevarskaya N (2011) Oncogenic TRP channels. Adv Exp Med Biol 704:929–945
4. Prevarskaya N, Zhang L, Barritt G (2007) TRP channels in cancer. Biochim Biophys Acta 1772(8):937–946
5. Shapovalov G, Lehen'kyi V, Skryma R, Prevarskaya N. TRP channels in cell survival and cell death in normal and transformed cells. Cell Calcium. 2011 Sep;50(3):295–302. Epub 2011 May 31. Review. PubMed PMID: 21628069.
6. Ding X et al (2010) Essential role of TRPC6 channels in G2/M phase transition and development of human glioma. J Natl Cancer Inst 102(14):1052–1068
7. Shi Y et al (2009) Critical role of TRPC6 channels in G2 phase transition and the development of human oesophageal cancer. Gut 58(11):1443–1450

8. Bomben VC, Sontheimer H (2010) Disruption of transient receptor potential canonical channel 1 causes incomplete cytokinesis and slows the growth of human malignant gliomas. Glia 58(10):1145–1156
9. Yang SL, Cao Q, Zhou KC, Feng YJ, Wang YZ (2009) Transient receptor potential channel C3 contributes to the progression of human ovarian cancer. Oncogene 28(10):1320–1328
10. Monet M et al (2010) Role of cationic channel TRPV2 in promoting prostate cancer migration and progression to androgen resistance. Cancer Res 70(3):1225–1235
11. Sharkey FE, Fogh J (1984) Considerations in the use of nude mice for cancer research. Cancer Metastasis Rev 3(4):341–360
12. Flanagan SP (1966) 'Nude', a new hairless gene with pleiotropic effects in the mouse. Genet Res 8(3):295–309
13. Bosma MJ, Carroll AM (1991) The SCID mouse mutant: definition, characterization, and potential uses. Annu Rev Immunol 9: 323–350
14. Fidler IJ (1986) Rationale and methods for the use of nude mice to study the biology and therapy of human cancer metastasis. Cancer Metastasis Rev 5(1):29–49
15. Cespedes MV, Casanova I, Parreno M, Mangues R (2006) Mouse models in oncogenesis and cancer therapy. Clin Transl Oncol 8(5):318–329
16. Wang X, Ponzio NM, Studzinski GP (1997) Long-term exposure of HL60 cells to 1,25-dihydroxyvitamin D3 reduces their tumorigenicity: a model for cancer chemoprevention. Proc Soc Exp Biol Med 215(4): 399–404

Chapter 25

Methods to Study Thermonociception in Rodents

Kata Bölcskei

Abstract

The study of thermonociception in conscious animals is based on the assessment of pain-avoiding behavior from noxious heat or cold stimuli. The conventional tests of heat nociception apply suprathreshold heat stimuli and measure the reflex latency of withdrawal reactions. A novel approach of heat sensitivity measurement is the application of slowly increasing heat stimulation to determine the noxious heat threshold which proved to be highly reproducible and sensitive to standard analgesics. The present chapter aims at providing a guide to the most widely used conventional thermonociceptive tests (constant-temperature hot plate, plantar test, tail-flick test), as well as an introduction to the novel methods, the increasing-temperature hot plate and water bath. In a third section, the methods to test noxious cold sensitivity are briefly described.

Key words: Thermonociception, Reflex latency, Hot plate, Plantar test, Tail-flick, Noxious heat threshold, Increasing-temperature hot plate, Increasing-temperature water bath, Cold plate

1. Introduction

The study of thermonociception in awake animals is based on the assessment of pain-avoiding (nocifensive) behavior from noxious heat or cold stimuli. In principle, the development of such methods seems to be an easy task, however, the tests measuring noxious heat/cold-evoked withdrawal reactions differ in various aspects (e.g., heat source, stimulus intensity, recorded parameter) and all of them have some limitations which need to be taken into account when choosing methods for a study.

The traditional methods for the study of heat nociception (constant-temperature hot plate, tail-flick, plantar test) apply a constant suprathreshold heat stimulus and measure the reflex latency of nocifensive reactions. The disadvantages of these tests is

Arpad Szallasi and Tamás Bíró (eds.), *TRP Channels in Drug Discovery: Volume II*, Methods in Pharmacology and Toxicology,
DOI 10.1007/978-1-62703-095-3_25,

that latency may be altered by factors unrelated to nociceptor responsiveness such as basal skin temperature, reaction time which themselves may be influenced by various other factors (for review see (1)). Latency may also vary considerably upon repeated measurements due to nociceptor sensitization, but habituation could also occur. All of these aspects could well be the reason why the pharmacological sensitivity of the hot plate or tail-flick tests is far from desirable, as they could only detect reliably the antinociceptive action of opioids but not of cyclooxygenase inhibitors (1). Another limitation of latency measurements is that the noxious threshold temperature cannot be exactly determined and these data cannot be compared with the thermal thresholds of nociceptors measured with electrophysiological techniques nor with heat pain thresholds determined in human experimental pain models.

Moreover, the antinociceptive effect of capsaicin pretreatment was controversial in rodents when assessed with the constant-temperature hot plate or tail-flick tests despite having a clear thermoanalgesic effect after topical pretreatment on the human skin (2). Therefore a new approach was introduced for the study of thermonociception, the measurement of the noxious heat threshold by increasing the heat stimulus in 1°C steps which revealed a clear dose-related thermal antinociception in rats pretreated with capsaicin (2, 3). The application of a continuously increasing heat stimulus to determine the noxious heat threshold in awake animals was only put into practice in a few other studies in the 1980s (4, 5) but they have never become widely used among pain researchers even though they proved to be more sensitive to standard analgesics than the conventional tests.

In the recent years, our workgroup at the University of Pécs (Pécs, Hungary) validated two novel methods which are suitable to determine the noxious heat threshold of conscious animals and measure the effect of analgesic drugs: the increasing-temperature hot plate (6) and the increasing-temperature water bath (7). In contrast to the conventional methods, repeated measurements with these novel techniques yielded remarkably reproducible threshold values which enhance their reliability. The most likely explanation of the excellent reproducibility is that the slow rate of heating fails to alter nociceptor responsiveness and the overall confounding effect of the abovementioned factors may have less impact on the measured value.

Noxious cold sensitivity has been less investigated in animal studies and the majority of studies explored neuropathic cold allodynia. In these experiments, the applied cold stimulus was not necessarily noxious, as robust nocifensive reaction was only seen in neuropathic but not in intact rats (8). Similar to the methods of heat nociception, the assessment of physiological cold nociception can be achieved by applying suprathreshold cold stimuli (<5°C) delivered by a constant-temperature cold plate or a cold bath and

measuring reflex latencies (9, 10) or by measuring the noxious cold threshold temperature with a decreasing-temperature plate (11).

The first part of the chapter aims at providing a guide to the most widely used conventional tests of heat nociception, as well as the description of the novel methods measuring noxious heat threshold. Advantages and disadvantages are presented in order to help the reader choose from the available methods, with practical advice on how to perform the tests and interpret results. A brief overview of the most frequently applied tests to study noxious cold sensitivity is also included at the end of the chapter.

2. Materials

2.1. Equipment

1. Hot/cold plate analgesia meter manufactured by IITC Life Science (Woodland Hills, CA, USA).

   The starting and cut-off temperatures of the plate can be set to any grade from 0 to 70°C and the rate of heating/cooling is also adjustable from 0 to 12°C/min. These features make the equipment suitable for constant-temperature hot or cold plate measurements or as an increasing/decreasing-temperature hot/cold plate.

   For constant-temperature hot/cold plate measurements, equipment from other manufacturers can equally be used.
2. Plantar test apparatus (various manufacturers, e.g., IITC Life Sciences, CA, USA; Ugo Basile, Italy).
3. Tail-flick apparatus (various manufacturers, e.g., IITC Life Sciences, CA, USA; Ugo Basile, Italy).
4. Thermostatically controlled water bath for constant-temperature paw/tail-immersion test.
5. Increasing-temperature water bath (SensoStress) manufactured by Experimetria Ltd. (Budapest, Hungary).

2.2. Animals

Rats of either gender can be used, except for the increasing-temperature hot plate, which was validated using female rats (see Note 1). All of the methods are suitable to test mice of either gender, however, paw immersion tests are not recommended due to the small size of the animal and the difficulty of restraining them properly for paw stimulation. The choice of strain in case of mice is also important as considerable difference in noxious heat sensitivity was demonstrated between different mouse strains (12).

Animals are brought to the laboratory at least a day before the experiment and they are provided with food and water ad libitum. Habituation to the measurement's conditions is essential, especially in case of methods involving restraint (Note 2). With rats, it

is generally sufficient to perform two measurements a day prior to the start of the study, mice, however, often require more habituation before they can be reliably tested (Note 3).

3. Methods

3.1. Methods to Study Heat Sensitivity: Latency Measurements

The general principle of these methods is to apply a suprathreshold heat stimulus to the animal's paw or tail and measure the reflex latency of the withdrawal reaction. An increase of the latency is considered as analgesia while the decrease of latency is regarded as hyperalgesia. The skin temperature eliciting a withdrawal reaction was found to be fairly constant in both humans and rats, between 42 and 45°C, independent of stimulus intensity. The reflex latency therefore is determined by two major components: the time required for heat transfer from the heat source to the skin and the reaction time (for review see (1)). The nature of the heat source (contact or radiant heat, immersion into hot water) and the stimulus intensity obviously determine the time-dependence of the first component. On the other hand, the experimenter must be aware that physiological/pathophysiological changes or drug effects can also strongly influence either component of the latency without having a direct effect on nociception. Basal skin temperature is a major influencing factor determined by cutaneous blood flow which is affected by changes of vasomotor tone or thermoregulation. The effect of the cutaneous temperature on reflex latencies have been demonstrated on the tail (for review see (13)) and on the paw as well (14). During restraint, tail temperatures of rats increased by as much as 8°C (13), but stress-induced decrease of the temperature of the tail and the extremities was also shown in another study (15). It is essential therefore to take special care to control ambient temperature and minimize handling-induced stress and possibly exclude any change or difference in thermoregulation or vasomotor tone.

3.1.1. Constant-Temperature Hot Plate

The constant-temperature hot plate consists of a metal plate which is heated up to a preset temperature and a plexiglass observation chamber. The applied temperature generally varies from 50 to 55°C, well above the noxious heat threshold. The advantage of the test is that it is easy and quick to perform and it does not require restraint of the animal. The end-point can be paw shaking, licking, or escape behavior such as jumping, all of which are supraspinally organized reactions. However, locomotion or even weight shifting can reduce contact with the plate adding another variable to the outcome of the latency measurement. As it has been mentioned, the main drawback of the method is the variability of the latency and the low pharmacological sensitivity. Using lower plate

temperatures has been shown to improve the sensitivity of the method to opioid partial agonists and cyclooxygenase inhibitors (1), however, variability of the latency is also increased at lower temperatures. Hyperalgesia models are rarely used with the constant-temperature hot plate, as hind paws cannot be independently stimulated.

Measurement of hot plate latency:

1. The plate is pre-heated to the chosen temperature.
2. The animal is gently placed into the chamber and the timer is immediately started.
3. On the first sign of nocifensive reaction (which is typically paw licking or shaking, see also Note 4) the timer is stopped and the animal is removed from the plate as quickly as possible to avoid heat injury. The animal should also be removed immediately if the cut-off time is reached without any reaction, in this case the cut-off time is used in the analysis (Note 5).
4. The animal is returned to its home cage between measurements. At least 10 min should be left before the same animal is tested again.
5. The mean of three measurements is regarded as control latency.

3.1.2. Plantar Test (Hargreaves Method)

The plantar test (16) uses controlled radiant heat as thermal stimulus: a focused light beam or infrared beam emitted from the movable stimulator unit of the apparatus. The method offers several advantages over the constant-temperature hot plate. Firstly, the heat stimulus is started by the experimenter and it ends upon paw withdrawal, therefore animals can be allowed to acclimate before the measurement and remain in the observation chamber between measurements. Secondly, only a small part of the body is heated, therefore hind paws can be tested separately. The latter aspect makes the equipment suitable to assess thermal hyperalgesia more reliably by comparing the latency of the inflamed/injured paw to the contralateral paw. The controlled delivery of the stimulus also yields more reproducible latency values, provided that measurements are not repeated at intervals of less than 5 min which is required for skin temperatures to return to pre-stimulus levels (17). A disadvantage of the glass surface is that it has a pronounced heat sink effect which lowers the basal skin temperature of the paw. Preheating of the glass to 30°C, however, has been shown to reduce the impact of the heat sink effect and maintain an even temperature of the paw ((17), Note 6). This function is now available in most models. Another considerable difficulty of the method is that locomotion or even changes of body position completely interfere with the stimulation, making the measurements unpredictably time-consuming, especially in mice.

Preliminary measurements should be made on a small group of animals to determine the adequate beam intensity. For practical reasons, the latency of control animals should be 8–10 s which leaves a sufficient range for shortening or lengthening of latency, allowing detection of hyperalgesia and analgesia as well. The cut-off is set to 20 s.

The plantar test is mainly used to assess thermal hyperalgesia in models of inflammatory pain induced by carrageenan (16) or Complete Freund's adjuvant (CFA) (18). Thermal hyperalgesia is also evoked after plantar incision which models postoperative pain (19). All of these conditions induce mechanical hyperalgesia/allodynia as well. Heat sensitivity can be measured in neuropathic pain models as well, however, one must be aware that while mechanical allodynia and signs of spontaneous pain are always robust, heat hyperalgesia is not consistently detected in all of the models (for review see (20), see also (14)).

Measurement of paw withdrawal latency with the plantar test:

1. The animals are placed into the observation chambers standing on a glass surface (pre-heated to 30°C) and they are allowed to acclimate for approximately 5–10 min, or until exploratory behavior ceases (Note 7).
2. Once the animal stays calm in the chamber (Note 8), the stimulator unit is positioned under the glass so that the beam aims at the middle of the plantar surface of the paw.
3. The heating is switched on by pressing the button on the stimulator which also starts the timer.
4. Paw withdrawal is detected automatically by a photocell (in most commercially available models) or manually by the experimenter (IITC Life Sciences model). The heating is immediately interrupted and the latency is recorded to the nearest 0.1 s. The heating is also automatically stopped if the cut-off value is reached without withdrawal, in this case the cut-off time is recorded as latency.
5. The duration of paw lifting/licking can also be measured by starting a stopwatch at the moment of withdrawal.
6. The animal is left in the chamber and the contralateral paw of the same animal is stimulated after approximately 1 min. However, the same paw should not be repeatedly measured within a 10-min interval.
7. The mean of three measurements is regarded as control.

Carrageenan-Induced Thermal Hyperalgesia (16)

Carrageenan injection into the paw induces inflammation which develops over the course of a few hours. After control measurements, a 3% λ-carrageenan solution is prepared in saline and it is administered intraplantarly at a volume of 100 µl to rats and 20 µl

to mice. Animals are returned to their home cages. Two hours afterwards, the paw is significantly swollen and thermal hyperalgesia develops by this time as well. The measurement is repeated 2 or 3 h after treatment. Thermal hyperalgesia is confirmed as a significant shortening of the paw withdrawal latency compared either to baseline latency of the same paw, or the actual latency of the contralateral paw. The withdrawal duration is also increased. Hyperalgesia is maintained for at least 8 h.

Complete Freund's Adjuvant-Induced Thermal Hyperalgesia (18)

CFA contains killed *Mycobacterium tuberculosis* suspended in mineral oil which induces chronic inflammation. A 1:1 emulsion is prepared with saline and it is administered intraplantarly at a volume of 100 µl to rats and 20 µl to mice after control measurements. Thermal hyperalgesia develops by 24 h and it is maintained for at least 5 days.

Plantar Incision-Induced Thermal Hyperalgesia (19)

Under anesthesia, a 1-cm incision is made on the plantar surface of the paw, starting at 0.5 cm from the heel, involving skin and muscle. The wound is closed with two sutures and animals are allowed to recover from anesthesia. Thermal hyperalgesia can be detected as early as 2 h after surgery and it is maintained for at least 7 days.

3.1.3. Tail-Flick Test

The tail-flick test also employs radiant heat to stimulate a small area of the tail and the latency of withdrawal reaction is determined. Along with the constant-temperature hot plate, it has been one of the most widespread methods for the study of thermonociception, but similarly unable to detect the antinociceptive effect of non-opioid analgesics (1). It is also quick and easy to perform, and contrary to the hot plate test, the stimulation is more controlled and the detection of the tail withdrawal can be automated. On the other hand, the test requires restraint of the animals, and the withdrawal reaction is a spinal reflex, not a complex nocifensive behavior involving supraspinal processing. The major disadvantages of tail stimulation are the previously discussed confounding effect of tail skin temperature changes (see Sect. 3.1) and the relative difficulty to induce hyperalgesia on the tail.

Intensity of the beam should be set to yield latency values of approximately 4 s in intact animals and the cut-off is set to 10 s.

Measurement of tail-flick latency:

1. Animals are put into a restrainer or wrapped in a piece of cloth and held by the experimenter (see also Note 2).
2. The site of stimulation is marked on the tail and it is positioned under the stimulator. The heating is switched on which also starts the timer.
3. Upon brisk withdrawal of the tail, the heating is interrupted and the latency is recorded to the nearest 0.1 s. The heating is

also interrupted if the cut-off time is reached without withdrawal, and the cut-off value is recorded as latency.

4. If a restrainer is used, the animal can remain inside until the next measurement. If the animal was held in the hand, it is returned to its home cage between measurements. The same animal should not be tested again within 10 min.
5. The mean of three measurements is regarded as control.

3.1.4. Tail/Paw-Immersion Test

A fixed-temperature water bath is also a classical method to deliver heat stimuli to the animals' paw or tail. Immersion into hot water induces a steep rise in skin temperature. Bath temperatures of 47–55°C have been used in different studies. The obvious disadvantage over the constant-temperature hot plate is the need to restrain animals, however, the heat transfer is more uniform, not affected by the behavior of individual rats or mice.

Measurement of paw/tail withdrawal latency with a hot water bath:

1. The water bath is pre-heated to the chosen temperature.
2. Animals are put into a restrainer or wrapped in a piece of cloth and held by the experimenter (see also Note 2).
3. The paw or the distal half of the tail is dipped into the bath, and a stopwatch is started at the same moment.
4. Upon brisk withdrawal of the paw/tail, the timer is stopped and the latency is recorded. If the cut-off time is reached without any reaction, the paw/tail is removed from the bath and the cut-off value is regarded as latency.
5. If a restrainer is used, the animal can remain inside until the next measurement. If the animal was held in the hand, it is returned to its home cage between measurements. The same animal should not be tested again within 10 min.
6. The mean of three measurements is regarded as control.

3.2. Methods to Study Heat Sensitivity: Noxious Heat Threshold Measurements

The basis of noxious heat threshold measurement is applying an increasing heat stimulus by slowly heating a metal plate or a water bath from subthreshold temperature until nocifensive behavior is observed. The corresponding plate or bath temperature is considered as the noxious heat threshold of the animal and it has been shown to be highly reproducible upon repeated measurements (6, 7). The threshold temperature of the paw ranged between 43–46 °C when determined with the hot plate and 42–45 °C when measured with the water bath. This is very close to the critical skin temperature which elicits pain reaction in humans and rats (see Sect. 3.1) which also supports the reliability of the method. The pharmacological sensitivity of the increasing-temperature hot plate also proved to be superior to the constant-temperature hot plate,

as the noxious heat threshold temperature was significantly increased by low doses of morphine or non-steroidal analgesics (4–6, 21).

The pharmacological sensitivity of nociceptive tests is generally increased after sensitization, therefore we have developed several thermal hyperalgesia models using noxious heat threshold measurement. Thermal hyperalgesia—detected as a decrease of heat threshold—induced by either the transient receptor potential vanilloid type 1 (TRPV1) receptor agonist, resiniferatoxin (RTX) (6), mild heat injury (7) or surgical incision of the paw (22) were all highly sensitive to standard analgesics and these models were also suitable to sensitively detect the antihyperalgesic effect of TRPV1 receptor antagonists (23).

In the following section, the protocols of the noxious heat threshold measurement with the two apparatuses and the three pharmacologically validated thermal hyperalgesia models are also presented.

3.2.1. Increasing-Temperature Hot Plate

The equipment consists of a steel plate (10 cm × 20 cm) with a microprocessor-controlled heating unit and a plexiglass observation chamber. Similar to the constant-temperature hot plate, animals move freely on the plate, but the slow rate of heating reduces the confounding effect of locomotion on heat transfer. In our experience, the noxious heat threshold temperature was independent of starting temperature or heating rate (6 or 12°C/min) and it was reproducible upon repeated measurements at intervals of 5 min, 30 min or 24 h (6). Very low heating rates are not recommended because the long duration of heat exposure may be too stressful for the animals (21).

Noxious heat threshold measurement with the increasing-temperature hot plate:

1. A starting temperature of 30°C and a heating rate of 12°C/min are used and the cut-off temperature is set to 50°C.
2. The animal is placed into the observation chamber and the heating is started immediately afterwards.
3. Heating is stopped by the experimenter at the moment when the animal shows any nocifensive behavior (typically paw licking or shaking) involving any of the hind paws and the animal is quickly removed from the plate (see also Note 4). The corresponding plate temperature is recorded as the noxious heat threshold of the animal. If the cut-off temperature is reached without any reaction, the heating is automatically interrupted. The animal is removed and the cut-off value is used in the analysis.
4. By the interruption of heating, the plate is rapidly cooled back automatically to the starting temperature while the threshold temperature remains visible on the display. Due to the rapid cooling process, successive measurements can be performed at intervals of approximately 2 min.

5. Measurements on the same animals can be reliably repeated at a 5-min interval. For control measurements, we use an interval of 30 min and the mean of two threshold values is considered as the control noxious heat threshold.

Resiniferatoxin-Induced Noxious Heat Threshold Drop (6)

RTX, the ultrapotent agonist of the TRPV1 receptor, is dissolved in ethanol (1 mg/ml) and further diluted with saline. Rats are injected 10 or 30 ng in 100 µl, while mice are given 6 ng in 20 µl intraplantarly. Immediately after RTX injection, nocifensive behavior (shaking and licking of the paw) of moderate intensity is observed, however, it declines during the first 5 min (Note 9). Meanwhile, the starting temperature of the plate is set to 25°C as the heat threshold may even drop below 30°C. Threshold measurements are repeated 5, 10, 15 and 20 min after injection. Typically the heat threshold decreases by 8–10°C at the 5-min measurement and gradually returns to control (Note 10).

The model was validated by pretreatment with standard analgesics (morphine, diclofenac or paracetamol i.p.) to measure the inhibitory effect on RTX-induced heat threshold drop. The sensitivity of the test is reflected by their minimum effective doses, all of which proved to be remarkably low (1, 1, 100 mg/kg i.p., respectively).

Other compounds were also found to induce an acute heat threshold drop, e.g., other TRPV1 receptor agonists such as N-oleoyl-dopamine (24) or 3-methyl-N-oleoyl-dopamine (25), as well as mediators which are known to sensitize nociceptors to heat (bradykinin, prostaglandin E_2, P2 purinoceptor agonists, etc.). Surprisingly, we were unable to measure reliably the heat threshold lowering effect of the classical TRPV1 receptor agonist, capsaicin on the increasing-temperature hot plate, most probably due to the very pronounced capsaicin-induced nocifensive reaction (see also Note 9). Nevertheless, the long-term desensitizing action of both capsaicin and RTX could be revealed as an elevation of the heat threshold (11). On the other hand, it is also noteworthy that no significant change of the noxious heat threshold was detected in carrageenan- or CFA-induced inflammation (Note 11).

3.2.2. Increasing-Temperature Water Bath

The equipment consists of a tap water-filled cylindrical container (12 cm inner diameter, 14 cm height) with a built-in heating unit in its bottom and a controlling unit. Two alternative starting temperatures (30 or 40°C) and three different heating rates (6, 12 or 24°C/min) can be set on the equipment. The rise of temperature proved to be nearly linear (7). The cut-off temperature is set to 53°C by the manufacturer. The controlling unit also has a display continuously showing the actual bath temperature measured by a thermocouple at a depth of 3 cm, which is approximately the depth to which the animal's paw (rats) or tail (mice) is immersed into the water.

The main difference from the increasing-temperature hot plate is the need to restrain animals (see Note 2). Similar to the methods of latency measurement, one must also consider that paw/tail withdrawal from the water is a spinal reflex while the nocifensive behavior of the freely moving animal involves supraspinal mechanisms.

Noxious heat threshold measurement with the increasing-temperature water bath:

1. The starting temperature and the heating rate are set to the chosen values (Note 12).
2. While the water is pre-heated to the starting temperature, the animals are removed from their home cage and gently restrained or put into the restrainer (see also Note 2).
3. A light on the controlling unit signals when the starting temperature is reached. The rat's paw or the mouse's tail is dipped into the bath approximately to the depth of the thermometer and the heating is started immediately.
4. Once the animal withdraws its paw/tail from the water, heating is quickly interrupted by a foot switch and the corresponding bath temperature remains on the display to be recorded. If the cut-off is reached without any reaction, the paw/tail is removed immediately from the bath and the cut-off temperature is regarded as noxious heat threshold.
5. If a restrainer is used, the animal can remain inside until the next measurement. If the animal was held in the hand, it is returned to its home cage between measurements.
6. After each measurement, the water bath is cooled back to the starting temperature by pumping cold water into the container while the excess water is drained through a spillway. Successive measurements can be performed at intervals of approximately 1.5 min.
7. Measurements on the same animals can be reliably repeated at a 10-min interval. For control measurements, we use an interval of 30 min and the mean of two threshold values is considered as the control noxious heat threshold.

Mild Heat Injury-Induced Noxious Heat Threshold Drop (7)

Mild heat injury models a first degree burn involving exactly the same skin area which is stimulated in the water bath. Rats are anesthetized with diethyl ether (in a chamber) or halothane (4%, via nose cone) and one of the hind paws is immersed into a constant, 51°C hot water bath for 20 s. After the paw is removed from the hot water, animals are returned to a cage lined with soft paper towel. They recover from anesthesia within minutes and threshold measurements are performed 10 and 20 min after injury to confirm the development of hyperalgesia which is typically a 7–8°C drop of the heat threshold. Anesthesia itself did not influence the noxious

heat threshold at the time of the measurement. Thermal hyperalgesia persists for up to 4 h afterwards.

The model was validated by administering standard analgesics (morphine, diclofenac, ibuprofen or paracetamol) as a post-treatment to measure the inhibitory effect on heat injury-induced heat threshold drop. Similar to the previous test, this one also proved to be highly sensitive to detect the antihyperalgesic effect of the tested compounds (minimum effective doses: 0.3, 0.3, 10 and 30 mg/kg i.p., respectively).

Plantar Incision-Induced Thermal Hyperalgesia (22)

The surgical procedure is exactly the same as described in Sect. 3.1.2. Animals are allowed to recover until the next day. A decrease of 5–7°C of the noxious heat threshold can be measured 18 h after incision which is maintained for at least a week. Morphine, diclofenac or paracetamol administered on the first day after surgery significantly reversed heat threshold drop at minimum effective doses of 0.3, 1 and 100 mg/kg i.p., respectively.

3.3. Methods to Study Cold Nociception

Cold nociception can be measured in animals applying the same approaches as those of heat nociceptive tests: measuring the latency of withdrawal reactions to suprathreshold cold stimuli (9, 10) or determining the noxious cold threshold by a decreasing temperature cold plate (11). A third approach is inducing spontaneous nocifensive behavior by cold exposure and measure the number or duration of paw licking/lifting, but the latter is mainly employed in the assessment of cold allodynia (8, 26). There is however an intriguing difference between heat and cold nociception: while the heat pain temperatures in humans and the noxious heat thresholds in animal studies are very close, a clear-cut nocifensive behavior to cold could only be evoked in animals by much lower temperatures. Humans report pain at 15°C (27), however, naïve rats only showed robust pain-avoiding behavior (paw licking) at 3°C on a constant-temperature cold plate (26) and at around 2°C on a decreasing-temperature plate (11). In a third study, paw lifting latency was measured in rats at different fixed temperatures and it was significantly shorter at 5°C compared to latencies at higher, non-noxious temperatures (10). All of these data suggest that the noxious cold temperature of rats is approximately 2–5°C on a cold plate. The study of physiological cold nociception of mice has gained interest since the discovery of cold sensitive TRP channels, TRPM8 and TRPA1 and the generation of gene-deleted mice lacking these receptors (28–32). The noxious cold sensitivity of wild-type mice varied between studies. Paw withdrawal latency was measured at 0°C in two studies, but latencies were markedly different: 7 s (30) and 50 s (32). Another group used a prolonged, 5-min exposure to a 0°C plate to induce nocifensive behavior (29), while in two other reports, paw licking or withdrawal was only observed at temperatures below 0°C (28, 31). Moreover, the involvement of TRPM8 and TRPA1 in noxious cold sensitivity

could not be unequivocally revealed in these studies which could also be explained by methodological differences. Cold nociceptive tests are less standardized and few comparative data are available on the sensitivity and validity of each test, therefore only a brief introduction to the simplest techniques is presented in the next section.

3.3.1. Constant-Temperature Cold Plate

The methodological advantages and disadvantages of the cold plate test are essentially the same as with the hot plate. The contact is influenced by locomotion and weight bearing. The latter is especially problematic in neuropathic pain models, as abnormal paw posture and paw guarding is often present in nerve injured animals.

Latency measurement on the cold plate:

1. The temperature of the plate is set to 0°C and the cut-off to 120 s. To assess cold allodynia, set the temperature to 10 or 15°C.
2. Follow the steps of latency measurement on the hot plate (see Sect. 3.1.1).

Cold-evoked spontaneous behavior on the cold plate:

1. The temperature of the plate is set to 5°C.
2. The animal is gently placed into the observation chamber and a stopwatch is started.
3. During the next 5 min, brisk paw lifts are counted.
4. The animal is removed from the plate and allowed to rest for 10 min.
5. The procedure is repeated three times and the mean of the three values is regarded as control.

3.3.2. Decreasing-Temperature Cold Plate

The decreasing-temperature cold plate is suitable to measure the noxious cold threshold by cooling the plate from room temperature to 0°C at a preset rate until the animal shows nocifensive behavior. The observed end-point is usually paw licking indistinguishable from a heat-evoked nocifensive reaction.

1. The starting temperature is set to 25°C and the cut-off temperature to 0°C. The rate is set to 6°C/min.
2. Follow the steps of noxious heat threshold measurement with the increasing-temperature hot plate (see Sect. 3.2.1).

3.3.3. Acetone-Induced Evaporative Cooling

The test was originally used to assess neuropathic cold allodynia, as intact rats show no or minimal reaction to acetone-induced cooling (8). On the other hand, intact mice respond with brief paw flinching or licking to acetone (see (28–31)). The difference could be explained by the findings that in rats skin temperature decreased by 7°C after acetone application (33), while it dropped by 10–12°C

in mice (30), however, it cannot be ruled out that chemical irritation also occurs in mice.

The steps of the acetone-test:

1. Animals are placed into observation chambers on a wire mesh floor and allowed to acclimate for 5–10 min.
2. 100 µl (rats) or 50 µl (mice) of acetone is sprayed onto the plantar surface of the hind paw with a repeating pipettor or syringe, taking care not to touch the paw to avoid mechanical stimulus.
3. The time spent licking and lifting the paw is recorded for 60 s.
4. Stimulation is repeated at least two times at 5-min intervals and the mean of the responses is regarded as control.

4. Notes

1. The reason for using female rats on the increasing-temperature hot plate is that in the case of male animals the skin of the scrotum (inevitably in contact with the hot plate) proved to be more sensitive than the paw which therefore produced a confounding effect. When developing the increasing-temperature water bath, we chose to continue the experiments with females to be able to compare the sensitivity of the two methods in the same gender.
2. Holding the animals by the skin of the back is not recommended for behavioral studies. For tests involving tail stimulation, animals can be restrained in commercially available plexiglass tubes or held loosely in the hand wrapped in a soft cloth. The latter requires certain experience and the same experimenter should handle all the animals during the entire study. The restraint obviously cannot be too loose, but if it is too tight, the animal may struggle more and an inexperienced experimenter may try to squeeze the animal more tightly. Care must be taken not to compress the chest. Rats can also be gently restrained by grasping their right shoulder between the index and middle fingers of the right hand while the thumb is placed under the other shoulder and the remaining fingers lightly embrace the body. For paw immersion tests in rats, the experimenter holds the animal in one hand and with the other supports the bottom while gently extending the hind limb. Rats generally tolerate restraint much better than mice, they show minimal or no struggle after two to three habituation sessions while mice are more stressed by repeated handling. Mogil and coworkers—with ample experience in mouse nociceptive tests—recommend a home-made cloth/cardboard

holder for mice which they found to be less stressful than plastic restrainers (34).

3. Mice tend to move around continuously in the observation chamber which hinders most of the testing procedures. We habituate mice to the box a few days prior to the experiment by placing them into chambers of identical sizes for at least an hour. In our experience, it has reduced agitation in consequent measurements. Mice do not habituate well to restraint either, they are obviously stressed and struggle more frequently. The most agitated mice may not habituate at all to restraint, even after repeated handling or prolonged confinement in the restrainer, making the measurements less reliable.
4. Licking of the fore paw could also occur as all four limbs are exposed to the hot plate but only hind paw licking should be accepted as an end-point. Grooming can be mistaken for nocifensive fore paw licking.
5. The measurement should be interrupted if the animal urinates on the plate as it changes heat transfer. Moreover, paw shaking, indistinguishable from a nocifensive reaction may also be seen if the animal steps into the puddle of urine.
6. In hyperalgesia models, animals may hold the affected paw in an elevated position which completely prevents the heat sink effect. It is recommended to start heat stimulation only when the paw is in contact with the glass.
7. If the animal urinates on the floor, it must be wiped dry before starting the measurement (see also Note 5).
8. In various assays on freely moving animals we have found that grooming considerably delays withdrawal reactions, apparently increases pain threshold, especially in mice. Though it would be convenient to stimulate the animal while it is grooming, as it stays in one place for a relatively longer period, it must be avoided in order to obtain reliable withdrawal reactions.
9. It is obvious that spontaneous nocifensive behavior interferes with noxious heat threshold measurement, especially on the increasing-temperature hot plate as it cannot be distinguished from the heat-evoked nocifensive reaction. The experimenter must make sure that spontaneous paw licking or lifting is absent before starting the measurement.
10. It has been a surprising observation that the pattern of nocifensive behavior on the increasing-temperature hot plate changed after the induction of hyperalgesia. During control measurements paw licking was typically the first pain-avoiding response but after RTX injection paw lifting was more frequently seen, and paw licking occurred only at higher plate temperatures (see (4)). We chose to accept paw lifting as an end-point, first because it is also a clear-cut nocifensive reaction, and secondly

because rats often held their paws in an elevated position after the first paw lifting reaction thus avoiding further contact with the plate.

11. The reason for the lack of noxious heat threshold drop in these models is not clear. It could be argued that thermal hyperalgesia determined by latency measurements is probably overestimated in these conditions, as basal skin temperature is definitely higher after inflammation (see Sect. 3.1). But a decrease of the threshold temperature to 38.5°C was also demonstrated in the carrageenan model (16). One possible explanation is that rats put less weight on the swollen paw reducing contact with the plate which consequently reduced heating of the skin.
12. If hyperalgesia is investigated, the starting temperature is set to 30°C and the rate is set to 12 or 24°C. A faster rate is necessary to reduce the duration of the measurement, otherwise restraint may become too stressful. On the other hand, if a heat threshold-elevating effect is studied, it is recommended to set the starting temperature to 40°C with the 6°C/min rate.

References

1. Le Bars D, Gozariu M, Cadden SW (2001) Animal models of nociception. Pharmacol Rev 53:597–652
2. Szolcsányi J (1985) Sensory receptors and the antinociceptive effects of capsaicin. In: Hakanson R, Sundler F (eds) Tachykinin Antagonists. Elsevier, Amsterdam, pp 45–54
3. Szolcsányi J (1987) Capsaicin and nociception. Acta Physiol Hung 69:323–332
4. Hunskaar S, Berge OG, Hole K (1986) A modified hot-plate test sensitive to mild analgesics. Behav Brain Res 21:101–108
5. Farré AJ, Colombo M, Gutiérrez B (1989) Maximum tolerated temperature in the rat tail: a broadly sensitive test of analgesic activity. Methods Find Exp Clin Pharmacol 11:303–307
6. Almási R, Pethő G, Bölcskei K, Szolcsányi J (2003) Effect of resiniferatoxin on the noxious heat threshold temperature in the rat: a novel heat allodynia model sensitive to analgesics. Br J Pharmacol 139:49–58
7. Bölcskei K, Horváth D, Szolcsányi J, Pethő G (2007) Heat injury-induced drop of the noxious heat threshold measured with an increasing-temperature water bath: a novel rat thermal hyperalgesia model. Eur J Pharmacol 564:80–87
8. Choi Y, Yoon YW, Na HS, Kim SH, Chung JM (1994) Behavioral signs of ongoing pain and cold allodynia in a rat model of neuropathic pain. Pain 59:369–376
9. Pizziketti RJ, Pressman NS, Geller EB, Cowan A, Adler MW (1985) Rat cold water tail-flick: a novel analgesic test that distinguishes opioid agonists from mixed agonist-antagonists. Eur J Pharmacol 119:23–29
10. Allchorne AJ, Broom DC, Woolf CJ (2005) Detection of cold pain, cold allodynia and cold hyperalgesia in freely behaving rats. Mol Pain 1:36
11. Bölcskei K, Tékus V, Dézsi L, Szolcsányi J, Pethő G (2010) Antinociceptive desensitizing actions of TRPV1 receptor agonists capsaicin, resiniferatoxin and N-oleoyldopamine as measured by determination of the noxious heat and cold thresholds in the rat. Eur J Pain 14:480–486
12. Mogil JS, Wilson SG, Bon K, Lee SE, Chung K, Raber P, Pieper JO, Hain HS, Belknap JK, Hubert L, Elmer GI, Chung JM, Devor M (1999) Heritability of nociception I: responses of 11 inbred mouse strains on 12 measures of nociception. Pain 80:67–82
13. Hole K, Tjølsen A (1993) The tail-flick and formalin tests in rodents: changes in skin temperature as a confounding factor. Pain 53:247–254
14. Luukko M, Konttinen Y, Kemppinen P, Pertovaara A (1994) Influence of various experimental parameters on the incidence of thermal and mechanical hyperalgesia induced by a constriction mononeuropathy of the sciatic nerve in lightly anesthetized rats. Exp Neurol 128:143–154

15. Vianna DM, Carrive P (2005) Changes in cutaneous and body temperature during and after conditioned fear to context in the rat. Eur J Neurosci 21:2505–2512
16. Hargreaves K, Dubner R, Brown F, Flores C, Joris J (1988) A new and sensitive method for measuring thermal nociception in cutaneous hyperalgesia. Pain 32:77–88
17. Dirig DM, Salami A, Rathbun ML, Ozaki GT, Yaksh TL (1997) Characterization of variables defining hindpaw withdrawal latency evoked by radiant thermal stimuli. J Neurosci Methods 76:183–191
18. Ren K, Hylden JL, Williams GM, Ruda MA, Dubner R (1992) The effects of a non-competitive NMDA receptor antagonist, MK-801, on behavioral hyperalgesia and dorsal horn neuronal activity in rats with unilateral inflammation. Pain 50:331–344
19. Zahn PK, Brennan TJ (1999) Primary and secondary hyperalgesia in a rat model for human postoperative pain. Anesthesiology 90: 863–872
20. Jaggi AS, Jain V, Singh N (2011) Animal models of neuropathic pain. Fundam Clin Pharmacol 25:1–28
21. Tjølsen A, Rosland JH, Berge OG, Hole K (1991) The increasing-temperature hot-plate test: an improved test of nociception in mice and rats. J Pharmacol Methods 25:241–250
22. Füredi R, Bölcskei K, Szolcsányi J, Pethő G (2009) Effects of analgesics on the plantar incision-induced drop of the noxious heat threshold measured with an increasing-temperature water bath in the rat. Eur J Pharmacol 605:63–67
23. Tékus V, Bölcskei K, Kis-Varga Á, Dézsi L, Szentirmay É, Visegrády A, Horváth C, Szolcsányi J, Pethő G (2010) Effect of transient receptor potential vanilloid 1 (TRPV1) receptor antagonist compounds SB705498, BCTC and AMG9810 in rat models of thermal hyperalgesia measured with an increasing-temperature water bath. Eur J Pharmacol 641:135–141
24. Szolcsányi J, Sándor Z, Pethő G, Varga A, Bölcskei K, Almási R, Riedl Z, Hajós G, Czéh G (2004) Direct evidence for activation and desensitization of the capsaicin receptor by N-oleoyldopamine on TRPV1-transfected cell, line in gene deleted mice and in the rat. Neurosci Lett 361:155–158
25. Almási R, Szőke É, Bölcskei K, Varga A, Riedl Z, Sándor Z, Szolcsányi J, Pethő G (2008) Actions of 3-methyl-N-oleoyldopamine, 4-methyl-N-oleoyldopamine and N-oleoylethanolamide on the rat TRPV1 receptor in vitro and in vivo. Life Sci 82:644–651
26. Jasmin L, Kohan L, Franssen M, Janni G, Goff JR (1998) The cold plate as a test of nociceptive behaviors: description and application to the study of chronic neuropathic and inflammatory pain models. Pain 75:367–382
27. Davis KD, Pope GE (2002) Noxious cold evokes multiple sensations with distinct time courses. Pain 98:179–185
28. Bautista DM, Jordt SE, Nikai T, Tsuruda PR, Read AJ, Poblete J, Yamoah EN, Basbaum AI, Julius D (2006) TRPA1 mediates the inflammatory actions of environmental irritants and proalgesic agents. Cell 124:1269–1282
29. Kwan KY, Allchorne AJ, Vollrath MA, Christensen AP, Zhang DS, Woolf CJ, Corey DP (2006) TRPA1 contributes to cold, mechanical, and chemical nociception but is not essential for hair-cell transduction. Neuron 50:277–289
30. Colburn RW, Lubin ML, Stone DJ Jr, Wang Y, Lawrence D, D'Andrea MR, Brandt MR, Liu Y, Flores CM, Qin N (2007) Attenuated cold sensitivity in TRPM8 null mice. Neuron 54:379–386
31. Dhaka A, Murray AN, Mathur J, Earley TJ, Petrus MJ, Patapoutian A (2007) TRPM8 is required for cold sensation in mice. Neuron 54:371–378
32. Bautista DM, Siemens J, Glazer JM, Tsuruda PR, Basbaum AI, Stucky CL, Jordt SE, Julius D (2007) The menthol receptor TRPM8 is the principal detector of environmental cold. Nature 448:204–208
33. Pradhan AA, Yu XH, Laird JM (2010) Modality of hyperalgesia tested, not type of nerve damage, predicts pharmacological sensitivity in rat models of neuropathic pain. Eur J Pain 14:503–509
34. Mogil JS, Wilson SG, Wan Y (2001) Assessing nociception in murine subjects. In: Kruger L (ed) Methods in pain research. CRC Press, Boca Raton, pp 11–39

Chapter 26

Methods for the Assessment of Heat Perception in Humans

Michael F. Crutchlow and Joel D. Greenspan

Abstract

Several transient receptor potential (TRP) ion channels are activated by heat and may potentially contribute to human heat perception though clinical data are currently either limited or absent. At least three of the identified heat-activated TRP channels are appealing drug targets for multiple potential therapeutic indications. Evaluation of heat perception in clinical development programs will improve drug characterization, highlight potential safety issues related to heat insensitivity, and clarify the role of these channels in human heat sensation. Multiple facets of heat perception may feasibly be assessed in the clinical research unit (CRU) setting using established methods and commercially available equipment including temperature-controlled contact thermodes and circulating water baths. Established methods are reviewed for the assessment of heat perception thresholds and multiple facets of heat perception. An exploratory approach to initial assessment of household burn risk is discussed as well.

Key words: Transient receptor potential (TRP) channels, Heat perception, Thermosensation, Noxious heat, Burn, Hyperalgesia, Human

1. Introduction

The role of transient receptor potential (TRP) ion channels in thermal sensation has and continues to be an area of very active research. Four of the identified TRP channels, TRPV1, V2, V3 and V4, are activated by temperatures perceived as warm or hot, and may plausibly play a role in human heat sensation. Extensive data from preclinical models have emerged in recent years and have progressively helped to define the role of the heat-activated TRP channels (reviewed in (1–4)). Key features of these channels specifically related to heat sensation are summarized in Table 1. Data from in vitro and in vivo models implicate TRPV1 (4–7), V3 (8–11) and V4 (12–15) in noxious heat sensation and in hyperalgesia to heat

Arpad Szallasi and Tamás Bíró (eds.), *TRP Channels in Drug Discovery: Volume II*, Methods in Pharmacology and Toxicology, DOI 10.1007/978-1-62703-095-3_26,

Table 1
Heat activated thermo-TRP channels

	Neuronal and cutaneous expression sites	In vitro thermal activation threshold	Demonstrated In vivo role in heat sensation?		
			Innocuous warmth	Noxious heat	Inflammatory heat hyperalgesia
TRPV1	• C, Aδ fibers • DRG[a] and TG[b]	~42°C	None	Yes[d]	Yes[d]
TRPV2	• DRG[a] • Brain	~53°C	None	None	None
TRPV3	• Keratinocytes • DRG[a] and TG[b]	~33°C	Yes	Yes	Yes
TRPV4	• Keratinocytes • DRG[a] and TG[b]	25–34°C[c]	Yes	Possibly at low-noxious temperatures (45–46°C)[c]	Yes at innocuous and low-noxious temperatures (37.5–42.5°C)

[a] *DRG* dorsal root ganglion
[b] *TG* trigeminal ganglion
[c] Conflicting results reported (12, 15)
[d] Demonstrated in humans

stimuli in the setting of inflammation. Available data suggest that TRPV4 may specifically play a role in these processes in a restricted, relatively low temperature range (13, 14). Both TRPV3 and V4 have also been implicated in the sensation of innocuous warmth (8, 13, 14). Though both the expression pattern of TRPV2 and its activation at high-noxious temperatures would be consistent with a role in noxious heat sensation (16), no thermosensory deficits have been identified in TRPV2 knockout mice (17).

Available clinical data with multiple pharmacologic inhibitors indicate that TRPV1 does indeed play roles in cutaneous perception of innocuous warmth and noxious heat as well as in inflammatory heat allodynia in humans (18–21). There is no publicly available data illuminating the role of TRPV2, V3, or V4 in human heat sensation. However, in light of the promise of the thermo-TRP channels as drug targets for multiple therapeutic indications, in particular TRPV1, V3, and V4, it is anticipated that they will be the focus of ongoing and future drug development efforts (1).

In the context of the development of drug candidates targeting one or more of the thermo-TRP channels, critical goals for assessment of effects on heat sensation include assessing drug target engagement, initial characterization of a therapeutic window in terms of heat insensitivity and burn risk, and elucidation of the role of the targeted TRP channel in human heat sensation. Though blunting of normal heat perception is not anticipated to be a desirable therapeutic effect, selective blunting of inflammatory allodynia (reduced pain thresholds) and hyperalgesia (increased response to painful stimuli) to heat stimuli may indicate early promise for analgesia and other indications related to inflammatory processes.

Well established and feasible methods exist for characterizing effects on non-noxious and noxious heat perception including heat perception thresholds, inflammatory heat allodynia, the intensity of perceived heat and pain associated with a heat stimulus and the affective perception of a stimulus as pleasant or unpleasant. Additionally, exploratory methods may be used to make an initial assessment of potential burn risk associated with identified deficits in heat perception.

2. Warm/Hot Thermal Detection Thresholds

2.1. Background

Thermal threshold assessments have been used to characterize minimum temperatures at which warm/hot stimuli are first perceived to be warm (warmth detection threshold [WDT]) and painful (heat pain threshold [HPT]). Normal skin temperature is 32–33°C (22) and heat stimuli are first perceived as warm just above this neutral temperature. Both the WDT and HPT vary

across body sites and with age, with central sites such as the face being both more sensitive (lower thresholds) and more resistant to age-related decreases in sensitivity than the extremities (23, 24).

Normative WDT and HPT data have been generated in healthy subjects (age 18–75 years; mean ± SD 38.9 ± 12.9 years; 61.1% female) using the contact thermode methodology (Method of Limits) described in detail below (23, 25). Mean cutaneous WDT was reported to be ~33, 34, and 36°C on the face, dorsum of the hand and dorsum of the foot, respectively, and mean cutaneous HPT was reported to be ~43, 44, and 45°C on the face, dorsum of the hand and dorsum of the foot, respectively (23). HPT was consistently higher in males vs. females (~1.6°C higher in males) while WDT was not meaningfully impacted by gender (25).

Studies assessing the impact of laterality (left vs. right or dominant vs. non-dominant side of body) on aspects of heat perception have been inconsistent in terms of identifying effect or lack of effect (23, 26). Though effects, where identified, have been quantitatively small, consistency with regard to the side of the body tested is likely optimal in terms of supporting comparisons. One additional nuance to skin location is the glabrous, nonhairy skin of the palms and soles, which have a higher HPT than adjacent hairy skin (27). This difference is likely explained, at least in part, by differential innervation, specifically the absence of myelinated Aδ (Type II) heat-sensing fibers in glabrous skin (3).

2.2. Methodology-Method of Limits

The most common method used for assessment of the cutaneous WDT and HPT is called the Method of Limits. This involves application of a temperature-controlled contact thermode with a small (generally ~10 cm^2) application surface (23, 28–30). The thermode is heated from a neutral starting temperature (~32°C) through an escalating temperature ramp (typically 0.5–1.0°C/s) to a maximum temperature of around 50°C, established as a test ceiling for safety purposes (23) (Fig. 1a). Subjects are instructed to push a button indicating their first perception of warmth (WDT) or their first perception of pain (HPT). The temperature when the button is pushed is the threshold value for that measurement. The thermode rapidly cools to the target temperature and the test may be repeated. The estimated threshold for a given assessment is typically the central estimate (mean or median) of multiple (usually ~3–6) measurements performed in succession.

Procedures for WDT and HPT Assessment (Method of Limits)

WDT and HPT assessment may be performed with a Thermal Sensory Analyzer (TSA, Medoc, Israel), a Thermotest (Somedic, Sweden), or other equivalent device. WDT and HPT assessment are performed using a nearly identical procedure with the key difference being the instructions to the study subject (Step 4b below). The specific approaches for assessing WDT and HPT provided below are adapted from the protocol developed by the German

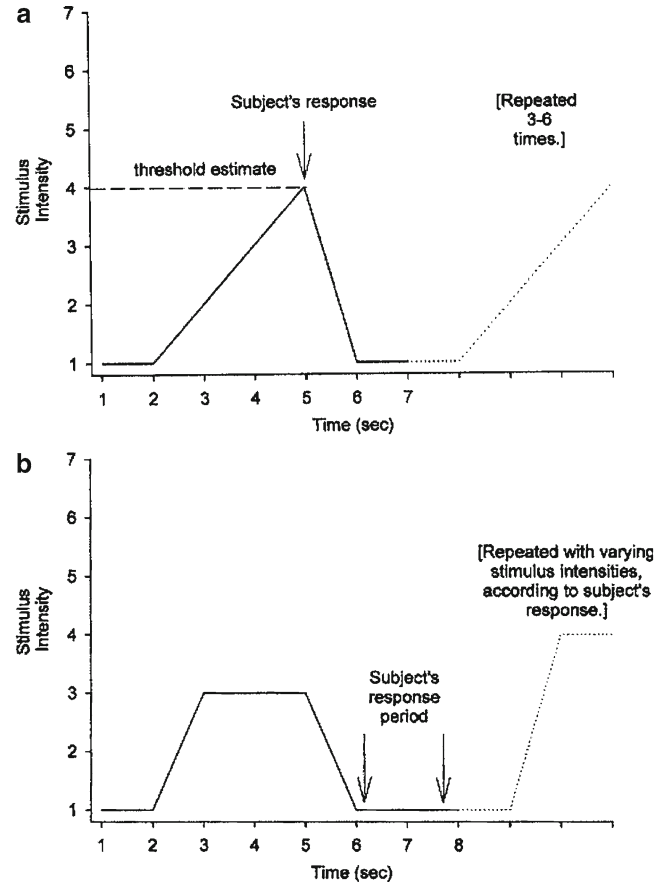

Fig. 1. Threshold determination protocols: general representation of Method of Limits and Method of Levels protocols for perception threshold determination. (**a**) Method of Limits protocol in which stimulus intensity increases until the subject indicates that the specified perception (i.e., warmth for warmth detection threshold [WDT] or pain for heat pain perception threshold [HPT]) has been reached after which the stimulus returns to the baseline level. (**b**) Method of Levels protocol in which a prescribed stimulus is presented for a fixed time after which the subject indicates whether a specified threshold (i.e., HPT) is exceeded. Depending on the response, subsequent stimuli are of either greater of lesser intensity. Reproduced from (28).

Research Network on Neuropathic Pain (DNFS), a protocol with well characterized performance characteristics (23, 25, 31).

1. The subject is informed of the goals of the procedure as follows:
   Now, we will test your ability to sense a change in temperature to "warm." A so-called temperature probe, which is a special appliance, can warm up your skin. This probe will be placed on your hands [feet, or any other area which is of interest]. *In addition, we will determine which temperatures you indicate as painfully hot.*

2. The thermode is brought to the neutral starting temperature of 32°C and then applied to the target skin site and the subject is questioned about the perceived temperature of the thermode:
   (a) *Please indicate if the probe on your skin feels warm, cold or indefinite.*
   (b) If the subject indicates the probe is indefinite (neither warm nor cool), proceed to Step 3. If not, wait up to 30 s and repeat the question in Step 2a (see Note 6 below).
3. The subject is instructed as follows:
   (a) For WDT: *Please press the mouse-button as soon as you start feeling a change in temperature towards "warm"* [or "warmer" if baseline perception is not indefinite—see Note 6 below]. *After this, the probe will cool again to the starting temperature. This procedure will start in a few seconds and will be repeated for three times in total.*
   (b) For HPT (after all WDT testing is complete): *Your skin will now be warmed up for a longer period. You may feel a "warm" sensation, quickly followed by a "hot" sensation. At a certain point, you may start feeling a sensation of "pain" in addition to the "hot" sensation, for example "burning" or "pricking." Please press the mouse button as soon as you start feeling such a painful sensation. After this, the probe will cool again to the starting temperature. This procedure will be repeated for three times in total.*
4. The thermode is then heated through an escalating temperature ramp (1°C/s to a maximum of 50°C) until the subject presses the mouse button at which time the thermode rapidly cools back to 32°C. The procedure is performed three times for each endpoint (WDT or HPT) with at least 1 min passing between stimulations.

Notes

1. The subject should be seated in a comfortable position throughout testing that permits application of the thermode to target skin sites.
2. The computer screen should be positioned that it cannot be seen by the study subject. If this is not possible, the subject should be instructed to look away from the computer screen.
3. For training purposes, a practice run-through of the planned testing should be performed on a skin site removed from the site planned for the actual experiment. It should be confirmed that the study subject understands the procedure before progressing to experimental testing.
4. The specific language used in instructing study subjects may be tailored to study specific goals, but investigators should be

aware that the wording of instructions (i.e., "pain" vs. "discomfort") will impact responses (28) and should be scripted and consistent throughout a study.

5. For HPT assessment it is critical to emphasize that the target threshold is the actual feeling of pain, not the sensation of warmth/heat or the threshold where pain becomes intolerable.
6. The purpose of asking the question in Step 3a is to assure the right adaptation of the skin to the probe. The 32°C temperature will typically be perceived as indefinite (neither warm nor cool). However, depending on skin temperature the thermode may initially be perceived as warm or cool. This should adapt to an indefinite sensation within the 30 s timeframe noted. If the sensation is indefinite prior to testing, the WDT is defined as when the subject perceives the transition from indefinite to warm. If the thermode is perceived to be warm or cool when testing initiates, the WDT is defined as when the subject feels the thermode transition to "warmer" than baseline perception.

2.3. Method of Levels

The Method of Limits is widely used in light of the ease and speed of testing though limitations have been noted. As the temperature of the thermode continues to rise in the time between when a subject perceives a threshold has been reached and when they push the mouse button, the measured threshold is higher than the actual perception threshold, making the measured threshold reaction time dependent (28, 32). Inclusion of the reaction component in the measured threshold could systematically confound results if, for example, a study drug is tested that could potentially impact reaction time (e.g., opiates) or comparisons are being made between young and elderly subjects. Therefore, depending on study goals, a reaction time-independent method referred to as the Method of Levels may be preferable. This involves application of a series of stimuli which are each fixed in duration and intensity and subsequently rated by the subject in terms of the target threshold (Fig. 1b). WDT or HPT measurement using the Method of Limits can be accomplished in 5–10 min while the Method of Levels typically takes 2–3 times longer. Details related to using the Method of Levels are reviewed elsewhere (28, 30).

2.4. Inflammatory Heat Allodynia

HPT assessment is also used to characterize inflammatory thermal allodynia through comparison of the HPT on experimentally inflamed skin vs. normal skin. Established models for inducing cutaneous inflammation include UVR, cutaneous application of capsaicin, and direct thermal burn (18, 33, 34). While UVR and thermal burn induce inflammation secondary to cutaneous injury, capsaicin produces a neurogenic inflammation, and also induces neuropathic effects (35, 36). The most appropriate method should be selected based on study goals.

UVR lowers the HPT in a dose-dependent fashion with relatively stable effects at 24 and 48 h after irradiation and may be a particularly useful model in the CRU setting (34). UVR is applied to a focal skin area using a UV source. An initial testing session is used to determine the minimal dose of UVR required to produce clearly demarcated erythema (minimum erythema dose [MED]) for each individual subject. Subsequently, predetermined multiples of the subject-specific MED (i.e., one- to threefold the MED) are used for testing inflammatory allodynia and/or hyperalgesia. UVR has been used in a clinical study of SB-705498, a TRPV1 antagonist, to assess effects on inflammatory heat allodynia (18).

Cutaneous (topical or intra-dermal) capsaicin application has been widely used as an experimental model of cutaneous inflammation and also robustly lowers the HPT (18, 34, 37). This may be most easily executed using topical application of a ~1% capsaicin preparation for 30 min under an occlusive dressing with HPT assessments being performed before and/or immediately after application. Notably, capsaicin is a direct activator of TRPV1. Therefore, the effects of TRPV1 antagonists in this model may not accurately reflect general effects on inflammatory hyperalgesia. Instead, the capsaicin model may be more useful for assessing direct target engagement of TRPV1 antagonists as has been done for antagonists of another molecule directly involved in the inflammatory response to capsaicin (36).

Thermal skin burn has also been used to induce cutaneous inflammation in experimental settings and does induce thermal allodynia and hyperalgesia (34). However, in light of the pain involved and the potential for more significant burn injury such as blistering, the available alternatives noted above may be considered first.

3. Perceived Intensity

3.1. Background

Human heat perception may be additionally characterized in terms of the perceived intensity of heat (how hot), pain (how painful), and its affective quality (how pleasant or unpleasant) experienced with warm/hot stimulus (22, 26). The highly dynamic relationship between temperature and perception intensity, and the interrelationship between these three facets of heat perception were illustrated in a study using the circulating water bath methodology described in greater detail below (22) (Fig. 2). The intensity of the heat experienced ("Thermal Intensity" Panel A) increased across the 35–47°C tested range. Temperatures ≤41°C were not painful, while those ≥43°C were painful with pain intensity increasing steeply with temperature ("Pain Intensity" Panel C). Increasing temperature was initially associated with increasing "pleasantness," but this diminished as temperatures approached the HPT and

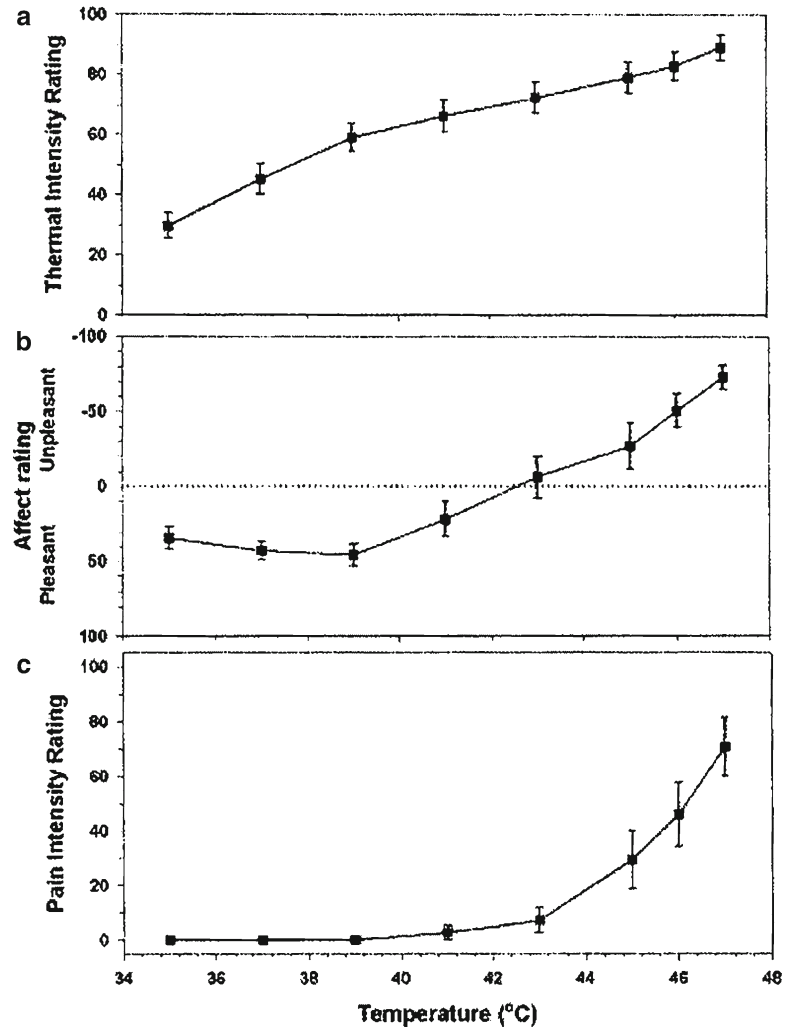

Fig. 2. The relationship between temperature and perception intensity. Ratings of thermal intensity (**a**), pleasantness/unpleasantness (**b**), and pain intensity (**c**) for the hand assessed across a range of temperatures. Thermal stimulus was delivered using immersion in circulating water baths and perception intensities were measured with timed visual analog scale (VAS) assessments. Warm/hot temperatures were 35, 37, 39, 41, 43, 45, 46, and 47°C. Adapted from (22).

temperatures were consistently perceived to be unpleasant at ≥43°C ("Affect" Panel B).

3.2. Methodology

3.2.1. Supra-Threshold Testing (STT) with Contact Thermode

STT is conducted to assess perceived pain intensity with a constant-temperature heat stimulus using the same type of temperature-controlled contact thermode used for WDT/HPT assessment. Therefore, STT and thermal threshold assessments can be performed in a single study with minimal impact on cost and complexity. Heat stimuli are set above the HPT (≥43°C, ranging up to a maximum of ~50°C) and applied to a target skin site (in many studies the volar forearm) for 1–5 s after which subjects are asked

to provide a rating that reflects their perceived pain intensity (38). This can be accomplished in several ways, but typically involves using a numeric rating scale (NRS; often 0–10 or 0–100). Another frequently used alternative is to indicate a point along a continuum with a visual reference of the scale, which is referred to as a visual analog scale (VAS) (22).

Procedure for STT Assessment

1. The subject is informed of the goals of the procedure using scripted language similar to the following, adapted as appropriate to the specific experiment:

   We want to test your sensitivity to heat applied to your arm. We can control the temperature of this device, which I will place on your forearm. At different times, the probe will heat up for 5 s and then cool down. If the temperature of the probe is too uncomfortable, you may ask for it to be removed before the 5 s is over. After the 5 s I will show you a scale from 1 to 100 for you to rate how painful it was. [show the pain VAS scale and give them time to look it over and read the descriptors].
   We will do this once as practice on your [skin site not being tested experimentally]. *Then we will do it a total of [intended number] times on* [experimental test site] *with different temperatures being applied in a random order.*
2. The thermode is brought to the neutral starting temperature of 32°C and then applied to the target skin site. After 30 s the thermode is rapidly heated to the target temperature, maintained at the target for 5 s, and then rapidly cooled to 32°C.
3. After each 5 s stimulus is complete, obtain and record the VAS pain rating.
4. The procedure is performed three times for each temperature being tested. If multiple temperatures are being tested, they may be applied in random sequence for blinding purposes (i.e., for three test temperatures, a total of nine stimulations are delivered in random sequence). At least approximately 1 min should pass between stimulations of the same skin site. Multiple distinct skin sites within a given area (i.e., along the volar forearm) may be used for faster completion of testing.

Notes

1. Notes 1–5 under Sect. 2.2 (Methodology for WDT and HPT Assessment) also apply to STT testing.
2. It is advantageous to assess responses to multiple supra-threshold temperatures during a single sitting. This permits subjects to experience a range of pain intensities and may thereby result in a more reliable use of the scale. This may also help identify deficits restricted to a discrete supra-threshold temperature range such as might hypothetically be seen with TRPV4 inhibition (see Table 1). The thermal sensory testing device can be preprogrammed with target temperature sequences.

3.2.2. Water Bath Immersion Testing

Heat intensity, pain intensity, and the affective component of heat perception may all be assessed using hand and/or foot immersion into temperature-controlled circulating water baths (Fig. 2) (22, 26). After equilibration at a neutral temperature (33°C), the hand/foot is immediately immersed into an adjacent bath at a target test temperature which may range from just above neutral (i.e., 35°C) to well above the noxious threshold (i.e., 49°C). At target time points after immersion in a test temperature, subjects rate the water bath with regard to heat intensity, pain, and pleasantness/unpleasantness using VAS scales (22). Testing may be performed with Fisher Isotemp Open Bath Circulators or other equivalent device. The procedures noted below are directly adapted from those previously published (22, 26).

Procedure for Water Bath Immersion Testing

1. A series of circulating water baths must be brought to the target temperatures in close proximity to one another. One bath must be neutral (33°C), and the others set to target test temperatures. The temperature settings must be obscured so that they are not visible to the participants.
2. Subjects should remove jewelry and watches from both hands/arms prior to testing.
3. The subject is informed of the goals of the procedure as follows:

   We will be testing your sensitivity to warm and hot water temperatures. At the appropriate times, I will instruct you to put one hand in a water bath. This will first be a neutral temperature bath, followed by a warmer bath. We are interested in knowing how the warmer bath feels to you and we will ask you questions about this while your hand is in the water. If you judge that the water temperature is too uncomfortable to tolerate, you may remove your hand. Otherwise, do not remove your hand until you are instructed to do so. The questions I will ask will be as follows:

   (a) *First, I will show you a scale from 1 to 100 for you to rate how warm or hot it was.* [show the warm/hot scale and give them time to look it over and read the descriptors].

   (b) *Second, I will show you a scale from 1 to 100 for you to rate how painful it was.* [show the warm/hot scale and give them time to look it over and read the descriptors].

   (c) *Third, I will show you a scale from 1 to 100 for you to rate how pleasant or unpleasant it was.* [show the pleasantness and unpleasantness scales and give them time to look it over and read the descriptors].
4. The subject places their hand into the neutral (33°C) water bath for 1 min. The hand should be submerged up to the wrist and not be in contact with the sides or bottom of the water bath.

5. After 1 min the subject is instructed to place their hand into one of the adjacent baths maintained at a target test temperature and a timer is started.
   (a) Thermal intensity assessment: Approximately 5 s after hand immersion in the test temperature, the subject is presented with the warmth-heat VAS and provides a rating of intensity from 0 [not at all warm] to 100 [extremely hot].
   (b) Pleasantness/unpleasantness assessment: At least 15 s after the thermal intensity scale is presented (longer if required for the response), the subject is asked whether the bath is pleasant, unpleasant, or neutral. If they indicate neutral, the pleasantness/unpleasantness rating is 0. Otherwise they are presented with the appropriate scale (pleasantness or unpleasantness) and provide a rating from 0 [not at all pleasant/unpleasant] to 100 [extremely pleasant/unpleasant].
   (c) Pain assessment: At least 15 s after the pleasantness/unpleasantness scale is presented, the subject is presented with the pain VAS and provides an intensity rating from 0 [not at all intense] to 100 [extremely intense].
6. The entire sequence for rating (steps 5a–c above) may be repeated a second time. When this is completed (approximately 1.5 min after the hand is placed in the test temperature), the subject is instructed to place their hand back in the neutral (33°C) bath and the sequence for rating (steps 5a–c) may be repeated a third time. Therefore, for the assessment of each individual test temperature, three sets of ratings are obtained—two for the test temperature and one for the neutral (33°C) temperature.
7. Approximately 45 s after hand immersion in the neutral (33°C) bath, the hand is removed and dried with a towel.
8. Two minutes after hand removal from the neutral (33°C) bath, steps 4 and 5 are repeated for the next test temperature using the opposite hand. The hand should be alternated between successive trials within each testing session.

Notes

1. The same approach outlined above may be used to test perception in the feet. The foot being tested should be submerged up to the ankle, and not touching the sides or bottom of the bath. A perforated surface such as Plexiglas has been used to elevate the foot above the bottom of the bath and permit contact between the circulating water and the bottom of the foot.
2. Though random sequencing of test temperatures would be optimal in terms of blinding, perceptions of lower/milder temperatures can be substantially blunted if they follow exposure to an extreme temperature. Therefore, a fixed ascending temperature sequence within each testing session has been

used though this may necessarily result in some degree of predictive anticipation.

3. Perceptual adaptation and/or augmentation over the timeframe of testing may be anticipated over the ~1.5 min of hand/foot immersion depending on the endpoint and the specific test temperature (26). Therefore, data collected with the first and second ratings during a given immersion should not be pooled unless there is a clear statistical rationale for doing so.

4. Withdrawal from/Avoidance of Potentially Injurious Heat

The methods noted above can substantially characterize deficits in heat perception. However, none specifically assesses whether heat perception deficits translate into significant impairment in the ability to avoid or withdraw from potentially injurious heat in the household setting, a potential safety concern for drugs inhibiting the activity of the heat-activated TRP channels (19, 21).

The HPT correlates closely with the threshold above which heat stimuli have potential to cause burn injury and exposure time required for second-degree burn dramatically shortens with incremental increases in temperature (39–41) (Table 2). For context in terms of heat encountered during normal daily living, 49°C is the recommended temperature setting for domestic hot water heaters, though temperatures as high as 60°C are commonly used (42).

Table 2
The relationship between temperature and the time to burn injury (41)

Temperature[a] (°C) F	Time to full thickness epidermal necrosis (second- or third-degree burn)
44.0°C	5–6 h
45.0°C	2–3 h
47.0°C	20–25 min
48.0°C	15–18 min
49.0°C	9.5 min
51.0°C	4 min
53.0°C	1.5 min
55.0°C	30 s
60.0°C	5 s

[a]Applied to anterior thorax or ventral forearm with flowing stream of hot water or oil

Second-degree burns are reported to occur within a plausible bathing timeframe (~9.5 min) at 49°C, and within 5 s at 60°C (39, 41). Food, drink, and heated surfaces are routinely encountered at much higher temperatures with potential to rapidly cause second- and third-degree burns (43). Notable variables impacting the relationship between temperature and time to burn include skin thickness, which varies across body sites and with age (44–46), and fundamental properties of the material delivering the heat stimulus to the skin (39).

The circulating water bath model is a reasonable surrogate for bathing, one of the common household scenarios in which burn risk may be encountered, and can be used to provide at least a preliminary assessment of risk in the bathing setting (19, 21). The general approach may be the same as noted above in Sect. 3.2.2 using a neutral temperature bath for equilibration and multiple test baths, with at least one at a temperature that may be encountered in bathing and has potential to cause significant burn injury (i.e., second-degree burn) in the plausible time frame of bathing. Temperatures in the 47–49°C range meet these criteria. Both are well above the noxious threshold and should be quickly perceived as intensely painful and unpleasant (22). Subjects may be instructed to remove their hand/foot if and when they perceive the bath to be "uncomfortable," a broad term selected based on the assumption that discomfort would lead to withdrawal and/or a lowering of the water temperature in the real bathing setting.

Procedures for Assessing Withdrawal from Noxious Heat

1. Same as Step 1 in Sect. 3.2.2 (bath preparation).
2. Same as Step 2 in Sect. 3.2.2 (watch/jewelry removal).
3. The subject is informed of the goals of the procedure using scripted language similar to the following:

   We will be testing your sensitivity to warm and hot water temperatures. At the appropriate times, I will instruct you to put one hand in a water bath. This will first be a neutral temperature bath, followed by a warmer bath. We are interested in knowing how the warmer bath feels to you. If you judge that the water temperature is uncomfortable enough to want to remove your hand, then just remove it. This is not a test to see how much you can tolerate. If your hand does not feel uncomfortable in a particular bath, leave it in the water until I tell you to remove it.
4. Same as Step 4 in Sect. 3.2.2 (1 min immersion in neutral [33°C] bath).
5. After 1 min the subject is instructed to place their hand into one of the adjacent baths maintained at a target test temperature and a timer is started.
6. Subject removes hand when discomfort is experienced or is instructed to remove their hand at a pre-established time limit

(see Note 1 below). The time from immersion to removal is captured.

7. If desired, perceived intensities may be assessed as exploratory endpoints (see Note 2 below).
8. Two minutes after hand removal from the test bath, steps 4–7 are repeated for the next test temperature using the opposite hand. The hand should be alternated between successive trials within each testing session. The different temperatures being tested may be applied in random sequence for blinding purposes.

Notes

1. There should be a fixed maximum exposure duration that ensures that no burn of any degree will occur at the maximum temperature tested. This is critical as first-degree burn could produce inflammatory allodynia/hyperalgesia and alter responses in subsequent testing and second-degree or greater burn would constitute significant injury to study subjects over a relatively large area of skin.
2. The same VAS scale approach described in Sect. 3.2.2 may be used to capture context with regard to what subjects were experiencing at the time of hand withdrawal. However, in the setting of a test drug that substantially blunts heat pain perception, the duration of hand immersion at the time VAS assessment would vary between treatments (i.e., placebo vs. study drug), thereby limiting the strength of between-treatment comparisons of these endpoints. Subjects may also be asked to rate the heat of the water bath relative to their preferred bathing temperature (i.e., "too hot," "optimal," "too cold") to provide additional "real world" context.
3. Some substantial weaknesses in terms of predicting household burn risk are notable. Neither this nor any other model of experimental heat pain has been validated in terms of predicting burn risk. Therefore, establishing criteria for concluding that burn risk may/may not exist must be based on the assumption that the extrapolation is valid. Additionally, the scenario tested is restricted in terms of temperature and the nature of heat exposure. Notably, much higher temperatures may be encountered in other daily-life scenarios (i.e., food, cooking, machinery, etc).

5. Lasers

Laser stimulation is an alternative to the use of contact thermodes for delivering a focused heat stimulus to the skin (47) and can be used for STT or thermal threshold assessment. One notable disadvantage of lasers is that they typically deliver a target stimulus

energy, and are not specifically controlled with regard to temperature. Key potential advantages to lasers include the lack of mechanoreceptor activation and more rapid heating than achieved with contact thermodes. Of particular interest, a recent study suggests that laser stimulation parameters can be set so as to selectively evoke monomodal heat pain mediated by *either* Aδ or C-fiber thermonociceptors (48), an approach that could potentially be leveraged to more selectively characterize drug-induced effects on heat sensation. Methodologies related to the use of lasers in assessing heat sensation are reviewed elsewhere (47).

6. Conclusions

Pharmacologic inhibition of heat-activated TRP channels has been the focus of substantial drug development efforts in light of potential promise for multiple therapeutic indications. Assessment of effects on human heat perception will be required to characterize the clinical profiles of drug candidates and to elucidate the role of TRP channels in human heat sensation. As discussed in this review, feasible well established methods are available for efficiently characterizing effects on heat perception thresholds, and multiple facets of heat perception (heat pain, thermal intensity, and pleasantness/unpleasantness). Further, exploratory approaches may be employed to make an initial assessment of the safety implications of identified deficits caused by a drug candidate. Collectively, these methodologies can support a robust early assessment of the impact of a drug candidate on human heat sensation.

References

1. Eid SR (2011) Therapeutic Targeting of TRP Channels—The TR(i)P to Pain Relief. Curr Top Med Chem 11(17):2118–2130
2. Pedersen SF, Owsianik G, Nilius B (2005) TRP channels: an overview. Cell Calcium 38(3–4):233–252
3. Schepers RJ, Ringkamp M (2010) Thermoreceptors and thermosensitive afferents. Neurosci Biobehav Rev 34(2):177–184
4. Szallasi A, Cortright DN, Blum CA, Eid SR (2007) The vanilloid receptor TRPV1: 10 years from channel cloning to antagonist proof-of-concept. Nat Rev Drug Discov 6(5):357–372
5. Caterina MJ, Schumacher MA, Tominaga M, Rosen TA, Levine JD, Julius D (1997) The capsaicin receptor: a heat-activated ion channel in the pain pathway. Nature 389(6653):816–824
6. Caterina MJ, Leffler A, Malmberg AB et al (2000) Impaired nociception and pain sensation in mice lacking the capsaicin receptor. Science 288(5464):306–313
7. Davis JB, Gray J, Gunthorpe MJ et al (2000) Vanilloid receptor-1 is essential for inflammatory thermal hyperalgesia. Nature 405(6783):183–187
8. Moqrich A, Hwang SW, Earley TJ et al (2005) Impaired thermosensation in mice lacking TRPV3, a heat and camphor sensor in the skin. Science 307(5714):1468–1472
9. Peier AM, Reeve AJ, Andersson DA et al (2002) A heat-sensitive TRP channel expressed in keratinocytes. Science 296(5575):2046–2049
10. Smith GD, Gunthorpe J, Kelsell RE et al (2002) TRPV3 is a temperature-sensitive

vanilloid receptor-like protein. Nature 418(6894): 186–190

11. Xu HX, Ramsey IS, Kotecha SA et al (2002) TRPV3 is a calcium-permeable temperature-sensitive cation channel. Nature 418(6894): 181–186
12. Guler AD, Lee HS, Iida T, Shimizu I, Tominaga M, Caterina M (2002) Heat-evoked activation of the ion channel, TRPV4. J Neurosci 22(15):6408–6414
13. Lee HS, Iida T, Mizuno A, Suzuki M, Caterina MJ (2005) Altered thermal selection behavior in mice lacking transient receptor potential vanilloid 4. J Neurosci 25(5):1304–1310
14. Todaka H, Taniguchi J, Satoh J, Mizuno A, Suzuki M (2004) Warm temperature-sensitive transient receptor potential vanilloid 4 (TRPV4) plays an essential role in thermal hyperalgesia. J Biol Chem 279(34): 35133–35138
15. Watanabe H, Vriens J, Suh SH, Benham CD, Droogmans G, Nilius B (2002) Heat-evoked activation of TRPV4 channels in a HEK293 cell expression system and in native mouse aorta endothelial cells. J Biol Chem 277(49):47044–47051
16. Caterina MJ, Rosen TA, Tominaga M, Brake AJ, Julius D (1999) A capsaicin-receptor homologue with a high threshold for noxious heat. Nature 398(6726):436–441
17. Park U, Vastani N, Guan Y, Raja SN, Koltzenburg M, Caterina MJ (2011) TRP vanilloid 2 knock-out mice are susceptible to perinatal lethality but display normal thermal and mechanical nociception. J Neurosci 31(32):11425–11436
18. Chizh BA, O'Donnell MB, Napolitano A et al (2007) The effects of the TRPV1 antagonist SB-705498 on TRPV1 receptor-mediated activity and inflammatory hyperalgesia in humans. Pain 132(1–2):132–141
19. Crutchlow MF, Dong Y, Schulz V et al. (2009) Pharmacologic Inhibition of TRPV1 impairs sensation of potentially injurious heat in healthy subjects. ASCPT 2009 in Gaylord National Resort and Convention Center on the Potomac, National Harbour, MD. 3-18-2009.
20. Krarup AL, Ny L, Astrand M et al (2011) Randomised clinical trial: the efficacy of a transient receptor potential vanilloid 1 antagonist AZD1386 in human oesophageal pain. Alim Pharmacol Ther 33(10):1113–1122
21. Rowbotham MC, Nothaft W, Duan WR et al (2011) Oral and cutaneous thermosensory profile of selective TRPV1 inhibition by ABT-102 in a randomized healthy volunteer trial. Pain 152(5):1192–1200
22. Greenspan JD, Roy EA, Caldwell PA, Farooq NS (2003) Thermosensory intensity and affect throughout the perceptible range. Somatosens Motor Res 20(1):19–26
23. Rolke R, Baron R, Maier C et al (2006) Quantitative sensory testing in the German Research Network on Neuropathic Pain (DFNS): standardized protocol and reference values. Pain 123(3):231–243
24. Stevens JC, Choo KK (1998) Temperature sensitivity of the body surface over the life span. Somatosens Motor Res 15(1):13–28
25. Magerl W, Krumova EK, Baron R, Tolle T, Treede RD, Maier C (2010) Reference data for quantitative sensory testing (QST): refined stratification for age and a novel method for statistical comparison of group data. Pain 151(3):598–605
26. Sarlani E, Farooq N, Greenspan JD (2003) Gender and laterality differences in thermosensation throughout the perceptible range. Pain 106(1–2):9–18
27. Taylor DJ, McGillis SLB, Greenspan JD (1993) Body site variation of heat pain sensitivity. Somatosens Motor Res 10(4):455–465
28. Greenspan JD (2007) Threshold determination protocols. In: Schmidt RF, Willis WD (eds) Encyclopedia of Pain. Springer, Berlin, pp 2479–2482
29. Hansson P, Backonja M, Bouhassira D (2007) Usefulness and limitations of quantitative sensory testing: clinical and research application in neuropathic pain states. Pain 129(3):256–259
30. Yarnitsky D (1997) Quantitative sensory testing. Muscle & Nerve 20(2):198–204
31. Geber C, Klein T, Azad S et al (2011) Test-retest and interobserver reliability of quantitative sensory testing according to the protocol of the German Research Network on Neuropathic Pain (DFNS): a multi-centre study. Pain 152(3):548–556
32. Yarnitsky D, Ochoa JL (1990) Studies of heat pain sensation in man—perception thresholds, rate of stimulus rise and reaction-time. Pain 40(1):85–91
33. Benrath J, Gillardon F, Zimmermann M (2001) Differential time courses of skin blood flow and hyperalgesia in the human sunburn reaction following ultraviolet irradiation of the skin. Eur J Pain (Lond) 5(2):155–167
34. Bishop T, Ballard A, Holmes H, Young AR, McMahon SB (2009) Ultraviolet-B induced inflammation of human skin: characterisation and comparison with traditional models of hyperlagesia. Eur J Pain 13(5):524–532
35. Nolano M, Simone DA, Wendelschafer-Crabb G, Johnson T, Hazen E, Kennedy WR (1999)

Topical capsaicin in humans: parallel loss of epidermal nerve fibers and pain sensation. Pain 81(1–2):135–145

36. Sinclair SR, Kane SA, Van der Schueren BJ et al (2010) Inhibition of capsaicin-induced increase in dermal blood flow by the oral CGRP receptor antagonist, telcagepant (MK-0974). Br J Clin Pharmacol 69(1):15–22
37. Chizh BA, Sang CN (2009) Use of sensory methods for detecting target engagement in clinical trials of new analgesics. Neurotherapeutics 6(4):749–754
38. Kim HS, Neubert JK, Miguel AS et al (2004) Genetic influence on variability in human acute experimental pain sensitivity associated with gender, ethnicity and psychological temperament. Pain 109(3):488–496
39. Bull JP, Lawrence JC (1979) Thermal conditions to produce skin burns. Fire Mater 3(2): 100–105
40. Diller KR, Pearce JA. Issues in modeling thermal alterations in tissues. Ann NY Acad Sci. 888:153–164
41. Moritz AHF (1947) Studies of thermal injury II. The relative importance of time and surface temperature in the causation of cutaneous burns. Am J Pathol 23:695–720
42. Levesque BLMJJ (2004) Residential water heater temperature: 49 or 60 degrees Celcius? Can J Infect Dis 15:11–12
43. Lee HS, O'Mahony M (2002) At what temperatures do consumers like to drink coffee?: mixing methods. J Food Sci 67(7): 2774–2777
44. Diller KR (2006) Adapting adult scald safety standards to children. J Burn Care Res 27(3):314–322
45. Seidenari S, Giusti G, Bertoni L, Magnoni C, Pellacani G (2000) Thickness and echogenicity of the skin in children as assessed by 20-MHz ultrasound. Dermatology 201(3): 218–222
46. Waller JM, Maibach HI (2005) Age and skin structure and function, a quantitative approach (I): blood flow, pH, thickness, and ultrasound echogenicity. Skin Res Technol 11(4): 221–235
47. Arendt-Nielsen L, Chen ACN (2003) Lasers and other thermal stimulators for activation of skin nociceptors in humans. Neurophysiol Clin 33(6):259–268
48. Tzabazis AZ, Klukinov M, Crottaz-Herbette S, Nemenov MI, Angst MS, Yeomans DC (2011) Selective nociceptor activation in volunteers by infrared diode laser. Mol Pain 7:18

Chapter 27

Collagen Antibody-Induced Arthritis: A Disease-Relevant Model for Studies of Persistent Joint Pain

Katalin Sandor, Kutty Selva Nandakumar, Rikard Holmdahl, and Camilla I. Svensson

Abstract

Rheumatoid arthritis (RA) is a complex autoimmune disease, with a prevalence of approximately 1% in the population worldwide. RA is a chronic inflammatory disease primarily affecting joints and patients suffer from a plethora of symptoms, including pain, fatigue and stiffness. Joint pain is one of the most egregious symptoms in RA. Animal models of RA are used extensively in research to understand the pathogenesis of inflammatory arthritis and in the assessment of potential disease-modifying agents. There is an increasing need for disease-relevant animal models for pain research and several of the RA animal models that previously were not used in pain research have now been characterized for this purpose. The most commonly used RA model is the collagen-induced arthritis (CIA) model. However, it has certain disadvantages when used for pain research. Here we describe an alternative model, the collagen antibody-induced arthritis (CAIA) model to study RA-induced pain. This model has been used to investigate disease pathology for more than 10 years, but has just recently been characterized as a pain model. In comparison to CIA, more mouse strains are susceptible to CAIA and the degree of joint pathology and systemic disease is less severe, making the assessment of arthritis-associated nociceptive behavior, such as paw withdrawal from mechanical or thermal stimuli, as well as changes in normal behavior such as locomotion more easily investigated. The aim of this chapter is to describe the CAIA model and several techniques used to study inflammatory pain-like behavior.

Key words: Collagen antibody-induced arthritis, Rheumatoid arthritis, Chronic pain, Mechanical hypersensitivity

1. Introduction

Rheumatoid arthritis (RA) is a complex, systemic autoimmune disease with genetic and environmental components, affecting approximately 1% of the population worldwide (three times more

Arpad Szallasi and Tamás Bíró (eds.), *TRP Channels in Drug Discovery: Volume II*, Methods in Pharmacology and Toxicology,
DOI 10.1007/978-1-62703-095-3_27,

common in women than in men). Arthritis in the articular joints is a devastating problem for patients, as it results in disability and pain, and thus reduces quality of life. Rheumatoid arthritis is characterized by inflammation primarily in the synovial joints, but may affect other tissues and organs throughout the body named as extra-articular manifestations. The disease is associated with proliferation and infiltration of multiple cell types including macrophages, neutrophils, mast cells, T and B cells in the synovium. The resulting inflammatory processes lead to swelling and pannus formation in the joint, as well as destruction of cartilage and bone. RA has been studied intensively but the precise pathological mechanisms remain unclear. Considering all symptoms of RA, pain is frequently reported to be the major physical problem and symptom of the patients. In fact, arthralgia (joint pain without inflammation) and the presence of serum autoantibodies (e.g., rheumatoid factors and anti-citrullinated protein antibodies) predate the development of RA (1, 2). The prognosis for RA has been dramatically improved since the introduction of "biologics," drugs that alter the progression of the disease. However, despite improved disease control, pain is still a major issue for RA patients. In a recent study 86% of the patients stated that their disease was "somewhat to completely controlled," yet 65% continued to rate their pain as a significant problem (3).

Chronic pain is often associated with sleep disturbances, depression, social isolation and reduced ability to work. Long-term pain is a major burden not only for the affected individual but also for the society; approximately 20% of the population worldwide suffers from chronic pain, which leads to enormous costs in the form of medical treatment, sick leave, and lost productivity (4, 5). Non-steroidal anti-inflammatory drugs (NSAIDs) and opioids, alone or in combination, are quite effective for treatment of short-lasting inflammatory pain. Unfortunately, these currently available treatments are often not sufficient for long-term pain, either because they do not provide adequate pain relief or because they are associated with problematic side effects. Thus it is critical to increase our understanding of how chronic pain is regulated in order to identify new targets for pain relief. By exploring the mechanisms of pain in RA we might be able to unravel targets with potential to attenuate chronic inflammatory joint pain. Hence, it is crucial to investigate chronic pain mechanisms using disease-relevant models.

Even though several experimental animal models exist for RA, there is no "universal model" due to the complexity, as well as genetic and molecular heterogeneity of the disease (6, 7). KRN mice, transgenic for a T cell receptor that recognizes an epitope of bovine RNAse peptide, develop arthritis spontaneously (8). Crossing KRN mice with non-obese diabetic (NOD) mice generates K/BxN mice that spontaneously develop severe joint inflammation of all distal

joints (9). Spontaneous inflammatory arthritis can be evoked by genetic modifications such as in TNF-α overexpressing mice (10) and in IL-1 receptor antagonist-deficient mice (11). Arthritis can also be induced by immunization, as in the collagen-induced arthritis model (12, 13). Intra-articular injection of zymosan, a polysaccharide derived from a bacterial cell wall, evokes biphasic arthritis in mice (14, 15). A single subcutaneous injection of pristane, a terpenoid alkane results in chronic arthritis in rats (16). Another way of inducing arthritis in rodents is sensitization to an antigen, followed by intra-articular injection of the same agent, such as proteoglycan (17) or bovine serum albumin (18).

The most commonly used RA animal model is the collagen-induced arthritis (CIA) model. Arthritis is induced in this model by immunizing mice or rats using collagen type II (CII), one of the major matrix proteins of the articular cartilage. Of note, the severity of CIA has been identified as a problem when focusing on pain-related behavioral experiments in the animals, as sickness may override readouts for nociception. In addition, the number of mouse strains that are susceptible to CIA is limited and this could pose a problem, especially as C57BL/6 mice are not susceptible and this genetic background often sets the framework for studies using genetically modified mice.

We are focusing on antibody-induced joint inflammation and have found that animal models of RA in which antibodies targeting proteins expressed in the joint are delivered systemically have several advantages in pain research. Antibodies, especially as constituents of immune complexes, play a central role in triggering inflammation but they can also directly cause the destruction of the target tissue preceding and independent of disease development and in the absence of any other pathogenic inflammatory factors or the action of immune cells (19). Serum transfer from the K/BxN mice reliably induces transient inflammatory arthritis in the joints of a wide range of mouse strains (8) due to transfer of autoantibodies against glucose-6-phosphate isomerase (9). Collagen antibody-induced arthritis (CAIA) is an extension of the CIA model, in which monoclonal antibodies against CII are injected instead of immunizing the mice against CII (20–22). These findings have led to defined cocktails of antibodies to standardize CAIA (23, 24). While both CAIA and K/BxN models are well established for disease-mechanistic studies in the RA field, we have recently characterized the K/BxN serum transfer arthritis (25, 26) and the CAIA model (Bas et al., manuscript in revision) as new experimental models of inflammatory joint pain. These models display pronounced and reproducible mechanical hypersensitivity during the phase of joint inflammation. As recipient mice receive the same quantity of antibodies at the same time, the CAIA and K/BxN serum transfer models have a predictable onset of signs of arthritis. Both models have a high incidence rate with a fast disease onset,

within days instead of weeks as with the CIA model (8, 27). The severity of the disease can be titrated based on the amount of antibodies injected and then the inflammatory phase reliably resolves as the antibodies are cleared and not replaced by B cells. Mice injected with CII antibodies or K/BxN serum display robust and highly reproducible mechanical hypersensitivity with an onset that correlates with joint and paw inflammation. Of note, the mechanical hypersensitivity does not return to baseline concurrent with the resolution of joint inflammation, but outlasts the signs of arthritis by at least 6 weeks. Thus, these two RA models provide an opportunity to study pain-like behavior and mechanisms of pain processing not only during the ongoing joint inflammation, but also in the post-inflammatory phase.

The K/BxN model was recently described from a pain perspective (25); hence in this chapter we are focusing on the CAIA model and accordingly the protocol describes the usage of the CAIA model as a model of persistent pain.

2. Materials

2.1. Mice

It is recommended to use adult mice, as mice under the age of 6–7 weeks show low incidence rate of collagen antibody-induced inflammation (28). In general, increasing age is associated with increased CAIA susceptibility and disease severity (22). Background strains that have been screened for susceptibility to CAIA include: BALB/c, C57BL/6, DBA/1, QB (BALB/c×B10.Q) F1, QD (B10.Q×DBA/1) F1, B10.Q, B10.RIII, C3H.Q, NFR/N, RIIIS/J and NOD.Q mice (22). If strains other than those listed above are preferred, pilot studies and appropriate controls should be undertaken as different strains may show different susceptibility to CAIA-mediated induction of hypersensitivity (and arthritis). It is also recommended to consider the choice of sex carefully. There are sex differences with regard to both basal and induced pain-like behavior in mice (29), as well as in CAIA susceptibility. In some strains male mice are more susceptible than females and this is thought to be dependent on estrogen's suppressive effect on CII antibody response (30) and on CAIA (22, 31). There are clear sex differences regarding social behavior. For example, fighting among males is more common than between female mice, and of importance, aggression enhances CIA susceptibility (32), also see Note 1.

2.2. Collagen Antibody Cocktail for Induction of Arthritis

(a) Antibody cocktail containing monoclonal antibodies against different epitopes of collagen type II.

While there are some variations in the cocktail composition between different manufacturers, the most common

cocktails contain IgG antibodies CIIC1, CIIC2, M2139 and UL1 against the $C1^{III}$, D3, J1 and U1 collagen epitopes (23). The highly conserved nature of these epitopes across the species originally formed the basis for the development of RA inducing reagents, as in mice and human RA patients the antibody response that best correlates with disease is directed against these epitopes (33). The first commercially available cocktail consisted of four antibodies and arthritis was inducible with these cocktails in several mouse strains, the best responders being DBA/1, BALB/c, QB and B10.RIII mice (22, 34). Later additional antibodies have been added to the cocktail to facilitate induction of RA in a broader range of mouse strains. The currently commercially available cocktails are listed in Table 1. CAIA cocktail is currently only available for mice.

(b) LPS from *Escherichia coli* serotype 055:B5 (Sigma-Aldrich) dissolved in saline or PBS.

(c) 1 ml syringe and 27 G needle for CII antibody cocktail and LPS injection.

(d) Restrainer for the injection of conscious mice.

(e) Infrared lamp to warm the tail prior to intravenous injection.

2.3. Assessment of Joint Swelling

(a) A plethysmometer is used to assess the degree of swelling. It consists of two Perspex chambers filled with conductive solution that are connected to each other and to a control unit. The device works on the principle of water displacement, the immersion of the paw into one chamber is reflected into the other chamber, which induces conductance between the two platinum electrodes. The control unit detects the conductivity changes and transforms it to the displaced volume.

(b) A caliper is used to measure the ankle/knee diameter.

2.4. Mechanical Hypersensitivity

(a) An elevated platform with open access from the bottom to the wire mesh surface.

(b) A clear Plexiglas enclosure on the top divided approximately into 15 × 15 cm boxes covered by Plexiglas lid. The Plexiglas boxes should provide enough space for the mouse to turn, walk and rear.

(c) A set of von Frey filaments. There are different types of synthetic plastic filaments, the most commonly known ones are the Stoelting filaments (0.04 g, 0.07 g, 0.16 g, 0.4 g, 0.6 g, 1.0 g and 2.0 g). The Marstock OptiHair filaments also are used frequently, the difference being that they are made of elastic optic glass fibers and therefore are not affected by temperature and humidity changes. The end of each filament is coated with

Table 1
Properties of the commercially available CAIA cocktails

Company	Epitopes	Antibodies	Dose	LPS	Mouse strain
Chondrex, Arthrogen CIA® 5-clone cocktail Kit	LyC1, LyC2 (on CB11 fragment)	3 IgG2a (A2-10, F10-21, D8-6) 1 IgG2b (D1-2G, D2-112)	1.5 mg i.v. or i.p.	25–50 μg i.p. (day 3)	B10.RIII, BALB/c, DBA/1, CB.17 scid/scid, 129/sv, C57BL/6, CBA
MDBiosciences ArthritoMAB™ antibody cocktail for inducing arthritis	$C1^{1b}$ (on CB11 fragment), U1 (CB8 fragment), J1, D3 (CB10 fragment)	3 IgG2a 1 IgG2b	2–8 mg, i.v. or i.p.	50–100 μg i.p. (day 3–6)	BALB/c, B10.RIII, B10.Q, C3H.Q, DBA, QB
MDBiosciences ArthritoMAB™ antibody cocktail for C57BL/6	$C1^{1b}$ (on CB11 fragment), U1 (CB8 fragment), J1, D3 (CB10 fragment)	3 IgG2a 1 IgG2b	2–8 mg, i.v. or i.p.	50–100 μg i.p. (day 3–6)	C57BL/6
Millipore ArthroMAB™	$C1^{1b}$ (on CB11 fragment), U1 (CB8 fragment), J1, D3 (CB10 fragment)	3 IgG2a 1 IgG2b	2–8 mg i.v.	25–50 μg i.p. (day 3–6)	DBA/1, BALB/c, B10.RIII, C57BL/6
ModiQuest, Arthritis Antibody Mix	Not listed	8 (IgG1, IgG2a, IgG2b)	2.4–3.2 mg i.p.	25 μg i.p. (day 3–6)	DBA/1, BALB/c, C57BL/6, 129/sv

The table shows the names of the antibody cocktails and companies providing the antibody cocktails for purchase. The antibody content of these cocktails, the dose range and the route of injection of the cocktail, the dose range and the day of the subsequent LPS injection, and a list of the mouse strains that have been reported to develop signs of arthritis subsequent to antibody cocktail injection are also listed

a small epoxy bead to ensure a constant contact surface of different fibers, as well as to avoid a potential stimulation of nociceptors when the filament is bent. The Marstock OptiHair filaments are calibrated to the following forces: 0.025 g, 0.051 g, 0.102 g, 0.204 g, 0.408 g, 0.815 g, 1.63 g and 3.26 g.

(d) An automatized von Frey device to assess mechanical hypersensitivity (alternative to manual filaments).

2.5. Pressure Application Measurement Device

The pressure application measurement device is designed to assess mechanical hypersensitivity in knee and ankle joints. It consists of a force transducer mounted on the researcher's thumb and a control unit.

2.6. Cold Hypersensitivity

It has been shown that RA patients develop hypersensitivity to innocuous cold (35); hence testing sensitivity to cold is of relevance in experimental models of RA. The mouse can be placed on a cold surface and the time to response is assessed. This test is commonly referred to as "the cold plate" test. Alternatively, cooling reagents, such as menthol or acetone, can be applied to the paw and the duration of response measured (36, 37).

(a) A cold plate to assess cold hypersensitivity or two cold plates connected to each other to assess temperature preference.

(b) 1 ml syringe and acetone or menthol for topical application to the paw.

(c) Grid or Plexiglas enclosure as testing environment for the acetone/menthol test.

2.7. Thermal Hypersensitivity

(a) Modified Hargreaves-type device. This includes a temperature variable glass surface upon which the mice are placed and a triggerable, movable focused heat source. Frequently this heat source is attached to a mirror to allow for easy visualization of the heat source on the appropriate portion of the footpad.

(b) A Plexiglas enclosure on the top divided approximately into 15×15 cm boxes covered by Plexiglas lid that can be placed on top of the thermal testing device.

(c) Timer.

2.8. Locomotor Activity

Besides the evoked mechanical hypersensitivity testing procedures, there is an increasing need to test changes in the spontaneous locomotion of mice, especially during long-term pain conditions. There are several methods to test locomotion, such as the catwalk system, the comprehensive laboratory animal monitoring system (CLAMS) or the laboratory animal behavior observation, registration and analysis system (LABORAS).

3. Methods

3.1. Induction of Arthritis

The antibody cocktail (PBS to the control group) can either be injected intravenously to the tail vein or intraperitoneally using a 1 ml syringe and a 27 G needle. Prior to intravenous injection, the mouse is gently restrained in a tube where they can breathe easily, but not turn around, leaving the tail accessible to the experimenter (see Note 2). To facilitate tail vein location and injection, the veins can be dilated by warming the tail with a tissue merged in warm water or using an infrared lamp to heat the tail for a couple of seconds. The recommended amount of antibodies and the injection volume are different and depend on the antibody cocktail composition and concentration, see Table 1. The day of the cocktail injection counts as day 0 in the experiment.

3.2. Synchronizing and Enhancing the Development of CAIA

Injection of LPS is optional in this model. However, it is commonly used as injection of LPS synchronizes the onset of visible inflammation, increases the disease severity and at the same time reduces the amount of monoclonal antibody required to induce arthritis (38). LPS is derived from *E. coli*, it is always part of the commercial package, the dosage and the recommended day of injection are described in Table 1. LPS is injected intraperitoneally with a 1 ml syringe and a 27 G needle. The first signs of inflammation usually appear within 1 day after injection of LPS. Mice in the control group are injected with the same volume of PBS or saline. It is recommended to include a control group injected with LPS alone, in particular if nociception is studied in the early phase of inflammation. LPS is associated with the release of pro-inflammatory cytokines, such as interleukin-1 (IL-1), which on its own may activate or sensitize nociceptors or cause release of other nociceptive mediators, e.g., prostaglandins (39). LPS also activates glia cells in the spinal cord, which have been implicated in pain processing (40). However, in our laboratory, 25 μg of LPS i.p. does not induce mechanical hypersensitivity (Fig. 1) and based on the low-dose single injection of LPS it is unlikely that LPS has a significant impact on pain thresholds at later time points in the model. Of note, following CII antibody cocktail injection, and in particular the day after LPS injection, the mice lose body weight, but normally they recover within 1 week of the experiment (see Note 3).

3.3. Arthritis Scoring

The degree of inflammation (redness and swelling) in the joints is assessed by visual inspection and scoring. There are different scoring systems, and in this chapter we describe two different methods. Scoring of the paws should be done prior to the injection of CII antibody cocktail and then regularly throughout the experiment (e.g., every third day). The signs of inflammation are quite obvious,

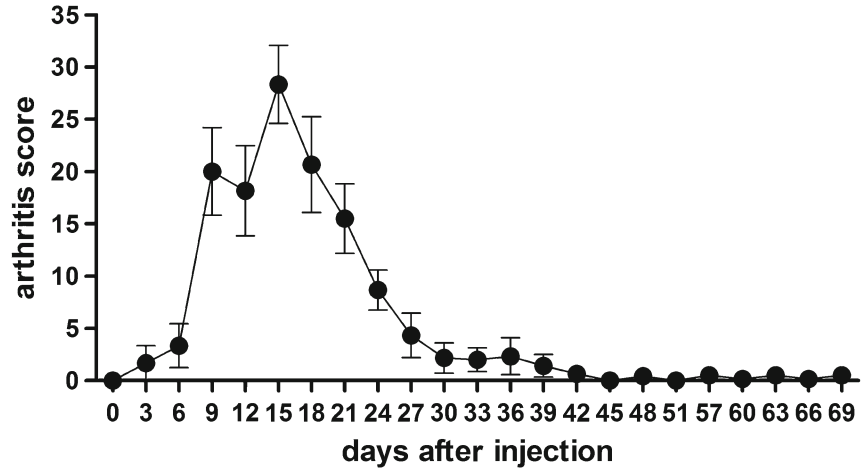

Fig. 1. Results of the mean arthritis scores in CAIA mice over time after injection. Visual signs of arthritis appeared already by day 3, reaching a maximum score of 30 on day 15 and gradually turned back to approach a score of 0 by day 40. PBS and LPS groups did not show signs of arthritis (Data points are expressed as mean ± SEM, $n = 6$ mice/group).

but it is recommended to practice with cross-checks between investigators, and to perform the scoring blinded.

The mouse is lightly restrained and the researcher carefully examines and records clinical signs according to method 1 or method 2 (described below). Data are presented as a total score per time point.

3.3.1. Method 1

Data presented in this protocol are recorded using method 1 (Fig. 1). This is an extended scoring protocol commonly used in research laboratories (41). Inflammation is defined as redness and swelling at the same time of the affected part of the leg (see Note 4). All four limbs are examined including the toes, the ankle and the dorsal mid-surface of the paw. Each leg can score a maximum of 15 points and each animal can score a maximum of 60 points. Points are given as follows:

- 1 point for each inflamed toe
- 1 point for each inflamed knuckle
- 5 points if the ankle is inflamed

3.3.2. Method 2

For each of the four limbs (maximum of 4 points per limb, up to a combined total of 16) score points (1–4) are given according to the presence of the following features with the greatest point value:

- 1 point if there is only redness of the bottom of the footpad.
- 2 points if there is visible thickening of the paw.
- 3 points if the swelling of the ankle is sufficient to make the ankle equal to or greater in width than the mid-footpad.
- 4 points if there is swelling of at least one digit.

3.4. Joint Swelling

Besides visual inspection and scoring, the degree of edema formation may be assessed.

(a) Plethysmometer
Mice are habituated to being restrained and having their paws immersed in water. Baseline testing should be performed before the cocktail injection. The mouse is restrained tightly and the experimenter gently holds and stretches the leg by the thigh, leaving the hind paws free. The paw is immersed in one of the chambers and held in a constant position until the displacement of solutions is stable on the display panel (shown in cm^3). In order to correctly assess edema, it is crucial to submerge the paw to the same depth of the chamber at each test session throughout the whole experiment. A reference point can be made by drawing a line above the ankle with a small fiber marker, dip the paw as deep as the line touches the surface of the solution; this way the same depth during the experiment can be ensured. Data can be presented as paw volume using cm^3 values, or as percent change from the baseline expressed as edema. The plethysmometer is designed to test paw edema and it is not suitable for measuring knee edema, because the leg cannot be submerged as deep as needed in the chamber.

(b) Caliper
The mouse is lightly restrained and the caliper is used to measure the diameter of the ankle and/or the knee joint. The caliper should be placed at the lateral sides of the ankle or the knee joint. Care should be taken to prevent compression of the tissue, the caliper should just touch the skin. A caliper without any spiral or with a weak spiral is preferable, as otherwise there may be a risk of tissue compression, which could cause tissue damage and confounded measurements. This method of edema assessment is not trivial; the joint can change position even due to weak pressure and therefore at least three recordings in each session are suggested. The test can be repeated as often as required. Data can be presented as diameter in mm, or as percent change compared to control.

3.5. Assessing Mechanical Hypersensitivity

1. Habituation
The mice are placed on a mesh surface in individual Plexiglas enclosures. The mice are habituated to the testing device for approximately 1–2 h on two different days prior to the recording of baselines and induction of arthritis. Habituation time differs between strains and research environments; hence the researcher should observe the mice during habituation in order to provide enough time to allow them to calm down and minimize their explorative behavior. Keeping the mice in the enclosure for a long time is not recommended, since the mesh surface could cause sensitization of the paw, and the absence of

food and water could affect the mice. At least three baseline measurements are suggested for calculation of average baseline thresholds prior to intravenous injection of CII antibody cocktail. Preferably the frequency of the baseline testing and testing during the experiment should be the same, e.g., every third day. Variation in nociceptive thresholds may be reduced by performing the tests during the same period of the day (also see Notes 5, 6 and 7).

2. von Frey filaments and the "up–down method"
Several sets of von Frey filaments exist, and this chapter describes the Dixon up–down method (42) modified by Chaplan and coworkers (43) and using the Marstock filaments. Each filament is applied perpendicular to the center of the plantar surface of the hindpaw for a maximum of 5 s, or until a response is observed. A response is defined as a clear and brisk withdrawal of the paw. In cases when the mouse steps or walks away, the testing is stopped and repeated 2–3 min later. When one paw is tested, it is recommended that the researcher tests the paw of another animal instead of testing the second paw of the same animal.

   (a) Testing begins with the middle filament (e.g., with 0.408 g in the Marstock series).

   (b) In the absence of paw withdrawal response ("o"), the next stronger filament in the series is applied (e.g., 0.815 g).

   (c) If a paw withdrawal is observed ("x"), the next weaker filament is chosen (e.g., 0.204 g).

   (d) When a response is observed after a non-responder filament, it has to be followed by four more filaments.

   These six recordings give a pattern of the sensitivity of the examined paw (e.g., "oxoxox"). This pattern is expressed as a certain factor in the appendix of the Chaplan paper (43) which belongs to the following formula:

$$50\%\ \text{g threshold} = (10^{[x_f + k\delta]}) / 10{,}000$$

where x_f is the value (in log units) of the final von Frey filament used, k is the value of the pattern in the appendix, and δ is the mean difference (in log units) between two filaments (see Note 8). This calculation results in the 50% threshold in grams, which means that at the calculated value there is a 50% chance to observe a positive withdrawal response. Even though it is mathematically not continuous, thus, considered to be non-parametrically distributed (43), very often data are analyzed according to parametrical features (44). The baseline 50% threshold varies between mouse strains and differs at different ages or between sexes, but generally it is not lower than 2 g or

higher than 4 g. Data can be presented as 50% threshold values in grams throughout the experiment, or as percent change from the baseline, which can be expressed as mechanical hypersensitivity.

3. Automatized von Frey device
   There are automated, digitalized devices to test hypersensitivity not using several filaments with different forces, length and diameters, but using one single filament, which is connected to and driven by a preset stimulator unit. The control unit is moved under the mouse with the help of a mirror attached, and once the unit is at the right place (the filament faces the middle of the hind paw), the button on the control unit is pressed and the filament lifts up until it reaches the plantar surface of the paw. Immediately after reaching the paw, the filament exerts an increasing upward force to a maximum value with a preset ramp (see Note 9) until the paw is withdrawn; thus, the filament falls back. The stimulator unit registers the force in grams and the time elapsed in seconds. Therefore, data can be presented as mechanical threshold in grams, as percent change from the baseline (expressed as mechanical hypersensitivity) or as response latency in seconds.

3.6. Assess Deep Pressure Sensitivity

A force transducer (with a 5 mm rounded probe) is mounted on the thumb of one hand and the mouse is lightly held with the other hand. The ankle or knee joint is gently positioned between one finger and the transducer, the latter being applied to the lateral side of the knee or the ankle joint. Once the proper position is set, the researcher applies increasing pressure on the joint (30 g/s) until the animal attempts to escape or withdraw the leg (see Note 10). In case the mouse does not respond the testing should be stopped at 8–10 s (240–300 g) to prevent tissue damage (45). With the help of a computer and a software the rate of force application can be preset and the linear increase of pressure visualized on the screen, thus, making the pressure application easier to control. Once a response is detected and the increase in pressure is discontinued, the control unit shows the force reached in grams and the latency in seconds. Data can be presented as pressure threshold in grams, as present change from baseline expressed as pressure hypersensitivity or as response latency in seconds.

3.7. Testing Cold Hypersensitivity

(a) Acetone drop test
   The mice are placed separately in an enclosure where they can move freely. The enclosure can be the same mesh surface and Plexiglas boxes that are used to assess mechanical hypersensitivity. One acetone drop is applied gently to the plantar side of one hind paw with the aid of a 1 ml syringe. It can be applied from beneath in case the mouse is sitting on a grid, or while the mouse is gently restrained. Frequently mice display an

immediate reaction to the cold and the reactive behavior may last for 60–90 s (continuous or in episodes). Hence the experimenter should prepare for immediate recording with a stopwatch. Typical reactions are lifting, licking, shaking or biting the paw. This test is subjected to a relatively high degree of variation when performed in mice, and it is recommended to repeat the test three times, with a 30 min test-free period in-between sessions, in order to get stable values. Data can be presented as time spent reacting to acetone in seconds. Noteworthy, this test has certain limitations. It is very difficult to adjust one drop of acetone precisely to the surface of the paw without touching it with the syringe, thus, the response might be due to cold sensation, chemical or touch stimulus (46).

(b) Cold plate
The mouse is placed on a metal plate set at room temperature (25°C) surrounded by an easily removable Plexiglas enclosure. The plate is set to decrease the temperature with a certain ramp and time (1°C/min), the mouse lifts and shakes one of the hind paws (as CAIA is polyarthritis model, both paws should be monitored). When a response is observed, the machine is stopped and the mouse is removed immediately to avoid tissue damage. It is highly recommended to set a cut-off temperature in order to discontinue the test session prior to tissue damage in case the mouse does not give any reaction. At least three baseline measurements are suggested, preferably taken on different days (see Note 11). Data can be presented as cold temperature threshold in degrees, as percent change from baseline expressed as cold hypersensitivity or as response latency in seconds.

(c) *Two-temperature preference device*
There is an increasing desire to develop a device to test ongoing cold hypersensitivity instead of evoked responses to noxious cold stimulus, as exemplified by the acetone and the cold plate tests. A temperature preference test gives the researcher the possibility to observe the rodent's spontaneous reaction to temperature changes. The set up consists of two hot/cold plates connected to each other within a common enclosure, in some cases complemented with an escape area in-between. The two plates are separately controlled and operated with different settings: one is set at room temperature and remains unchanged, while the other is set to gradually decrease the surface temperature from 32°C to lower degrees, usually stepwise during 30–60 min. Noteworthy, although the cold plate is very often used at low temperatures, around 0–5°C, this test shows temperature preferences already at relatively high (around 20°C) temperatures (47, 48). The mouse is placed in the middle of

the two plates at the start of the test session. With a help of a video camera the testing is recorded; thus, the mouse can be left undisturbed and undistracted. It is important to test baselines several times and to alternate the plate settings between trials to avoid the mice getting habituated to the settings (see Note 12). Data can be presented as time spent on each plate in seconds, or as relative time spent on each plate compared to each other in percentage.

3.8. Thermal Hypersensitivity

Here we describe assessment of thermal thresholds using a Hargreaves-type testing device (49). Mice are placed on the glass surface in Plexiglas containers and allowed to habituate to the test environment three times prior to baseline testing and for a minimum of an hour (depending upon strains) prior to each test session. The experimenter must ensure that mice are calm and are no longer displaying explorative behavior.

(a) When the mouse is sitting still with both hind paws flat on the glass surface, position the light source to point to the middle of the foot pad.

(b) Initiate the thermal nociceptive stimulus (here, a focused projection bulb under the glass surface) coincident with starting the timer.

(c) Terminate the stimulus and timer upon a brisk withdrawal of the paw. If the mouse is walking away during testing, the test should be repeated after 2–3 min.

(d) When one paw is tested, it is recommended that the researcher tests the paw of another animal instead of testing the second paw of the same animal.

(e) When the withdrawal latency is assessed for one paw of all mice, the time to response of the second paw is measured.

Thermal latency is defined as the time required to generate a paw withdrawal and is measured in seconds. By changing the heat ramp (by altering the amperage of the bulb) different stimulus intensity can be achieved. Average baseline values typically fall within 8–12 s. To prevent thermal exposure damage, a cut-off time of 20 s or 55°C is recommended. Data can be presented as paw withdrawal latency in seconds or paw withdrawal temperature in degrees.

3.9. Illustrative Data

In this section, we give an illustration of our experiments with the CAIA mouse model. We used B10.RIII male mice. On day 0 (at the time of intravenous injection) mice were 15–17 weeks old. Each mouse was given 4 mg antibodies (150–200 μl) intravenously to the tail vein (this cocktail is commercially available from MD Biosciences, see Table 1). On day 5 mice were injected intraperitoneally with 25 μg LPS dissolved in 100 ml saline. The control groups were either

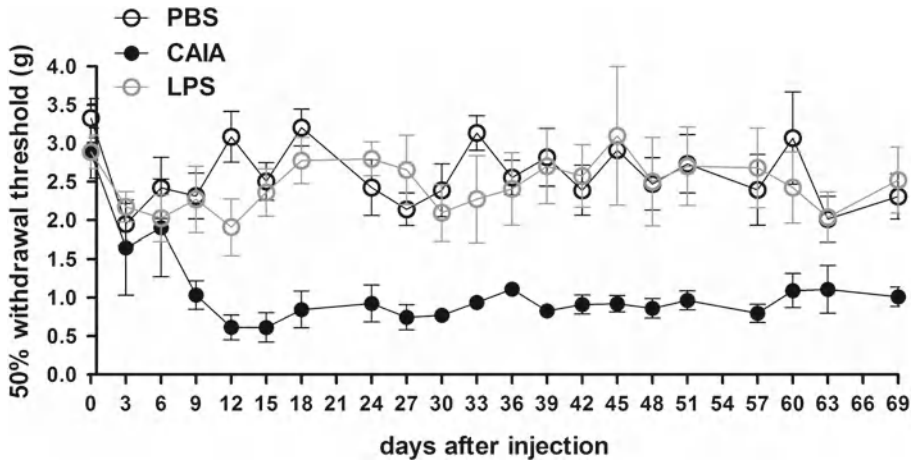

Fig. 2. Results of 50% withdrawal threshold over time after injection show a significant mechanical hypersensitivity in CAIA mice compared to PBS group throughout the whole study. LPS mice were not statistically different from the PBS group. Two-way ANOVA followed by Bonferroni's post hoc test was used for statistical analysis, $p<0.05$ was considered to be significant (Data points are expressed as mean ± SEM, $n=6$ mice/group).

given PBS on both days 0 and 5 or PBS on day 0 and LPS on day 5, thus, there were a CAIA (CAIA + LPS), a PBS and an LPS group. Mechanical hypersensitivity and clinical scores were assessed every third day. B10.RIII mice developed mild signs of arthritis prior to injection of LPS. After injecting LPS, CAIA mice showed a prominent increase in clinical score, reaching around 30 points by day 15, whilst there was no inflammation in the PBS or the LPS group. The arthritis score began to decrease from day 18 with visual signs of inflammation completely resolved by day 40 (Fig. 1).

Meanwhile, mechanical hypersensitivity (tested with Marstock von Frey filaments) was present in CAIA mice already by day 2 with an almost 40% drop in tactile threshold (though both saline and LPS control group showed hypersensitivity as early as day 2). Mice were the most sensitive to touch stimulus around days 15–18, with hypersensitivity reaching 70% reduction from baseline values. Even though the clinical signs of inflammation resolved, hypersensitivity remained pronounced throughout the whole study until the experimental endpoint on day 69 (Fig. 2). The saline and LPS groups showed some variations in tactile thresholds between testing days, but generally remained unchanged throughout the study compared to the CAIA group (Fig. 2).

4. Notes

1. Separation of the animals from their home cages resolves the aggression, but may introduce changes in the behavior related

to isolation, which could lead to confounding factors in the testing environment.

2. Injection can also be performed in anesthetized mice; however, it is more difficult, as veins contract due to the reduced blood pressure. In this case, warming the tail with a warm tissue or with the infrared lamp facilitates injection to the same extent as in conscious mice.
3. Measuring body weight is a good marker for disease severity. Difficulties for the mice to reach and grab standard rodent pellets placed high in the cage can cause weight loss subsequent to induction of arthritis. This can be prevented by providing powder food or wet pellets at the bottom of the cage. The recommended allowance for reduction in body weight without taking measures is 10%. One way to stimulate food intake and weight gain is to provide a sweet addition to the food, such as jam or jello. However, care should be taken if using such an approach as sugar could affect the experimental outcome.
4. Redness and swelling should be observed at the same time in order for the observation to be considered a sign of inflammation. In some strains, especially in albino mice, the toes and paws are naturally pink and may be mistaken for red. In such cases the observer has to take extra caution to ensure that the toes are also swollen when given a score and it is always good to compare inflamed paws with normal paws from naïve mice, if the experimenter is in doubt of inflammation. More detailed information about the degree of inflammation can be achieved by examining if the knuckles are inflamed. However, this can be difficult to distinguish; therefore, more extensive training in arthritis score assessment may be required.
5. The amount of explorative behavior in different mouse strain varies and is also dependent on the testing environment. Thus, the duration of time before the mice can be subjected to the von Frey-filament test may vary. It is important to set the experiment according to the mouse strain being examined. The duration of the testing session is crucial, as after a certain time the mice may change their behavior due to lack of food and water. Maybe more importantly, mice may become sensitized when standing on a mesh surface for a long time, which could result in confounded values. The effect of testing frequency should also be evaluated. We are using a paradigm where the mice are tested every third day, if test-induced sensitization is suspected, testing should be performed less frequently (e.g., every sixth day).
6. It has to be taken into consideration that each setting differs in males and females. Testing in both sexes should be performed in different rooms or on different days, and if possible, in different testing devices. Females need slightly more time to acclimatize and get anxious easier. According to our observations, they also are more sensitive to frequent testing.

7. Mechanical hypersensitivity can only be assessed in the hind paws. Currently there is no device or method to test evoked response in the forepaws properly.
8. The 50% threshold calculation in the Chaplan et al. 1994 paper is made for the Stoelting series of filaments, modification of the calculation (recalculation of the δ value) is required when using other sets of filaments.
9. Different settings for this type of systems can be used, but it is important to note that the ramp should not be too high, since it can cause a different, pushing sensation for the mice instead of tactile stimulus. There also has to be a preset maximum force value, otherwise it reaches a force that can cause serious damages on the paw skin. If the filament reaches the maximum force without the paw being removed, the testing has to be stopped manually, so the filament can fall down to the original position.
10. As the pressure is applied on the leg of a restrained animal, attempts to escape from the position are more frequently observed than withdrawal. It is strongly suggested that the experimenter goes through a training period to become familiar with the responses mice show to this type of stimulus and that the mice are habituated to the test situation to minimize stress.
11. Response of mice to cold sensation can vary individually, some mice jump or paddle instead of lifting the paw and therefore it is important to record several baselines before the experiment starts to become familiar to their response.
12. As in all preference type of tests, standardizing the environment (the right place for the device, standard room temperature, humidity conditions, etc.) is of high importance.

Acknowledgments

This work was supported by grants from The Swedish Research Council (CIS, RH, KSN), Swedish Foundation for Strategic Research (CIS), Marie Curie International Reintegration grant (CIS), Olle Engkvist Byggmästares Foundation (CIS), Wenner-Gren Foundation (KS) and The Swedish Rheumatism Association (CIS, KSN).

References

1. Rantapaa-Dalqvist S, de Jong BA, Berglin E et al (2003) Antibodies against cyclic citrullinated peptide and IgA rheumatoid factor predict the development of rheumatoid arthritis. Arthritis Rheum 48:2741–2749
2. Uysal H, Nandakumar KS, Kessel C et al (2010) Antibodies to citrullinated proteins: molecular interactions and arthritogenicity. Immunol Rev 233:9–33

3. Taylor P, Manger B, Alvaro GG et al (2010) Patient perceptions concerning pain management in the treatment of rheumatoid arthritis. J Int Med Res 38:1213–1224
4. Ricci JA, Stewart WF, Chee E et al (2005) Pain exacerbation as a major source of lost productive time in US workers with arthritis. Arthritis Rheum 53:673–681
5. Swedish Council on Technology Assessment in Healthcare (2006) Methods of Treating Chronic Pain. Report No: 177/1þ2
6. Kollias G, Papadaki P, Apprailly F et al (2011) Animal models for arthritis: innovative tools for prevention and treatment. Ann Rheum Dis 70:1357–1362
7. Nandakumar KS (2012) Antibody mediated arthritis and new therapeutic avenues. In: Pathak Y, Benita S (eds) Antibody-Mediated Drug Delivery Systems: Concepts, Technology, and Applications. John Wiley & Sons Inc., New Jersey, pp 407–425
8. Kouskoff V, Korganow AS, Duchatelle V et al (1996) Organ-specific disease provoked by systemic autoimmunity. Cell 87:811–822
9. Matsumoto I, Staub A, Benoist C, Mathis D (1999) Arthritis provoked by linked T and B cell recognition of a glycolytic enzyme. Science 286:1732–1735
10. Keffer J, Probert L, Cazlaris H et al (1991) Transgenic mice expressing human tumour necrosis factor: a predictive genetic model of arthritis. EMBO J 10:4025–4031
11. Koenders MI, Devesa I, Marijnissen RJ et al (2008) Interleukin-1 drives pathogenic Th17 cells during spontaneous arthritis in interleukin-1 receptor antagonist-deficient mice. Arthritis Rheum 58:4361–3470
12. Trentham DE, Townes AS, Kang AH (1977) Autoimmunity to type II collagen an experimental model of arthritis. J Exp Med 146:857–868
13. Courtenay JS, Dallman MJ, Dayan AD et al (1980) Immunisation against heterologous type II collagen induces arthritis in mice. Nature 283:666–668
14. Keystone EC, Schorlemmer HU, Pope C, Allison AC (1977) Zymosan-induced arthritis: a model of chronic proliferative arthritis following activation of the alternative pathway of complement. Arthritis Rheum 20:1396–1401
15. Frasnelli ME, Tarussio D, Chobaz-Peclat V et al (2005) TLR2 modulates inflammation in zymosan-induced arthritis in mice. Arthritis Res Ther 7:370–379
16. Vingsbo C, Sahlstrand P, Brun JG et al (1996) Pristane-induced arthritis in rats: a new model for rheumatoid arthritis with a chronic disease course influenced by both major histocompatibility complex and non-major histocompatibility complex genes. Am J Pathol 149:1675–1683
17. Glant TT, Finnegan A, Mikecz K (2003) Proteglycan-induced arthritis: immune regulation, cellular mechanisms, and genetics. Crit Rev Immunol 23:199–250
18. Kannan K, Ortmann RA, Kimpel D (2005) Animal models of rheumatoid arthritis and their relevance to human disease. Pathophysiology 12:167–181
19. Nandakumar KS (2010) Pathogenic antibody recognition of cartilage. Cell Tissue Res 339:213–220
20. Holmdahl R, Rubin K, Klareskog L et al (1986) Characterization of the antibody response in mice with type II collagen-induced arthritis, using monoclonal anti-type II collagen antibodies. Arthritis Rheum 29:400–410
21. Terato K, Hasty KA, Reife RA et al (1992) Induction of arthritis with monoclonal antibodies to collagen. J Immunol 148:2103–2108
22. Nandakumar KS, Svensson L, Holmdahl R (2003) Collagen type II-specific monoclonal antibody-induced arthritis in mice. Am J Pathol 163:1827–1837
23. Nandakumar KS, Holmdahl R (2005) Efficient promotion of collagen induced arthritis (CAIA) using four monoclonal antibodies specific for the major epitopes recognized in both collagen induced arthritis and rheumatoid arthritis. J Immunol Methods 304: 126–136
24. Hutamekalin P, Saito T, Yamaki K et al (2009) Collagen antibody-induced arthritis in mice: development of a new arthritogenic 5-clone cocktail of monoclonal anti-type II collagen antibodies. J Immunol Methods 343:49–55
25. Christianson CA, Corr M, Firestein GS et al (2010) Characterization of the acute and persistent pain state present in K/BxN serum transfer arthritis. Pain 151:394–403
26. Christianson C.A. et al. (2012) K/BxN serum transfer arthritis as a model of inflammatory joint pain. In: Luo ZD (ed) Pain Research, Methods and Protocols, Methods in Molecular Biology, Springer Science, New York
27. Khachigian LM (2006) Collagen-antibody-induced arthritis. Nat Protoc 1:2512–2516
28. Holmdahl R, Jansson L, Gullberg D et al (1985) Incidence of arthritis and autoreactivity of anti-collagen antibodies after immunization of DBA/1 mice with heterologous and autologous collagen II. Clin Exp Immunol 62:639–646
29. Mogil JS, Bailey AL (2010) Sex and gender differences in pain and analgesia. Prog Brain Res 186:141–157

30. Holmdahl R, Jansson L, Meyerson B et al (1987) Oestrogen induced suppression of collagen arthritis: I. Long term oestradiol treatment of DBA/1 mice reduces severity and incidence of arthritis and decreases the anti type II collagen immune response. Clin Exp Immunol 70:372–378
31. Jochems C, Islander U, Erlandsson M et al (2011) Effects of oestradiol and raloxifene on the induction and effector phases of experimental postmenopausal arthritis and secondary osteoporosis. Clin Exp Immunol 165:121–129
32. Holmdahl R, Bockermann R, Bäcklund J et al (2002) The molecular pathogenesis of collagen-induced arthritis in mice—a model for rheumatoid arthritis. Ageing Res Rev 1:135–147
33. Rowley MJ, Nandakumar KS, Holmdahl R (2008) The role of collagen antibodies in mediating arthritis. Mod Rheumatol 18:429–441
34. Nandakumar KS, Holmdahl R (2007) Collagen antibody induced arthritis. Methods Mol Med 136:215–223
35. Leffler AS, Kosek E, Lerndal T et al (2002) Somatosensory perception and function of diffuse noxious inhibitory controls (DNIC) in patients suffering from rheumatoid arthritis. Eur J Pain 6:161–176
36. Tajino K, Matsumura K, Kosada K et al (2007) Application of menthol to the skin of whole trunk in mice induces autonomic and behavioral heat-gain responses. Am J Physiol Regul Integr Comp Physiol 293:2128–2135
37. Vissers K, Meert T (2005) A behavioral and pharmacological validation of the acetone spray test in gerbils with a chronic constriction injury. Anesth Analg 101:457–464
38. Terato K, Harper DS, Griffiths MM et al (1995) Collagen-induced arthritis in mice: synergistic effect of *E. coli* lipopolysaccharide bypasses epitope specificity in the induction of arthritis with monoclonal antibodies to type II collagen. Autoimmunity 22:137–147
39. Wolf G, Yirmiya R, Goshen I et al (2003) Impairment of interleukin-1 (IL-1) signaling reduces basal pain sensitivity in mice: genetic, pharmacological and developmental aspects. Pain 104:471–480
40. Deleo JA, Yezierski RP (2001) The role of neuroinflammation and neuroimmune activation in persistent pain. Pain 90:1–6
41. Holmdahl R et al (1998) Genetic analysis of mouse models for rheumatoid arthritis. In: Adolph KW (ed) Human Genome Methods. CRC, New York, p 215
42. Dixon WJ (1980) Efficient analysis of experimental observations. Ann Rev Pharmacol Toxicol 20:441–462
43. Chaplan SR, Bach FW, Pogrel JW et al (2004) Quantitative assessment of tactile allodynia in the rat paw. J Neurosci Methods 53:55–63
44. Vickers AJ (2005) Parametric versus non-parametric statistics in the analysis of randomized trials with non-normally distributed data. BMC Med Res Methodol 5:35–46
45. Leuchtweis J, Imhof AK, Montechiaro F et al (2010) Validation of the digital pressure application measurement (PAM) device for detection of primary mechanical hyperalgesia in rat and mouse antigen-induced knee joint arthritis. Methods Find Exp Clin Pharmacol 32:575–583
46. Walczak JS, Beaulieu P (2006) Comparison of three models of neuropathic pain in mice using a new method to assess cold allodynia: the double plate technique. Neurosci Lett 399:240–244
47. Knowlton WM, Bifolck-Fisher A, Bautista DM, McKemy DD (2010) TRPM8, but not TPA1, is required for neural and behavioral responses to acute noxious cold temperatures and cold mimetics in vivo. Pain 150:340–350
48. Noe J, Zimmermann K, Busserolles J et al (2009) The mechano-activated Kþ channels TRAAK and TREK-1 control both warm and cold perception. EMBO J 28:1308–1318
49. Dirig DM, Salami A, Rathbun ML et al (1997) Characterization of variables defining hindpaw withdrawal latency evoked by radiant thermal stimuli. J Neurosci Methods 76:183–191

Chapter 28

Animal Models of Muscular Dystrophy

Yuko Iwata and Shigeo Wakabayashi

Abstract

Muscular dystrophy is a severe degenerative disorder of the skeletal muscle, characterized by progressive muscle weakness. One subgroup of this disease is caused by a defect in the genes encoding the components of the dystrophin–glycoprotein complex. Such a defect results in a significant disruption of membrane integrity and/or stability and, consequently, a sustained increase in cytosolic Ca^{2+} concentration ($[Ca^{2+}]_i$). Abnormal Ca^{2+} homeostasis, especially under mechanical stress, is believed to be a key molecular event in the pathology of muscular dysgenesis. In this chapter, we will review the animal models of muscular dystrophy useful for understanding the pathophysiology of the disease. Particularly, we will focus on stretch-activated TRP channels, which were reported to have critical pathological significance, and discuss the therapeutic potential of these channels for muscle dystrophy. We will also briefly summarize in vivo and in vitro procedures using dystrophic animal models, isolated muscle fibers, and cultured myotubes.

Key words: Dystrophin–glycoprotein complex, Muscular dystrophy, Stretch-activated channel, TRPV, TRPC, Cell damage, Mechanical stress, Membrane fragility, Sarcoglycan

1. Introduction

Muscular dystrophy is a severe disease with no known cure, characterized by weakness and wasting of skeletal muscle (1). Patients with muscular dystrophy have high levels of cytosolic muscle enzymes in the serum, and, on muscular biopsy, show ongoing muscle degeneration and regeneration, fibrosis, and interstitial fibrosis. More than 30 forms of muscle dystrophy are known according to the genetic basis of classification. The most frequent form is Duchenne muscular dystrophy (DMD), a lethal and X-linked recessive type caused by dystrophin deficiency, occurring in 1 of 3,500 men. Another form is limb-girdle muscle dystrophy (LGMD), including its autosomal dominant (LGMD type 1) or autosomal recessive (LGMD type 2) type, which affects roughly 1 out of 15,000. Many LGMDs are caused by mutations

Arpad Szallasi and Tamás Bíró (eds.), *TRP Channels in Drug Discovery: Volume II*, Methods in Pharmacology and Toxicology,
DOI 10.1007/978-1-62703-095-3_28, © Springer Science+Business Media, LLC 2012

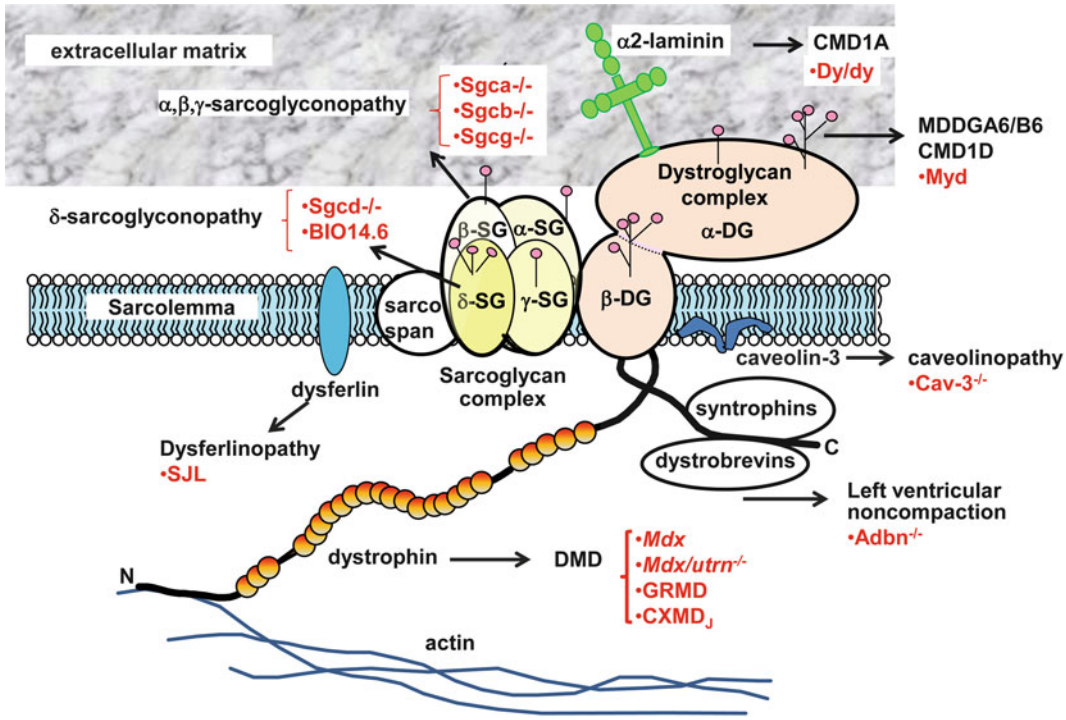

Fig. 1. Animal models of muscular dystrophy associated with the dystrophin–glycoprotein complex and membrane repair.

in genes encoding the dystrophin–glycoprotein complex (DGC) (Fig. 1) or the membrane cytoskeleton. Interestingly, many of these genes are known to be also associated with cardiomyopathy. Since there are significant structural and functional similarities between cardiac and skeletal muscles, a common signaling pathway leading to muscle dysgenesis may be involved in these two muscle degenerative disorders. Recently, we identified candidate proteins that may link DGC defects to downstream Ca^{2+} abnormality and the consequent occurrence of muscle dysgenesis in two animal models, dystrophin-deficient *mdx* mice and δ-sarcoglycan (δ-SG)-deficient BIO14.6 hamsters. In this chapter, we will review the features of known animal models of muscular dystrophy, the available procedures for evaluating the disease, and finally the trials for drug target identification.

2. Animal Models of Muscular Dystrophy

Table 1 shows the currently available animal models for human diseases, as well as their genes and products involved in muscular dystrophy. The table also shows that disruption of some of these genes can also lead to heart failure, especially dilated cardiomyopathy.

Table 1
Animal models of muscular dystrophy

Animal model	Human disease	Abnormal protein/gene	Skeletal dystrophy	Cardiomyopathy	Remarks
Mdx	DMD	Dystrophin	Mild/moderate	Mild	amelioration by calcineurin activation
Mdx/utrn$^{-/-}$	DMD	Dystrophin/utrophin	Severe	Severe	more resemble DMD than mdx
GRMD (canine)	DMD	Dystrophin	Severe	Severe	
GXMD$_J$ (canine)	DMD	Dystrophin	Severe	Severe	
BIO14.6 (hamster)	δ-Sarcoglycanopathy	δ-Sarcoglycan	Severe	Severe	LGMD2F, amelioration by calcineurin inhibition, vascular abnormality
Sgcd$^{-/-}$	δ-Sarcoglycanopathy	δ-Sarcoglycan	Severe	Severe	LGMD2F, amelioration by calcineurin inhibition, vascular abnormality
Sgca$^{-/-}$	α-Sarcoglycanopathy	α-Sarcoglycan	Moderate	None	LGMD2D
Sgcb$^{-/-}$	β-Sarcoglycanopathy	β-Sarcoglycan	Severe	Severe	LGMD2E, vascular abnormality
Sgcg$^{-/-}$	γ-Sarcoglycanopathy	γ-Sarcoglycan	Severe	Severe	LGMD2C
Adbn$^{-/-}$	LV noncompaction	α-Dystrobrevin	Mild/moderate	Hypertrophic/ dilated	Muscle-cell signaling disruption
Cav-3$^{-/-}$	Caveolinopathy	Caveolin-3	Mild	Progressive	LGMD1C, hyperCKemia, distal myopathy, rippling muscle disease
Dy/dy	CMD1A	α2-Laminin	Severe	Rare	dy^{2J},dy^{W},dy^{3K}
Myd	MDDGA6/B6	LARGE	Moderate	Dilated	CMD1D, glycosyl transferase CMD1D
SJL	Dysferlinopathy	Dysferlin	Mild	Severe	Miyoshi distal/LGMD2B

In DMD, dystrophin is defective and dystrophin-associated proteins are greatly reduced (2). Other types of muscular dystrophy are also caused by mutations in the genes encoding DGC components (3–5). DGC is a multi-subunit complex (3, 6, 7) that spans the sarcolemma to structurally link the extracellular matrix laminin and the actin cytoskeleton (8) (Fig. 1) and provides mechanical strength to muscle cell membranes. Therefore, disruption of the DGC could significantly disrupt membrane integrity or stability during contraction/relaxation and therefore cause cell damage. Importantly, defects in different genes cause similar symptoms at the end stages of disease development, i.e., muscle dysgenesis. Despite the advances in understanding the molecular basis of muscular dystrophy, no definitive medical treatment is available yet. Animal models for these disorders are highly useful for studies on muscular dystrophy because they allow extensive preclinical studies on the safety and functionality of various therapeutic approaches as well as understanding the mechanism of muscle dysgenesis.

2.1. Animal Models Associated with the DGC and Membrane Repair

2.1.1. Dystrophinopathy

The most widely used animal model for dystrophy is the *mdx* mouse, which carries an X-linked mutation in the dystrophin gene, thus mimicking the DMD genotype in humans. This mutation causes a lack of dystrophin in the sarcolemma. Previous studies with *mdx* mice revealed that the acute onset of pathology starts at around 3 weeks of age and that massive muscle degeneration/necrosis occurs at approximately 4 weeks of age (9, 10). Muscles continue to go through cycles of necrosis and regeneration throughout the life span of the *mdx* mouse; after 12 weeks, muscle degeneration becomes milder. Muscle pathology is most pronounced between 3 and 10 weeks of age, a period characterized by the presence of extensive necrosis, regenerated centrally nucleated fibers, and high serum levels of creatine kinase (CK), a biochemical marker of muscle necrosis. The deterioration of the skeletal and cardiac muscles of the *mdx* mouse is relatively much milder than that of human cases of DMD mainly due to the presence of revertant fibers (11) and an upregulation of utrophin (a smaller analogue of dystrophin) (12). As a result, the fibrosis and infiltration of inflammatory cells in the skeletal muscle at later stages tend to be much less than that observed in human DMD patients. A double mutant lacking both dystrophin and utrophin (*mdx*/utrn$^{-/-}$) has been generated, which displays a phenotype closer to that of human DMD patients and appears to be a more valid model for DMD (13).

Canine models of DMD have also been extensively studied (14–16). Two major breeding colonies of dystrophic dogs have been established, bearing the same mutation in different genetic backgrounds: one is a colony of large golden retriever muscular dystrophy (GRMD) dogs and another is of medium-sized beagle (canine X-linked muscular dystrophy in Japan [CXMD$_J$]) dogs,

which was developed through artificial insemination of frozen GRMD semen. GRMD dogs carry a point mutation at the intron 6 splice acceptor site in the canine dystrophin gene, which causes a premature transcription stop codon. As a result, no dystrophin is produced in the affected muscles. These dystrophic dogs show progressive skeletal muscle weakness and atrophy, as well as electrocardiographic abnormality and cardiac fibrosis like those seen in DMD, and represent a more attractive animal model for DMD than murine models because of their larger size, severity of muscle degeneration, and cardiac involvement.

2.1.2. Sarcoglycanopathy

The BIO14.6 hamster was identified in 1962 as a model of recessively inherited dystrophic myopathy that affects both cardiac and skeletal muscles (17). The skeletal muscle of BIO14.6 hamster displays classic signs of muscular dystrophy, including necrosis, central nucleation, and variably sized muscle fibers (18), and this strain has been recognized as a model for LGMD 2F with δ-SG deficiency (5). On the other hand, disruption of SGs has been carried out in mice, providing models for all known sarcoglycanopathies. All SG-null animals display progressive muscular dystrophy of variable severity. These models share the property of a significant secondary reduction in the expression of the other members of the SG-sarcospan complex as well as variable degrees of disruption of other components of the DGC. In most of these models, membrane integrity is disrupted and can be measured by permeation of a dye marker. Importantly, unlike Sgca-null mice, Sgcb-, Sgcg-, and Sgcd-null mouse models display a cardiac phenotype, and coronary artery perfusion studies have revealed abnormal vascular functions in Sgcb- and Sgcd-null mice, thus providing new insights into the complexity of the pathological mechanisms of LGMD 2E and 2F. Sgcg-null mice also show severe muscular dystrophy and cardiomyopathy; however, these conditions differ from those seen in other models in that the expression of dystroglycans (DGs) is not altered and the mice show normal resistance to mechanical stress and no evidence of contraction-induced injury after exercise (19).

2.1.3. Dystroglycanopathy

DG is posttranslationally cleaved into an extracellular α-DG and a transmembrane β-DG subunit, and is a key link between the cytoskeleton and extracellular matrix proteins such as laminin, agrin, and neurexin. DGs are considered the most broadly expressed DGC components and are crucial in the early stages of development. DG deficiency in mice leads to embryonic lethality (20); chimeric mice, lacking DG only in skeletal muscle, develop progressive muscle pathology similar to human muscular dystrophy (21). Accumulating evidence now shows that posttranslational modification of α-DG and its binding to the extracellular matrix protein laminin are required for normal muscle function.

The myodystrophy (myd) mouse, myd (Large^{myd}), is an animal model for DG hypoglycosylation that lacks only O-glycan, which binds the laminin-globular domain, because of a deficiency in the like-acetylglucosaminyltransferase (LARGE) protein. Mutations in the human *LARGE* gene cause a severe congenital muscular dystrophy–dystroglycanopathy with mental retardation (MDDGB6) or brain and eye anomaly (MDDGA6), previously designated as severe congenital muscular dystrophy type 1D (CMD1D) (22–24). The myd mice were also found to show late-onset focal myocardial necrosis/fibrosis and myocyte damage (25, 26). In addition to these disorders, dystroglycanopathy includes CMD1C, Walker–Warburg syndrome, muscle-eye-brain (MEB) disease, Fukuyama-type congenital muscular dystrophy (FCMD), and LGMD2I, 2K, 2M, 2N, 2O. An important characteristic of these disorders is hypoglycosylation of α-DG. To date, six genes, protein *O*-mannosyltransferases 1 and 2 (*POMT1* and *POMT2*), protein *O*-mannose *N*-acetylglucosaminyltransferase 1 (*POMGnT1*), *fukutin*, fukutin-related protein (*FKRP*), and *LARGE* have been implicated in dystroglycanopathies and all are thought to be involved in α-DG glycosylation. *POMGnT1* and *POMT1/2* are known to have glycosyltransferase activities that place *O*-mannosyl sugar chains on α-DG. However, the functions of *fukutin*, *FKRP*, and *LARGE* are still unknown. Recently, it was reported that myd, FCMD, and MEB have common defects characterized by postphosphoryl modification of phosphorylated O-linked mannose in α-DG, which is mediated by the LARGE protein (27). More recently, a DG missense mutation was reported in a woman with LGMD and cognitive impairment (28), which was also related to a defect in postphosphoryl modification by the LARGE protein.

2.1.4. Merosin (Laminin-2)-Deficient Muscular Dystrophy

As mentioned above, α-DG binds to the basement membrane protein laminin-2 (composed of laminin α2, β1, and γ1 chains). Several laminin-2-defective mice, including dy/dy (dystrophia-muscularis) and dy^{2J}/dy^{2J} (an allelic mutant of the dy mouse), have been used as models for human merosin-deficient CMD (CMD1A). Interestingly, these mice showed no signs of sarcolemmal damage; that is, no significant abnormal dye accumulation was observed (29) despite their severe clinical phenotype. Two further mouse models have been generated by homologous recombination: the dy^{W}/dy^{W} mouse expresses small amounts of a truncated laminin α2 chain, whereas the dy^{3K}/dy^{3K} mouse is completely deficient in the laminin α2 chain. Both mouse strains develop severe muscle dystrophy and die within a few weeks after birth. Laminin-2 is also expressed in the heart, but there has been only one report where one out of six patients had significant cardiac involvement with congestive cardiomyopathy at 1.4 years of age (30).

2.1.5. Other DGC Components

Deficiency of α-dystrobrevin, a cytoplasmic protein linked to dystrophin, leads to skeletal and cardiac myopathies, defects of neuromuscular junction maturation, abnormal myotendinous junctions, and impaired biochemical association between dystrophin and β-DG despite the structurally intact DGC in the sarcolemma in adbn-null mice (31). A missense mutation was found in four generations of a Japanese family with left ventricular noncompaction (32), a type of cardiomyopathy often associated with neuromuscular disorders (33).

Caveolin-3 is a muscle-specific caveolin isoform and an essential component of caveolae. Caveolin-3-deficiency, known as a caveolinopathy, causes mild muscular dystrophy and progressive cardiomyopathy with hypertrophy, dilation, and fibrosis (34, 35).

2.1.6. Dysferlinopathy

Besides DGC or other membrane cytoskeleton proteins, dysferlin plays an important role in Ca^{2+}-dependent membrane repair, which maintains sarcolemmal integrity through DGC-independent mechanisms. A deletion in the dysferlin gene has been identified in spontaneous dystrophic mice (SJL mice). These mice spontaneously develop progressive muscular dystrophy primarily affecting the proximal muscle groups and represent a model for LGMD 2B and Miyoshi myopathy. Dysferlin is also involved in cardiomyocyte membrane repair and its deficiency leads to cardiomyopathy (36). Such a cardiac involvement has also been reported in human patients (37).

2.2. Animal Models of Muscular Dystrophy Associated with Ion Channels

In a recent study (38), overexpression of TRPC3 resulted in a muscular dystrophy phenotype that is nearly identical to that observed in dystrophic animal models with abnormal DGC, and transgene-mediated inhibition of TRPC channels dramatically reduced the dystrophic phenotype in animal models. These results suggest that Ca^{2+} itself through TRPC channels is sufficient to induce muscular dystrophy in vivo, and that TRPC channels are also therapeutic targets for muscular dysgenesis. Mice lacking the scaffolding protein Homer-1, interacting with TRPC1, exhibit a myopathy associated with increased spontaneous cation influx (39).

2.3. Therapeutic Approaches Toward Different Phenotypes of Muscular Dystrophy

Various therapeutic approaches to muscular dystrophy have been challenged thus far, and some of them show great promise. These treatments can be divided into three categories: (1) chemical drugs; (2) gene therapy with an adeno-associated virus vector or exon skipping by antisense oligonucleotides; and (3) cell therapy in the preclinical or clinical stage (40). Drugs for DMD patients are currently almost completely restricted to glucocorticoids (steroid hormones) as the gold standard. Steroids such as prednisone, prednisolone, and deflazacort have been used (41), although the precise mechanism by which they improve dystrophy is not clear. Recently, some papers reported that steroid treatment for skeletal

muscle dystrophy accelerated the progression of cardiomyopathy in a δ-SG-deficient mouse model and BIO14.6 hamster, as well as in *mdx* mice (42–44). Although animal models may not entirely replicate the human cases, more attention should be given to use of chemicals because many myopathic patients simultaneously exhibit cardiomyopathy. Furthermore, it is important to know whether treatments are appropriate for different types of muscular dystrophy. For example, calcineurin inhibitors such as cyclosporine A may have different effects among different animal models: inhibition of calcineurin can reduce myofiber death by inhibition of necrosis in a model of LGMD, but it apparently has neither beneficial nor detrimental effect on the *mdx* mouse model (45).

3. Methods for Evaluation of Muscle Dysgenesis

Unifying experimental protocols from different laboratories into standardized operating procedures is helpful in evaluating the effects of new treatments in animal models. Such standard experimental protocols have been established for *mdx*, GRMD (as a DMD model), and *dy* (as a CMD model) mice (http://www.treat-nmd.eu/research/preclinical/).

In this chapter, we introduce easily evaluable procedures for model animals and cells that we have used, with special focus on an assay method using cultured myotubes, to search for effective drugs and to understand the mechanism of muscle dysgenesis.

3.1. In Vivo Assay

The use of mouse models in evaluating the effects of drugs on muscle dystrophy has two big advantages.

1. Taking blood samples from the tail vein of a mouse is an easy task, and the selected mouse can be followed without killing the animal. Serum CK level in *mdx* mice changes according to age or days since drug administration. In *mdx* mice, the extent of muscle degeneration reaches the first peak in 3–4 weeks, then declines because of regeneration, and again increases to reach the second peak at ~10 weeks, based on serum CK levels.
2. Measurement of muscle function can be easily performed without causing any injury to the animals. The forelimb grip strength of *mdx* mice is assessed by timing how long they could support their body weight while holding onto a fine wire net.

3.2. In Vitro Assay

3.2.1. DGC Abnormality

Since many muscular dystrophy types show DGC abnormality, it is important to assay DGC abnormality by using a small amount of muscle tissue (0.1–0.2 g). For example, we have previously reported that the physical association between dystrophin and DG in the

heart of BIO14.6 hamsters was very weak (46). The protocols are as follows:

1. Homogenize ventricles (0.1–0.2 g) for 30 s, three times, with Physcotron NS-60 at 25,000 rpm in 0.5–1 ml buffer A (1% digitonin, 0.5 M NaCl, 50 mM Tris–HCl [pH 7.4], 0.25 mM phenylmethanesulfonyl fluoride, 1.5 mM benzamidine, 2.5 μg/ml leupeptin, 2.5 μg/ml aprotinin, and 2.5 μg/ml pepstatin A).
2. After centrifugation at 540,000×*g* (max), incubate the supernatant (20 mg protein) overnight at 4°C either with dystrophin immunoaffinity beads; antimouse IgG Sepharose beads (50 μl) (Sigma) carrying antidystrophin antibody (NCL-DYS2) or with wheat germ agglutinin (WGA) Sepharose 6MB beads (100 μl) (Pharmacia-LKB). Then, wash the beads extensively with buffer A and elute with an SDS sample buffer (100 μl) containing 4% SDS, 200 mM DTT, and 20% glycerol.
3. Load samples on an SDS-PAGE gel and then perform immunoblotting (see Note 1).

3.2.2. Functional Analysis with Model Cell Systems

We introduced an in vitro system to study the effect of δ-SG deficiency on various cellular functions, including ion flux and degeneration under some stresses during a relatively short period. We characterized the biochemical and pathological properties of culture myotubes from δ-SG-deficient BIO14.6 and normal hamsters. Myotubes from both animal models have well-developed myofibrils. As observed in native muscles, dystrophin, syntrophin, and β-DG were detected in BIO14.6 myotubes, although δ-SG was completely absent. However, the expression and sarcolemmal localization of the other DGC components α-, β-, and γ-SGs were greatly reduced (Fig. 2a) (47). By using these myotubes, ion flux, gene transfer, stress-induced cell signaling, and cell damage (Fig. 2b–d) (47–49) can be measured as described below.

Cell Isolation and Cultured Myotubes

Satellite cells from gastrocnemius muscles of 30–40-day-old hamsters are prepared by enzymatic dissociation, as follows:

1. Cut the muscles (0.3 g) into small pieces (~1 mm^2) with microscissors.
2. Incubate minced muscles in 1 ml Ham's F12 medium containing 2 U/ml dispase and 1% collagenase for 45 min at 37°C.
3. Dilute the muscle slurry with 10 ml Ham's F12 medium (GIBCO BRL, Gaithersburg, MA) and spun at 350×*g* to sediment the dissociated cells.
4. Resuspend the cells in growth medium (see Note 2) and filter through a fine-mesh nylon filter (100 μm).

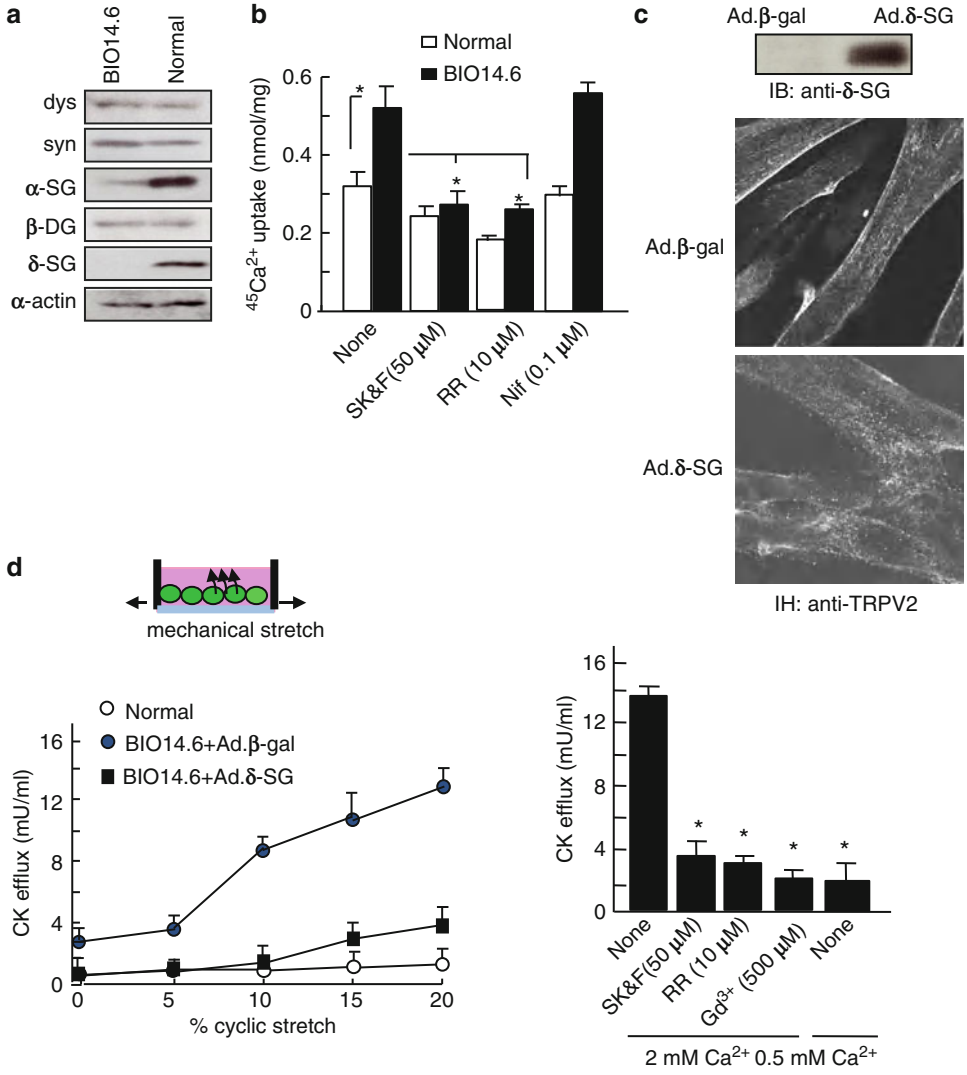

Fig. 2. Evaluation of muscle dysgenesis by using cultured dystrophic myotubes. (**a**) Comparison of the expression levels of cytoskeletal proteins between normal and BIO14.6 myotubes. Myotube homogenates (40 μg each) were subjected to SDS-PAGE followed by immunoblot analysis with the respective antibodies. (**b**) $^{45}Ca^{2+}$ uptake into normal or BIO14.6 myotubes measured under resting conditions with or without SK&F96365 (SK&F), ruthenium red (RR), or nifedipine. Gd^{3+}-inhibitable fractions are shown. (**c**) Immunoblot assay and immunohistochemistry (IH) of BIO14.6 myotubes infected with Ad.β-gal or Ad.δ-SG. (**d**) Cyclic stretch-induced creatine kinase (CK) efflux in normal myotubes or BIO14.6 myotubes infected with Ad. β-gal or Ad.δ-SG (*left*). CK efflux from BIO14.6 myotubes subjected to cyclic stretch under the indicated conditions (*right*).

5. Preplate for 1 h at 37°C to remove fibroblasts (differential adhesion).
6. Plate nonadhering (satellite rich) cells onto collagen-coated (100 mg/ml collagen type I; Sigma) culture dishes at a density of 5,000 cells/cm^2.

7. When myoblasts reach 80% confluence, trypsinize them and then plate on collagen-coated dishes for the experiments (see Note 3).
8. After 1–2 days, change the medium to DMEM (GIBCO BRL) containing 2% horse serum (Hyclone Laboratories, Logan, UT) to initiate differentiation (see Note 4).

Fiber Isolation

1. Take out the flexor digitorum brevis (FDB) muscles.
2. Incubate muscles for 40 min at 37°C in Krebs solution containing 124 mM NaCl, 1.2 mM $MgCl_2$, 5.9 mM KCl, 11.5 mM glucose, 11.5 mM HEPES-Na, 1.5 mM $CaCl_2$, and 0.2% collagenase type IV (Sigma-Aldrich).
3. Remove the muscle samples, wash twice in Krebs buffer, and suspend in Ham's F12/DMEM (Sigma-Aldrich) supplemented with 2% FCS.
4. Dissociate the single fibers mechanically by repeatedly passing the muscle samples through fire-polished Pasteur pipettes.
5. Plate the dissociated fibers onto glass-bottomed dishes coated with BDcell-Tak™ (BD Biosciences) and allow them to adhere to the bottom of the dish for 2 h.

Intracellular Ca^{2+} Measurement

1. Load myotubes (see Note 5) with 4 μM fura-2 acetoxymethyl ester (fura-2/AM) in balanced salt solution (BSS) for 30 min at 37°C, and maintain in BSS (146 mM NaCl, 4 mM KCl, 2 mM $MgCl_2$, 0.5 mM $CaCl_2$, 10 mM glucose, 0.1% bovine serum albumin, and 10 mM HEPES/Tris [pH 7.4]).
2. Measure fura-2 fluorescence by a ratiometric fluorescence method using a fluorescence image processor (Aquacosmos, Hamamatsu Photonics). Alternate the excitation wavelength at 340 and 380 nm (1 Hz) and detect the emitted fluorescence light at 510 nm. Then, calculate the fluorescence ratio at 340/380 nm.
3. To test the involvement of TRPV2, perform stimulation with the TRPV agonist 2-aminoethoxydiphenyl borate (2-APB) (see Note 6).

Measurement of ^{45}Ca Uptake

1. Culture myotubes from skeletal muscles on collagen I-coated 24-well dishes and preincubate at 37°C for 30 min in BSS (146 mM NaCl, 4 mM KCl, 2 mM $MgCl_2$, 1 mM $CaCl_2$, 10 mM glucose, 0.1% bovine serum albumin, and 10 mM HEPES/Tris [pH 7.4]) containing 0 or 0.5 mM $GdCl_3$ (see Note 7).
2. Start $^{45}Ca^{2+}$ uptake reaction into cells by switching the medium into BSS containing $^{45}CaCl_2$ (10 μCi/ml).

3. After appropriate intervals, wash the wells with attached cells four times with ice-cold 5 mM $LaCl_3$ and 10 mM HEPES/Tris (pH 7.4), to terminate $^{45}Ca^{2+}$ uptake.
4. Lyse the cells with 0.1 N NaOH and take aliquots for the determination of protein concentration and radioactivity.
5. Calculate the Gd^{3+}-inhibitable fraction of $^{45}Ca^{2+}$ uptake by subtracting the uptake in the absence of Gd^{3+} from that in its presence, which accounts for about 20% of total uptake.

Gene Transfection

1. Ligate full-length cDNAs of hamster δ-SG or β-galactosidase (βgal) into the Adeno-X™ viral vector (Clontech) according to the manufacturer's protocol.
2. Infect 1-day-old myotubes in differentiated medium with adenoviruses at a multiplicity of infection of 5–10 viral particles per cell for 24 h and then culture them for an additional 36–48 h (see Note 8).

Stretch-Induced Cell Damage

1. Attach the collagen I-coated silicon chambers with a transparent bottom (200 μm thick), containing the cultured myotubes from skeletal muscles, to a stretching apparatus driven by a computer-controlled stepping motor (Fig. 2d).
2. Preincubate myotubes in BSS containing 0.5 or 2 mM Ca^{2+} with or without drugs for the appropriate time and apply to the silicon chamber a constant strength from 5 to 20% elongation at 1 Hz for the appropriate time.
3. To assay cell damage with stretch stimulation (see Note 9), measure CK activity (see Note 10) in the medium by using an in vitro colorimetric assay kit (CK test kit; Wako Pure Chem. Co., Osaka, Japan) according to the protocol provided by the manufacturer.

3.2.3. Others

Immunoblotting and Immunohistochemistry

1. Visualize proteins on the blotting membranes by using an enhanced chemiluminescence detection system (Amersham Biosciences) after blotting, blocking with phosphate-buffered saline (PBS) containing 5% nonfat milk, and incubation with the appropriate primary and horseradish peroxidase-conjugated secondary antibodies.
2. For immunohistochemistry, obtain frozen muscle sections (5–6 μm thick) and incubate them for 1 h with the appropriate primary and fluorescein isothiocyanate (FITC)-conjugated or rhodamine-conjugated secondary antibodies.
3. For the immunostaining of myotubes or isolated fibers, fix fibers immobilized on glass slides with MeOH or 4% paraformaldehyde for 15 min at room temperature, permeabilize with 0.1% Triton X-100, and then stain with the appropriate antibody followed by an FITC-conjugated secondary antibody.

4. Observe stained samples under a confocal laser scanning microscope (FLUOVIEW FV1000, Olympus) mounted on an objective lens (Olympus).

Histology

1. Fix the skeletal muscle in PBS containing 10% formalin and embed in paraffin.
2. Stain serial sections (5 μm) with hematoxylin and eosin or Masson's trichrome.
3. For measurement of Evans blue dye (EBD) uptake to evaluate membrane permeability, inject EBD in PBS (10 mg/ml) intraperitoneally into each kind of animal (0.1 ml/10 g body weight). Kill animals 24 h after injection, excise muscles and embed in optimal cutting temperature compound (Tissue-Tek, Torrance, CA) and snap-freeze with liquid nitrogen. Slice the frozen blocks into 6-μm-thick sections, dry for 10 min, and wash briefly in PBS. EBD is detected as a red autofluorescence.

Quantification of Histological Data

1. View stained serial sections under a light microscope (OLYMPUS BX41) and analyze images by using a computer-assisted imaging system (FLOVEL Filing System) (see Note 11).
2. For the determination of the extent of muscle regeneration, count the number of fibers with central nuclei.
3. For the determination of the variability in fiber size, average the standard deviations of the area from the myofiber cross-sectional views (>1,000 fibers) of 3–4 animals per group.
4. For detection of apoptosis, stain muscle fibers with TUNEL, using an apoptosis detection kit (Takara Biomedical).
5. For detection of fibrosis, measure the Masson's trichrome-positive area. Convert color images to binary images by setting a threshold so that only blue-stained fibrotic areas are detected.

4. Therapeutic Targets for Muscular Dystrophy

Myocyte degeneration has been reported to be possibly caused by increased membrane permeability to Ca^{2+}, which is probably linked with membrane weakness. Many studies on DMD patients and *mdx* mice have reported chronic elevation in $[Ca^{2+}]_i$ underneath the sarcolemma, or within other intracellular compartments in skeletal muscle fibers or in myotubes (50–52). The $[Ca^{2+}]_i$ in muscles is regulated by numerous ion channels, Ca^{2+}pumps, and transporters in the sarcolemma and the sarcoplasmic reticulum (SR). Among them, attention has been focused on sarcolemmal Ca^{2+}-permeable channels (Ca^{2+}-specific leak channels) or mechanosensitive nonselective cation channels, which contribute to abnormal

Ca^{2+} handling in dystrophic myocytes. Abnormalities of mechanosensitive stretch-activated channels (SACs) have been detected in recordings from muscle biopsy samples from DMD patients (53, 54) as well as myotubes and fibers from *mdx* mice (55) and myotubes from BIO14.6 hamsters (49). These results suggest that SACs are important for pathological Ca^{2+} entry into DGC-deficient muscles at early stages of the disease process.

4.1. TRPV

We have shown that stretch-sensitive cation-selective channels similar to those recorded in *mdx* skeletal muscles are active in cultured myotubes prepared from BIO14.6 hamsters (49). Either a positive or a negative pressure largely increases the probability of opening this channel in BIO14.6 myotubes. We identified the candidate channel, which was previously reported as growth factor responsive channel (GRC) (56) and later renamed as the TRP vanilloid type 2 (TRPV2) channel. TRPV2 is activated by mechanical stimuli and plays a critical role in the pathogenesis of muscular dystrophy and cardiomyopathy (47, 57). TRPV2 is normally localized in intracellular membrane compartments, but translocates into the plasma membrane in response to stretch or growth factor stimulation. Importantly, TRPV2 was accumulated in the sarcolemma of skeletal muscles with muscular dystrophy from human patients, BIO14.6 hamsters, and *mdx* mice (47), thus contributing to a sustained $[Ca^{2+}]_i$ in diseased myocytes. Although other types of TRPV channels have not been reported in terms of their relationship with muscular dystrophy, *TRPV4* was recently identified as a responsive gene of inherited neurodegenerative disease, which indirectly causes muscle atrophy (58, 59).

4.2. Method for TRPV2 Inhibition

To determine whether TRPV2 is a responsive molecule causing Ca^{2+}-induced muscle damage, it is important to determine whether specific inhibition of TRPV2 prevents muscle damage. However, at present, specific inhibitors against TRPV2 are not available.

4.2.1. Dominant-Negative Mutant Strategy

1. Generate loss-of-function TRPV2 mutants in the pore region, which has a dominant-negative effect on channel function by forming nonfunctional tetramers, thereby abrogating the activity of endogenous TRPV2 (Fig. 3a).
2. Introduce these dominant-negative TRPV2 mutants into *mdx* mice by using a transgenic strategy (cross a transgenic [Tg] mouse expressing a TRPV2 mutant in muscle with an *mdx* mouse) or into BIO14.6 hamsters by adenoviral transfer (see Note 12).

4.2.2. Development of Inhibitors

Two approaches can be used to develop channel inhibitors (Fig. 4). Both strategies are available for inhibition of TRPV2 in dystrophic muscles or cultured cells, because TRPV2 is concentrated and activated in the plasma membranes. Specific inhibitors against TRPV2

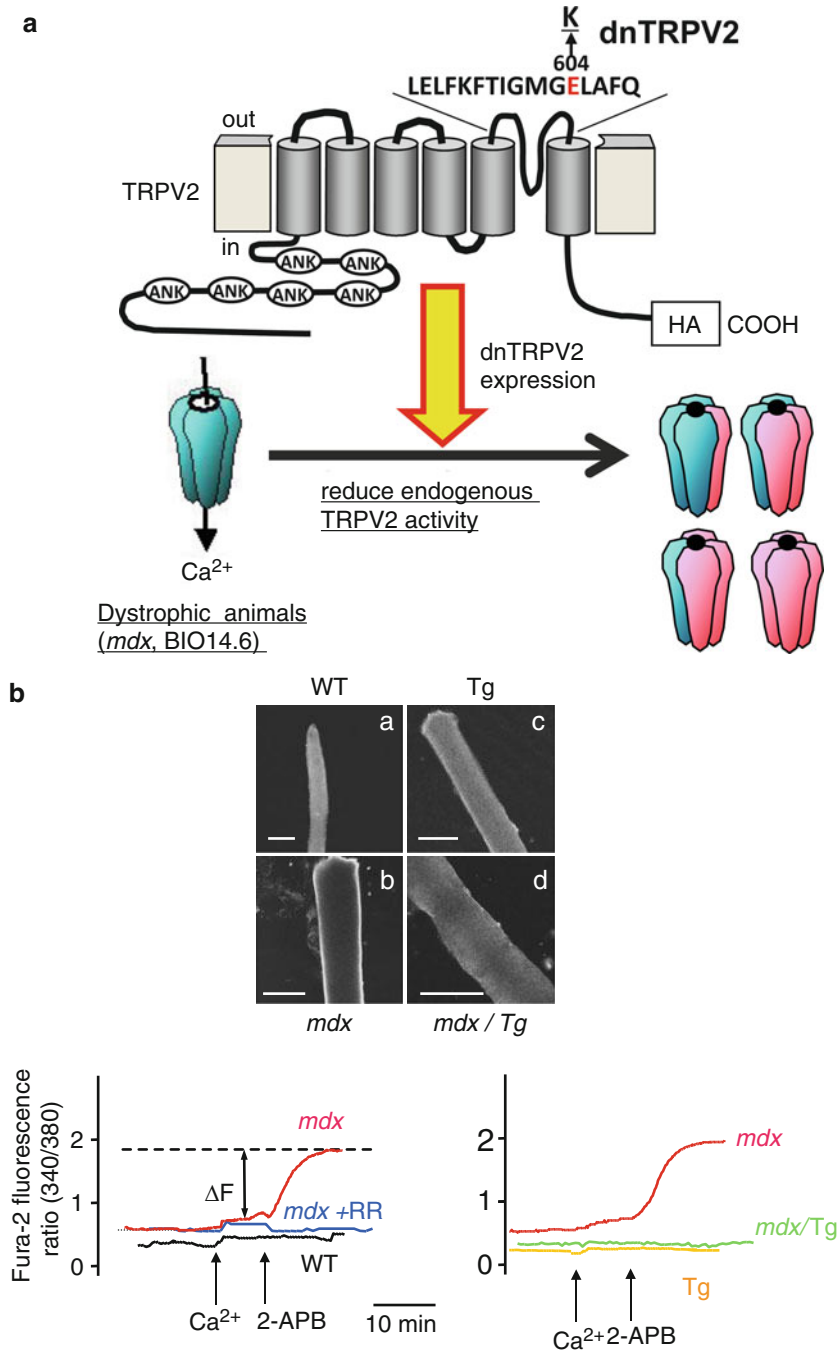

Fig. 3. Production of a dominant-negative (dn) TRPV2 mutant. (**a**) Transgenic (Tg) mice overexpressing a TRPV2 mutant, with a mutation in the putative pore region (Glu604), were produced. These mice were crossed with *mdx* mice to introduce dnTRPV2 and to inhibit endogenous TRPV2 activity. ANK, ankyrin repeat domain. HA, epitope tag. (**b**) FDB muscle fibers isolated from wild-type (**a**), *mdx* (**b**), Tg (**c**), and mdx/Tg (**d**) mice were visualized by immunofluorescence staining with anti-TRPV2 antibody (**a**–**d**). Scale, 100 μm. Agonist (2-APB)-induced $[Ca^{2+}]_i$ increase in isolated flexor digitorum brevis fibers from *mdx* mice was inhibited by ruthenium red (RR) (*left*). Note that no $[Ca^{2+}]_i$ increase was detected in fibers from wild-type mice. Such $[Ca^{2+}]_i$ increase was markedly reduced by expressing dnTRPV2 (*mdx*/Tg) (*right*) (68).

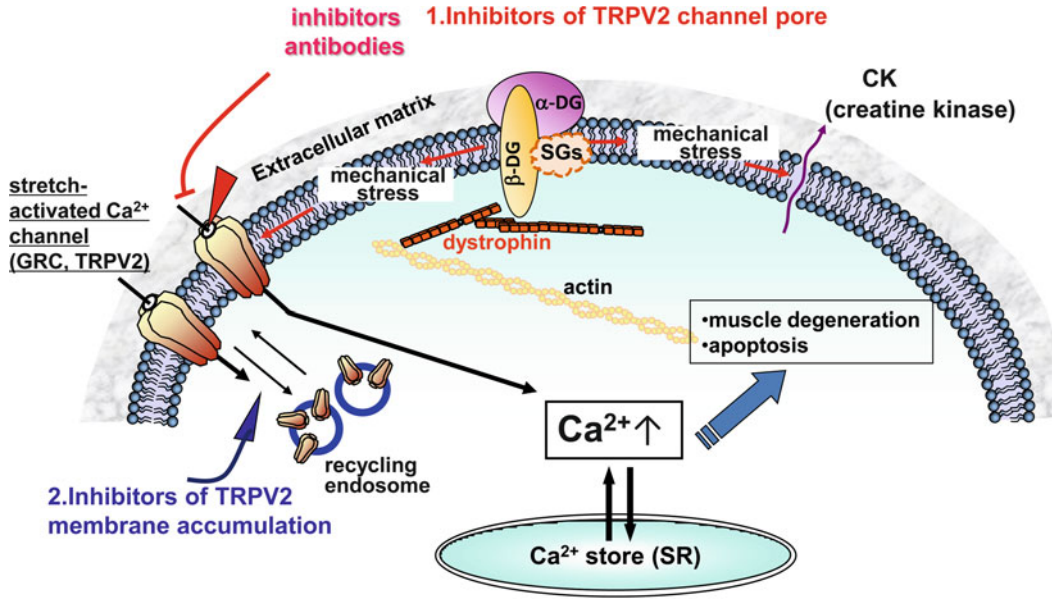

Fig. 4. Therapeutic strategies for inhibiting TRPV2 activity involve inhibition of the TRPV2 channel pore by using specific inhibitors or antibodies, and inhibition of TRPV2 membrane accumulation.

could be potentially useful and effective for the treatment of various muscle degenerative diseases as well as hereditary diseases:

1. By inhibiting the channel pore itself, for example, using specific antibodies or chemical inhibitors (see Note 13).
2. By inhibiting membrane accumulation (see Note 14).

4.3. TRPC

TRPC channels are also important candidate therapeutic targets. TRPC1, TRPC4, and TRPC6 are expressed in the sarcolemma of skeletal muscles (60). Knockdown of TRPC1 and TRPC4, but not TRPC6, was reported to reduce abnormal Ca^{2+} influx in dystrophic fibers (60). TRPC1 has been shown to form SACs (61), although controversial data also exist (62). TRPC1 together with its binding partner caveolin-3 accumulate at high levels in the sarcolemma of dystrophin-deficient muscle and contribute to abnormal Ca^{2+} influx, which is activated by reactive oxygen species and Src kinase (63). Further, mice lacking the scaffolding protein Homer-1, interacting with TRPC1, exhibit a myopathy associated with increased spontaneous cation influx (39). A recent study (38) also reported that overexpression of TRPC3 resulted in a phenotype of muscular dystrophy nearly identical to that observed in dystrophic animal models with abnormal DGC, and transgene-mediated inhibition of TRPC channels dramatically reduced the dystrophic phenotype in animal models. These results suggest that Ca^{2+} itself through TRPC channels is sufficient to induce muscular dystrophy in vivo, and TRPC channels are also therapeutic targets for muscular dysgenesis.

4.4. Others

Drugs for muscular dystrophy, e.g., steroids and antioxidants such as coenzyme Q10 and Debio-025(cyclosporine analogue), are already clinically or preclinically used. As mentioned above, a Ca^{2+} modulator may also become a target, for example to reduce the effects associated with chronic Ca^{2+} leakage from activated channels and membrane rupture, to increase the rates of Ca^{2+} reuptake into the SR by overexpressing the SR Ca^{2+}-pump SERCA1. Indeed, in a previous study, transgenic overexpression of SERCA1 dramatically rescued the dystrophic phenotype of δ-SG-null mice (64). Furthermore, Ca^{2+} removal by adenovirus-mediated overexpression of SERCA1a reduced the susceptibility to contraction-induced damage in *mdx* mice (65). Thus, control of $[Ca^{2+}]_i$ would provide a universal therapeutic strategy for reducing the dystrophic phenotype.

5. Notes

1. Despite having no sugar conjugates, dystrophin is retained on WGA Sepharose together with β-DG, α-SG, and α-DG from normal hamster ventricles, because the DGC is intact. However, dystrophin is not detectable in myopathic hamster ventricles because the DGC is incomplete even when dystrophin and β-DG are intact. A similar situation occurs on analysis using dystrophin-immunoaffinity beads. β-DG, α-SG, and α-DG are detected together with dystrophin from normal ventricular homogenates, while these dystrophin-associated proteins are not detected from myopathic ventricular homogenates.
2. The growth medium for myoblasts consist of Ham's F12 medium supplemented with 20% FCS and 2.5 ng/ml bFGF (Promega BRL, Madison, WI) and 1% chick embryo extract (GIBCO BRL).
3. During the first several passages of the primary cultures, myoblasts can be enriched by preplating.
4. Myoblasts begin to fuse and form myotubes in culture within 24 h. The formed myotubes are available for use in experiments by 2–5 days.
5. For muscle fibers, it is better to incubate the samples with 4 μM fura-2/AM in BSS for 1 h at room temperature. Use the medium containing 50 μM *N*-benzyl-*p*-toluene sulfonamide, an inhibitor of myosin II ATPase, as the working medium.
6. Stimulate myotubes or fibers with 2-APB in BSS containing 5 mM $CaCl_2$ (pH 6.8). A large $[Ca^{2+}]_i$ increase will be evident only in dystrophic myotubes or fibers (Fig. 3b).
7. For measurement of exchangeable Ca^{2+}, load myotubes with $^{45}CaCl_2$ for 4 h at 37°C. Measure the cellular $^{45}Ca^{2+}$ content after rinsing the myotubes five times with 1 ml of ice-cold La^{3+}

solution containing 146 mM choline chloride, 4 mM KCl, 2 mM $MgCl_2$, 10 mM glucose, 10 mM HEPES/Tris (pH 7.4), and 1 mM $LaCl_3$.

8. When BIO14.6 myotubes are infected with an adenoviral vector carrying δ-SG cDNA, the elevated sarcolemmal TRPV2 levels are downregulated (Fig. 2c), and the stretch-induced CK efflux are significantly suppressed (Fig. 2d).
9. Osmotic stress (e.g., 70% hypo)-induced cell damage can be measured in myotubes preloaded with 5 μM calcein-AM (Molecular Probes) to measure bleb formation (48). Under hypo-osmotic stress (70% osmolarity), extensive cell bleb formation is seen in BIO 14.6 myotubes, but not in the control ones (48). Similar bleb formation is also seen in *mdx* fibers, but not in control fibers.
10. By cyclic stretching up to 20% elongation for 1 h, creatine phosphokinase (CK) efflux (a maker of cell damage) increases with increasing strength of stretch only in BIO14.6 myotubes (Fig. 2d). Such cell damage in *mdx* myotubes has also been reported by other groups (66, 67).
11. All histochemical analyses should be done by investigators blinded to the genotypes.
12. These approaches significantly reduce the increase in resting intracellular Ca^{2+} concentration ($[Ca^{2+}]_i$) as well as the increase in $[Ca^{2+}]_i$ induced by high Ca^{2+} and the TRPV2 agonist 2-APB, which are observed in dystrophic muscles (Fig. 3b). Histological, biochemical, and physiological indices characterizing dystrophic pathologies, such as an increased number of central nuclei and fiber size variability/fibrosis/apoptosis, elevated serum CK levels (68), and reduced muscle performance (69), are all ameliorated in *mdx*/Tg mice. Similar beneficial effects are also observed in the muscles of BIO14.6 hamsters infected with adenovirus carrying the mutant TRPV2 (68).
13. A nonselective cation channel blocker, tranilast, has been shown to be an effective inhibitor for TRPV2 (48). Oral administration of tranilast reduced various symptoms of muscular dystrophy such as elevated serum CK level, progressive muscle degeneration, and increased infiltration of immune cells (48).
14. We are now looking for candidates that can inhibit the membrane accumulation of TRPV2.

References

1. Manzur AY, Muntoni F (2009) Diagnosis and new treatments in muscular dystrophies. Postgrad Med J 85:622–630
2. Ervasti JM, Kahl SD, Campbell KP (1991) Purification of dystrophin from skeletal muscle. J Biol Chem 266:9161–9165
3. Campbell KP (1995) Three muscular dystrophies: loss of cytoskeleton-extracellular matrix linkage. Cell 80:675–679
4. Duclos F, Straub V, Moore SA, Venzke DP, Hrstka RF, Crosbie RH, Durbeej M, Lebakken CS, Ettinger AJ, van der Meulen J, Holt KH, Lim LE, Sanes JR, Davidson BL, Faulkner JA, Williamson R, Campbell KP (1998) Progressive muscular dystrophy in alpha-sarcoglycan-deficient mice. J Cell Biol 142:1461–1471
5. Nigro V, Okazaki Y, Belsito A, Piluso G, Matsuda Y, Politano L, Nigro G, Ventura C, Abbondanza C, Molinari AM, Acampora D, Nishimura M, Hayashizaki Y, Puca GA (1997) Identification of the Syrian hamster cardiomyopathy gene. Hum Mol Genet 6:601–607
6. Campbell KP, Kahl SD (1989) Association of dystrophin and an integral membrane glycoprotein. Nature 338:259–262
7. Tinsley JM, Blake DJ, Zuellig RA, Davies KE (1994) Increasing complexity of the dystrophin-associated protein complex. Proc Natl Acad Sci USA 91:8307–8313
8. Ervasti JM, Campbell KP (1993) Dystrophin and the membrane skeleton. Curr Opin Cell Biol 5:82–87
9. Dangain J, Vrbova G (1984) Muscle development in mdx mutant mice. Muscle Nerve 7:700–704
10. Tanabe Y, Esaki K, Nomura T (1986) Skeletal muscle pathology in X chromosome-linked muscular dystrophy (mdx) mouse. Acta Neuropathol (Berl) 69:91–95
11. Hoffman EP, Morgan JE, Watkins SC, Partridge TA (1990) Somatic reversion/suppression of the mouse mdx phenotype in vivo. J Neurol Sci 99:9–25
12. Weir AP, Burton EA, Harrod G, Davies KE (2002) A- and B-utrophin have different expression patterns and are differentially up-regulated in mdx muscle. J Biol Chem 277: 45285–45290
13. Grady RM, Teng H, Nichol MC, Cunningham JC, Wilkinson RS, Sanes JR (1997) Skeletal and cardiac myopathies in mice lacking utrophin and dystrophin: a model for Duchenne muscular dystrophy. Cell 90:729–738
14. Kornegay JN, Tuler SM, Miller DM, Levesque DC (1988) Muscular dystrophy in a litter of golden retriever dogs. Muscle Nerve 11: 1056–1064
15. Sharp NJ, Kornegay JN, Van Camp SD, Herbstreith MH, Secore SL, Kettle S, Hung WY, Constantinou CD, Dykstra MJ, Roses AD et al (1992) An error in dystrophin mRNA processing in golden retriever muscular dystrophy, an animal homologue of Duchenne muscular dystrophy. Genomics 13:115–121
16. Shimatsu Y, Katagiri K, Furuta T, Nakura M, Tanioka Y, Yuasa K, Tomohiro M, Kornegay JN, Nonaka I, Takeda S (2003) Canine X-linked muscular dystrophy in Japan (CXMDJ). Exp Anim 52:93–97
17. Homburger F, Baker JR, Nixon CW, Wilgram G (1962) New hereditary disease of Syrian hamsters. Primary, generalized polymyopathy and cardiac necrosis. Arch Intern Med 110:660–662
18. Straub V, Duclos F, Venzke DP, Lee JC, Cutshall S, Leveille CJ, Campbell KP (1998) Molecular pathogenesis of muscle degeneration in the delta-sarcoglycan-deficient hamster. Am J Pathol 153:1623–1630
19. Durbeej M, Campbell KP (2002) Muscular dystrophies involving the dystrophin-glycoprotein complex: an overview of current mouse models. Curr Opin Genet Dev 12:349–361
20. Williamson RA, Henry MD, Daniels KJ, Hrstka RF, Lee JC, Sunada Y, Ibraghimov-Beskrovnaya O, Campbell KP (1997) Dystroglycan is essential for early embryonic development: disruption of Reichert's membrane in Dag1-null mice. Hum Mol Genet 6:831–841
21. Cote PD, Moukhles H, Lindenbaum M, Carbonetto S (1999) Chimaeric mice deficient in dystroglycans develop muscular dystrophy and have disrupted myoneural synapses. Nat Genet 23:338–342
22. Longman C, Brockington M, Torelli S, Jimenez-Mallebrera C, Kennedy C, Khalil N, Feng L, Saran RK, Voit T, Merlini L, Sewry CA, Brown SC, Muntoni F (2003) Mutations in the human LARGE gene cause MDC1D, a novel form of congenital muscular dystrophy with severe mental retardation and abnormal glycosylation of alpha-dystroglycan. Hum Mol Genet 12:2853–2861
23. Clement E, Mercuri E, Godfrey C, Smith J, Robb S, Kinali M, Straub V, Bushby K, Manzur A, Talim B, Cowan F, Quinlivan R, Klein A, Longman C, McWilliam R, Topaloglu H, Mein R, Abbs S, North K, Barkovich AJ, Rutherford M, Muntoni F (2008) Brain involvement in muscular dystrophies with defective dystroglycan glycosylation. Ann Neurol 64:573–582

24. Clarke NF, Maugenre S, Vandebrouck A, Urtizberea JA, Willer T, Peat RA, Gray F, Bouchet C, Manya H, Vuillaumier-Barrot S, Endo T, Chouery E, Campbell KP, Megarbane A, Guicheney P (2011) Congenital muscular dystrophy type 1D (MDC1D) due to a large intragenic insertion/deletion, involving intron 10 of the LARGE gene. Eur J Hum Genet 19:452–457
25. Holzfeind PJ, Grewal PK, Reitsamer HA, Kechvar J, Lassmann H, Hoeger H, Hewitt JE, Bittner RE (2002) Skeletal, cardiac and tongue muscle pathology, defective retinal transmission, and neuronal migration defects in the Large(myd) mouse defines a natural model for glycosylation-deficient muscle-eye-brain disorders. Hum Mol Genet 11:2673–2687
26. Kabaeva Z, Meekhof KE, Michele DE (2011) Sarcolemma instability during mechanical activity in Largemyd cardiac myocytes with loss of dystroglycan extracellular matrix receptor function. Hum Mol Genet 20:3346–3355
27. Yoshida-Moriguchi T, Yu L, Stalnaker SH, Davis S, Kunz S, Madson M, Oldstone MB, Schachter H, Wells L, Campbell KP (2010) O-mannosyl phosphorylation of alpha-dystroglycan is required for laminin binding. Science 327:88–92
28. Hara Y, Balci-Hayta B, Yoshida-Moriguchi T, Kanagawa M, Beltran-Valero de Bernabe D, Gundesli H, Willer T, Satz JS, Crawford RW, Burden SJ, Kunz S, Oldstone MB, Accardi A, Talim B, Muntoni F, Topaloglu H, Dincer P, Campbell KP (2011) A dystroglycan mutation associated with limb-girdle muscular dystrophy. N Engl J Med 364:939–946
29. Straub V, Rafael JA, Chamberlain JS, Campbell KP (1997) Animal models for muscular dystrophy show different patterns of sarcolemmal disruption. J Cell Biol 139:375–385
30. Gilhuis HJ, ten Donkelaar HJ, Tanke RB, Vingerhoets DM, Zwarts MJ, Verrips A, Gabreels FJ (2002) Nonmuscular involvement in merosin-negative congenital muscular dystrophy. Pediatr Neurol 26:30–36
31. Grady RM, Grange RW, Lau KS, Maimone MM, Nichol MC, Stull JT, Sanes JR (1999) Role for alpha-dystrobrevin in the pathogenesis of dystrophin-dependent muscular dystrophies. Nat Cell Biol 1:215–220
32. Ichida F, Tsubata S, Bowles KR, Haneda N, Uese K, Miyawaki T, Dreyer WJ, Messina J, Li H, Bowles NE, Towbin JA (2001) Novel gene mutations in patients with left ventricular noncompaction or Barth syndrome. Circulation 103:1256–1263
33. Stollberger C, Finsterer J (2004) Subclinical cardiac involvement in myotonic dystrophy. Neuromuscul Disord 14:694–695, author reply 695–696
34. Woodman SE, Park DS, Cohen AW, Cheung MW, Chandra M, Shirani J, Tang B, Jelicks LA, Kitsis RN, Christ GJ, Factor SM, Tanowitz HB, Lisanti MP (2002) Caveolin-3 knock-out mice develop a progressive cardiomyopathy and show hyperactivation of the p42/44 MAPK cascade. J Biol Chem 277:38988–38997
35. Ohsawa Y, Toko H, Katsura M, Morimoto K, Yamada H, Ichikawa Y, Murakami T, Ohkuma S, Komuro I, Sunada Y (2004) Overexpression of P104L mutant caveolin-3 in mice develops hypertrophic cardiomyopathy with enhanced contractility in association with increased endothelial nitric oxide synthase activity. Hum Mol Genet 13:151–157
36. Han R, Bansal D, Miyake K, Muniz VP, Weiss RM, McNeil PL, Campbell KP (2007) Dysferlin-mediated membrane repair protects the heart from stress-induced left ventricular injury. J Clin Invest 117:1805–1813
37. Kuru S, Yasuma F, Wakayama T, Kimura S, Konagaya M, Aoki M, Tanabe M, Takahashi T (2004) A patient with limb girdle muscular dystrophy type 2B (LGMD2B) manifesting cardiomyopathy. Rinsho Shinkeigaku 44:375–378
38. Millay DP, Goonasekera SA, Sargent MA, Maillet M, Aronow BJ, Molkentin JD (2009) Calcium influx is sufficient to induce muscular dystrophy through a TRPC-dependent mechanism. Proc Natl Acad Sci USA 106: 19023–19028
39. Stiber JA, Zhang ZS, Burch J, Eu JP, Zhang S, Truskey GA, Seth M, Yamaguchi N, Meissner G, Shah R, Worley PF, Williams RS, Rosenberg PB (2008) Mice lacking Homer 1 exhibit a skeletal myopathy characterized by abnormal transient receptor potential channel activity. Mol Cell Biol 28:2637–2647
40. Arnett AL, Chamberlain JR, Chamberlain JS (2009) Therapy for neuromuscular disorders. Curr Opin Genet Dev 19:290–297
41. Angelini C, Fanin M, Pegoraro E, Freda MP, Cadaldini M, Martinello F (1994) Clinical-molecular correlation in 104 mild X-linked muscular dystrophy patients: characterization of sub-clinical phenotypes. Neuromuscul Disord 4:349–358
42. Guerron AD, Rawat R, Sali A, Spurney CF, Pistilli E, Cha HJ, Pandey GS, Gernapudi R, Francia D, Farajian V, Escolar DM, Bossi L, Becker M, Zerr P, de la Porte S, Gordish-Dressman H, Partridge T, Hoffman EP, Nagaraju K (2010) Functional and molecular effects of arginine butyrate and prednisone on muscle and heart in the mdx mouse model of

Duchenne Muscular Dystrophy. PLoS One 5:e11220

43. Rotundo IL, Faraso S, De Leonibus E, Nigro G, Vitiello C, Lancioni A, Di Napoli D, Castaldo S, Russo V, Russo F, Piluso G, Auricchio A, Nigro V (2011) Worsening of cardiomyopathy using deflazacort in an animal model rescued by gene therapy. PLoS One 6:e24729
44. Bauer R, Blain A, Greally E, Lochmuller H, Bushby K, MacGowan GA, Straub V (2010) Attenuation of adverse cardiac effects in prednisolone-treated delta-sarcoglycan-deficient mice by mineralocorticoid-receptor-antagonism. Neuromuscul Disord 20:21–28
45. Parsons SA, Millay DP, Sargent MA, Naya FJ, McNally EM, Sweeney HL, Molkentin JD (2007) Genetic disruption of calcineurin improves skeletal muscle pathology and cardiac disease in a mouse model of limb-girdle muscular dystrophy. J Biol Chem 282:10068–10078
46. Iwata Y, Nakamura H, Mizuno Y, Yoshida M, Ozawa E, Shigekawa M (1993) Defective association of dystrophin with sarcolemmal glycoproteins in the cardiomyopathic hamster heart. FEBS Lett 329:227–231
47. Iwata Y, Katanosaka Y, Arai Y, Komamura K, Miyatake K, Shigekawa M (2003) A novel mechanism of myocyte degeneration involving the Ca2+-permeable growth factor-regulated channel. J Cell Biol 161:957–967
48. Iwata Y, Katanosaka Y, Shijun Z, Kobayashi Y, Hanada H, Shigekawa M, Wakabayashi S (2005) Protective effects of Ca(2+) handling drugs against abnormal Ca(2+) homeostasis and cell damage in myopathic skeletal muscle cells. Biochem Pharmacol 70:740–751
49. Nakamura TY, Iwata Y, Sampaolesi M, Hanada H, Saito N, Artman M, Coetzee WA, Shigekawa M (2001) Stretch-activated cation channels in skeletal muscle myotubes from sarcoglycan-deficient hamsters. Am J Physiol Cell Physiol 281:C690–C699
50. Brown RH Jr (1997) Dystrophin-associated proteins and the muscular dystrophies. Annu Rev Med 48:457–466
51. Mallouk N, Jacquemond V, Allard B (2000) Elevated subsarcolemmal Ca2+ in mdx mouse skeletal muscle fibers detected with Ca2+-activated K+ channels. Proc Natl Acad Sci USA 97:4950–4955
52. Robert V, Massimino ML, Tosello V, Marsault R, Cantini M, Sorrentino V, Pozzan T (2001) Alteration in calcium handling at the subcellular level in mdx myotubes. J Biol Chem 276:4647–4651
53. Vandebrouck C, Duport G, Cognard C, Raymond G (2001) Cationic channels in normal and dystrophic human myotubes. Neuromuscul Disord 11:72–79
54. Vandebrouck C, Duport G, Raymond G, Cognard C (2002) Hypotonic medium increases calcium permeant channels activity in human normal and dystrophic myotubes. Neurosci Lett 323:239–243
55. Franco-Obregon A Jr, Lansman JB (1994) Mechanosensitive ion channels in skeletal muscle from normal and dystrophic mice. J Physiol 481(Pt 2):299–309
56. Kanzaki M, Zhang YQ, Mashima H, Li L, Shibata H, Kojima I (1999) Translocation of a calcium-permeable cation channel induced by insulin-like growth factor-I. Nat Cell Biol 1:165–170
57. Muraki K, Iwata Y, Katanosaka Y, Ito T, Ohya S, Shigekawa M, Imaizumi Y (2003) TRPV2 is a component of osmotically sensitive cation channels in murine aortic myocytes. Circ Res 93:829–838
58. Deng HX, Klein CJ, Yan J, Shi Y, Wu Y, Fecto F, Yau HJ, Yang Y, Zhai H, Siddique N, Hedley-Whyte ET, Delong R, Martina M, Dyck PJ, Siddique T (2010) Scapuloperoneal spinal muscular atrophy and CMT2C are allelic disorders caused by alterations in TRPV4. Nat Genet 42:165–169
59. Landoure G, Zdebik AA, Martinez TL, Burnett BG, Stanescu HC, Inada H, Shi Y, Taye AA, Kong L, Munns CH, Choo SS, Phelps CB, Paudel R, Houlden H, Ludlow CL, Caterina MJ, Gaudet R, Kleta R, Fischbeck KH, Sumner CJ (2010) Mutations in TRPV4 cause Charcot-Marie-Tooth disease type 2C. Nat Genet 42:170–174
60. Vandebrouck C, Martin D, Colson-Van Schoor M, Debaix H, Gailly P (2002) Involvement of TRPC in the abnormal calcium influx observed in dystrophic (mdx) mouse skeletal muscle fibers. J Cell Biol 158:1089–1096
61. Maroto R, Raso A, Wood TG, Kurosky A, Martinac B, Hamill OP (2005) TRPC1 forms the stretch-activated cation channel in vertebrate cells. Nat Cell Biol 7:179–185
62. Gottlieb P, Folgering J, Maroto R, Raso A, Wood TG, Kurosky A, Bowman C, Bichet D, Patel A, Sachs F, Martinac B, Hamill OP, Honore E (2008) Revisiting TRPC1 and TRPC6 mechanosensitivity. Pflugers Arch 455:1097–1103
63. Gervasio OL, Whitehead NP, Yeung EW, Phillips WD, Allen DG (2008) TRPC1 binds to caveolin-3 and is regulated by Src kinase - role in Duchenne muscular dystrophy. J Cell Sci 121:2246–2255
64. Goonasekera SA, Lam CK, Millay DP, Sargent MA, Hajjar RJ, Kranias EG, Molkentin JD

(2011) Mitigation of muscular dystrophy in mice by SERCA overexpression in skeletal muscle. J Clin Invest 121:1044–1052

65. Morine KJ, Sleeper MM, Barton ER, Sweeney HL (2010) Overexpression of SERCA1a in the mdx diaphragm reduces susceptibility to contraction-induced damage. Hum Gene Ther 21:1735–1739
66. Menke A, Jockusch H (1991) Decreased osmotic stability of dystrophin-less muscle cells from the mdx mouse. Nature 349:69–71
67. Petrof BJ, Shrager JB, Stedman HH, Kelly AM, Sweeney HL (1993) Dystrophin protects the sarcolemma from stresses developed during muscle contraction. Proc Natl Acad Sci USA 90:3710–3714
68. Iwata Y, Katanosaka Y, Arai Y, Shigekawa M, Wakabayashi S (2009) Dominant-negative inhibition of Ca2+ influx via TRPV2 ameliorates muscular dystrophy in animal models. Hum Mol Genet 18:824–834
69. Zanou N, Iwata Y, Schakman O, Lebacq J, Wakabayashi S, Gailly P (2009) Essential role of TRPV2 ion channel in the sensitivity of dystrophic muscle to eccentric contractions. FEBS Lett 583:3600–3604

Concluding Remarks

As highlighted in the introduction to this book, much remains to be discovered about the Transient Receptor Potential (TRP) superfamily of ion channels. Even the most thoroughly characterized member of the family continues to provide controversy and surprises. Our goal is to summarize the current state of the art in regard to the literature as well as methods. This comprehensive collection provides up-to-date information on targets that are being pursued in human clinical trials (TRPV1 and TRPA1) as well as less-explored family members that may serve as the next generation of "hot" drug targets. Of particular interest are the TRP channels that human genetic data implicate in disease. These include TRPML1 (mucolipidosis type IV), TRPC6 (focal segmental glomerular sclerosis), TRPP2 (polycystic kidney disease), TRPV4 (varied peripheral neuropathies and spinal dysplasias), and TRPM4 (progressive familial heart block type 1). We expect the material presented here will help investigators as they think about targeting TRP channels to improve human health and will promote discussion of this exciting and diverse family of proteins.

Arpad Szallasi and Tamás Bíró (eds.), *TRP Channels in Drug Discovery: Volume II*, Methods in Pharmacology and Toxicology,
DOI 10.1007/978-1-62703-095-3, © Springer Science+Business Media, LLC 2012

INDEX

A

Arpad Szallasi and Tamás Bíró (eds.), *TRP Channels in Drug Discovery: Volume II*, Methods in Pharmacology and Toxicology,
DOI 10.1007/978-1-62703-095-3, © Springer Science+Business Media, LLC 2012

B

C

D

E

F

G

H

I

K

L

M

N

O

P

R

S

T

U

V

W

Z